DISSERTATION ZUR ERLANGUNG DES DOKTORGRADES
DER FAKULTÄT FÜR CHEMIE UND PHARMAZIE
DER LUDWIG-MAXIMILIANS-UNIVERSITÄT MÜNCHEN

Synthesis and Characterization of New Energetic Materials Based on Various Energetic Building Blocks and Investigation of Different Industrial RDX Synthesis

Jasmin Theresia Lechner
aus
Heilbronn, Deutschland
2023

Erklärung

Diese Dissertation wurde im Sinne von § 7 der Promotionsordnung vom 28. November 2011 von Herrn Prof. Dr. Thomas M. Klapötke betreut.

Eidesstattliche Versicherung

Diese Dissertation wurde eigenständig und ohne unerlaubte Hilfe erarbeitet.

München, ...29.11.2023.....

_____

(Jasmin T. Lechner)

Dissertation eingereicht am 12.10.2023

1. Gutachter: Prof. Dr. Thomas M. Klapötke

2. Gutachter: Prof. Dr. Konstantin L. Karaghiosoff

Mündliche Prüfung am 23.11.2023

Für Oma Theresia und Oma Inge ❤

– zwei inspirierende und starke Frauen –

DANKSAGUNG

Zuallererst möchte ich mich bei meinem Doktorvater, Herrn Prof. Dr. Thomas M. Klapötke bedanken. Vielen Dank für die Möglichkeit meine Promotion bei Ihnen im Arbeitskreis machen zu dürfen und für Ihr Vertrauen in mich und meine Arbeit. Ich habe mich oft gefordert, doch stets gefördert und vor allem immer gut aufgehoben gefühlt. Vielen Dank für Ihre ruhige, unkomplizierte, positive und immer absolut nahbare Art. Bei jeder kleinen, aber auch größeren Herausforderung konnte ich mir Ihrer Unterstützung immer gewiss sein.

Mein weiterer großer Dank gilt Herrn Prof. Dr. Konstantin Karaghiosoff für die Übernahme des Zweitgutachtens, aber vielmehr für seine aufgeschlossene und stets optimistische Art sowie der Hilfe bei jeglichen Problemen.

Daneben danke ich Frau Prof. Dr. Silvija Markic, Herrn Prof. Dr. Hans-Christian Böttcher, Herrn Prof. Dr. Oliver Trapp und Frau Prof. Dr. Ivana Ivanović-Burmazović für die Bereitschaft an der Prüfungskommission teilzunehmen.

Ein weiterer Dank geht an Herrn Dr. Burkhard Krumm. Vielen Dank für die Hilfe bei verschiedenen NMR-Messungen sowie deren Auswertung.

Für praktische sowie mentale Unterstützung möchte ich mich bei Herrn Dr. Jörg Stierstorfer bedanken. Du bist zwar nicht mein Doktorvater, jedoch auf jeden Fall mein „Doktorpapa“. Vielen Dank für deine Unterstützung, sei es beim Fertigstellen der Kristallstrukturen oder beim Korrekturlesen der Manuskripte, wenn ich dich gebraucht habe, warst du immer zu Stelle. Danke aber auch für die unzähligen Tipps und Gespräche sowohl über Uniinternes aber auch Uniexternes.

Als nächstes geht mein Dank an unsere Sekretärin Frau Irene Scheckenbach. Vielen Dank, dass Sie den Arbeitskreis so zusammen und am Laufen erhalten. Es ist wirklich nicht einfach bei dem Bürokratiewirrwarr der Uni durchzusteigen aber Sie wissen immer Bescheid, was man wie, wo, bei wem beantragen muss. Vielen Dank für Ihre stets positive und sympathische Art sowie stetige Hilfsbereitschaft.

Ein weiterer Dank geht an Prof. Klapötke und Jörg für die Möglichkeit neben der klassischen Forschung im Arbeitskreis auch ein Teil bzw. Mitarbeiter der EMTO GmbH gewesen sein zu dürfen. Mir haben meine Kooperationen und Projekte immer viel

Spaß gemacht und ich konnte neben dem Arbeiten am Abzug auch meine Organisation und Management Fähigkeiten erweitern.

Außerdem möchte ich mich bei Herrn Dr. Moritz Mühlemann sowie Herrn Guillaume Lemarchand der Firma BIAZZI S.A. bedanken. Vielen Dank für die tolle Zusammenarbeit in verschiedenen Projekten, die Einladung in die Schweiz und nach Italien und die allgemeine Unterstützung während meiner Promotion.

Dem chemisch technischen Assistenten unseres Arbeitskreises, Herrn Stefan Huber, möchte ich auch meinen Dank widmen. Lieber Stefan, vielen Dank für deine lustige und aufgeschlossene Art mit der du das ein oder andere Sensitivitätsmessen zu einem richtigen Erlebnis gemacht hast. Vielen Dank auch für die unzähligen witzigen Gespräche und deinen Beitrag zu den „green energetics“ durch das ständige Umtopfen und Verteilen deiner Fittonie.

„Wenn die Chemie stimmt, stimmt auch die Reaktion.“ Genau das beschreibt unseren Arbeitskreis perfekt. So viele verschiedene Charaktere und trotzdem harmonieren wir perfekt miteinander und sind ein unschlagbares Team. Mein riesengroßer Dank geht an alle aktuellen, aber auch ehemalige Mitglieder des Arbeitskreises Klapötke. Natürlich liebe ich es am Abzug zu stehen und Chemie zu machen, aber vor allem die Gruppenmitglieder haben dazu beigetragen, dass ich mich jeden Morgen gefreut habe in die Uni zu fahren. Mein Dank geht an: Lukas Bauer, Lukas Eberhardt, Markus Rösch, Simon Endraß, Jelena Reinhart, Jan „Willi“ Cremers, Simon Thamm, Marcus Lommel, Tobias Lenz, Andreas Bartonek, Chris Riedelsheimer, Andi Neuer, Alex Schweiger, Jonathan Tietze, Alexander Gisnapp, Maurus Völkl, sowie Dr. Maxi Benz, Michi Gruhne, Dr. Alex Harter, Dr. Moritz Kofen, Dr. Cornelia Unger, Dr. Anne Friedrichs und Dr. Teresa Bölter. Ihr seid alle tolle Menschen und habt euren ganz eigenen Beitrag zur Gruppe geleistet. Ich finde es ist nicht selbstverständlich, dass man seine Kollegen auch als Freunde bezeichnen kann und ich bin sehr dankbar, dass ich ein Teil dieser Gruppe sein durfte.

Hervorheben möchte ich hier Likas und Simson, die beiden EXPLO Experten unseres Arbeitskreises. Die gemeinsame Geschäftsreise nach Zagreb, wenn auch ohne Gepäck, war mir ein Fest!

Ganz besonders möchte ich mich an diese Stelle aber bei Chris bedanken! Jeden Tag meiner Promotion warst du an meiner Seite und hast mit mir jeden witzigen Moment

erlebt aber auch jede Krise durchgestanden. Du warst mir mit deiner ruhigen und besonnenen Art eine riesige Unterstützung, hast dir aber auch immer die Zeit genommen mit mir zu tigern oder sonstigen Schmarrn zu unternehmen. Ich schätze dich chemisch sowie persönlich extrem und bin jetzt schon traurig, wenn ich an den Tag denke, an dem ich dich nicht mehr meinen Kollegen nennen darf. Ich wünsche dir für deine Zukunft wirklich nur das aller Beste und alles Glück der Welt!

Mein weiterer Dank geht an meine Praktikanten Katharina Solohub, Leon „Bre“ Walter Bernhard Stanislawski, Nina Gerold und Jennifer Heidrich. Es war mir stets eine Freude mit euch zusammen zu arbeiten und mein Wissen an euch weiterzugeben. Eure Arbeit im Labor hat einen großen Beitrag zu dieser Arbeit geliefert.

Mein weiterer besonderer Dank geht an alle Mitglieder der „Lab Fam“. Liebe*r Leon, Nina, Jenny, Melina, Darya und Julia, die Zeit mit euch im Labor war unvergleichlich aufregend, witzig und schön. Ihr seid alle sehr tüchtig und engagiert und euch vor allem für nichts zu schade. Auf euch war einfach immer Verlass und ich muss wirklich sagen ich bin sehr stolz auf jeden von euch!

Außerdem möchte ich mich noch bei ein paar Leuten abseits der Uni bedanken. Zuerst einmal bei allen Mitgliedern des Zeltlager Billigheims. Diese zwei Wochen im Jahr sind mein absoluter Happy Place, an dem ich abschalten und einfach glücklich sein kann. Vielen Dank an alle die es jedes Jahr möglich machen diesen Happy Place wieder für mich zu erschaffen. Ein besonderer Dank an dieser Stelle geht an Saskia Müller und Mario Mayerhöffer, Danke für eure Unterstützung und das Rückenstärken.

Mein weiterer Dank geht an Tessa! Wahre Freundschaft ist keine Selbstverständlichkeit und deshalb möchte ich dir Danke sagen! Danke, dass es dich gibt und du immer für mich da bist! Danke für dein gut Zureden, Motivieren, Unterstützen und Aufbauen und Danke, dass ich immer auf dich zählen kann! Danke, dass du, auch wenn ich mal wieder was Komisches gemacht habe, mich verstehst und mir den Rücken stärkst!

Zweifellos wäre diese Arbeit nicht möglich gewesen ohne die Unterstützung meiner Familie, LIEBE. ♥. Ich möchte mich deshalb vor allem bei meiner Mutter Judith, bei meinem Vater Jürgen bedanken. Liebe Mama, lieber Papa, Danke für die unglaubliche Unterstützung die ich von euch bekomme. Danke dass ihr immer für mich da seid und Danke dass ihr immer an mich glaubt. Danke für eure Geduld und euer Verständnis

und Danke, dass ihr mir beigebracht habt was wichtig ist im Leben. Danke euch, dass ihr mich zu dem Menschen gemacht habt, der ich heute bin. Außerdem möchte ich mich bei meinem Zwillingsbruder Julian bedanken, auch mit wenig Worten (wahrscheinlich durch die Zwillingsverbindung) verstehen wir uns blind und wissen meistens was der andere gerade braucht oder denkt. Natürlich geht mein Dank auch an meine Schwägerin Mareike, Danke, dass ich mich immer auf euch verlassen kann. Und zuletzt geht mein Dank an meine Oma Inge, der ich zum Teil auch diese Arbeit gewidmet habe. Liebe Omi, du bist einfach unvergleichlich und unersetzlich. Danke für alle Weisheiten, die du mir gegeben hast und für alles was du mir beigebracht hast.

Table of Content

1 Introduction

The world of energetic materials is large and manifold. Especially because of its diversity, there are many different ways to divide the field of high-energy materials. For example, one possibility is to divide them depending on their area of application into energetic materials for civilian applications or military applications. Another division, probably the most common one, is the division according to their type of application. Here, as shown in Figure 1, there are three main areas: **Explosives**, **pyrotechnics** and **propellants**.[1-5]

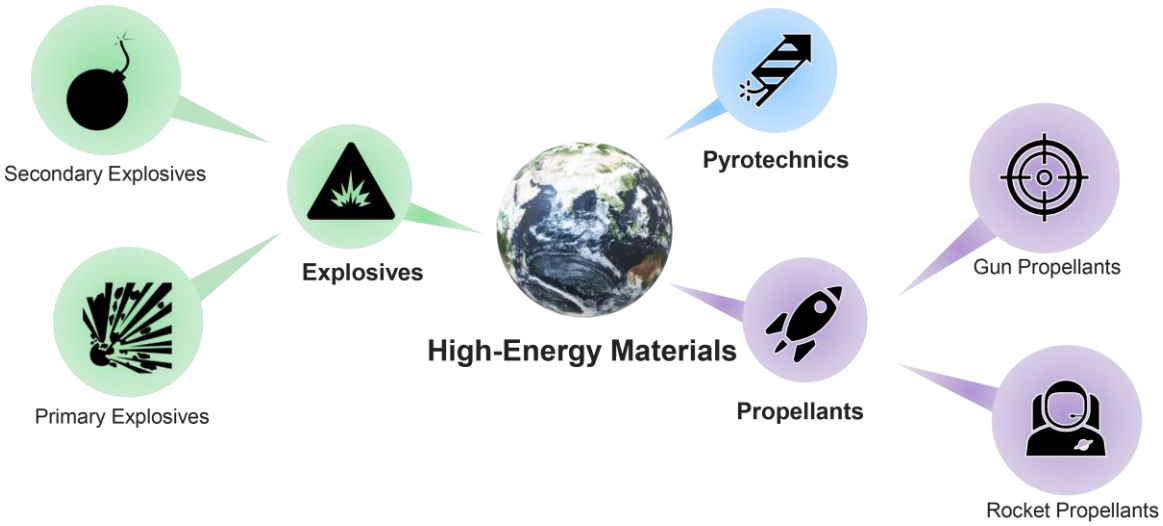

Figure 1. Division of high-energy materials according to their type of application.

The word **pyrotechnics** is derived from the Greek word '*pyr*' which translates as 'fire'. These are substances or mixtures of substances that can generate light, heat, sound, gas, smoke or combinations thereof. The specific properties such as burning color are controlled by the individual components or by additives, but basically the pyrotechnic mixtures always consist of an oxidizer and a reducing agent.[1,2,6-8]

The section of **propellants**, as shown in Figure 1, can be further subdivided into **gun propellants** and **rocket propellants** depending on type of their subsequent area of application. Both subareas often use similar formulations with the same components, but the difference between the two sections is in their burning behavior. While gun propellants undergo rapid deflagration, rocket propellants combust in a more controlled manner. This can be seen especially in the burn rate,

which is much faster for gun propellants, resulting in a drastically increased pressure. The pressure during isochoric deflagration of gun propellants is approximately 50 times higher than that of rocket propellants.[1,4,9-11] Moreover, the group of rocket propellants can be further subdivided, but here a distinction is made according to the aggregate condition of propellant mixture and is divided into solid propellants and liquid propellants. While liquid propellants are then divided into hypergolic and non-hypergolic component mixtures,[12,13] solid propellants are subdivided into heterogeneous propellants and homogeneous propellants.[11,14,15] Figure 2 shows the main difference between homogeneous and heterogeneous solid propellant mixtures. Heterogeneous propellant mixtures, as shown in Figure 2 on the left, are mixtures of several components that can be mixed well but are still present individually in the mixture. The best-known example are the so-called composite propellants. One component is a polymer binder, in most cases HTPB (hydroxyl-terminated polybutadiene). Into this binder, a crystalline oxidizer, usually ammonium perchlorate (NH_4ClO_4), and a fuel, in this case aluminum (Al) powder, are admixed.[1, 4, 11, 16]

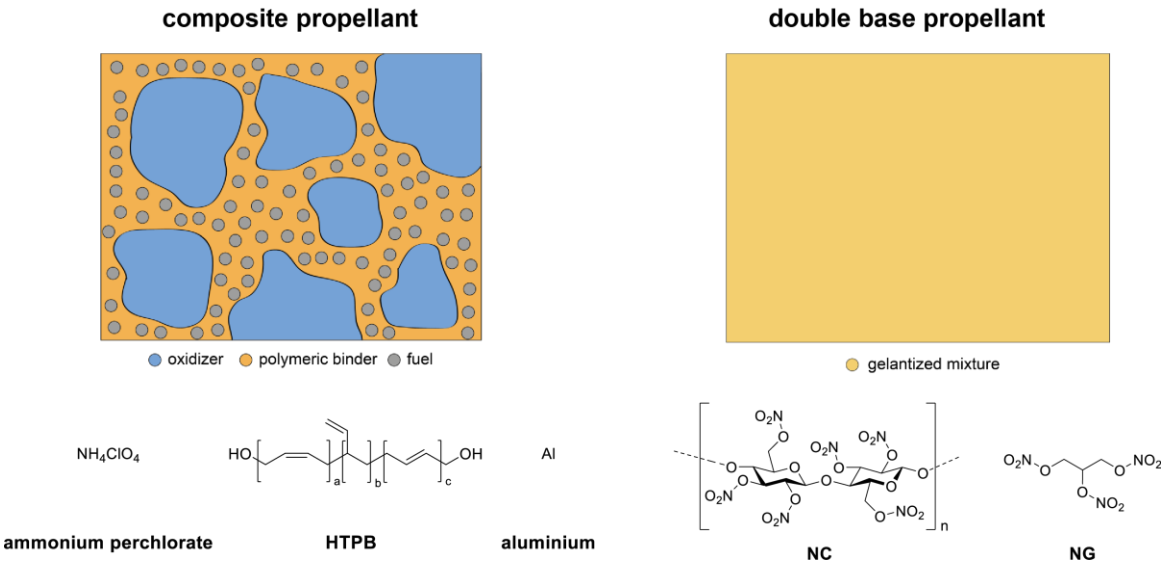

Figure 2. Examples of heterogeneous (left) and homogeneous (right) propellants with molecular structures of exemplary components.

Figure 2 on the right shows an example of a homogeneous propellant mixture. The example shows a double base propellant, consisting of a mixture of nitrocelluloce (NC) and nitroglycerin (NG). In the figure the main difference between the

homogeneous propellants and the heterogeneous propellants can be seen. When the homogeneous propellant components are mixed, they gelantize and thus an inseparable homogeneous formulation is formed.[1,4,11,17]

Additives can be added to such homogeneous propellant mixtures to modify their properties or adapt them to the desired values. For example, nitroguanidine (NQ) can be added (known as triple base propellants) to increase the impact sensitivity of the mixture, making it more handleable or to decrease its thermal stability.[18,19] Basically there are five groups of possible additives: oxidizers, fuels, stabilizers, burn rate modifiers and plasticizers. The name of the group already describes its modification possibilities.[18, 20] For the group of the plasticizers, in general, there is a difference between energetic and inert plasticizers, some examples of energetic plasticizers can be seen in Figure 3.[18, 21]

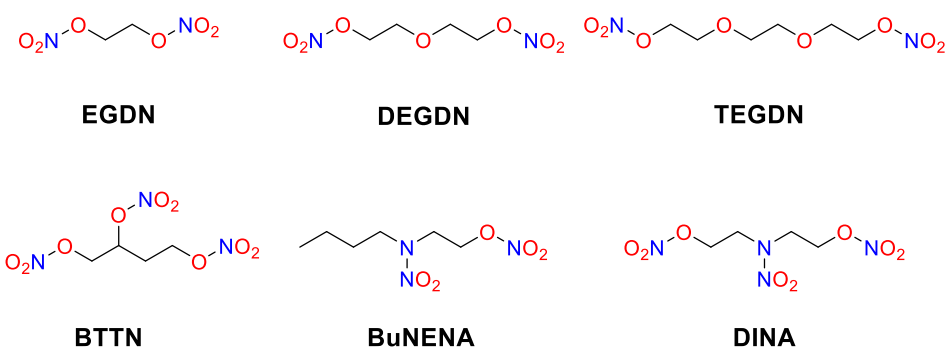

Figure 3. Molecular structures of the energetic plasticizers EGDN (ethylene glycol dinitrate), DEGDN (diethylene glycol dinitrate), TEGDN (triethylene glycol dinitrate), BTTN (butanetriol trinitrate), BuNENA (*n*-butyl nitroxyethylnitramine) and DINA (dinitroxyethyl nitramine dinitrate).

Looking at the structures of the energetic plasticizers, it is obvious that they have very similar structures to the main components of the double base propellants NC and NG. Ethylene glycol dinitrate (EGDN), diethylene glycol dinitrate (DEGDN), triethylene glycol dinitrate (TEGDN) and butanetriol trinitrate (BTTN) each have at least two nitric esters as functional groups. Similar to nitroglycerin, they are liquid at room temperature and gelatinize well with nitrocellulose.[1,4,18] With regard to the processing of the final propellant mixture, this offers advantages because the consistency of the finished mixture can be easily adjusted with less sensitive components. Especially TEGDN and BTTN show advantages, due to their lower volatility, lower sensitivity and higher thermal stability compared to

nitroglycerin.[22-24] *n*-Butyl nitroxyethylnitramine (BuNENA) and dinitroxyethyl nitramine dinitrate (DINA) belong to the group of the nitroxyethyl nitramines (NENAs), which combine a nitramine unit and a nitric ester functional group in one molecule. These compounds also gelatinize well with nitrocellulose, changing the properties of the mixture. Nevertheless, they are also of particular interest because they produce high burning rates at reduced flame temperatures in the final formulations.[18, 22, 25]

Continuing with the section of **explosives**, these are divided into the two main categories of **primary explosives** and **secondary explosives**.[1-5] Both areas differ significantly in the sensitivities and performance parameters of the compounds but also in their decomposition behavior. Primary explosives are easy to initiate due to their low sensitivity and undergo very fast deflagration to detonation transition (DDT), generating a large heat or shock wave which is then able to initiate secondary explosives.[26, 27] Deflagration derives from the Latin word '*deflagrare*' which can be translated as 'burning', detonation comes from Latin '*detonare*' which translates as 'thundering'. Based on this these translations, the difference between the two processes can be derived. Deflagration is a kind of rapid burning under pressure development, but the velocity remains below the speed of sound of the surrounding medium. In the case of a detonation, the burning process is faster than the speed of sound, which produces a sound or thunder.[1, 26] Usually, primary explosives are, as already mentioned, significantly more sensitive towards heat, impact and friction, but at the same time have a lower detonation velocity and detonation pressure than secondary explosives.[1, 26, 27] In an ignition system, therefore, their properties are used in such a way that they are placed before the main charge to transfer the detonation to the less sensitive secondary explosive.[1, 26, 28] Examples of common primary explosives can be seen in Figure 4.

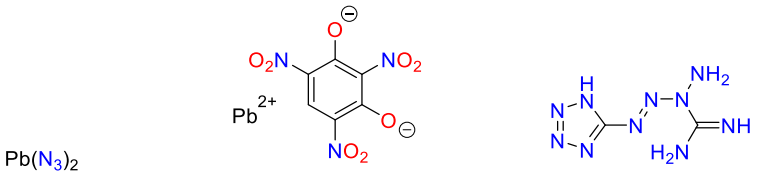

Figure 4. Molecular structures of the common primary explosives lead azide (LA), lead styphnate (LS) and tetrazene.

Lead azide is used, for example, in detonators. Here, a pyrotechnical mixture is initiated by an ignitor, for example an electrical match. This pyrotechnical mixture, which simply consists of a mixture of oxidizer (e.g. potassium nitrate) and a fuel (e.g. magnesium powder), then initiates the primary explosive, which then propagates the shockwave to the secondary explosive. In such detonators, PETN is usually used as the secondary explosive. This detonator then ignites the main charge, in some cases a booster charge is placed in between for reinforcement.[1, 26] Since lead azide is very sensitive towards external stimuli, it is phlegmatized in industry when it is synthesized in larger quantities for safe handling while manufacturing. By the addition of dextrin during the production of lead azide, crystal growth can be controlled to avoid formation of the extremely sensitive needles.[1, 29] Lead styphnate is used, for example, in primers. It is less powerfull than lead azide but is much easier to initiate, especially by flame. In primers based on lead styphnate, tetrazene is often added as sensitizer, as it is very sensitive towards friction and thus the primer's response can be improved.[1, 26, 29]

Secondary explosives have moderate sensitivities compared to primaries and cannot be ignited as easily by heat or shock compared to primary explosives. According to the definition their impact sensitivity is greater than or equal to 4 J and the friction sensitivity is greater than or equal to 50 N.[1] However, as mentioned before, they have better performance parameters than primary explosives. The most important parameters for secondaries are the detonation velocity (V_{det} in m s^{-1}), the detonation pressure (P in kbar) and the heat of explosion (Q in kJ kg^{-1}).[1-5, 30-32] For these parameters in military grade explosives there is the general aim ‘the higher the better’, which is why secondaries are also known as high explosives. There are many different areas of application for this class of explosives, so their properties can differ strongly and be of varying importance. Such a special application is, for example, blasting under hot conditions such as oil deposits. Here, thermally stable secondaries are required. An example of such a secondary is hexanitrostilbene (HNS), which is thermally stable up to above 300°C.[5] Another special area of secondaries are the so-called melt-castable compounds. Probably the best-known example here is 2,4,6-trinitrotoluene (TNT), which is still widely used. Another example is 2,4-dinitroanisole (DNAN). The compounds in this area should be solid at room temperature, but should be able to melt in a water bath at about 80°C. For safety reasons, their thermal stability should

be about 100 degrees higher than the melting temperature.[5, 33] In booster charges, so-called booster explosives are required, an example of these is pentaerythritol tetranitrate (PETN).[1, 26, 34] This group of substances is somewhat more sensitive towards impact and friction than common secondaries, but still offers a high detonation velocity and pressure and can be easily initiated for example by detonators. As the name booster explosive already suggests, they then reinforce the initiation towards the main charge. Figure 5 shows several examples of industrially applied secondary explosives.[1, 26, 34]

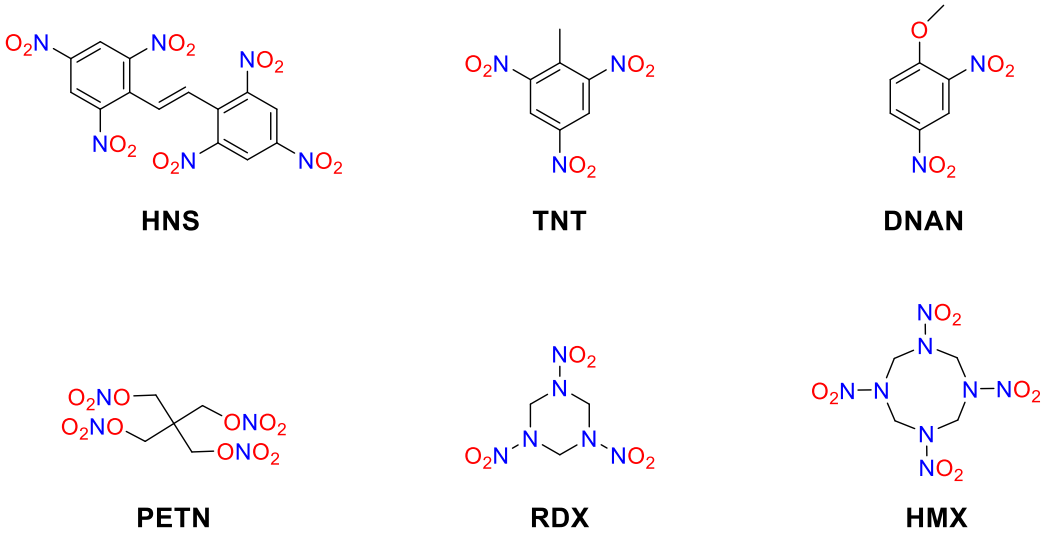

Figure 5. Molecular structures of the common secondary explosives hexanitrostilbene (HNS), 2,4,6-trinitrotoluene (TNT), 2,4-dinitroanisole (DNAN), pentaerythritol tetranitrate (PETN), 1,3,5-trinitro-1,3,5-triazine (RDX) and 1,3,5,7-tetranitro-1,3,5,7-tetrazocine (HMX).

The safe handling of explosives is a very important issue, especially in large-scale industrial manufacturing, but also in the transport or preparation of blasting activities. This is the reason why secondary explosives such as hexogen (RDX) and also octogen (HMX) are incorporated into so-called plastic bonded explosives (PBX).[1, 35] Here, the solid explosives are embedded in a polymer matrix, this is why PBX is sometimes also referred as polymer-bonded explosive. Established PBX formulations are Composition C4, Composition B or SEMTEX.[1] In the latter, for example, the polymer matrix consists of non-energetic polyisobutylene (PIB) and besides the main components PETN and RDX for preparation reasons also a non-energetic plasticizer is added.[1, 5, 36]

Although **research on new energetic materials** has been going on for many years, substances such as TNT, RDX or lead azide are still used today even they are known for a very long time and have different disadvantages. There are various reasons for this. On the one hand, it is very difficult to develop new compounds that outperform the existing substances in all their properties. In addition, there are many requirements that are set for new compounds. According to the slogan "higher, faster, further", compounds are always searched for which surpass everything that has existed so far, but at the same time the corresponding compound should also be very safe, stable, non-toxic and easy to synthesize. In particular, the toxicity and environmental impact of the high-energy materials used so far represent a major disadvantage. Figure 6 shows some of the main disadvantages of currently used substances.[1]

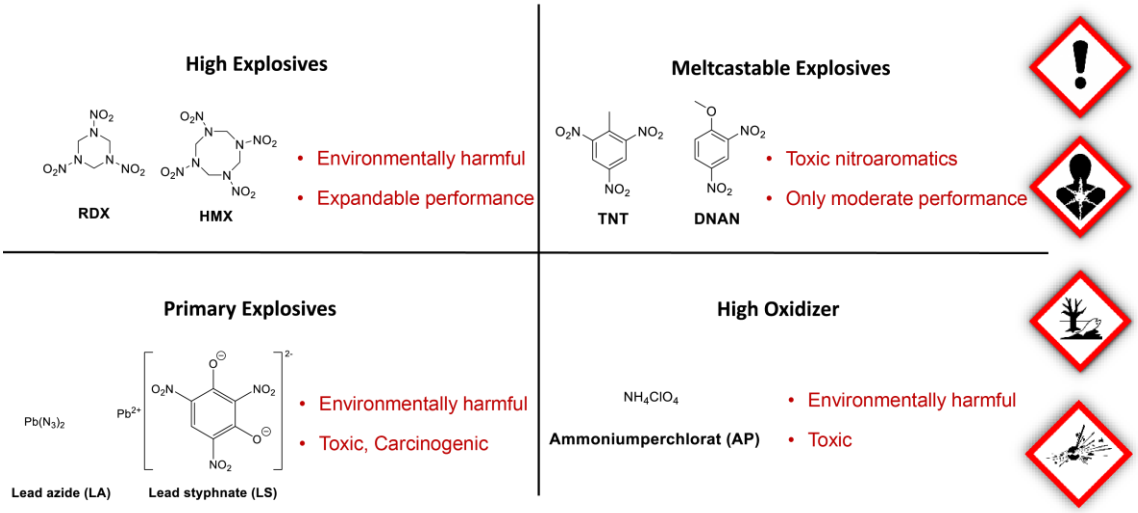

Figure 6. Nowadays used energetic materials of the different categories with their disadvantages.

In general, the research of new energetic materials can be divided into two parts. On the one hand, the part of the research which is of **industrial interest** and on the other hand, which is **academically relevant**.

The academic interest applies to research on substances that are far too exotic or expensive to ever find any application in real life, but whose properties are very interesting to study. An example of this is the isotopic modification with ^{2}D or ^{13}C of energetic materials or the synthesis of substances which are only stable at certain temperature or atmospheric conditions.

Industrially relevant is for example research work, which deals with synthesis optimization in terms of a simple, cheap and safe reaction pathway. For RDX, for instance, there is half a dozen of different synthesis routes. Two of them are used industrially: the Woolwich process and the Bachmann process, which can be seen in Figure 7.[1, 37-39]

Woolwich Process:

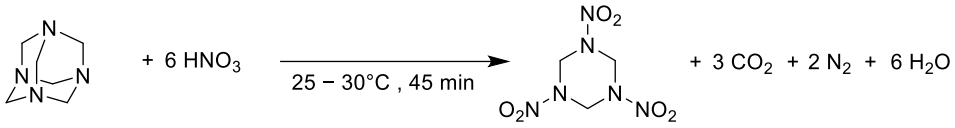

Bachmann Process:

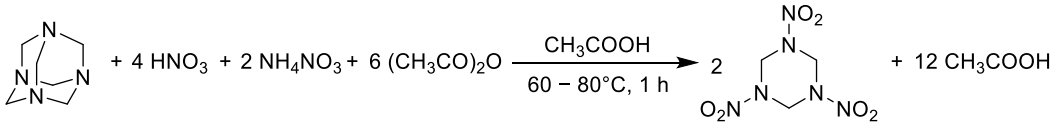

Figure 7. Synthetic pathways of the industrial used Woolwich and Bachmann Process for RDX synthesis.

Both synthesis routes start with the same starting material: hexamine. In the Woolwich process, however, nitration is achieved directly with nitric acid, while in the Bachman process nitration is achieved with a mixture of ammonium nitrate, acetic acid anhydride and nitric acid. Due to the different nitration conditions, the Bachmann process requires less nitric acid, which is significantly more cost-efficient. However, this synthesis route also produces different by-products which then have to be removed by purification steps.[1, 37, 39] A study of the exact reaction conditions and ratios as well as experimental influences such as filter steps can lead to an improvement of already established syntheses.

Moreover, the complete and further characterization of already known and used energetics in order to better understand their behavior and properties is of interest for the industry. Especially the synthesis of new energetic materials as possible substitutes for nowadays used energetics which overcome their plays a major role of industrial interest in energetic materials research. In the following, possible substitutes in different categories of high-energy materials are given.

Research on new high explosives is focused on the search for replacements of RDX (and HMX). RDX and also its decomposition products are harmful to the environment as well as weakly toxic to the human body.[40] Furthermore, RDX with a detonation velocity of about 8800 m s^{-1} and HMX with 9200 m s^{-1} have good performance parameters, but there is still potential for improvement here as well.[30] Dihydroxylammonium-5,5′-bistetrazolyl-1,1′-diolate (TKX-50) is a possible substitution for RDX and HMX, it was first prepared in 2012 by the research group of *Prof. Klapökte* in Munich. It shows promising properties, having a higher detonation velocity than RDX of about 9700 m s^{-1} while being less sensitive towards impact and having a slightly higher thermal stability.[41] However, a lot of optimization and testing must still be done. Like scaling up and working out a possible industrial synthesis as well as many experimental tests to verify the theoretical performance parameters. Also, 1,1-diamino-2,2-dinitroethylene (FOX-7) which was developed by FOI in Sweden shows promising properties, has a slightly weaker performance than RDX but is much less sensitive and easier to synthesize.[30, 42] Hexanitrohexaazaisowurtzitane (CL-20) which was developed by China Lake facility is a possible HMX substitute and has a even higher detonation velocity of about 9500 m s^{-1}, nevertheless the synthesis of CL-20 is very complex and expensive.[30, 43]

In research for new melt-castable energetics, replacements for TNT and also DNAN are searched. Both nitroaromatics, and in this case especially their decomposition products, are toxic to the environment and humans.[44] In addition, the two have only very low performance parameters, which can still be significantly increased, such as a velocity of detonation of TNT of only about 6900 m s^{-1}.[30] As already mentioned, in this special area other parameters are more important than a good performance, for example, suitable melting and decomposition temperatures. A possible substitute here is 1,3,3-trinitroazetidine (TNAZ), which was first synthesized by *Archibald et al.* in 1990.[45, 46]

The two most commonly used primary explosives are lead azide and lead styphnate. These are both lead compounds and are therefore toxic to the environment and humans due to the heavy metal nature of lead.[1, 47] Possible substitutes are therefore also needed in this area. One possible compound is copper(I) 5-nitrotetrazolate (DBX-1), which was first published in 2011. It is said to have an equivalent or better output than LA at the same volume.[48]

The search for substitutes is also being performed in the field of propellants, especially for ammonium perchlorate. In this case the perchlorate anion is the main problem. Despite the great properties for use as an oxidizer, it is toxic and environmentally harmful.[1, 49] A possible replacement in this case is TNEF, which provides a good oxygen balance combined with moderate sensitivities.[50] The structures of the substitutes mentioned above can be seen in Figure 8.

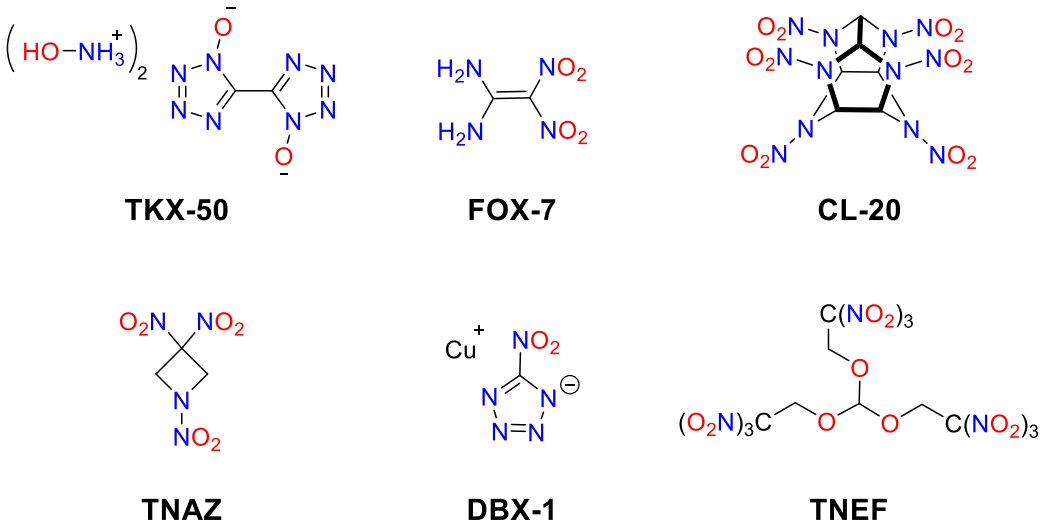

Figure 8. Molecular structures of dihydroxylammonium-5,5′-bistetrazolyl-1,1′-diolate (TKX-50), 1,1-diamino-2,2-dinitroethylene (FOX-7), hexanitrohexaazaisowurtzitane (CL-20), 1,3,3-trinitroazetidine (TNAZ), copper(I) 5-nitrotetrazolate (DBX-1) and trinitroethyl formate (TNEF).

The substitutes shown above have promising properties and thus a possible chance for industrial application. However, as already mentioned, the path from discovery to real industrial synthesis and manufacture is very long and complex. Moreover, there is always the possibility of an even better replacement, thus the search for new and possibly even better substitutes is still ongoing.

There are various **synthesis strategies** for the research of new energetic materials.[1-5] On the one hand, strategies are needed to bring energy into the chemical structure, as the name high energy materials already suggests. At the same time, however, also strategies to stabilize the chemical structure, so that they become handleable, are needed. Looking at the long known as well as the new energetic compounds presented above, many structural similarities can be seen. A high nitrogen content, for example, leads to an increased energy in the molecule, since a lot of energy is released during its decomposition when N_2 is formed. In

addition, ring and cage strain contribute to an increase of the energy content in the compound. In the synthesis of energetic materials, at least one nitration reaction is present in almost all synthesis routes. This is because the oxidation of a CHNO-backbone, the introduction of nitro groups into a compound, can also increase the energy content. However, to find the right compromise between increased energy content and stability, stabilization strategies must also be considered. One example here is the introduction of amino groups close to nitro groups. Intermolecular interactions of the two functional groups with each other lead to stabilization. Also, the formation of salts of energetic anions with energetic but also metal cations leads to the stabilization of the compound due to the corresponding enhanced lattice energy.[1-5] When designing new energetic compounds, various **building blocks** can be used, considering the strategies mentioned above, to synthesize promising new compounds.[1-5, 37] Some, but not all, possible examples of building blocks of energetic materials are shown in Figure 9.

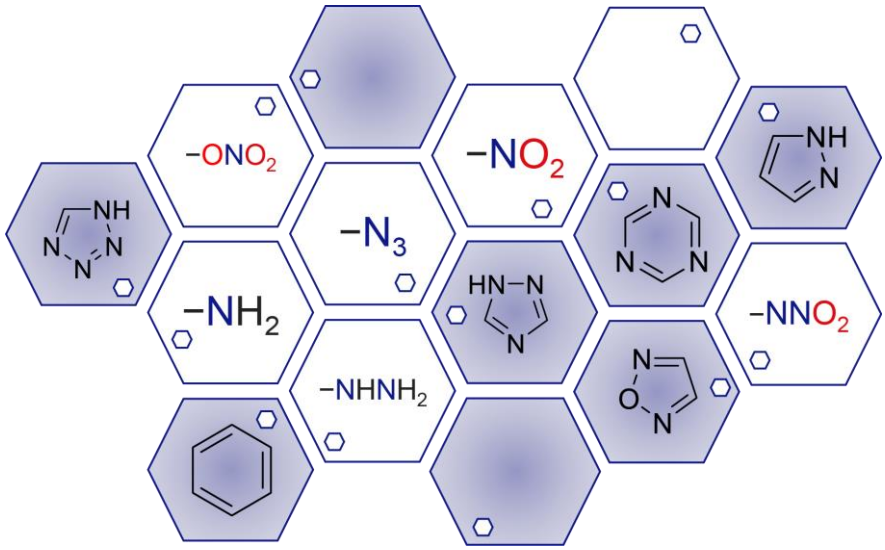

Figure 9. Different building blocks for the synthesis of new energetic materials.

The white boxes show different examples of energetic functional groups. Covalent bonded azides (-N_3), for example, increase the nitrogen content of a compound. While nitro groups (-NO_2) or nitric esters (-ONO_2) as well as nitramines (-NNO_2) increase the energy by oxidation to nitro compounds. Amino groups (-NH_2) or also hydrazines (-$NHNH_2$) increase the nitrogen content while additionally stabilizing through intramolecular interaction at the same time. These functional groups are

then in most cases attached to various CHNO-based building blocks when designing new energetic compounds. These building blocks can be open-chain or, as shown here in the blue boxes, various cyclic basic building blocks. As examples, different azoles such as pyrazole, 1,2,4-triazole and tetrazole or 1,2,5-oxadiazole are shown in Figure 9. Moreover, six-membered ring compounds such as triazine or benzene are depicted. Due to the cage strain of the rings shown here, their use in the corresponding energetic materials leads to an increase of the energy content. In the cases of the N-based heterocycles, it also to an increase of the nitrogen content.[1-5, 37] Thus, by combining these energetic building blocks, new promising compounds can be designed.

1.1 References

[1] T. M. Klapötke, *Chemistry of High Energy Materials*, 6th ed., de Gruyter, Berlin/Boston, **2022**.

[2] E.-C. Koch, *High Explosives, Propellants, Pyrotechnics,* 1st ed., de Gruyter, Berlin/Boston, **2021**.

[3] J. Akhavan, *The Chemistry of Explosives*, 4th ed., Royal Society of Chemistry, Cambridge, **2022**.

[4] J. P. Agrawal, *High Energy Materials: Propellants, Explosives and Pryotechnics*, 1st ed., USA Wiley-VCH New Jersey, **2010**.

[5] R. Meyer, J. Köhler, A. Homburg, *Explosivstoffe*, 10th ed., Wiley-VCH, Weinheim, **2008**.

[6] S. Kanitkar, D. Haynes, E. M. Sabolsky, B. Chorpening, *Prop., Explos., Pyrotech.* **2023**, e202300012.

[7] G. Steinhauser, T. M. Klapötke, Angew. Chem. Int. Ed. **2008**, *47*, 3330−3347.

[8] J. J. Sabatini, *Prop., Explos., Pyrotech.* **2018**, *43*, 28−37.

[9] V. Gettwert, M. A. Bohn, H. Schubert, *Propellants*. in *Ullmann's Encyclopedia of Industrial Chemistry*, Wiley, **2015**.

[10] N. Kubota, *Propellants and Explosives*, Wiley-VCH, Weinheim, **2007**.

[11] J. Liu, *Nitrate Esters Chemistry and Technology*, Springer, **2019**.

[12] A. de laco Veris, *Fundamental Concepts of Liquid-Propellant Rocket Engines*, Springer, **2021**.

[13] Q. Zhang, J. M. Shreeve, *Chem. Eur. J.* **2013**, *19*, 15446−15451.

[14] A. Davenas, *J. Propuls. Power.* **2003**, *19*, 1108−1128.

[15] J. P. Agrawal, H. Singh, *Prop., Explos., Pyrotech.* **1993**, *18*, 106−110.

[16] T. L. Boggs, R. L. Derr, M. W. Beckstead, *AIAA Journal* **1970**, *8*, 370−372.

[17] I. S. Tseng, V. Yang, *Combust. Flame.* **1994**, *96*, 325−342.

[18] J. J. Sabatini, E. C. Johnson, *ACS Omega* **2021**, *6*, 11813−11821.

[19] D. Trache, A. F. Trachoun, *J. Mater. Sci.* **2018**, *53*, 100−123.

[20] R. Steinberger, P. D. Drechsel, *Adv. Chem.* **1969**, *88*, 1−28.

[21] A. M. A. Maraden, P. Stojan, J. Zigmund, R. Matyas, *Cent. Eur. J. Energ. Mater.* **2018**, *15*, 485−500.

[22] G. Bikelytė, M. A. Härtel, M. Holler, A. Neuer, T. M. Klapötke, *J. Chem. Eng. Data* **2021**, *66*, 1709-1716.

[23] M. A. Härtel, T. M. Klapötke, J. Stierstorfer, L. Zehetner, *Prop. Explos., Pyrotech.* **2019**, *44*, 484−492.

[24] F. J. Pisacane, NSWC TR 82−380; Defense Technical Information Center, **1982**.

[25] R. V. Cartwright, *Prop., Explos., Pyrotech.* **1995**, *20*, 51−57.

[26] R. Matyas, J. Pachman, *Primary Explosives*, 1st ed., Springer, Heidelberg/New York/Dordrecht/London, **2013**.

[27] Q.-u.-N. Tariq, S. Manzoor, M.-u.-N. Tariq, W.-L. Cao, W.-S. Dong, F. Arshad, J.-G. Zhang, *ChemistrySelect* **2022**, *7*, e202200017.

[28] K. D. Oyler, *Green Primary Explosives in Green Energetic Materials*, **2014**, 103−131.

[29] N. Mehta, K. Oyler, G. Cheng, A. Shah, J. Marin, K. Yee, *Z. anorg. allg. Chem.* **2014**, *64*, 1309−1313.

[30] T. M. Klapötke, *Energetic Materials Encyclopedia*, 2nd ed., DeGruyter, Berlin/Boston, **2021**.

[31] N. V. Muravyev, D. R. Wozniak, D. G. Piercy, *J. Mater. Chem. A* **2022**,*10*, 11054−11073.

[32] S. Zeman, M. Jungová, *Prop. Explos., Pyrotech.* **2014**, *41*, 426−451.

[33] P. Ravi, D. M. Badgujar, G. M. Gore, S. P. Tewari, A. K. Sikder, *Prop. Explos. Pyrotech.* **2011**, *36*, 393−403.

[34] T. M. Klapötke, G. Lemarchand, T. Lenz, M. Mühlemann, J. Stierstorfer, F. Venetz, R. Weber, J. Wutke, *Prop., Explos., Pyrotech.* **2023**, *48*, e202200288.

[35] J. J. Pietron, P. B. Mirkarimi, *Prop., Explos., Pyrotech.* **2022**, *47*, e202100379.

[36] A. Elbeih, S. Zeman, M. Jungova, P. Vávra, Z. Akstein, *Prop., Explos., Pyrotech.* **2012**, 37: 676−684.

[37] J. P. Agrawal; R. D. Hodgson, *Organic Chemistry of Explosives*, 1st ed., USA Wiley-VCH, **2007**.

[38] W. de. C. Crater, *Ind. Eng. Chem.*, **1948**, *40*, 1627–1635.

[39] W. E. Bachmann, J. C. Sheehan, *J. Am. Chem. Soc.*, **1949**, *71*, 1842–1845.

[40] E. L. Etnier, *Regulat. Toxicol. Pharmacol.* **1989**, *9*, 147–157.

[41] N. Fischer, D. Fischer, T. M. Klapötke, D. G. Piercey, J. Stierstorfer, *J. Mater. Chem.* **2012**, *22*, 20418–20422.

[42] A. J. Bellamy, *FOX-7 (1,1-Diamino-2,2-dinitroethene). in High Energy Density Materials: Structure and Bonding*, Springer, Berlin/ Heidelberg, **2007**.

[43] U. R. Nair, R. Sivabalan, G. M. Gore, *Combust. Explos. Shock Waves* **2005** *41*, 121–132.

[44] L. A. Smock, D. L. Stoneburner, J. R. Clark, *Water Research* **1976**, *10*, 537–543.

[45] T. G. Archibald, R. Gilardi, K. Baum, C. George, *J. Org. Chem.* **1990**, 55, 2920–2924.

[46] D. S. Viswanath, T. K. Ghosh, V. M. Boddu, *1,3,3-Trinitroazetidine (TNAZ). in Emerging Energetic Materials: Synthesis, Physicochemical, and Detonation Properties*, Springer, Dordrecht, **2018**.

[47] L. T. Fairhall, W. V. Jenrette, S. W. Jones, E. A. Pritchard, *Public Health Reports (1896-1970)*, **1943**, *58*, 607-617.

[48] J. W. Fronabarger, M. D. Williams, W. B. Sanborn, J. G. Bragg, D. A. Parrish, M. Bichay, *Prop. Explos., Pyrotech.* **2011**, *36*, 541–550.

[49] P. Niziński, A. Błażewicz, J. Kończyk, R. Michalski, *Environ. Health*, **2021**, *36*, 199–222.

[50] D. E. Dosch, K. Andrade, T. M. Klapötke, B. Krumm, *Prop., Explos., Pyrotech.* **2021**, *46*, 895–898.

2 Motivation and Objectives

The objective and target of this work was to contribute to all areas of research on high-energy materials shown in Figure 1. The work is also structured according to this principle.

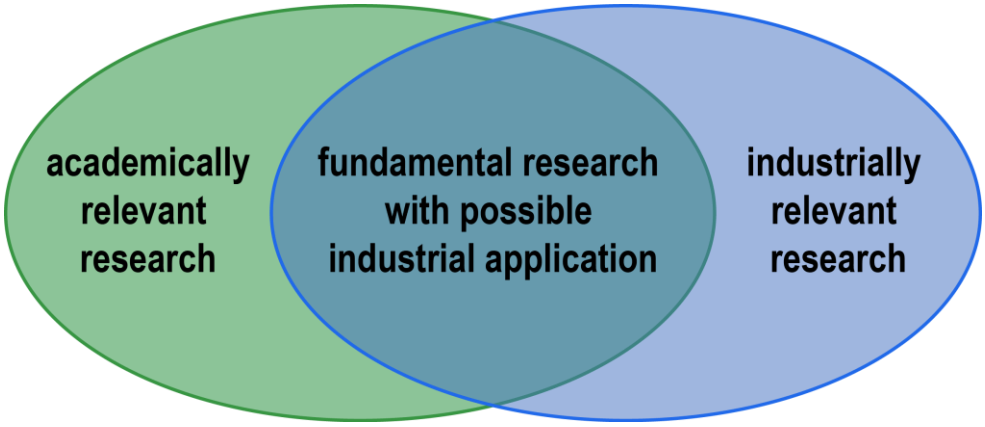

Figure 1. Research areas in the field of high-energy material research.

The first chapters deal with academically relevant research, the goal in this part was to label the promising energetic material FOX-7 with both ^{2}D and ^{13}C isotopes. The main objective here was to investigate the changed properties due to the isotopic labeling. In addition, however, the aim was to use the substances in a cooperation with the University of Hawaii at Mānoa to study their decomposition process under specific conditions. This is followed by a chapter where the already known and widely used energetic plasticizers EGDN, DEGDN and TEGDN were crystallized in order to better understand their behavior at low temperatures and thus provide new safety information for the industry. The main part of the thesis deals with fundamental research on the synthesis of new energetic materials based on the strategies previously described and using the building blocks shown above. However, this fundamental research is always carried out with a perspective of possible application and the compounds are investigated for their possible use as substitutes. As already mentioned before, this design of new substitutes is not that easy. In addition to various requirements on the properties of the compound itself, there is also a list of requirements on the synthesis of the compound in order to make a real application or industrial production possible. Some of these

requirements along the path from discovery towards industrial application can be seen in Figure 2.

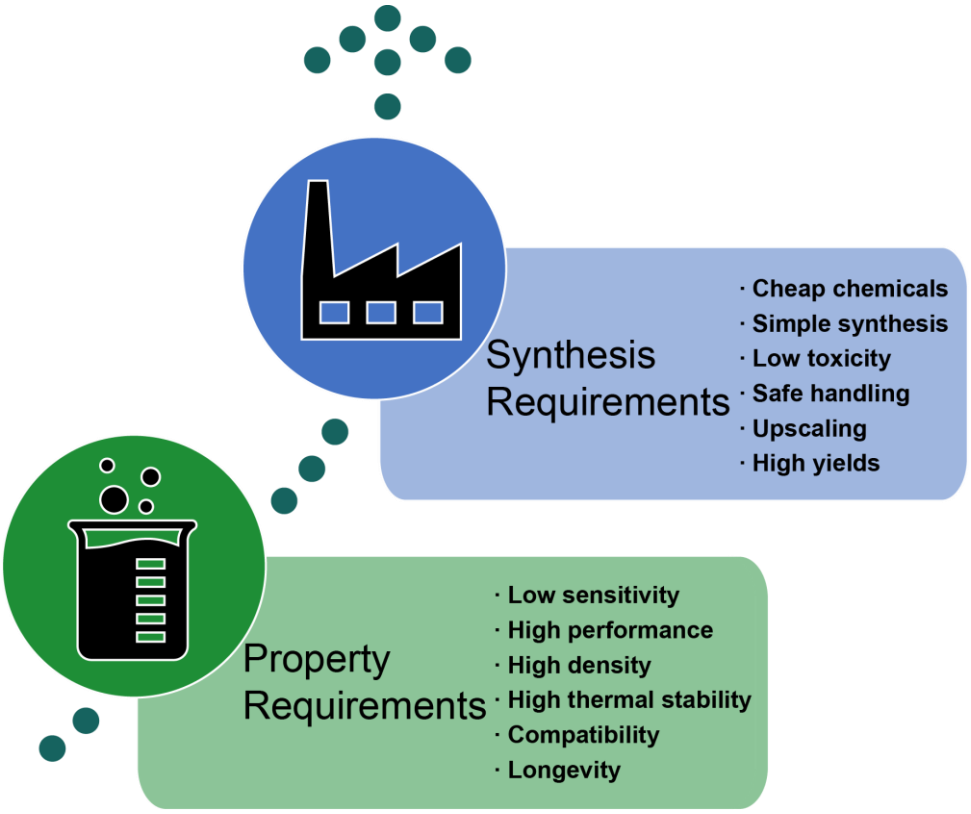

Figure 2. Property and synthesis requirements for new high-energy materials.

The requirements on the properties are relatively simple to define, the compound should have as much power as possible while being relatively insensitive towards external stimuli such as impact, friction but also heat. A high density contributes to a good performance, so this is always favored. In addition, the compound should be compatible with various other energetic materials as well as binders and plasticizers for later use in formulations. The requirements on the synthesis are mainly that the synthesis is kept relatively simple. This means few synthesis steps, few purification steps and, if feasible, no needed inert atmosphere. The synthesis should therefore also be easy to scale up and relatively safe for the operator working on it. In addition, all reactants, products and by-products used should be cheap and of course non-toxic. The aim of the main part of the work was to synthesize the new substances and, above all, to investigate them with regard to the property requirements described above and moreover to compare and discuss

them as possible substitutes. The last part of the thesis deals mainly with the industrially relevant research area. On the one hand, a possible new synthesis route for RDX was investigated and compared with the processes already used in industry. Furthermore, the last chapter shows a cooperation project with the industry, in which the Bachmann process for RDX and HMX synthesis was studied and different process variations, for example the filter temperature, and their impact on the product were investigated.

3 Investigation of Deuterated FOX-7 – Changes in Structural Behavior and Energetic Characteristics after Deuteration under Ambient Conditions

Thomas M. Klapötke*, Burkhard Krumm, Jasmin T. Lechner and Jörg Stierstorfer

as published in *Dalton Transactions* **2022**, *51*, 5788−5791

DOI: 10.1039/D2DT00490A

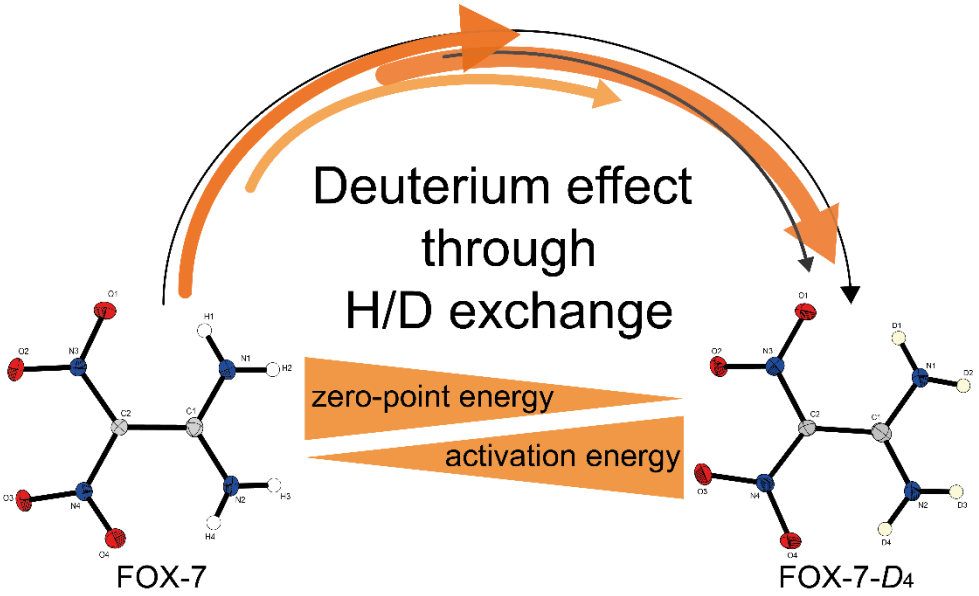

Abstract: For an investigation of the deuterium effect of *N*-deuterated compounds on the structural and thermal behavior, 1,1-diamino-2,2-dinitroethylene (FOX-7) was deuterated by deprotonation in heavy water and subsequent acidification with D_2SO_4. The status of deuteration progress was monitored by infrared spectra analysis and the deuteration level was determined *via* ^{1}H q-NMR. The properties of FOX-7-D_4 were studied by single crystal X-ray diffraction and differential thermal analysis. In addition, the activation energy of thermal decomposition was determined, and the heat of formation and zero-point energy were calculated.

3.1 Introduction

In the past, various energetic materials have been isotopically modified with deuterium, some of which are shown in Figure 1. The main reason for deuteration was to investigate their different physical and chemical properties compared to the "normal" hydrogenated homologues. Interestingly, in all of the examples shown in Figure 1, only C-H bonds were deuterated.

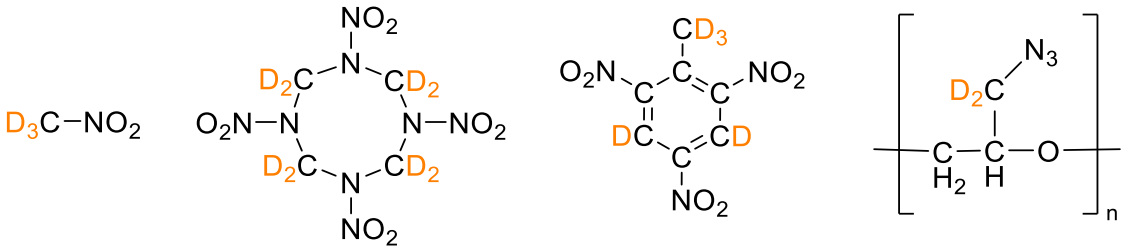

Figure 1. Molecular structures of deuterated energetic materials, which have been reported previously in the literature.[1–4]

The previously reported examples not only classical secondary explosives such as HMX[1] (octahydro-1,3,5,7-tetranitro-1,3,5,7-tetrazocine) and TNT[2] (2,4,6-trinitrotoluene), but also propellant ingredients as nitromethane[3] as well as the energetic polymer GAP[4] (glycidyl azide polymer). In the research of energetic materials, the decomposition process has one of the most important roles and therefore it is important to elucidate the mechanism which occurs. For example, by understanding which decomposition products are formed and in which

composition, allows knowledge about the long-term stability, explosion performance and sensitivity of the compounds. For such investigations, it is necessary for the hydrogenated compound to be compared with the deuterated one. For example, Kaiser *et al.* studied nitromethane and nitromethane-d_3 as the simplest model and example of energetic nitro-*CDNO*-compounds.[3]

However, the deuteration of energetic materials not only allows a better understanding of their decomposition mechanism, but also shows the influence of the deuterium effect on the structure and thermal stability. This deuterium effect, or kinetic isotope effect in general, is observed when bonds to isotopes are built or broken, as the case in the thermal decomposition process of explosives.[5] This effect is particularly significant for cases in which exchange of hydrogen by deuterium occurs, since the mass of the atom is directly doubled by the isotope exchange involving H and D. The primary kinetic isotope effect states that bonds with deuterium have a significantly lower zero-point energy but at the same time a significantly higher activation energy than the same bond with hydrogen, because a C-H (D^0_{298}: 338.4 kJ mol^{-1}) bond breaks several times faster than a C-D (D^0_{298}: 341.4 kJ mol^{-1}) bond.[5] For energetic materials, this would mean that an energetic compound should show an increase in its energetic properties by a simple H/D exchange.

In this work, for the first time the influence of deuteration on the structural properties and the energetic characteristics of nitrogen-deuterium bonds was investigated using the well-known energetic compound FOX-7 (1,1-diamino-2,2-dinitroethylene) as an example.

3.2 Results and Discussion

3.2.1 Synthesis

For the synthesis of deuterated FOX-7, its acid-base equilibrium known from literature was exploited.[6] For this purpose, sodium deuteroxide solution was first prepared by dissolving elemental sodium in heavy water. FOX-7 was then dissolved in this solution and deprotonated *in situ* to give its conjugate base. After addition of concentrated deuterated sulfuric acid, the equilibrium was shifted again and the compound could be deuterated.[7]

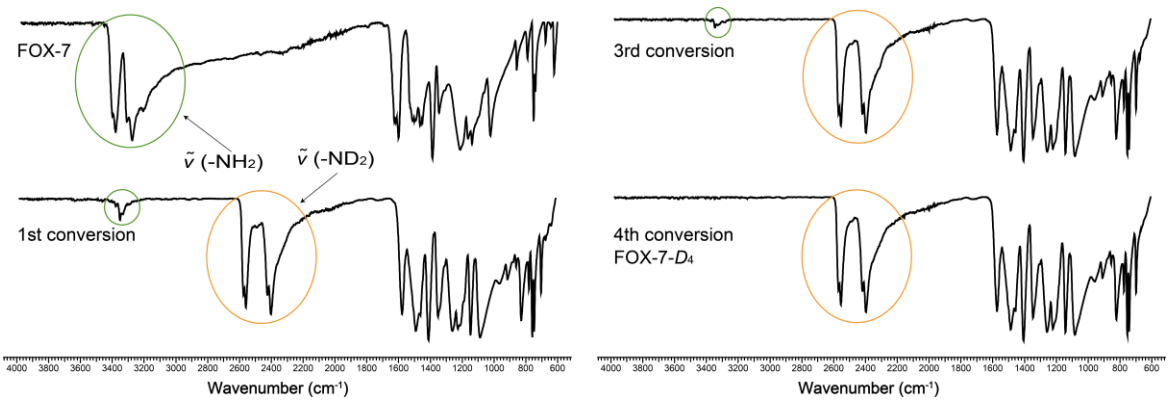

Figure 2. Infrared spectra of the different conversion steps from FOX-7 into FOX-7-*D*4.

As indicated in Scheme 1, this synthesis was iteratively repeated four times in order to obtain the deuteration level as high as possible.

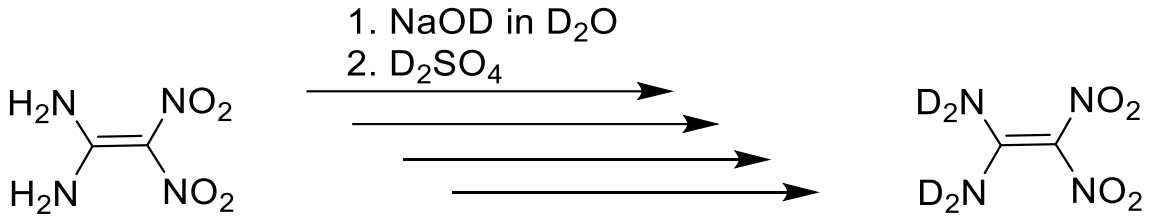

Scheme 1. Repeated (4 times) synthesis for the preparation of FOX-7-*D*4.

Since the amount of deuterated FOX-7-*D*4 is exponentially increasing with each repetition and therefore only little amount of FOX-7 is left for deuteration, the process needed to be repeated only four times.

3.2.2 Characterization

The successful isotope labeling can be followed particularly well using IR spectroscopy, shown in Figure 2 with the different conversion steps.

The replacement of an atom by a heavier isotope leads to a downshift in wavenumbers.[8] In the IR spectra this red shift of the -NH_2 vibrations at 3500−3200 cm^{-1} to the -ND_2 vibrations at 2600−2200 cm^{-1} is clearly visible. Moreover, using IR spectroscopy the conversion was monitored, the -NH_2 peaks decrease with each repetition, while the -ND_2 peaks increase.

A comparison of the NMR spectra in DMSO-D_6 of FOX-7-D_4 with those of FOX-7 reveals only minimal differences. In the ^{14}N NMR spectrum only the resonance of the nitro group is visible for both at −25 ppm with no effect on NH or ND. In the ^{13}C NMR spectrum only a very small difference is detected for the amino bound carbon resonance (158.1 to 158.0 ppm for FOX-7-D_4). The carbon bound to the nitro groups remains at the same position for both isotopomers at 128.0 ppm. The deuterium resonance in the ^{2}D NMR spectrum (in DMSO-H_6) is detected as broadened singlet at 8.6 ppm.

For a determination of the exact isotopic purity, a quantitative ^{1}H NMR (q-NMR) was recorded using ethylene carbonate as external standard. According to equation for calculation of q-NMR,[9] the isotopic purity of FOX-7-D_4 is 95.7%.

3.2.3 Crystal Structure

It was possible to obtain single crystals of the deuterated species of FOX-7 (CCDC 2150220) by slow crystallization. FOX-7-D_4 crystallizes in the orthorhombic space group *Pna*2$_1$ as pale yellow blocks. This is somewhat surprising, in general it was expected that crystallization in the same space group as FOX-7 occur. Since hydrogen and deuterium do not differ in their electronic properties but only in the mass of the nucleus, FOX-7 and FOX-7-D_4 are by definition isosteric (same atomic number, electron number and atomic shells).[10] FOX-7, however, crystallizes in the monoclinic space group *P*2$_1$/*n* published in 1998.[11] The density of FOX-7-D_4 recalculated to room temperature is 1.902 g cm^{-3}, which is as expected slightly higher than that of FOX-7 with 1.872 g cm^{-3} at room temperature, the recalculation method of the densities is explained in more detail in the Supporting Information (SI). The crystal structures of FOX-7 and FOX-7-D_4, as well as the corresponding Newman projections along the C=C axis and a section of their crystal package are shown in Figure 3. If the molecular structures of the two FOX-7 derivatives are compared, it can be concluded that the structure of the individual molecules do not significantly differ. The Newman projection highlights, that the -NH_2 and the -ND_2 groups are located in the C=C plane. In addition, in both compounds one of the two nitro groups almost lies in this plane, whereas the second nitro group is clearly twisted out of this plane. Comparing the dihedral angels of both compounds, the nitro groups in FOX-7-D_4 are slightly more twisted out the plane than in the non-

deuterated FOX-7. A view at the two different crystal packings shows for both ABA zig-zag layers. However, after close examination, those of FOX-7 appear to lie identically parallel on top of each other with only a slight twist in the y axis. The layers of FOX-7-D_4, on the other hand, differ more clearly. The B layers are rotated and shifted by 180 degrees to the A layers. This could possibly be the reason that FOX-7-D_4 crystallizes in a different space group.

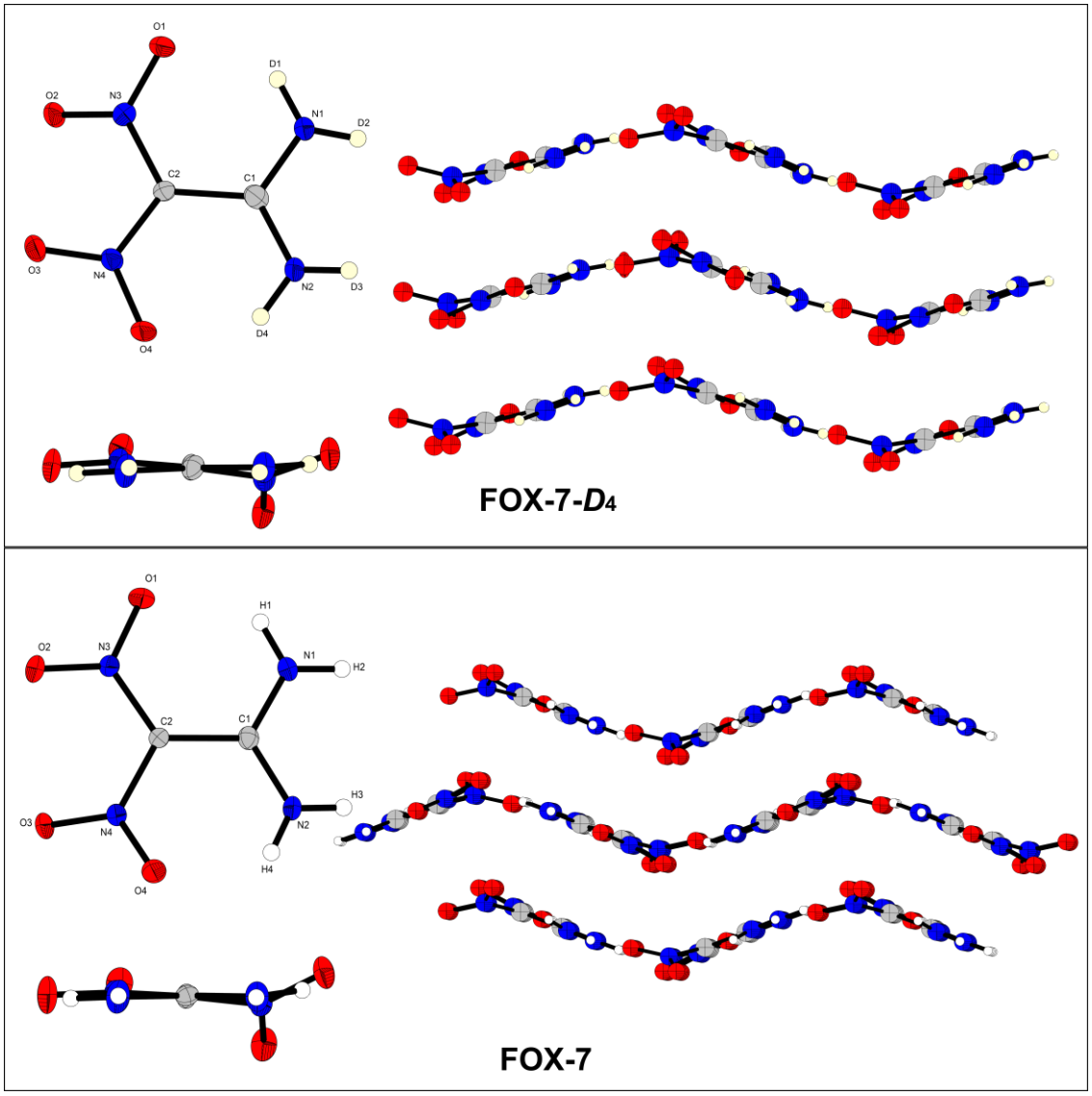

Figure 3. Top: Molecular structure, Newman projection and crystal package of FOX-7-D_4; Bottom: Molecular structure, Newman projection and crystal package of FOX-7[11]; Thermal ellipsoids of non-hydrogen atoms in all structures are set to the 50% probability level. Selected dihedral angels of FOX-7-D_4 (°): O4−N4−C2−N3 168.7(3), O3−N4−C2−C1 168.7(3), O1−N3−C2−N4 154.6(3), O2−N3−C2−C1 148.7(4). Selected dihedral angels of FOX-7 (°): N3−C2−N4−O4 −171.78(15), C1−C2−N4−O3 −171.03(15), N4−C2−N3−O1 −148.00(15), C1−C2−N3−O2 −143.57(16).

The experimentally determined (X-ray) solid state structures of FOX-7 and FOX-7-D_4 show one slightly shorter and one longer C-NO_2 bond, as well as one shorter and one longer C-NH_2/C-ND_2 bond. Both structures with their bond lengths are shown in Figure 4.

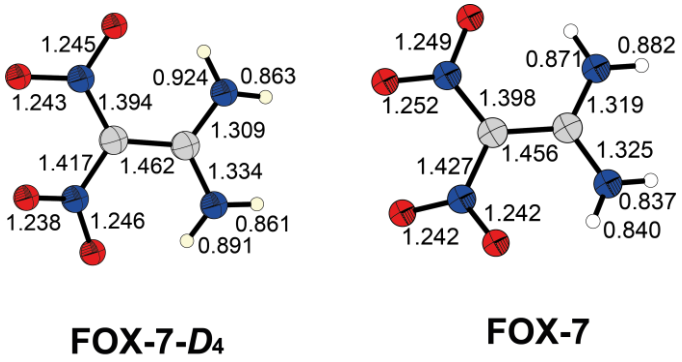

Figure 4. Molecular structures of FOX-7-D_4 and FOX-7[11] with their bond lengths.

3.2.4 Thermal Analysis

The thermal behavior of FOX-7 has been extensively studied in the past. For example, two high-temperature modifications beta and gamma FOX-7 have been discovered.[6] The phase transition from alpha to beta can be observed at ca. 115°C, whereas the transition from beta to gamma occurs at ca. 173°C and decomposition being observed at about 228°C. By comparison of the DTA spectra of FOX-7 and FOX-7-D_4, Figure 5 shows that the deuterated compound has a decomposition temperature of 255°C, which is about 30°C higher than that of the non-deuterated compound.

As mentioned before, hydrogen bonds require less energy to be cleaved compared to deuterium bonds, which explains the higher thermal stability. The deuterated species also shows an endothermic signal at 114°C, which suggests a phase transition also for FOX-7-D_4 to another polymorph (which was not yet further investigated).

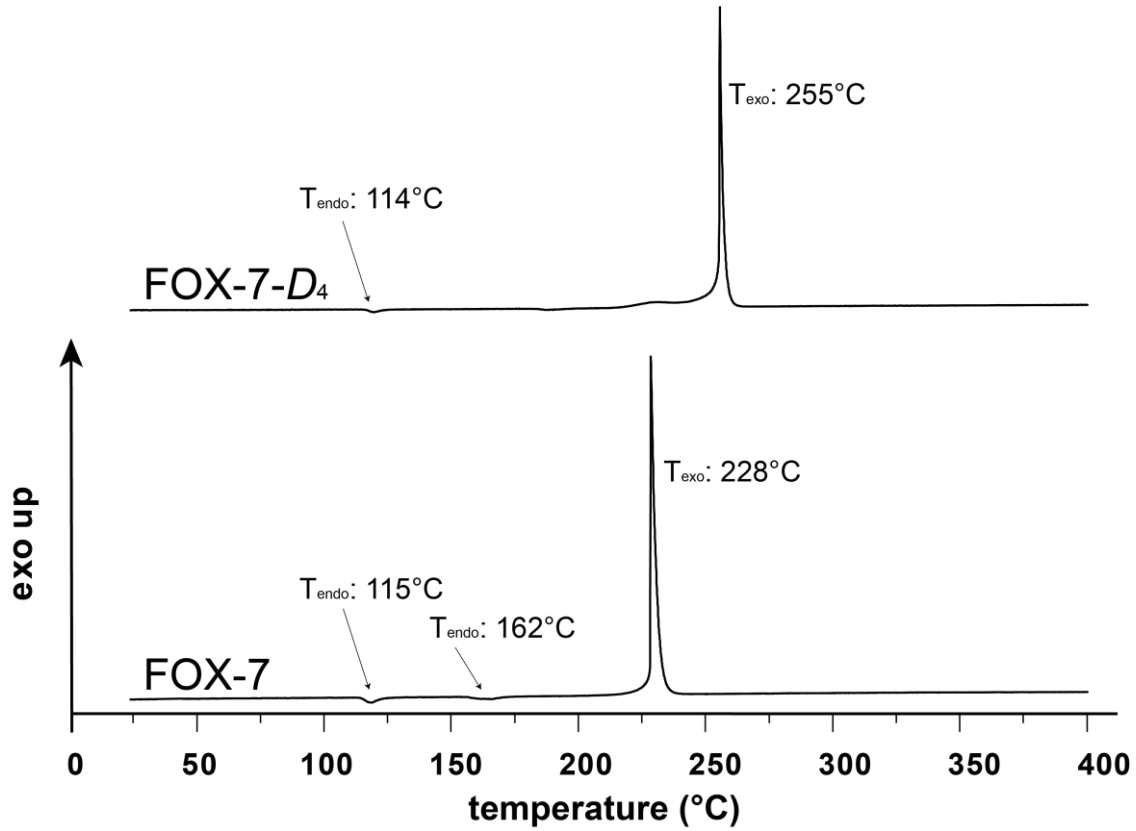

Figure 5. Differential thermal analysis spectra of FOX-7-D_4 and FOX-7 with their onset temperatures measured in the range from 25°C to 400°C with a heating rate of 5°C min^{-1}.

The activation energy of the thermal decomposition as function of the conversion of FOX-7 and FOX-7-D_4 was determined using the NETZSCH Kinetics Neo software,[13] therefore thermal gravimetric analysis (TGA) measurements were performed. The Friedman method was chosen, since overall it provided the best fit values and activation energies for FOX-7 of 90 kJ mol^{-1} and for FOX-7-D_4 of 225 kJ mol^{-1} were obtained. The previously made assumption that the activation energy for deuterated compounds is higher could therefore be confirmed experimentally.

3.2.5 Quantum Chemical Calculations

All performed quantum chemical calculations are explained in more detail in the SI. Table 1 shows the results of the various calculations. Because the W1BD method is the most accurate one, only the results obtained using this method will be discussed in more detail. The zero-point energy of FOX-7 (237.3 kJ mol^{-1}) is higher

than that of FOX-7-D_4 (202.6 kJ mol^{-1}) in agreement with the expectation that deuterated compounds show lower ZPEs than the non-deuterated analogue. The calculated HOF of FOX-7-D_4 (−114.0 kJ mol^{-1}) is also lower than that of FOX-7 (−91.0 kJ mol^{-1}). Calculations of the detonation parameters in this case would be very interesting but they are ongoing, since no code is available for the calculation of deuterated explosives now.

Table1. Heat of formation and zero-point energy calculation of FOX-7 and FOX-7-D_4.

	method	$-H^{298}$ [a] /a.u.	$\Delta_f H°$(g) [b] /kJ mol^{-1}	$\Delta_f H°$(s) [c] /kJ mol^{-1}	ZPE [d] /kJ mol^{-1}
FOX-7	CBS-4M	597.60	+ 12.1	− 82.2	257.2
	CBS-QB3	597.55	− 15.3	− 109.6	241.9
	W1BD	598.54	+ 3.30	− 91.0	237.3
FOX-7-D_4	CBS-4M	597.62	− 7.2	− 106.5	218.2
	CBS-QB3	597.57	− 33.2	− 133.0	206.5
	W1BD	598.55	− 14.7	− 114.0	202.6

[a] Electronic enthalpy; [b] Gas phase enthalpy of formation; [c] Standard solid state enthalpy of formation calculated by applying Trouton´s rule[12]; [d] Zero-point energy.

3.3 Conclusion

In conclusion in this work, FOX-7 was deuterated to form FOX-7-D_4. The deuteration level was determined to be greater than 95% by ^{1}H q-NMR. Furthermore, it was possible to determine the crystal structure of FOX-7-D_4, it unexpectedly crystallized in a different space group than the non-deuterated FOX-7. The structures of both compounds were compared and discussed. In addition, the thermal stability was compared, here it was found that the deuterated FOX-7-D_4 exhibiting a decomposition temperature 30°C higher than the hydrogenated form. Moreover, the activation energy of thermal decomposition of both compounds was determined, as well as the enthalpies of formation and zero-point energies of both were calculated using different methods. Here it was shown that the previously established theory that deuterated compounds, in contrast to their hydrated derivatives, have a lower zero-point energy but a higher activation energy also applies to *N* deuterated compounds. For future studies, it would be definitely

interesting to calculate the energetic parameters such as detonation velocity or detonation pressure for deuterated compounds, or in general for isotopically labeled compounds, to see how isotopic labeling affects the performance properties.

3.4 Acknowledgement

For financial support of this work by Ludwig Maximilian University (LMU), the Office of Naval Research (ONR) under grant no. ONR N00014-19-1-2078 and the Strategic Environmental Research and Development Program (SERDP) under contract no. W912HQ19C0033 are gratefully acknowledged. Open Access funding enabled and organized by Projekt DEAL.

3.5 References

[1] a.) B. C. Tappan, P. R. Bowden, V. W. Manner, J. A. Leiding, M. S. Jakulewicz, *Propellants Explos. Pyrotech.* **2017**, *42*, 1–8; b) M. D. Coburn, D. G. Ott, *J. Labelled Compd. Radiopharm.* **1981**, 18, 1423–1427.

[2] a.) S. A. Shackelford, J. W. Beckmann, J. S. Wilkers, *J. Org. Chem.* **1977**, *42*, 4201–4206; b) Z. Fang,S. Li, J. Liu, *Propellants Explos.Pyrotech.* **2021**, *46*, 1581–1588.

[3] P. Maksyutenko, L. G. Muzangwa, B. M. Jones, R. I. Kaiser, *Phys. Chem. Chem. Phys.* **2015**, *17*, 7514−7527.

[4] S. Ringuette, R. Stowe, C. Dubois, G. Charlet, Q. Kwok, D. E. G. Jones, *J. Energ. Mater.* **2006**, *24*, 307−320.

[5] a.) P. *Atkins, J. de Paula*, Atkins' Physical Chemistry **2006**, *8th ed. Oxford University Press.; b) Y.-R. Luo, Handbook of Bond Dissociation Energies in Organic Compounds **2002**,* CRC Press Inc, Bosa Roca.

[6] a.) Q. Axthammer, B. Krumm, T. M. Klapötke, *J. Phys. Chem. A* **2017**, *121*, 3567−3579; b) A. Bellamy, T. M. Klapötke, *FOX-7 (1,1-Diamino-2,2-dinitroethene) in High Energy Density Materials*, Springer Berlin/Heidelberg: **2007**; Vol. 125, pp. 1−33; c) J. Evers, T. M. Klapötke, P. Mayer, G. Oehlinger, J. M. Welch, *Inorg. Chem.* **2006**, *45*, 4996−5007; d) M.-J. Crawford, J. Evers, M. Göbel, T. M.

Klapötke, P. Mayer, G. Oehlinger, J. M. Welch, *Propellants, Explos., Pyrotech*. **2007**, 32, 478−49.

[7] S. Hunter, P. L. Coster, A. J. Davidson, D. I. A. Millar, S. F. Parker, W. G. Marshall, R. L. Smith, C. A. Morrison, C. R. Pulham, *J. Phys. Chem. C* **2015**, *119*, 2322−2334.

[8] S. Quillard; G. Louarn; J. P. Buisson; M. Boyer, M. Lapkowski; A. Pron; S. Lefrant, *Synth. Met.* **1997**, *84*, 805−806.

[9] S. K. Bharti, R. Roy, *Trends Anal. Chem.* **2012**, *35*, 5−26.

[10] I. Langmuir. *J. Am. Chem. Soc.* **1919**, *41*, 1543−1559.

[11] U. Bemm, H. Östmark, *Acta Crystallogr.* **1998***, 54,* 1997−1999*.*

[12] F. Trouton, *Philos. Mag.* (1876-1900) **1884**, *18*, 54-57; b) M. S. Westwell, M. S. Searle, D. J. Wales, D. H. Willimas, *J. Am. Chem. Soc.* **1995**, *117*, 5013-5015.

[13] NETZSCH Kinetics Neo software, version 2.5.0.1, **2021**.

3.6 Supporting Information

3.6.1 Experimental Information

All chemicals and solvents were employed as received (Sigma-Aldrich, Fluka, Acros). ^{1}H, ^{2}D, ^{13}C and ^{14}N NMR spectra were recorded at ambient temperature using a Bruker TR 400 instrument. The chemical shifts quoted in ppm in the text refer to tetramethylsilane, D_2O or nitromethane. Dehydration, melting and decomposition temperatures of the described compounds were measured through differential thermal analysis (DTA) with an OZM Research DTA 552-Ex instrument. The samples were measured in a range of 25–400°C at a heating rate of 5 °C min^{-1}. The activation energies of the compounds were determines by thermal gravimetric analysis (TGA) with a PerkinElmer TGA4000 and usage of the NETZSCH Kinetics Neo software (version 2.5.0.1).[S1] Infrared spectra were measured with pure samples on a Perkin-Elmer BXII FT-IR system with a Smith DuraSampler IR II diamond ATR.

FOX-7-*D*$_4$

For the preparation of NaOD, elemental sodium (1.84 g, 0.08 mol) was carefully dissolved in D_2O (75 mL) under ice cooling. FOX-7 (6.00 g, 0.04 mol) was then added to this solution and stirred for 1 h at room temperature. The mixture was acidified with conc. D_2SO_4 (5 mL) until a pH of about 3 was reached. The precipitate which formed was filtered and washed with a small amount of D_2O and acetone-*D*$_6$. To achieve the highest possible isotopic content, these steps were iteratively repeated four times. FOX-7-*D*$_4$ (5.23 g, 85%) with a deuteration level of 95.7% was obtained as a light-yellow solid in good yield. Crystals of FOX-7-*D*$_4$ were obtained by slow crystallization of the D_2SO_4 solution.

^{2}D NMR (61 MHz, DMSO-*H*$_6$): δ (ppm) 8.62 (s, 4D, ND2); ^{13}C NMR (101 MHz, DMSO-*D*$_6$): δ (ppm) 128.4 (C2, C(NO2)2), 158.0 (C1, C(ND2)2); ^{14}N NMR (28.9 MHz, DMSO-*D*$_6$): δ (ppm) −25 (2N, C(NO2)2);; IR (ATR): $\tilde{\nu}$ = 2579 (s), 2564 (s), 2427 (s), 2405 (s), 1574 (s), 1487 (vs), 1463 (s), 1457 (s), 1406 (vs), 1345 (s), 1256 (vs), 1219 (vs), 1140 (vs), 1079 (vs), 954 (m), 905 (m), 850 (m), 817 (s), 769 (s), 747 (vs), 735 (vs), 692(s) cm^{-1}; DTA (5° min^{-1}) = T(endo): 114°C; T(exo): 255 °C.

3.6.2 IR Spectroscopy

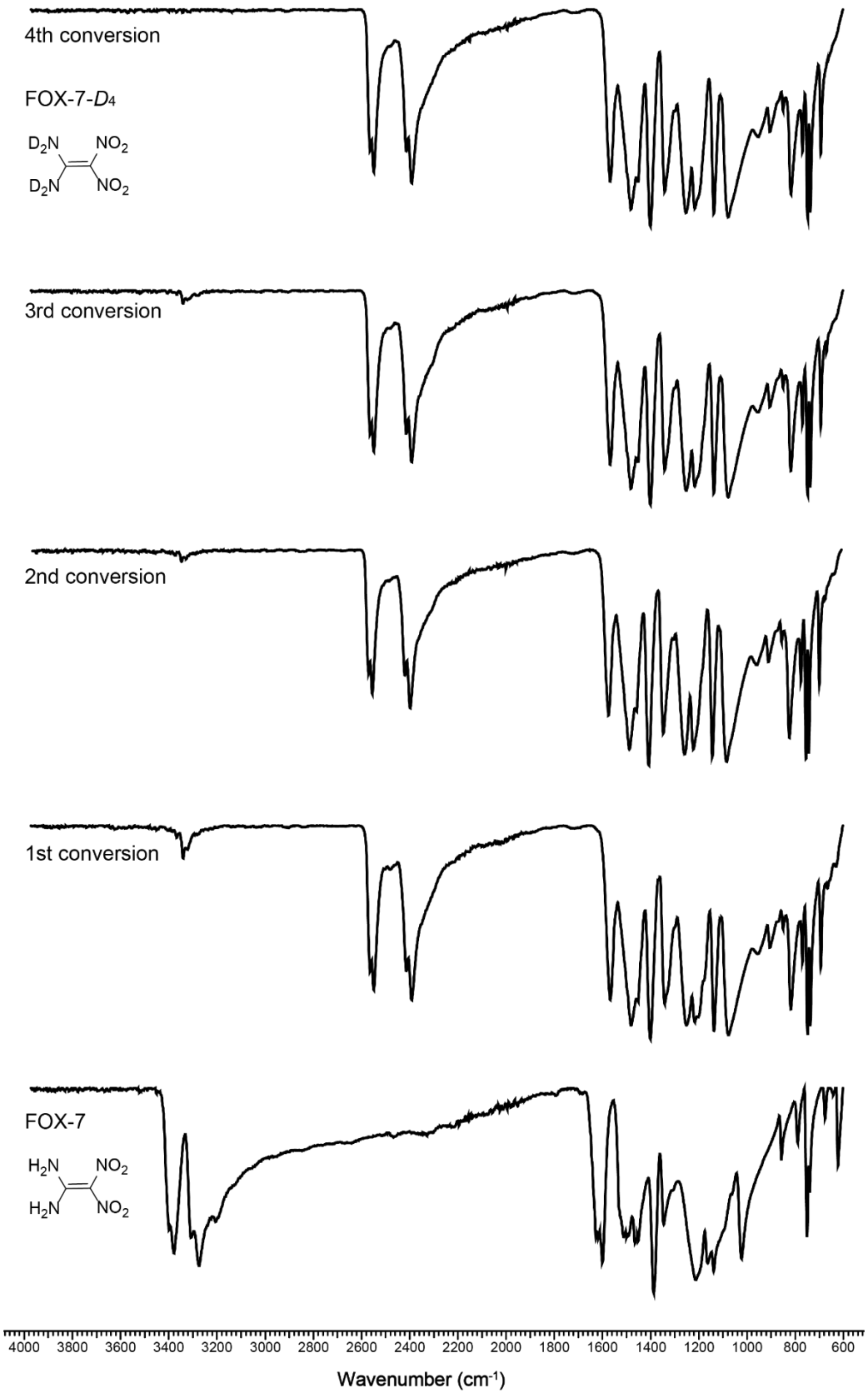

Figure S1. IR spectra of al conversion steps from FOX-7 to FOX-7-*D*4.

3.6.3 ^{1}H q-NMR Measurements

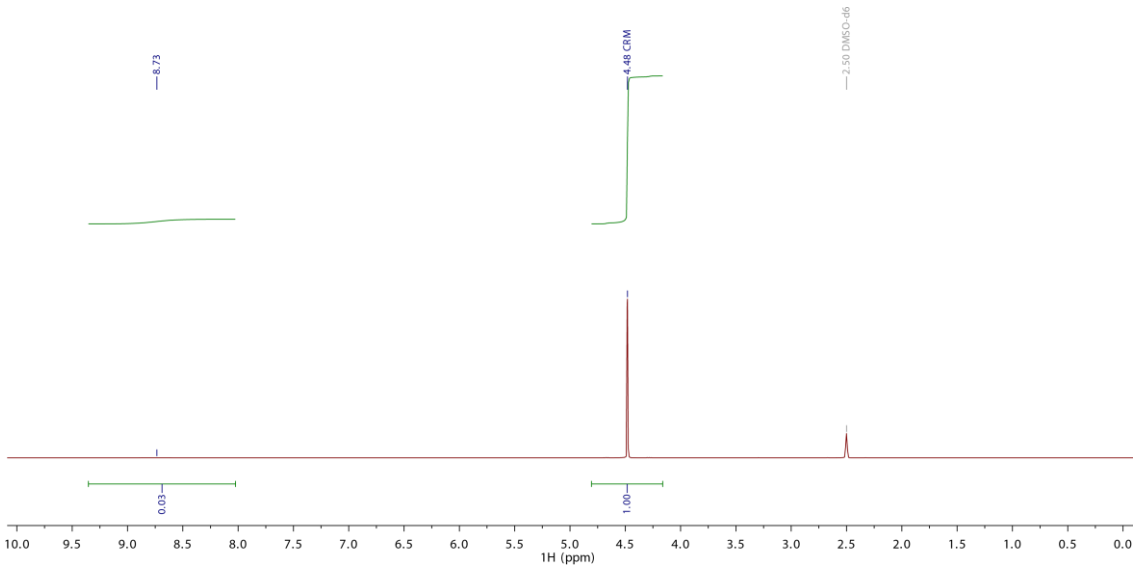

Figure S2. ^{1}H q-NMR of FOX-7-D_4.

Certified Reference Materials (CRM): Ethylene carbonate

$$P_{sample} = \frac{S_{sample}}{S_{standard}} \times \frac{N_{standard}}{N_{sample}} \times \frac{m_{standard}}{m_{sample}} \times \frac{M_{sample}}{M_{standard}} \times P_{standard}$$

$$= \frac{212896.86}{6744429.09} \times \frac{4}{4} \times \frac{10.412}{12.434} \times \frac{148.08}{88.06} \times 0.9992$$

$$= 0.043$$

S = integrated area of the peak

N = number of protons

m = prepared mass

M = molecular weight

P = purity

→ deuteration level: 95.7 %

3.6.4 TGA Measurements

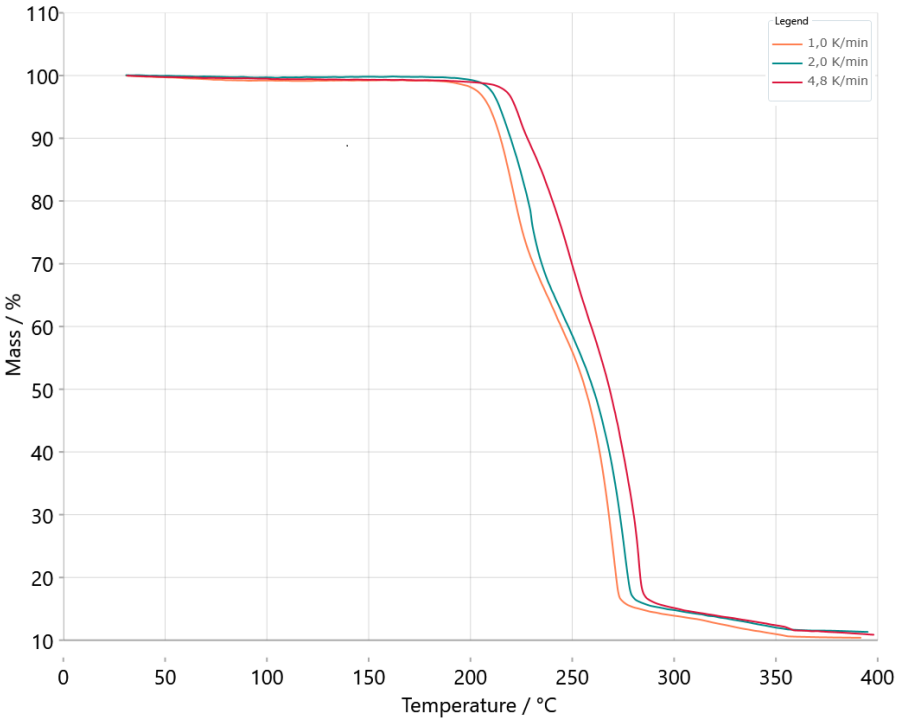

Figure S3. TGA measurement of FOX-7-D_4.

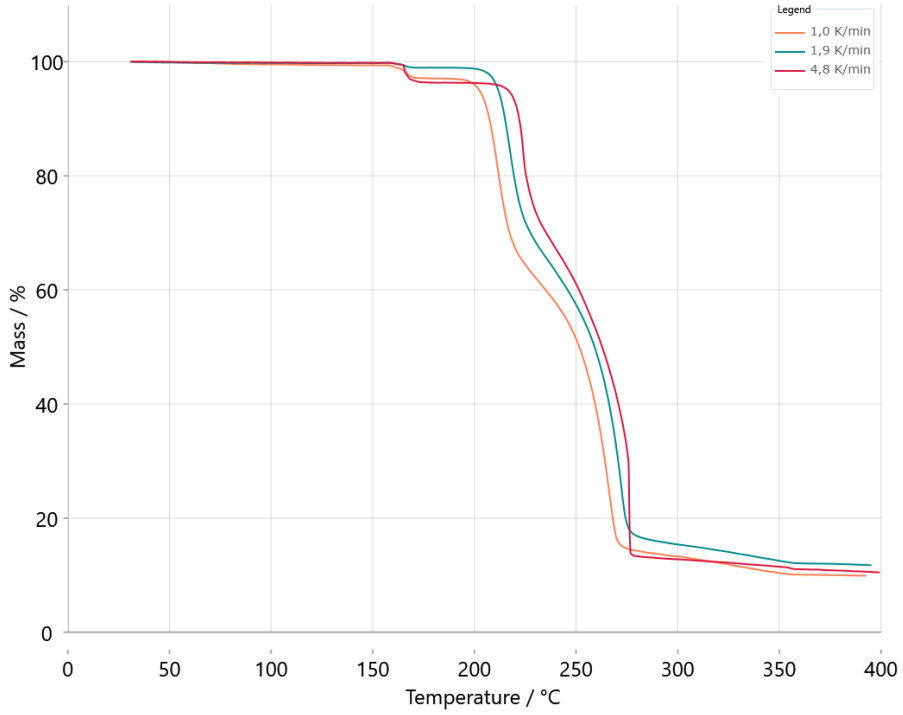

Figure S4. TGA measurement of FOX-7.

3.6.5 Activation Energy

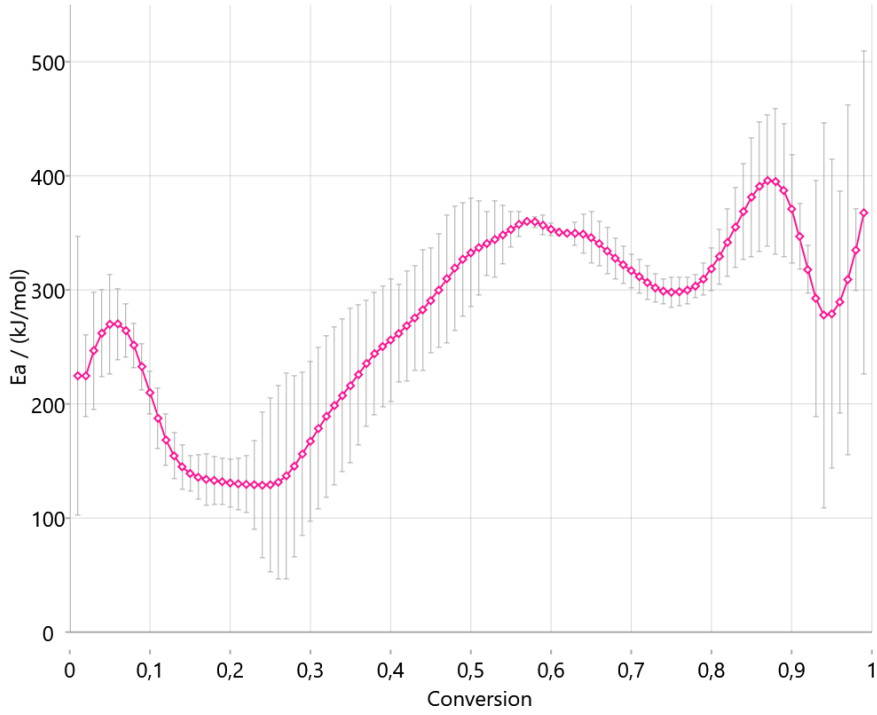

Figure S5. TGA measurement of FOX-7-D_4.

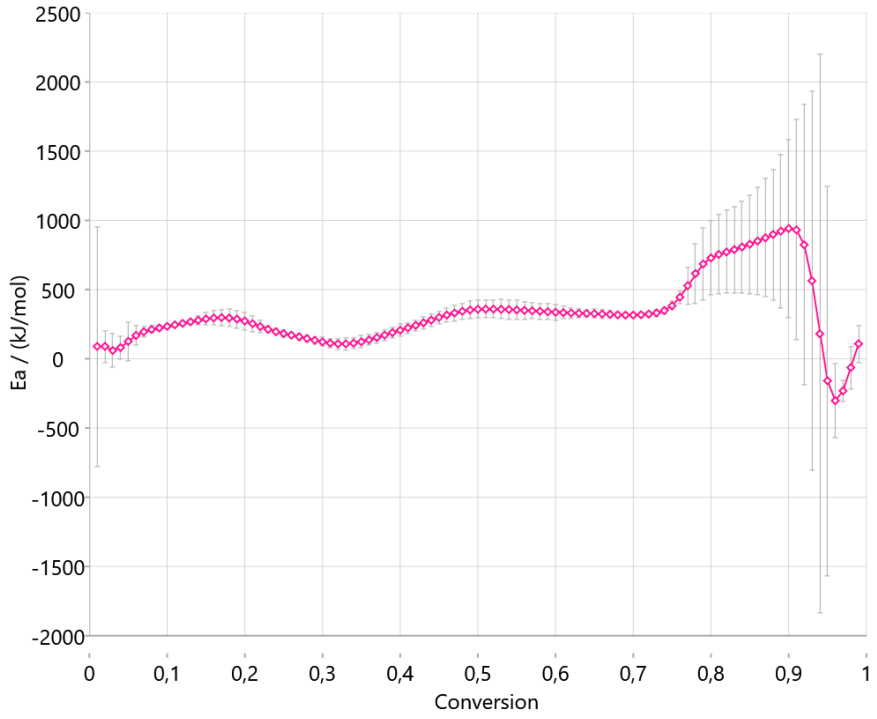

Figure S6. TGA measurement of FOX-7.

3.6.6 X-Ray Diffraction

For the crystalline compound FOX-7-D_4, an Oxford Xcalibur3 diffractometer with a CCD area detector with a multilayer monochromator, a Photon 2 detector and a rotating-anode generator were employed for data collection using Mo-$K\alpha$ radiation (λ = 0.71073 Å). On the Oxford device, data collection and reduction were carried out using the CRYSALISPRO software.[S2]. The structures were solved by direct methods (SIR-92[S3], SIR-97[S4] or SHELXT[S5]) and refined by full-matrix least-squares on $F2$ (SHELXL[S5]) and finally checked using the PLATON software[S6] integrated in the WinGX[S7] software suite. The absorptions were corrected by a SCALE3 ABSPACK or SADABS Bruker APEX3 multiscan method.[S8,9] All DIAMOND2 plots are shown with thermal ellipsoids at the 50 % probability level and hydrogen atoms are shown as small spheres of arbitrary radius.

Table S1. Crystallographic data and structure refinement details of FOX-7-D_4.

	FOX-7-D_4
Formula	$C_2D_4N_4O_4$
FW [g mol^{-1}]	152.12
Crystal system	orthorhombic
Space group	*Pna*2$_1$
Color / Habit	pale yellow block
Size [mm]	0.05 x 0.25 x 0.50
a [Å]	6.5238(13)
b [Å]	6.9618(8)
c [Å]	11.3592(9)
α [°]	90
β [°]	90
γ [°]	90
***V* [Å^3]**	515.91(13)
Z	4
$\rho_{calc.}$ [g cm^{-3}]	1.958
μ [mm^{-1}]	0.181
F(000)	304
$\lambda_{MoK\alpha}$ [Å]	0.71073
T [K]	101
θ Min-Max [°]	3.4, 28.3
Dataset	-8: 8 ; -9: 9 ; -15: 15
Reflections collected	8171
Independent refl.	1279
***R*$_{int}$**	0.063
Observed reflections	1090
Parameters	107
***R*$_1$ (obs)[a]**	0.0442
w*R*$_2$ (all data)[b]	0.0937
***S* [c]**	1.07
Resd. dens [e Å^{-3}]	-0.22, 0.27
Device type	Xcalibur, Sapphire3
Solution	SIR-92
Refinement	SHELXL-2018/3
Absorption correction	multi-scan
CCDC	2150220

[a]R1 = Σ||F0|−|Fc||/Σ|F0|; [b]wR2 = [Σ[w(F02−Fc2)2]/Σ[w(F0)2]]1/2; w = [σc2(F02)+(xP)2+yP]−1 and P=(F02+2Fc2)/3; [c]S = {Σ[w(Fo2−Fc2)2]/(n−p)}1/2 (n = number of reflections; p = total number of parameters).

3.6.7 Heat of Formation Calculations

All quantum chemical calculations were carried out using the Gaussian G09 program.[S10] The enthalpies (H) and zero-point energies (ZPE) were calculated using the complete basis set (CBS) method and the W1 method of *Petersson et al*.[S11] assuming a C_2 symmetry.

Heats of formation (HOF) were calculated using the atomization method (Equation S1) using room temperature enthalpies.[S12]

$$\Delta_f H°_{(g,\,M,\,298)} = H_{(Molecule,\,298)} - \sum H°_{(Atoms,\,298)} + \sum \Delta_f H°_{(Atoms,\,298)} \quad (S1)$$

Table S2. Enthalpies for atoms C, H, N, O and D and their literature values for atomic $\Delta_f H°_{298}$.[S12]

	H^{298K} CBS-4M [a.u.]	H^{298K} CBS-QB3 [a.u.]	H^{298K} W1BD [a.u.]	Δ_fH°(atoms) [kJ mol^{-1}]
C	-37.786153	-37.783015	-37.850513	218.0
H	-0.500991	-0.497457	-0.497634	716.7
N	-54.522456	-54.518173	-54.608828	472.7
O	-74.991184	-74.985259	-75.108878	249.2
D	-0.500991	-0.497457	-0.497634	221.7

The standard molar enthalpy of formation of the FOX-7 derivatives were calculated using Δ_fH(g) subtracting the enthalpy of sublimation estimated by applying Trouton´s rule.[S13]

3.6.8 Calculation of Density at 298 K

The room temperature density was recalculated from the corresponding crystal densities by Equation S2 (a_v = 1.5x10^{-4} K).

$$d_{298K} = \frac{d_T}{1+ \alpha_v(298-T_0)} \quad \text{(S2)}$$

d_T = insert X-ray density in g cm^{-3}

T_0 = insert X-Ray temperatur in K

α_v = correction factor

Table S3. X-Ray and recalculated densities of FOX-7 and FOX-7-*D*$_4$.

	X-Ray density [g cm-3]	Density recalculated to 298K [g cm^{-3}]
FOX-7-*D*$_4$	(@ 101K) 1.958	1.902
FOX-7[S14]	(@ 173K) 1.907	1.872

3.6.9 References SI

[S1] NETZSCH Kinetics Neo software, version 2.5.0.1, **2021**.

[S2] CrysAlisPro, Oxford Diffraction Ltd., version 171.33.41, **2009**.

[S3] A. Altomare, G. Cascarano, C. Giacovazzo, A. Guagliardi, *J. Appl. Crystallogr*. **1992**, *26*, 343–350.

[S4] a) A. Altomare, G. Cascarano, C. Giacovazzo, A. Guagliardi, A. G. G. Moliterni, M. C. Burla, G. Polidori, M. Camalli, R. Spagna, SIR97, **1997**; b) A. Altomare, M. C. Burla, M. Camalli, G. L. Cascarano, C. Giacovazzo, A. Guagliardi, A. G. G. Moliterni, G. Polidori, R. Spagna, *J. Appl. Crystallogr.* **1999**, *32*, 115–119.

[S5] a) G. M. Sheldrick, SHELXL-97, Program for the Refinement of Crystal Structures, University of Göttingen, Germany, **1997**; b) G. M. Sheldrick, *Acta Crystallogr. Sect. A* **2008**, *64*, 112–122.

[S6] A. L. Spek, PLATON, A Multipurpose Crystallographic Tool, Utrecht University, The Netherlands, **1999**.

[S7] L. J. Farrugia, *J. Appl. Cryst.* **2012**, *45*, 849–854.

[S8] Empirical absorption correction using spherical harmonics, implemented in SCALE3 ABSPACK scaling algorithm (CrysAlisPro Oxford Diffraction Ltd., Version 171.33.41, 2009).

[S9] APEX3. Bruker AXS Inc., Madison, Wisconsin, USA.

[S10] M. J. Frisch, G. W. Trucks, H. B. Schlegel, G. E. Scuseria, M. A. Robb, J. R. Cheeseman, G. Scalmani, V. Barone, B. Mennucci, G. A. Petersson, H. Nakatsuji, M. Caricato, X. Li, H.P. Hratchian, A. F. Izmaylov, J. Bloino, G. Zheng, J. L. Sonnenberg, M. Hada, M. Ehara, K. Toyota, R. Fukuda, J. Hasegawa, M. Ishida, T. Nakajima, Y. Honda, O. Kitao, H. Nakai, T. Vreven, J. A. Montgomery, Jr., J. E. Peralta, F. Ogliaro, M. Bearpark, J. J. Heyd, E. Brothers, K. N. Kudin, V. N. Staroverov, R. Kobayashi, J. Normand, K. Raghavachari, A. Rendell, J. C. Burant, S. S. Iyengar, J. Tomasi, M. Cossi, N. Rega, J. M. Millam, M. Klene, J. E. Knox, J. B. Cross, V. Bakken, C. Adamo, J. Jaramillo, R. Gomperts, R. E. Stratmann, O. Yazyev, A. J. Austin, R. Cammi, C. Pomelli, J. W. Ochterski, R. L. Martin, K. Morokuma, V. G. Zakrzewski, G. A. Voth, P. Salvador, J. J. Dannenberg, S. Dapprich, A. D. Daniels, O. Farkas, J.B. Foresman, J. V. Ortiz, J. Cioslowski, D. J. Fox, Gaussian 09 A.02, Gaussian, Inc., Wallingford, CT, USA, **2009**.

[S11] a) J. W. Ochterski, G. A. Petersson, and J. A. Montgomery Jr., *J. Chem. Phys.* **1996**, *104*, 2598–2619; b) J. A. Montgomery Jr., M. J. Frisch, J. W. Ochterski G. A. Petersson, *J. Chem. Phys.* **2000**, *112*, 6532–6542; c) E.C. Barnes, G. A. Petersson, J. A. Montgomery Jr, M. J. Frisch, J. M. L. Martin, *J. Chem. Theor. Comput.* **2009**, *5*, 2687−2693.

[S12] a) P. J. Linstrom, W. G. Mallard (Editors), NIST Standard Reference Database Number 69, http://webbook.nist.gov/chemistry/ (May 2011); b) J. D. Cox, D. D. Wagman, V. A. Medvedev, CODATA Key Values for Thermodynamics, Hemisphere Publishing Corp., New York, **1984**.

[S13] F. Trouton, *Philos. Mag.* (1876-1900) **1884**, *18*, 54-57; b) M. S. Westwell, M. S. Searle, D. J. Wales, D. H. Willimas, *J. Am. Chem. Soc.* **1995**, *117*, 5013-5015.

[S14] U. Bemm, H. Östmark, *Acta Crystallogr.* **1998**, *54*, 1997−1999.

4 Synthesis and Characterization of ^{13}C Isotopically Labeled $^{13}C_2$-FOX-7 (1,1-diamino-2,2-dinitroethylene)

unpublished results from a cooperation project with

Prof. Ralf I. Kaiser from the University of Hawai‘i at Mānoa

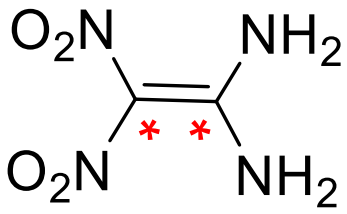

$^{13}C_2$-FOX-7

4.1 Motivation

This project aims to develop a synthetic pathway to obtain double ^{13}C-labeled FOX-7, with the main goal of exploring its different properties. Since the regular synthetic pathway towards FOX-7 starts from 4,6-dihydroxyl-2-methyl-pyrimidine, which however is not commercially available in labeled form, another synthetic pathway had to be found. The synthesis was designed to start from 1,2-^{13}C-labeled acetonitrile to proceed via a two-step process to the known FOX-7 precursor 4,6-dihydroxyl-2-methyl-pyrimidine.
For financial reasons, all experiments were first carried out and optimized with unlabeled chemicals before running them with the isotope-labeled compounds.

4.2 Results and Discussion

4.2.1 Synthesis

The first objective was to synthesize acetamidine hydrochloride (**2**) starting from acetonitrile. The first synthesis variant attempted used a method developed by *Bernthsen*,[1] in which the reaction mixtures were heated in an autoclave-like process in a pressure vessel at various temperatures (see Scheme 1) for one to five days. However, none of these synthesis attempts were successful. Increasing the temperature resulted in negligible amounts of the desired product and its isolation was not possible. At 180° C, the reaction yielded only a black, highly viscous mass that could not be further characterized.

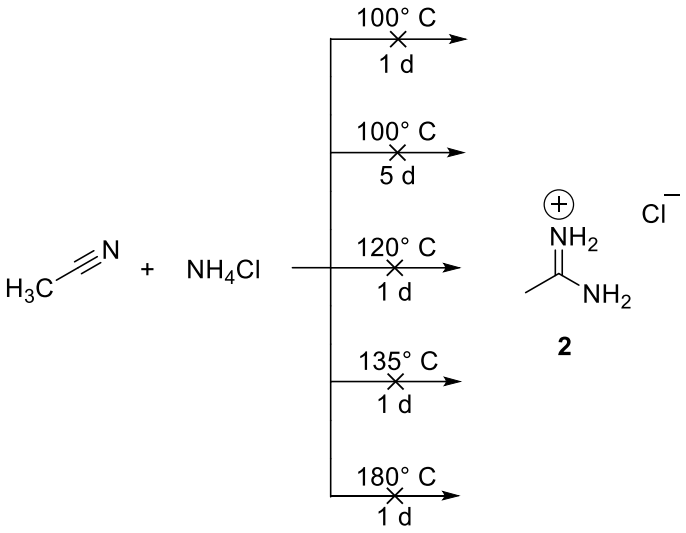

Scheme 1. Overview of synthesis attempts using a method developed by Bernthsen.[1]

After the failed experiments shown in Scheme 1, this route was discarded in favor of a two-step procedure suggested by *W. Dox*.[2] First, acetonitrile was treated with hydrochloric acid in ethanol, yielding ethyl acetimidate hydrochloride (**1**) . According to Dox, the next step should be carried out with an alcoholic ammonia solution, but due to initial failures, we decided to switch to gaseous ammonia. Compound **1** was therefore suspended in ethanol and treated with pure ammonia to replace the alcohol functionality with an amine, as shown in Scheme 2. Thus, compound **2** could be obtained pure after separation from ammonium chloride.

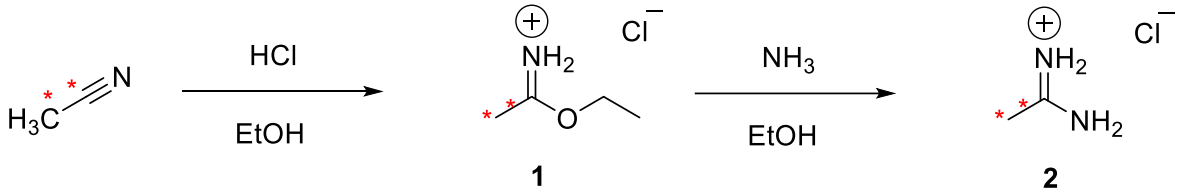

Scheme 2. Synthesis of acetamidine hydrochloride (**2**) via compound **1**.

The pyrimidine was synthesized following *Allentoff* et al. by condensation of acetamidine hydrochloride (**2**) with diethyl malonate using sodium methanolate as base as can be seen in Scheme 3.[3]

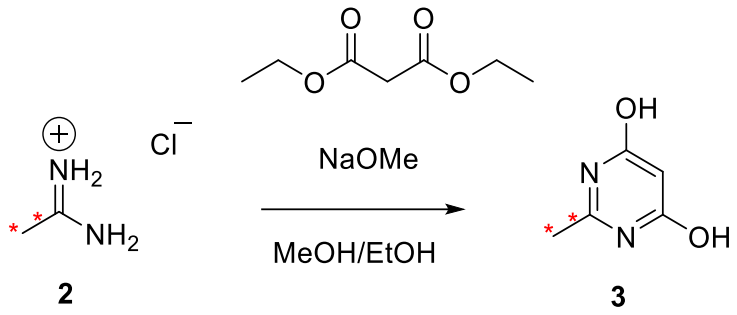

Scheme 3. Synthesis pathway towards 4,6-dihydroxyl-2-methyl-pyrimidine.

The labeled $^{13}C_2$-FOX-7 was synthesized in accordance with *Latypov et al.* and *Astrat'ev et al.* as can be seen in Scheme 4. [4,5] Reaction of 4,6-dihydroxyl-2-methyl-pyrimidine (**3**) with mixed acid gives a tetranitro intermediate which then hydrolyzes directly and cleaves. This yields dinitro methane, carbon dioxide and the desired target compound FOX-7.

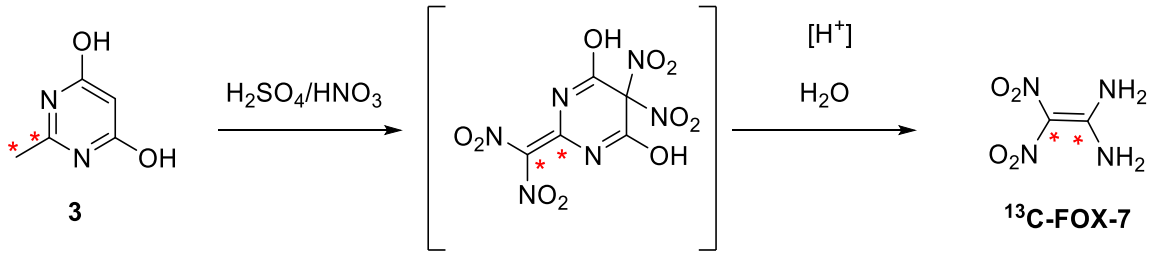

Scheme 4. Synthesis pathway towards $^{13}C_2$-FOX-7 starting from compound **3**.

4.2.2 NMR Spectroscopy

To study the target compound, ^{1}H and ^{13}C NMR measurements in deuterated DMSO were determined.

The proton NMR is shown in Figure 1 and corresponds to that of unlabeled FOX-7. At 8.76 ppm a broad signal can be seen which can be assigned the -NH_2 groups. The singlet at 3.35 ppm can be assigned to water.

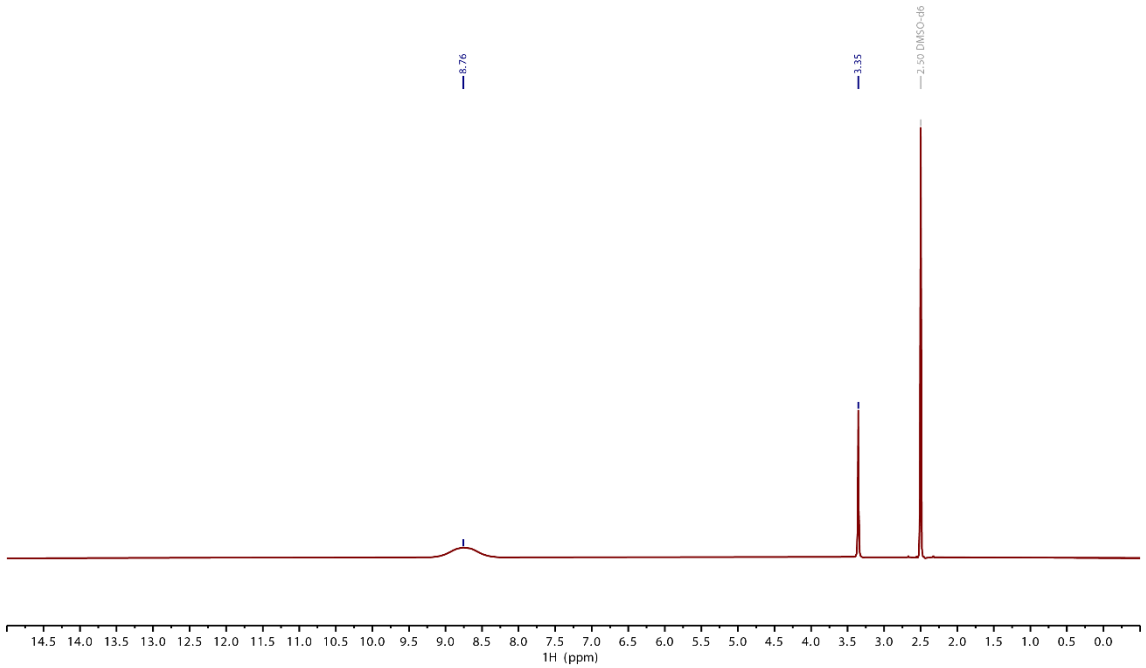

Figure 1. ^{1}H NMR of $^{13}C_2$-FOX-7 in DMSO-D_6.

In Figure 2 the ^{13}C spectrum of $^{13}C_2$-FOX-7 is shown, showing a peculiarity due to the isotopic labeling. At 158.0 and 127.9 ppm two duplets can be seen. In the case of unlabeled FOX-7 only two singlets can be seen in these areas.

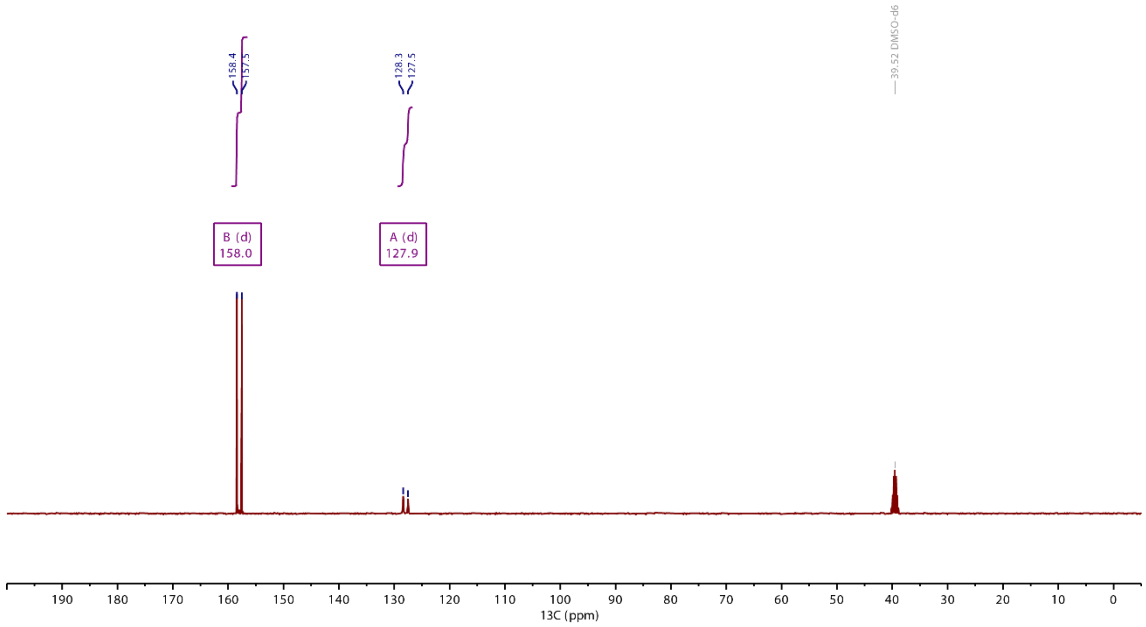

Figure 2. ^{13}C NMR of $^{13}C_2$-FOX-7 in DMSO-D_6.

^{12}C is the main isotope of carbon with a natural abundance of almost 99%. However, due to its spin quantum number of zero, it is not magnetically active and therefore cannot be detected by NMR. The isotope ^{13}C which is stable too, has a spin quantum number of $^{1}/_{2}$, like ^{1}H, and can therefore be detected in NMR. The drawback here is, that this isotope has a natural abundance of only about 1.1%. This leads to the fact that ^{13}C NMR measurements take much longer than ^{1}H NMR measurements.[6] In normal compounds such as the unmacerated FOX-7, ^{13}C-^{13}C pairs are very rare, so that no splitting of the signals occurs and no multiplicity can be detected in a normal ^{13}C NMR but only singletons occur. In our case, however, we have achieved such a rare case by ^{13}C isotope maceration. As known from the multiplicity rule (n+1) for nuclei with a nuclear spin of $^{1}/_{2}$, the two signals split into a duplet as shown in Figure 2, because they have one carbon as neighbor in each case. The duplet at 127.9 ppm (d, $^{1}J_{C,C}$ = 89.3 Hz) can be assigned to the carbon having the two nitro groups attached, the duplet at 158.0 ppm (d, $^{1}J_{C,C}$ = 89.2 Hz) to the carbon with the amino groups.

4.2.3 IR Spectroscopy

Figure 3 shows the IR spectrum of $^{13}C_2$-FOX-7.

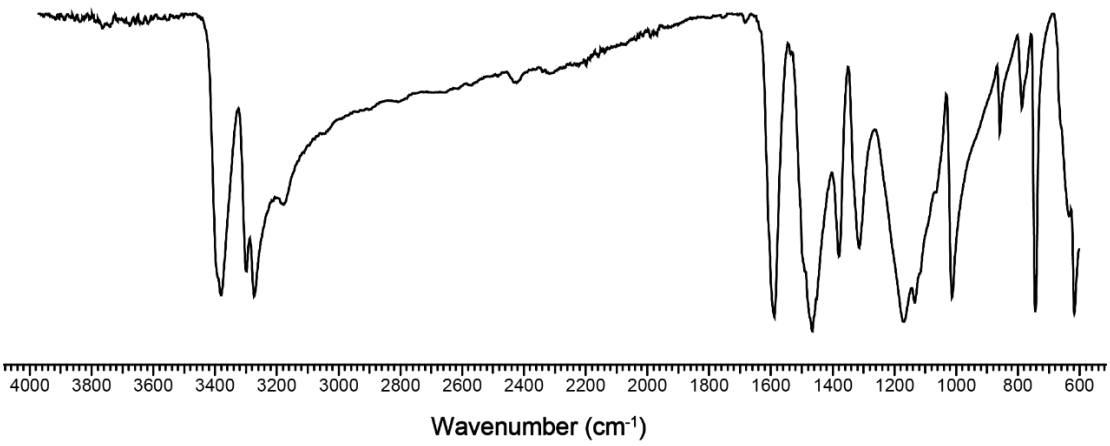

Figure 3. IR spectra of $^{13}C_2$-FOX-7.

4.2.4 Differential Thermal Analysis (DTA)

Furthermore, the thermal properties of the compounds were investigated using differential thermal analysis. The graph of the measurement in the range from 25°C to 400°C with a heating rate of 5°C min^{-1} is shown in Figure 4.

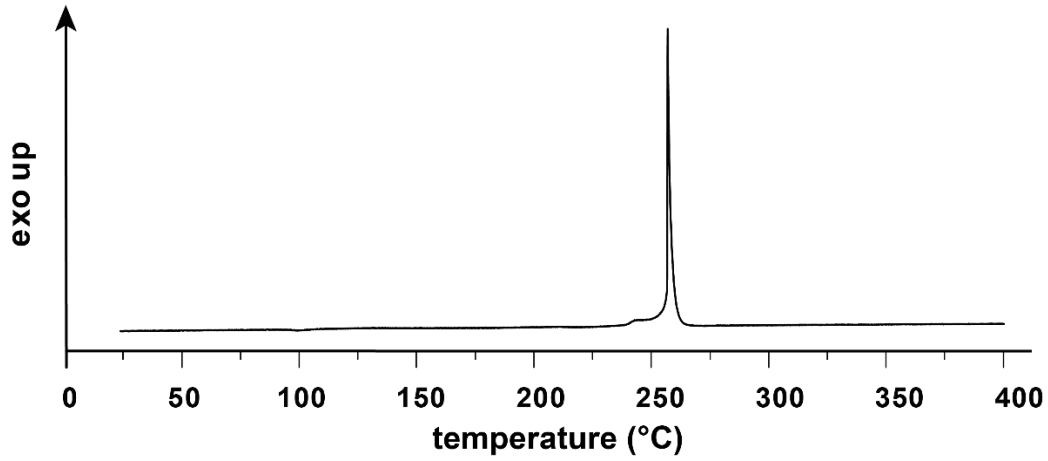

Figure 4. DTA measurement of $^{13}C_2$-FOX-7.

As already seen in the case of the deuterated compound, the ^{13}C isotopic labeled compound has a better thermal stability due to the kinetic isotope effect compared to the unlabeled compound.[7] While normal FOX-7 decomposes at 228°C, the deuterated one decomposes at 255°C and the ^{13}C- labeled FOX-7 at 257°C.

4.3 Experimental Section

^{13}C Labeled acetonitrile (1.00 g, 1.287 mL, 23.2 mmol, 1.0 eq) was mixed with ethanol (100%, 3 mL) and cooled to 0 °C using an ice bath. Under nitrogen counter stream, HCl was introduced to the solution for 1 h. The reaction vessel was sealed with a glass pipe filled with $CaCl_2$ and stored at 5°C overnight. The resulting solid was filtered and dried on a filter paper to obtain compound **1** as colorless chunks. Compound **1** (about 1.70 g) was resuspended in ethanol (100%, 6 mL), cooled to 0 °C using an ice bath and ammonia was inserted to the solution under nitrogen counter stream for 1 h. The mixture was reduced by transferring to a crystallization bowl and evaporation in the fume hood. The crude solid containing the desired product and NH_4Cl was suspended in cold ethanol (100%, 10 mL) and stirred at

0 °C for 1 h. The solid (NH_4Cl, sparingly soluble in cold ethanol) was filtered and the alcoholic solution was used for the next step without further purification.
The yield was determined by weighing the solid before and after the workup step, in which the NH_4Cl was eliminated.
Sodium (1.07 g, 46.5 mmol, 3.0 eq) was dissolved in methanol (80 mL). A solution of **2** (1.49 g, 15.5 mmol, 1.0 eq; slight contamination with NH_4Cl was expected) in ethanol (30 mL) from the previous reaction step and diethyl malonate (2.24 g, 2.13 mL, 14.0 mmol, 0.9 eq) was added in one portion at 0 °C. The mixture was stirred for 2 d at room temperature before being reduced using a rotary evaporator. The obtained solid was dissolved in water (40 mL) and aqueous HCl was added until a pH of 2 was obtained. The suspension was stirred for 1 h at room temperature, cooled to 0 °C and filtered to obtain compound **3**.
Compound **3** (0.55 g, 4.37 mmol, 1.0 eq) was dissolved in concentrated sulfuric acid (3.7 mL). After all solid was in solution, it was cooled to 0 °C using an ice bath. Fuming nitric acid (0.78 mL) was added dropwise keeping the temperature below 10 °C. After the addition the ice bath was removed and the mixture was stirred for 4 h at room temperature. During this time, precipitation from the yellowish solution starts. After cooling to 0 °C the solid was filtered and washed with concentrated sulfuric acid (5 mL) on a glass filter chute. After drying for 20 min, the acid wet yellow solid was transferred in a beaker and dissolved in ice water (5 mL). After stirring for 1 h (strong formation of CO_2), the mixture was cooled to 0 °C and the formed FOX-7 was filtered and dried in the fume hood.
Yield: 89 mg.
The filtrate was concentrated and the precipitate was filtered again and washed with a small amount of cold water.
Yield: 250 mg.

$^{13}C_2$-FOX-7

^{1}H NMR (400 MHz, DMSO-d_6): δ (ppm) 8.76 (s, 4H, NH2); ^{13}C NMR (101 MHz, DMSO-d_6): δ (ppm) 128.0 (d, 1C, C(NO2)2), 158.0 (d, 1C, C(NH2)2); IR (ATR): $\tilde{\nu}$ = 3403 (s), 3320 (s), 3294 (s), 3233 (m), 3199 (s), 2445 (w), 2435 (w), 1595 (vs), 1495 (s), 1471 (vs), 1384 (s), 1318 (s), 1172 (vs), 1136 (vs), 1067 (m), 1014 (s), 858 (m), 786 (w), 742 (vs), 632 (s), 615 (vs); DTA (5 °C min^{-1}) onset: 257 °C (dec.).

4.4 Conclusion

In this project, double ^{13}C isotope-labeled $^{13}C_2$-FOX-7 was successfully synthesized. After various attempted synthesis routes, the following was chosen. Starting from acetonitrile, acetamidine hydrochloride was synthesized via ethyl acetimidate hydrochloride. The typical FOX-7 precursor 4,6-dihydroxyl-2-methyl-pyrimidine was then prepared and after reaction with mixed acid, the isotope-labeled FOX-7 could be isolated. It was investigated by IR and NMR spectroscopy and for that compound a splitting was observed in the ^{13}C NMR spectrum due to the isotopic labelling. In the thermal investigation by differential thermal analysis (DTA) it was found that the thermal stability was increased by the kinetic isotope effect and therefore the decomposition temperature was increased by about 30°C compared to the un-labeled FOX-7.

4.5 References

[1] A. Bernthsen, *Justus Liebigs Ann. Chem.* **1877**, *184*, 290–320.

[2] W. Dox, *Org. Synth.* **1928**, *8*, 1.

[3] A. J. Allentoff, M. W. Lago, M. Ogan, B. C. Chen, R. Zhao, R. A. Iyer, L. J. Christopher, J. K. Rinehart, B. Balasubramanian, S. J. Bonacorsi, *J. Label. Compd. Radiopharm.* **2008**, *51*, 41–47.

[4] N. V. Latypov, M. Johansson, E. Holmgren, E. V. Sizova, V. V. Sizov, A. J. Bellamy, *Org. Process Res. Dev.* **2007**, *11*, 56–59.

[5] A. A. Astrat'ev, D. V. Dashko, A. Y. Mershin, A. I. Stepanov, N. A. Urazgil'deev, *Russ. J. Org. Chem.* **2001**, *37*, 729–733.

[6] R. M. Silverstein; G. C. Bassler; T. C. Morrill*, Spectrometric Identification of Organic Compounds,* Wiley, New York, **1191**.

[7] T. M. Klapötke, B. Krumm, J. T. Lechner, J. Stierstorfer *Dalton Transactions* **2022**, *51*, 5788-5791.

5 Crystal Structures of the Commonly Used Plasticizers Ethylene Glycol Dinitrate, Diethylene Glycol Dinitrate and Triethylene Glycol Dinitrate − Characterization and Discussion of their Structural Behavior

Jasmin T. Lechner, Andreas Neuer, Valentin Bockmair, Jörg Stierstorfer, and Thomas M. Klapötke*

as published in *Crystal Growth and Design* **2022**, *22,* 6215–6223

DOI: 10.1021/acs.cgd.2c00775

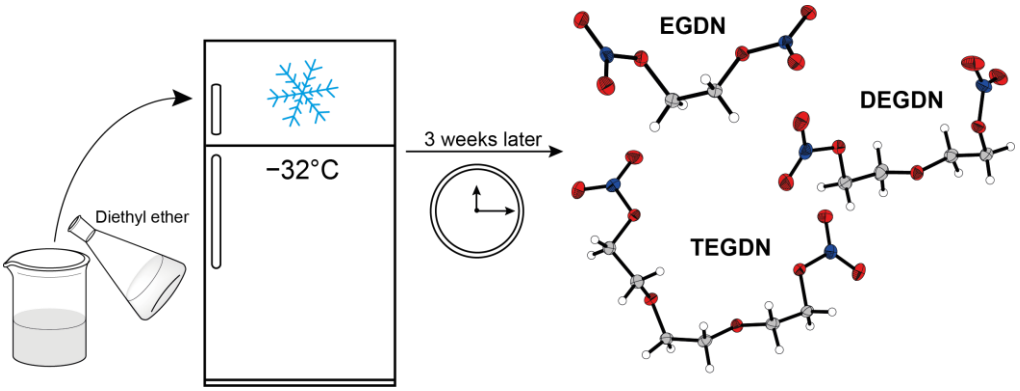

Abstract: Ethylene glycol dinitrate (EGDN), diethylene glycol dinitrate (DEGDN) and triethylene glycol dinitrate (TEGDN) are used as plasticizers in propellant mixtures and have been known for more than 100 years. Despite the industrial application and the long history of these compounds, the crystal structures of all three compounds, which are liquids at room temperature, have not been determined. Therefore, in this work the crystal structures were examined by low-temperature X-ray diffraction and thus the bonding properties and crystal packing in the solid state could be compared and discussed for the first time. Furthermore, the compounds were characterized by NMR spectroscopy and infrared spectroscopy. The thermal properties were investigated by DTA measurements and the experimental vapor pressures were measured with the chromatography assisted transpiration method. The densities at room temperature (for the liquids) were measured by gas pycnometry and the energetic properties were calculated using the EXPLO5 code. Moreover, a more in-depth analysis of the different sensitivities through discussion of the Hirshfeld surfaces, created based on their crystal structures, was made to compare their sensitivities in the solid state.

5.1 Introduction

The purpose of a propellant is to provide the energy to enable an object to fly a certain distance.[1] There are several known propellant mixtures; the most popular ones are shown in Figure 1.[1–3]

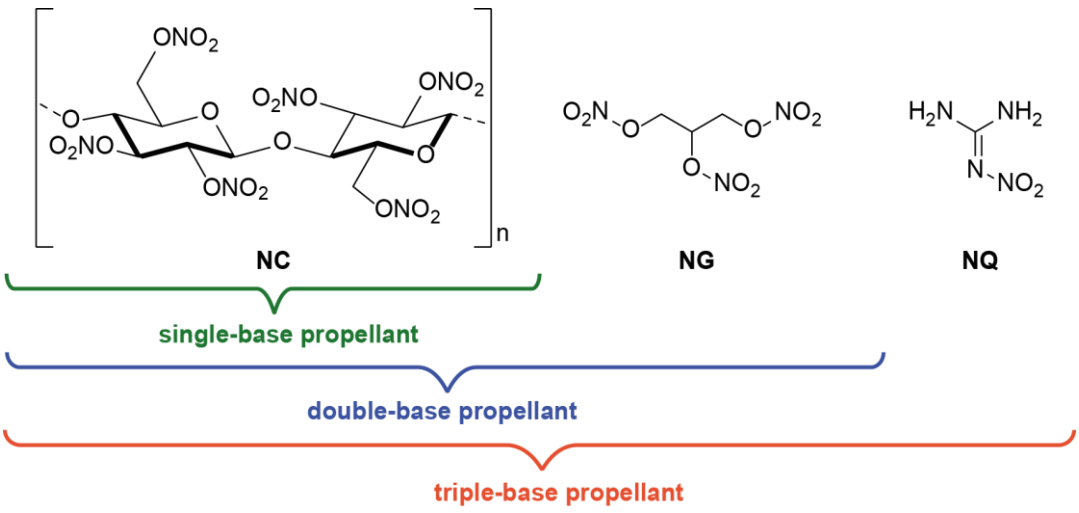

Figure 1. Components of single-base (SB), double-base (DB) and triple-base (TB) propellants.

First of all, single-base propellants, obtained by the reaction of high-purity cellulose with nitric acid, result in the well-known compound nitrocellulose (NC).[1,2] Depending on the acid concentration used in its production, NC can be synthesized with different nitrogen contents (11.5–14.0%) dependent on the degree of nitration.[4,5] NC with lower nitrogen content is very stable and insensitive toward impact and friction.[6] Consequently, NC with different nitrogen contents allows various applications in the field of energetic materials.[2,7,8]

Second, double-base (DB) propellants consist of a mixture of NC with nitroglycerin (NG). NG is absorbed by NC, and a gelled mixture is obtained.[1,3] Depending on the amount of NG present in the formulation, DB propellants can be used in gun and rocket munitions.[2,4,9] Pure NG is very difficult to handle; due to the very low impact sensitivity of the liquid, countless accidents have occurred in the past.[2,10,11]

Triple-base (TB) propellants are mixtures of NC, NG, and nitroguanidine (NQ).[12] In this case, NQ is not absorbed in the NC/NG mixture but is imbedded as a fine powder in the double-base propellant gelled mixture.[13] The addition of NQ is mainly to compensate the high impact sensitivity of the NC/NG mixture and at the same time to increase the thermal stability.[1] There are also other components that are added to propellant mixtures to adjust the properties as desired. For example, burn rate modifiers can be added, which are mostly metal powders to reduce the decomposition temperature of the mixture in order to obtain high levels of thrust; moreover stabilizers can be added to reduce or even eliminate the known autocatalytic decomposition process of nitrate esters.[14−17]

Furthermore, plasticizers can be added to increase the impact and friction sensitivity value of the formulations.[2,3,6] Several examples of energetic plasticizers are shown in Figure 2.

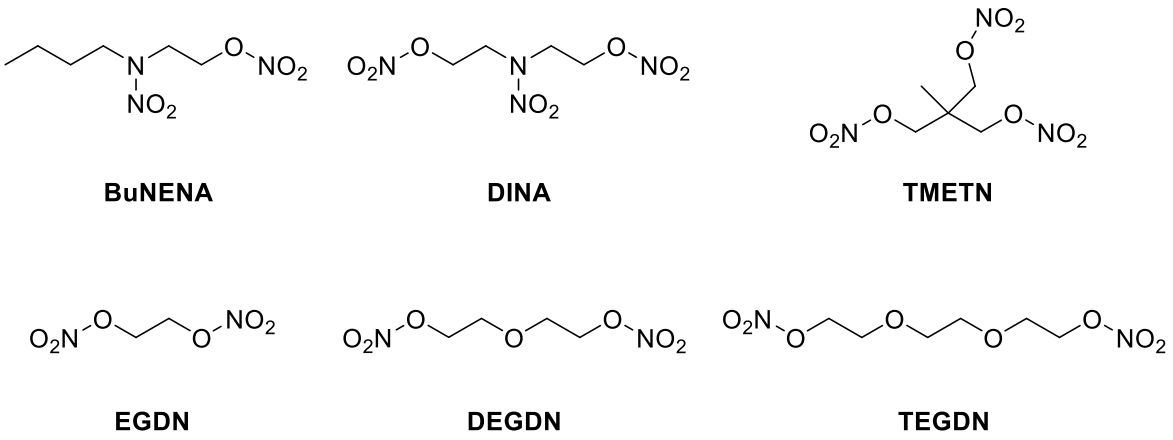

Figure 2. Molecular structures of the plasticizers *n*-butyl nitroxyethylnitramine (BuNENA), di(1-nitratoeth-2-yl) nitramine (DINA), trimethyloltrinitrate (TMETN), ethylene glycol dinitrate (EGDN), diethylene glycol dinitrate (DEGDN), and triethylene glycol dinitrate (TEGDN).

The addition of such plasticizers to propellent mixtures is therefore to plasticize the formulation and make it safer to handle or easier to manufacture.

Three examples of energetic plasticizers are the ethylene-bridged glycols ethylene glycol dinitrate (EGDN), diethylene glycol dinitrate (DEGDN), and triethylene glycol dinitrate (TEGDN). Due to the apparent analogue molecular construction, it could be assumed that the ethylene glycol nitrates have similar properties to NG. In fact, they show a worse performance and also have a lower oxygen balance. However, they also have advantages compared to NG; all three gelatinize much better with NC than NG, and by adding them, the freezing point of NG (14 °C) can be significantly reduced.[1] They are not handled as NG replacements for this very reason but used as additives to the propellant mixtures to increase the sensitivity values and enable easier handling. At the same time, they lower the freezing point of the formulations.[18–21] Depending on which properties are desired for the final formulation, different ethylene glycol dinitrates are added. They differ from each other in such a way that the performance decreases with the increase of the length of the bridging carbon chain, while the sensitivity values increase.[1,2]

Although the three propellant additives have been known and used for over 100 years in civil as well as military application, the structural studies and thermochemical properties are not yet available in the literature.[22–25]

Therefore, in this work, the crystal structures of the three compounds mentioned above were measured at low temperatures and their properties like vapor pressure or thermal behavior were fully investigated.

5.2 Results and Discussion

5.2.1 Synthesis

The three different ethylene glycol dinitrates were all prepared according to the same procedure. They were slowly added to a mixed acid (3 parts nitric acid (100%) and 2 parts concentrated sulfuric acid) under cooling. An excess of the nitrating mixture was always used, in a ratio of 3.6 mass % mixed acid to the 1 mass % of the diols. The reaction scheme of the synthesis can be seen in Scheme 1.

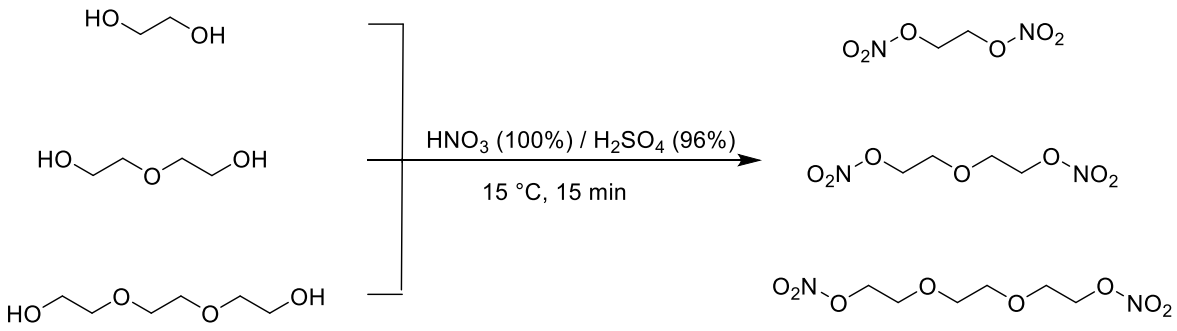

Scheme 1. Preparation and Nitration of EGDN, DEGDN, and TEGDN

5.2.2 Characterization

The three compounds were investigated by nuclear magnetic resonance (NMR) spectroscopy as well as infrared vibrational spectroscopy.

he NMR spectral recordings of ^{1}H, ^{13}C, and ^{14}N NMR were commissioned using a Bruker AVANCE 400 MHz instrument. For this purpose, samples of all compounds were dissolved in acetone-d_6. The purity χ_{an} of the ethylene glycol nitrates was tested by the ^{1}H qNMR technique. For each substance, three samples between 2 mg and 20 mg and around 10 mg of the certified reference material 1,3,5-trimethoxybenzene (TMB, Sigma-Aldrich) were weighed with a Mettler Toledo

XP26DR scale (0.002/0.01 mg) and dissolved in 0.75 mL of $(CD_3)_2CO$. Each sample was transferred into a clean 5 mm NMR tube and measured with a temperature-controlled Bruker AVANCE 400 MHz NMR instrument at 25 °C. The NMR instrument was operated with a z-gradient using a 90°-pulse with a pulse width of 11.85 µs. In total, 65,536 data points were acquired with a spectrum size of 2048 K (2097152). Samples were not spinned, and the acquisition time was set to 6.5012 s. To ensure that the relaxation duration would be exceeded five to seven times, a relaxation delay (D1) of 60 s was chosen. In each measurement, 64 scans were performed. For processing, the MestReNova software was used. Before Fourier transformation, linear group delay was applied and zero filling spectrum size to 2048 K was executed. After manual phase correction and Bernstein polynomial of 5th order baseline adjustment, manually edited sum integration was performed including the ^{13}C satellites for the analyte and TMB. The spectra of each sample were independently processed five times. The chemical purity was calculated manually with Microsoft Excel according to the work of Schoenberger.[26] The uncertainty was calculated considering the buoyancy corrected weighing, the general uncertainty created by the scale, the uncertainty of the determination of the molar mass according to Wieser, and finally the uncertainty of the reference material given by the manufacturer.[27] The result of the purity determination is shown in Table 1. The purities were determined to assess the presence of possible disturbances and to enable adjustment of the analytical calibration for the determination of the thermochemical properties—like the vapor pressure. No interfering impurities were detected, and the determined purity was used to adjust the VO-GC/MS-assisted quantification. The corresponding spectra are shown in the Supplementary Information (SI). In the ^{14}N spectra, it could be seen that with increasing chain length from EGDN to TEGDN, the nitrogen of the nitrato group is shifted to lower fields.

Table 1. Mass Fraction Purity χ_{an} of the Ethylene Glycol Nitrates Investigated in This Work, As Determined by the ^{1}H qNMR Technique.

	IUPAC name	CAS #	$\chi_{an} \pm U(P_{an})$ [a]
EGDN	Ethane-1,2-diyl dinitrate	628-96-6	0.9983 (±0.0026)
DEGDN	Oxydi(ethane-2,1-diyl) dinitrate	693-21-0	0.9969 (±0.0047)
TEGDN	2,2'-(Ethane-1,2-diylbis (oxy))bisethyl dinitrate	111-22-8	0.9881 (±0.0058)

[a]Expended uncertainties are reported with a confidence level of 0.95 (k = 2).

Considering vibrational spectroscopy, all expected symmetric and asymmetric stretching vibrations can be detected, shown in Figure 3.

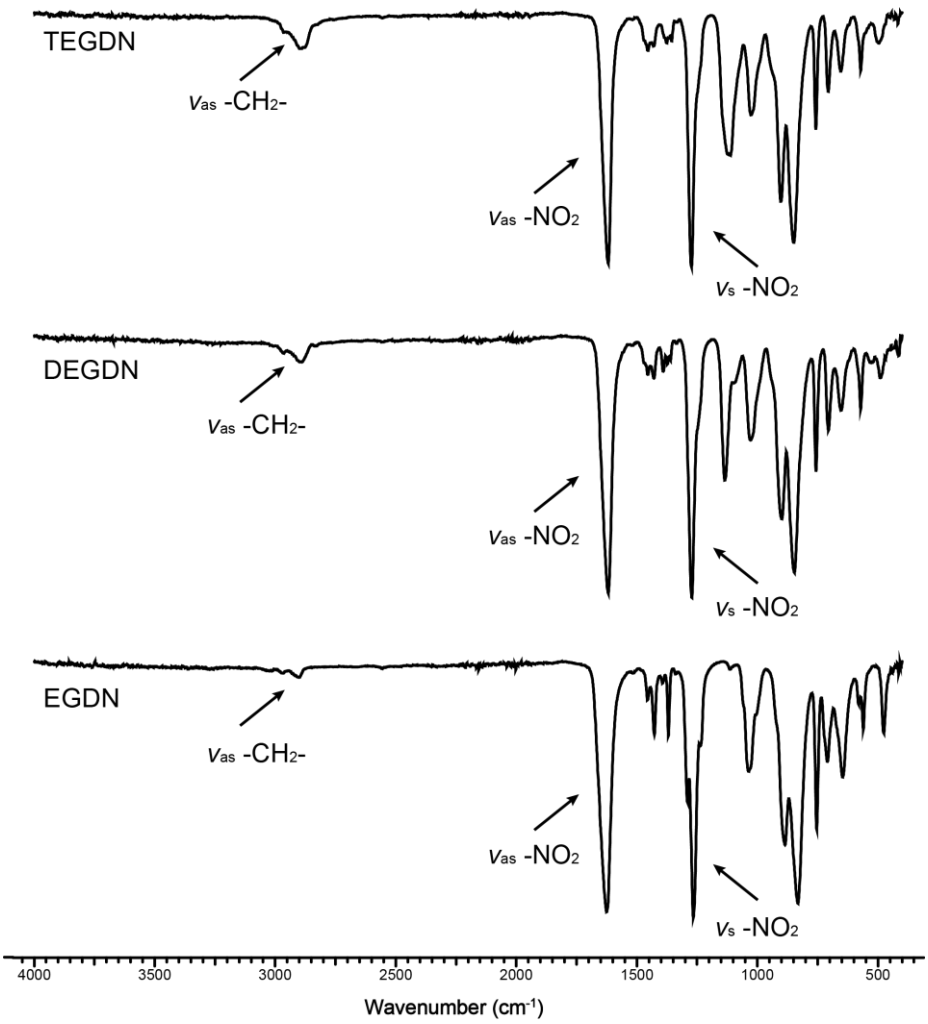

Figure 3. IR spectra of EGDN, DEGDN, and TEGDN.

The stretching vibrations for saturated −CH_2 groups are expected at about 2900 cm^{-1} (ν_{as} ~ 2930 cm^{-1}; ν_s ~ 2850 cm^{-1}) as a weak signal and can be assigned at this energy in the spectra for all compounds.[28] In addition, it can be seen that the signal TEGDN is the most intense one representing 6 −CH_2 groups, whereas the least intense is for EGDN representing only two −CH_2 groups. The asymmetric stretching vibration for nitro groups bonded to an oxygen is expected at about 1630 cm^{-1}, and the symmetric stretching vibration at about 1275 cm^{-1}.[28] These are also clearly identifiable in the spectra for all three compounds.

5.2.3 X-Ray Diffraction

For the first time, the single-crystal X-ray structure of the three different ethylene glycol dinitrates EGDN, DEGDN, and TEGDN could be determined. For this purpose, a low-temperature crystallization method was used. The compounds were mixed with diethyl ether in a ratio of one to one and allowed to crystallize at 241.15 K for over 3 weeks. The crystals were then picked under nitrogen counterflow at low temperatures and measured at about 100 K. The crystallographic data can be seen in Table 2.

Table 2. Crystallographic Data of EGDN, DEGDN, and TEGDN.

	EGDN	**DEGDN**	**TEGDN**
Formula	$C_2H_4N_2O_6$	$C_4H_8N_2O_7$	$C_6H_{12}N_2O_8$
FW [g mol^{-1}]	152.06	196.12	240.17
Crystal system	monoclinic	monoclinic	monoclinic
Space group	$P2_1/c$	$P2_1/c$	$P2_1/c$
Color / Habit	colorless plate	colorless block	colorless plate
Size [mm]	0.29 x 0.68 x 0.79	0.50 x 0.50 x 0.75	0.10 x 0.30 x 0.40
a [Å]	10.4565(7)	12.5584(9)	7.4093(7)
b [Å]	5.4581(4)	9.0354(4)	18.4268(14)
c [Å]	20.5859(14)	15.6231(11)	7.7865(6)
α [°]	90	90	90
β [°]	103.562(7)	109.944(8)	105.062(8)
γ [°]	90	90	90
V [Å^3]	1142.13(14)	1666.4(2)	1026.57(15)
Z	8	8	4
Z'	2	2	1
ρ_{calc} [g cm^{-3}]	1.769	1.564	1.554
μ [mm^{-1}]	0.182	0.153	0.146
F (000)	624	816	504
$\lambda_{MoK\alpha}$ [Å]	0.71073	0.71073	0.71073
T [K]	103	100	100
θ Min-Max [°]	2.0, 26.4	2.6, 26.4	2.9, 26.4
Dataset	-13:11; -6:6; -25:25	-11:15;-10:11; -19:19	-9:9; -23:22; -9:9
Reflections coll.	8507	13253	8123
Independent refl.	2330	3422	2101
R_{int}	0.024	0.026	0.035
Parameters	214	299	193
*R*1 (obs)[a]	0.0294	0.0280	0.0325
w*R*2 (all data)[b]	0.0709	0.0728	0.0774
S [c]	1.10	1.04	1.02
Resd. Dens. [e Å^{-3}]	-0.21, 0.22	-0.28, 0.21	-0.18, 0.17
Device type	Xcalibur, Sapphire 3	Xcalibur, Sapphire 3	Xcalibur, Sapphire 3
Solution	SHELXT 2018/2	SHELXT 2018/2	SHELXT 2018/2
Refinement	ShelXL 2018/3	ShelXL 2018/3	ShelXL 2018/3
Absorption corr.	multi-scan	multi-scan	multi-scan
CCDC	2171114	2171116	2171115

[a] $R1 = \Sigma||F0|-|Fc||/\Sigma|F0|$; [b] $wR2 = [\Sigma[w(F02-Fc2)2]/\ \Sigma[w(F0)2]]1/2$; $w = [\sigma c2(F02)+(xP)2+yP]-1$ and $P=(F02+2Fc2)/3$; [c] $S = \{\Sigma[w(Fo2-Fc2)2]/(n-p)\}1/2$ (n = number of reflections; p = total number of parameters).

All three compounds crystallize in the same monoclinic space group $P2_1/c$, with the only difference that EGDN and DEGDN have two independent molecules in the asymmetric unit, whereas TEGDN only has one. The densities at 100 K decrease in the row from EGDN (1.77 g cm^{-3}) via DEGDN (1.56 g cm^{-3}) to TEGDN (1.55 g cm^{-3}).

The unit cell of EGDN includes two independent molecules in its asymmetric unit with different torsional angles of the nitro groups (Figure 4).

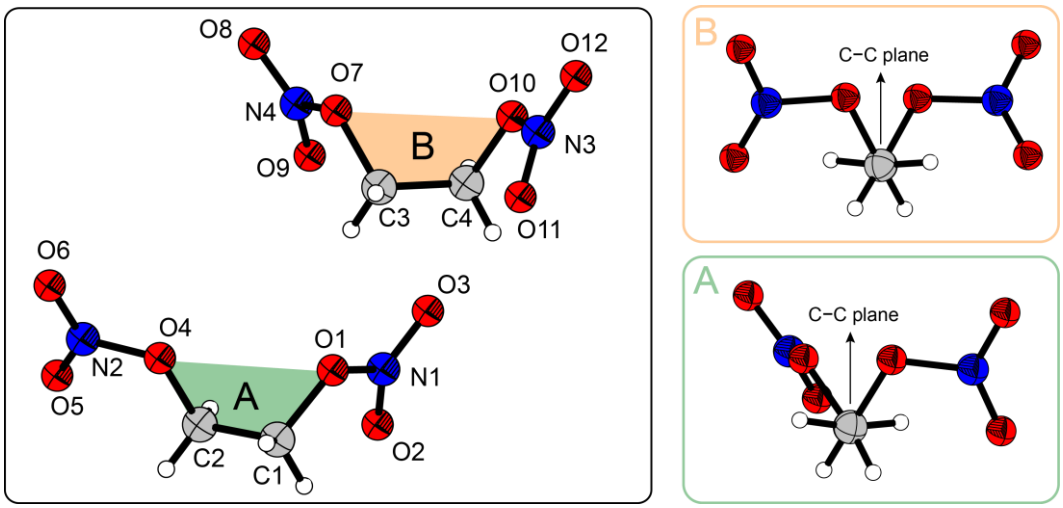

Figure 4. Left: molecular structure of EGDN with selected angles (°): O1–C1–C2 112.05(11), O4–C2–C1 104.26(11), O7–C3–C4 112.06(11), O10–C4–C3 112.64(11), O1–C1–C2–O4–65.59(14), and O7–C3–C4–O10 55.93(15); right top: view of species B along the C–C bond; right bottom: view of species A along the C–C bond.

Since both species show comparable sp^3 hybridized C–C bonds and C–O bonds as well as similar bonds in the nitro group, their difference can only be explained by the rotation of the nitro groups.

Although the nitro groups in both varieties are positioned *cis* to each other, in the first moiety (A), the nitro groups are quite unsymmetrically twisted, while it seems to be almost symmetrically twisted in the second moiety (B). By looking at the angle between the carbons and the bridging oxygen, this can be clearly seen. Species A has angles of 112.1° (O1–C1–C2) and 104.3° (O4–C2–C1), whereas species B has almost identical angles of 112.1° (O7–C3–C4) and 112.6° (O10–C4–C3). The angles inside the nitro groups are again almost the same for both species.

Looking at the three-dimensional arrangement of the two species, it can be seen that the crystal is built up in layers as shown in Figure 5. Each layer is built up in an AA BB AA pattern, but the same species side by side are always mirrored vertically. Thus, the nitro group (O2–N1–O3) of species A is next to the nitro group (O11–N3–O12) of species B, and the second nitro group (O8–N4–O9) of this same molecule is next to another molecule B oriented to the nitro group (O8–N4–O9). This pattern then continues. The layers are arranged in such a way that one species A is exactly between the two molecules of species B which are next to each other and the other way around.

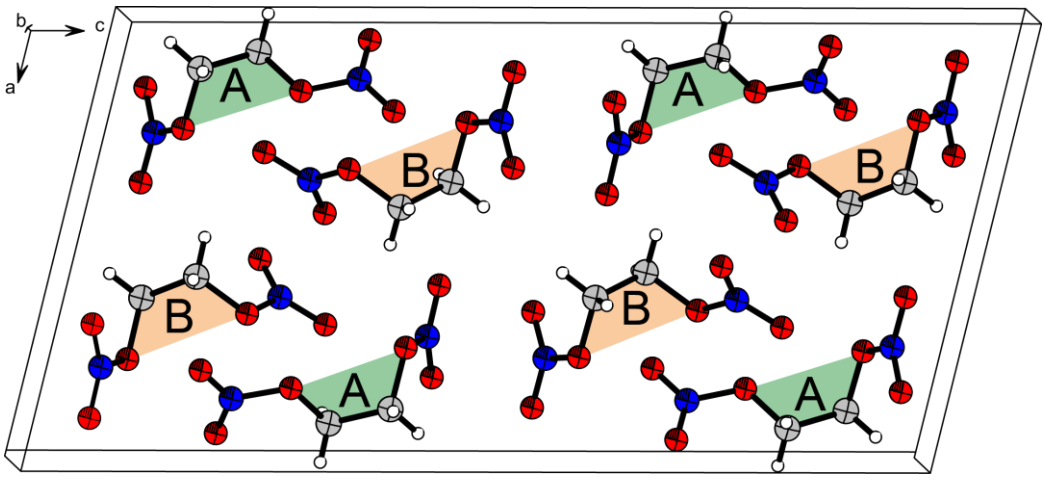

Figure 5. View of the unit cell of EGDN along the *b* axis.

The same behavior as for EGDN can also be observed for DEGDN, and again two different species are present in the crystalline state at low temperatures (100 K) in one unit cell, shown in Figure 6.

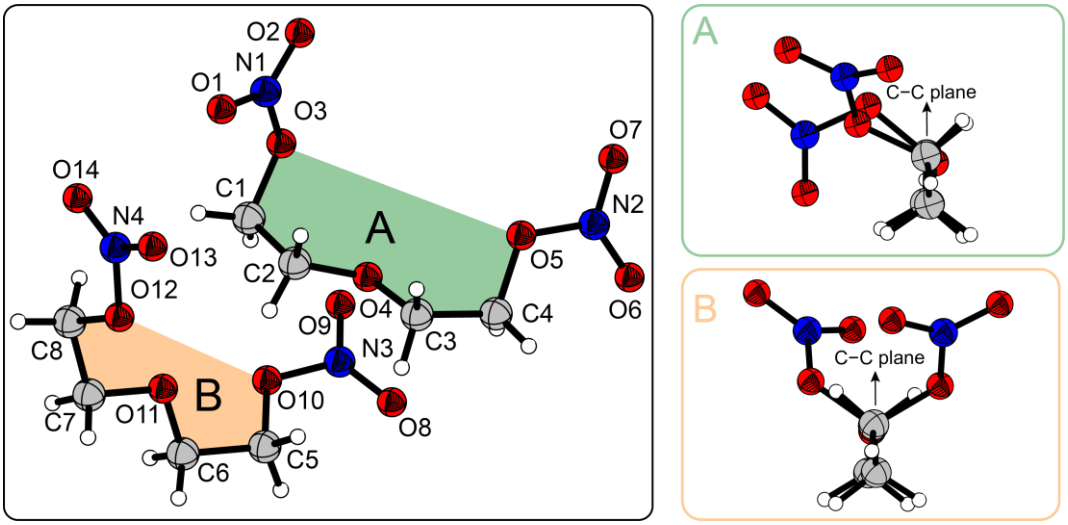

Figure 6. Molecular structure of DEGDN with selected angles (°): C3–O4–C2 111.91(8), C6–O11–C7 111.81(8), O3–C1–C2 111.50(9), O5–C4–C3 105.38(9), O10–C5–C6 104.83(8), O12–C8–C7 105.87(8), O4–C2–C1–O3–64.78(11), O5–C4–C3–O4 71.48(11), O10–C5–C6–O11–63.57(11), and O11–C7–C8–O12–68.83(10); right top: view of species A along the C–C plane; right bottom: view of species B along the C–C plane.

In this case, again the nitro groups are positioned *cis* to each other and, viewed along the C–C axis, are aligned once asymmetrically (A) and once symmetrically (B) to each other. However, even though the species are twisted differently, no difference in bond lengths can be seen. Comparable to EGDN, the difference lies in the angles of the C–C bond toward the oxygen which is bound to the nitro groups. In species A, there are two clearly different angles of 111.5° (O3–C1–C2) and 105.4° (O5–C4–C3), whereas in species B, the angles of 104.8° (O10–C5–C6) and 105.8° (O12–C8–C7) differ only slightly.

Looking at the three-dimensional arrangement of DEGDN, we see that this structure is also built up in layers. As shown in Figure 7 on the top, there are always four molecules aligned in an ABBA pattern. In addition, this block is then repeated layer by layer as can be seen in Figure 7 on the bottom.

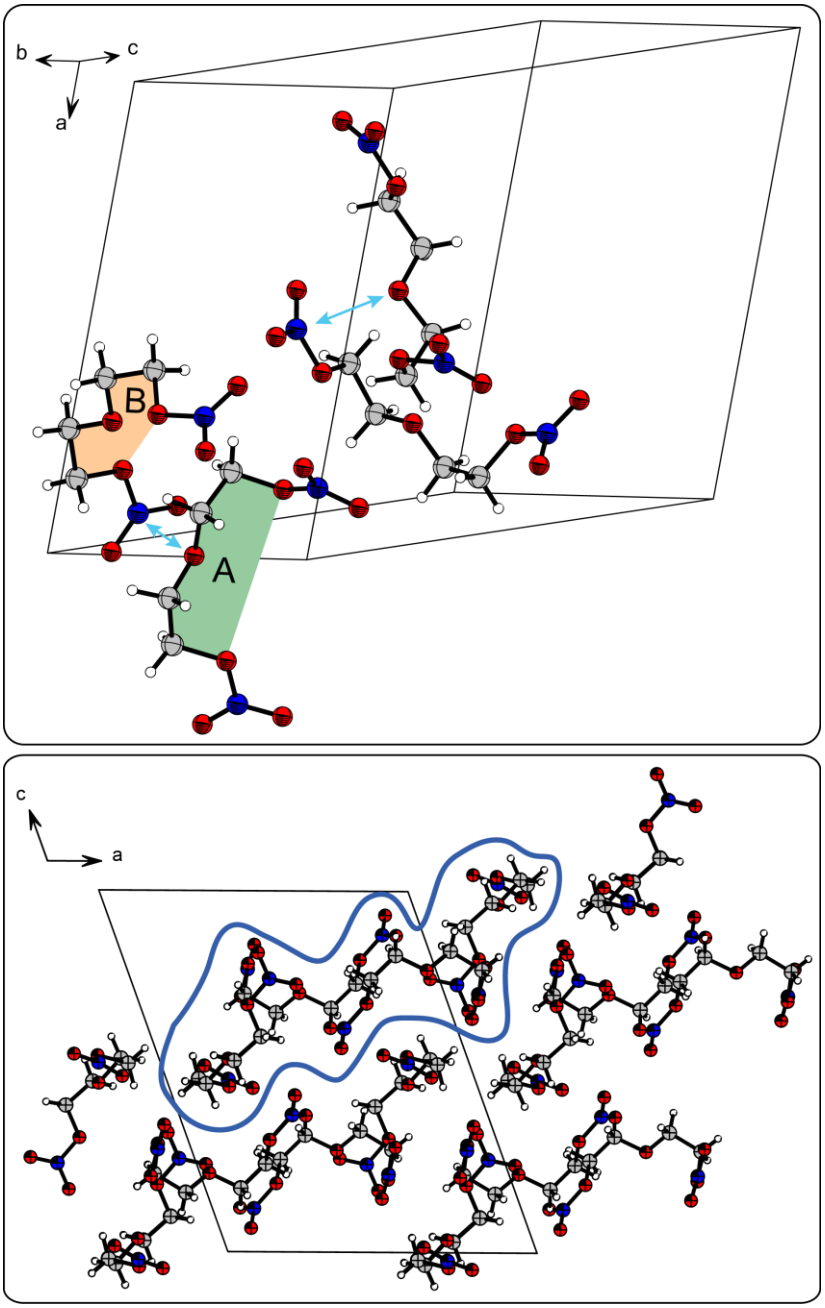

Figure 7. View of the unit cell of DEGDN along the axis between *b* and *c* axes (top) and along the *b* axis (bottom).

In this structure, it is particularly noticeable that N3 of the nitro group of species B is always aligned with the bridging oxygen O4 of species A. The distance of the two atoms with 3.07 Å almost corresponds to the combined van-der-Waals radii of oxygen (1.52 Å) and nitrogen (1.55 Å); thus, in this compound, van-der-Waals interactions are present.

In the structure of TEGDN, there is now only one species in the crystal structure at 100 K. However, the nitro groups are arranged *cis* to each other as before, shown in Figure 8.

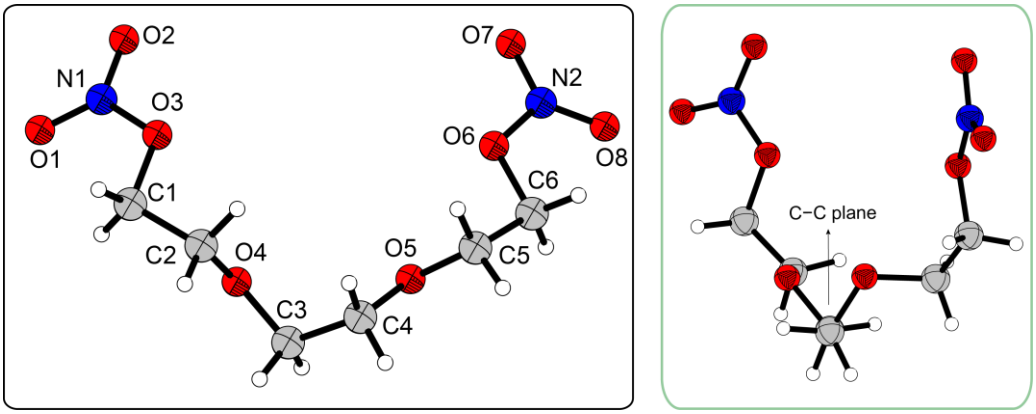

Figure 8. Molecular structure of TEGDN with selected angles (°): O3–C1–C2 106.18(12), O6–C6–C5 105.97(12), O4–C2–C1–O3–75.34(15), and O6–C6–C5–O5 67.59(15); right: view of TEGDN along the C–C plane.

Looking at the structure of TEGDN along the central C–C bond (C3–C4), it can be seen that the nitro groups in this structure are not symmetrically twisted to each other. Viewed three-dimensionally, an arrangement in layers can also be seen here, as shown in Figure 9.

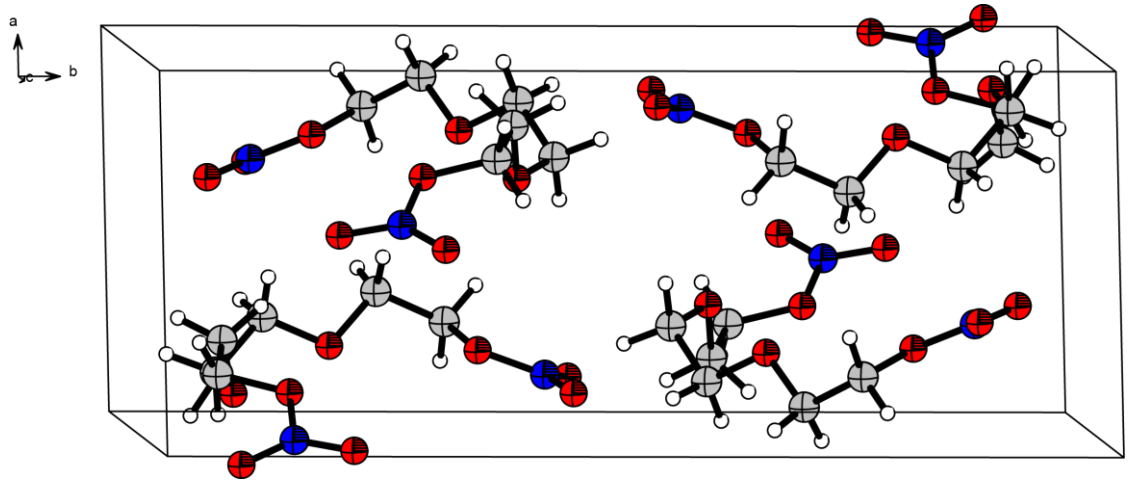

Figure 9. View of the unit cell of TEGDN along the *c* axis.

In this structure, it is noticeable that the molecules next to each other and on top of each other are rotated by 180°. The opening of the court-iron-shaped connection

thus points once to the right and then to the left, as can be seen, for example, in Figure 9.

However, in addition to the differences in the 3D arrangement of the investigated ethylene glycol dinitrates, there are also similarities. If the nitro groups of the three compounds are compared with the values for nitrate esters in the literature,[29] the bond lengths and angles differ only slightly from the literature values (Figure 10). As a trend, it can be seen that the bond length from the carbon to the ester oxygen becomes longer with increasing chain length from EGDN to TEGDN. In contrast, the length between the ester oxygen and nitrogen decreases from EGDN to TEGDN.

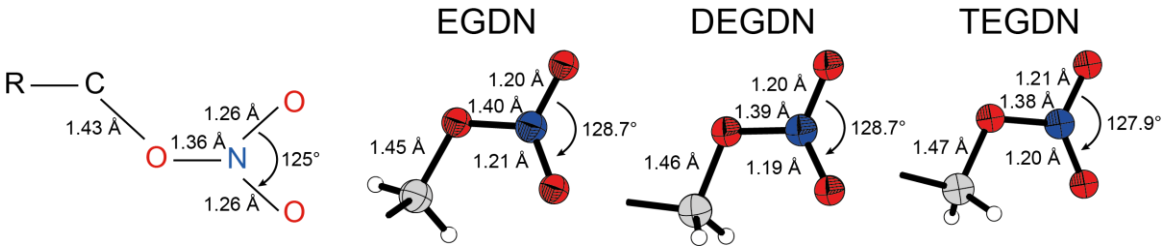

Figure 10. Structural behavior of the nitrato groups of the three compounds compared to literature values[29] on the left.

5.2.4 Thermal Analysis

For thermal analysis, DTA measurements were performed for all three compounds. The range of 25–400 °C was investigated and measured with a heating rate of 5°C per minute. The endothermic and exothermic onset signals and the melting points from the literature are shown in Table 3.

Table 3. Literature Melting Point of EGDN, DEGDN, and TEGDN[30] as well as Endothermic and Exothermic Onset Points of the DTA Measurements with a Heating Rate of 5 °C per minute.

	T_{melt}[30] [°C]	T_{endo}[a] [°C]	T_{exo}[b] [°C]
EGDN	−22	190	–
DEGDN	−11	–	184
TEGDN	−19	–	193

[a] endothermic onset point; [b] exothermic onset point.

Here, it is noticeable that DEGDN and TEGDN decompose as usual by means of an exothermic signal. Looking at the DTA plots in Figure 11, it can be seen that EGDN only shows a broadened clear endothermic signal, and EGDN does not decompose during the DTA measurement, only evaporates, which is why the endothermic signal at 190 °C can be identified as its boiling point. The fact that EGDN does not decompose can also be seen when comparing the DTA tubes after the measurement, while for DEGDN, the decomposition can be seen by dark residues, and for EGDN, no decomposition residues can be observed.

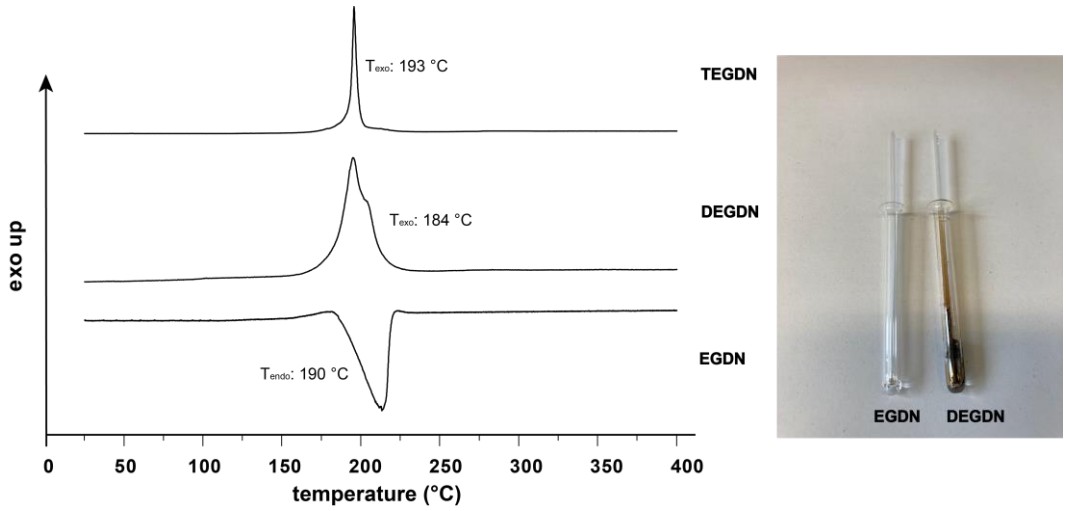

Figure 11. DTA plots of EGDN, DEGDN, and TEGDN as well as the DTA tubes of EGDN and DEGDN after measurement.

However, it is of course the case that EGDN can also be brought to decomposition. All that is needed is a very fast heating rate that preempts the vapor pressure. Comparing pictures of the hot-plate tests of the three compounds, shown in Figure 12, it can be seen that EGDN deflagrates. The intensity of the flame decreases from EGDN to TEGDN.

Figure 12. Hot-plate test of the investigated ethylene glycol dinitrates.

5.2.5 Vapor Pressure

The experimental vapor pressures p_{sat} as well as the thermochemical properties such as molar enthalpies of vaporization $\Delta_l^g H_m^\circ(T)$ and molar entropies of vaporization $\Delta_l^g S_m^\circ(T)$ of the investigated ethylene glycol dinitrates were determined using the transpiration method with coupled quantification via vacuum-outlet gas-chromatographic mass spectroscopy (VO-GC/MS). The results were presented in Table 4. The exact method description can be found elsewhere and the VO-GC/MS parameters can be found in the Supporting Information.[31,32]

Table 4. Comparison of the Thermodynamic Properties of the Compounds EGDN, DEGDN, and TEGDN Obtained in This Work via the Transpiration Method: Vapor Pressure p_{sat} and Molar Enthalpies of Vaporization $\Delta_l^g H_m^\circ$ at the Average Experimental Temperature T_{avg} and at 298.15 K.

	EGDN	**DEGDN**	**TEGDN**
T-Range [K]	274.1–318.2	274.5–323.1	288.3–328.2
T_{avg} [K]	294.3	297.9	310.0
$\Delta_l^g H_m^\circ(T_{avg})$[a] [kJ mol^{-1}]	65.4	88.6	91.9
$\Delta_l^g H_m^\circ(298.15\ \mathrm{K})$[b] [kJ mol^{-1}]	65.1 ± 0.3	88.4 ± 1.3	93.1 ± 1.1
p_{sat}[c] [mPa]	12.10×10^3	220.31	12.50

[a] Molar enthalpy of vaporization at average temperature. [b] Molar enthalpies of vaporization were adjusted according to *Chickos et al.*[33] with values of $\Delta_l^g C_{p,m}^\circ$, $C_{p,m}^\circ$(l) stated in Table S1. Uncertainties for molar enthalpies of vaporization at reference temperatures are expressed as expanded uncertainties with confidence level of 0.95 (k = 2). [c] Vapor pressure at 298.15 K extrapolated from the p-T-data.

EDGN: The vaporization behavior of EGDN was measured by Härtel in the temperature range of 274.1 to 318.2 K.[31] The values of the molar enthalpy of

vaporization ((65.1 ± 0.3) kJ mol^{-1}) and extrapolated vapor pressure at a reference temperature of 298.15 K (12.1 Pa) were determined. A detailed consideration of the literature values was carried out by Härtel, to which reference is drawn here.[32] DEGDN: The VO-GC/MS-coupled transpiration method was used to determine the vaporization behavior of DEGDN in the temperature range of 275.5 to 323.1 K (for further information see the Supporting Information). In Table S2, the absolute vapor pressures p_{sat} and thermodynamic properties of vaporization including the Clark–Glew fit function are presented. From these results, values of the molar enthalpy of vaporization ((88.4 ± 1.3) kJ mol^{-1}) and extrapolated vapor pressure at a reference temperature of 298.15 K (220.31 mPa) were derived.

The obtained results were compared with the literature data of Vacek and Crater in Table S3 and Figure S10, respectively.[34,35] Vacek only gave the Antoine fit function without specifying the used method.[34] In contrast, Crater used a comparable transpiration method, with gravimetric quantification.[35] Here, each of the five temperature points was reproduced once, and the mean value was taken to create a linear logarithmic pressure against the temperature plot. In some cases, the reproduced data points were up to 20% apart. The same data points are plotted in Figure S4 and compared with Vacek fit function and our experimental data. Since both literature sources did not calculate the molar enthalpy of vaporization, this calculation was performed in an analogous manner to our procedure. An extrapolation of the vapor pressure to room temperature was also carried out in this way. This resulted in 98.0 kJ mol^{-1} for the molar enthalpy of vaporization and in 143.54 mPa for the extrapolated vapor pressure at a reference temperature of 298.15 K for the values of Vacek and in 70.2 kJ mol^{-1} for the molar enthalpy of vaporization and in 829.08 mPa for the extrapolated vapor pressure at a reference temperature of 298.15 K for the values of Crater. By comparing the literature sources with the experimental data of this work, a discrepancy can be found. However, since both literature sources show deficits, in the data set of Vacek, the determination of the fit function cannot be reconstructed and experimental data points are not given at all, and in the data set of Crater, it can be clearly recognized that neither the described linear behavior is present nor the reproduction of the data points has taken place to a satisfactory extent. In contrast, our method has been evaluated several times, and in previous work, the thermochemical properties of well-characterized compounds have been reliably reproduced.[31,32]

TEGDN: The VO-GC/MS-coupled transpiration method was used to determine the vaporization behavior of TEGDN in the temperature range of 288.3 to 328.2 K (for further information, see the Supporting Information). In Table S4, the absolute vapor pressures p_{sat} and thermodynamic properties of vaporization including the Clark–Glew fit function are presented. From these results, values of the molar enthalpy of vaporization ((93.1 ± 1.1) kJ mol^{-1}) and extrapolated vapor pressure at a reference temperature of 298.15 K (12.50 mPa) were derived.

The results were mapped into the existing literature by Woodman.[36] Nine data points between 303.4 and 348.0 K were recorded via a piston manometer apparatus by Ernsberger and Pitman.[37] These experimental data points were processed in the same manner as in this work. This means that the experimental data points were used to calculate the resulting molar enthalpy of vaporization to be 91.6 kJ mol^{-1} and the extrapolated vapor pressure at a reference temperature of 298.15 K to be 12.86 mPa according to the Clarke–Glew fit function considering the heat capacity difference (see Table S1). The experimental *p*–*T* data points and the processing data from this work are compared in Figure S11 and Table S5 with the reported data points of Woodman.[36] Examination of the determined enthalpies of both this work and the literature, as well as visualization of the *p*–*T* data sets, revealed rough agreement with the literature values. The marginal deviations of the literature values from our results are plausible by considering the limits of the piston manometer[38] and the insufficient number of data points in comparison with the versatile evaluated transpiration method in this work.[31,32,39]

Comparison: The experimental *p*–*T* data of the compounds of interest are depicted in Figure 13. Corresponding thermodynamic properties are compiled in Table 4. By comparing the similar ethylene glycol dinitrates, which differ only in the number of ethylene glycol bridges, the trend becomes apparent that the vapor pressure is lowered by an order of magnitude by inserting another ethylene glycol bridge (see Table 4). This is accompanied by an increase in the molar phase transition enthalpy and an offset shift of the underlying Clark–Glew fit function to the left-hand side (see Figure 13). This trend in the thermodynamic behavior can be plausibly explained by the increase in molar mass and the associated reduction in volatility. Nevertheless, this work shows for the first time how the introduction of such a bridge affects the behavior and corrects existing deficiencies in the existing literature.

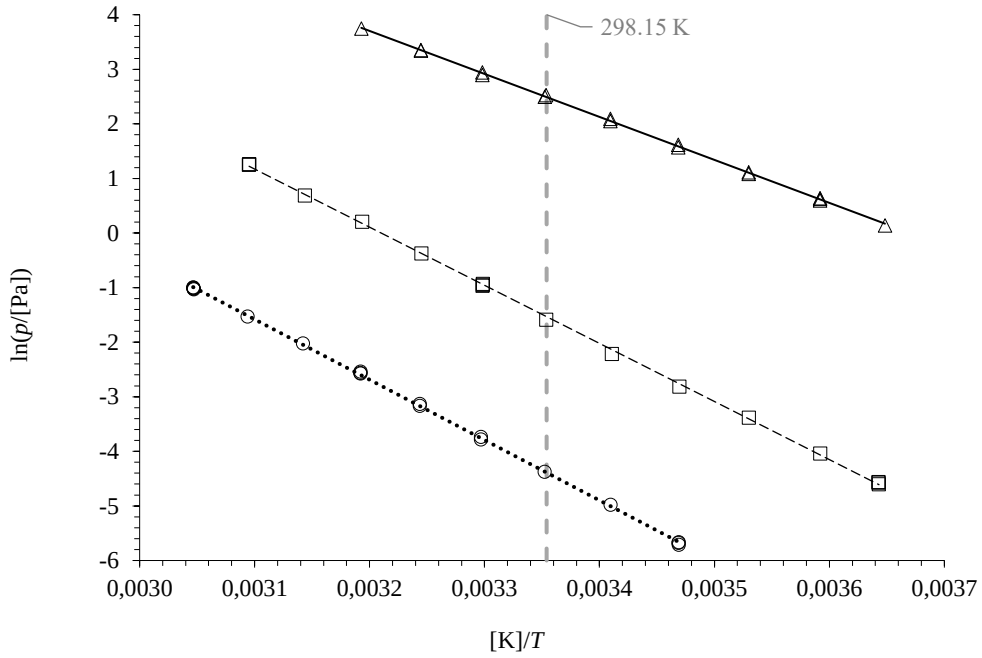

Figure 13. Comparison of the experimental vapor pressure values of the investigated ethylene glycol dinitrates. Here, the black open triangle and solid line represent EGDN; the black open square and dashed line represent DEGDN; and the black open circle and dotted line represent TEGDN. The gray line was included for guidance and is not related to the calculated values.

5.2.6 Sensitivities and Energetic Properties

The sensitivities of the three title compounds toward impact and friction were measured at room temperature in the liquid state. Since all three compounds are liquid at room temperature, they are all insensitive toward friction. However, they differ in their impact sensitivities. While TEGDN with the longest chain (and highest carbon content) with a sensitivity higher than 40 J can be classified as insensitive, DEGDN with 10 J and also EGDN with 5 J must be classified as sensitive according to the "UN Recommendations on the Transport of Dangerous Goods".[40] The sensitivities are gathered in Table 5.

Table 5. Sensitivities toward Friction and Impact of EGDN, DEGDN, and TEGDN.

	EGDN	**DEGDN**	**TEGDN**
IS [J] [a]	5	10	>40
FS [N] [b]	>360	>360	>360

[a] impact sensitivity according to the BAM drophammer (method 1 of 6); [b] friction sensitivity according to the BAM friction tester (method 1 of 6).

Table 6 shows the energetic parameters of the investigated ethylene glycol dinitrates calculated with the EXPLO5 code.(41) The room-temperature densities used were measured with a gas pycnometer. The densities decrease significantly from EGDN to TEGDN. Conversely, the enthalpy of formation decreases significantly from EGDN to TEGDN. This means that EGDN is energetically favored compared to TEGDN. Looking at the calculated parameters, it is not surprising that EGDN shows the best energetic parameters. For example, the detonation velocity of TEGDN is 1000 m s^{-1} lower than that of EGDN. Furthermore, the oxygen balance of EGDN compared to TEGDN is significantly lower. While EGDN still has a ″perfect″ oxygen balance toward CO_2 of 0%, that of TEGDN is −66.6%.

Table 6. Energetic Properties of EGDN, DEGDN, and TEGDN.(30)

	EGDN	**DEGDN**	**TEGDN**
Formula	$C_2H_4N_2O_6$	$C_4H_8N_2O_7$	$C_6H_{12}N_2O_8$
FW [g mol^{-1}]	152.06	196.12	240.17
ρ (298 K)[a] [g cm^{-3}]	1.49	1.38	1.32
T_{dec} [°C][b]	190 (T_{boil})	184	193
$\Delta_f H°$ [kJ mol^{-1}][c]	−241.0	−430.0	−606.1
EXPLO5 V6.06.01			
P_{CJ} [GPa][d]	20.9	17.5	14.1
V_{det} [m s^{-1}][e]	7519	6911	6475
$-\Delta_{ex}U°$ [kJ kg^{-1}][f]	6426	4870	4318
T_{det} [K][g]	4441	3312	2853
V_0 [L kg^{-1}][h]	810	850	851
Ω_{CO} [%][i]	21	−8.2	−26.6
Ω_{CO2} [%][i]	0	−40.8	−66.6

[a] Density measured by gas pycnometer; [b] Temperature of decomposition indicated by exothermic event according to DTA (onset temperatures at a heating rate of 5 °C min^{-1}); [c] Heat of formation values from the EXPLO5 database;40 [d] Detonation pressure; [e] Detonation velocity; [f] Energy of explosion; [g] Explosion temperature; [h] Assuming only gaseous products; [i] Oxygen balance assuming formation of CO or CO_2.

5.2.7 *Hirshfeld* Analysis

Structural properties can also provide information about the sensitivities toward external stimuli of similar compounds.(42) Therefore, based on the crystal structures

of the three compounds, *Hirshfeld* surfaces were generated as well as 2D fingerprint plots of their interactions, which are shown in Figure 14.

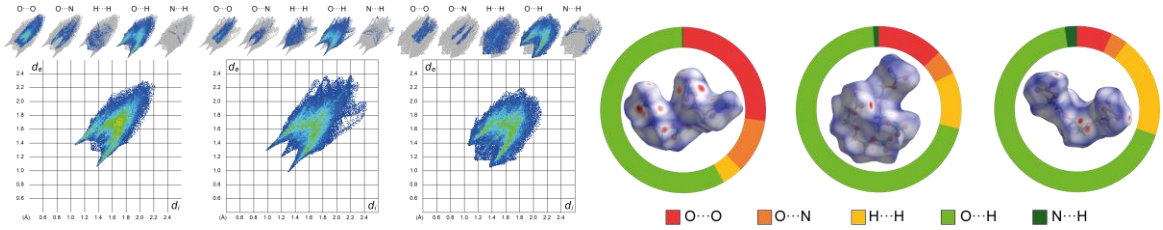

Figure 14. Left: two-dimensional fingerprint plots of the corresponding crystal structures of EGDN, DEGDN, and TEGDN. Right: distribution of the close contacts as a ring diagram and the corresponding *Hirshfeld* surfaces (d_e: distance from the *Hirshfeld* surface to the nearest atom exterior; d_i: distance from the *Hirshfeld* surface to the nearest atom interior).

The 2D fingerprint plots show distances and the types of different interactions of atoms in the crystal structure with surrounding atoms. Here, a distinction should be drawn between positive and negative interactions. The general trend is that multiple negative interactions lead to more sensitive compounds and the other way around. Homoatomic interactions are to be classified as negative interactions, but of course the size of the atoms also plays a role here. The occurring O···O interactions have a more negative influence than the occurring H···H interactions, but they all lead to a destabilization of the compound. In contrast, intermolecular hydrogen bonds like O···H and N···H lead to a stabilization in the molecule, which results in a more insensitive behavior. This is due to the additionally formed interactions between the molecules. Comparing the three compounds, the destabilizing O···O interactions decrease significantly from EGDN (27.1%) via DEGDN (13.0%) to TEGDN (6.9%). In contrast, the stabilizing O···H interactions increase in the same direction from EGDN (58.0%) to DEGDN (70.1%). However, the O···H interactions of DEGDN (70.1%) and TEGDN (67.5%) are almost consistent. Nevertheless, the stabilizing N···H interactions from DEGDN (1.1%) to TEGDN (2.4%) also increase. Therefore, the *Hirshfeld* analysis predicts that the sensitivity of EGDN via DEGDN to TEGDN stabilizes and becomes in that row more insensitive for the compounds in the solid state.

5.3 Conclusion

In this work, for the first time, it was possible to determine the crystal structures of the energetic plasticizers EGDN, DEGDN, and TEGDN, using a low-temperature crystallizing method. XRD studies at 100 K showed that all crystallized in monoclinic space group $P2_1/c$ with densities in the row EGDN (1.77 g cm^{-3}), DEGDN (1.56 g cm^{-3}), and TEGDN (1.55 g cm^{-3}). Furthermore, the obtained crystal structures were used to obtain new information about the properties in the solid state, for which *Hirshfeld* analyses were performed. These showed that even in the solid state, EGDN is the most sensitive, followed by DEGDN, while TEGDN is the most insensitive. In addition, all three compounds were fully characterized. When analyzing the thermal properties, it was noticed that EGDN only evaporates at a heating rate of 5 degrees per minute and does not decompose. Therefore, vapor pressure measurements were performed. For the ethylene glycol dinitrates DEGDN and TEGDN, the experimental vapor pressures and the resulting molar enthalpies of vaporization were reported and integrated in the existing literature, as well as discussed in the case of discrepancies. In addition, the glycol nitrates were categorized in the existing literature of the related ethylene glycol EGDN. The thermochemical properties of the compounds were measured in the ambient temperature range using the transpiration method in conjunction with VO-GC/MS quantification. The study revealed the trend that the introduction of further ethylene glycol bridges leads to a decrease in the volatility accompanied by an increase in the molar enthalpy of vaporization.

5.4 Acknowledgement

For financial support of this work by Ludwig Maximilian Universi-ty (LMU), the Office of Naval Research (ONR) under grant no. ONR N00014-19-1-2078 and the Strategic Environmental Re-search and Development Program (SERDP) under contract no. W912HQ19C0033 are gratefully acknowledged. Moreover, the authors want to thank Dr. B. Krumm for ^{1}H-qNMR measurements.

5.5 References

(1) Sabatini, J. J.; Johnson, E. C. A Short Review of Nitric Esters and Their Role in Energetic Materials. *ACS Omega* **2021**, *6*, 11813−11821.

(2) Klapötke, T. M. *Chemistry of High Energy Materials*, 6th, deGruyter, Berlin, **2022**.

(3) Kubota, N. *Propellants and Explosives*, Wiley-VCH, Weinheim, **2007**.

(4) Zheng, Y.; Gao, H.; Cao, X.; Wang, B.; Nan, F. Study on the Method of Measuring Nitrocellulose Nitrogen Content. *J. Phys.: Conf. Ser.* **2021**, 012072.

(5) Lopez-Lopez, M.; Alegre, J. M. R.; Garcia-Ruiz, C.; Torre, M. Determination of the nitrogen content of nitrocellulose from smokeless gunpowders and collodions by alkaline hydrolysis and ion chromatography. *Anal. Chim. Acta* **2011**, *685*, 196−203.

(6) Agrawal, J. P. *High Energy Materials*, Wiley-VCH, Weinheim, **2010**.

(7) Sanghavi, R. R.; Pillai, A. G. S.; Velapure, S. P.; Singh, A. Studies on Different Types of Nitrocellulose in Triple Base Gun Propellant Formulations. *J. Energ. Mater.* **2003**., *21*, 87−95.

(8) Sovizi, M. R.; Hajimirsadeghi, S. S.; Naderizadeh, B. Effect of particle size on thermal decomposition of nitrocellulose. *J. Hazard. Mat.* **2009**, *168*, 1134−1139.

(9) Volk, F.; Bohn, M.; Wunsch, G. Determination of Chemical and Mechanical Properties of Double Base Propellants during Aging. *Propellants Explos. Pyrotech.* **1987**, *12*, 81−87.

(10) Agrawal, J. P.; Singh, H. Qualitative Assessment of Nitroglycerin Migration from Double-Base and Composite Modified Double-Base Rocket Propellants: Concepts and Methods of Prevention. *Propellants Explos. Pyrotech.* **1993**, *18*, 106−110.

(11) Sućeska, M.; Musanic, S. M., Houra, I. F. Kinetics and enthalpy of nitroglycerin evaporation from double base propellants by isothermal thermogravimetry. *Thermochim. Acta* **2010**, *510*, 9−16.

(12) Mueller, D. Method and apparatus for producing single-base or multibase propellants. DE3242301 **1982**.

(13) Fong, C. W.; Warren, R. C. An Interphasic Region between Nitrocellulose and Nitroguanidine in Triple Base Propellant. *Propellants Explos. Pyrotech.* **1985**, *10*, 69−73.
(14) Bellerby, J. M.; Sammour, M. H. Stabilizer Reactions in Cast Double Base Rocket Propellants. Part I: HPLC Determination of Stabilizers and their Derivatives in a Propellant Containing thc Stabilizer Mixture para-Nitro-N-Methylaniline and 2-Nitrodiphenylamine Aged at 80°C and 90°C. *Propellants Explos. Pyrotech.* **1991**, *16*, 235−239.
(15) Boers, M. N.; de Klerk, W. P. C. Lifetime Prediction of EC, DPA, Akardite II and MNA Stabilized Triple Base Propellants, Comparison of Heat Generation Rate and Stabilizer Consumption. *Propellants Explos. Pyrotech.* **2005**, *30*, 356−362.
(16) Lindblom, T.; Christy, A. A.; Libnau, F. O. Quantitative determination of stabiliser in a single base propellant by chemometric analysis of Fourier transform infrared spectra. *Chemometrics Intell. Lab. Sys.* **1995**, *29*,243−254.
(17) Soliman, A. A.-W. 2,4,6-Triphenyl- thiazolo [3,2-a]-s-Triazine as a Stabilizer for Single Base Propellant. *Propellants Explos. Pyrotech.* **1985**, *10*, 82−83.
(18) Agrawal, J.P.; Hodgson, R. D. *Organic Chemistry of Explosives*, Wiley-VCH, Weinheim, **2007**.
(19) Reese, D. A.; Groven, L. J.; Son, S. F. Formulation and Characterization of a New Nitroglycerin - Free Double Base Propellant. *Propellants Explos. Pyrotech.* **2014**, *39*, 205−210.
(20) Volk, W.; Wunsch, G. Determination of the Decomposition Behavior of Double-Base Propellants at Low Temperatures. *Propellants Explos. Pyrotech.* **1985**, *10*, 181−186.
(21) Townend, D. J.; Warren, R. C. Relaxations in double base propellants. *Polymer* **1985**, *26*, 79−83.
(22) Cowper, R. On the action of alcohol on mercuric nitrate. *J. Chem. Soc. Trans.*, **1881**, *39*, 242−247.
(23) Rinkenbach, Wm. H. Preparation and Properties of Diethyleneglycol Dinitrate. *Ind. Eng. Chem.* **1927**, *19*, 925–927.
(24) Will, W.; Lenze, F. Nitrirung von Kohlehydraten. *Chem. Ber.* **1898**, *31*, 68–90.
(25) Steinberger, R.; Carder, K. E. Surface Temperature of Burning Liquid Nitrate Esters. *J. Phys. Chem.* **1955**, *59*, 255–257.

(26) Schoenberger, T. Determination of standard sample purity using the high-precision ^{1}H-NMR process. *Anal. Bioanal. Chem.* **2012**, *403*, 247–254.
(27) Wieser, M. E.; Holden, N.; Coplen, T. B.; Böhlke, J. K.; Berglund, M.; Brand, W. A.; De Bièvre, P.; Gröning, M.; Loss, R. D.; Meija, J. Atomic weights of the elements 2011.*Pure Appl. Chem.* **2013**, *85*, 1047–1078.
(28) Bienz, S.; Bigler, L.; Fox, T. *Spektroskopische Methoden in der organischen Chemie*, 9 *ed*., Thieme, Stuttgart, **2016**.
(29) Liu, J. *Nitrate Esters Chemistry and Technology*, Springer, **2019**.
(30) Klapötke, T. M. *Energetic Materials Encyclopedia*, 2nd Edition, DeGruyter, Berlin/Boston, **2021**.
(31) Bikelytė, G.; Härtel, M. A. C.; Holler, M.; Neuer, A.; Klapötke, T. M. Thermodynamic Properties of Energetic Plasticizers: Experimental Vapor Pressures of Methyl-, Ethyl-, and Butyl-Nitroxyethyl Nitramines. *J. Chem. Eng. Data* **2021**, *66*, 1709-1716.
(32) Härtel, M. A.; Klapötke, T. M.; Stierstorfer, J.; Zehetner, L. Vapor Pressure of Linear Nitrate Esters Determined by Transpiration Method in Combination with VO-GC/MS. *Propellants, Explos., Pyrotech.* **2019**, *44*, 484−492.
(33) Acree, W.; Chickos, J. S. Phase Transition Enthalpy Measurements of Organic and Organometallic Compounds. Sublimation, Vaporization and Fusion Enthalpies From 1880 to 2010. *J. Phys. Chem. Ref. Data* **2010**, *39*, 043101.
(34) Vacek, J.; Stanek, J. Vapor pressures of some organic nitrates. *Chem. Prum.* **1959**, *9*, 286−.
(35) Crater, W. d. The Vapor Pressures of Glycerol Trinitrate and Certain Glycol Dinitrates. *Ind. Eng. Chem.* **1929**, *21*, 674−676.
(36) Woodman, A. L.; Adicoff, A. Vapor Pressure of Tiracetin, Triethylene Glycol Dinitrate, and Metriol Trinitrate. J. Chem. Eng. Data 1963, 8, 241−242.
(37) Ernsberger, F. M.; Pitman, H. W. New Absolute Manometer for Vapor Pressures in the Micron Range. *Rev. Sci. Instrum.* **1955**, *26*, 584−589.
(38) Steckelmacher, W. The calibration of vacuum gauges. *Vacuum* **1987**, *37*, 651−657.
(39) Östmark, H.; Wallin, S.; Ang, H. G. Vapor pressure of explosives: a critical review. *Propellants Explos. Pyrotech.* **2012**, *37*, 12−23.
(40) Impact: insensitive > 40 J, less sensitive ≥ 35 J, sensitive ≥ 4 J, very sensitive ≤ 3 J, Friction: insensitive > 360 N, less sensitive = 360 N, sensitive < 360 N and >

80 N, very sensitive ≤ 80 N, extremely sensitive ≤ 10 N. According to the UN Recommendations on the Transport of Dangerous Goods, (+) indicates not safe for transport.
(41) Sućeska, M. EXPLO5 V6.06.01, Zagreb (Croatia) **2021**.
(42) Bauer, L.; Benz, M.; Klapötke, T. M.; Lenz, T.; Stierstorfer J. Polyazidomethyl Derivatives of Prominent Oxadiazole and Isoxazole Scaffolds: Synthesis, Explosive Properties, and Evaluation. *J. Org. Chem.* **2021**, *86*, 6371−6380.

5.6 Supporting Information

5.6.1 Experimental Information

All chemicals and solvents were employed as received (*Sigma-Aldrich*, *Acros*, VWR). ^{1}H,^{13}C and ^{14}N NMR spectra were recorded at ambient temperature using a *Bruker* TR 400 instrument. The chemical shifts quoted in ppm in the text refer to typical standards such as tetramethylsilane or nitromethane (^{1}H, ^{13}C, ^{14}N). Infrared spectra were measured with pure samples on a *Perkin-Elmer* BXII FT-IR system with a *Smith* DuraSampler IR II diamond ATR. Determination of the carbon, hydrogen, and nitrogen contents was carried out by combustion analysis using an *Elementar Vario* El (nitrogen values determined are often lower than the calculated ones due to their explosive behavior). Impact sensitivity tests were carried out according to *STANAG* 4489[1] modified instruction [2] using a *BAM* (Bundesanstalt für Materialforschung) drophammer.[3] Friction sensitivity tests were carried out according to *STANAG* 4487[4] modified instruction[5] using the BAM friction tester. The classification of the tested compounds results from the “UN Recommendations on the Transport of Dangerous Goods”.[6]

CAUTION! All investigated compounds are potentially explosive energetic materials, which show partly increased sensitivities towards various stimuli (e.g. elevated temperatures, impact, or friction). Therefore, proper security precautions (safety glass, face shield, earthed equipment and shoes, leather coat, Kevlar gloves, Kevlar sleeves, and earplugs) have to be applied while synthesizing and handling the described compounds.

Ethylene glycol dinitrate (EGDN)

Mixed acid (3.6 mass %) was prepared under ice-cold conditions by slowly adding fuming nitric acid (10.80 g, 7.15 mL) to concentrated sulfuric acid (7.20 g, 3.91 mL). Ethylene glycol (5.00 g, 80.55 mmol) was added dropwise to the reaction mixture while maintaining the temperature below 15 °C. After stirring at 15 °C for 5 min, the reaction was quenched on ice (15 mL). DCM (25 mL) was added to the organic phase to enlarge it. The two-phase mixture was separated in a separating funnel, followed by washing the organic phase with water (2 x 25 mL) and a saturated $NaHCO_3$ solution (2 x 25 mL). The organic phase was dried over magnesium sulfate and the solvent was removed *in vacuo*. Ethylene glycol dinitrate (5.92 g, 38.93 mmol, 48 %) was obtained as colorless oil.

^{1}H NMR (400 MHz, acetone-d_6) δ 4.89 (s, 4H, CH_2); ^{13}C NMR (101 MHz, acetone-d_6) δ 70.1; ^{14}N (29 MHz, acetone-d_6) δ −44; EA ($C_2H_4N_2O_6$, 152.06): calcd: C 15.80, H 2.65, N 18.42 %; found: C 15.56, H 2.72, N 15.29 %, *BAM* drophammer: 4 J; friction tester: >360 N.

Diethylene glycol dinitrate (DEGDN)

Diethylene glycol (5.00 g, 47.12 mmol) was added dropwise to mixed acid under ice-cold conditions. The mixed acid (3.6 mass %) contained fuming nitric acid (10.80 g, 7.15 mL) and concentrated sulfuric acid (7.20 g, 3.91 mL). The reaction mixture was stirred at 15 °C for 15 min and quenched on ice (15 mL). The organic phase was extended by addition of DCM (25 mL) and both were separated. Then the organic phase was washed with water (2 x 25 mL) and a saturated $NaHCO_3$ solution (2 x 25 mL). The organic phase was then dried over magnesium sulfate and removed *in vacuo*. Diethylene glycol dinitrate (5.18 g, 26.41 mmol, 56 %) was obtained as a colorless oil.

^{1}H NMR (400 MHz, acetone-d_6) δ 4.69 (m, 4H, CH_2ONO$_2$), 3.83 (m, 4H, CH_2); ^{13}C NMR (101 MHz, acetone-d_6) δ 73.4 (CH_2ONO$_2$), 67.9 (CH_2); ^{14}N (29 MHz, acetone-d_6) δ −42; EA ($C_4H_8N_2O_7$, 196.12): calcd: C 24.50, H 4.11, N 14.28 %; found: C 24.34, H 4.05, N 13.55 %; *BAM* drophammer: 10 J, friction tester: >360 N.

Triethylene glycol dinitrate (TEGDN)

Triethylene glycol (5.00 g, 33.30 mmol) was added dropwise to mixed acid under ice-cold conditions. The mixed acid (3.6 mass%) contained fuming nitric acid

(10.80 g, 7.15 mL) and concentrated sulfuric acid (7.20 g, 3.91 mL). The reaction mixture was stirred at 15 °C for 15 min and quenched on ice (15 mL). To enlarge the organic phase DCM (25 mL) wad added. After separation of the two-phase mixture, the organic phase was washed with water (2 x 25 mL) and a saturated $NaHCO_3$ solution (2 x 25 mL). The organic phase was then dried over magnesium sulfate and removed *in vacuo*. Triethylene glycol dinitrate (3.26 g, 13.60 mmol, 41 %) was obtained as colorless oil.

^{1}H NMR (400 MHz, acetone-d_6) δ 4.67 (m, 4H, CH_2ONO$_2$), 3.79 (m, 4H, OCH_2CH$_2$ONO$_2$), 3.64 (s, 4H, O-CH_2-CH_2-O); ^{13}C NMR (101 MHz, acetone-d_6) δ 73.6, 71.2, 67.7; ^{14}N (29 MHz, acetone-d_6) δ −40; EA ($C_6H_{12}N_2O_8$, 240.17): calcd: C 30.01, H 5.04, N 11.66 %; found: C 29.74, H 4.98, N 11.56 %; *BAM* drophammer: >40 J, friction tester: >360 N.

5.6.2 NMR Spectroscopy

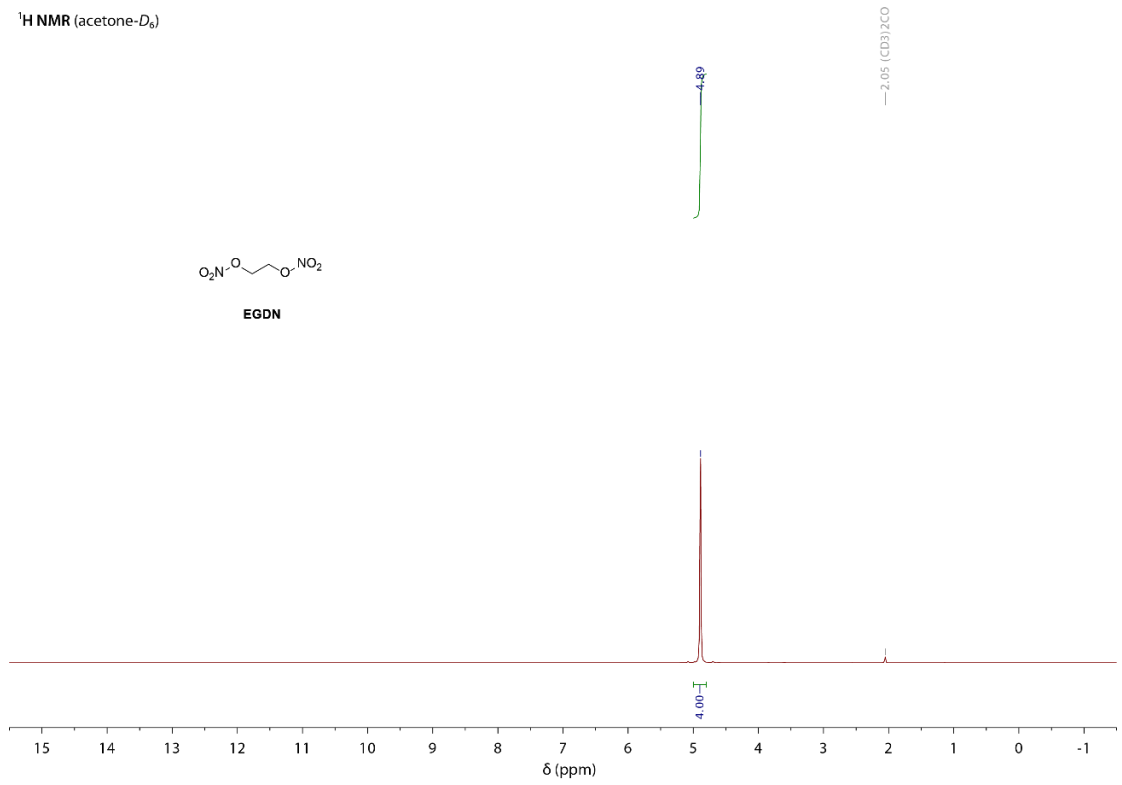

Figure S1. ^{1}H NMR spectrum of EGDN in acetone-D_6.

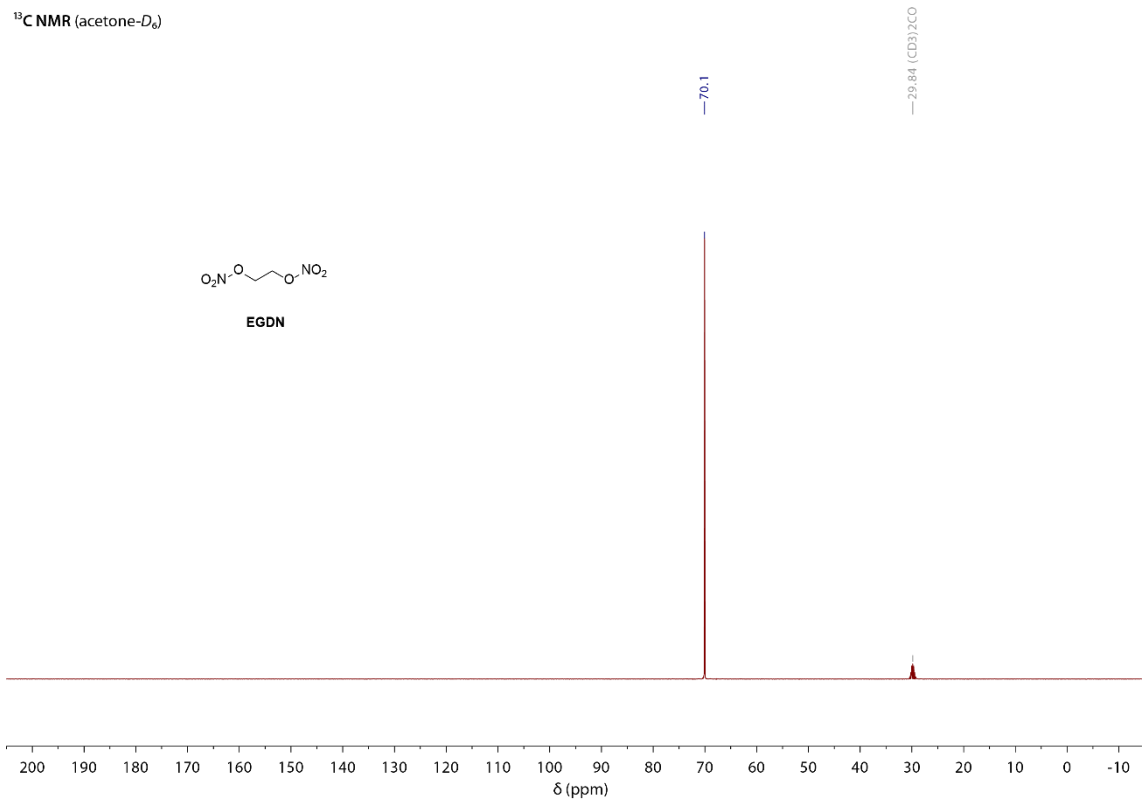

Figure S2. $^{13}C\{^{1}H\}$ NMR spectrum of **EGDN** in acetone-D_6.

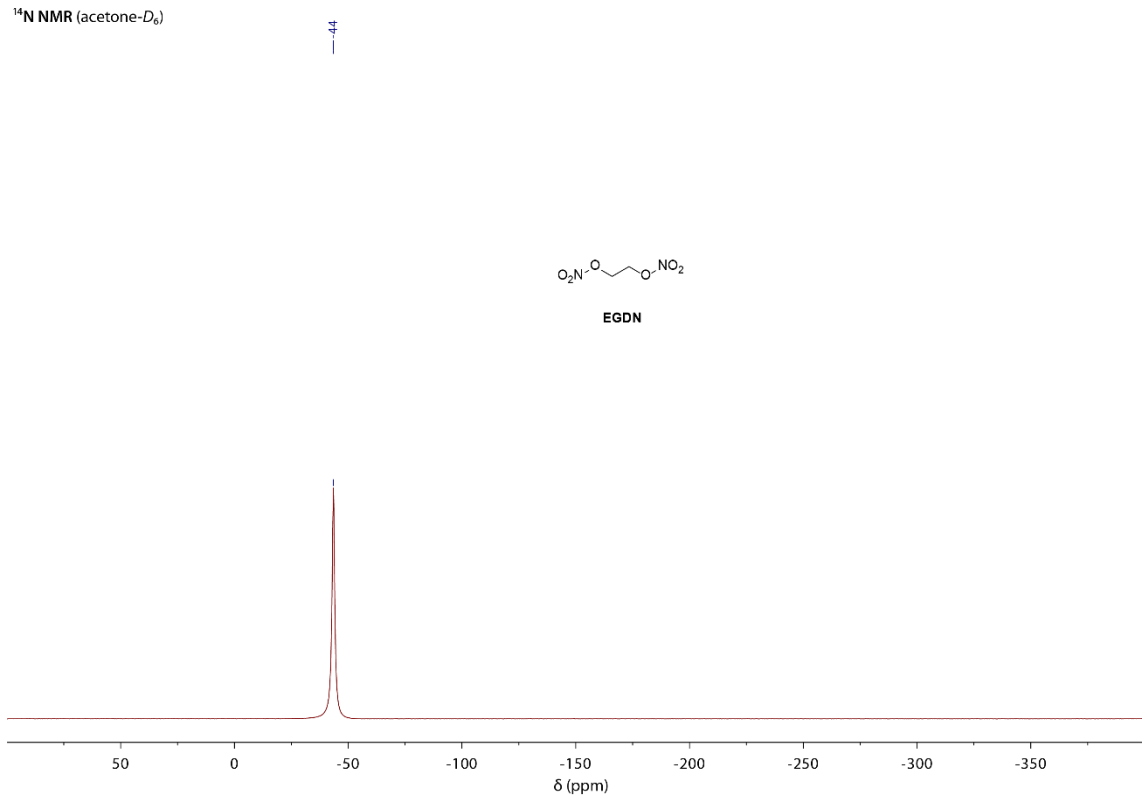

Figure S3. ^{14}N NMR spectrum of **EGDN** in acetone-D_6.

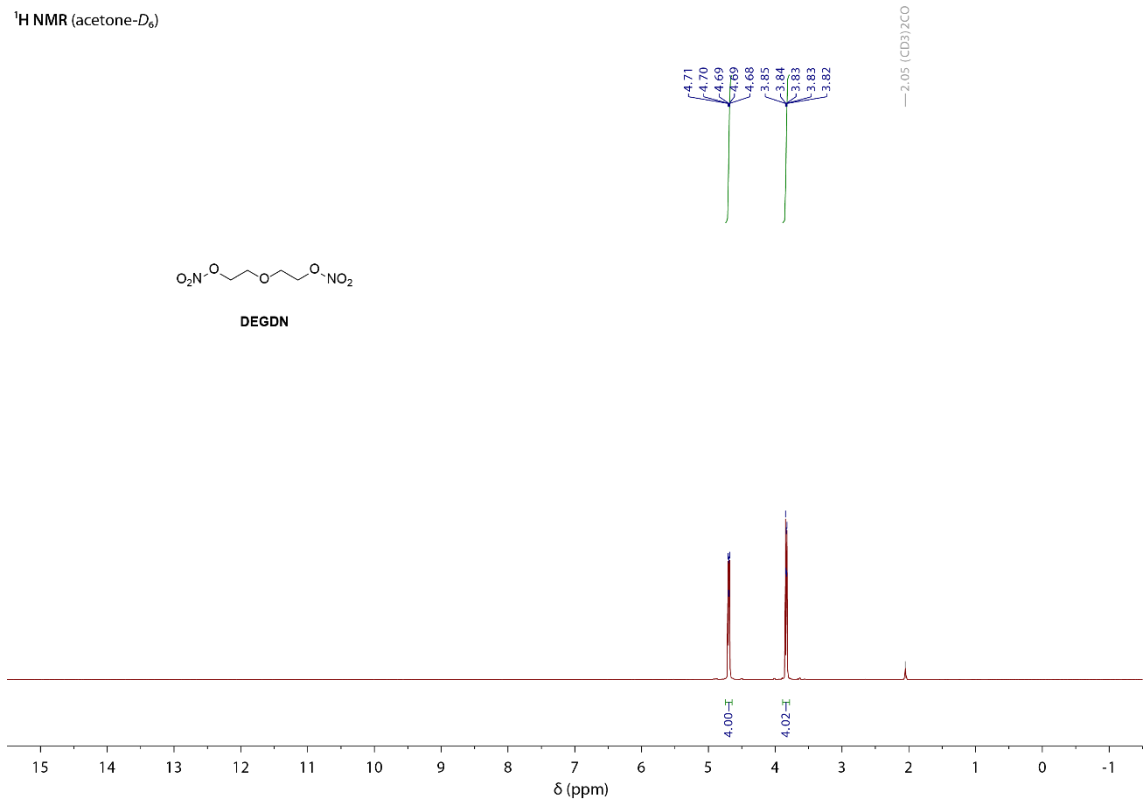

Figure S4. ^{1}H NMR spectrum of **DEGDN** in acetone-D_6.

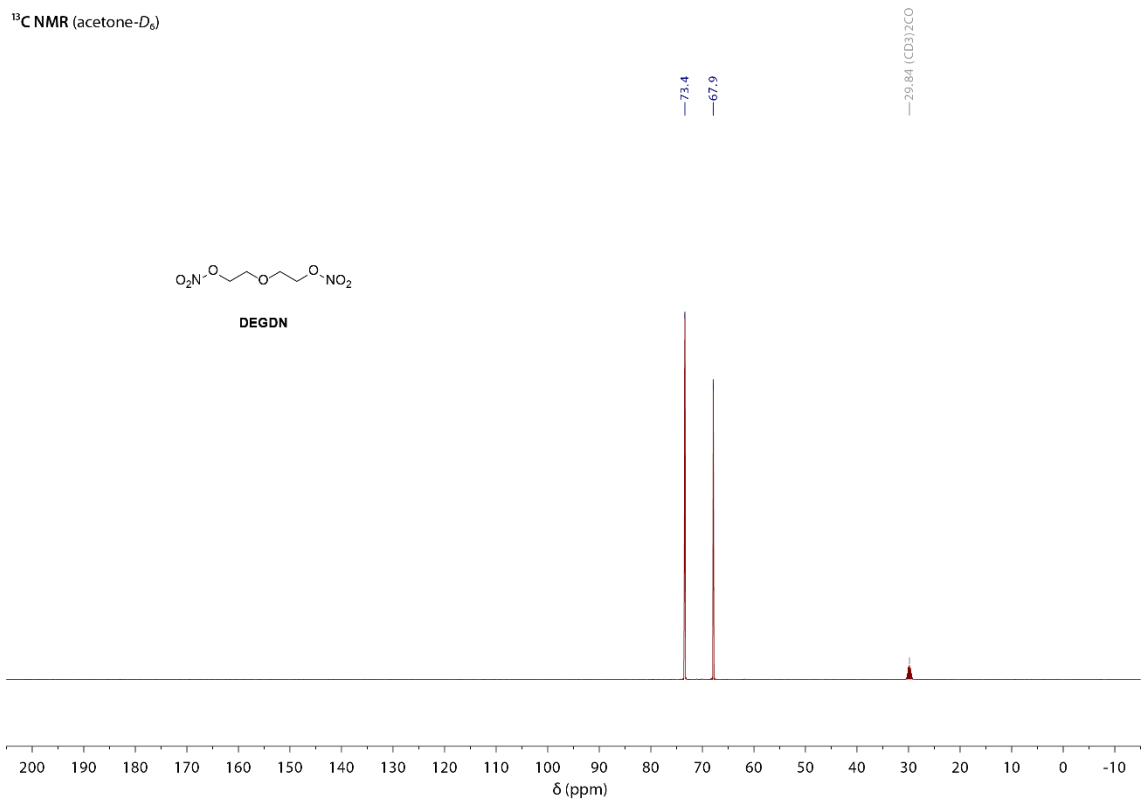

Figure S5. $^{13}C\{^{1}H\}$ NMR spectrum of **DEGDN** in acetone-D_6.

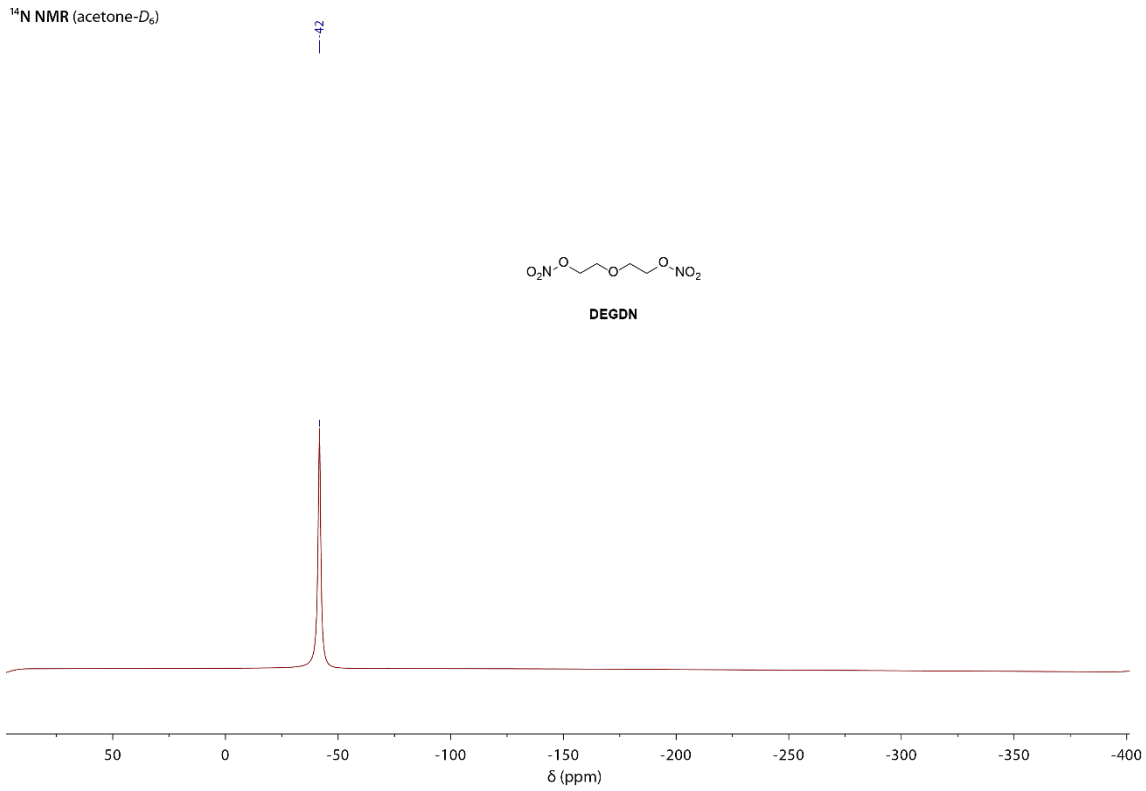

Figure S6. ^{14}N NMR spectrum of **DEGDN** in acetone-D_6.

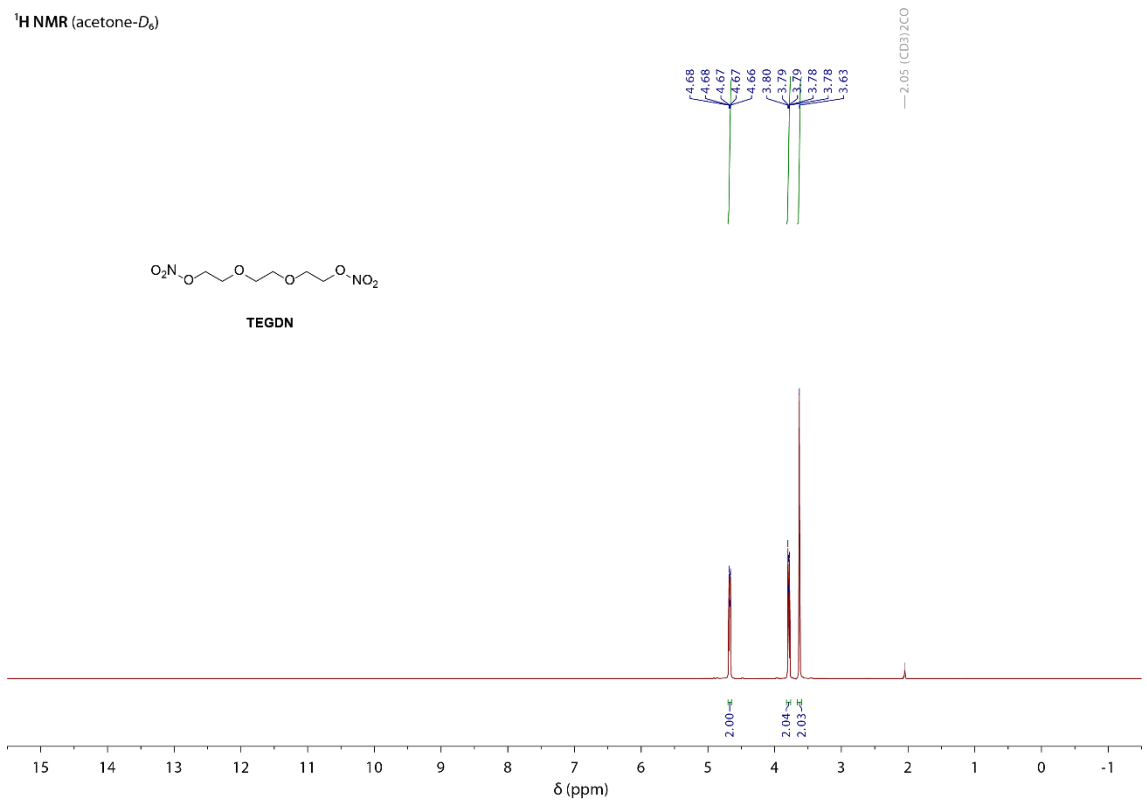

Figure S7. ^{1}H NMR spectrum of **TEGDN** in acetone-D_6.

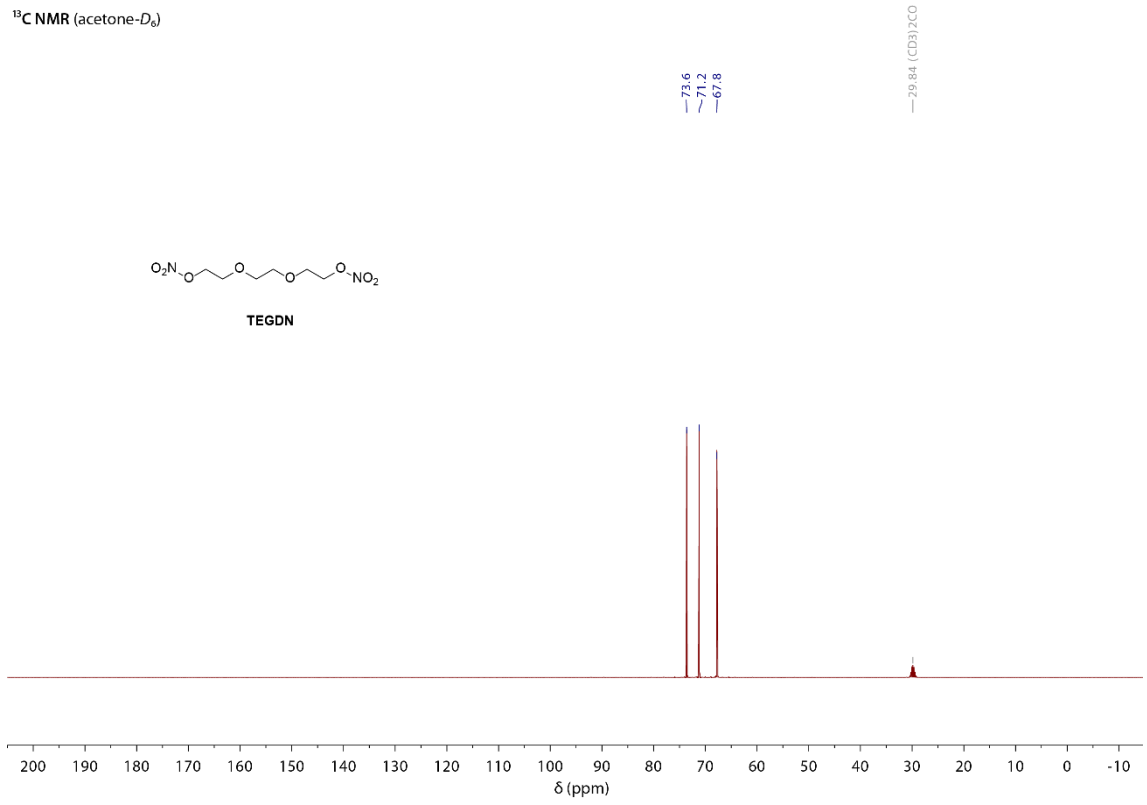

Figure S8. ^{13}C{^{1}H} NMR spectrum of **TEGDN** in acetone-D_6.

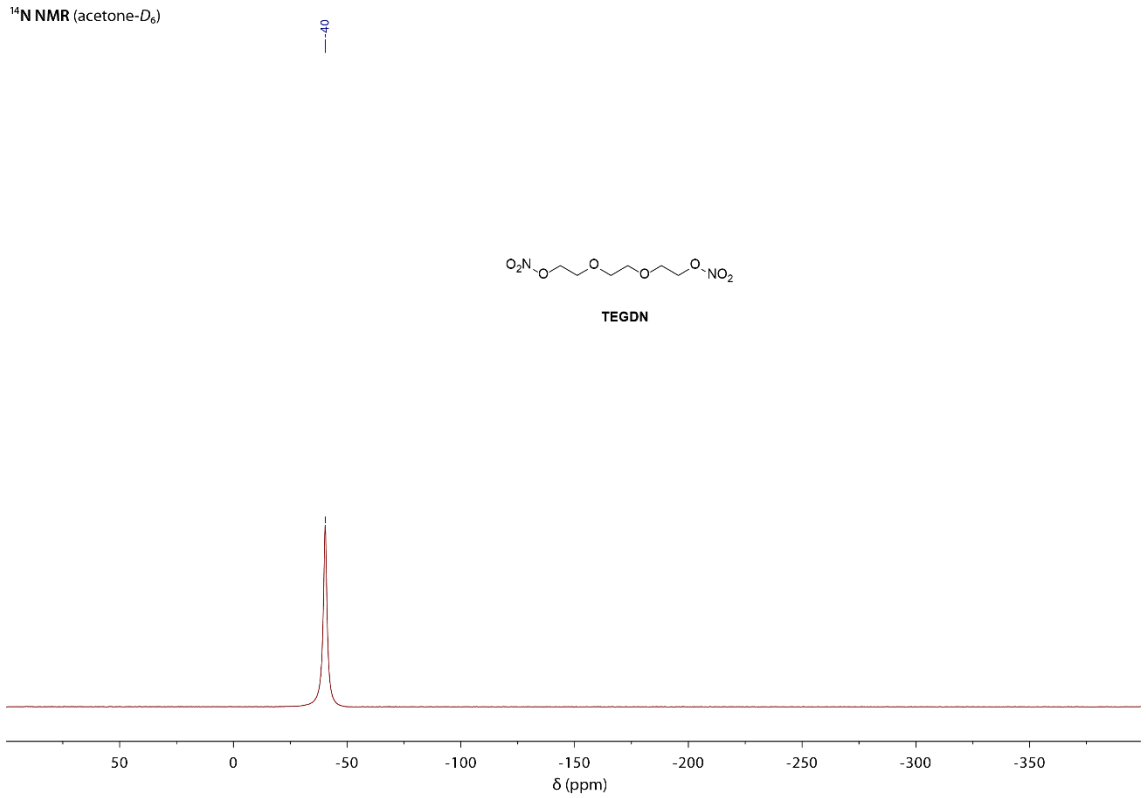

Figure S9. ^{14}N NMR spectrum of **TEGDN** in acetone-D_6.

5.6.3 X-Ray Diffraction

For all crystalline compounds, an *Oxford* Xcalibur3 diffractometer with a CCD area detector or *Bruker* D8 Venture TXS diffractometer equipped with a multilayer monochromator, a Photon 2 detector, and a rotating-anode generator was employed for data collection using Mo-Kα radiation (λ = 0.71073 Å). On the *Oxford* device, data collection and reduction were carried out using the *CRYSALISPRO* software.[7] On the *Bruker* diffractometer, the data were collected with the *Bruker* Instrument Service v3.0.21, the data reduction was performed using the *SAINT* V8.18C software (*Bruker* AXS Inc., 2011). The structures were solved by direct methods (*SIR*-92, [8] *SIR*-97[9] or *SHELXT*[9,10]) and refined by full-matrix least-squares on F2 (*SHELXL*[10,11]) and finally checked using the *PLATON* software[12] integrated into the *WinGX*[13] software suite. The non-hydrogen atoms were refined anisotropically and the hydrogen atoms were located and freely refined. The absorptions were corrected by a *SCALE3* ABSPACK or SADABS *Bruker* APEX3 multiscan method.[14] All DIAMOND2 plots are shown with thermal ellipsoids at the 50 % probability level and hydrogen atoms are shown as small spheres of arbitrary radius.

5.6.4 Vapor Pressure Determination

After the isolation of the three different ethylene glycol dinitrates, purity was tested via elemental analysis and complemented by ^{1}H-qNMR techniques (see Main Paper). After determining sufficient purity, the heat capacity difference of vaporization $\Delta_{\mathrm{l}}^{\mathrm{g}}C_{\mathrm{p,m}}^{\circ}$ of the respective substances – required for the *Clark-Glew* fit function – was calculated according to the method of *Chickos,* since no literature values were accessible.[15] The values were presented in Table S1.

Table S1. Estimated molar heat capacities and their differences for the ethylene glycol dinitrate compounds (T = 298.15 K).

Compound	$C_{\mathrm{p,m}}^{\circ}(l)$ [a]	$-\Delta_{\mathrm{l}}^{\mathrm{g}}C_{\mathrm{p,m}}^{\circ}$ [b]
	Calc.	Calc.
	J·mol^{-1}·K^{-1}	J·mol^{-1}·K^{-1}
EGDN	240.6	73.1
DEGDN	334.2	97.5
TEGDN	427.8	121.8

a: Calculated according to the group additivity approach by *Chickos et al.*[15] b: calculated by $-\Delta_{\mathrm{l}}^{\mathrm{g}}C_{\mathrm{p,m}}^{\circ} = 10.58 + C_{\mathrm{p,m}}^{\circ}(l) \times 0.26$[2].

The experimental vapor pressures as well as the thermochemical properties such as molar enthalpies of vaporization $\Delta_{\mathrm{l}}^{\mathrm{g}}H_{\mathrm{m}}^{\circ}(T)$ and molar entropies of vaporization $\Delta_{\mathrm{l}}^{\mathrm{g}}S_{\mathrm{m}}^{\circ}(T)$ were reported in Table S2 for DEGDN, Table S4 for DEGDN. The corresponding literature comparison can be found in Table S3 and Figure S10 for DEGDN, in Table S5 and Figure S11 for TEGDN. An analog report can be found for EGDN in the Supporting Information of *Härtel's* publication.[17]

5.6.4.1 *p-T* data obtained in this work for DEGDN

Table S2. Experimental conditions and *Clark-Glew* fit function resulting in absolute vapor pressures p_{sat} and thermochemical properties of vaporization (molar enthalpy of vaporization $\Delta_{\mathrm{l}}^{\mathrm{g}}H_m^{\circ}$ and molar entropy of vaporization $\Delta_{\mathrm{l}}^{g}S_m^{\circ}$). Obtained from the measurements of DEGDN by the Transpiration Method[a].

DEGDN: $\Delta_{\mathrm{l}}^{\mathrm{g}}H_{\mathrm{m}}^{\circ}$ (298.15 K) = (88.4 ± 1.3) kJ·mol^{-1}

$$\ln p_{\mathrm{sat}}/p^0 = \frac{381.4}{R} - \frac{117476.1}{RT} - \frac{97.5}{R} ln \frac{T}{298.15\ \mathrm{K}}$$

T[b]	m[c]	V_{N2}[d]	T_{amb}[e]	Flow	p_{sat}[f]	$u(p_{\mathrm{sat}})$[g]	$\Delta_{\mathrm{l}}^{\mathrm{g}}H_m^{\circ}(T)$	$\Delta_{\mathrm{l}}^{g}S_m^{\circ}(T)$
K	mg	dm³	K	dm³·h^{-1}	Pa	Pa	kJ·mol^{-1}	J·mol^{-1}·K^{-1}
274.5	0.058	74.2	299.1	4.2	0.010	0.001	90.72	196.5
274.5	0.058	71.9	299.5	3.6	0.010	0.001	90.72	196.7
274.5	0.062	76.2	299.8	4.8	0.010	0.001	90.72	196.8
278.4	0.017	12.5	299.1	4.8	0.018	0.001	90.34	195.2
283.3	0.018	6.73	299.4	4.8	0.034	0.001	89.86	193.4
288.2	0.018	3.73	297.9	4.8	0.060	0.003	89.38	191.0
293.2	0.018	2.08	297.9	4.8	0.109	0.005	88.90	189.1
298.2	0.019	1.20	298.2	4.8	0.204	0.009	88.41	187.6
303.2	0.037	1.20	298.1	4.8	0.386	0.017	87.93	186.4
303.2	0.111	3.58	298.0	4.8	0.393	0.017	87.93	186.5
303.2	0.048	1.60	298.2	4.8	0.379	0.016	87.93	186.2
308.1	0.065	1.20	298.9	4.8	0.687	0.030	87.44	184.9
313.1	0.117	1.20	295.2	4.8	1.223	0.053	86.96	183.7
318.1	0.286	1.83	299.1	4.8	1.978	0.085	86.47	181.8
323.1	0.162	0.59	299.0	2.3	3.507	0.151	85.99	180.9
323.1	0.187	0.67	298.4	2.7	3.517	0.151	85.99	180.9
323.1	0.205	0.75	298.9	3.0	3.482	0.150	85.98	180.8

[a] Experimental conditions: T is saturation temperature; *m* is mass of the transferred sample quantified via VO-GC/MS experiments; V_{N2} is volume of the carrier gas and T_{amb} is ambient temperature. The uncertainties for *T*, *V*, and *m* are standard uncertainties. The uncertainty of the molar enthalpy of vaporization is the standard uncertainty with a confidence level of 0.95 (k = 2), calculated including uncertainties of vapor pressure, uncertainties from the fitting equation, and the uncertainty of temperature adjustment to T = 298.15 K. Detailed information on the methods of calculations was published previously[3,5]. [b] Saturation temperature ($u(T)$ = 0.1 K). [c] Mass of transferred sample condensed at 243 K. [d] Volume of nitrogen ($u(V)$ = 0.005 dm³) used to transfer *m* ($u(m)/m$ = 1.5 %) of the sample. [e] T_{amb} is the temperature of the soap film flowmeter used for measurement of the gas flow. [f] Vapor pressure at temperature *T,* calculated from the *m* and the residual vapor pressure at the condensation temperature, calculated by an iteration procedure; p° = 1 Pa. [g] Relative standard uncertainty with confidence level 0.95 (k = 2) for p_{sat} was calculated to be $u(p)/p$ = 4.31 % (see Supporting Information).

Table S3. Comparison of thermodynamic properties of DEGDN: Vapor pressure p_{sat} and molar enthalpies of phase transition $\Delta_l^g H_m^\circ$ at 298.15 K.

Experiment	T-Range	$\Delta_l^g H_m^\circ(298.15\ \mathrm{K})$[a]	p_{sat}[b]
	K	kJ·mol^{-1}	mPa
Vacek[6]	-	98.0[c]	143.54[c]
Crater[7]	288.2 – 328.2	70.2[c]	829.08[c]
This Work	275.5 – 323.1	88.4 ± 1.3	220.31

[a] Molar enthalpies of vaporization were adjusted according to *Chickos et al.*[2] with values of $\Delta_l^g C_{p,m}^\circ$, $C_{p,m}^\circ$(l) stated in Table S1. Uncertainties for molar enthalpies of phase transition at average and reference temperatures are expressed as expanded uncertainties with confidence level of 0.95 (k = 2). [b] Vapor pressure at 298.15 K extrapolated from the p-T-data. [c] Calculation according to previous published procedures.[16,17]

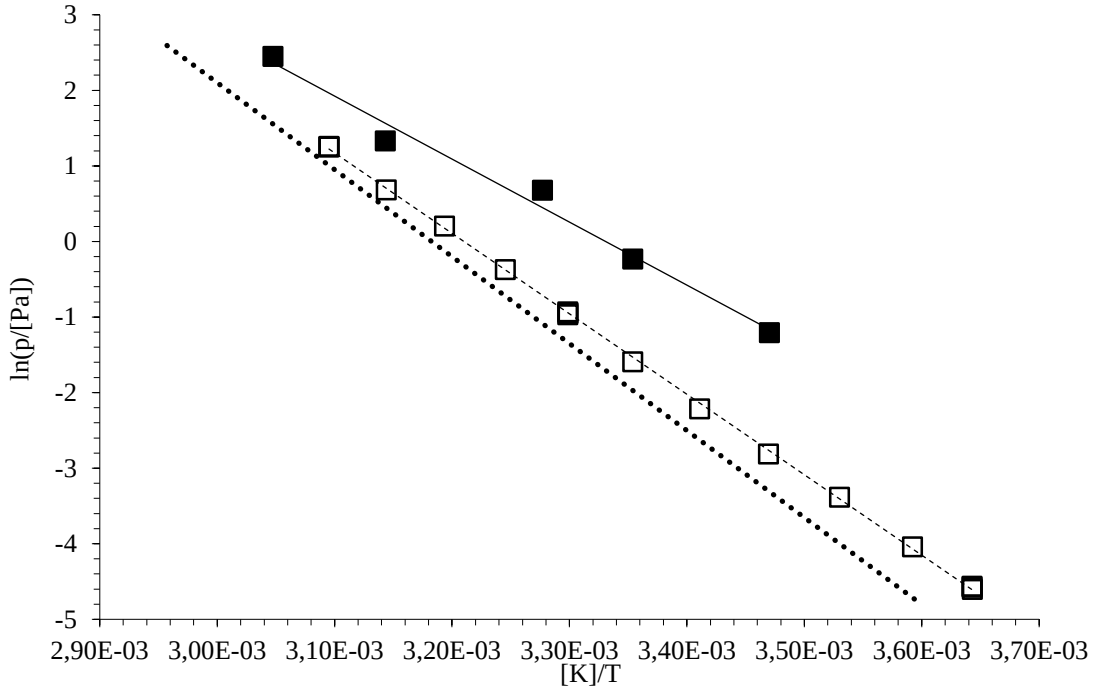

Figure S10. Comparison of the experimental vapor pressure Values of DEGDN with the reported thermodynamic function according to *Vacek* and the experimental findings according to *Crater*.[18,19] Here □ and dashed line are the experimental values taken from this work; dotted line represents the thermodynamic function according to *Vacek* and ■ and solid line represent the findings according to *Crater*.

5.6.4.2 *p-T* data obtained in this work for TEGDN

Table S4. Experimental conditions and *Clark-Glew* fit function resulting in absolute vapor pressures p_{sat} and thermochemical properties of vaporization (molar enthalpy of vaporization $\Delta_{\mathrm{l}}^{\mathrm{g}}H_m^{\circ}$ and molar entropy of vaporization $\Delta_{\mathrm{l}}^{g}S_m^{\circ}$). Obtained from the measurements of TEGDN by the Transpiration Method[a].

TEGDN: $\Delta_{\mathrm{l}}^{\mathrm{g}}H_{\mathrm{m}}^{\circ}$ (298.15 K) = (93.1 ± 1.1) kJ·mol^{-1}

$$\ln p_{\mathrm{sat}}/p^0 = \frac{397.8}{R} - \frac{129455.1}{RT} - \frac{121.8}{R} ln \frac{T}{298.15\ \mathrm{K}}$$

T[b]	m[c]	V_{N2}[d]	T_{amb}[e]	Flow	p_{sat}[f]	$u(p_{\mathrm{sat}})$[g]	$\Delta_{\mathrm{l}}^{\mathrm{g}}H_m^{\circ}(T)$	$\Delta_{\mathrm{l}}^{g}S_m^{\circ}(T)$
K	mg	dm³	K	dm³·h^{-1}	Pa	Pa	kJ·mol^{-1}	J·mol^{-1}·K^{-1}
288.3	0.029	87.74	297.0	4.9	0.003	0.001	94.34	184.4
288.3	0.037	114.9	298.3	5.2	0.003	0.001	94.34	184.1
288.3	0.042	129.5	300.0	5.5	0.003	0.001	94.34	184.3
293.3	0.051	77.79	298.6	4.9	0.007	0.001	93.73	182.4
298.3	0.024	19.38	296.9	4.8	0.013	0.001	93.12	180.0
303.3	0.027	12.13	297.7	4.9	0.023	0.001	92.51	177.8
303.3	0.036	15.66	297.7	4.9	0.024	0.001	92.51	178.2
308.3	0.025	6.124	298.9	4.9	0.042	0.002	91.91	176.1
308.3	0.032	7.603	296.7	4.9	0.044	0.002	91.90	176.4
313.3	0.059	7.668	296.8	4.8	0.079	0.003	91.30	174.6
313.3	0.024	3.230	297.0	4.8	0.076	0.003	91.30	174.3
313.3	0.031	4.110	296.9	4.8	0.077	0.003	91.30	174.4
318.2	0.023	1.825	299.7	5.5	0.132	0.006	90.69	172.4
323.2	0.025	1.212	297.2	4.8	0.216	0.009	90.09	170.3
328.2	0.042	1.219	297.0	4.9	0.355	0.016	89.48	168.3
328.2	0.043	1.214	296.9	4.9	0.363	0.016	89.48	168.5
328.2	0.043	1.221	299.3	4.9	0.366	0.016	89.48	168.6
328.2	0.042	1.215	298.1	4.9	0.359	0.016	89.48	168.4
328.2	0.049	1.370	298.2	5.5	0.369	0.016	89.47	168.6

[a] Experimental conditions: T is saturation temperature; *m* is mass of the transferred sample quantified via VO-GC/MS experiments; V_{N2} is volume of the carrier gas and T_{amb} is ambient temperature. The uncertainties for *T*, *V*, and *m* are standard uncertainties. The uncertainty of the molar enthalpy of vaporization is the standard uncertainty with a confidence level of 0.95 (k = 2), calculated including uncertainties of vapor pressure, uncertainties from the fitting equation, and the uncertainty of temperature adjustment to T = 298.15 K. Detailed information on the methods of calculations was published previously[3,5]. [b] Saturation temperature ($u(T)$ = 0.1 K). [c] Mass of transferred sample condensed at 243 K. [d] Volume of nitrogen ($u(V)$ = 0.005 dm³) used to transfer *m* ($u(m)/m$ = 1.5 %) of the sample. [e] T_{amb} is the temperature of the soap film flowmeter used for measurement of the gas flow. [f] Vapor pressure at temperature *T,* calculated from the *m* and the residual vapor pressure at the condensation temperature, calculated by an iteration procedure; p° = 1 Pa. [g] Relative standard uncertainty with confidence level 0.95 (k = 2) for p_{sat} was calculated to be $u(p)/p$ = 4.38 % (see Supporting Information).

Table S5. Comparison of thermodynamic properties of TEGDN: vapor pressure p_{sat} and molar enthalpies of phase transition $\Delta_l^g H_m^\circ$ at 298.15 K.

Experiment	T-Range	$\Delta_l^g H_m^\circ(298.15\ \mathrm{K})$[a]	p_{sat}[b]
	K	kJ·mol^{-1}	mPa
Woodman[8]	303.4 – 348.0	91.6	12.86
This Work	288.3 – 328.2	93.1 ± 1.1	12.50

[a] Molar enthalpies of vaporization were adjusted according to *Chickos et al.*[2] with values of $\Delta_l^g C_{p,m}^\circ$, $C_{p,m}^\circ$(l) stated in Table S1. Uncertainties for molar enthalpies of phase transition at average and reference temperatures are expressed as expanded uncertainties with confidence level of 0.95 (k = 2). [b] Vapor pressure at 298.15 K extrapolated from the *p*-*T*-data.

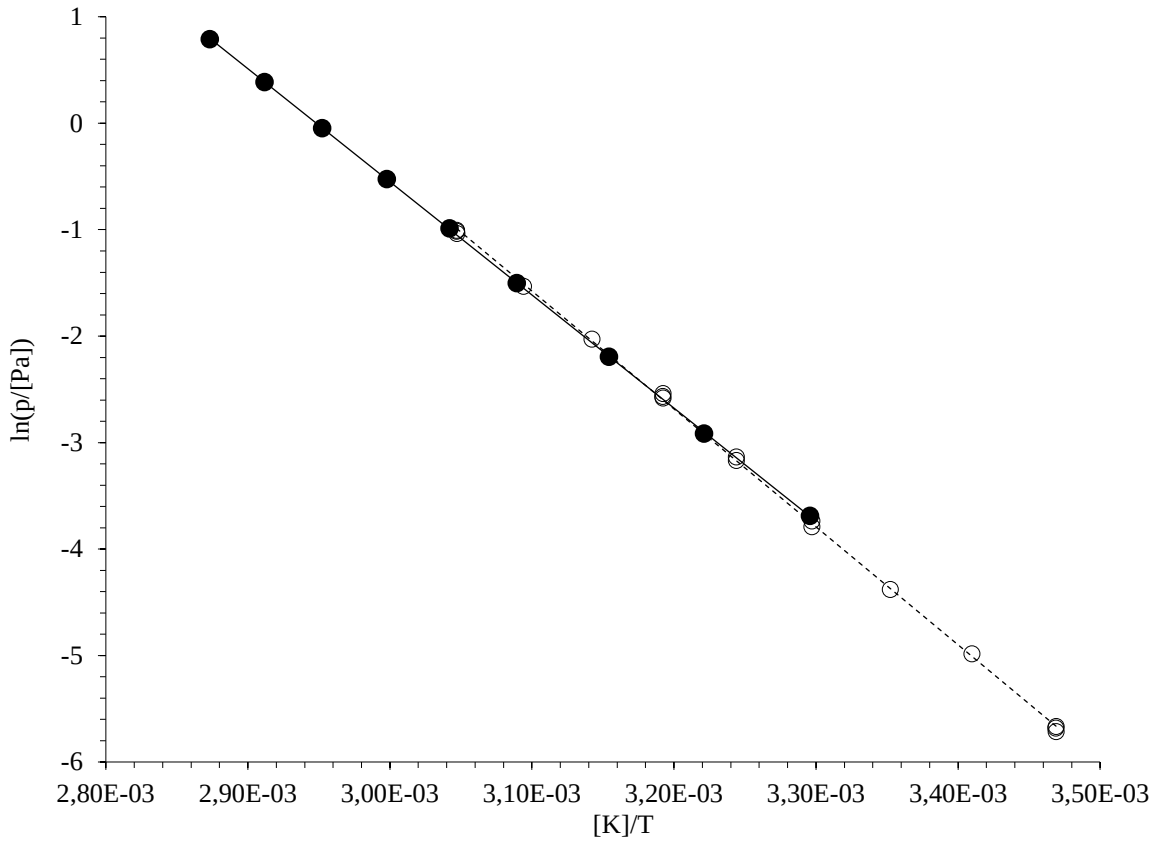

Figure S11. Comparison of the experimental vapor pressure values of TEGDN with the experimental findings according to Woodman[8]. Here ○ and dashed line are the experimental values taken from this work; ● and solid line represent the findings according to Woodman.[20]

5.6.4.3 VO-GC/MS Parameters

Compilation of the VO-GC/MS setup is presented in Table S6 and the parameters which were used in the experiments are compiled in Table S7.

Table S6. VO-GC/MS Setup used for the mass quantification.

GC/MS	*Shimadzu QP2010SE®;* software *LabSolution GCMSsolution v4.11*
Injector	Atas Optic 4; software *Evolution Workstation v4.1*
Liner	10 mm V2A stainless steel tube, 5 mm wall thickness, equipped with silanized glass wool (2 mm injection needle penetration into wool)
Restriction	0.05 mm capillary, 10.57 mm length (*Restek* #10097)
Column connector	*SGE* Siltite µ-Union® (*Restek* #073562)
Analytical column	*Restek* RTX-TNT 1® (3 m, 0.53 mm, 1.5 µm)
Restriction	0.05 mm capillary, 10.57 mm length (*Restek* #10097)
Virtual column	100 m, 0.25 µm film thickness, 0.20 mm i.d. (entry for GCMSsolution)
Split ratio	150.0 (entered in GCMSsolution)
Purge flow	10 mL/min
Ion source	200 °C
MS interface	200 °C

Table S7. Compilation of VO-GC/MS parameters used for transpiration experiment of the different analytes.

	DEGDN	**TEGDN**
Standard	Undecane	Undecane
Oven program	40 °C (hold 0.10 min) → 274 °C (rate 60 °C/min, hold 1.00 min), total program time 5.00 min	40 °C (hold 0.10 min) → 274 °C (rate 60 °C/min, hold 1.00 min), total program time 5.00 min
Head pressure	92 kPa	92 kPa
Flow	3.97 mL/min	3.97 mL/min
Injection volume	1 µL	1 µL
MS mode	SIM mode (event time 100 ms); DEGDN: 1.20 – 2.00 min; m/z 73.00; Undecane: 0.70 – 1.10 min; m/z 71.00 (standard).	SIM mode (event time 100 ms); TEGDN: 1.70 – 2.30 min; m/z 90.00; Undecane: 0.70 – 1.60 min; m/z 71.00 (standard).

5.6.5 Calculation of Energetic Performance

The detonation parameters were calculated with the *EXPLO5* (version 6.06.01) computer code.[21] The necessary enthalpies of formation of the corresponding compounds were taken from the *EXPLO5* database. This calculation code is based on the steady-state model of equilibrium and uses the *Becker–Kistiakowski–Wilson* equation of state.[22] It calculates the detonation parameters at the *Chapman–Jouguet* (CJ) point, which itself is found from the *Hugoniot* curve of the system by its first derivative. These calculations are based on the density measured at room temperature by gas pycnometer.

Table S8. Enthalpies of formation of **EGDN**, **DEGDN** and **TEGDN** from the *EXPLO5* database.

	$\Delta_f H°$ [kJ mol^{-1}]
EGDN	−241.0
DEGDN	−430.0
TEGDN	−606.1

Table S9. Measured gas pycnometer densities of **EGDN**, **DEGDN** and **TEGDN**.

	Density @ 298 K [g cm^{-3}]
EGDN	1.49
DEGDN	1.38
TEGDN	1.32

5.6.6 References SI

[S1] NATO standardization agreement (STANAG) on explosives, impact sensitivity tests, no. 4489, 1st ed, Sept. 17, **1999**.

[S2] WIWEB-Standardarbeitsanweisung 4-5.1.02, Ermittlung der Explosionsgefährlichkeit, hier der Schlagempfindlichkeit mit dem Fallhammer. Nov. 8, **2002**.

[S3] "http://www.bam.de", accessed March **2022**.

[S4] NATO standardization agreement (STANAG) on explosive, friction sensitivity tests. no. 4487, 1st ed., Aug. 22, **2002**.

[S5] WIWEB-Standardarbeitsanweisung 4-5.1.03, Ermittlung der Explosionsgefährlichkeit oder der Reibeempfindlichkeit mit dem Reibeapparat. Nov. 8, **2002**.

[S6] Impact: insensitive > 40 J, less sensitive ≥ 35 J, sensitive ≥ 4 J, very sensitive ≤ 3 J, Friction: insensitive > 360 N, less sensitive = 360 N, sensitive < 360 N and > 80 N, very sensitive ≤ 80 N, extremely sensitive ≤ 10 N. According to the UN Recommendations on the Transport of Dangerous Goods, (+) indicates not safe for transport.

[S7] CrysAlisPro, Oxford Diffraction Ltd., version 171.33.41, **2009**.

[S8] Altomare, A.; Cascarano, G.; Giacovazzo, C.; Guagliardi, A. Completion and refinement of crystal structures with SIR 92. *J. Appl. Crystallogr* **1993**, *26*, 343−350.

[S9] a) Altomare, A.; Cascarano, G.; Giacovazzo, C.; Guagliardi, A.; Moliterni, A. G. G. SIR97 **1997**; b) Altomare, A.; Burla, M. C.; Camalli, M.; Cascarano, G. L.; Giacovazzo, C. SIR97: a new tool for crystal structure determination and refinement *J. Appl. Crystallogr*. **1999**, *32*, 115−119.

[S10] Sheldrick, G. M. A short history of SHELX. *Acta Crystallogr. Sect. A* **2008**, *A64*, 112−122.

[S11] Sheldrick, G. M. SHELXL-97, Program for the Refinement of Crystal, University of Göttingen, Germany, **1997**.

[S12] Spek, A. L. PLATON, A Multipurpose Crystallographic Tool, Utrecht University **1999**.

[S13] Farrugia, L. J. WinGX and ORTEP for Windows: an update. *J. Appl. Cryst.* **2012**, *45*, 849−854.

[S14] a) Empirical absorption correction using spherical harmonics, implemented in SCALE3 ABSPACK scaling algorithm (CrysAlisPro Oxford Diffraction Ltd., Version 171.33.41, 2009); b) APEX3. Bruker AXS Inc., Madison, Wisconsin, USA.

[S15] Acree, W.; Chickos, J. S. Phase Transition Enthalpy Measurementsof Organic and Organometallic Compounds. Sublimation, Vaporizationand Fusion Enthalpies From 1880 to 2010. *J. Phys. Chem. Ref. Data* **2010**, *39*, 043101.

[S16] Bikelytė, G.; Härtel, M. A. C.; Holler, M.; Neuer, A.; Klapötke, T. M. Thermodynamic Properties of Energetic Plasticizers: Experimental Vapor Pressures of Methyl-, Ethyl-, and Butyl-Nitroxyethyl Nitramines. *J. Chem. Eng. Data* **2021**, *66* (4), 1709−1716.

[S17] Härtel, M. A.; Klapötke, T. M.; Stierstorfer, J.; Zehetner, L. Vapor Pressure of Linear Nitrate Esters Determined by Transpiration Method in Combination with VO-GC/MS. *Propellants, Explos., Pyrotech.* **2019**, *44*, 484−492.

[S18] Vacek, J.; Stanek, J. Vapor pressures of some organic nitrates. *Chem. Prum.* **1959**, *9*, 286.

[S19] Crater, W. d. The Vapor Pressures of Glycerol Trinitrate and Certain Glycol Dinitrates. *Ind. Eng. Chem.* **1929**, *21* , 674-676.

[S20] Woodman, A. L.; Adicoff, A. Vapor Pressure of Tiracetin, Triethylene Glycol Dinitrate, and Metriol Trinitrate. *J. Chem. Eng. Data* **1963**, *8*, 241−242.

[S21] Sućeska, M. EXPLO5 V6.06.01, Zagreb (Croatia) **2021**.

[S22] Sućeska, M. Calculation of the Detonation Properties of C−H−N−O explosives. *Propellants, Explos., Pyrotech.* **1991**, *16*, 197–202.

6 Synthesis and Properties of Bis(nitrocarbamoylethyl) Nitramine – A New Energetic Open-Chain Nitrocarbamate

Prof. Dr. Thomas M. Klapötke*, Dr. Burkhard Krumm*, Jasmin T. Lechner, Christian Riedelsheimer

as published in *Chemistry Select* **2022**, *7*, e20220223

DOI: 10.1002/slct.202202232

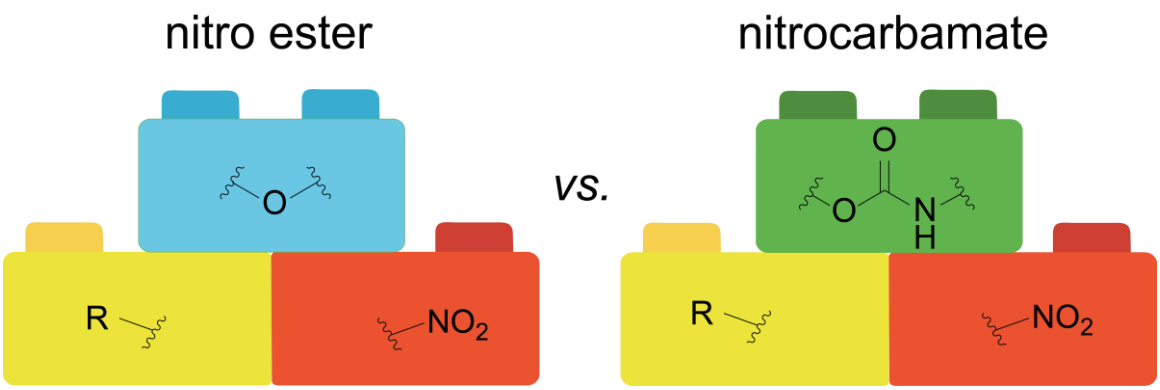

Abstract: The nitrocarbamate derivative of the well-known and intensively investigated nitro ester DINA was prepared and studied. Starting with bis(hydroxyethyl) nitramine obtained from DINA, the corresponding carbamate was obtained by treatment with chlorosulfonyl isocyanate (CSI). Using fuming nitric acid only as nitration reagent, the target compound bis(nitrocarbamoylethyl) nitramine was synthesized. Furthermore, a route to the salt bis(nitrocarbamoylethyl)ammonium nitrate by a simple two step synthesis starting from diethanolamine was revealed. The compounds were fully characterized by NMR spectroscopy, X-ray diffraction, differential thermal analysis, vibrational analysis and elemental analysis. The sensitivities towards impact and friction of the energetic compounds were measured, as well as their energetic properties determined by using the energies of formation, calculated on the CBS4-M level of theory, with the EXPLO5 computer code.

6.1 Introduction

The discovery of nitroglycerine (NG) and nitrocellulose (NC) ultimately formed the foundation for modern propellants.[1-3] The strategy for developing new energetic nitro esters changed slightly due to the need to increase the energy levels of the existing propellant mixtures. Therefore, other nitro esters were added to nitroglycerine to lower its freezing point while increasing the impact and friction sensitivity values, leading to overall safer handling.[1, 3, 4] Ethylene glycol dinitrate (EGDN) for example is a plasticizer used as such an additive. While this plasticizer appears to have similar building blocks like NG, their properties differ.

EGDN (7456 m s^{-1}) has a lower detonation velocity value than NG (7694 m s^{-1}), but is generally more stable and less sensitive towards impact, shown in Figure 1.[5] Although EGDN has a higher volatility, it has a good oxygen balance (OB), which is defined as the relative amount of oxygen excess (+) or deficit (−) remaining after combustion of the energetic material. Nitroglycerine, on the other hand, is an explosive with a positive OB value (Ω_{CO2}=+3.5 %). Accordingly, it seemed reasonable to combine NG with oxygen-deficient explosives such as nitrocellulose to obtain a more balanced OB value.[1,3−4]

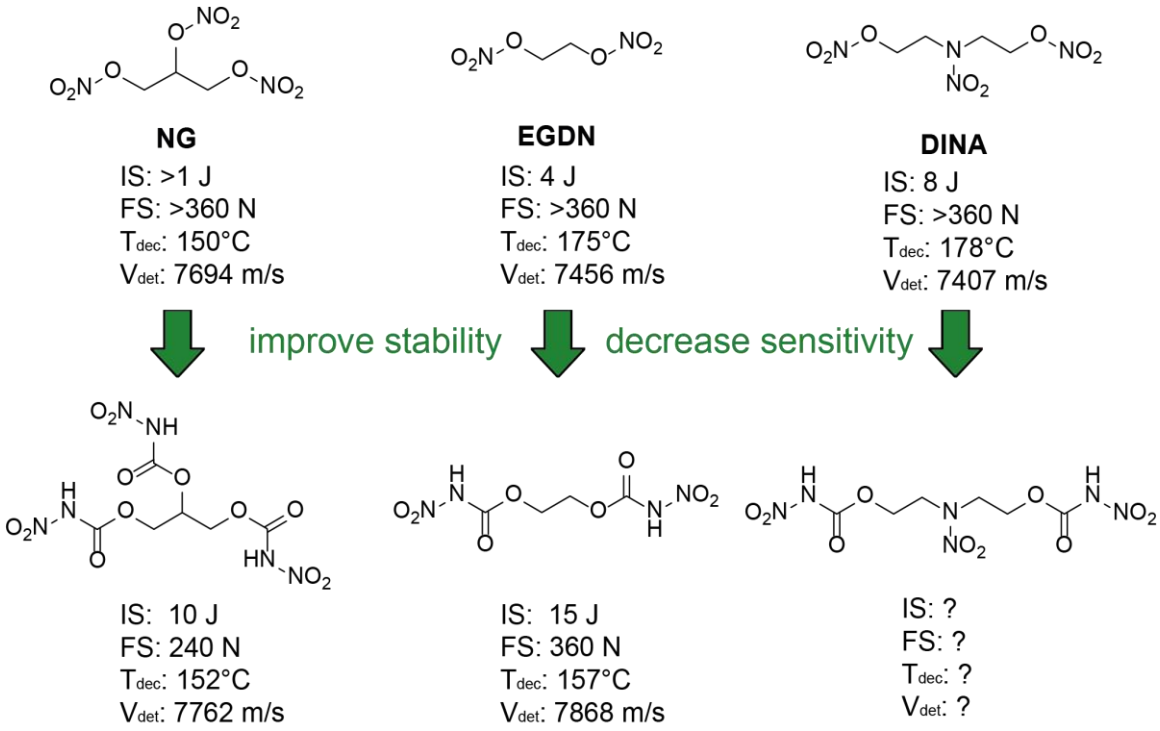

Figure 1. Nitro esters NG, EGDN and DINA with their properties in comparison to their corresponding nitrocarbamates (values are calculated with the newest EXPLO5 version: V6.06.01).[5]

In the 1940s, the nitroxyethylnitramine (NENA) plasticizers were described, which are characterized by containing both nitro ester and nitramine functionalities, making them some of the most powerful explosives available.[6] Dinitrooxyethylnitramine dinitrate (DINA), shown in Figure 1, has a similar explosive performance to RDX and is used as a substitute for NG due to its higher energy, larger specific volume, lower combustion temperature, and good thermal stability.[7] Moreover, DINA is used as an ingredient in the production of double base propellant to improve mechanical properties at low temperatures,[8-11] and has a conveniently low melting point that enables melt casting.[4]

Unfortunately, the advantageous and powerful properties of nitro esters are not without several drawbacks. Not only they are more sensitive than their *C*-nitro counterparts and often undergo thermal decomposition, they also lack in chemical stability.[2] Nitro esters hydrolyze in the presence of acids or bases, and are not resistant to prolonged exposure to water or moisture. Given these disadvantages, long-term storage of these substances is difficult. However, the amount of autocatalytic decomposition can be limited by adding stabilizers to the propellant

composition, which trap the nitrous decomposition products and convert them into stable compounds, ultimately delaying the decomposition process.[12]

Considering the disadvantages associated with nitro esters, there is an obvious need to increase the stability of propellants, therefore the group of nitrocarbamates will be discussed in more detail below. The carbamate functionality exhibits characteristic properties of amides and esters as it contains a carbonyl function directly linked to an amino function, which can be nitrated to form *N*-nitrocarbamates.[11, 13] These were first reported in 1895[14] and more thoroughly investigated by us in 2016, by converting alcohols (some well-known precursors of their nitro esters), into carbamates and further into nitrocarbamates.[15] Thereby, the thermal stability as well as sensitivity values towards impact and friction are increased. In addition, the new nitrocarbamates have good physical properties and are more stable to acid hydrolysis due to the functionality of the carbonyl group.[15, 16] The structure of the corresponding nitrocarbamates of NG and EGDN with their properties are shown in Figure 1. However, the oxygen balance often decreases, but the nitrogen content increases, which can result in a higher detonation performance as in the case of the corresponding nitrocarbamates of NG and EGDN.[15] Therefore, in this work, the preparation of the corresponding nitrocarbamate of DINA was attempted and the physical and energetic properties have been compared with the nitro esters DINA and EGDN.

6.2 Results and Discussion

6.2.1 Synthesis

The starting material diethanolamine (DEA) was converted into the corresponding carbamate, bis(carbamoylethyl) amine (**1**) by reaction with chlorosulfonyl isocyanate (CSI) according to the established method.[13]

For the nitration of all three amino groups of **1** various reagents were tested. Harsh conditions such as mixtures of nitric acid with oleum or acetic acid anhydride[17] failed due to decomposition. Milder conditions such as the combination of ammonium nitrate with trifluoroacetic acid[18] or N_2O_5[19] were also not successful. Treatment with fuming nitric acid resulted in formation of the nitrate salt **2**

(Scheme 1). While the carbamate moiety is nitrated, the secondary nitrogen is protonated only.

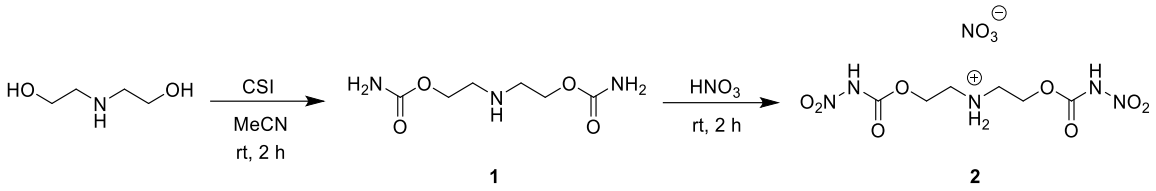

Scheme 1. Preparation and nitration of bis(carbamoylethyl) amine (**1**).

Based on this observation, an approach via the known nitramine bis(hydroxyethyl) nitramine was pursued. This potential precursor is accessible from the corresponding nitro ester bis(nitratoethyl) nitramine (**3**, DINA, Figure 1).

DINA is usually synthesized from diethanolamine by employing mixtures of HNO_3/MgO[10] or HNO_3/Ac_2O.[17, 20, 21] For this purpose, MgO or Ac_2O are used as dehydrating agents.[17] Starting from the HNO_3/MgO approach[10], diethanolamine is first converted into diethanolamine dinitrate (DIA) via *O*-nitration[2, 22] by heating and addition of NaCl as a catalyst. Further *N*-nitration[23] leads to the formation of DINA.

This reaction has several disadvantages, requiring both a catalyst[20] and heat source to form the product. Moreover, the product could only be obtained with low yield and poor purity. The sticky consistency can be attributed to the undesirable formation of $Mg(OH)_2$.[17] The two-step synthesis also leads to the formation of the intermediate DIA. DIA was shown to have a lower thermal stability than DINA[24], therefore a potential risk and its accumulation should be avoided.[17]

The traditional HNO_3/Ac_2O method[21, 24] was optimized in 2019.[17] Here, the starting material diethanolamine is replaced by diethanolamine hydrochloride (DEAHC), which previously served as a catalyst for the synthesis of DEA to DINA.[20, 21] This chloride salt is the reagent of choice for the nitration to DINA (**3**) with minimized safety concerns.

This synthesis was pursued and switched from continuous flow[17] to a conventional batch synthesis to test the efficiency and compare the two approaches. Care was taken to dose DEAHC and HNO_3 in a controlled manner. Considering that a higher molar ratio of Ac_2O to reactant benefits the overall process by improving the safety

and yield of the synthesis, excess of Ac_2O was applied, which is in accordance with the molar ratio reported in the continuous flow procedure.[17] The nitration was carried out without the addition of heat, in fact, cooling was only applied when the reactants were added (Scheme 2). The batch synthesis was successfully carried out as DINA (**3**) was obtained with high purity and yield.

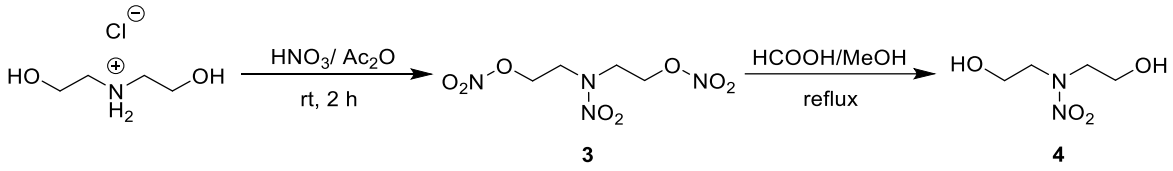

Scheme 2. Nitration to form DINA (**3**) and further hydrolysis to form bis(hydroxyethyl) nitramine (**4**).

Further controlled hydrolysis of **3** to the desired nitramine **4** was achieved *via* a combination of known procedures.[25, 26] DINA was first refluxed with formic acid which reduced exclusively the *O*-nitratomethyl units back to the hydroxymethyl moiety. After removal of formic acid, additional refluxing in methanol is required. Isolation and purification of **4** is performed by column chromatography. Storage of **4** is required at low temperatures.

Now, with this precursor available, a conversion to the corresponding bis(carbamoylethyl) nitramine (**5**) is performed as described earlier. Followed by nitration at 0 °C for one hour the desired nitrocarbamate bis(nitrocarbamoylethyl) nitramine (**6**) was obtained and isolated (Scheme 3).

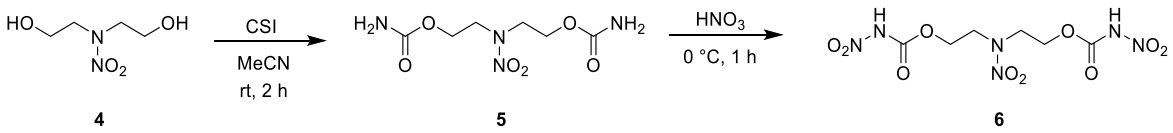

Scheme 3. Carbamoylation and nitration of **4** to form the nitrocarbamate **6**.

6.2.2 NMR Spectroscopy

All materials were characterized by $^{1}H/^{13}C$ NMR and nitro group containing compounds also by ^{14}N NMR spectroscopy in DMSO-D_6 as solvent (for assignments see Experimental Section). Additionally, the ^{15}N NMR spectrum of **6** was recorded in acetone-D_6 (Figure 2) and is discussed in more detail.

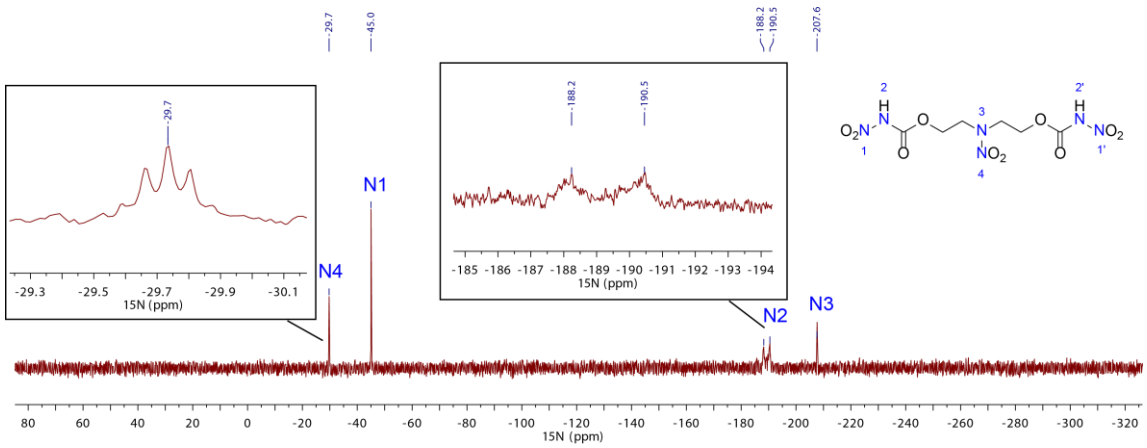

Figure 2. ^{15}N NMR spectrum of bis(nitrocarbamoylethyl) nitramine (**6**) in acetone-D_6.

The four resonances, two nitro and two amine resonances, are observed in the typical regions around −35 and −200 ppm. The central nitro resonance at −29.7 ppm is split into a quintet ($^3J_{N,H}$=2.9 Hz) due to coupling with the two methylene groups attached to the nitramine unit. The terminal nitro groups resonate at −45.0 ppm as a singlet. The nitrocarbamate nitrogen resonance is detected at −189.4 ppm as a broadened dublet ($^1J_{N,H}$=89.9 Hz), whereas that of the central nitramine nitrogen is observed at −207.7 ppm as a singlet.

6.2.3 Single Crystal Analysis

A single-crystal X-ray diffraction analysis was performed for **2**, **5** and **6** (Table 1).

Table 1. Crystallographic data of **2**, **5** and **6**.

	2	**5**	**6**
Formula	$C_6H_{12}N_6O_{11}$	$C_6H_{12}N_4O_6$	$C_6H_{10}N_6O_{10}$
FW [g mol^{-1}]	344.22	236.20	326.18
Crystal system	triclinic	monoclinic	monoclinic
Space group	*P*-1	*C*2/*c*	$P2_1$
Color / Habit	colorless block	colorless plate	colorless plate
Size [mm]	0.20x0.17x0.08	1.0x0.76x0.10	0.12x0.08x0.02
a [Å]	7.4011(5)	8.1385(15)	6.4019(6)
b [Å]	9.0114(6)	6.0196(11)	9.6138(9)
c [Å]	11.1321(7)	20.395(4)	10.1326(9)
α [°]	76.213(5)	90	90
β [°]	79.670(5)	98.973(16)	104.705(3)
γ [°]	66.974(6)	90	90
V [Å^3]	660.52(8)	986.9(3)	603.20(10)
Z	2	4	2
ρ_{calc} [g cm^{-3}]	1.731	1.590	1.796
μ [mm^{-1}]	0.167	0.142	0.17
F (000)	356	496	336
$\lambda_{MoK\alpha}$ [Å]	0.71073	0.71073	0.71073
T [K]	101	102	173
θ Min-Max [°]	1.89, 26.37	2.02, 26.4	2.97, 25.4
Dataset	−9 ≤ 9; −11 ≤ 11; −13 ≤ 13	−9 ≤ 10; −7 ≤ 7; −20 ≤ 25	−7 ≤ 7; −11 ≤ 0; −12 ≤ 0
Reflections coll.	9723	3050	37891
Independent refl.	1959	1181	1160
R_{int}	0.040	0.048	0.025
Parameters	256	98	200
*R*1 (obs)[a]	0.0778	0.0663	0.039
w*R*2 (all data)[b]	0.1156	0.1448	0.1017
S [c]	1.025	1.175	1.196
Resd. Dens. [e Å^{-3}]	−0.206, 0.343	−0.295, 0.315	−0.22, 0.27
Device type	Xcalibur, Sapphire 3	Xcalibur, Sapphire 3	D8 Venture
Solution	SHELXT 2018/2	SHELXT 2018/2	SHELXT 2018/2
Refinement	ShelXL 2018/3	ShelXL 2018/3	ShelXL 2018/3
Absorption corr.	multi-scan	multi-scan	multi-scan
CCDC	2169524	2169525	2169523

[a] *R*1 = Σ||F0|−|Fc||/Σ|F0|; [b] w*R*2 = [Σ[w(F02−Fc2)2]/Σ[w(F0)2]]1/2; w = [σc2(F02)+(xP)2+yP]−1 and P=(F02+2Fc2)/3; [c] *S* = {Σ[w(Fo2−Fc2)2]/(n−p)}1/2 (n = number of reflections; p = total number of parameters).

Bis(nitrocarbamoylethyl)ammonium nitrate (**2**) crystallizes in the triclinic space group of $P\bar{1}$ (Figure 3) with two molecules in its unit cell.

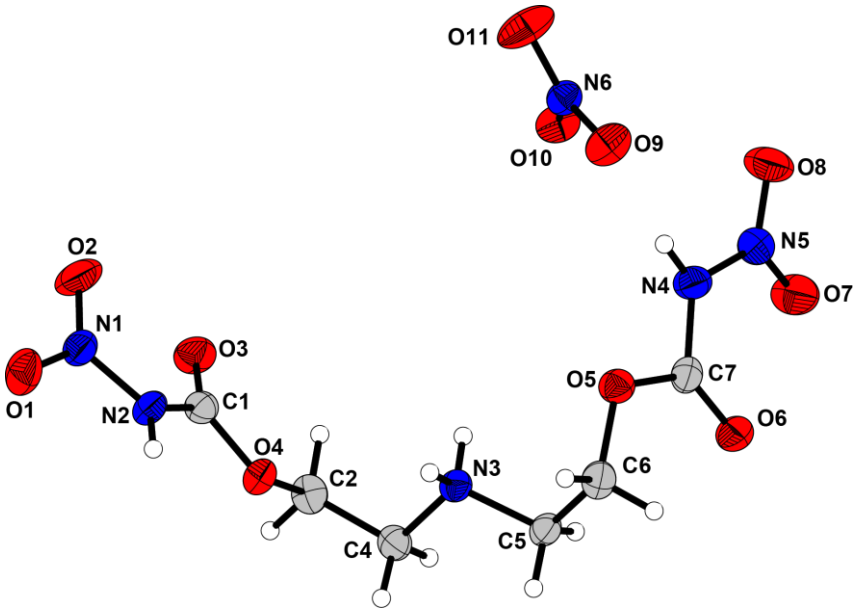

Figure 3. Molecular structure of **2**. Selected bond lengths (Å): N2-C1 1.384(3), N1-N2 1.370(3), O1-N1 1.222(3), N1-O2 1.217(3), N4-C7 1.385(3), N5-N4 1.374(3), O7-N5 1.211(3), O8-N5 1.222(3), N3-C4 1.490(3), N3-C5 1.491(3). Selected angles (°): O3-C1-N2 127.0(2), O6-C7-N4 127.6(2), O1-N1-N2-C1 158.5(2), O2-N1-N2-C1 −21.2(3), O7-N5-N4-C7 17.7(4), O8-N5-N4-C7 -161.9(2).

Bis(carbamoylethyl) nitramine (**5**) crystallizes in the monoclinic space group *C*2/*c* with four molecules per unit cell (Figure 4).

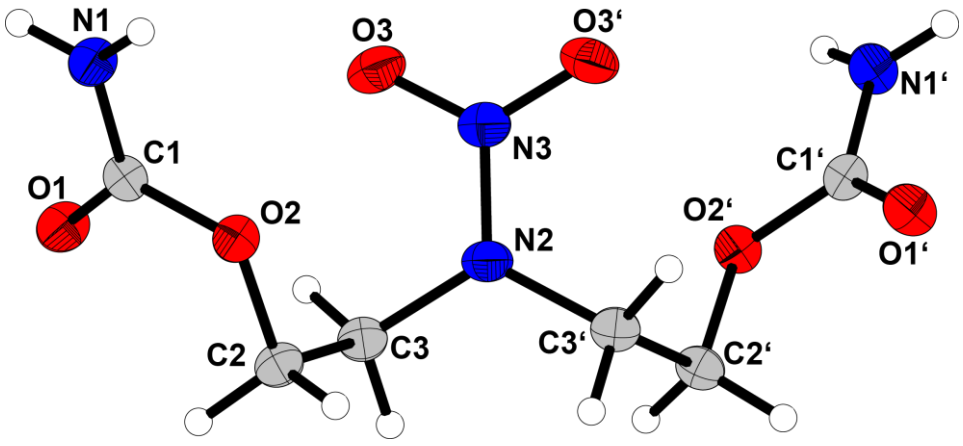

Figure 4. Molecular structure of **5**. Selected bond lengths (Å): N1-C1 1.325(3), N3-N2 1.338(4), O3-N3 1.241(2). Selected angles (°): O1-C1-N1 124.6(2), O3-N3-N2-C3 176.66(14).

Bis(nitrocarbamoylethyl) nitramine (**6**) crystallizes in the monoclinic space group $P2_1$ with one molecule per unit cell (Figure 5).

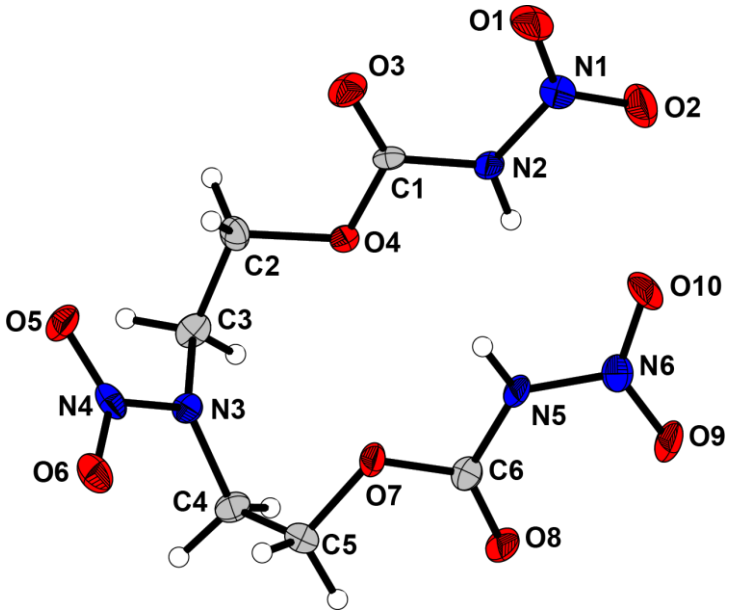

Figure 5. Molecular structure of **6**. Selected bond lengths (Å): N2-C1 1.370(6), N3-N4 1.358(6), N1-N2 1.386(6), O5-N4 1.237(6), N1-O1 1.201(7). Selected angles (°): O3-C1-N2 126.4(5),O8-C6-N5 126.9(5) O5-N4-N3-C3 −10.9(6), O1-N1-N2-C1 9.9(7), O9-N6-N5-C6 −11.8(7), O2-N1-N2-C1 −170.1(5), O10-N6-N5-C6 169.0(5), N1-N2-C1-O4 177.4(5).

The bond lengths in the carbamate units of N1-C1 in **5** (1.325(3) Å) and N2−C1 in **6** (1.370(5) Å), differ by 0.045 Å. The longer bond of **6** is due to the electron withdrawing effect of the nitro group in **6**.

The bond angles of magnetically equivalent atoms in the same substance may differ, thus the nitrocarbamates **2** and **6** will be discussed in more detail. For this purpose, the two oxygen atoms of the nitro group are distinguished, depending on which is closer to the corresponding carbonyl group. The torsion angles of the O-atom facing the carbonyl are −21.2(3)° for O2-N1-N2-C1 and 17.7(4)° for O7-N5-N4-C7. This results in a difference of 3.6°. The torsion angle of the oxygen atom farther from the carbonyl oxygen is 158.5(2)° for O1-N1-N2-C1 and −161.9(2)° for O8-N5-N4-C7. This results in an overall difference of 3.4°. Compound **6** shows the same trend, although the difference is much smaller compared to **2**. The oxygen atoms facing the carbonyl group show a difference of 1.9° (O1-N1-N2-C1 9.9(7)°, O9-N6-N5-C6 −11.8(7)°) and the oxygen atoms farther away from the carbonyl

group showing a difference of 1.1° (O2-N1-N2-C1 −170.1(5)°, O10-N6-N5-C6 169.0(5)°).

A difference between the bond angles of carbamate **5** and nitrocarbamate **6** can also be observed. The O=C−N angles of **6** are 126.4(5)° for O3-C1-N2 and 126.9(5)° for O8-C6-N5, whereas that of **5** is 124.6(2)° for O1-C1-N1. The angles of **6** differ only slightly by 0.5°. However, the difference between **5** and **6** is in the range of 1.8-2.3°, indicating that the nitration of the carbamate strongly influences this angle.

6.2.4 Thermal Analysis

A differential thermal analysis (DTA) study was performed for the thermal characterization of **1**, **2**, **3**, **5** and **6**. A heating rate of 5 °C per minute was used for this purpose. The endothermic and exothermic onset points are listed in Table 2 and plots of all DTAs can be found in the Supporting Information (Figure S18).

Table 2. Endothermic[a] and exothermic[b] onset points of the DTA measurements.

	T_{endo}[a] [°C]	T_{exo}[b] [°C]
1	207	234
2	-	150
3	50	184
5	175	262
6	142	153

The endothermic signals of carbamates **1** and **5** (**1**: 207 °C, **5**: 175 °C) can be identified as melting points. The nitramine group of **5** evidently has a great influence on the melting point, since this functional group is the only structural difference between these two compounds. Decomposition occurs in both, which is reflected in the exothermic signals (**1**: 234 °C, **5**: 262 °C).

The salt **2** exhibits only an exothermic signal at 150 °C. However, it can be concluded, that the ionic compound undergoes a gradual exothermic conversion. The nitrocarbamate **6** shows both an endothermic (142 °C) and exothermic signal (153 °C). It can be assumed that the endothermic event initiates the exothermic

decomposition of the structure. The DTA measurement shows that this compound does not decompose directly in one step, but first breaks down into smaller components. In summary, **2** and **6** have very similar thermal stability.

6.2.5 Sensitivities and Energetic Properties

The sensitivities towards impact (IS) and friction (FS) were determined and shown in Table 3.

Table 3. Sensitivities towards friction and impact of **2**, **3**, **5**, and **6**.

	2	**3**	**5**	**6**
IS [J] [a]	5	8	>40	6
FS [N] [b]	>360	>360	>360	>360

[a] impact sensitivity according to the BAM drophammer (method 1 of 6); [b] friction sensitivity according to the BAM friction tester (method 1 of 6).

The nitrocarbamates **2** (5 J) and **6** (6 J) have to be classified as impact sensitive. With an impact sensitivity of >40 J, substance **5** can be classified as insensitive.[24, 27] Moreover, the friction sensitivity for all is >360 J, which implies insensitive towards friction.

The EXPLO5 code version 6.06.01[28] was used to calculate the energetic properties. The EXPLO5 calculations are performed based on the molecular formula, densities, and enthalpy of formation of the compounds. The comparison of **2** and **6** demonstrates how the properties affect the EXPLO5 calculation, since these two substances have a similar molecular formula, but differ in other characteristics. The enthalpy of formation of **6** (−683.3 kJ mol^{-1}) is greater than that of **2** (−1193.1 kJ mol^{-1}). At the same time the ionic compound **2** (1.68 g cm^{-3}) has a lower density than **6** (1.76 g cm^{-3}), which is why **2** (7251 m s^{-1}) has a lower detonation velocity value than **6** (7804 m s^{-1}).

The detonation velocity of **2** is lower compared to EGDN (7456 m s^{-1}) and DINA (7407 m s^{-1}). However, compound **6** was able to achieve the desired properties and has a higher detonation velocity compare to DINA or EGDN of 7804 m s^{-1}. The energetic properties are listed in Table 4.

Table 4. Energetic properties of **2** and **6**, EGDN and DINA for comparison.[5]

	2	**6**	**EGDN**	**DINA (3)**
Formula	$C_6H_{12}N_6O_{11}$	$C_6H_{10}N_6O_{10}$	$C_2H_4N_2O_6$	$C_4H_8N_4O_8$
FW [g mol^{-1}]	344.19	326.18	152.06	240.13
ρ (298 K) [g cm^{-3}]	1.68[a]	1.76[a]	1.48	1.49
$T_{dec.}$ [°C][b]	150	153	175	184
$\Delta_f H°$ [kJ mol^{-1}][c]	−1193.1	−683.3	−241.0	−329.0
EXPLO5 V6.06.01				
P_{CJ} [GPa][d]	20.1	25.0	20.9	21.7
V_{det} [m s^{-1}][e]	7251	7804	7456	7407
$-\Delta_{ex}U°$ [kJ kg^{-1}][f]	3151	4071	6258	5156
T_{det} [K][g]	2403	2871	4371	3589
V_0 [L kg^{-1}][h]	782	743	810	833
Ω_{CO2} [%][i]	−32.5	−34.3	0	−26.6

[a] X-ray density converted to RT; [b] temperature of decomposition indicated by exothermic event according to DTA (onset temperatures at a heating rate of 5 °Cmin^{-1}); [c] calculated (CBS-4M) heat of formation; [d] detonation pressure; [e] detonation velocity; [f] Energy of explosion; [g] Explosion temperature; [h] Assuming only gaseous products; [i] Oxygen balance ($\Omega = (xO-2yC-1/2zH)M/1600$).

Although EGDN and DINA (**3**) may have different structures and molecular formulas, the enthalpies of formation values are quite close (EGDN: −241.0 kJ mol^{-1}, DINA: −329.0 kJ mol^{-1}) and the densities are virtually identical (~1.48 g cm^{-3}). Thus, it is no surprise that the detonation velocities of EGDN and DINA are similar, although EGDN has an even higher detonation velocity than DINA owing to its higher enthalpy of formation.

6.3 Conclusion

In this work, the main goal was the synthesis and thorough characterization of the corresponding nitrocarbamate of the nitro ester DINA (dinitroxyethylnitramine dinitrate, **3**), bis(nitrocarbamoylethyl) nitramine (**6**).

In general, nitrocarbamates often show a higher thermal stability compared to the corresponding nitro esters.[15] Therefore, the thermal stability should be enhanced for **2** and **6** compared to DINA. However, this statement could not be confirmed by analytical measurements. On the contrary, DTA measurements revealed that DINA (184 °C) has indeed a higher thermal stability than its nitrocarbamate counterparts **2** (150 °C) and **6** (153 °C).

However, if the detonation parameters are compared, it can be seen that the higher nitrogen content and the better density of the nitrocarbamate **6** results in better detonation velocities compared with DINA (**3**). Further important calculated values of the nitrate salt **2** and nitrocarbamate **6** are compared to DINA with a bar chart in Figure 6.

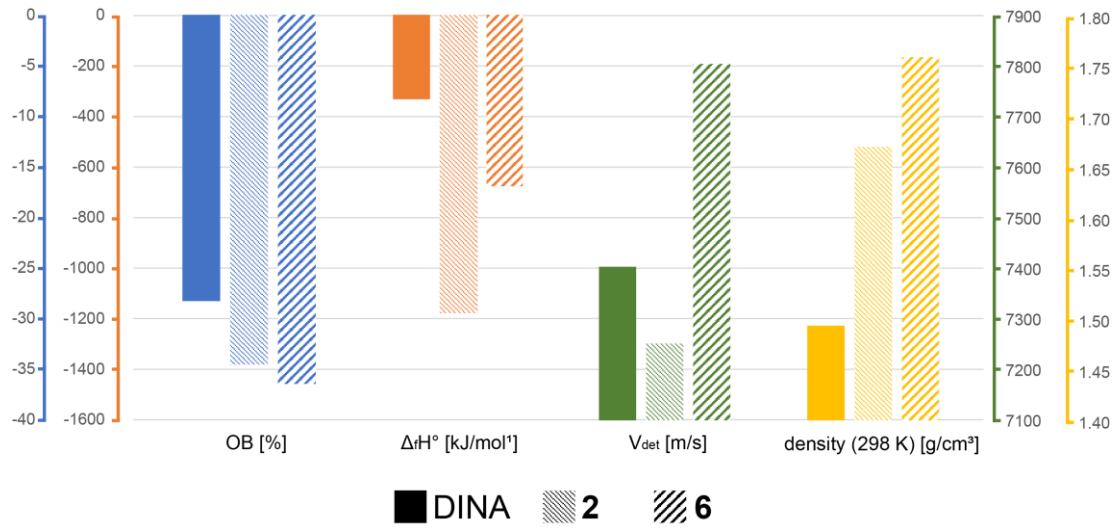

Figure 6. Bar chart comparing four different properties of DINA (**3**), **2** and **6**. OB: Oxygen balance (Ω=(xO-2yC-1/2zH)M/1600) [%]; $\Delta_f H°$: calculated (CBS-4M) heat of formation [kJ mol^{-1}]; V_{det}: detonation velocity [m s^{-1}]; calc. density (298 K).

6.4 Acknowledgments

Financial support of this work is gratefully acknowledged from the Ludwig-Maximilians-Universität, the Office of Naval Research (ONR) under grant no. ONR N00014-19-1-2078 and the Strategic Environmental Research and Development Program (SERDP) under contract number W912HQ19C0033. We also would like to thank Dr. Peter Mayer and Marcus Lommel M.Sc. for their help with X-ray measurements.

6.5 References

[1] T. M. Klapötke, *Chemistry of High Energy Materials,* 5th., deGruyter, Berlin, **2019**.

[2] R. Boschan, R. T. Merrow, R.W. van Dolah, *Chem Rev.* **1955**, *55*, 485−510.

[3] J. P. Agrawal, *High Energy Materials*, Wiley-VCH, Weinheim, **2010**.

[4] J. P. Agrawal, R. D. Hodgson, *Organic Chemistry of Explosives*, Wiley-VCH, Weinheim, **2007**.

[5] T. M. Klapötke, *Energetic Materials Encyclopedia*, 2nd Edition, DeGruyter, Berlin/Boston, **2021**.

[6] J. J. Sabatini, E. C. Johnson, *ACS Omega* **2021**, *6*, 11813−11821.

[7] Z. Wu, N. Liu, W. Zheng, J. Chen, X. Song, J. Wang, C. Cui, D. Zhang, F. Zhao, *Propellants Explos. Pyrotech.* **2020**, *45*, 92−100.

[8] J. Zhang, B. B. Xue, G. N. Rao, L. P. Chen, W. H. Chen, *J. Therm. Anal. Calorim.* **2018**, 727−735

[9] A. Książczak, M. Ostrowski, W. Tomaszewski, *J. Therm. Anal. Calorim.* **2008**, 275−279.

[10] F. Gao, B. Zhao, L. Hu, B. Chen, Y. Pan, P. Li, Y. Wang, *J. Chem. Eng. Data* **2020**, *65*, 3216−3220.

[11] P. Kočovský, *Tetrahedron Letters* **1986**, 5521−5524.

[12] D. Trache, A. F. Tarchoun, *J. Mater. Sci.* **2018**, *53*, 100−123.

[13] Q. J. Axthammer, T. M. Klapötke, B. Krumm, *Z. Anorg. Allg. Chem.* **2016**, *642*, 211−218.

[14] A. L. J. Thiele, *Justus Liebig Ann. Chem.* **1895**, *288*, 267−311.

[15] a) Q. J. Axthammer, T. M. Klapötke, B. Krumm, *Chem. Asian J.* **2016**, *11*, 568−575; b) Q. J. Axthammer, PhD Thesis, LMU Munich **2016**; c) Q. J. Axthammer, B. Krumm, T. M. Klapötke, *J. Org. Chem.* **2015**, *80*, 6329−6335.

[16] a) G. Gattow, W. K. Knoth, *Z. Anorg. Allg. Chem.* **1983**, *499*, 194−204; b) H. M. Curry, J. P. Mason, *J. Am. Chem. Soc.* **1951**, *73*, 5043−5046.

[17] W. Li, W. Feng, J. Hao, Z. Gao, L. Chen, W. Chen, *Org. Proc. Res. Dev.* **2019**, *23*, 2388−2393.

[18] G. Zhao, D. Kumar, P. Yin, C. He, G. H. Imler, D. A. Parrish, J. M. Shreeve, *Org. Lett.* **2019**, *21*, 1073−1077.

[19] D. Fischer, T. M. Klapötke, J. Stierstorfer, *Angew. Chem. Int. Ed.* **2014**, *53*, 8172−8175.

[20] W. J. Chute, G. E. Dunn, J. C. MacKenzie, G. S. Myers, G.N.R. Smart, J. W. Suggit, G. F. Wright, *Can. J. Res. Sect. B* **1948**, *26*, 114−137.

[21] G. E. Dunn, J. C. MacKenzie, G. F. Wright, *Can. J. Res.* **1948**, *26b*, 104−113.

[22] D. E. Chavez, M. A. Hiskey, D. L. Naud, D. Parrish, *Angew. Chem., Int. Ed.* **2008**, *47*, 8307−8309.

[23] a) L. Zhai, X. Qu, B. Wang, F. Bi, S. Chen, X. Fan, G. Xie, Q. Wei, S. Gao, *ChemPlusChem* **2016**, *81*, 1156−1159; b) Y. Liu, J. Zhang, K. Wang, J. Li, Q. Zhang, J. M. Shreeve, *Angew. Chem., Int. Ed.* **2016**, *55*, 11548−11551.

[24] J. Zhou, L. Ding, X. Wang, Y. Zhu, B. Wang, J. Zhang, *ChemistryOpen* **2018**, *7*, 527−532.

[25] N. Dai, A. D. Shah, L. Hu, M. J. Plewa, B. McKague, W. A. Mitch, *Environ. Sci. Technol.* **2012**, *46*, 9793−9801.

[26] R. G. Pews, *J. Org. Chem.* **1967**, *32*, 2914−2915.

[27] Impact: insensitive > 40 J, less sensitive ≥ 35 J, sensitive ≥ 4 J, very sensitive ≤ 3 J, Friction: insensitive > 360 N, less sensitive = 360 N, sensitive < 360 N and > 80 N, very sensitive ≤ 80 N, extremely sensitive ≤ 10 N. According to the UN Recommendations on the Transport of Dangerous Goods, (+) indicates not safe for transport.

[28] M. Sućeska, EXPLO5 V6.06.01, Zagreb (Croatia), **2021**.

6.6 Supplementary Information

6.6.1 Experimental Information

All chemicals and solvents were employed as received (Sigma-Aldrich, Fluka, Acros, ABCR). ^{1}H,^{13}C, ^{14}N and ^{15}N NMR spectra were recorded at ambient temperature using a Bruker TR 400 instrument and are referenced with respect to Me_4Si ($^{1}H/^{13}C$) and $MeNO_2$ ($^{14}N/^{15}N$). Melting and decomposition temperatures of the described compounds were measured through differential thermal analysis (DTA) with an OZM Research DTA 552-Ex instrument. The samples were measured in a range of 25–400 °C at a heating rate of 5 °C min^{-1}. Infrared spectra were measured with pure samples on a Perkin-Elmer BXII FT-IR system with a Smith DuraSampler IR II diamond ATR. Determination of the carbon, hydrogen, and nitrogen contents was carried out by combustion analysis using an Elementar Vario El (nitrogen values determined are often lower than the calculated due to their explosive behavior). Impact sensitivity tests were carried out according to STANAG 4489[1] modified instruction[2] using a BAM (Bundesanstalt für Materialforschung) drophammer.[3] Friction sensitivity tests were carried out according to STANAG 4487[4] modified instruction[5] using the BAM friction tester. The classification of the tested compounds results from the “UN Recommendations on the Transport of Dangerous Goods”.[6]

CAUTION! All investigated compounds are potentially explosive energetic materials, which show partly increased sensitivities towards various stimuli (e.g. elevated temperatures, impact or friction). Therefore, proper security precautions (safety glass, face shield, earthed equipment and shoes, leather coat, Kevlar gloves, Kevlar sleeves, and ear plugs) have to be applied while synthesizing and handling the described compounds.

Bis(carbamoylethyl) amine (**1**)

CSI (9.91 mL, 2.4 eq) was added to MeCN (130 mL) under ice-cold conditions using a syringe. Diethanolamine (5.00 g, 47.6 mmol, 1 eq) was pre-dissolved in 30 mL MeCN and added to the reaction mixture. The solution was stirred at 0 °C for 5 minutes and at room temperature for two hours. Ice water (100 mL) was used to

quench the reaction. Acetonitrile was reduced *in vacuo*. The remaining aqueous phase was neutralized by addition of pure $NaHCO_3$, since pH 7 is required for precipitation of the colorless solid. This solid was filtered and washed with water to remove the residual $NaHCO_3$. The carbamate **1** (8.82 g, 97 %) was obtained as a colorless solid, after drying for two days at 80 °C.

DTA (5 °C min^{-1}) onset: 207 °C (endo), 234 °C (dec.); ^{1}H NMR (400 MHz, DMSO-D_6) δ = 6.51 (s, 4H, NH_2), 5.88 (s, 1H, NH), 3.95 (t, $^{3}J_{H,H}$ = 6.0 Hz, 4H, CH_2O), 3.37 (t, 4H, NCH_2) ppm; $^{13}C\{^{1}H\}$ NMR (101 MHz, DMSO-D_6) δ = 156.6 (*C*O), 61.9 (*C*H_2O), 46.7 (N*C*H_2) ppm; IR (ATR): $\tilde{\nu}$ = 3453 (w), 3439 (w), 3383 (w), 3327 (w), 3165 (w), 3085 (vw), 2979 (vw), 2164 (vw), 2146 (vw), 1709 (m), 1687 (vs), 1620 (m), 1607 (m), 1585 (s), 1508 (m), 1469 (m), 1437 (s), 1421 (vs), 1377 (s), 1338 (m), 1325 (s), 1316 (s), 1303 (m), 1290 (m), 1214 (m), 1183 (w), 1150 (m), 1118 (m), 1092 (vs), 1069 (vs), 1055 (s), 935 (w), 901 (w), 879 (w), 797 (w), 779 (w), 768 (w), 738 (w), 686 (w), 674 (w), 611 (m) cm^{-1}; elemental analysis calcd (%) for $C_6H_{13}N_3O_4$: C 37.69, H 6.85, N 21.98; found: C 34.86, H 5.54, N 23.16.

Bis(nitrocarbamoylethyl)ammonium nitrate (**2**)

The carbamate **1** (4.88 g, 25.5 mmol) was added dropwise to fuming nitric acid (20 mL) under ice-cold conditions. The reaction mixture was stirred at 0 °C for 5 minutes and at room temperature for two hours. The reaction was quenched on ice and extracted with EtOAc (3 x 150 mL). The solvent was dried over magnesium sulfate and reduced *in vacuo*. This mixture was left for crystallization, and colorless needles were formed. The needles (2.55 g, 31 %), suitable for X-ray diffraction, were filtered and washed with a small amount of cold water.

DTA (5 °C min^{-1}) onset: 150 °C (dec.); ^{1}H NMR (400 MHz, DMSO-D_6) δ = 13 (b, 2H, NH), 8.8 (b, 2H, NH_2^+), 4.43 (t, $^{3}J_{H,H}$ = 5.0 Hz, 4H, CH_2O), 3.4 (b, 4H, NCH_2) ppm; $^{13}C\{^{1}H\}$ NMR (101 MHz, DMSO-D_6) δ = 148.9 (*C*O), 61.7 (*C*H_2O), 45.9 (N*C*H_2) ppm; ^{14}N NMR (29 MHz, DMSO-D_6) δ = −5 (NO_3^-), −41 (NO_2) ppm. IR (ATR): $\tilde{\nu}$ = 3078 (m), 2979 (w), 2941 (w), 2852 (w), 2812 (w), 2742 (w), 1777 (m), 1753 (s), 1590 (s), 1472 (m), 1453 (s), 1419 (m), 1402 (m), 1388 (m), 1353 (s), 1321 (s), 1295 (s), 1269 (m), 1219 (m), 1181 (vs), 1149 (vs), 1116 (s), 1100 (s), 1064 (m), 1056 (m), 1021 (m), 985 (s), 917 (m), 897 (m), 886 (s), 817 (s), 792 (m), 771 (m), 745 (s), 728 (s), 702 (s) cm^{-1}; elemental analysis calcd (%) for

$C_6H_{12}N_6O_{11}$: C 20.94, H 3.51, N 24.42; found: C 20.75, H 3.55, N 24.05; BAM drophammer: 5 J; friction tester: >360 N.

Bis(nitratoethyl) nitramine (**3**, DINA)

Under ice-cold conditions, fuming nitric acid (2.14 mL) was added to acetic anhydride (23.6 mL). Diethanolamine hydrochloride (5.00 g, 159 mmol) and HNO_3 (4.29 mL) were added alternatingly in portions. During this process, the temperature was kept below 10 °C. The reaction mixture was stirred at room temperature for two hours and quenched on ice. The colorless solid of **3** (8.05 g, 94 %) was filtered and washed with ice-cold water (3 x 20 mL).

DTA (5 °C min^{-1}) onset: 50 °C (endo), 184 °C (dec.); ^{1}H NMR (400 MHz, DMSO-D_6) δ = 4.78 (t, $^{3}J_{H,H}$ = 5.0 Hz, 2H, CH_2O), 4.19 (t, 2H, NCH_2) ppm; $^{13}C\{^{1}H\}$ NMR (101 MHz, DMSO-D_6) δ = 69.9 (CH_2O), 49.0 (NCH_2) ppm; ^{14}N NMR (29 MHz, DMSO-D_6) δ = −29 (NO_2), −43 (ONO_2) ppm; elemental analysis calcd (%) for $C_4H_8N_4O_8$: C 20.01, H 3.36, N 23.33; found: C 20.01, H 3.21, N 21.77; BAM drophammer: 8 J, friction tester: >360 N.

Bis(hydroxyethyl) nitramine (**4**)

DINA (9.60 g, 40.0 mmol) was refluxed for 12 h in formic acid (150 mL, 97 %). Then the formic acid was reduced *in vacuo*, and the crude product again refluxed in methanol (30 mL) for 48 hours and again reduced *in vacuo*. The crude product was purified by column chromatography (SiO_2, EtOAc: MeOH 9.5:0.5). The nitramine **4** (4.78 g, 46%) was obtained as a colorless liquid.

^{1}H NMR (400 MHz, DMSO-D_6) δ = 4.95 (t, $^{3}J_{H,H}$ = 5.2 Hz, 2H, OH), 3.85 (t, $^{3}J_{H,H}$ = 5.7 Hz, 4H, NCH_2), 3.64 (td, 4H, CH_2OH) ppm; $^{13}C\{^{1}H\}$ NMR (101 MHz, DMSO-D_6) δ = 57.2/54.6 (CH_2) ppm; ^{14}N NMR (29 MHz, DMSO-D_6) δ = −29 (NO_2) ppm.

Bis(carbamoylethyl) nitramine (**5**)

Into ice-cold acetonitrile (130 mL) was added CSI (3.33 mL, 2.4 eq) in portions, then **4** (2.40 g, 16.0 mmol, 1 eq), pre-dissolved in acetonitrile (10 mL) also added in portions while the temperature was kept below 10 °C. The reaction mixture was stirred at 0 °C for 5 min and at room temperature for two hours. Ice-cold water (100 mL) was added to quench the reaction, forming a precipitate. After the reaction

was stirred overnight, the colorless solid **5** (6.03 g, 83 %) was filtered and washed with water.

DTA (5 °C min^{-1}) onset: 175 °C (endo), 262 °C (dec.); ^{1}H NMR (400 MHz, DMSO-D_6) δ = 6.6 (br, 4H, NH_2), 4.16 (t, $^{3}J_{H,H}$ = 5.4 Hz, 4H, CH_2), 3.97 (t, 4H, CH_2) ppm; ^{13}C{^{1}H} NMR (101 MHz, DMSO-D_6) δ = 156.3 (CO), 59.6 (NCH_2), 51.2 (CH_2O) ppm; ^{14}N NMR (29 MHz, DMSO-D_6) δ = −30 (NO_2) ppm; IR (ATR): $\tilde{\nu}$ = 3417 (m), 3369 (w), 3360 (w), 3334 (w), 3265 (m), 3213 (m), 3086 (vw), 3025 (vw), 3010 (vw), 2966 (w), 1778 (vw), 1757 (w), 1693 (vs), 1616 (s), 1500 (s), 1472 (m), 1453 (m), 1444 (s), 1420 (s), 1411 (s), 1358 (vs), 1330 (s), 1300 (m), 1285 (s), 1259 (s), 1194 (s), 1157 (s), 1127 (m), 1085 (vs), 1056 (s), 1046 (vs), 944 (w), 922 (m), 830 (m), 780 (m), 757 (m), 718 (w), 687 (w), 679 (w) cm^{-1}; elemental analysis calcd (%) for $C_6H_{12}N_4O_6$: C 30.01, H 5.12, N 23.72; found: C 30.05, H 5.04, N 23.81; BAM drophammer: >40 J; friction tester: >360 N.

Bis(nitrocarbamoylethyl) nitramine (**6**)

Nitramine **5** (0.985 g, 4.17 mmol) was added in portions to HNO_3 (10 mL) under stirring at ice-cold conditions. After stirring at 0 °C for 1 h, the reaction mixture was placed on ice (150 g). The aqueous solution was extracted with EtOAc (3 x 150 mL), dried over magnesium sulfate, and reduced *in vacuo*. The remaining solution was crystallized with ice-cold conditions. The nitrocarbamate **6** was obtained after filtration as a colorless solid (0.597 g, 44 %).

DTA (5 °C min^{-1}) onset: 142 °C (endo), 153 °C (dec.); ^{1}H NMR (400 MHz, acetone-D_6) δ = 13.35 (s, 2H, NH), 4.54 (t, $^{3}J_{H,H}$ = 5.1 Hz, 4H, CH_2), 4.22 (t, 4H, CH_2); ^{13}C{^{1}H} NMR (101 MHz, acetone-D_6) δ = 149.2 (CO), 63.9 (CH_2O), 51.6 (NCH_2) ppm; ^{15}N NMR (41 MHz, acetone-D_6) δ = −29.7 (t, $^{3}J_{N,H}$ = 2.9 Hz, NNO_2), −45.0 ($NHNO_2$), −189.4 (d, $^{1}J_{N,H}$ = 89.9 Hz, $NHNO_2$), −207.7 (NNO_2) ppm; IR (ATR): $\tilde{\nu}$ = 3242 (m), 3193 (m), 3035 (vw), 1745 (vs), 1609 (vs), 1522 (s), 1456 (s), 1430 (s), 1411 (m), 1403 (m), 1383 (w), 1360 (w), 1325 (s), 1290 (s), 1278 (vs), 1210 (s), 1181 (s), 1152 (s), 1062 (m), 994 (m), 982 (m), 970 (s), 946 (m), 858 (s), 811 (w), 797 (w), 758 (s), 727 (w), 623 (m) cm^{-1}; elemental analysis calcd (%) for $C_6H_{10}N_6O_{10}$: C 22.09, H 3.09, N 25.77; found: C 22.24, H 2.87, N 25.67; BAM drophammer: 6 J; friction tester: >360 N.

6.6.2 NMR Spectroscopy

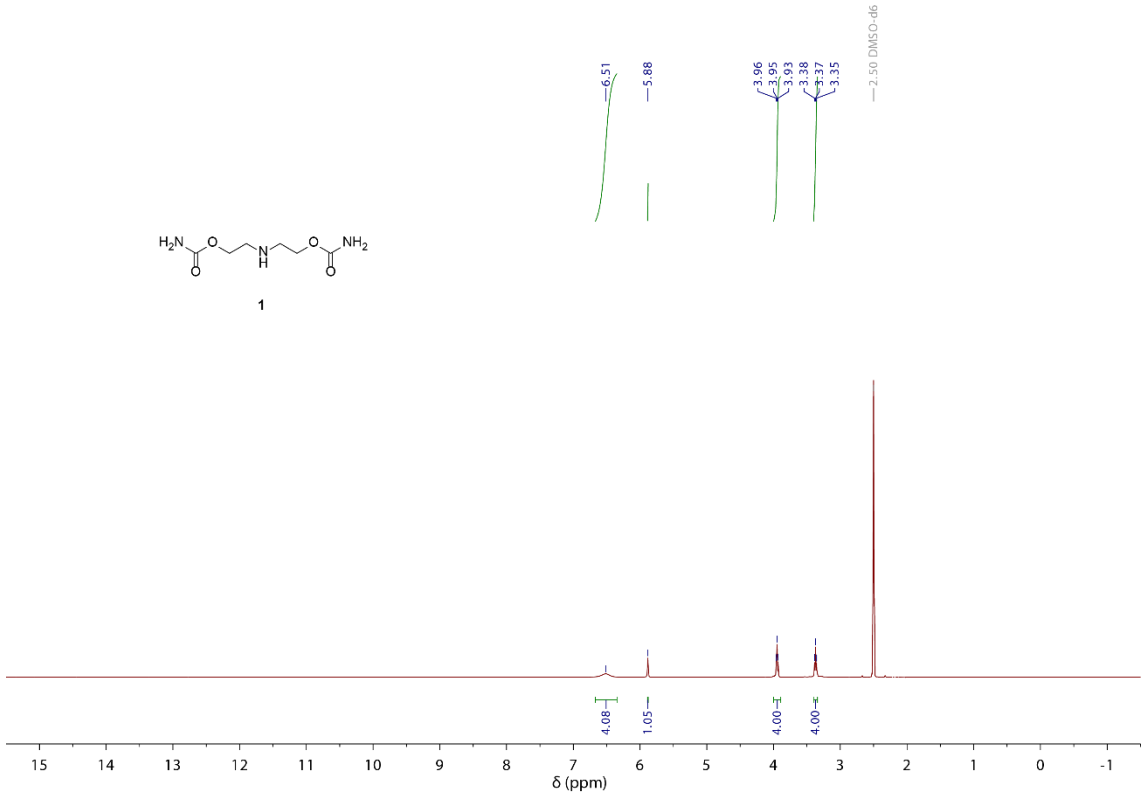

Figure S1. ^{1}H NMR spectrum of **1** in DMSO-D_6.

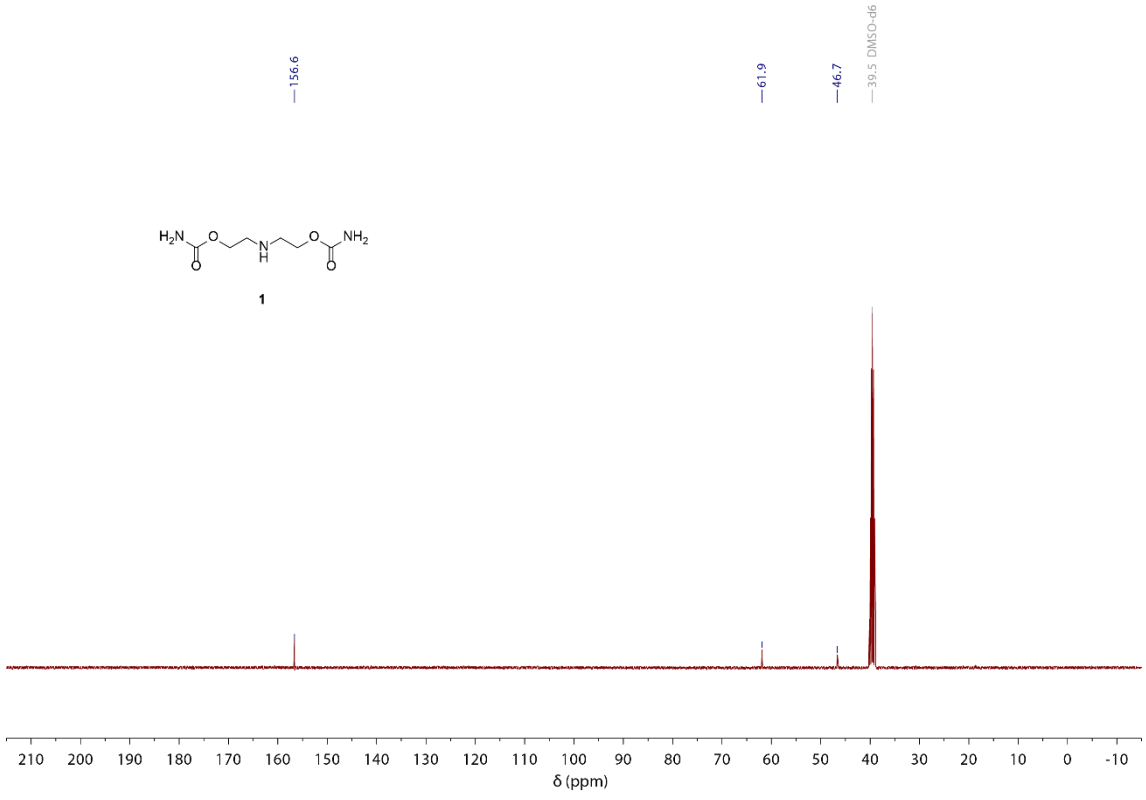

Figure S2. ^{13}C{^{1}H} NMR spectrum of **1** in DMSO-D_6.

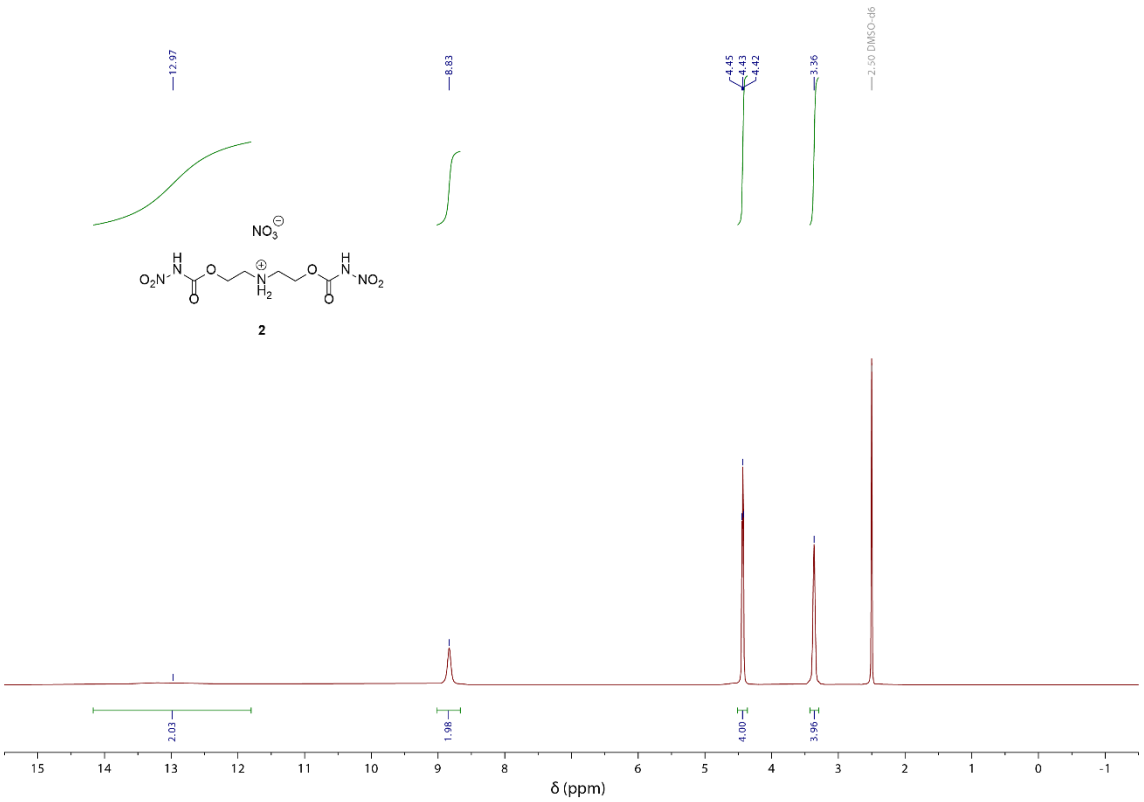

Figure S3. ^{1}H NMR spectrum of **2** in DMSO-D_6.

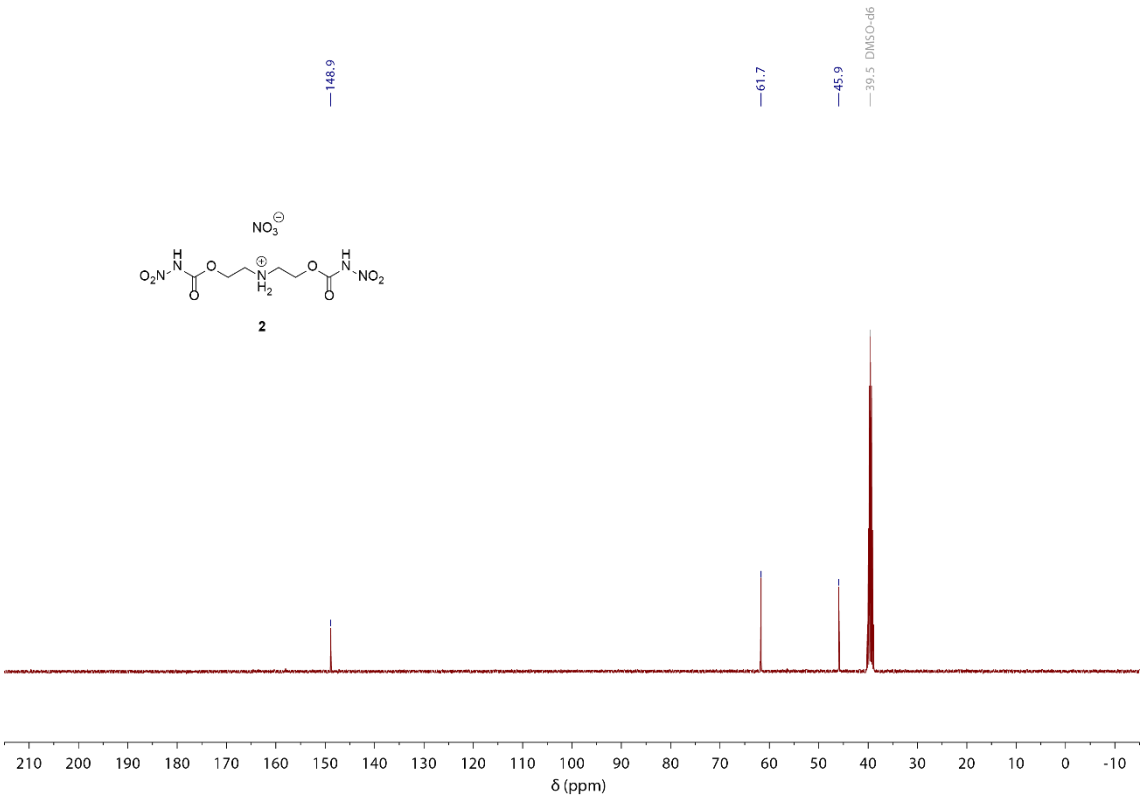

Figure S4. ^{13}C{^{1}H} NMR spectrum of **2** in DMSO-D_6.

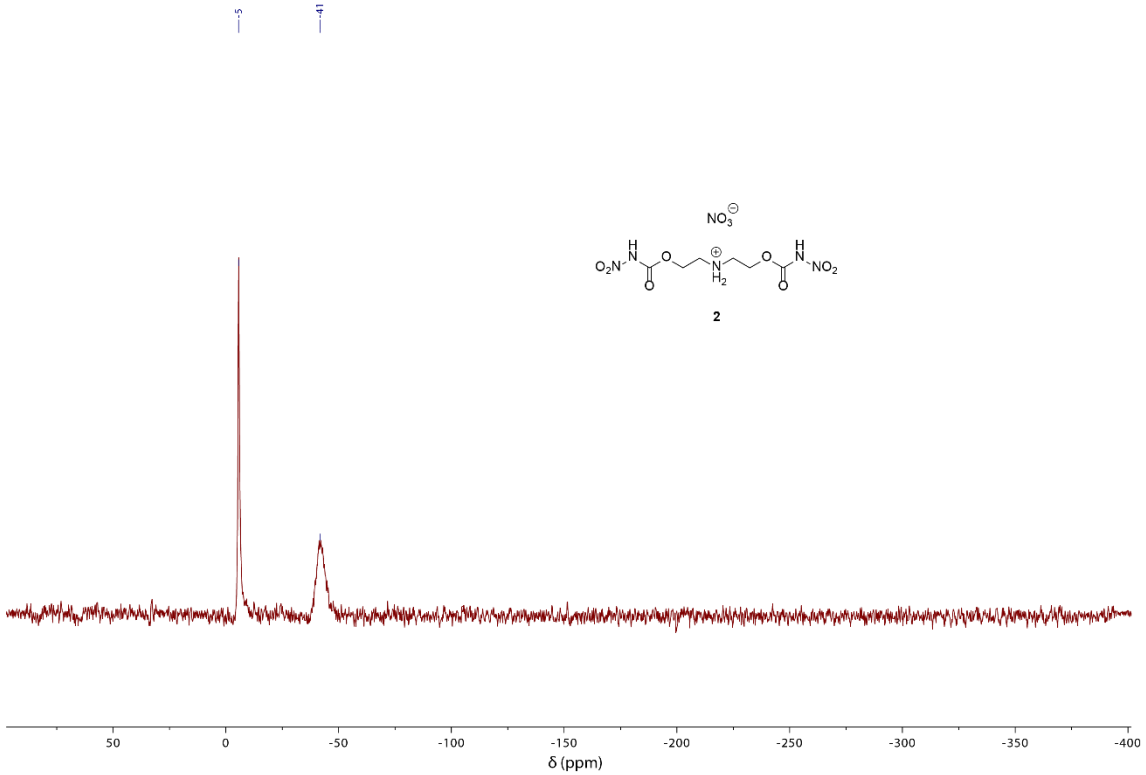

Figure S5. ^{14}N NMR spectrum of **2** in DMSO-D_6.

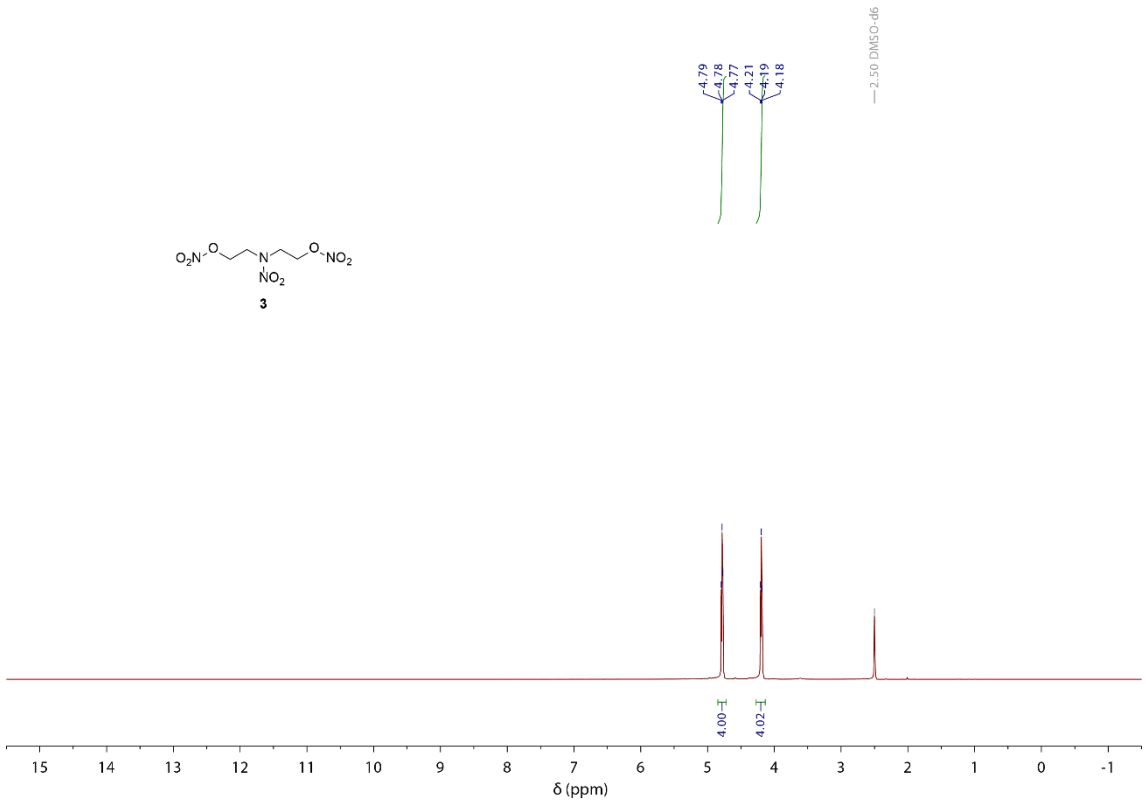

Figure S6. ^{1}H NMR spectrum of **3** in DMSO-D_6.

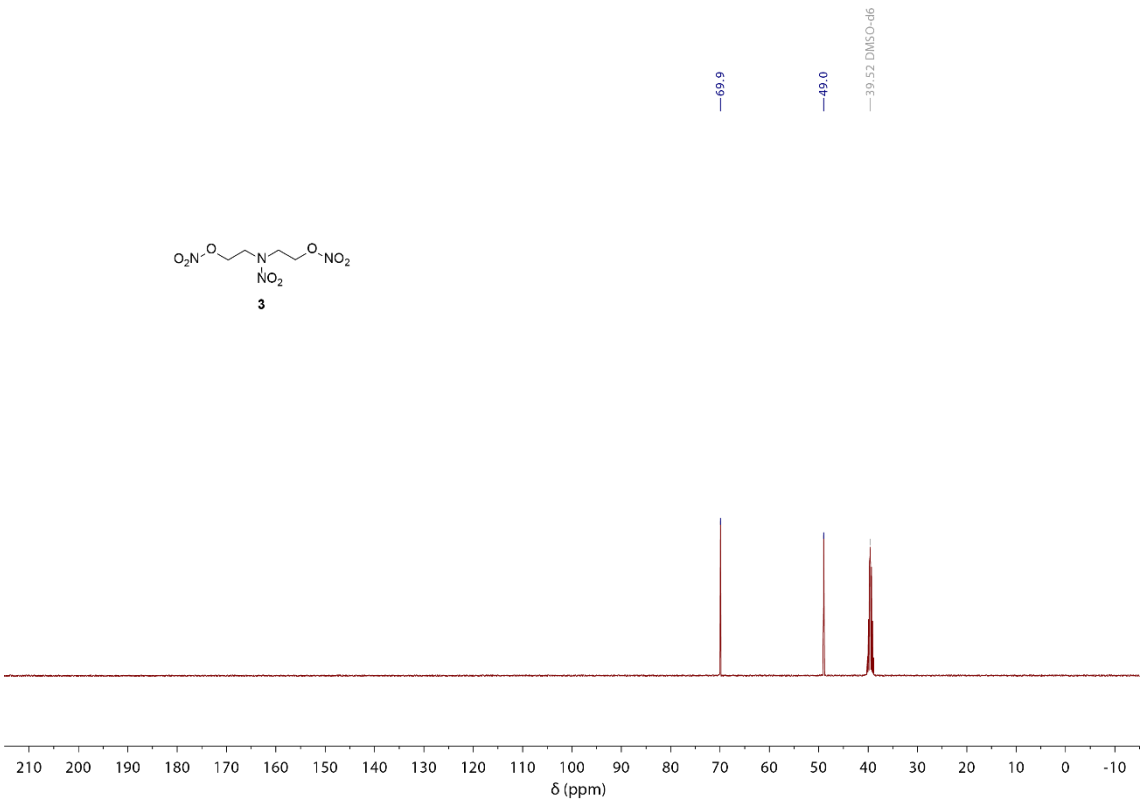

Figure S7. $^{13}C\{^{1}H\}$ NMR spectrum of **3** in DMSO-D_6.

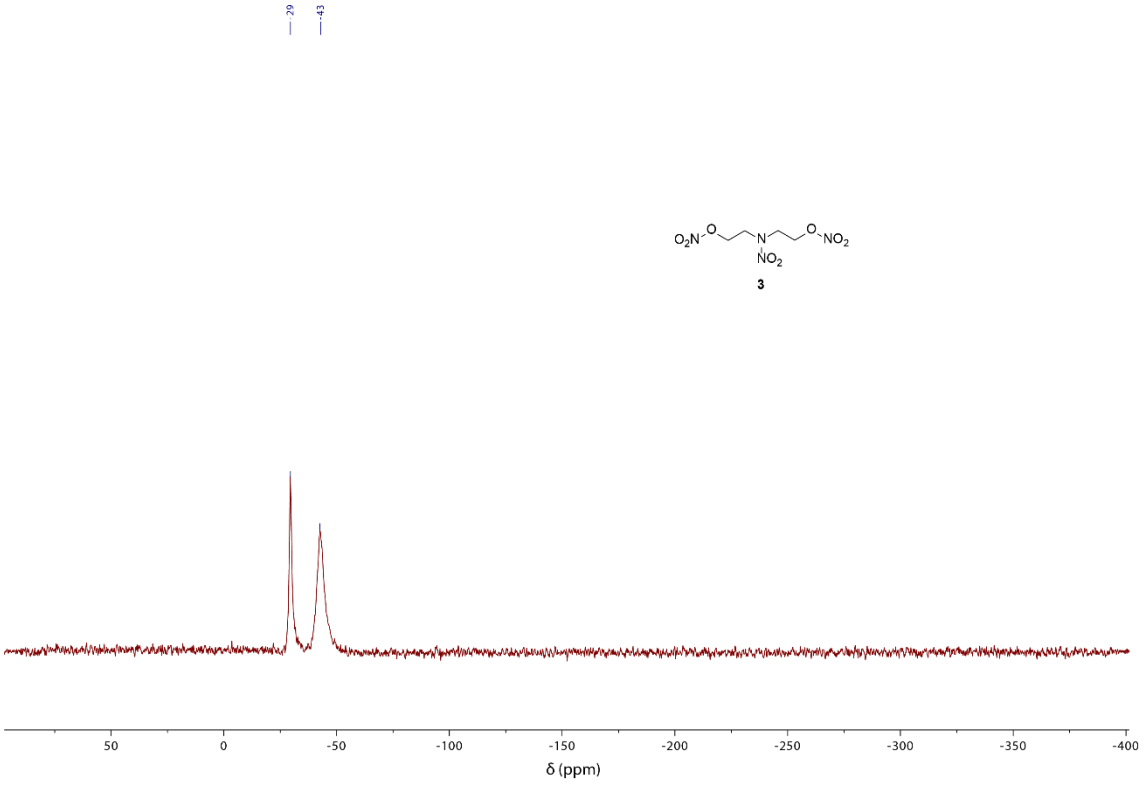

Figure S8. ^{14}N NMR spectrum of **3** in DMSO-D_6.

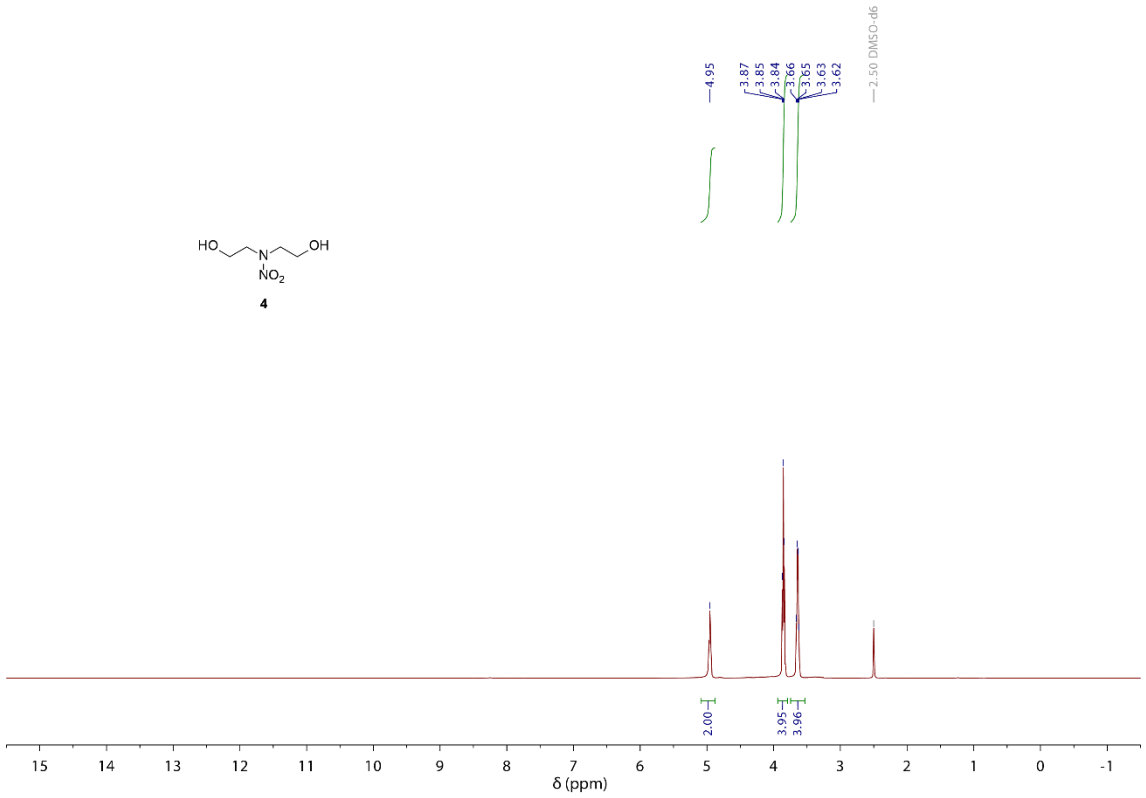

Figure S9. ^{1}H NMR spectrum of **4** in DMSO-D_6.

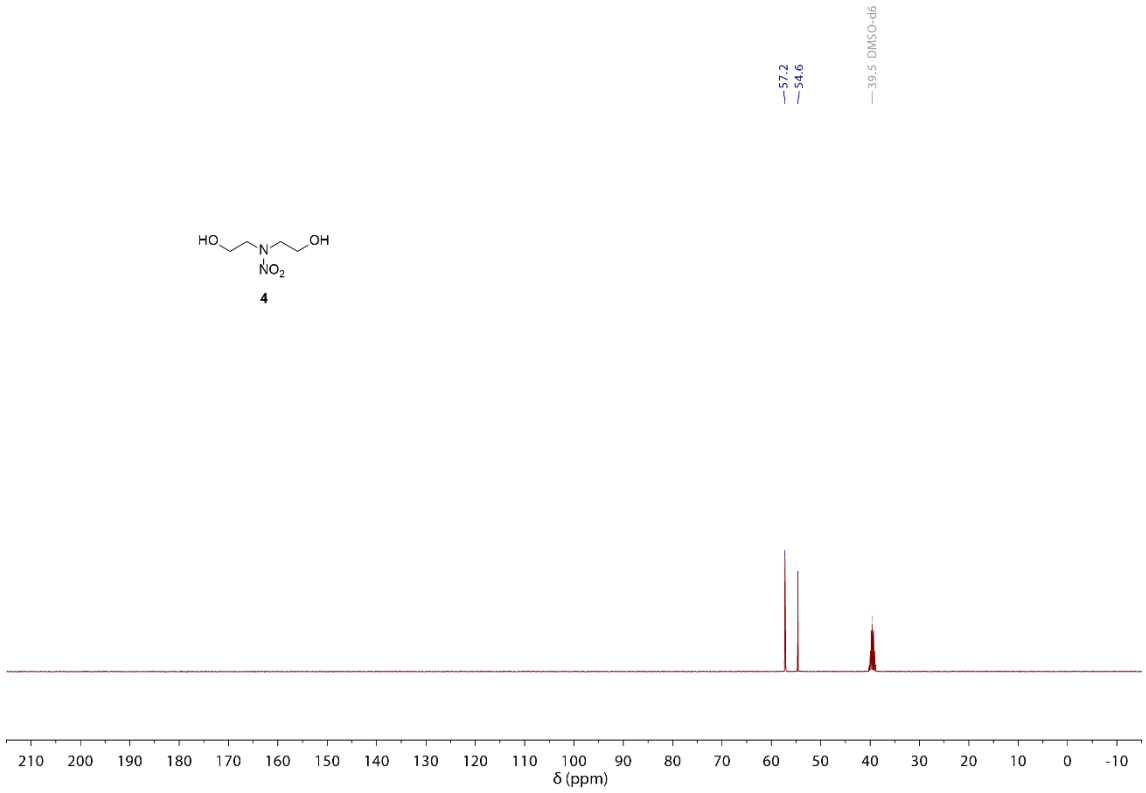

Figure S10. ^{13}C{^{1}H} NMR spectrum of **4** in DMSO-D_6.

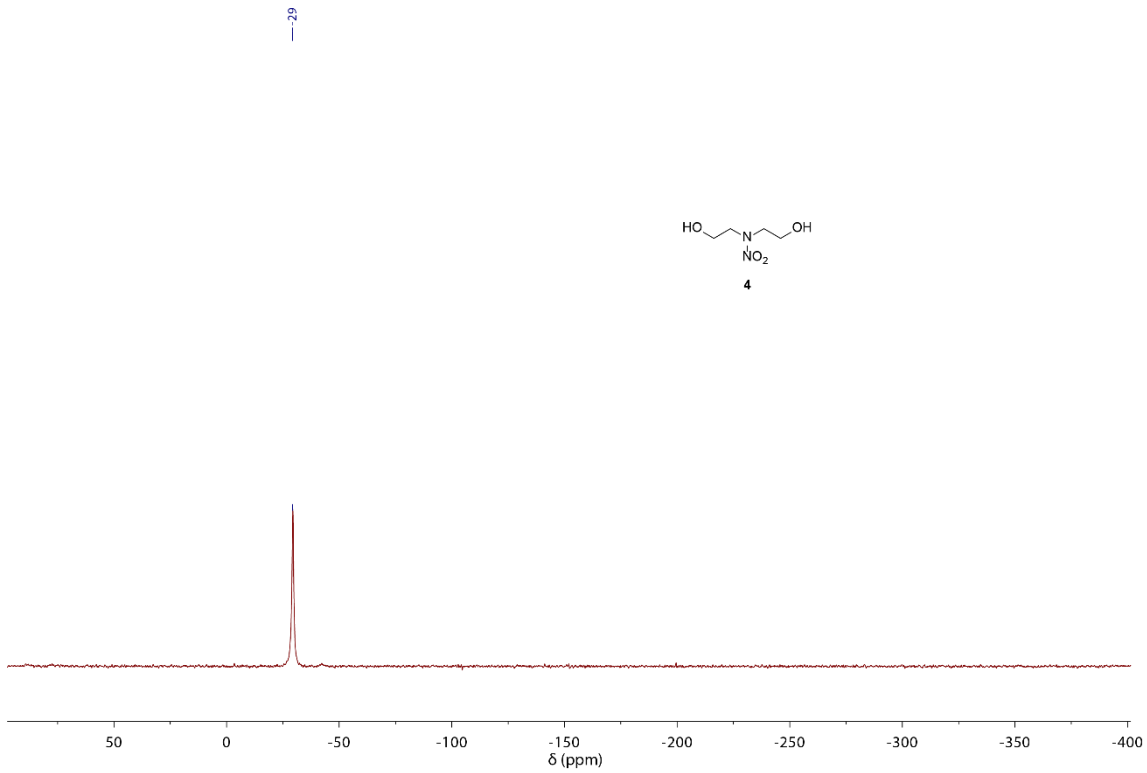

Figure S11. ^{14}N NMR spectrum of **4** in DMSO-D_6.

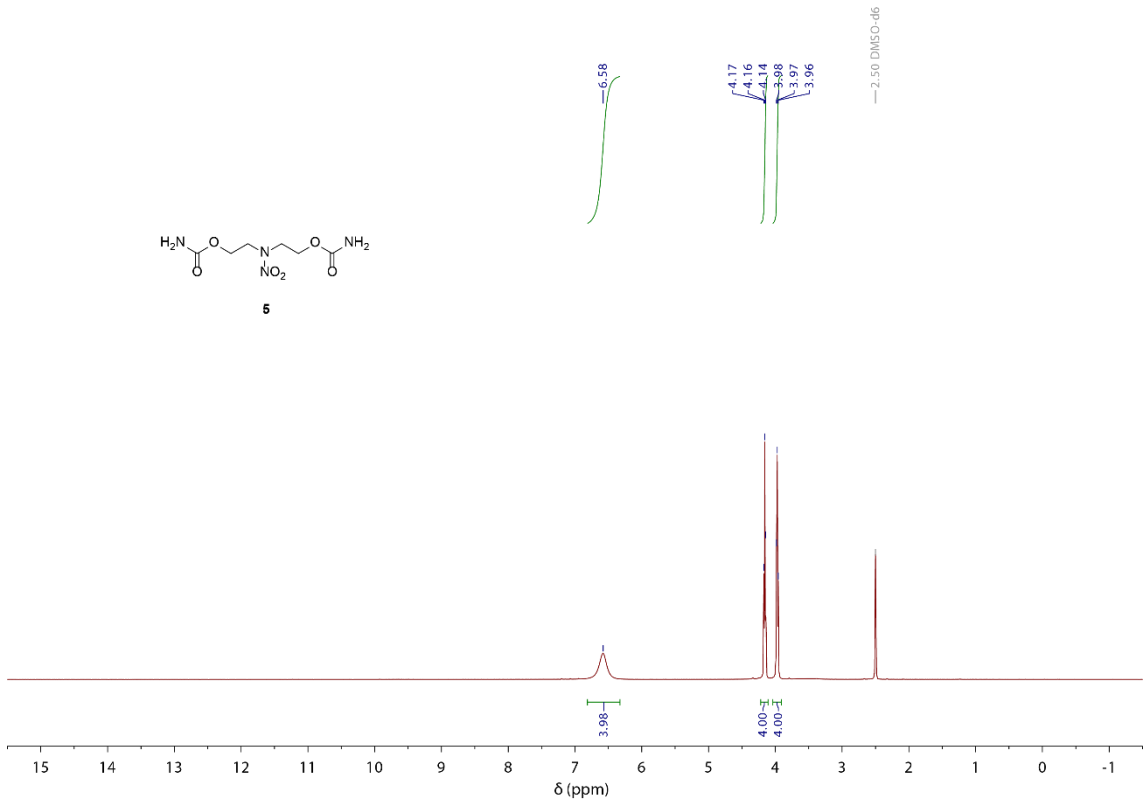

Figure S12. ^{1}H NMR spectrum of **5** in DMSO-D_6.

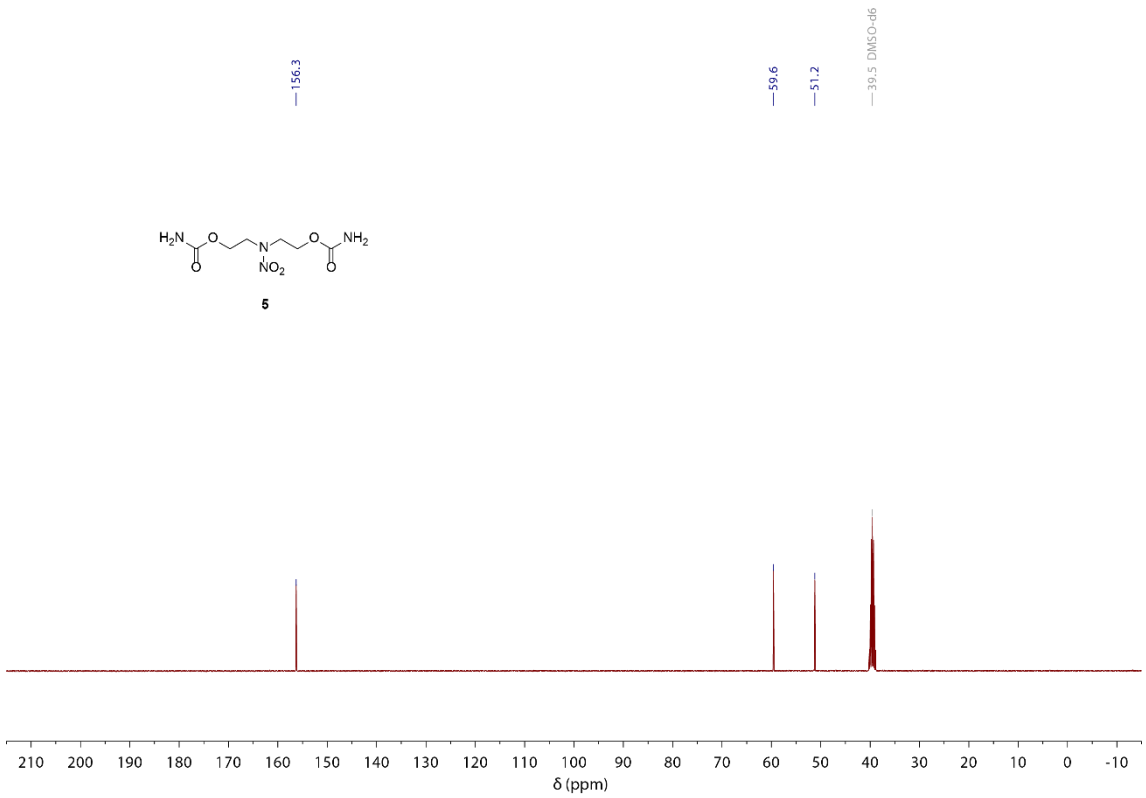

Figure S13. $^{13}C\{^{1}H\}$ NMR spectrum of **5** in DMSO-D_6.

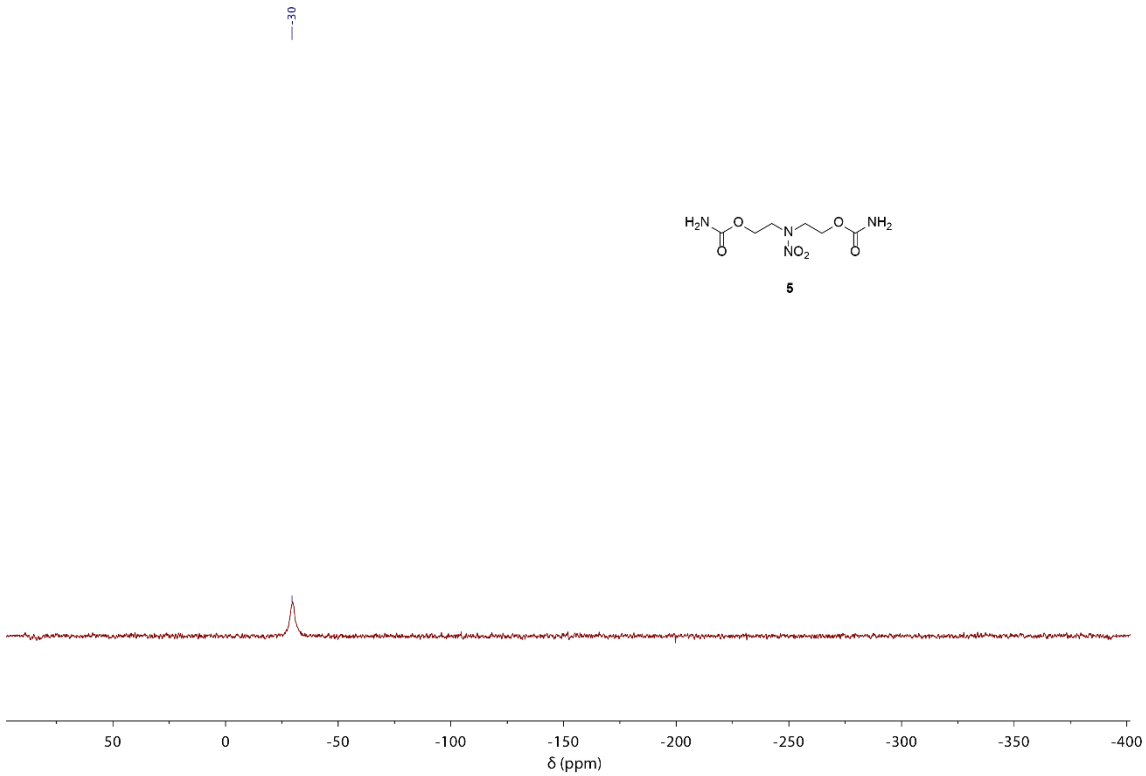

Figure S14. ^{14}N NMR spectrum of **5** in DMSO-D_6.

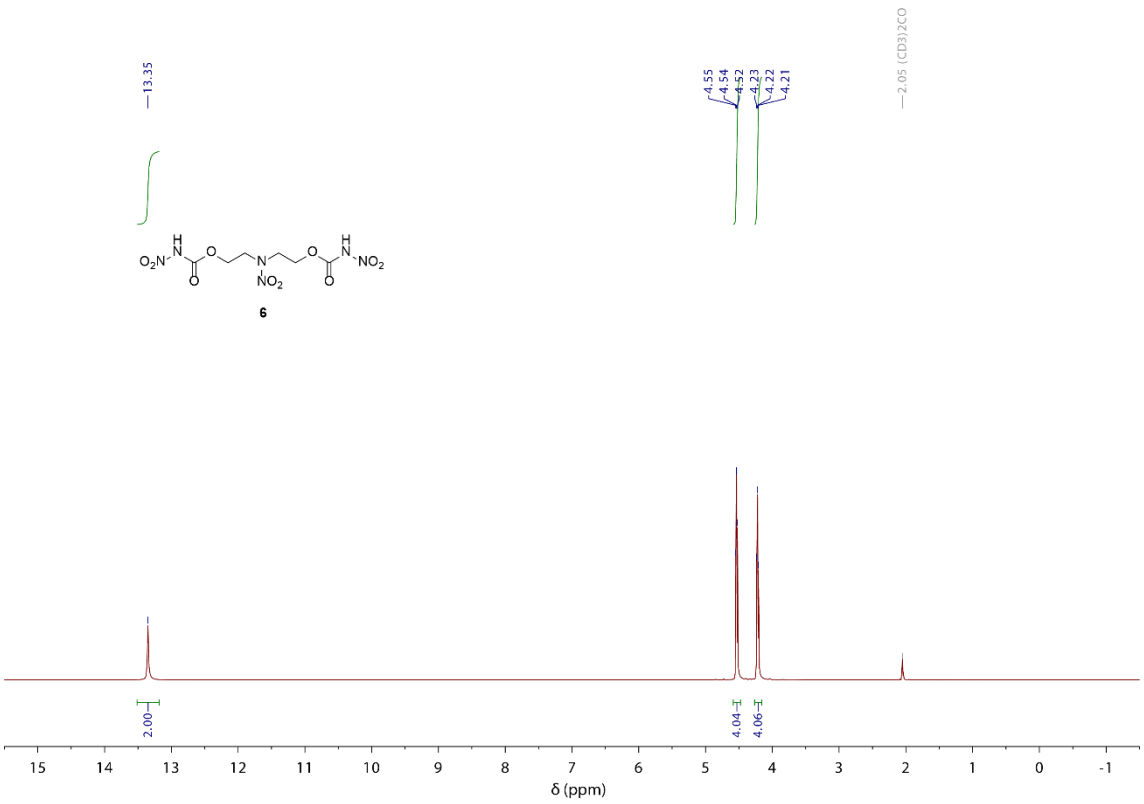

Figure S15. ^{1}H NMR spectrum of **6** in acetone-D_6.

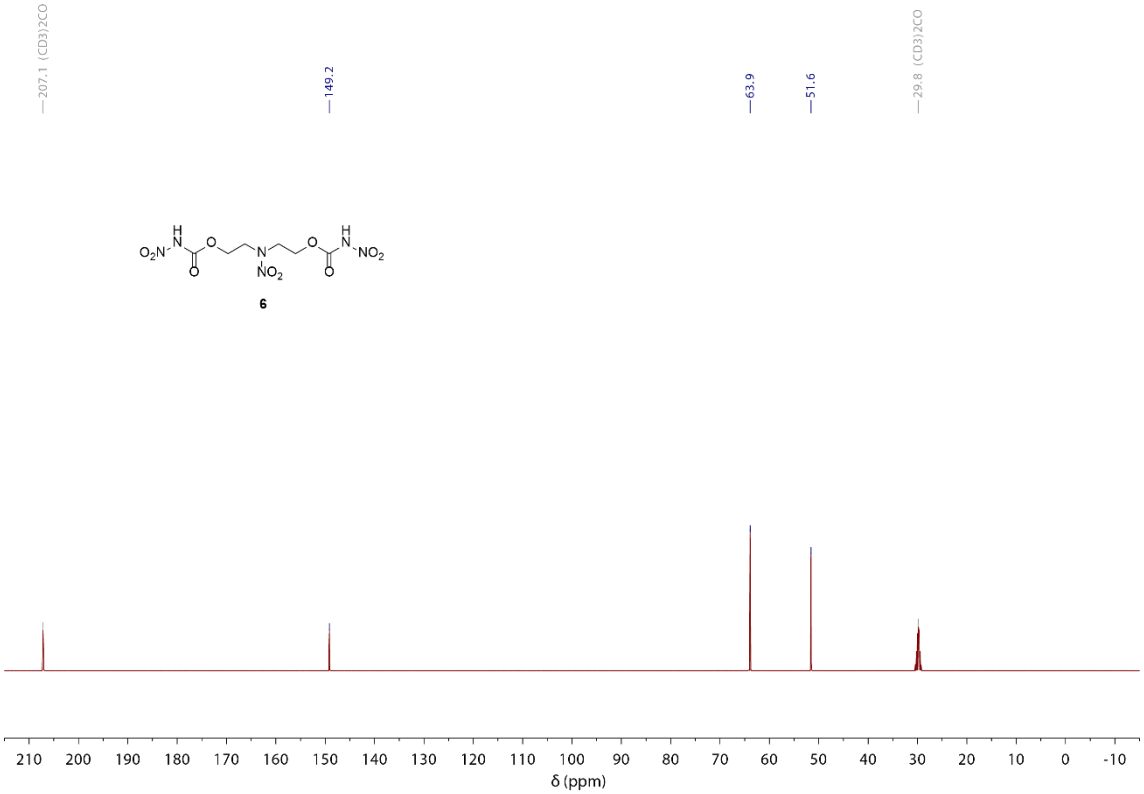

Figure S16. ^{13}C{^{1}H} NMR spectrum of **6** in acetone-D_6.

6.6.3 IR Spectroscopy

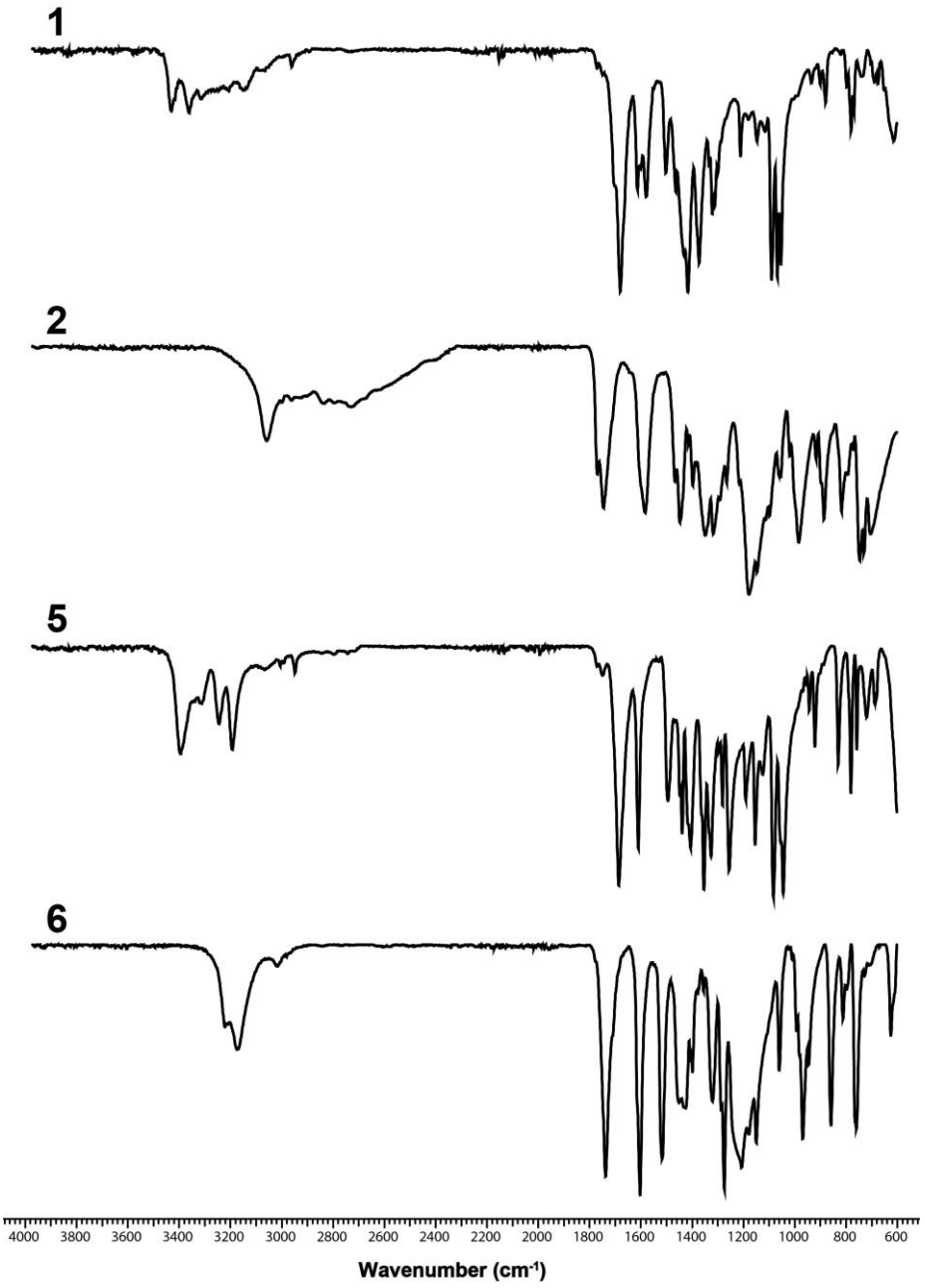

Figure S17. **IR spectra of** 1**,** 2**,** 5 **and** 6**.**

6.6.4 DTA Measurements

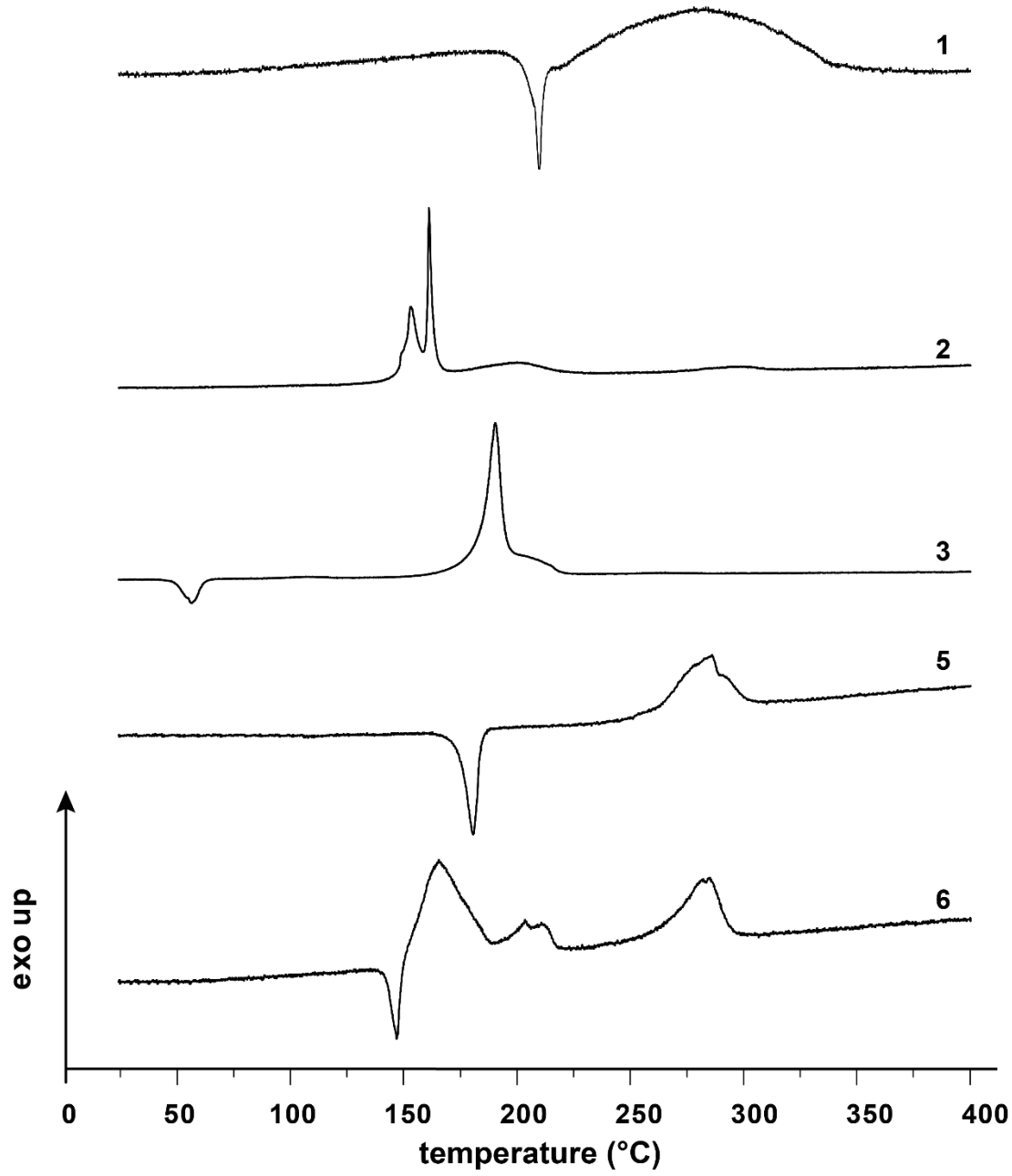

Figure S18. DTA measurements of **1**, **2**, **3**, **5** and **6**.

6.6.5 X-Ray Diffraction

For all crystalline compounds, an Oxford Xcalibur3 diffractometer with a CCD area detector or Bruker D8 Venture TXS diffractometer equipped with a multilayer monochromator, a Photon 2 detector, and a rotating-anode generator was employed for data collection using Mo-Kα radiation (λ = 0.71073 Å). On the Oxford device, data collection and reduction were carried out using the CRYSALISPRO software.[7] On the Bruker diffractometer, the data were collected with the Bruker Instrument Service v3.0.21, the data reduction was performed using the SAINT V8.18C software (Bruker AXS Inc., 2011). The structures were solved by direct methods (SIR-92, [8] SIR-97[9] or SHELXT[9,10]) and refined by full-matrix least-squares on F2 (SHELXL[10,11]) and finally checked using the PLATON software[12] integrated into the WinGX[13] software suite. The non-hydrogen atoms were refined anisotropically and the hydrogen atoms were located and freely refined. The absorptions were corrected by a SCALE3 ABSPACK or SADABS Bruker APEX3 multiscan method. [14] All DIAMOND2 plots are shown with thermal ellipsoids at the 50 % probability level and hydrogen atoms are shown as small spheres of arbitrary radius.

6.6.6 Heat of Formation Calculations

All quantum chemical calculations were carried out using the Gaussian G09 program package.[15] The enthalpies (H) and free energies (G) were calculated using the complete basis set (CBS) method of *Petersson* and coworkers to obtain very accurate energies.[16] The CBS models are using the known asymptotic convergence of pair natural orbital expressions to extrapolate from calculations using a finite basis set to the estimated CBS limit. CBS-4 starts with an HF/3-21G(d) geometry optimization; the zero-point energy is computed at the same level. It then uses a large basis set SCF calculation as base energy, and an MP2/6-31+G calculation with a CBS extrapolation to correct the energy through second order. A MP4(SDQ)/6-31+(d,p) calculation is used to approximate higher-order contributions. In this study, we applied the modified CBS-4M method.
Heats of formation were calculated using the atomization method (Equation S1) using room temperature CBS-4M enthalpies, which are summarized in Table S1.[16]

$$\Delta_f H°_{(g,\,M,\,298)} = H_{(Molecule,\,298)} - \sum H°_{(Atoms,\,298)} + \sum \Delta_f H°_{(Atoms,\,298)} \quad (S1)$$

Table S1. CBS-4M enthalpies for atoms C, H, N, and O and their literature values for atomic $\Delta H°_f{}^{298}$ / kJ mol^{-1}.

	$-H^{298}$ / a.u.	NIST
H	0.500991	218.2
C	37.786156	717.2
N	54.522462	473.1
O	74.991202	249.5

For ionic compounds, the lattice energy (U_L) and lattice enthalpy (ΔH_L) are calculated from the corresponding X-ray molecular volumes (converted to RT) according to the equations provided by *Jenkins* and *Glasser*.[17] With the calculated lattice enthalpy, the gas-phase enthalpy of formation was converted into the solid-state (standard conditions) enthalpy of formation. The calculation results are summarized in Table S2.

Table S2. Heat of formation calculations.

	$-H^{298}$ [a] /a.u.	$\Delta_f H°$(g,M) [b] /kJ mol^{-1}	$\Delta_f H°$(s) [c] /kJ mol^{-1}	$\Delta_f U$(s) [d] /kJ kg^{-1}
2 cation	1109.755165	–550.9	–	–
NO_3^-	280.080446	–314.1	–	–
2	–	–	–1193.1	–1157.2
5	–904.992446	–795.0	–879.2	–851.9
6	–1313.501571	–605.2	–605.2	–651.1

[a] CBS-4M electronic enthalpy; [b] gas phase enthalpy of formation; [c] standard solid state enthalpy of formation; [d] solid state energy of formation.

6.6.7 Calculation of Energetic Performance

The detonation parameters were calculated with the EXPLO5 (version 6.06.01) computer code.[18] This calculation code is based on the steady-state model of equilibrium and uses the Becker–Kistiakowski–Wilson equation of state.[19] It calculates the detonation parameters at the Chapman–Jouguet (CJ) point, which itself is found from the Hugoniot curve of the system by its first derivative. These calculations are based on the density recalculated from the corresponding crystal densities by Equation S2 (av = 1.5x10^{-4} K) and on the calculated enthalpies of formation.

$$d_{298K} = \frac{d_T}{1+ \alpha_v(298-T_0)} \quad \text{(S2)}$$

d_T = insert X-ray density in g cm^{-3}

T_0 = insert X-Ray temperature in K

α_v = correction factor

Table S3. X-Ray and recalculated densities of **2**, **5** and **6**.

	X-Ray density [g cm-3]	Density recalculated to 298K [g cm^{-3}]
2	(@ 101K) 1.731	1.681
5	(@ 102K) 1.590	1.589
6	(@ 173K) 1.796	1.763

6.6.8 References SI

[S1] NATO standardization agreement (STANAG) on explosives, impact sensitivity tests, no. 4489, 1st ed, Sept. 17, **1999**.

[S2] WIWEB-Standardarbeitsanweisung 4-5.1.02, Ermittlung der Explosionsgefährlichkeit, hier der Schlagempfindlichkeit mit dem Fallhammer. Nov. 8, **2002**.

[S3] "http://www.bam.de", accessed March **2022**.

[S4] NATO standardization agreement (STANAG) on explosive, friction sensitivity tests. no. 4487, 1st ed., Aug. 22, **2002**.

[S5] WIWEB-Standardarbeitsanweisung 4-5.1.03, Ermittlung der Explosionsgefährlichkeit oder der Reibeempfindlichkeit mit dem Reibeapparat. Nov. 8, **2002**.

[S6] Impact: insensitive > 40 J, less sensitive ≥ 35 J, sensitive ≥ 4 J, very sensitive ≤ 3 J, Friction: insensitive > 360 N, less sensitive = 360 N, sensitive < 360 N and > 80 N, very sensitive ≤ 80 N, extremely sensitive ≤ 10 N. According to the UN Recommendations on the Transport of Dangerous Goods, (+) indicates not safe for transport.

[S7] CrysAlisPro, Oxford Diffraction Ltd., version 171.33.41, **2009**.

[S8] A. Altomare, G. Cascarano, C. Giacovazzo, A. Guagliardi, *J. Appl. Crystallogr* **1993**, *26*, 343−350.

[S9] a) A. Altomare, G. Cascarano, C. Giacovazzo, A. Guagliardi, A. G. G. Moliterni, SIR97 **1997**; b) A. Altomare, M. C. Burla, M. Camalli, G. L. Cascarano, C. Giacovazzo, A., *J. Appl. Crystallogr*. **1999**, *32*, 115−119.

[S10] G. M. Sheldrick, *Acta Crystallogr. Sect. A* **2008**, *A64*, 112−122.

[S11] G. M. Sheldrick, SHELXL-97, Program for the Refinement of Crystal, University of Göttingen, Germany, **1997**.

[S12] A. L. Spek, PLATON, A Multipurpose Crystallographic Tool, Utrecht University **1999**.

[S13] L. J. Farrugia, *J. Appl. Cryst.* **2012**, *45*, 849−854.

[S14] a) Empirical absorption correction using spherical harmonics, implemented in SCALE3 ABSPACK scaling algorithm (CrysAlisPro Oxford Diffraction Ltd., Version 171.33.41, 2009); b) APEX3. Bruker AXS Inc., Madison, Wisconsin, USA.

[S15] M. J. Frisch, G. W. Trucks, H. B. Schlegel, G. E. Scuseria, M. A. Robb, J. R. Cheeseman, G. Scalmani, V. Barone, B. Mennucci, G. A. Petersson, H. Nakatsuji, M. Caricato, X. Li, H.P. Hratchian, A. F. Izmaylov, J. Bloino, G. Zheng, J. L. Sonnenberg, M. Hada, M. Ehara, K. Toyota, R. Fukuda, J. Hasegawa, M. Ishida, T. Nakajima, Y. Honda, O. Kitao, H. Nakai, T. Vreven, J. A. Montgomery, Jr., J. E. Peralta, F. Ogliaro, M. Bearpark, J. J. Heyd, E. Brothers, K. N. Kudin, V. N. Staroverov, R. Kobayashi, J. Normand, K. Raghavachari, A. Rendell, J. C. Burant, S. S. Iyengar, J. Tomasi, M. Cossi, N. Rega, J. M. Millam, M. Klene, J. E. Knox, J. B. Cross, V. Bakken, C. Adamo, J. Jaramillo, R. Gomperts, R. E. Stratmann, O. Yazyev, A. J. Austin, R. Cammi, C. Pomelli, J. W. Ochterski, R. L. Martin, K. Morokuma, V. G. Zakrzewski, G. A. Voth, P. Salvador, J. J. Dannenberg, S. Dapprich, A. D. Daniels, O. Farkas, J.B. Foresman, J. V. Ortiz, J. Cioslowski, D. J. Fox, Gaussian 09 A.02, Gaussian, Inc., Wallingford, CT, USA, **2009**.

[S16] a) J. W. Ochterski, G. A. Petersson, and J. A. Montgomery Jr., *J. Chem. Phys.* **1996**, *104*, 2598−2619; b) J. A. Montgomery Jr., M. J. Frisch, J. W. Ochterski G. A. Petersson, *J. Chem. Phys.* **2000**, *112*, 6532−6542; c) L. A. Curtiss, K. Raghavachari, P. C. Redfern, J. A. Pople, *J. Chem. Phys.* **1997**, *106*, 1063−1079; d) E. F. C. Byrd, B. M. Rice, *J. Phys. Chem. A* **2006**, *110*, 1005–1013; e) B. M. Rice, S. V. Pai, J. Hare, *Comb. Flame* **1999**, *118*, 445–458.

[S17] a) H. D. B. Jenkins, H. K. Roobottom, J. Passmore, L. Glasser, *Inorg. Chem.* **1999**, *38*, 3609–3620; b) H. D. B. Jenkins, D. Tudela, L. Glasser, *Inorg. Chem.* **2002**, *41*, 2364–2367.

[S18] M. Sućeska, EXPLO5 V6.06.01, Zagreb (Croatia) **2021**.

[S19] M. Sućeska, *Propellants, Explos., Pyrotech.* **1991**, *16*, 197–202.

7 Nitraza/Oxa-propylene- and Hydrazonemethylene-bridged 1,2,4-Nitraminotriazoles and Selected Salts

Alexander G. Harter, Thomas M. Klapötke,* Burkhard Krumm, Jasmin T. Lechner, Christian Riedelsheimer

as published in *European Journal of Organic Chemistry* **2023**, *26*, e202300302

DOI: 10.1002/ejoc.202300302

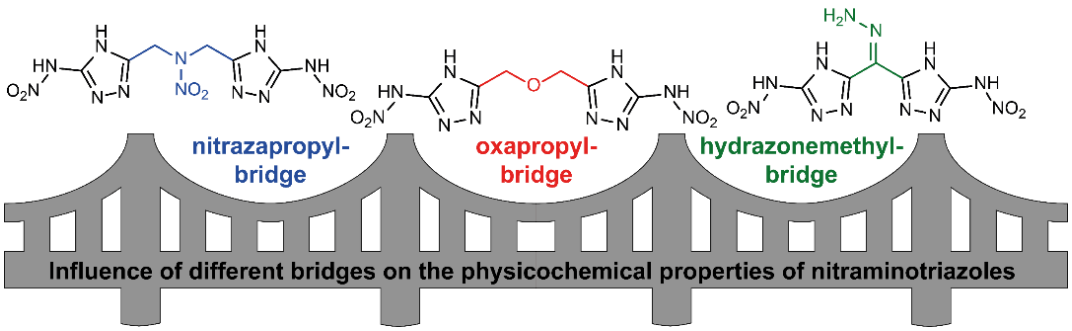

Abstract: Two new bridged nitraminotriazoles with bridging oxapropylene and nitrazapropylene moieties were synthesized, and converted into several salts, as well as from the hydrazonemethylene bridged nitraminotriazole. All compounds were fully characterized by NMR and IR spectroscopy, elemental analysis as well as differential thermal analysis. The sensitivity towards friction and impact were determined according to BAM standard technics and the energetic properties were calculated by using the EXPLO5 computer code. The neutral compounds as well as the various salts were examined in terms of their physicochemical properties and detonation performance to each other and compared to the commonly used secondary explosive RDX.

7.1 Introduction

Energetic materials are widely used in both civilian and military applications. For this reason, there is a constant search for production improvements of already known compounds, but there is also research on new energetic compounds exhibiting better properties, such as easier synthesis, or more environmentally friendly production.[1-3] Current research shows that nitrogen-rich heterocycles such as triazoles, tetrazoles or oxadiazoles are promising units for new high-energy materials (HEMs), because of their high heat of formation, good densities, high thermal stability, good detonation performance and low sensitivities.[4-7] In addition, these HEMs mainly decompose into non-toxic nitrogen gas, which is very important in terms of green chemistry.[7]

HEMs based on 1,2,4-triazoles are of interest for new potential secondary explosives. Their main advantages stem from typically low sensitivity towards heat or mechanical stimuli.[7] One of the best known and studied examples is nitrotriazolone (NTO), which exhibits low sensitivity as well as high thermal stability, and further can be used as a stabilizer for more sensitive and thermally labile compounds. [8] Other examples are PATO (3-picrylamino-1,2,5-triazoles) and NNTF (3-nitro-4-(5-nitro-1,2,4-triazol-3-yl)furazan), which show potential for use as secondary explosives (Figure 1). [9,10]

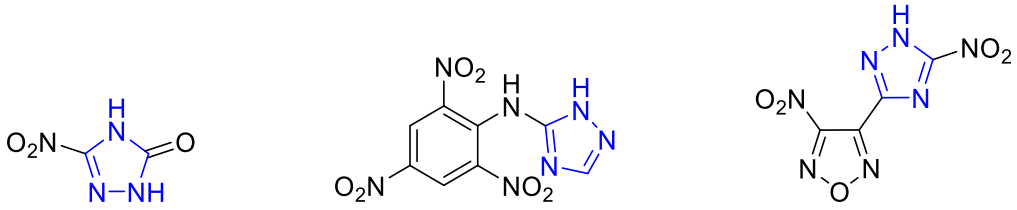

Figure 1. Examples of 1,2,5-triazole based secondary explosives.

In order to further improve specific properties, bridged azoles became of more interest. By variation of azoles and bridging moieties, a wide selection of new energetic molecules is possible with varying properties.[11-13] Azo bridges for example increase the nitrogen content and energy of the molecule, but can lead on the other hand to an increased sensitivity compared to the azole itself.[14] In contrast, short alkyl bridges can increase thermal stability, but could decrease the sensitivity.[15] A selection of various bridging moieties are shown in Figure 2, such as the methylene, azo, oxapentylene and nitrazapropylene bridging unit.

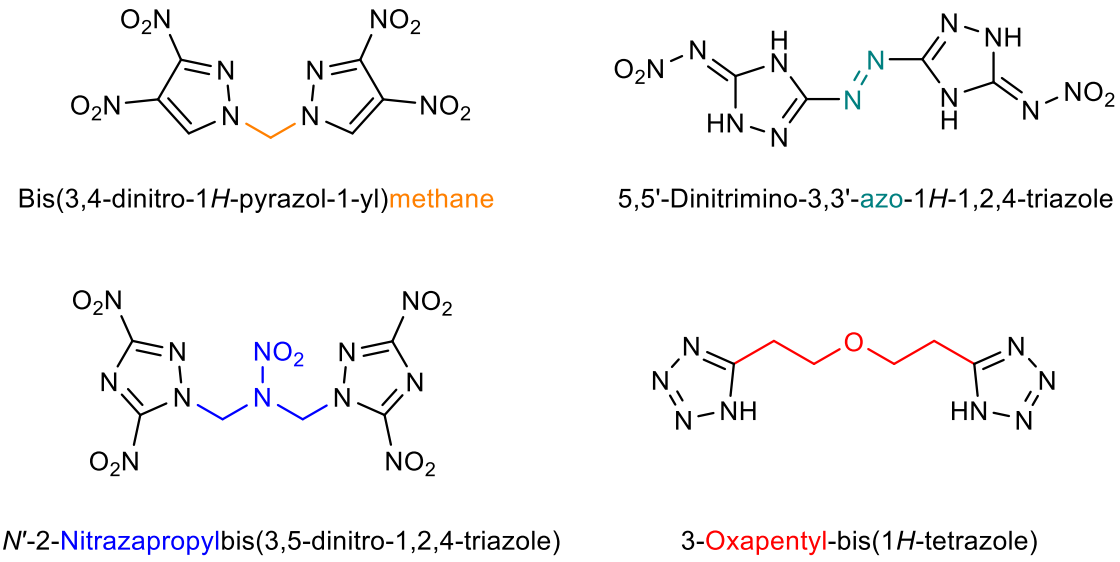

Figure 2. A selection of various bridged azoles.[15-18]

By using different bridges with the same azole moiety, the properties of the new compounds may vary. Since 1,2,4-triazoles have good properties, such as low sensitivity and high thermal stability, this work aims to synthesize and characterize new bridged nitramino-1,2,4-triazoles and compare their properties with each

other. The bridging units were selected to vary the oxygen and nitrogen content for a comparison in terms of thermal stability, sensitivities and energetic performance. In addition, several salts could be accessible via the acidic hydrogen of the nitramine moiety and their properties discussed.

7.2 Results and Discussion

7.2.1 Synthesis

Via a three-step procedure as shown in Scheme 1, starting from easily available iminodiacetic acid, diacetylnitramino dihydrazide was prepared.[19] Subsequent reaction with freshly synthesized *N*-methyl-*N*-nitroso-*N*′-nitro-guanidine[20] resulted in the formation of diacetylnitramino-bis-*N*-amino-nitroguanidine (**1**). The cyclization to the nitrazapropylene bridged triazole was accomplished under basic conditions, followed by nitration to the nitraminotriazole 1,3-bis(3-nitramino-4*H*-1,2,4-triazol-5-yl) 2-nitrazapropane (**2**, BNATNP) (Scheme 1).

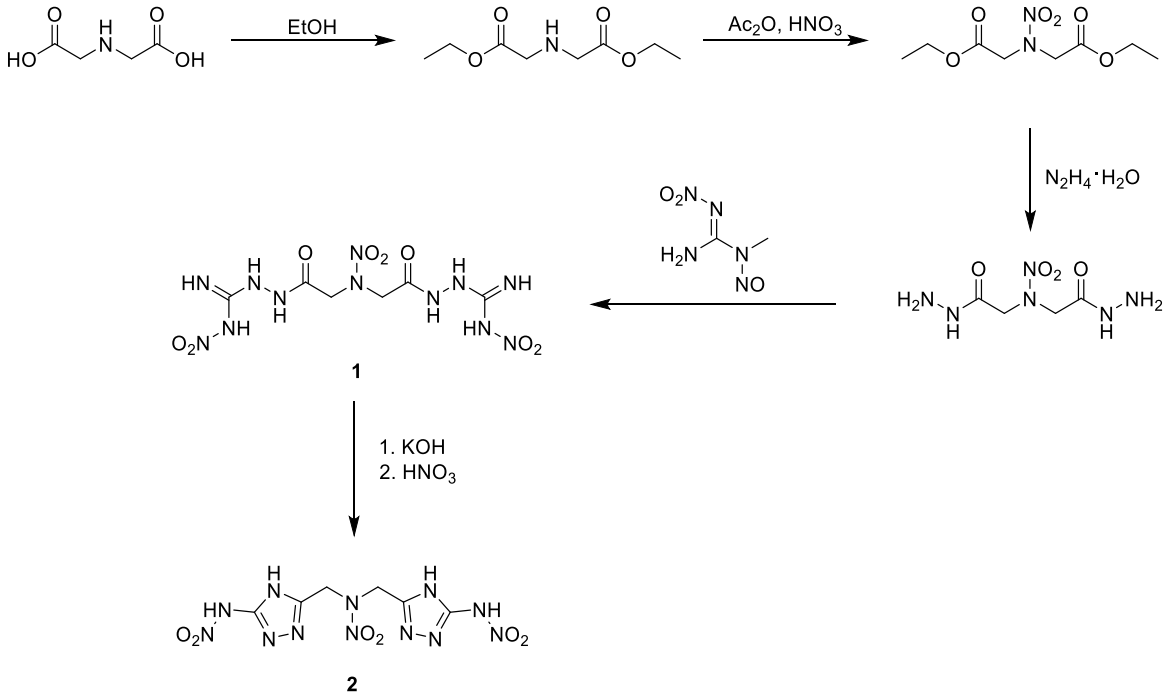

Scheme 1. Synthetic route towards 1,3-bis(3-nitramino-4*H*-1,2,4-triazol-5-yl) 2-nitrazapropane (**2**, BNATNP) starting from iminodiacetic acid.

The acidic hydrogen atoms of the nitraminotriazole **2** can be deprotonated with selected organic and inorganic bases to form the corresponding salts **3**–**8** (Scheme 3). The salts were obtained pure and in quantitative yield, except for the hydroxylammonium salt, because here a mixture was obtained, which could not be further purified.

Diglycolic acid is converted into the corresponding dihydrazide in two steps.[21, 22] In a similar fashion as described before, subsequent reaction with *N*-methyl-*N*-nitroso-*N′*-nitro-guanidine furnished diacetyloxa-bis-*N*-amino-nitroguanidine (**9**). Similarly, the cyclization to the nitraminotriazole was performed to give 1,3-bis(3-nitramino-4*H*-1,2,4-triazol-5-yl) 2-oxapropane (**10**, BNATOP) (Scheme 2).

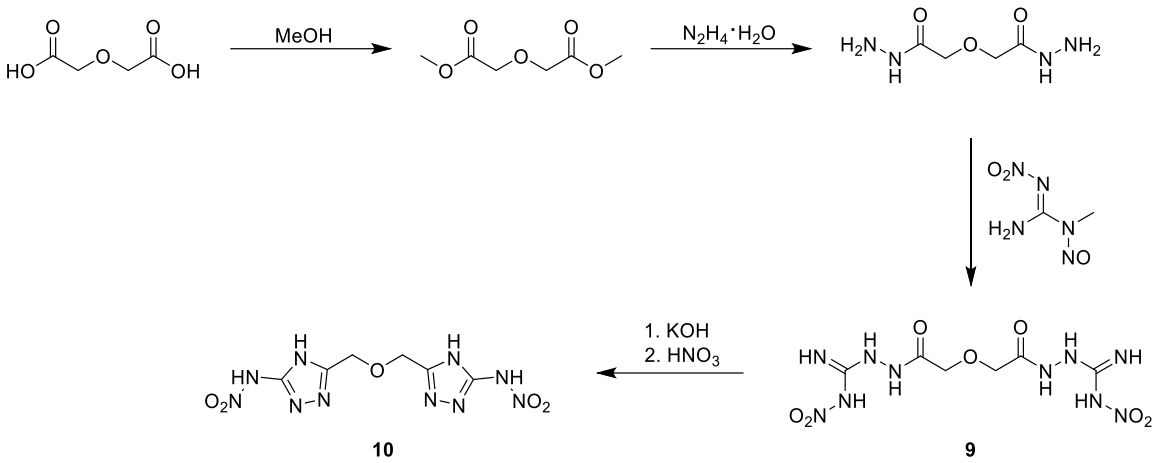

Scheme 2. Synthetic pathway towards 1,3-bis(3-nitramino-4*H*-1,2,4-triazol-5-yl) 2-oxapropane (**10**, BNATOP) starting from diglycolic acid.

The nitraminotriazole **10** is converted into salts **11–17** with same bases (Scheme 3).

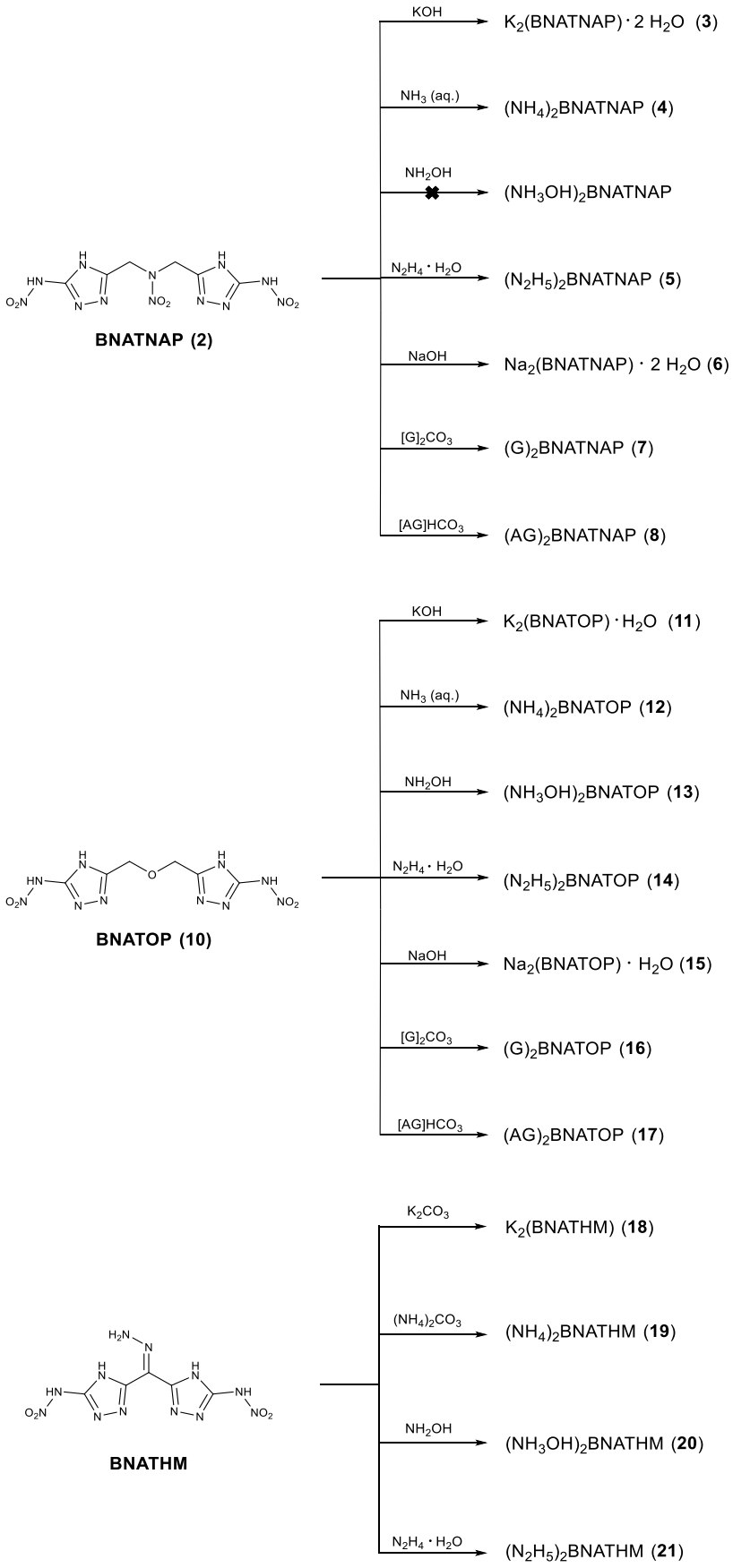

Scheme 3. Salt formation overview for BNATNAP **2** (**3**–**8**), BNATOP **10** (**11**–**17**) and BNATHM (**18**–**21**).

Finally, the hydrazono bridged nitraminotriazole, 1,3-bis(3-nitramino-4*H*-1,2,4-triazol-5-yl) hydrazonemethane (BNATHM), available in three steps from diethyl 2,2-diazidomalonate,[23] was converted into four salts **18**–**21** as shown in Scheme 3. The reaction with the other bases as applied before, did not result in uniform products.

7.2.2 NMR Spectroscopy

The characterization was performed by ^{1}H and ^{13}C{^{1}H} NMR spectroscopy in DMSO-d_6, however the restricted solubility prevented the detection of the ^{14}N resonances of the nitro groups.

Both bridging units in **2** and **10** contain methylene groups, adjacent to either nitrogen or oxygen. Those in **2** are observed in the range of 5.22–4.60 ppm, whereas those in **10** are detected at 4.62–3.94 ppm. The resonances of the nitramine and triazole hydrogen atoms are found in the region of 14.2–12.7 ppm. The corresponding ^{13}C NMR resonances were observed for the CH_2 groups at 53.7–47.2 ppm for the nitrazapropylene units and at 65.3–62.3 ppm for the oxapropylene units. The triazole resonances attached to the nitramine group are detected at 157–147 ppm and those attached to the nitraza/oxapropylene units at 159–153 ppm.

7.2.3 Crystal Structure

Suitable crystals for X-ray determination were obtained for the aminoguanidinium salt **17** by recrystallization from water. The salt crystallizes in the monoclinic space group *C*2/*c* with a density of 1.60 g cm^{-3} at 174 K. The structure as well as two different views onto the unit cell are shown in Figure 3.

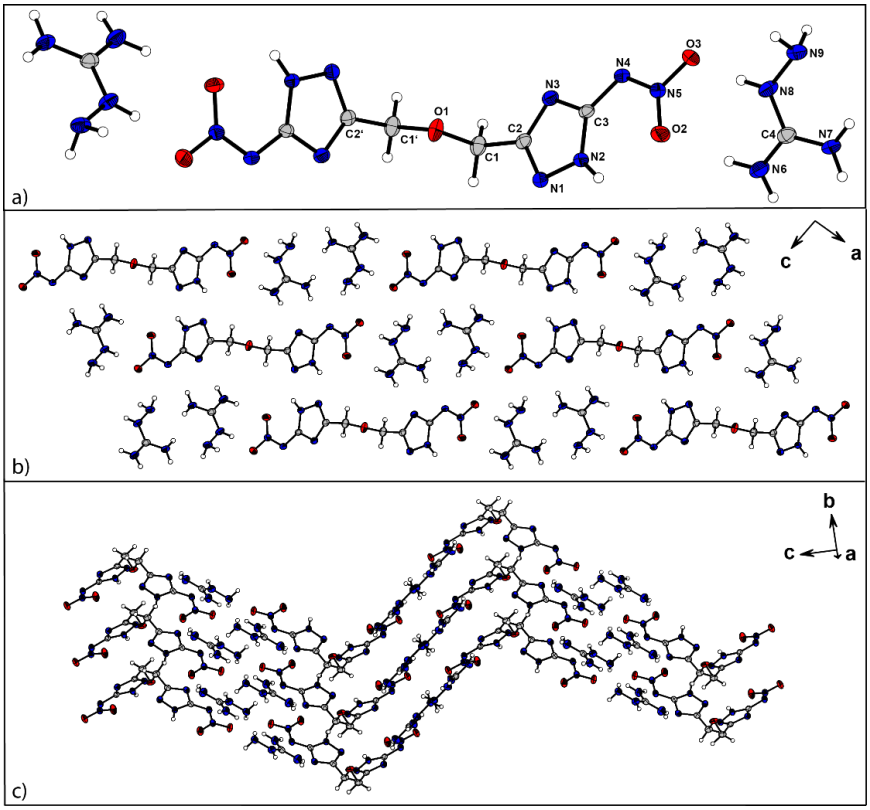

Figure 3. (a) Crystal structure of the aminoguanidinium salt **17**, showing the atom labeling. (b) View of the unit cell along the *b* axis to show the stacking. (c) View of the unit cell slightly shifted from the *a* axis to show the zigzag layers.

The C−N bond lengths of the triazole are in the range of 1.32–1.36 Å, which is quite exactly in the middle between a C−N single and double bond length.[24] For the N−N bond of the ring, the bond length is 1.36 Å, which fits perfectly for typical N−N bond length of 1,2,4-triazoles.[25] The torsions angles N3−N1−C2−N3 −0.41° and C3−N2−N1−C2 −0.03° demonstrate that the five-membered ring is nearly planar.
For the aminoguanidinium cation, same trends can be observed as for the 1,2,4-triazole ring in terms of C−N bond lengths as well as for the planarity of the molecule. The C−N bond length is between 1.32-1.34 Å, which is again in the middle of a C−N single and double bond length and the torsion angles N9−N8−C4−N7 0.0° and N9−N8−C4−N6 −179.73° indicate the planarity.
Moreover, the unit cell illustrates that along the b axis the molecules stack perfectly, and each bridged triazole is surrounded by two aminoguanidinium cations. Furthermore, in Figure 3 on the bottom (c) shows the formation of zigzag layers, in which the oxapropylene bridging units form the corners.

7.2.4 Physiochemical Properties

A full characterization in regard to the physicochemical properties was performed for all energetic compounds. This includes their sensitivities towards impact and friction, the thermal behavior, heats of formation and detonation parameters. Those were determined and compared to the state-of-the-art secondary explosive in industrial use, RDX, shown in Table 1 and Table 2. The sensitivity values towards impact and friction were determined with the 1 out of 6 method according to BAM standards.[26] The thermal properties of all compounds were determined by differential thermal analysis (DTA) in the temperature range of 25–400 °C with a heating rate of 5 °C.

Table 1. Physicochemical properties of **2**, **10** and BNATHM compared to RDX.[24]

	2	**10**	**BNATHM**	**RDX**
Formula	$C_6H_8N_{12}O_6$	$C_6H_8N_{10}O_5$	$C_5H_6N_{12}O_4$	$C_3H_6N_6O_6$
M [g·mol^{-1}]	344.21	300.20	298.18	222.12
IS[a] [J]	3	4	2.5	7.5
FS[b] [N]	360	360	360	120
N+O[c] [%]	76.72	73.31	77.83	81.06
Ω_{CO2}[d] [%]	−46	−59	−34	−22
T_{endo}[e]/ $T_{exo.}$[f] [°C]	−/159	−/187	–/177	203/208
ρ[g] [g·cm^{-3}]	1.76	1.73	1.81	1.82
$\Delta_f H°$[h] [kJ·mol^{-1}]	438	266	541	87
EXPLO5 V6.05				
$-\Delta_E U°$[i] [kJ·kg^{-1}]	6378	5664	5137	5816
$T_{C\text{-}J}$ [j] [K]	3295	2987	3624	3758
$p_{C\text{-}J}$ [k][GPa]	26.6	23.2	31.0	34.5
$D_{C\text{-}J}$ [l] [m·s^{-1}]	8233	7818	8654	8898
V_0 [m] [dm^3·kg^{-1}]	773	767	766	780

[a] Impact sensitivity (BAM drophammer, method 1 of 6); [b] friction sensitivity (BAM friction tester, method 1 of 6); [c] combined nitrogen and oxygen content; [d] oxygen balance toward carbon dioxide (Ω_{CO2}=(nO-2xC-yH/2)(1600/M)); [e] endothermic peak (DTA, β=5 °C·min^{-1}); [f] temperature of decomposition (DTA, β=5 °C·min^{-1}); [g] Densities measured by gas pycnometry; [h] standard molar enthalpy of formation; [i] detonation energy; [j] detonation temperature; [k] detonation pressure; [l] detonation velocity; [m] volume of detonation gases at standard temperature and pressure conditions.

Table 2. Physical and energetic properties of **3**–**21**.

	T_{endo}[a] [°C]	$T_{exo.}$[b] [°C]	ρ[c] [g·cm^{-3}]	$D_{C\text{-}J}$[l] [m·s^{-1}]	$p_{C\text{-}J}$ [k][GPa]	IS[d] [J]	FS[e] [N]	$\Delta_f H°$[h] [kJ·mol^{-1}]
3·2H_2O	64	207	−	−	−	20	>360	−
4	−	176	1.73	8467	26.7	6	288	312
5	−	181	1.74	8663	27.4	3	160	618
6·2H_2O	123, 132	193	−	−	−	40	>360	−
7	−	182	1.56	7460	19.1	40	>360	260
8	−	212	1.60	7903	21.7	20	>360	447
11·H_2O	143	195	−	−	−	15	>360	−
12	181	225	1.72	8263	24,4	5	280	63
13	−	191	1.72	8400	26.7	3	288	188
14	−	195	1.68	8502	25.9	5	240	358
15·H_2O	155	208	−	−	−	40	>360	−
16	−	268	1.57	7367	18.1	40	>360	41
17	−	220	$1.57^{x\text{-ray}}$	7704	20.0	25	>360	279
18	−	205	1.93	7271	20.2	10	>360	106
19	−	175	1.69	8355	25.2	2	252	399
20	−	170	1.73	8701	29.1	5	288	567
21	−	181	1.75	9197	31.4	3	252	702

[a] endothermic peak (DTA, β = 5 °C·min^{-1}); [b] temperature of decomposition (DTA, β = 5 °C·min^{-1}); [c] Densities measured by gas pycnometer if not otherwise noted; [d] detonation velocity; [e] detonation pressure; [f] Impact sensitivity (BAM drophammer, method 1 of 6); [g] friction sensitivity (BAM friction tester, method 1 of 6), [h] standard molar enthalpy of formation.

The three neutral nitraminotriazoles **2**, **10** and BNATHM differ only in the bridging unit, containing either more or less nitrogen or oxygen. This is reflected in the nitrogen and oxygen content, where it can be seen that BNATHM has the largest content with 78 %, closely followed by **2** with 77 %. Not surprisingly, **10** shows the lowest value of 73 %, since it contains only one oxygen atom in the bridging unit. However, despite the lower oxygen and nitrogen content, **10** shows a very similar sensitivity as the other compounds. All compounds show no sensitivity towards friction, but a high sensitivity towards impact in the range of 2.5–4 J. Thus, these neutral triazoles have an increased sensitivity compared to RDX, even though RDX has a higher oxygen and nitrogen content.

There were no endothermic events observed in the DTA, which could be assigned to melting points. The highest decomposition temperature shows **10** with 187 °C, followed by BNATHM with 177 °C. The lowest value was observed for **2** (159 °C), which could be due to the nitramino group of the bridging unit, which are often thermally labile.

Regarding the densities, the triazoles show quite similar values of 1.73–1.81 g cm^{-3}, which are in the same range as RDX. Based on the densities, obtained by gas pycnometer, and the heats of formation, obtained by CBS-4M calculations, the energetic properties were calculated with EXPLO5 (V6.05).[27] The calculated detonation velocities and pressures follow the same trend as the nitrogen and oxygen content. BNHATHM shows the highest N+O content (78 %) as well as the highest energetic parameters ($D_{C\text{-}J}$=8654 m s^{-1}, $p_{C\text{-}J}$=31.0 GPa), whereas **10** shows the lowest N+O content (73 %) and in turn the lowest detonation velocity and pressure ($D_{C\text{-}J}$=7818 m s^{-1}, $p_{C\text{-}J}$=32.2 GPa). In summary, BNATHM shows the best values, which cannot surpass RDX. However, **10** shows higher thermal stability, as well as lower sensitivities than BNATHM, which is also associated with lower energetic properties.

For the total of 17 new salts, there is a clear trend towards increased thermal stability, with the exception of salts **18**–**21** based on BNATHM, which decompose in the same range as the neutral compound. The highest decomposition temperature was observed for guanidinium salt **16** with 268 °C followed by ammonium salt **12** with 225 °C. All salts containing crystal water (**3**, **6**, **11**, **15**) and the ammonium salt **12** also show an endothermic event.

For all salts, the sensitivities towards impact and friction were measured. It was found that most salts are not sensitive towards friction, except for the ammonium, hydrazinium and hydroxylammonium salts (**4**–**5**, **12**–**14**, **19**–**21**), which show low sensitivities in the range of 240–290 N. The hydrazinium salt **5** is the only salt to show a higher sensitivity towards friction with a value of 160 N. For the sensitivity towards impact, the same trend was observed. The metal, guanidinium and aminoguanidinium salts (**7**–**8**, **16**–**17**, **18**) show a moderate sensitivity towards impact in the range of 10–40 J. The ammonium, hydrazinium and hydroxylammonium salts (**4**–**5**, **12**–**14**, **19**–**21**) are very sensitive towards impact with values of 2–5 J, which are in the range of primary explosives.

For the salts without crystal water, the densities were determined using a gas pycnometer, except for **16**. The density of aminoguanidinium salt **16** was recalculated to room temperature from the crystal structure. For the salts of **2** and **10**, the densities of the ammonium, hydrazinium and hydroxylammonium salts (**4**–**5**, **12**–**14**) are in the same range as the neutral compounds and for the guanidinium and aminoguanidinium salts (**7**–**8**, **16**–**17**), the densities are slightly lower. The densities of the salts of BNATHM (**18**–**21**) are lower compared to the neutral compound, except for the potassium salt **18**, which shows the highest value of all new compounds with 1.92 g cm^{-3}.

After determining the densities and calculating the heat of formation, the different energetic parameters were calculated for the various salts. The highest values were obtained again for the ammonium, hydroxylammonium and hydrazinium salts (**4**–**5**, **12**–**14**, **19**–**21**) with values above 8200 m s^{-1}. Overall, the hydrazinium salts (**5**, **14** and **21**) show the highest values from 8500 m s^{-1} for **14** to 9200 m s^{-1} for **21**. The guanidinium and aminoguanidinium salts (**7**–**8**, **16**–**17**) show the lowest values from 7200–7900 m s^{-1}, which are even lower compared to their neutral compounds.

In summary, the hydrazinium salts show the best overall properties in terms of thermal stability and energetic parameters. However, these compounds are also very sensitive to impact.

7.3 Conclusion

Two new nitrazapropylene and oxapropylene bridged nitraminotriazoles, as well as the hydrazonemethylene bridged derivative, along with some of their salts were prepared and characterized. From easily available starting materials iminodiacetic and diglycolic acids, via the corresponding nitroguanidines, the triazoles are accessible. Furthermore, a detailed investigation on their physicochemical and energetic properties was performed. As a result from the comparison of the bridging units, the nitrazapropylene bridge has the lowest thermal stability, probably due to the thermally labile nitram ino group, though improving the energetic parameters. The oxapropylene bridge prevents an increase in the energetic properties, but increases the thermal stability. The overall most balanced

nitraminotriazole is BNATHM, with moderate thermal stability and the best energetic properties.

The salts confirm the same trends but with increased thermal stability; for those with nitrogen-rich cations, the energetic properties are also further enhanced. However, the triazoles and salts with a detonation velocity exceeding 8000 m s^{-1} are very sensitive towards impact in the range of primary explosives.

7.4 Experimental Section

Solvents, deuterated solvents and all further chemicals were used as received from suppliers, without further purification. The hydrazide precursors for **1** and **9** were synthesized according to literature procedures.[19, 21, 22]

^{1}H and $^{13}C\{H\}$ NMR spectra were recorded with a Bruker 400 MHz spectrometer at ambient temperature. The chemical shifts were referenced with respect to external Me_4Si (^{1}H 399.8 MHz; ^{13}C 100.5 MHz).

Infrared spectra were recorded at ambient temperature in the range 4000–400 cm^{-1} on a Perkin-Elmer Perkin-Elmer BXII FTIR system with a Smith DuraSampler IR II diamond ATR.

Analyses of C/H/N contents were performed with an Elementar vario EL or Elementar vario micro cube. Melting and decomposition temperatures of the described compounds were measured through differential thermal analysis (DTA) with an OZM Research DTA 552-Ex instrument. The samples were measured in a range of 25–400 °C at a heating rate of 5 °C min^{-1}.

The sensitivities towards impact and friction were determined with a BAM drop hammer[28] and a BAM friction tester.[29]

Single crystal X-ray diffraction study was performed on an Oxford Diffraction Xcalibur3 diffractometer with a generator (voltage 50 kV, current 40 mA) and a KappaCCD area detector operating with Mo−Kα radiation (λ=0.7107 Å). The data collection was performed using the CRYSTALIS RED software.[30] The solution of the structure was performed by direct methods and refined by full-matrix least-squares on F2 (SHELXT)[31] implemented in the OLEX2 software suite.[32] All non-hydrogen atoms were refined anisotropically and the hydrogen atoms were located and freely refined. DIAMOND plots are shown with thermal ellipsoids at the 50 %

probability level and the hydrogen atoms are shown as small spheres of arbitrary radius.

Information on the X-ray measurements and refinements are given in the Supporting Information. Deposition Number 2247722 (for **17**) contains the supplementary crystallographic data for this paper. These data are provided free of charge by the joint Cambridge Crystallographic Data Centre and Fachinformationszentrum Karlsruhe Access Structures service.

All quantum chemical calculations were carried out using the Gaussian G09 program package.[33] The enthalpies (H) and free energies (G) were calculated using the complete basis set (CBS) method of Petersson and co-workers in order to obtain very accurate energies. The CBS models are using the known asymptotic convergence of pair natural orbital expressions to extrapolate from calculations using a finite basis set to the estimated CBS limit. CBS-4 starts with an HF/3-21G(d) geometry optimization; the zero-point energy is computed at the same level. It then uses a large basis set SCF calculation as a base energy, and an MP2/6-31+G calculation with a CBS extrapolation to correct the energy through second order. A MP4(SDQ)/6-31+ (d,p) calculation is used to approximate higher order contributions. In this study, we applied the modified CBS-4M.[34, 35]

Caution: The compounds discussed here are sensitive materials. Therefore, it is recommended to carry out all reactions on a small scale, using the proper safety equipment, including ear, hand and body protection.

Diacetylnitramino-bis-*N*-amino-nitroguanidine (1): A suspension of *N*-methyl-*N*-nitroso-nitroguanidine (720 mg, 7.06 mmol, 2.1 equiv.) in 10 mL of water was added to a solution of diacetylnitramino dihydrazide (693 mg, 3.36 mg, 1 equiv.) in 10 mL of water and heated to 55 °C for 2 h during which a grey precipitate formed. Cooling to room temperature, filtration and washing with water yielded **1** as an off-white solid (1.03 g, 79 %). **^{1}H NMR** (400 MHz, DMSO-d_6): δ (ppm)=10.37 (s, 2H, N*H*), 9.77 (s, 2H, N*H*), 8.76 (s, 2H, N*H*), 8.17 (s, 2H, N*H*), 4.60 (s, 4H, CH_2); **^{13}C{^{1}H} NMR** (101 MHz, DMSO-d_6): δ (ppm)=166.4 (*C*O), 160.9 (*C*(NH)), 53.7 (*C*H); **IR** (ATR, rel. int.): $\tilde{\nu}$ (cm^{-1})=3963 (w), 3909 (w), 3826 (w), 3783 (w), 3692 (w), 3468 (m), 3393 (w), 3297 (w), 3198 (w), 3069 (w), 2988 (w), 2952 (w), 2617 (w), 2486 (w), 2432 (w), 2336 (w), 2228 (w), 2173 (w), 2126 (w), 2095 (w), 2044 (w), 1993 (w), 1880 (w), 1845 (s), 1714 (s), 1629 (s), 1516 (s), 1420 (s), 1380 (s), 1348 (s),

1286 (m), 1244 (m), 1152 (m), 1083 (s), 1025 (s), 970 (s), 812 (s), 774 (s), 703 (s), 646 (s), 558 (s), 493 (s); **Elemental analysis**: calcd. (%) for $C_6H_{18}N_{12}O_{11}$ (380.24 g mol^{-1}): C 16.59, H 4.18, N 38.70; found C 16.80, H 4.09, N 38.40; **DTA** (5 °C min^{-1}): T_{endo}=111 °C, T_{exo}=154 °C.

1,3-Bis(3-nitramino-4*H*-1,2,4-triazol-5-yl) 2-nitrazapropane (2): A suspension of **1** (937 mg, 2.40 mmol, 1 equiv.) in 10 mL of water was added to a solution of potassium hydroxide (345 mg, 6.10 mmol, 3 equiv.) in 10 mL of water. The resulting crimson solution was stirred at room temperature for 24 h. Afterwards the solution was cooled to 0 °C and brought to pH 4 using nitric acid (65 %) during which a crimson precipitate formed. The solution was immediately filtered and the filtrate was stirred at room temperature for 1 h during which an off-white precipitate formed. Filtration and washing with water and cold ethanol yielded an off-white solid. The crude product was recrystallized from methanol to yield **2** as an off-white powder (232 mg, 28 %). **^{1}H NMR** (400 MHz, DMSO-d_6): δ (ppm)=14.21 (s, 2H, N*H*), 5.22 (s, 4H, CH_2); **^{13}C{^{1}H} NMR** (101 MHz, DMSO-d_6): δ (ppm)=153.1 (*C*−CH_2), 146.0 (*C*-NH), 47.2 (*C*H_2); **IR** (ATR, rel. int.): $\tilde{\nu}$(cm^{-1})=3587 (m), 3536 (m), 3363 (m), 3202 (m), 3145 (m), 3038 (m), 2962 (m), 2825 (s), 2719 (s), 2583 (m), 2183 (m), 2129 (m), 2095 (w), 2008 (w), 1973 (w), 1863 (w), 1721 (w), 1604 (w), 1544 (w), 1505 (w), 1417 (w), 1323 (w), 1228 (w), 1092 (w), 1017 (w), 990 (w), 937 (w), 849 (w), 762 (w), 707 (w), 655 (w), 616 (w), 449 (w); **Elemental analysis**: calcd. (%) for $C_6H_8N_{12}O_6$ (344.21 g mol^{-1}): C 20.94, H 2.34, N 48.83; found C 21.17, H 2.25, N 48.55; **Sensitivities** (grain size 100–500 µm): impact 3 J, friction 360 N; **DTA** (5 °C min^{-1}): T_{exo}=164 °C.

Salt formation of 2 – General Procedure

The bis-triazole **2** (0.500 g, 1.45 mmol) was suspended in 5 mL water and two equivalents of various bases (potassium/sodium hydroxide, 2 M ammonia solution, hydrazine monohydrate, guanidinium carbonate and aminoguanidinium bicarbonate) were added. The mixtures were stirred until the liquid turned clear. Afterwards, the solvent was removed at 80 °C overnight to obtain the desired salt in 94 % for **5** (562 mg), and quantitative yield for **3** · 2 H_2O (662 mg), **4** (548 mg), **6** · 2 H_2O (615 mg), **7** (670 mg), **8** (714 mg).

Diglycolic acid-bis(*N*-amino-nitroguanidine) (9): Diglycolic acid dihydrazide (1.62 g, 10.0 mmol, 1 equiv.) was dissolved in water (20 mL) and N-methyl-N-nitroso-N'-nitroguanidine (2.94 g, 20.0 mmol, 2 equiv.), suspended in water (50 mL) was added. The mixture was stirred for 3 h at 95 °C, cooled to 0 °C, the precipitate filtered and washed with cold water and cold EtOH. After drying at room temperature, **9** (2.66 g, 79 %) was obtained as a colorless solid. **^{1}H NMR** (400 MHz, DMSO-d_6): δ (ppm)=10.03 (s, 2H, NH), 9.7 (br, 2H, NH), 8.7 (br, 2H, NH), 8.2 (br, 2H, NH), 4.14 (s, 4H, CH_2); **^{13}C{^{1}H} NMR** (101 MHz, DMSO-d_6): δ (ppm)=168.8 (*C*O), 161.1 (*C*<*C*->NH), 69.8 (*C*H_2); **IR** (ATR, rel. int.): $\tilde{\nu}$ (cm^{-1})=3387(m), 3351(w), 3332(w), 3301(m), 3255(w), 3182(m), 3176(m), 3062(m), 2970(w), 2930(w), 1738(w), 1699(s), 1642(s), 1587(s), 1564(m), 1507(m), 1423(m), 1378(s), 1352(s), 1318(vs), 1272(s), 1244(s), 1187(s), 1187(s), 1085(s), 1048(m), 1031(m), 990(w), 923(w), 784(w), 753(s), 616(vs), 564(m), 537(s), 507(m), 481(vs), 437(s); **Elemental analysis**: calcd. (%) for $C_6H_{12}N_{10}O_7$ (336.23 g mol^{-1}): C 21.43; H 3.60; N 40.80. Found: C 21.49; H 3.84; N 40.80; **DTA** (5 °C min^{-1}): T_{exo}=193 °C.

1,3-Bis(3-nitramino-4*H*-1,2,4-triazol-5-yl) 2-oxapropane (10):

Diglycolic-di-*N*-amino-nitroguanidine (**9**) (1.00 g, 2.94 mmol, 1 equiv.) was dissolved in water (20 mL) and KOH (500 mg, 8.93 mmol, 3.0 equiv.), dissolved in water (15 mL), was added. The mixture was stirred overnight at 80 °C. The clear solution was cooled to 50 °C and acidified to pH 3 with HNO_3 (65 %). The resulting suspension was cooled to 0 °C, the precipitate filtered, washed with cold water and dried for two days at 100 °C to yield **10** (610 mg, 68 %) as a beige solid.**^{1}H NMR** (400 MHz, DMSO-d_6): δ (ppm)=14.2 (br, 2H, NH), 4.62 (s, 4H, CH_2);**^{13}C{^{1}H} NMR** (101 MHz, DMSO-d_6): δ (ppm)=153.0 (*C*−CH_2), 147.5 (*C*-NNO_2), 62.4 (*C*H_2); **IR** (ATR, rel. int.): $\tilde{\nu}$ (cm^{-1})=3341(w), 3223(w), 2665(w), 2578(w), 1607(s), 1567(s), 1501(m), 1447(m), 1427(m), 1412(m), 1309(s), 1234(vs), 1210(s), 1127(s), 1098(s), 1015(m), 995(s), 951(m), 905(m), 870(m), 853(m), 803(w), 774(s), 774(s), 748(w), 713(s), 688(s), 665(m), 655(m), 603(m), 591(m), 575(m), 570(m), 545(m), 528(m), 484(m), 467(s), 444(s), 426(w), 420(w); **Elemental analysis**: calcd. (%) for $C_6H_8N_{10}O_5$ (300.20 g mol^{-1}): C 24.01; H 2.69; N 46.66; found: C 23.84; H 2.76;

N 46.30; **Sensitivities** (grain size 100–500 µm): impact 4 J, friction >36 N; **DTA** (5 °C min^{-1}): T_{exo}=187 °C.

Salt formation of **10** – General Procedure

The bis-triazole **10** (0.500 g, 1.67 mmol) was suspended in 5 mL water and two equivalents of various bases (potassium/sodium hydroxide, 2 M ammonia solution, 50 % aqueous hydroxylamine solution, hydrazine monohydrate, guanidinium carbonate and aminoguanidinium bicarbonate) were added. The mixtures were stirred until the liquid turned clear. Afterwards, the solvent was removed at 60 °C overnight to obtain the desired salt in 73 % (**11** · $2H_2O$, 480 mg), 63 % (**12**, 352 mg), 67 % (**13**, 410 mg), 72 % (**14**, 438 mg), 86 % (**15** · H_2O, 520 mg), 89 % (**16**, 622 mg) and 91 % (**17**, 681 mg) yield.

Salt formation of BNATHM – General Procedure

Bis(3-nitramino-4*H*-1,2,4-triazol-5-yl) hydrazonemethane (BNATHM, 0.200 g, 0.67 mmol) was suspended in 10 mL water and two equivalents of various bases (potassium hydroxide, ammonium carbonate, 50 % aqueous hydroxylamine solution, hydrazine monohydrate) were added. The mixtures were stirred for 1 h at 80 °C. Afterwards, the solvent was removed at 50 °C overnight to obtain the desired salt in 70 % (**18**, 177 mg), 46 % (**19**, 102 mg), 68 % (**20**, 167 mg), 72 % (**21**, 176 mg) yield.

7.5 Acknowledgments

For financial support of this work by the Ludwig-Maximilian University (LMU), the Office of Naval Research (ONR) under grant no. ONR N00014-19-1-2078 and the Strategic Environmental Research and Development Program (SERDP) under contract no. W912HQ19C0033 are gratefully acknowledged. The authors thank Stefan Huber for his help with the sensitivity measurement, as well as research students Marc Fimm and Luca Parziale for working on parts of this project. Open Access funding enabled and organized by Projekt DEAL.

7.6 References

[1] D. M. Badgujar, M. B. Talawar, S. N. Asthana, P. P. Mahulikar, *J. Hazard. Mater.* **2008**, *151*, 289-305.

[2] M. B. Talawar, R. Sivabalan, T. Mukundan, H. Muthurajan, A. K. Sikder, B. R. Gandhe, A. S. Rao, *J. Hazard. Mater.* **2009**, *161*, 589-607.

[3] P. F. Pagoria, G. S. Lee, A. R. Mitchell, R. D. Schmidt, *Thermochim. Acta* **2002**, *384*, 187-204.

[4] Y. Tang, Z. Yin, A. K. Chinnam, R. J. Staples, J. M. Shreeve, *Inorg. Chem.* **2020**, *59*, 17766-17774.

[5] M. Benz, T. M. Klapötke, J. Stierstorfer, M. Voggenreiter, *ACS Appl. Eng. Mater.* **2022**, *1*, 3-6.

[6] H. Dou, P. Chen, C.-l. He, S.-p. Pang, *Energetic Materials Frontiers* **2022**, *3*, 154-160.

[7] T. M. Klapötke, *Chemistry of High-Energy Materials*, 6 ed., De Gruyter, Berlin, **2022**.

[8] R. R. Sirach, P. N. Dave, *Chem. Heterocycl. Compd.* **2021**, *57*, 720-730.

[9] P. Leonard, P. Bowden, M. Shorty, M. Schmitt, *Propellants Explos. Pyrotech.* **2019**, *44*, 203-206.

[10] Z. Xu, G. Cheng, H. Yang, J. Zhang, J. M. Shreeve, *Chem. Eur. J.* **2018**, *24*, 10488-10497.

[11] Q. Xue, F.-q. Bi, J.-l. Zhang, Z.-j. Wang, L.-j. Zhai, H. Huo, B.-z. Wang, S.-y. Zhang, *Front. Chem.* **2020**, *7*, 942.

[12] S. Zhang, Z. Gao, D. Lan, Q. Jia, N. Liu, J. Zhang, K. Kou, *Molecules* **2020**, *25*, 3475.

[13] Q. Lai, T. Fei, P. Yin, J. M. Shreeve, *Chem. Eng. J.* **2021**, *410*, 128148.

[14] A. K. Chinnam, Q. Yu, G. H. Imler, D. A. Parrish, J. M. Shreeve, *Dalton Trans.* **2020**, *49*, 11498-11503.

[15] M. F. Bölter, T. M. Klapötke, T. Kustermann, T. Lenz, J. Stierstorfer, *Eur. J. Inorg. Chem.* **2018**, 4125-4132.

[16] A. Dippold, T. M. Klapötke, F. A. Martin, *Z. Anorg. Allg. Chem.* **2011**, *637*, 1181-1193.

[17] T. M. Klapötke, A. Penger, C. Pflüger, J. Stierstorfer, M. Sućeska, *Eur. J. Inorg. Chem.* **2013**, *2013*, 4667-4678.

[18] A. Chafin, D. J. Irvin, M. H. Mason, S. L. Mason, *Tetrahedron Lett.* **2008**, *49*, 3823-3826.

[19] T. M. Klapötke, B. Krumm, T. Reith, *Propellants Explos. Pyrotech.* **2018**, *43*, 685-693.

[20] A. F. McKay, G. F. Wright, *J. Am. Chem. Soc.* **1947**, *69*, 3028-3030.

[21] X. X. Sun, Y. C. Li, L. Li, Y. Hu, *Adv. Mater. Res.* **2012**, *430-432*, 205-208.

[22] B. D. Parthiban, S. Saxena, M. Chandran, P. S. Jonnalagadda, R. Yadav, R. R. Srilakshmi, Y. Perumal, S. Dharmarajan, *Chem. Biol. Drug Des.* **2016**, *87*, 265-274.

[23] A. G. Harter, T. M. Klapötke, C. Riedelsheimer, J. Stierstorfer, S. M. Strobel, M. Voggenreiter, *Eur. J. Inorg. Chem.* **2022**, e202200100.

[24] F. H. Allen, O. Kennard, D. G. Watson, L. Brammer, A. G. Orpen, R. Taylor, *J. Chem. Soc., Perkin Trans. 2* **1987**, S1-S19.

[25] E. Garcia, K.-Y. Lee, *Acta Crystallogr.* **1992**, *C48*, 1682-1683.

[26] Test methods according to the UN Recommendations on the Transport of Dangerous Goods., *Manual of Test and Criteria*, 4th revised ed., United Nations Publication: New York and Geneva, 2003, ISBN 92-1-139087-7, Sales No. E.03.VIII.2; 13.4.2 Test 3 a (ii) BAM Fallhammer.

[27] M. Sućeska, *EXPLO5 V6.05 program*, Brodarski Institute: Zagreb, Croatia, **2020**.

[28] NATO Standardization Agreement 4489 (STANAG 4489), *Explosives, Friction Sensitivity Tests*, Brussels, Belgium, **1999**.

[29] NATO Standardization Agreement 4487 (STANAG 4487), *Explosives, Friction Sensitivity Tests*, Brussels, Belgium, **2002**.

[30] *CrysAlisPro*, Oxford Diffraction Ltd., *version 171.33.41*, **2009**.

[31] G. M. Sheldrick, *Acta Crystallogr.* **2015**, *A71*, 3-8.

[32] O. V. Dolomanov, L. J. Bourhis, R. J. Gildea, J. A. K. Howard, H. Pushmann, *J. Appl. Cryst.* **2009**, *42*, 339-341.

[33] M. J. Frisch, G. W. Trucks, H. B. Schlegel, G. E. Scuseria, M. A. Robb, J. R. Cheeseman, G. Scalmani, V. Barone, G. A. Petersson, H. Nakatsuji, X. Li, M. Caricato, A. V. Marenich, J. Bloino, B. G. Janesko, R. Gomperts, B. Mennucci, H. P. Hratchian, J. V. Ortiz, A. F. Izmaylov, J. L. Sonnenberg, Williams, F. Ding, F.

Lipparini, F. Egidi, J. Goings, B. Peng, A. Petrone, T. Henderson, D. Ranasinghe, V. G. Zakrzewski, J. Gao, N. Rega, G. Zheng, W. Liang, M. Hada, M. Ehara, K. Toyota, R. Fukuda, J. Hasegawa, M. Ishida, T. Nakajima, Y. Honda, O. Kitao, H. Nakai, T. Vreven, K. Throssell, J. A. Montgomery Jr., J. E. Peralta, F. Ogliaro, M. J. Bearpark, J. J. Heyd, E. N. Brothers, K. N. Kudin, V. N. Staroverov, T. A. Keith, R. Kobayashi, J. Normand, K. Raghavachari, A. P. Rendell, J. C. Burant, S. S. Iyengar, J. Tomasi, M. Cossi, J. M. Millam, M. Klene, C. Adamo, R. Cammi, J. W. Ochterski, R. L. Martin, K. Morokuma, O. Farkas, J. B. Foresman, D. J. Fox, *Gaussian 16 Rev. C.01*, Wallingford, CT, **2016**.

[34] J. A. Montgomery, M. J. Frisch, J. W. Ochterski, G. A. Petersson, *J. Chem. Phys.* **2000**, *112*, 6532-6542.

[35] J. W. Ochterski, G. A. Petersson, J. A. M. Jr., *J. Chem. Phys.* **1996**, *104*, 2598-2619.

7.7 Supporting Information

7.7.1 Characterization Details for Salts 3-8 and 11-21

Potassium 1,3-bis(3-nitramino-4H-1,2,4-triazole-5-yl) 2-nitrazapropane (**3·2H$_2$O**):

^{1}H NMR (400 MHz, DMSO-*d*$_6$): δ (ppm) = 12.81 (s, 2H, N*H*), 4.95 (s, 4H, C*H*$_2$); **^{13}C{^{1}H} NMR** (101 MHz, DMSO-*d*$_6$): δ (ppm) = 157.4 (*C*-CH$_2$), 154.0 (*C*-NNO$_2$), 48.6 (*C*H$_2$); **IR** (ATR, rel. int.): $\tilde{\nu}$ (cm^{-1}) = 3947 (w), 3907 (w), 3843 (w), 3803 (w), 3759 (w), 3676 (w), 3507 (w), 3159 (m), 3021 (w), 2896 (w), 2837 (w), 2457 (w), 2372 (w), 2265 (w), 2222 (w), 2177 (w), 2151 (w), 2084 (w), 2040 (w), 2002 (w), 1950 (w), 1831 (w), 1787 (w), 1688 (m), 1518 (m), 1427 (s), 1277 (s), 1133 (m), 1078 (m), 1001 (m), 938 (m), 862 (m), 759 (m), 656 (m), 602 (m), 560 (m), 455 (m); **Elemental analysis**: calcd. (%) for $C_6H_6K_2N_{12}O_6 \cdot 2\ H_2O$ (456.42 g mol^{-1}): C 15.79, H 2.21, N 36.83; found C 15.52, H 2.39, N 36.59; **Sensitivities** (grain size 100–500 µm): impact 20 J, friction >360 N; **DTA** (5 °C min^{-1}): T_{endo} = 64 °C, T_{exo1} = 207 °C, T_{exo2} = 231 °C.

Ammonium 1,3-bis(3-nitramino-4H-1,2,4-triazole-5-yl) 2-nitrazapropane (4):

^{1}H NMR (400 MHz, DMSO-*d*$_6$): δ (ppm) = 12.9 (br, 2*H*, N*H*) 7.18 (s, 8H, N*H*$_4$), 4.98 (s, 4H, C*H*$_2$); **^{13}C{^{1}H} NMR** (101 MHz, DMSO-*d*$_6$): δ (ppm) = 157.9 (*C*-CH$_2$), 154.8 (*C*-NNO$_2$), 48.6 (*C*H$_2$); **IR** (ATR, rel. int.): $\tilde{\nu}$ (cm^{-1}) = 3948 (w), 3891 (w), 3851 (w), 3801 (w), 3732 (w), 3696 (w), 3586 (s), 3394 (w), 3345 (w), 3286 (w), 3254 (w), 3212 (w), 2789 (w), 2582 (w), 2538 (w), 2504 (w), 2469 (w), 2384 (w), 2311 (w), 2271 (w), 2190 (w), 2142 (w), 2096 (w), 1982 (w), 1932 (w), 1893 (w), 1829 (m), 1627 (m), 1513 (s), 1441 (s), 1310 (s), 1238 (s), 1133 (w), 1079 (w), 1004 (w), 945 (w), 861 (w), 804 (w), 762 (w), 717 (w), 658 (w), 630 (w), 489 (w), 445 (w); **Elemental analysis**: calcd. (%) for $C_6H_{14}N_{14}O_6$ (378.27 g mol^{-1}): C 19.05, H 3.73, N 51.84; found C 18.94, H 3.48, N 51.75; **Sensitivities** (grain size 100–500 µm): impact 6 J, friction >288 N; **DTA** (5 °C min^{-1}): T_{exo1} = 176 °C, T_{exo2} = 217 °C.

Hydrazinium 1,3-bis(3-nitramino-4H-1,2,4-triazole-5-yl) 2-nitrazapropane (5):

^{1}H NMR (400 MHz, DMSO-d_6): δ (ppm) = 4.95 (s, 4H, CH_2); **^{13}C{^{1}H} NMR** (101 MHz, DMSO-d_6): δ (ppm) = 157.8 (*C*-CH_2), 154.7 (*C*-NNO_2), 48.6 (*C*H_2); **IR** (ATR, rel. int.): $\tilde{\nu}$ (cm^{-1}) = 3964 (w), 3873 (w), 3742 (w), 3676 (w), 3645 (w), 3604 (w), 3553(m), 3513 (m), 3318 (m), 3053 (m), 3001 (w), 2742 (w), 2630 (w), 2166 (w), 2104 (w), 2031 (w), 1986 (w), 1943 (w), 1751 (m), 1609 (s), 1509 (s), 1440 (s), 1300 (s), 1241 (m), 1125 (s), 1075 (s), 1004 (s), 945 (s), 859 (m), 807 (m), 759 (m), 717 (m), 666 (m), 451 (m); **Elemental analysis**: calcd. (%) for $C_6H_{16}N_{16}O_6$ (408.30 g mol^{-1}): C 17.65, H 3.95, N 54.89; found C 17.85, H 3.78, N 54.64; **Sensitivities** (grain size 100–500 µm): impact 3 J, friction 160 N; **DTA** (5 °C min^{-1}): T_{exo1} = 181 °C, T_{exo2} = 217 °C.

Sodium 1,3-bis(3-nitramino-4H-1,2,4-triazole-5-yl) 2-nitrazapropane (**6·2H_2O**): **^{1}H NMR** (400 MHz, DMSO-d_6): δ (ppm) = 12.80 (s, 2H, N*H*), 4.95 (s, 4H, CH_2); **^{13}C{^{1}H} NMR** (101 MHz, DMSO-d_6): δ (ppm) = 157.8 (*C*-CH_2), 154.8 (*C*-NNO_2), 48.7 (*C*H_2); **IR** (ATR, rel. int.): $\tilde{\nu}$ (cm^{-1}) = 3977 (w), 3910 (w), 3868 (w), 3779 (w), 3731 (s), 3341 (w), 3287 (w), 3253 (w), 3213 (w), 2496 (w), 2431 (w), 2380 (w), 2336 (w), 2313 (w), 2274 (w), 2183 (w), 2147 (w), 2094 (w), 2005 (w), 1974 (w), 1932 (w), 1882 (w), 1838 (s), 1637 (s), 1515 (m), 1443 (s), 1314 (w), 1272 (m), 1249 (w), 1137 (m), 1081 (w), 1005 (w), 942 (w), 864 (w), 804 (w), 758 (w), 712 (w), 657 (w), 616 (s), 451 (w); **Elemental analysis**: calcd. (%) for $C_6H_6Na_2N_{12}O_6$ ·2 H_2O (458.43 g mol^{-1}): C 16.99, H 2.38, N 39.62; found C 17.25, H 2.54, N 39.35; **Sensitivities** (grain size 100–500 µm): impact 40 J, friction >360 N; **DTA** (5 °C min^{-1}): T_{endo} = 123 °C, T_{exo1} = 193 °C, T_{exo2} = 253 °C.

Guanidinium 1,3-bis(3-nitramino-4H-1,2,4-triazole-5-yl) 2-nitrazapropane (7): **^{1}H NMR** (400 MHz, DMSO-d_6): δ (ppm) = 12.90 (s, 2H, N*H*), 6.94 (s, 12H, NH_2), 4.97 (s, 4H, CH_2); **^{13}C{^{1}H} NMR** (101 MHz, DMSO-d_6): δ (ppm) = 158.0 (*C*-CH_2), 157.0 (*C*-NH_2), 153.8 (*C*-NNO_2), 48.7 (*C*H_2); **IR** (ATR, rel. int.): $\tilde{\nu}$ (cm^{-1}) = 3986 (w), 3946 (w), 3907 (w), 3832 (w), 3773 (w), 3715 (w), 3675 (w), 3626 (w), 3539 (m), 3507 (m), 3440 (m), 3325 (w), 3147 (w), 2860 (w), 2816 (w), 2750 (w), 2577 (w), 2538 (w), 2505 (w), 2452 (w), 2389 (w), 2323 (w), 2289 (w), 2233 (w), 2186 (w), 2140 (w), 2099 (w), 2059 (w), 2001 (w), 1966 (w), 1897 (m), 1862 (m), 1827 (w), 1780 (m), 1683 (w), 1637 (w), 1595 (w), 1522 (m), 1489 (w), 1435 (w), 1377 (w),

1324 (w), 1272 (w), 1238 (w), 1133 (w), 1075 (w), 1007 (w), 972 (w), 934 (w), 861 (w), 793 (w), 752 (w), 704 (w), 652 (m), 612 (w), 578 (m), 541 (m), 467 (s); **Elemental analysis**: calcd. (%) for $C_8H_{18}N_{18}O_6$ (462.35 g mol^{-1}): C 20.78, H 3.92, N 54.53; found C 21.00, H 3.64, N 54.32; **Sensitivities** (grain size 100–500 µm): impact 40 J, friction >360 N; **DTA** (5 °C min^{-1}): T_{exo1} = 182 °C, T_{exo2} = 207 °C.

Aminoguanidinium 1,3-bis(3-nitramino-4H-1,2,4-triazole-5-yl) 2-nitrazapropane (8): ^{1}H NMR (400 MHz, DMSO-*d*$_6$): δ (ppm) = 12.80 (s, 2H, N*H*), 8.6 (br, 2H, N*H*), 7.54–6.75 (m, 8H, N*H*$_2$) 4.95 (s, 4H, C*H*$_2$), 4.69 (s, 4H, N*H*$_2$); **^{13}C{^{1}H} NMR** (101 MHz, DMSO-*d*$_6$): δ (ppm) = 158.8 (*C*-CH$_2$), 157.6 (*C*-NH$_2$), 154.7 (*C*-NNO$_2$), 48.7 (*C*H$_2$); **IR** (ATR, rel. int.): $\tilde{\nu}$ (cm^{-1}) = 3945 (w), 3896 (w), 3858 (w), 3801 (w), 3735 (w), 3660 (w), 3633 (m), 3589 (m), 3560 (m), 3517 (m), 3342 (w), 3303 (w), 3276 (w), 3215 (w), 3164 (w), 2885 (w), 2777 (w), 2341 (w), 2292 (w), 2222 (w), 2172 (w), 2110 (w), 2084 (w), 2041 (w), 2000 (w), 1915 (w), 1889 (w), 1844 (w), 1808 (w), 1757 (w), 1666 (s), 1519 (s), 1441 (m), 1370 (s), 1318 (s), 1278 (m), 1236 (m), 1206 (m), 1126 (m), 1060 (m), 1005 (m), 931 (m), 864 (m), 795 (m), 755 (s), 701 (m), 642 (m), 557 (m), 513 (s), 462 (s); **Elemental analysis**: calcd. (%) for $C_8H_{20}N_{20}O_6$ (492.38 g mol^{-1}): C 19.51, H 4.09, N 56.89; found C 19.78, H 3.83, N 56.83; **Sensitivities** (grain size 100–500 µm): impact 20 J, friction >360 N; **DTA** (5 °C min^{-1}): T_{exo} = 212 °C.

Potassium 1,3-bis(3-nitramino-4*H*-1,2,4-triazole-5-yl) 2-oxapropane hydrate (11·H$_2$O): **^{1}H NMR** (400 MHz, DMSO-*d*$_6$): δ (ppm) = 12.7 (br, 2H, N*H*), 4.36 (s, 4H, C*H*$_2$); **^{13}C{^{1}H} NMR** (101 MHz, DMSO-*d*$_6$): δ (ppm) = 157.6 (*C*-CH$_2$), 157.3 (*C*-NNO$_2$), 65.1 (*C*H$_2$); **IR** (ATR): $\tilde{\nu}$ (cm^{-1}) = 3331(w), 3252(w), 3231(w), 1738(w), 1726(w), 1521(m), 1436(m), 1379(s), 1316(vs), 1274(m), 1251(s), 1237(s), 1229(s), 1141(m), 1131(m), 1087(s), 1061(s), 1035(m), 1017(m), 996(s), 859(m), 764(m), 728(m), 728(m), 713(m), 462(m), 453(m), 448(m); **Elemental analysis**: calcd. (%) for $C_6H_6N_{10}O_5K_2 \cdot H_2O$ (394.39 g mol^{-1}): C 18.27; H 2.04; N 35.52 found: C 18.30; H 2.16; N 35.60; **Sensitivities** (grain size 300−1000 µm): impact 15 J, friction >360 N; **DTA** (onset, 5 °C min^{-1}): T_{endo} = 143 °C, T_{exo} = 195 °C.

Ammonium 1,3-bis(3-nitramino-4*H*-1,2,4-triazole-5-yl) 2-oxapropane (12): **^{1}H NMR** (400 MHz, DMSO-*d*$_6$): δ (ppm) = 13.1 (br, 2H, N*H*), 7.3 (br, 8H, N*H*$_4$), 4.41

(s, 4H, C*H*$_2$); **^{13}C{^{1}H} NMR** (101 MHz, DMSO-*d*$_6$): δ (ppm) = 156.8 (*C*-CH$_2$), 155.5 (*C*-NNO$_2$), 64.7 (*C*H$_2$); **IR** (ATR): $\tilde{\nu}$ (cm^{-1}) = 3141(m), 3026(m), 2863(m), 1739(w), 1618(w), 1505(m), 1461(m), 1421(s), 1371(s), 1312(vs), 1284(vs), 1229(vs), 1134(s), 1096(s), 1026(s), 1001(vs), 861(m), 764(m), 719(s), 655(m), 512(m), 471(m), 461(m), 461(m), 444(m); **Elemental analysis**: calcd. (%) for $C_6H_{14}N_{12}O_5$ (334.25 g mol^{-1}): C 21.56; H 4.22; N 50.29 found: C 21.66, H 4.10, N 50.05; **Sensitivities** (grain size 300−1000 µm): impact 5 J, friction >288 N; **DTA** (onset, 5 °C min^{-1}): T_{endo} = 181 °C, T_{exo} = 225 °C.

Hydroxylammonium 1,3-bis(3-nitramino-4*H*-1,2,4-triazole-5-yl) 2-oxapropane (13): **^{1}H NMR** (400 MHz, DMSO-*d*$_6$): δ (ppm) = 8.7 (br, 10H, N*H*, N*H*$_3$O*H*), 4.42 (s, 4H, C*H*$_2$); **^{13}C{^{1}H} NMR** (101 MHz, DMSO-*d*$_6$): δ (ppm) = 156.8 (*C*-CH$_2$), 155.4 (*C*-NNO$_2$), 64.7 (*C*H$_2$); **IR** (ATR): $\tilde{\nu}$ (cm^{-1}) = 3183(m), 3154(m), 3134(m), 3111(m), 3091(m), 3075(m), 3030(m), 3013(m), 2985(m), 2975(m), 2936(m), 2688(m), 2507(m), 1519(m), 1453(m), 1441(m), 1415(m), 1369(m), 1348(s), 1335(s), 1301(vs), 1263(s), 1245(s), 1245(s), 1216(s), 1141(s), 1129(s), 1093(vs), 1042(m), 1024(m), 1001(vs), 860(m), 825(m), 770(m), 757(m), 736(m), 710(m), 463(m); **Elemental analysis**: calcd. (%) for $C_6H_{14}N_{12}O_7$ (366.11 g mol^{-1}): C 19.68; H 3.85; N 45.89 found: C 19.76, H 4.09, N 45.66; **Sensitivities** (grain size 300−1000 µm): impact 3 J, friction >288 N; **DTA** (onset, 5 °C min^{-1}): T_{exo1} = 191 °C, T_{exo2} = 208 °C.

Hydrazinium 1,3-bis(3-nitramino-4*H*-1,2,4-triazole-5-yl) 2-oxapropane (14): **^{1}H NMR** (400 MHz, DMSO-*d*$_6$): δ (ppm) = 12.7 (br, 2H, N*H*), 6.5 (br, 10H, N$_2$*H*$_5$), 4.40 (s, 4H, C*H*$_2$); **^{13}C{^{1}H} NMR** (101 MHz, DMSO-*d*$_6$): δ (ppm) = 157.0 (*C*-CH$_2$), 156.0 (*C*-NNO$_2$), 64.8 (*C*H$_2$); **IR** (ATR): $\tilde{\nu}$ (cm^{-1}) = 3385(m), 3366(m), 3316(m), 3255(w), 3210(w), 3191(w), 3121(m), 2971(m), 2941(m), 2870(m), 2763(m), 2687(m), 2634(m), 1739(w), 1726(w), 1613(w), 1529(s), 1473(m), 1454(m), 1387(s), 1326(vs), 1290(vs), 1229(s), 1229(s), 1147(s), 1126(s), 1091(vs), 1045(w), 1020(s), 1004(s), 968(s), 858(w), 763(w), 692(s), 621(m), 461(w); **Elemental analysis**: calcd. (%) for $C_6H_{16}N_{14}O_5$ (364.29 g mol^{-1}): C 19.78; H 4.43; N 53.83 found: C 19.93, H 4.33, N 53.54; **Sensitivities** (grain size 300−1000 µm): impact 5 J, friction >240 N; **DTA** (onset, 5 °C min^{-1}): T_{exo} = 196 °C.

Sodium 1,3-bis(3-nitramino-4*H*-1,2,4-triazole-5-yl) 2-oxapropane hydrate (15·H_2O): **^{1}H NMR** (400 MHz, DMSO-d_6): δ (ppm) = 12.7 (br, 2H, N*H*), 4.36 (s, 4H, CH_2); **^{13}C{^{1}H} NMR** (101 MHz, DMSO-d_6): δ (ppm) = 157.8 (*C*-CH_2), 157.4 (*C*-NNO_2), 65.2 (*C*H_2); **IR** (ATR): $\tilde{\nu}$ (cm^{-1}) = 3224(m), 3190(m), 3173(m), 3140(m), 3124(m), 1738(m), 1727(w), 1526(m), 1453(m), 1350(vs), 1329(vs), 1264(s), 1231(m), 1218(m), 1141(m), 1085(s), 1032(w), 1005(s), 869(m), 760(m), 729(m), 673(m), 468(m), 468(m); **Elemental analysis**: calcd. (%) for $C_6H_6N_{10}O_5Na_2 \cdot H_2O$ (362.17 g mol^{-1}): C 19.90; H 2.23; N 38.67 found: C 19.82, H 2.36, N 38.47; **Sensitivities** (grain size 300−1000 µm): impact 40 J, friction >360 N; **DTA** (onset, 5 °C min^{-1}): T_{endo} = 155 °C, T_{exo} = 208 °C.

Guanidinium 1,3-bis(3-nitramino-4*H*-1,2,4-triazole-5-yl) 2-oxapropane (16): **^{1}H NMR** (400 MHz, DMSO-d_6): δ (ppm) = 12.82 (s, 2H, N*H*), 7.14 (s, 12H, NH_2), 4.37 (s, 4H, CH_2); **^{13}C{^{1}H} NMR** (101 MHz, DMSO-d_6): δ (ppm) = 157.9 (*C*-NH_2), 157.3 (*C*-CH_2), 157.3 (*C*-NNO_2), 65.3 (*C*H_2); **IR** (ATR): $\tilde{\nu}$ (cm^{-1}) = 3386(m), 3351(m), 3141(m), 3123(m), 1650(m), 1523(m), 1504(m), 1455(m), 1443(m), 1379(m), 1350(m), 1327(vs), 1263(s), 1236(s), 1221(m), 1143(s), 1100(m), 1087(m), 1062(m), 1023(m), 1005(s), 994(m), 971(m), 971(m), 863(m), 767(w), 745(m), 740(w), 543(m), 481(m), 457(s); **Elemental analysis**: calcd. (%) for $C_8H_{18}N_{16}O_5$ (418.34 g mol^{-1}): C 22.97; H 4.34; N 53.57. Found: C 23.16; H 4.22; N 53.49; **Sensitivities** (grain size 300−1000 µm): impact 40 J, friction >360 N; **DTA** (onset, 5 °C min^{-1}): T_{exo} = 268 °C.

Aminoguanidinium 1,3-bis(3-nitramino-4*H*-1,2,4-triazole-5-yl) 2-oxapropane (17): **^{1}H NMR** (400 MHz, DMSO-d_6): δ (ppm) = 12.8 (br, 2H, N*H*-C), 8.8 (br, 2H, NH_2-NH), 7.2 (br, 8H, NH_2-C), 4.70 (s, 4H, NH_2-NH), 4.38 (s, 4H, CH_2); **^{13}C{^{1}H} NMR** (101 MHz, DMSO-d_6): δ (ppm) = 158.9 (*C*-NH_2), 157.3 (*C*-CH_2), 157.3 (*C*-NNO_2), 65.3 (*C*H_2); **IR** (ATR): $\tilde{\nu}$ (cm^{-1})= 3437(w), 3322(m), 3223(m), 3147(m), 3019(m), 2924(m), 2874(m), 2768(w), 1671(vs), 1666(s), 1523(m), 1509(s), 1459(m), 1442(s), 1351(s), 1333(s), 1300(vs), 1261(vs), 1235(s), 1147(s), 1103(m), 1079(s), 1005(vs), 1005(vs), 994(s), 863(m), 803(m), 766(m), 749(m), 734(m), 688(m), 673(w), 584(w), 498(m), 486(m), 483(m), 453(s); **Elemental analysis**: calcd. (%) for $C_8H_{20}N_{18}O_5$ (448.37 g mol^{-1}): C 21.43; H 4.50; N 56.23.

Found: C 21.60; H 4.65; N 56.06; **Sensitivities** (grain size 300−1000 µm): impact 25 J, friction >360 N; **DTA** (onset, 5 °C min^{-1}): T_{exo} = 220 °C.

Potassium bis(3-nitramino-4*H*-1,2,4-triazole-5-yl) hydrazonemethane (18): ^{1}H NMR (400 MHz, DMSO-d_6): δ (ppm) = 11.2 (br, 2H, N*H*), 8.6 (br, 2H, NH_2); **^{13}C{^{1}H} NMR** (101 MHz, DMSO-d_6: δ (ppm) = 159.0 (*C*-NNO_2), 152.7 (*C*-CH_2), 116.6 (*C*-NNH_2); **IR** (ATR, rel. int.): $\tilde{\nu}$ (cm^{-1}) = 3338 (m), 1624 (w), 1533 (m), 1498 (w), 1451 (m), 1327 (s), 1229 (s), 1157 (s), 1076 (s), 934 (s), 854 (m), 767 (s), 495 (s), 453 (s); **Elemental analysis**: calcd. (%) for $C_5H_4K_2N_{12}O_4$ (374.36 g mol^{-1}): C 16.04, H 1.08, N 44.90; found: C 15.84, H 1.38, N 43.32; **Sensitivities** (grain size 500–1000 µm): impact 10 J, friction >360 N; **DTA** (5 °C min^{-1}): T_{exo} = 205 °C.

Ammonium bis(3-nitramino-4*H*-1,2,4-triazole-5-yl) hydrazonemethane (19): ^{1}H NMR (400 MHz, DMSO-d_6): δ (ppm) = 9.2 (br, 4H, N*H*, NH_2), 7.29 (br, 2H, NH_4); **^{13}C{^{1}H} NMR** (101 MHz, DMSO-d_6): δ = 155.9 (*C*-NNO_2), 153.5 (*C*-CH_2), 121.0 (*C*-NNH_2); **IR** (ATR, rel. int.): $\tilde{\nu}$ (cm^{-1}) = 3182 (m), 3035 (m), 1532 (m), 1436 (m), 1314 (s), 1222 (s), 1157 (s), 1076 (s), 1003 (m), 934 (s), 854 (m), 667 (m), 620 (m), 497 (s); **Elemental analysis**: calcd. (%) for $C_5H_{12}N_{14}O_4$ (332.24 g mol^{-1}): C 18.08, H 3.64, N 59.02; found: C 17.78, H 3.60, N 54.68; **Sensitivities** (grain size 500–1000 µm): impact 2 J, friction 252 N; **DTA** (5 °C min^{-1}): T_{exo} = 175 °C.

Hydroxylammonium bis(3-nitramino-4*H*-1,2,4-triazole-5-yl) hydrazonemethane (20): ^{1}H NMR (400 MHz, DMSO-d_6): δ (ppm) = 9.31 6 (br, 2H, NH_2); **^{13}C{^{1}H} NMR** (101 MHz, DMSO-d_6): δ (ppm) = 155.9 (*C*-NNO_2), 154.3 (*C*-CH_2), 119.2 (*C*-NNH_2); **IR** (ATR, rel. int.): $\tilde{\nu}$ (cm^{-1}) = 3143 (m), 2916 (m), 2708 (m), 1594 (w), 1513 (s), 1453 (m), 1315 (s), 1160 (s), 1082 (s), 996 (s), 937 (m), 858 (s), 771 (s), 628 (s), 446 (s); **Elemental analysis**: calcd. (%) for $C_5H_{12}N_{14}O_6$ (364.24 g mol^{-1}): C 16.49, H 3.32, N 53.85; found: C 16.41, H 3.33, N 51.71; **Sensitivities** (grain size 100–500 µm): impact 5 J, friction 288 N; **DTA** (5 °C min^{-1}): T_{exo} = 177 °C.

Hydrazinium bis(3-nitramino-4*H*-1,2,4-triazole-5-yl) hydrazonemethane (21): ^{1}H NMR (400 MHz, DMSO-d_6): δ (ppm) = 9.08 (br, 10H, N_2H_5), 8.11 (br, 4H, N*H*,

N*H*$_2$); **^{13}C{^{1}H} NMR** (101 MHz, DMSO-*d*$_6$): δ (ppm) = 156.8 (*C*-NNO$_2$), 155.8 (*C*-CH$_2$), 122.7 (*C*-NNH$_2$); **IR** (ATR, rel. int.): $\tilde{\nu}$ (cm^{-1}) = 3315 (w), 3079 (w), 1606 (w), 1506 (m), 1448 (w), 1320 (m), 1238 (m), 1159 (m), 1076 (s), 934 (s), 855 (m), 763 (m), 630 (m), 444 (s); **Elemental analysis**: calcd. (%) for $C_5H_{14}N_{16}O_4$ (362.27 g mol^{-1}): C 16.58, H 3.90, N 61.86; found: C 16.42, H 4.08, N 58.28; **Sensitivities** (grain size 100–500 µm): impact 3 J, friction 252 N; **DTA** (5 °C min^{-1}): T_{exo} = 181 °C.

7.7.2 X-ray Diffraction

Table S1. Crystallographic data and structure refinement details for **17**.

	17
formula	$C_8H_{20}N_{18}O_5$
FW [g mol^{-1}]	448.42
T [K]	174
λ [Å]	0.71073
crystal system	monoclinic
space group	*C*2/*c*
crystal size [mm]	0.25 x 0.1 x 0.03
crystal habit	colorless needle
a [Å]	17.1468(6)
b [Å]	4.17070(10)
c [Å]	26.0973(9)
α [deg]	90
β [deg]	95.105(1)
γ [deg]	90
V [Å^3]	1858.92(10)
Z	4
$\rho_{calc.}$ [g cm^{-3}]	1.602
μ [mm^{-1}]	0.13
F(000)	936
2Θ range [deg]	2.97 – 26.37
index ranges	$-21 \leq h \leq 19$ $-5 \leq k \leq 5$ $-32 \leq l \leq 32$
reflections collected	18747
reflections unique	15943
parameters	181
GooF	1.1460
R_1/wR_2 [I>2σ(I)]	0.0351 / 0.0872
R_1/wR_2 (all data)	0.0370 / 0.0884
Resd. Dens [Å^{-3}]	–0.27 / 0.20
CCDC	2247722

7.7.3 NMR Spectroscopy

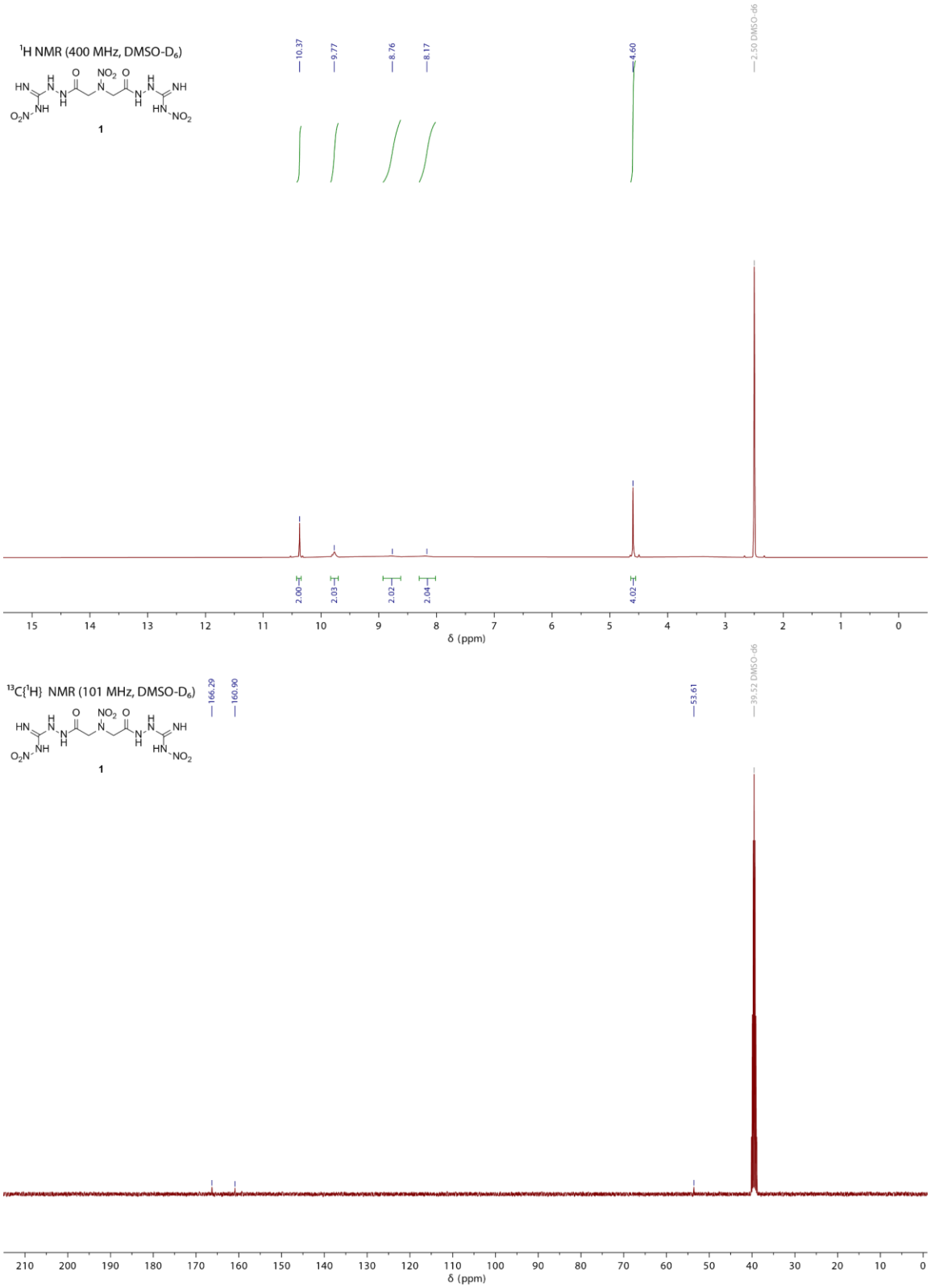

Figure S1. ^{1}H and ^{13}C{^{1}H} NMR spectra of **1**.

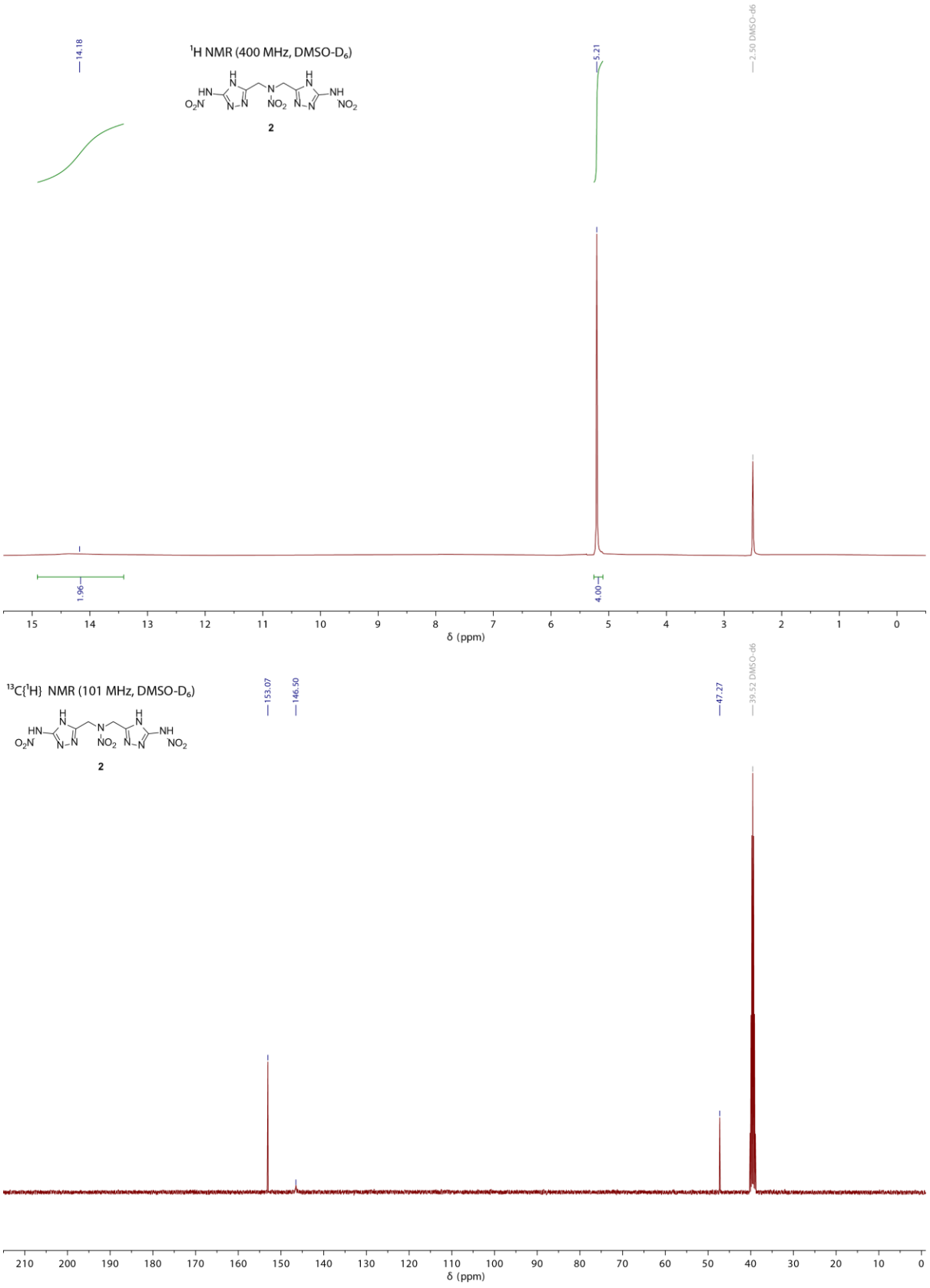

Figure S2. ^{1}H and ^{13}C{^{1}H} NMR spectra of **2**.

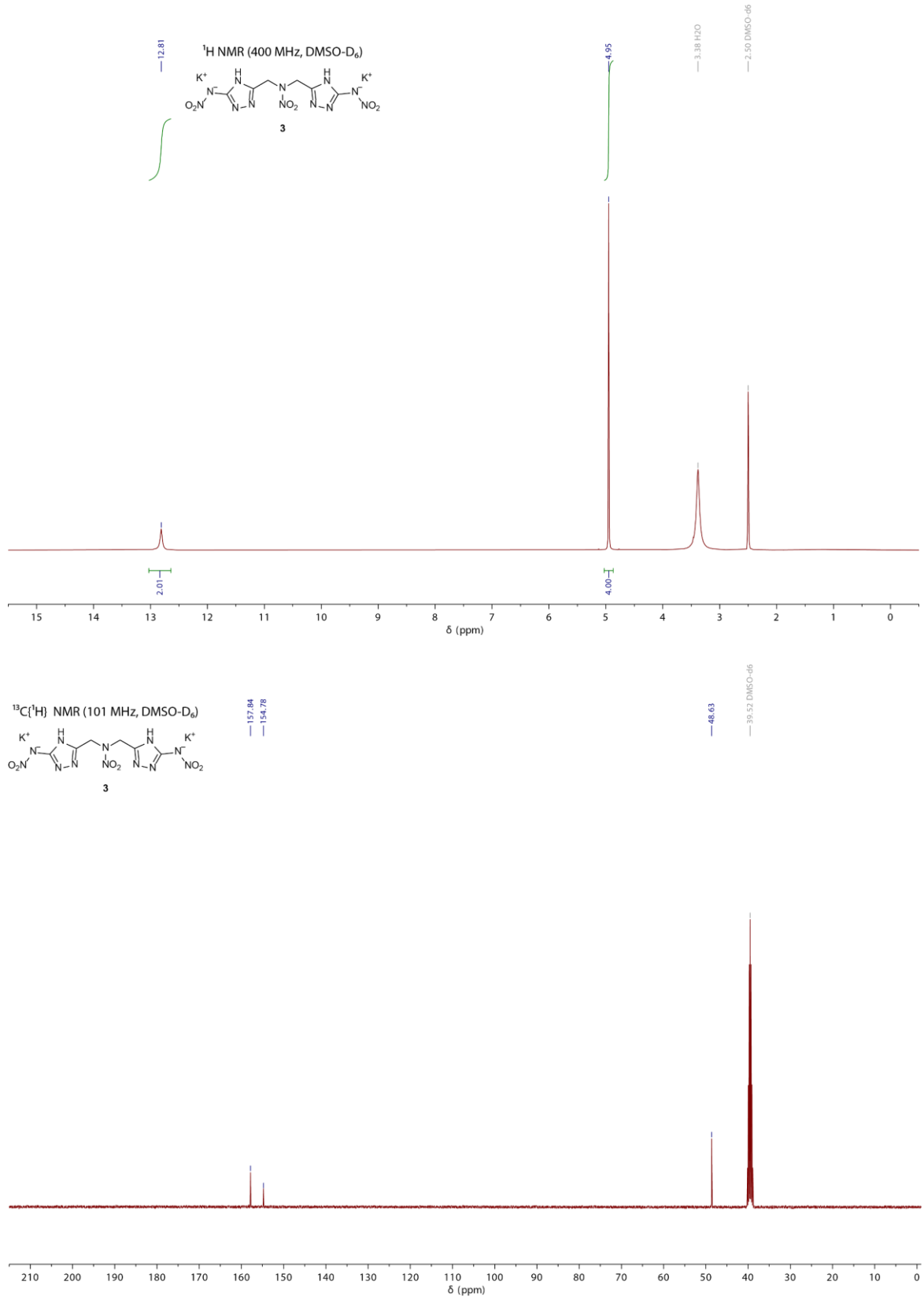

Figure S3. ^{1}H and ^{13}C{^{1}H} NMR spectra of **3**.

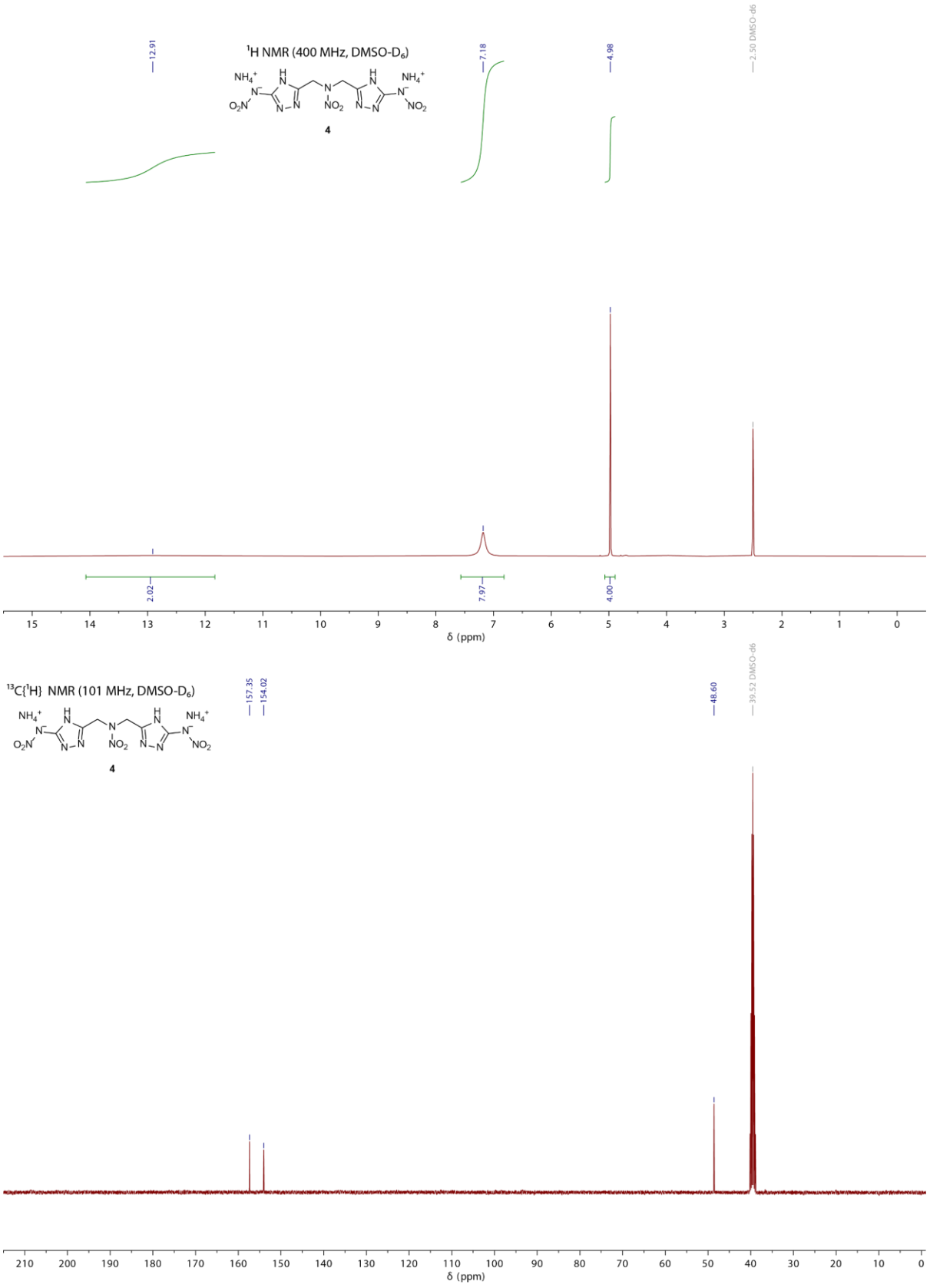

Figure S4. ^{1}H and ^{13}C{^{1}H} NMR spectra of **4**.

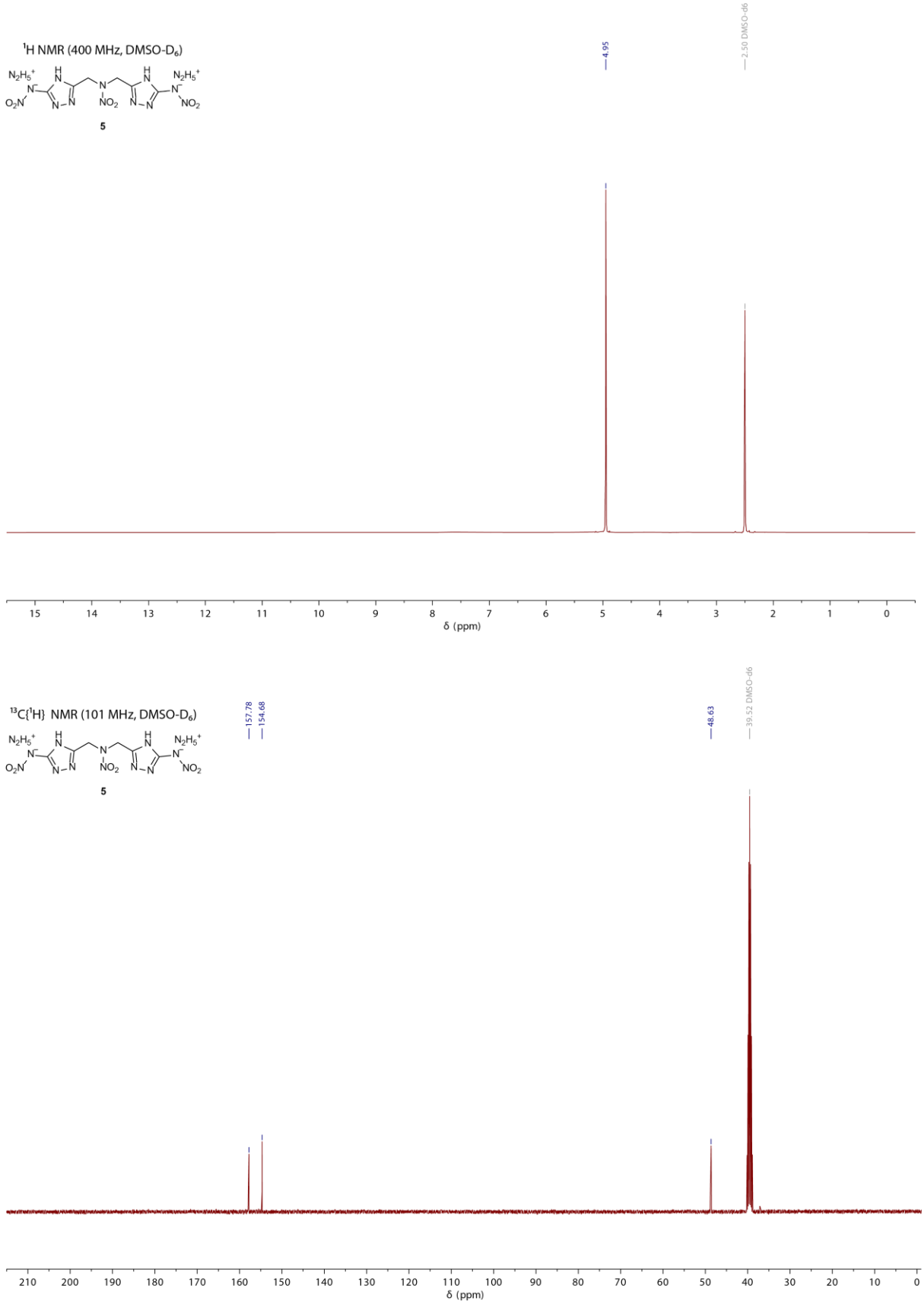

Figure S5. ^{1}H and ^{13}C{^{1}H} NMR spectra of **5**.

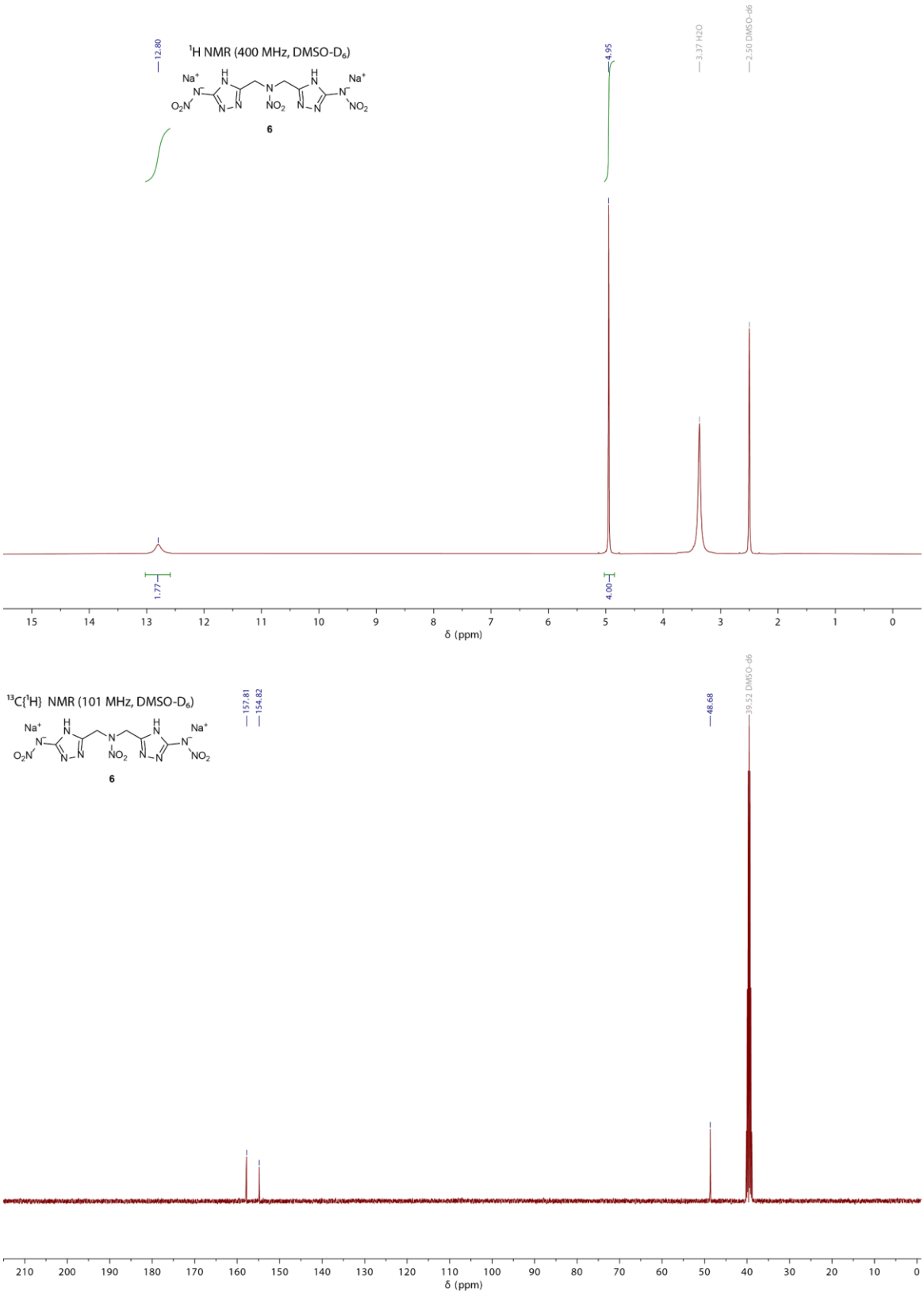

Figure S6. ^{1}H and ^{13}C{^{1}H} NMR spectra of **6**.

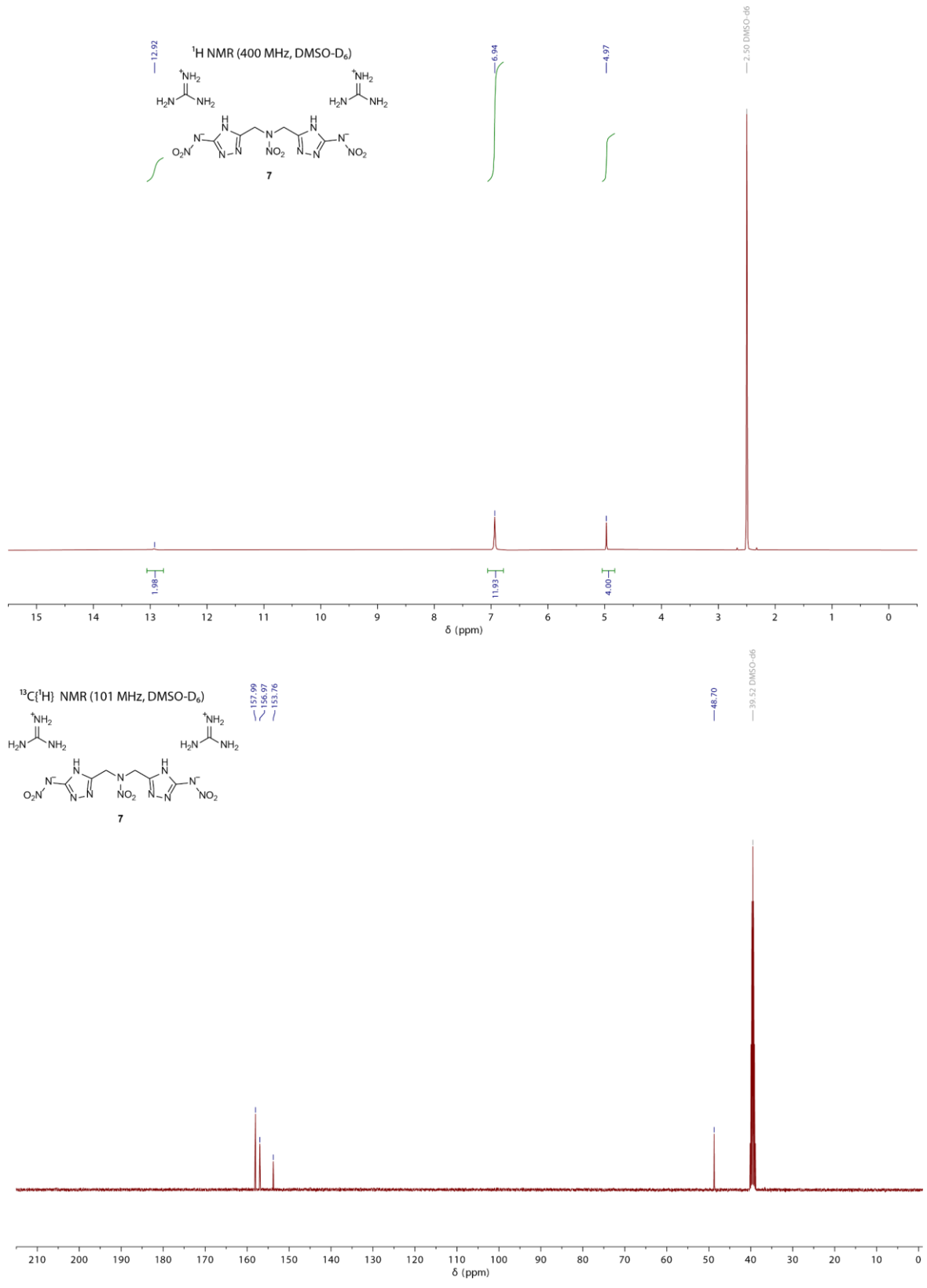

Figure S7. ^{1}H and ^{13}C{^{1}H} NMR spectra of **7**.

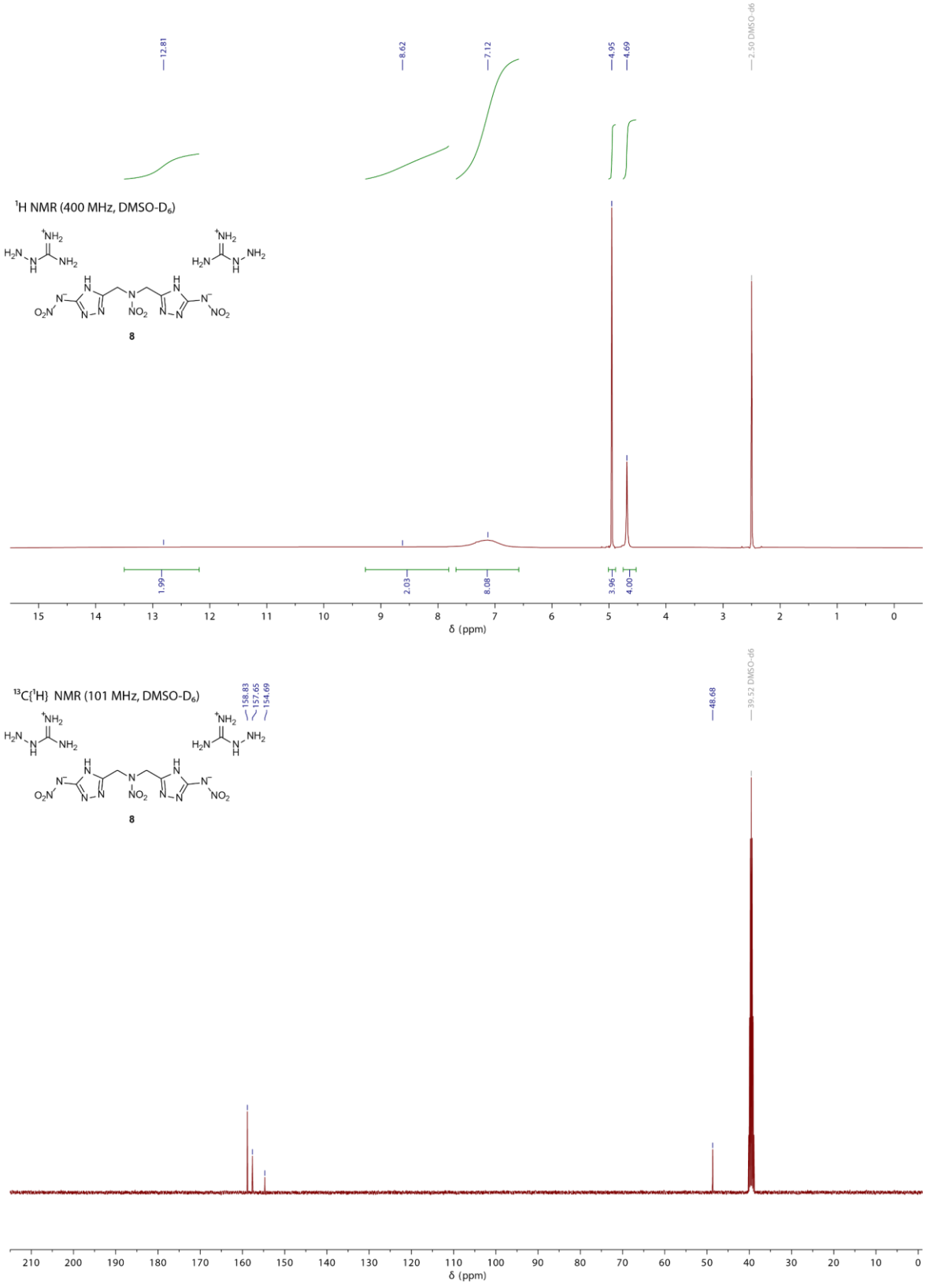

Figure S8. ^{1}H and ^{13}C{^{1}H} NMR spectra of **8**.

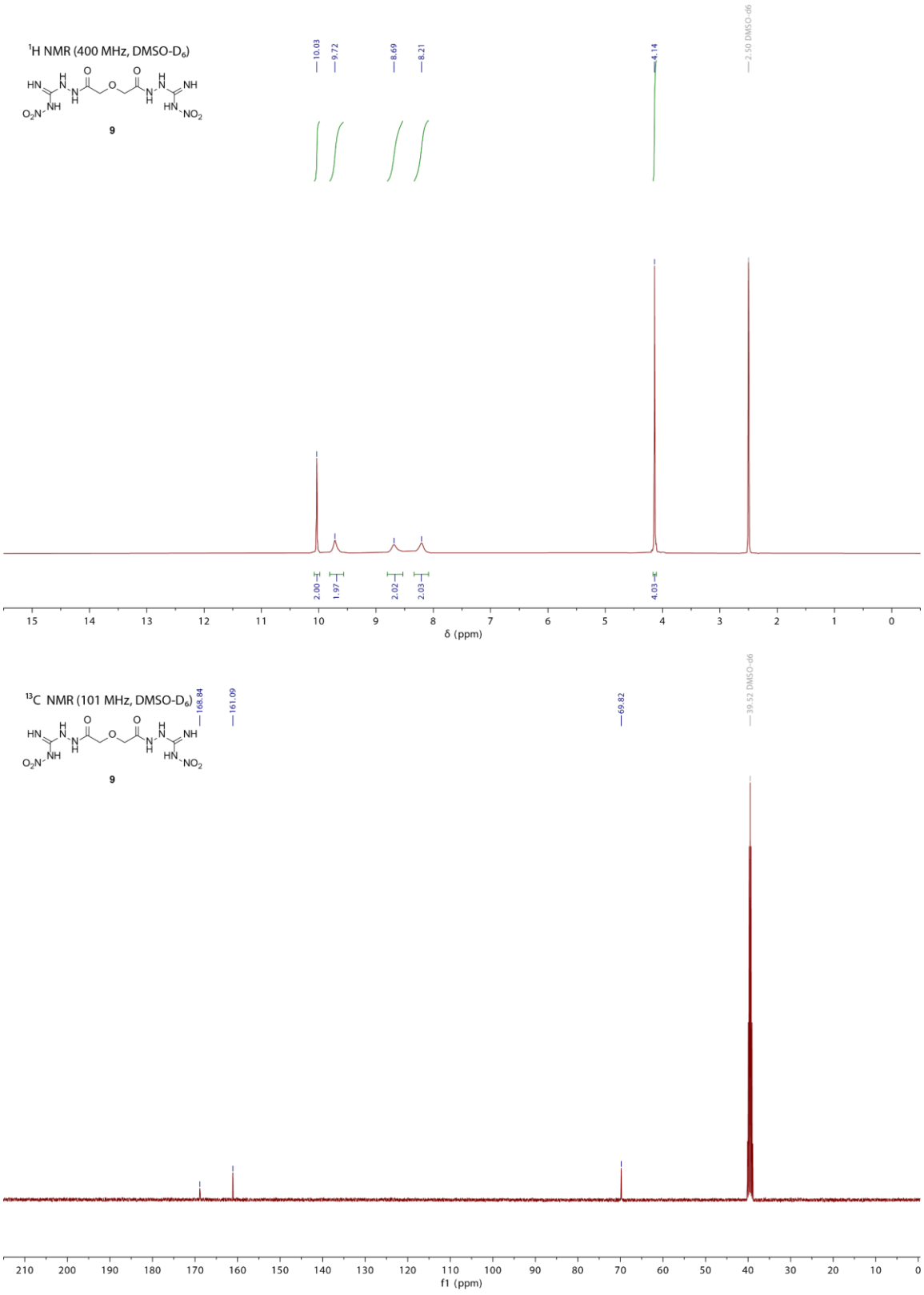

Figure S9. ^{1}H and ^{13}C{^{1}H} NMR spectra of **9**.

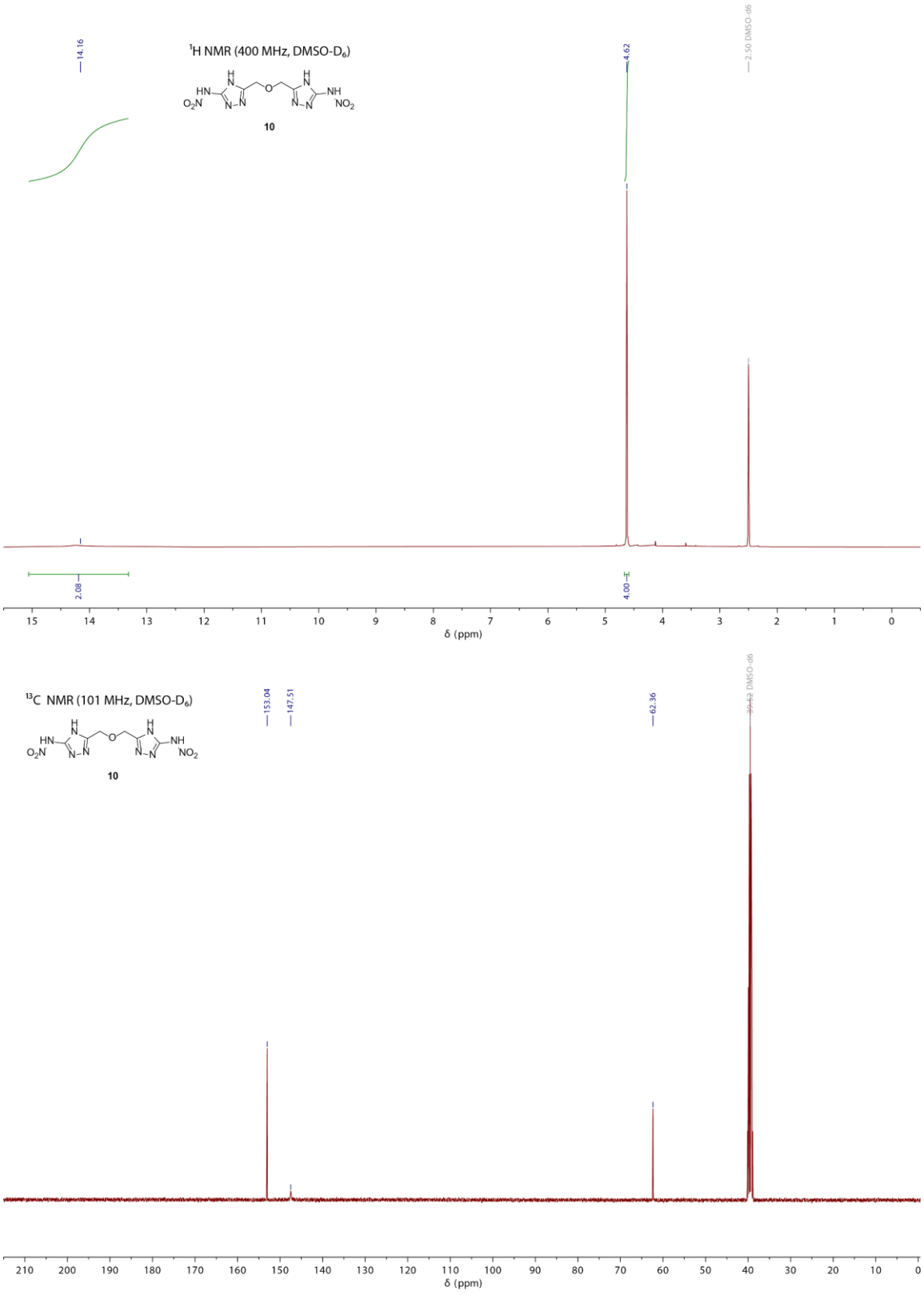

Figure S10. ^{1}H and ^{13}C{^{1}H} NMR spectra of **10**.

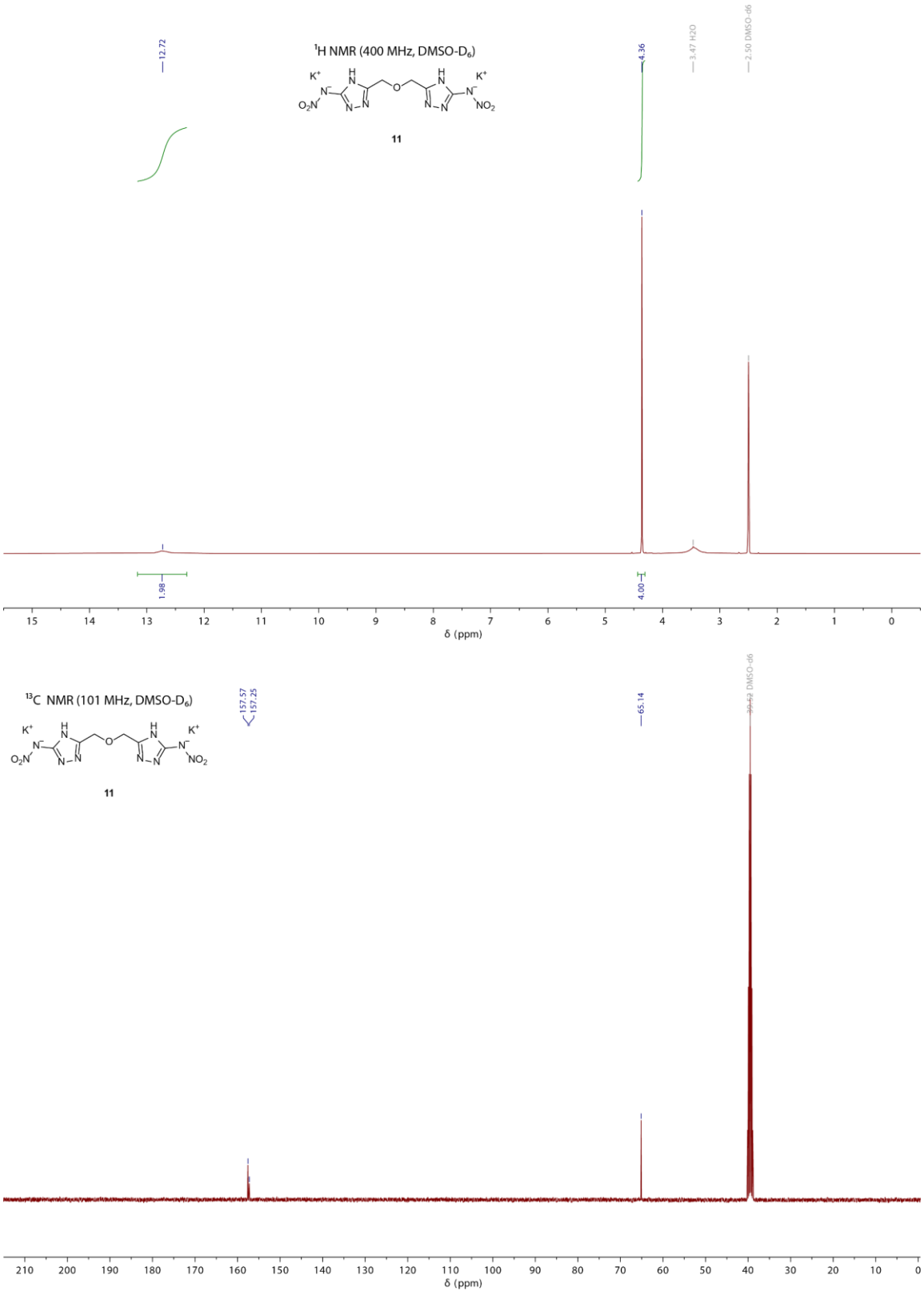

Figure S11. ^{1}H and ^{13}C{^{1}H} NMR spectra of **11**.

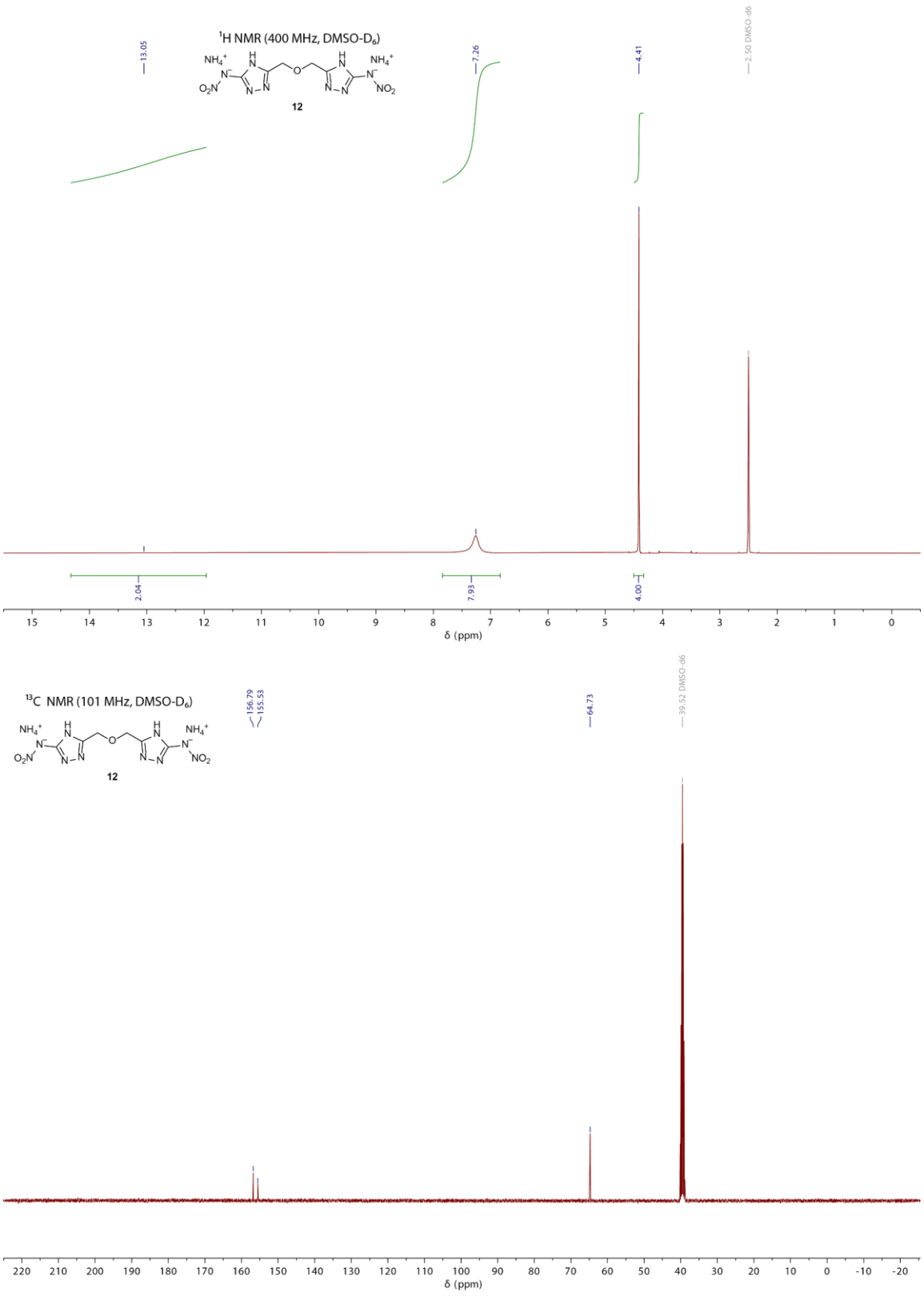

Figure S12. ^{1}H and ^{13}C{^{1}H} NMR spectra of **12**.

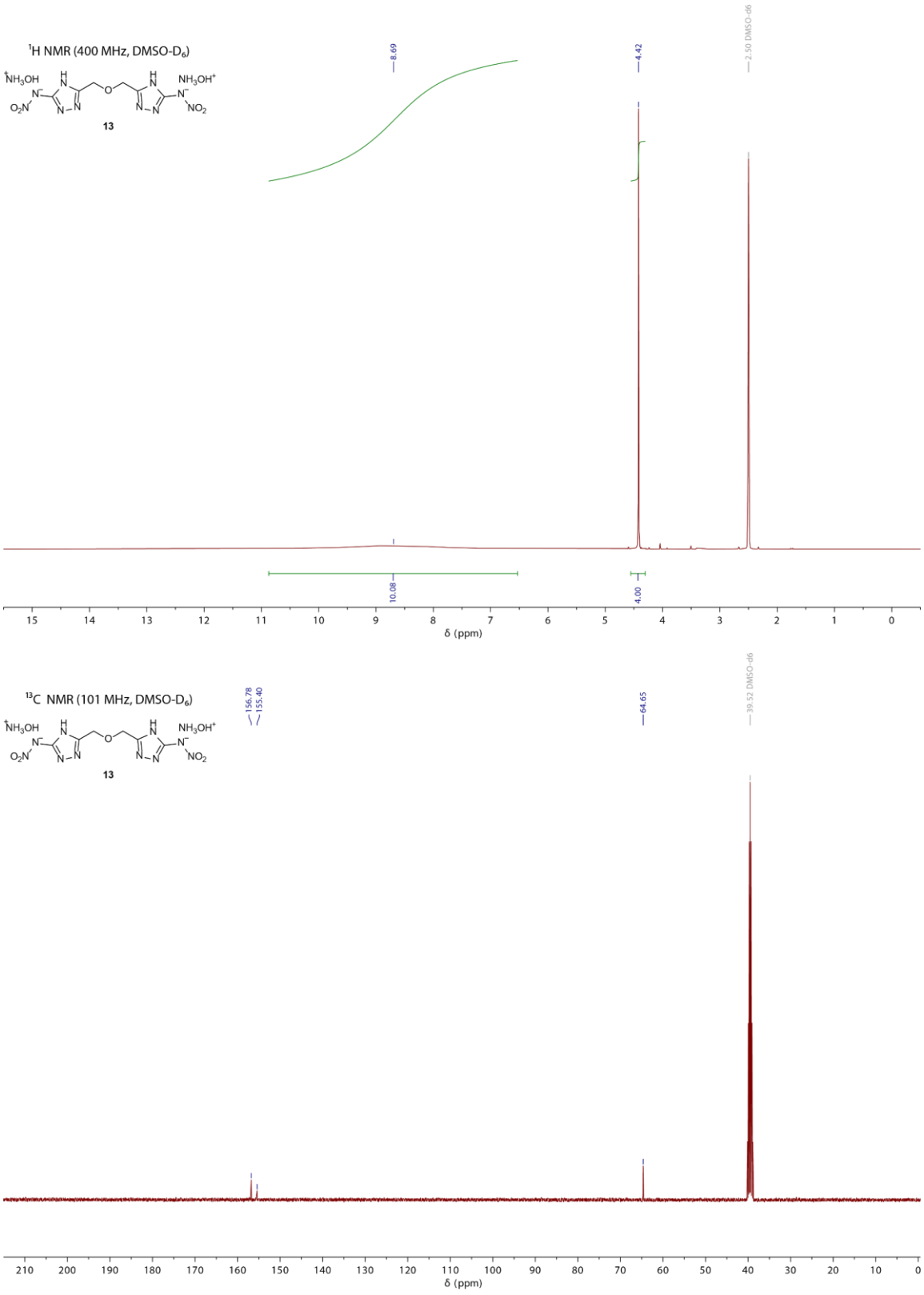

Figure S13. ^{1}H and ^{13}C{^{1}H} NMR spectra of **13**.

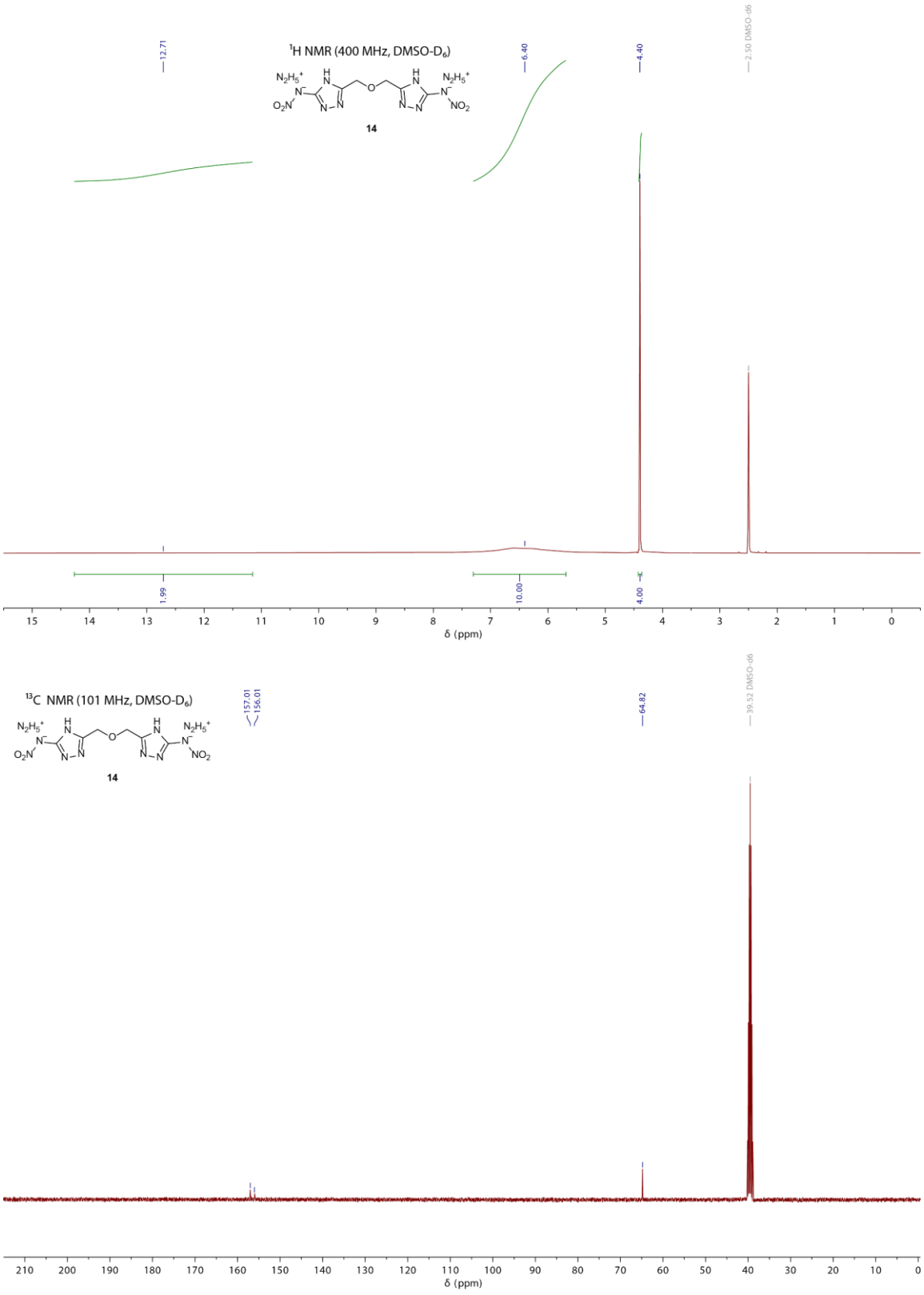

Figure S14. ^{1}H and ^{13}C{^{1}H} NMR spectra of **14**.

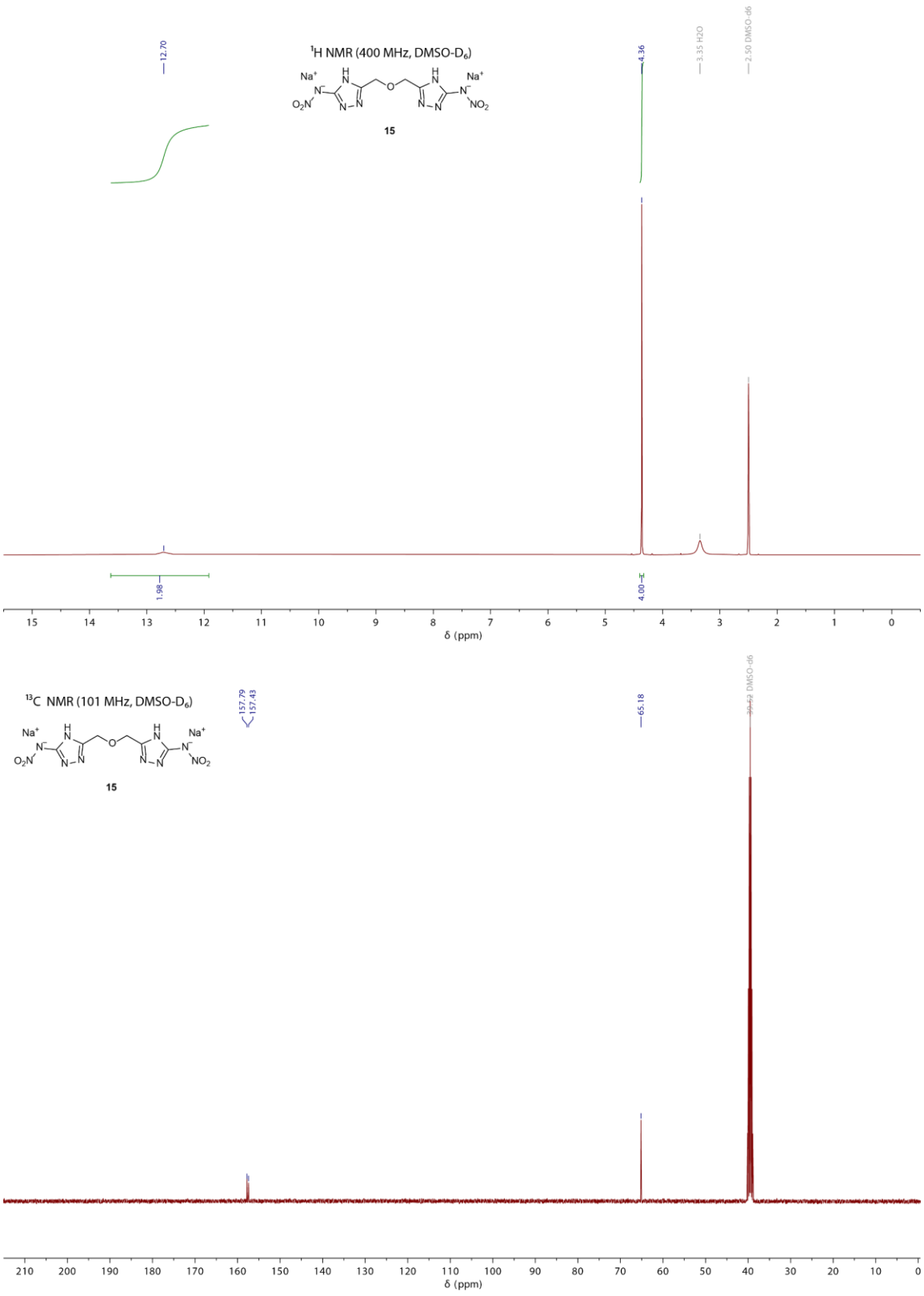

Figure S15. ^{1}H and ^{13}C{^{1}H} NMR spectra of **15**.

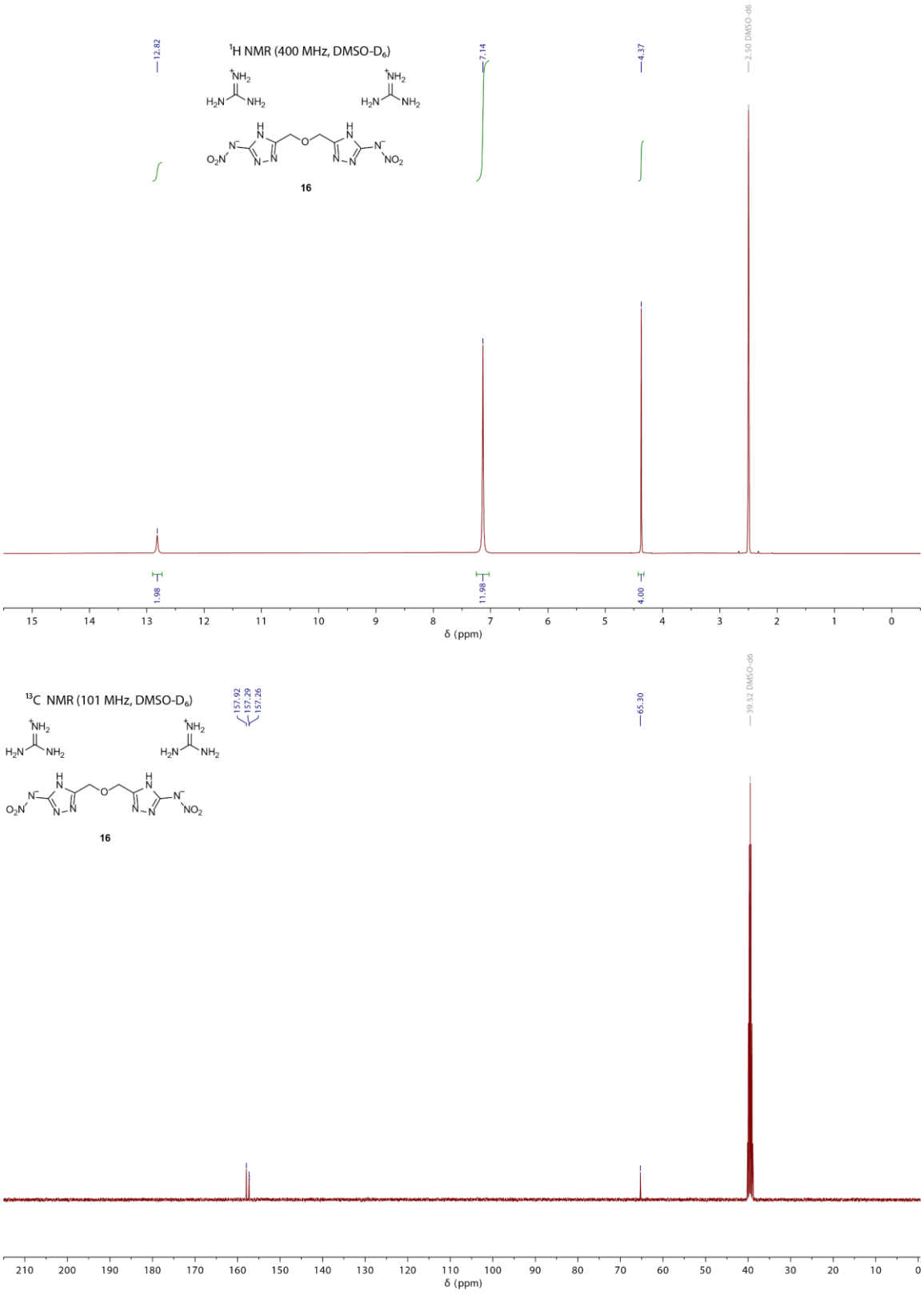

Figure S16. ^{1}H and ^{13}C{^{1}H} NMR spectra of **16**.

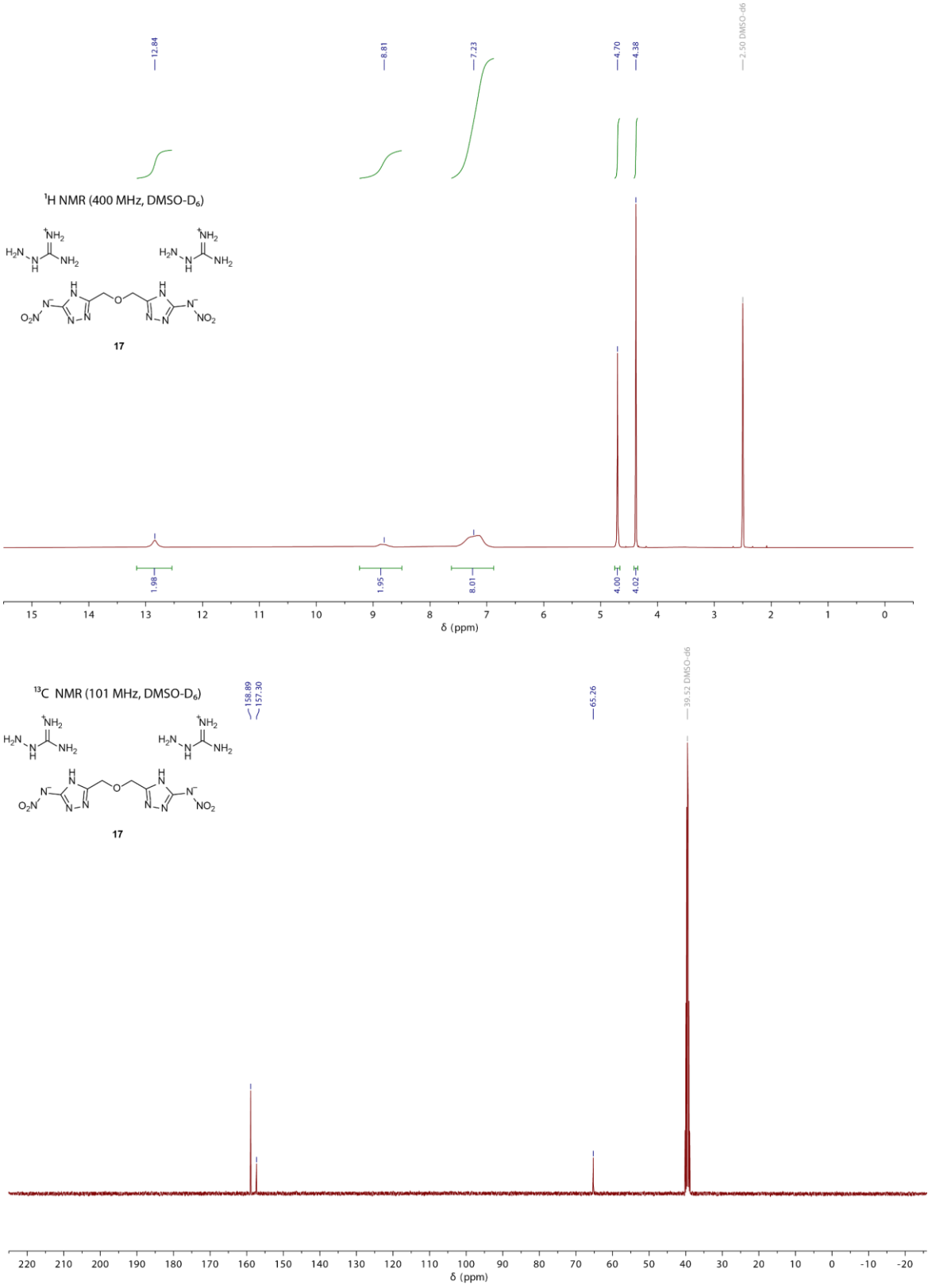

Figure S17. ^{1}H and ^{13}C{^{1}H} NMR spectra of **17**.

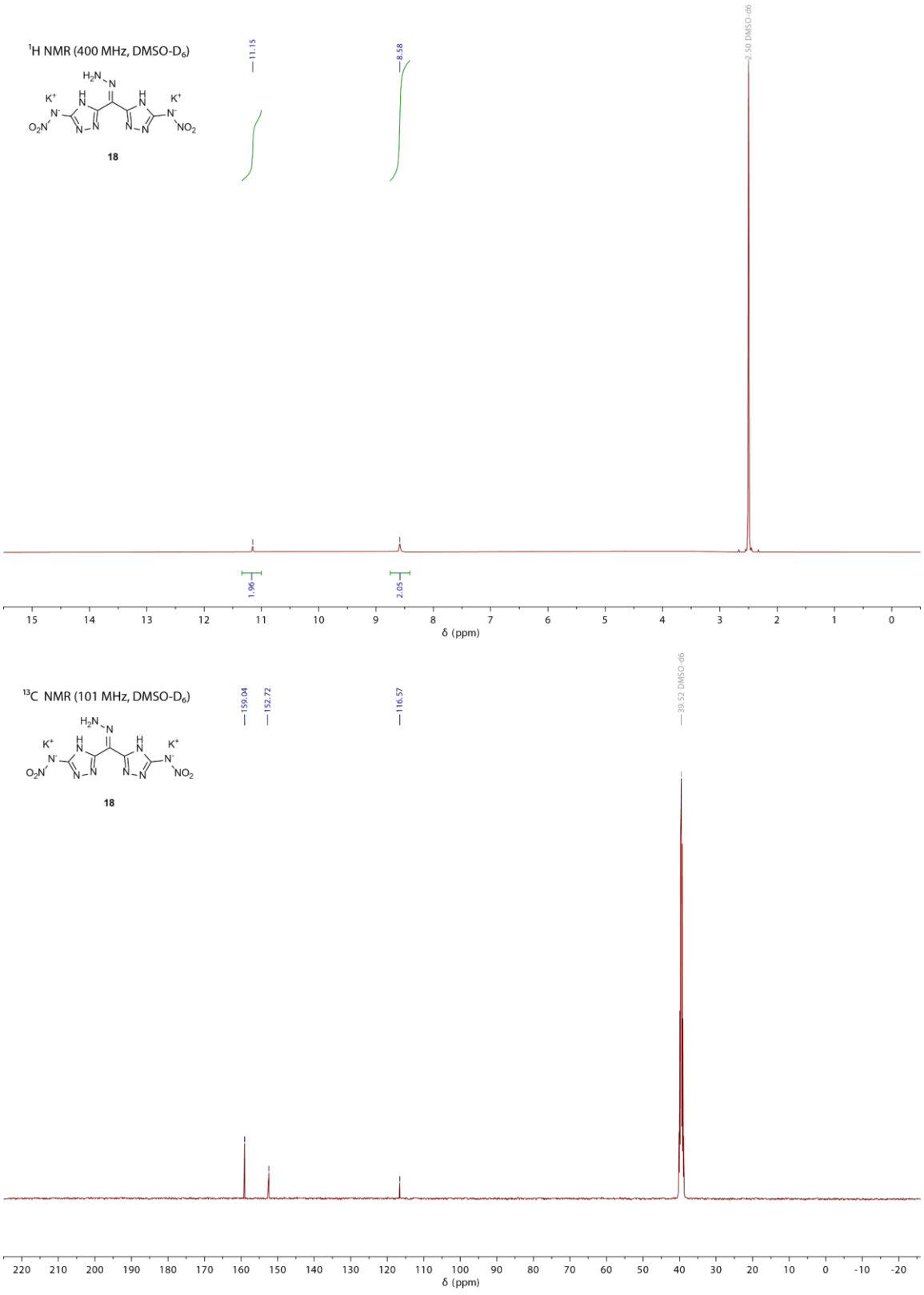

Figure S18. ^{1}H and ^{13}C{^{1}H} NMR spectra of **18**.

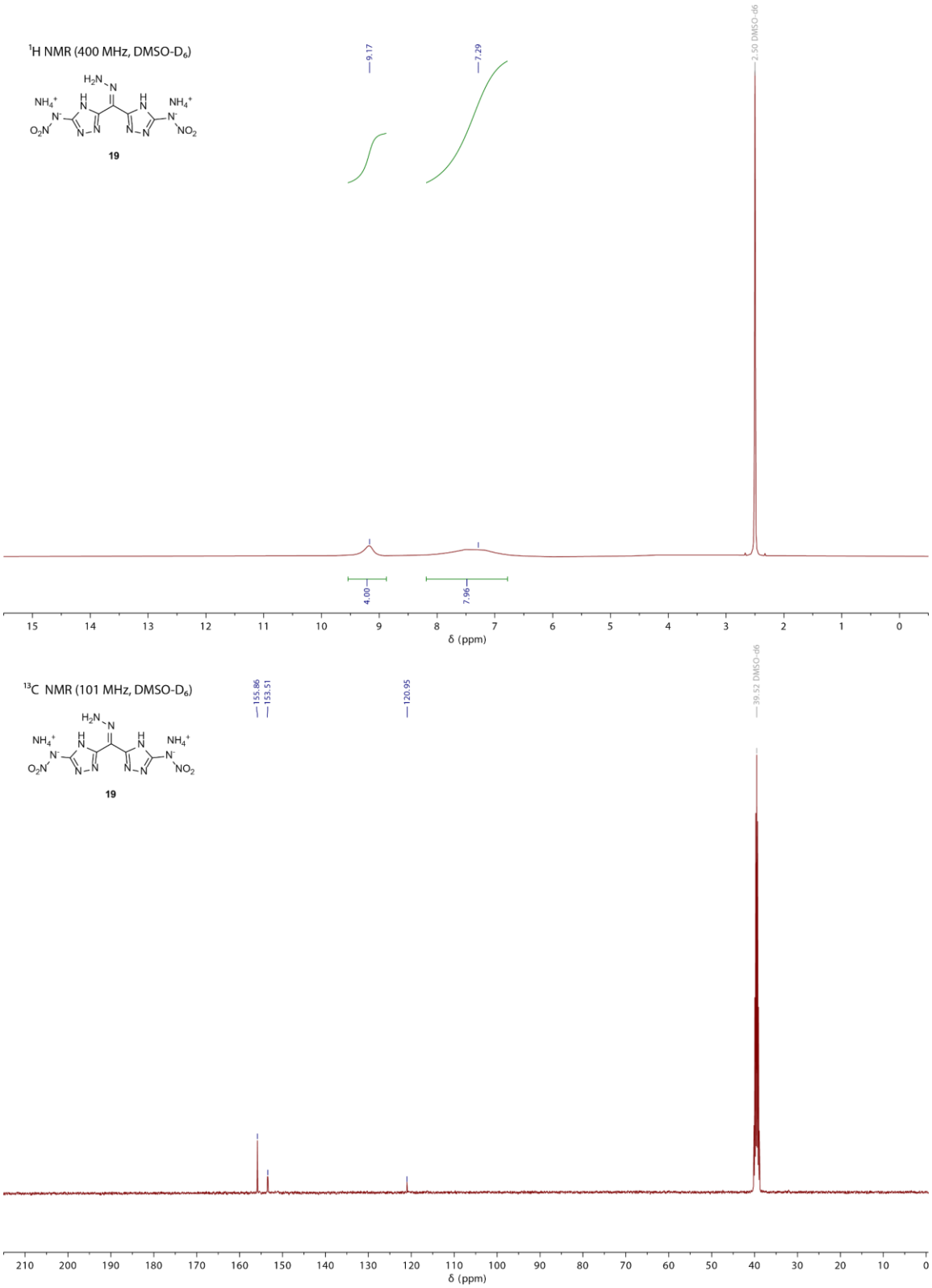

Figure S19. ^{1}H and ^{13}C{^{1}H} NMR spectra of **19**.

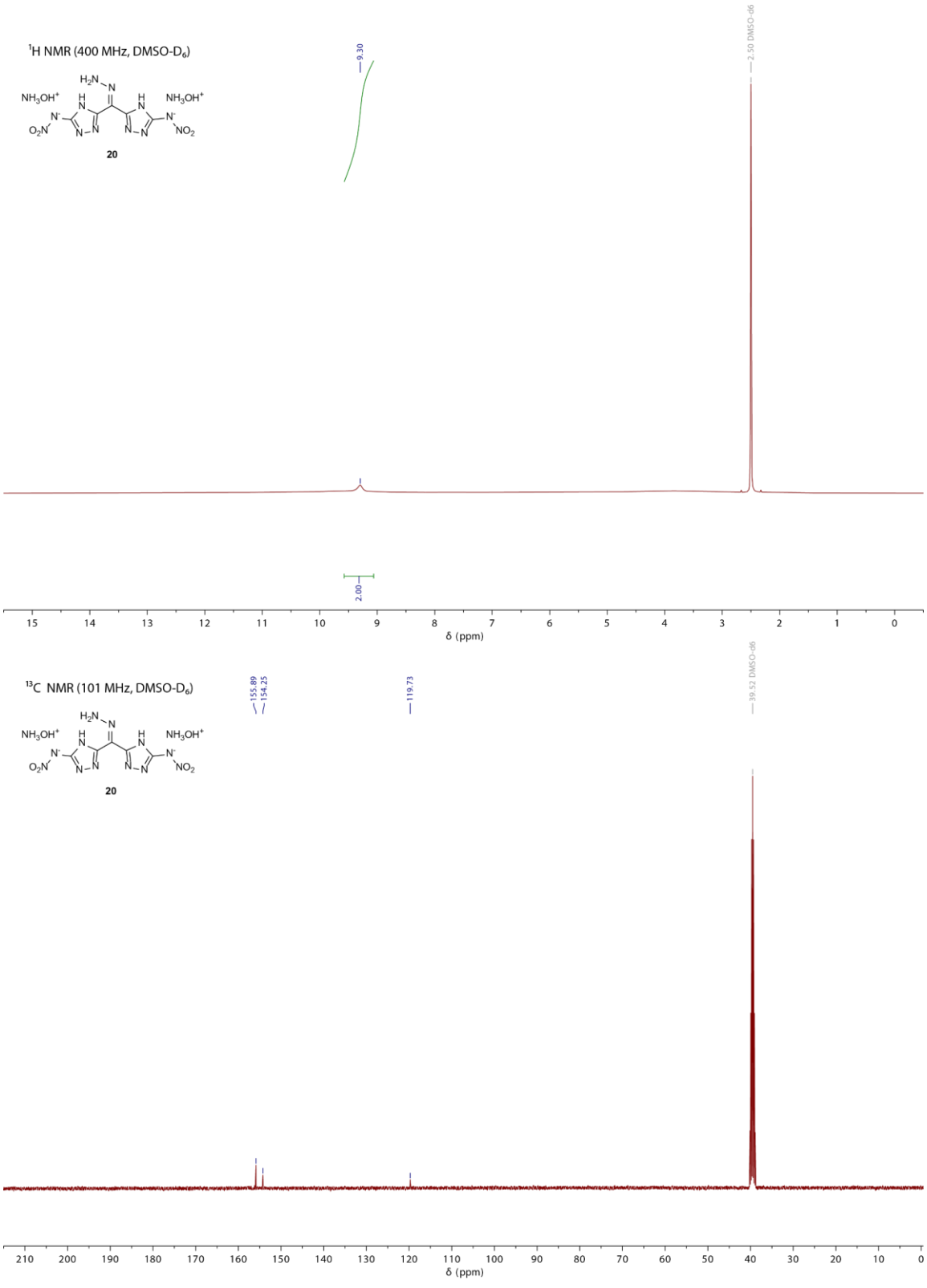

Figure S20. ^{1}H and ^{13}C{^{1}H} NMR spectra of **20**.

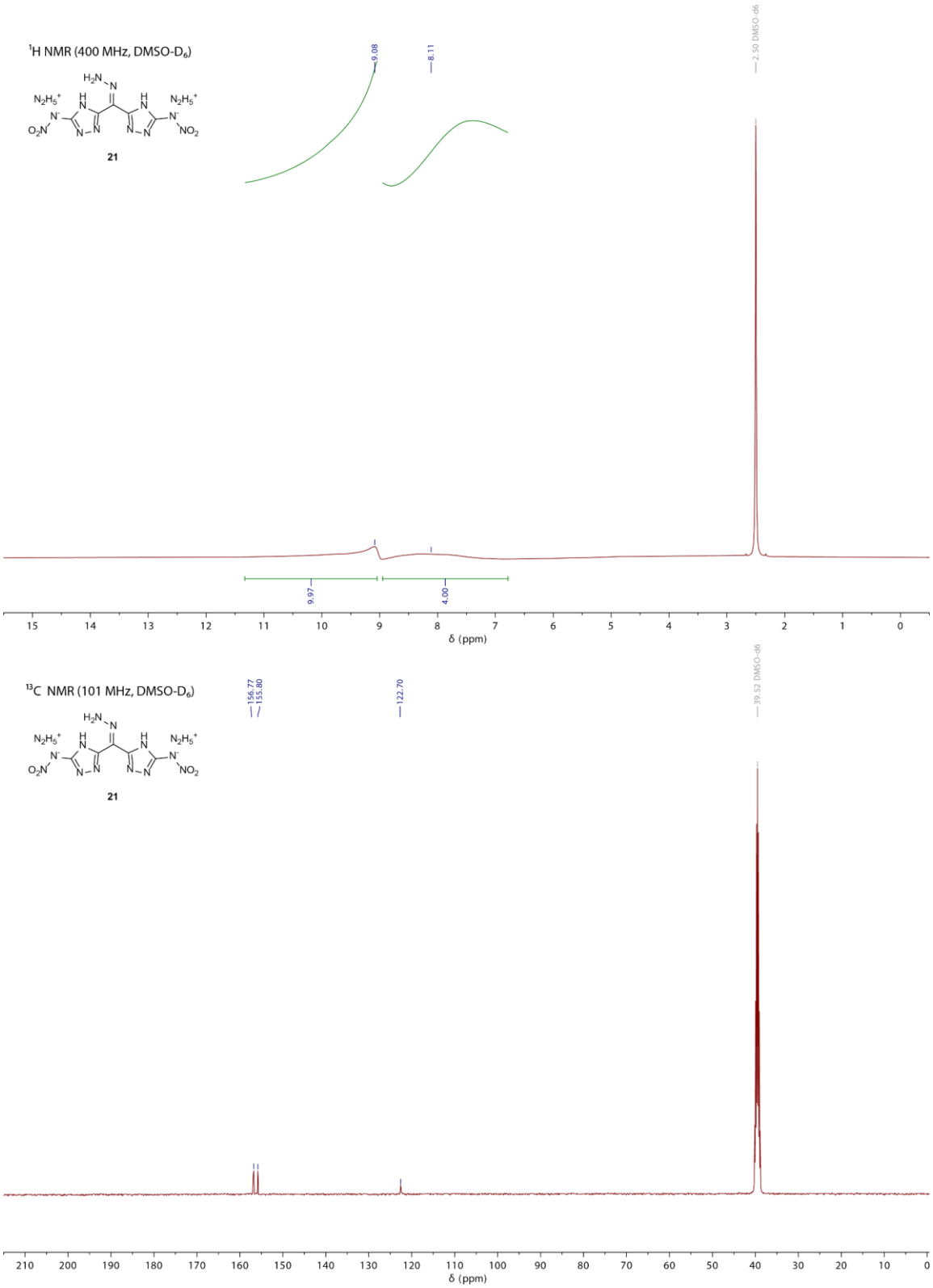

Figure S21. ^{1}H and ^{13}C{^{1}H} NMR spectra of **21**.

7.7.4 DTA measurements

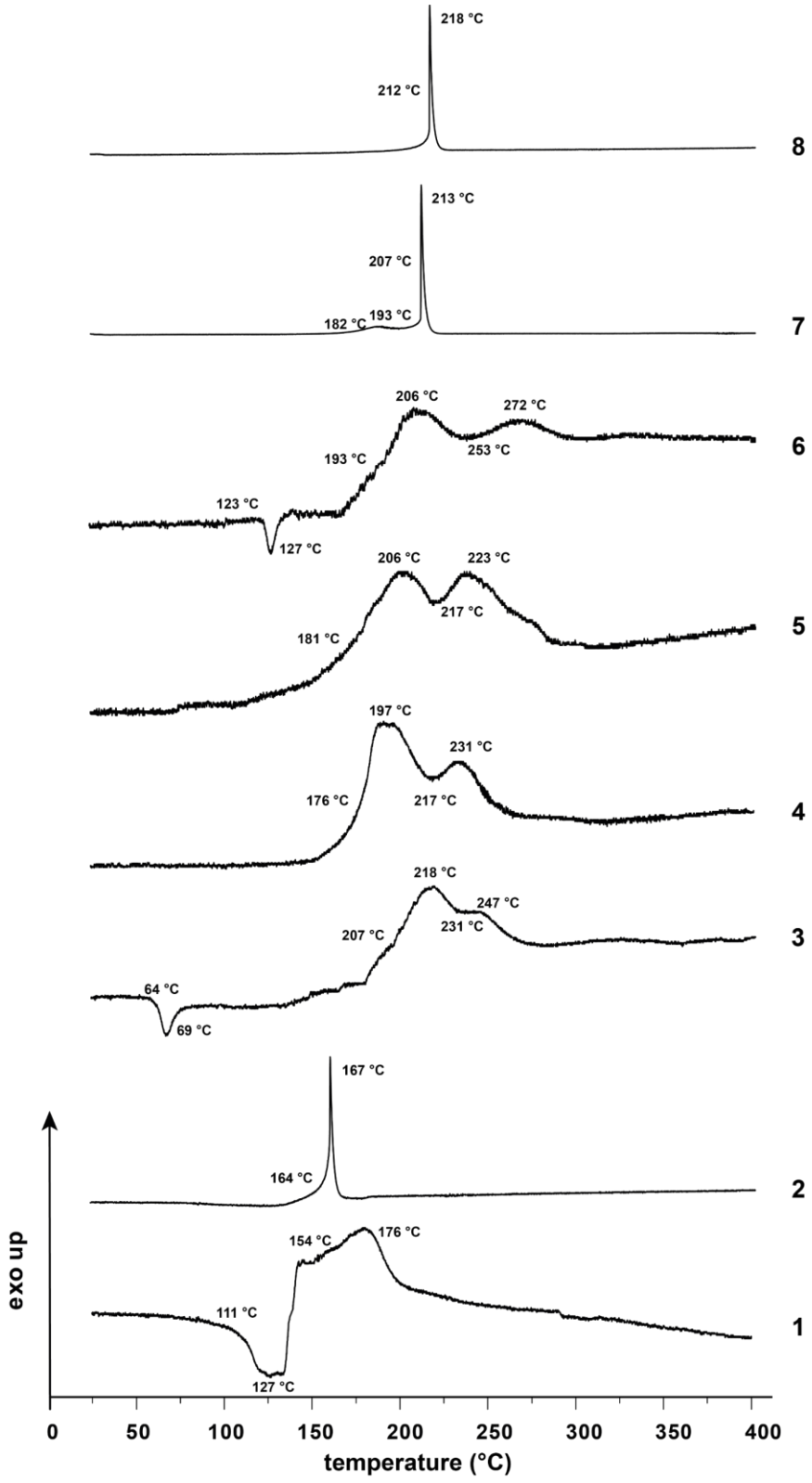

Figure S22. DTA measurements of **1**–**8** with their onset and peak temperatures.

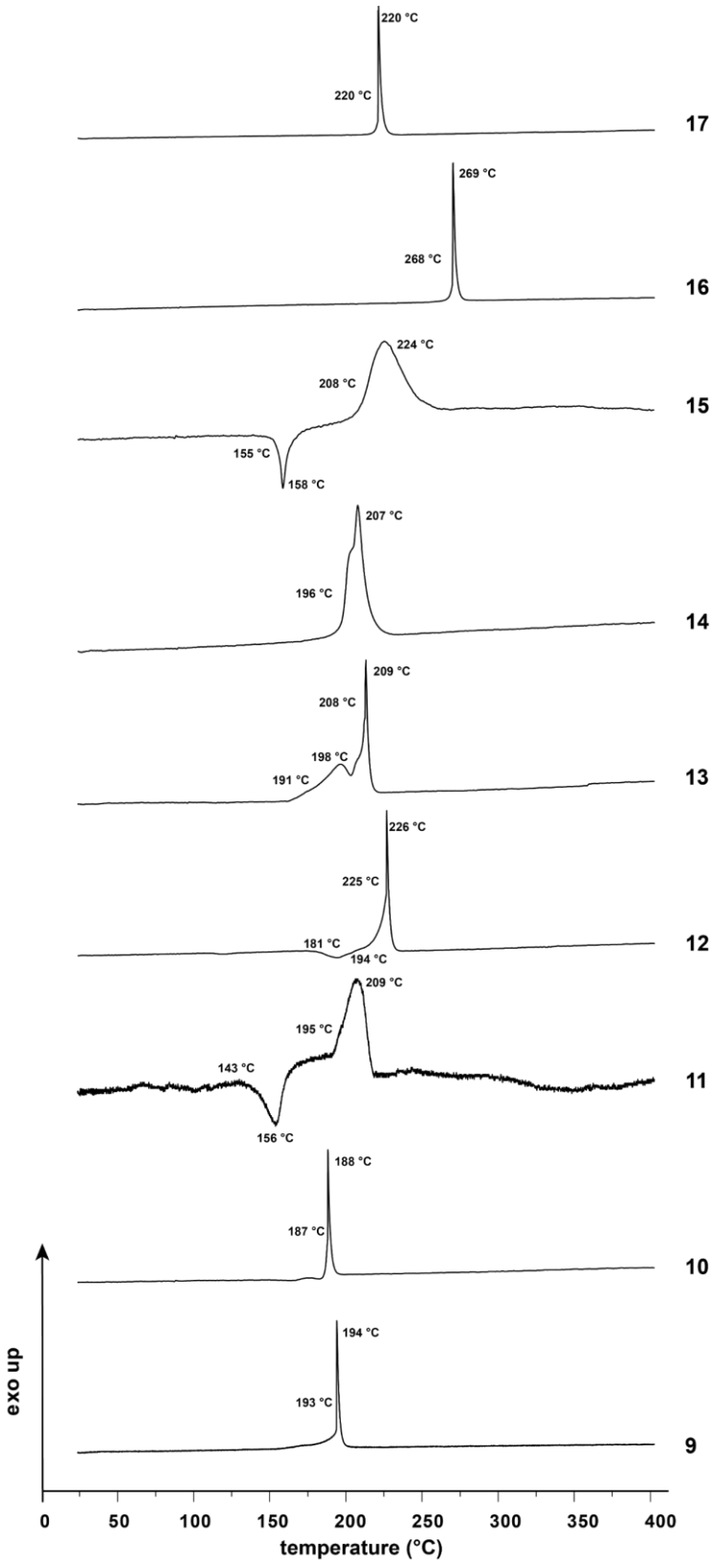

Figure S23. DTA measurements of **9**−**17** with their onset and peak temperatures.

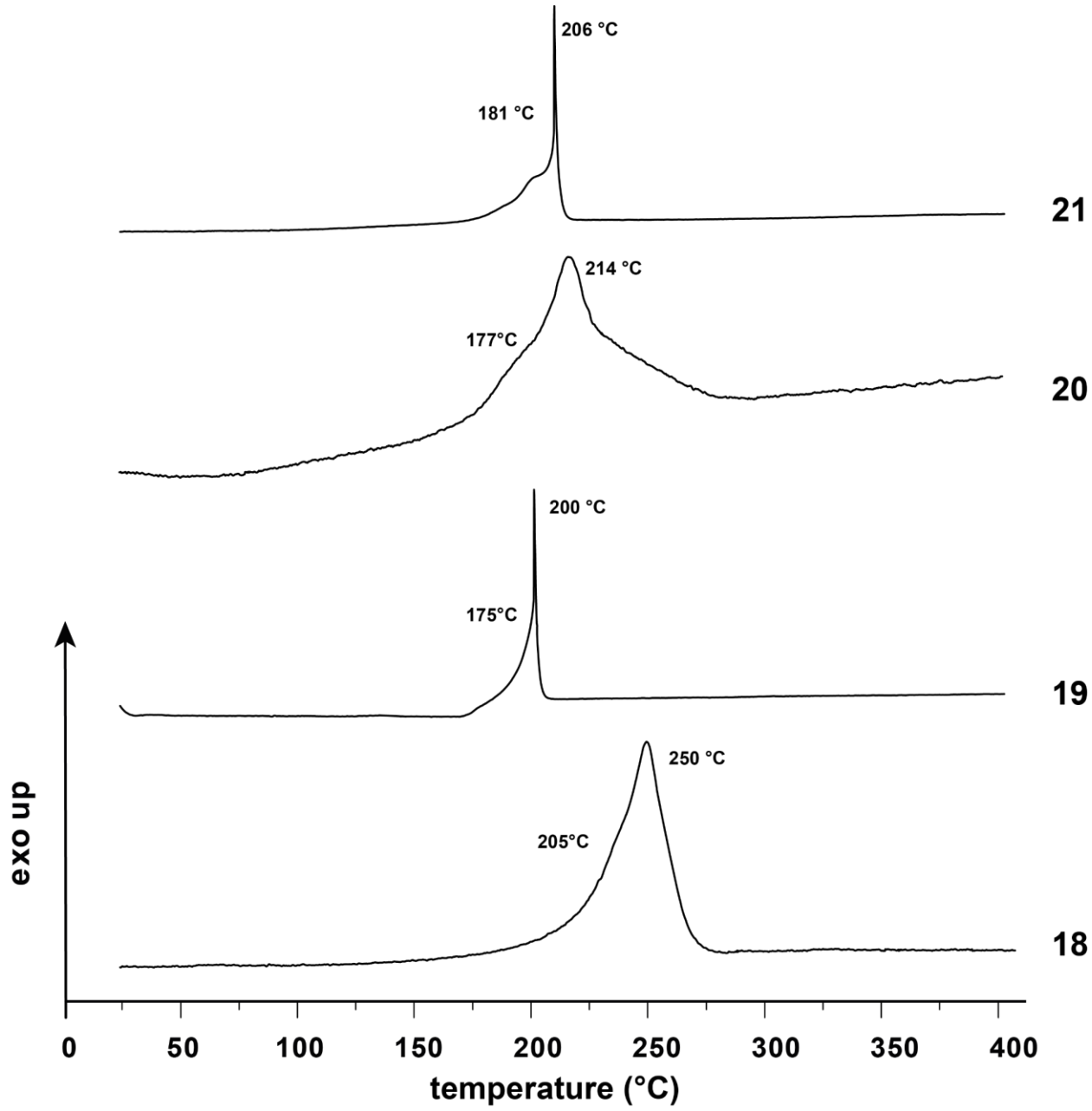

Figure S24. DTA measurements of **18**−**21** with their onset and peak temperatures.

7.7.5 Heat of Formation Calculations

All quantum chemical calculations were carried out using the Gaussian G09 program.[S1] The enthalpies (H) and zero-point energies (ZPE) were calculated using the complete basis set (CBS) method and the W1 method of *Petersson et al*.[S2] assuming a C_2 symmetry.

Heats of formation (HOF) were calculated using the atomization method (Equation S1) using room temperature enthalpies.[S3]

$$\Delta_f H°_{(g,\,M,\,298)} = H_{(Molecule,\,298)} - \sum H°_{(Atoms,\,298)} + \sum \Delta_f H°_{(Atoms,\,298)} \quad (S1)$$

Table S2. Enthalpies for atoms C, H, N, O and D and their literature values for atomic $\Delta_f H°^{298}$.[S3]

	H^{298K} CBS-4M [a.u.]	NIST
C	-37.786153	218.0
H	-0.500991	716.7
N	-54.522456	472.7
O	-74.991184	249.2

The standard molar enthalpy of formation were calculated using $\Delta_f H(g)$ subtracting the enthalpy of sublimation estimated by applying Trouton´s rule.[S4]

For ionic compounds, the lattice energy (U_L) and lattice enthalpy (ΔH_L) are calculated from the corresponding X-ray molecular volumes (converted to RT) according to the equations provided by *Jenkins* and *Glasser*.[S5] With the calculated lattice enthalpy, the gas-phase enthalpy of formation was converted into the solid-state (standard conditions) enthalpy of formation. The calculation results are summarized in Table S3.

Table S3. Heat of formation calculations.

	$-H^{298}$ [a] /a.u.	$\Delta_f H°$(g,M) [b] /kJ mol^{-1}	$\Delta_f H°$(s) [c] /kJ mol^{-1}	$\Delta_f U$(s) [d] /kJ kg^{-1}
2	–1339.775803	519.2	437.9	1365.9
4	–	–	311.9	935.8
5	–	–	617.9	1628.8
7	–	–	259.6	674.0
8	–	–	446.8	1023.2
10	–1155.348084	352.8	266.2	981.9
12	–	–	62.6	302.3
13	–	–	188.4	626.0
14	–	–	358.1	1102.0
16	–	–	40.5	212.5
17	–	–	278.6	740.3
18	–	–	106.0	349.4
19	–	–	398.8	1312.4
20	–	–	567.2	1666.0
21	–	–	702.2	2055.2

[a] CBS-4M electronic enthalpy; [b] gas phase enthalpy of formation; [c] standard solid state enthalpy of formation; [d] solid state energy of formation.

7.7.6 Calculation of Density at 298 K

The room temperature density was recalculated from the corresponding crystal density by Equation S2 (a_v = 1.5x10^{-4} K).

$$d_{298K} = \frac{d_T}{1+ \alpha_v(298-T_0)} \quad \text{(S2)}$$

d_T = insert X-ray density in g cm^{-3}

T_0 = insert X-Ray temperature in K

α_v = correction factor

Table S3. X-Ray and recalculated densities of **17**.

	X-Ray density [g cm^{-3}]	Density recalculated to 298K [g cm^{-3}]
17	(@ 174K) 1.602	1.573

7.7.7 References SI

[S1] M. J. Frisch, G. W. Trucks, H. B. Schlegel, G. E. Scuseria, M. A. Robb, J. R. Cheeseman, G. Scalmani, V. Barone, B. Mennucci, G. A. Petersson, H. Nakatsuji, M. Caricato, X. Li, H.P. Hratchian, A. F. Izmaylov, J. Bloino, G. Zheng, J. L. Sonnenberg, M. Hada, M. Ehara, K. Toyota, R. Fukuda, J. Hasegawa, M. Ishida, T. Nakajima, Y. Honda, O. Kitao, H. Nakai, T. Vreven, J. A. Montgomery, Jr., J. E. Peralta, F. Ogliaro, M. Bearpark, J. J. Heyd, E. Brothers, K. N. Kudin, V. N. Staroverov, R. Kobayashi, J. Normand, K. Raghavachari, A. Rendell, J. C. Burant, S. S. Iyengar, J. Tomasi, M. Cossi, N. Rega, J. M. Millam, M. Klene, J. E. Knox, J. B. Cross, V. Bakken, C. Adamo, J. Jaramillo, R. Gomperts, R. E. Stratmann, O. Yazyev, A. J. Austin, R. Cammi, C. Pomelli, J. W. Ochterski, R. L. Martin, K. Morokuma, V. G. Zakrzewski, G. A. Voth, P. Salvador, J. J. Dannenberg, S. Dapprich, A. D. Daniels, O. Farkas, J.B. Foresman, J. V. Ortiz, J. Cioslowski, D. J. Fox, Gaussian 09 A.02, Gaussian, Inc., Wallingford, CT, USA, **2009**.

[S2] a) J. W. Ochterski, G. A. Petersson, and J. A. Montgomery Jr., *J. Chem. Phys.* **1996**, *104*, 2598–2619; b) J. A. Montgomery Jr., M. J. Frisch, J. W. Ochterski G. A. Petersson, *J. Chem. Phys.* **2000**, *112*, 6532–6542; c) E.C. Barnes, G. A. Petersson, J. A. Montgomery Jr, M. J. Frisch, J. M. L. Martin, *J. Chem. Theor. Comput.* **2009**, *5*, 2687−2693.

[S3] a) P. J. Linstrom, W. G. Mallard (Editors), NIST Standard Reference Database Number 69, http://webbook.nist.gov/chemistry/ (May 2011); b) J. D. Cox, D. D. Wagman, V. A. Medvedev, CODATA Key Values for Thermodynamics, Hemisphere Publishing Corp., New York, **1984**.

[S4] F. Trouton, *Philos. Mag.* **1884**, *18*, 54-57; b) M. S. Westwell, M. S. Searle, D. J. Wales, D. H. Willimas, *J. Am. Chem. Soc.* **1995**, *117*, 5013-5015.

[S5] a) H. D. B. Jenkins, H. K. Roobottom, J. Passmore, L. Glasser, *Inorg. Chem.* **1999**, *38*, 3609–3620; b) H. D. B. Jenkins, D. Tudela, L. Glasser*, Inorg. Chem.* **2002**, *41*, 2364–2367.

8 Investigation and Characterization of Nitrazapropane-, Oxapropane- and Trinitrazaheptane-Bridged Nitro Esters

Jasmin T. Lechner, Christian Riedelsheimer, Nina M. Gerold, Jennifer Heidrich, Burkhard Krumm, Jörg Stierstorfer and Thomas M. Klapötke*

as published in *European Journal of Organic Chemistry* **2023**, e202300890

DOI: 10.1002/ejoc.202300890

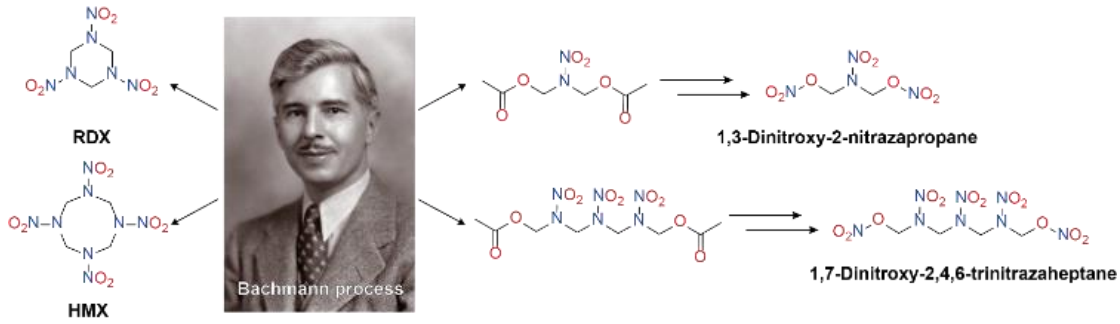

Abstract: In this work, 1,3-dinitroxy-2-nitrazapropane and 1,7-dinitroxy-2,4,6-trinitrazaheptane were synthesized and investigated. Starting from hexamine, the open-chain compounds were prepared by a modified Bachmann procedure which is commonly used for the synthesis of hexogen (RDX) and octogen (HMX). All new compounds were characterized by NMR spectroscopy, X-ray diffraction, vibrational analysis and elemental analysis. Their thermal behavior was studied by differential thermal analysis (DTA) and thermogravimetric analysis (TGA). The sensitivities towards impact (IS) and friction (FS) were determined according to the BAM (Bundesanstalt für Materialforschung und -prüfung) standard method. Their energetic properties, which were determined from the energies of formation at the CBS-4 M level, were calculated using the EXPLO5 computer code. Moreover, 1,3-dinitroxy-2-oxapropane was synthesized and investigated. The various compounds were compared with each other and with the commonly used explosives in terms of their physicochemical properties and detonation behavior.

8.1 Introduction

RDX, also known as hexogen, is one of the best-researched and most-used secondary explosives.[1] It has several applications in the civilian as well as military sector, for example in combination with a binder used as plastic-bonded explosives (PBX).[1, 2, 3] With a moderate sensitivity towards external stimuli and high detonation performance RDX (1,3,5-trinitro-1,3,5-triazinane) is a popular energetic material. In addition, the preparation is quite facile. Nowadays, there are many procedures known for RDX synthesis.[1, 4]

Two of the most studied and in industry used synthesis are the Woolwich process and the Bachmann process.[1, 4-6] In the Woolwich synthesis, RDX is obtained using hexamine as starting material and only nitric acid as the nitration agent.[1, 6] In the Bachmann process a mixture of nitric acid, ammonium nitrate and acetic anhydride is used as a nitration mixture.[4, 7] The Bachmann process, however, allows not only the targeted production of RDX starting from hexamine, but also its eight-membered ring derivative HMX (1,3,5,7-tetranitro-1,3,5,7-tetrazocane), by adjusting the reaction conditions.[8, 9] As can be seen from Figure 1, a lower reaction temperature during nitration is more suitable to obtain HMX as the main

product. In addition, the preferred synthesis of HMX uses a lower acidity and a smaller amount of ammonium nitrate.[1, 9-11]

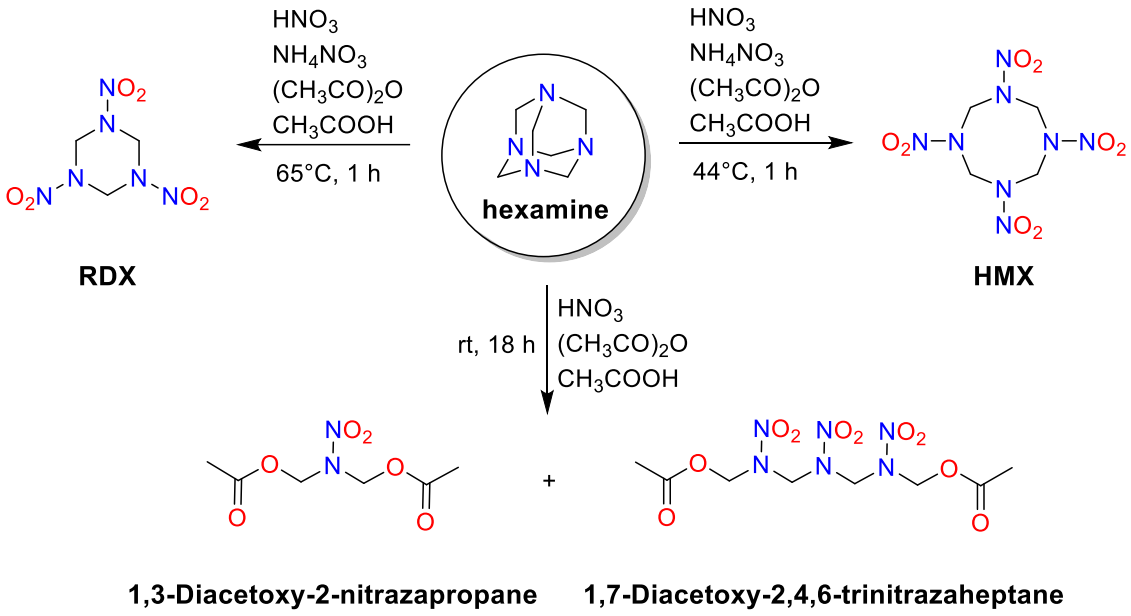

Figure 1. Products obtained from the nitration of hexamine with different reaction conditions.

This modification of the reaction conditions is especially advantageous because two different products can be produced at the same industrial plant using the same chemicals just by changing a few conditions. As shown in Figure 1, the conditions can also be changed in such a way that the open-chain nitramines 1,3-diacetoxy-2-nitrazapropane and 1,7-diacetoxy-2,4,6-trinitrazaheptane are formed preferentially.[12, 13] Here the reaction temperature is significantly lower than the temperature of the other two reactions. In addition, no ammonium nitrate is required, but reaction time necessitates 18 hours, while the synthesis of RDX and HMX is finished after only one hour.[12, 13]

In this work, attempts were made to synthesize new energetic materials based on these open-chain nitramines, displayed in Figure 1. From these precursors, further promising derivatives could be produced at existing Bachmann plants and thus, may find versatile applications. Already known from the literature are the corresponding diazido derivatives, which are, however, difficult for a possible application due to their very high sensitivity.[12] The goal in this work, was to look for a route to the corresponding nitro esters, which are very similar to

nitroxyethylnitramine (NENA) compounds and could represent promising energetic materials by combining both nitro ester and nitramine moiety in one compound.[14, 15] 1,3-Dinitroxy-2-nitrazapropane is mentioned once in literature but apparently was impossible to isolate due to its instability.[16] Furthermore, attempts were made to synthesize the corresponding oxapropane-bridged dinitroxy compound which is also only mentioned once in literature without analysis or further characterization.[16] Due to its similar structure to the widely used plasticizers EGDN (ethylene glycol dinitrate), DEGDN (diethylene glycol dinitrate), and TEGDN (triethylene glycol dinitrate), this could be a potential application area for 1,3-dinitroxy-2-oxapropane.[17, 18] In addition, compounds with oxapropane bridges should show better thermal stability compared to nitrazapropane bridged compounds, which would make them even more promising for a potential application in safety concerns.[19]

8.2 Results and Discussion

8.2.1 Synthesis

1,3-Diacetoxy-2-nitrazapropane (**1**) and 1,7-diacetoxy-2,4,6-trinitrazaheptane (**2**) were prepared by a modified literature procedure.[12, 13] Starting from hexamine, the Bachmann nitration reaction was modified to give the open-chain nitramines as the main products. After 18 hours according to Scheme 1, **2** can be easily separated by filtration. From the remaining filtrate, **1** is obtained by vacuum distillation at elevated temperatures of around 170 °C. Afterward, both acetoxy functionalized **1** and **2** were chlorinated using hydrogen chloride to obtain 1,3-dichloro-2-nitrazapropane (**3**) and 1,7-dichloro-2,4,6-trinitrazaheptane (**4**).

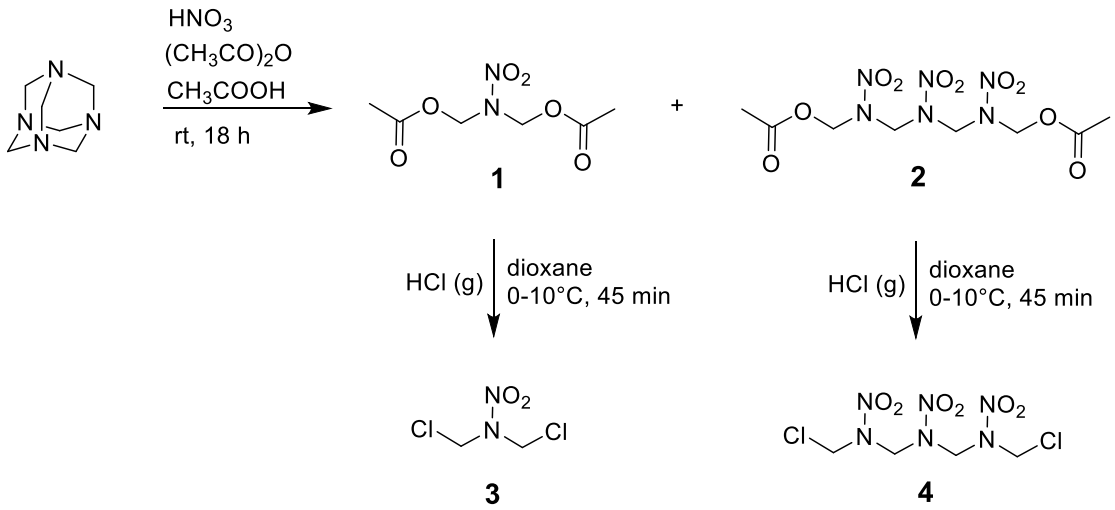

Scheme 1. Synthetic route to the chloromethyl substituted nitramines **3** and **4**.

In order to obtain the corresponding nitro esters **5** and **6** starting from **3** and **4**, different approaches were attempted for the nitrazapropane and trinitrazaheptane compounds. First, a classical nitration reaction using fuming nitric acid as nitration agent was attempted in each case, shown in Scheme 2. This was successful for both, the nitrazapropane and the trinitrazaheptane derivatives and **5** and **6** were obtained through a nucleophilic substitution reaction. In both cases, however, it should be noted that a short reaction time in nitric acid is crucial, and that even after separation of the products it is essential to ensure extensive washing with water, until free of acid to avoid decomposition. As known from literature, accidents have occurred because residual acid in nitro esters has led to uncontrolled autocatalytic decomposition reactions.[18, 20, 21] As shown in Scheme 2 for reaction pathway II, alternatively the chloromethyl groups can be converted into the nitro esters (nitroxy or nitratomethyl groups) by reaction with silver nitrate in acetonitrile. In this so-called Victor-Meyer reaction,[22] it was taken advantage of the poor solubility of silver chloride in organic solvents. The reaction mechanism here also follows an S_N2 mechanism and **5** and **6** were obtained pure after filtration and extraction.

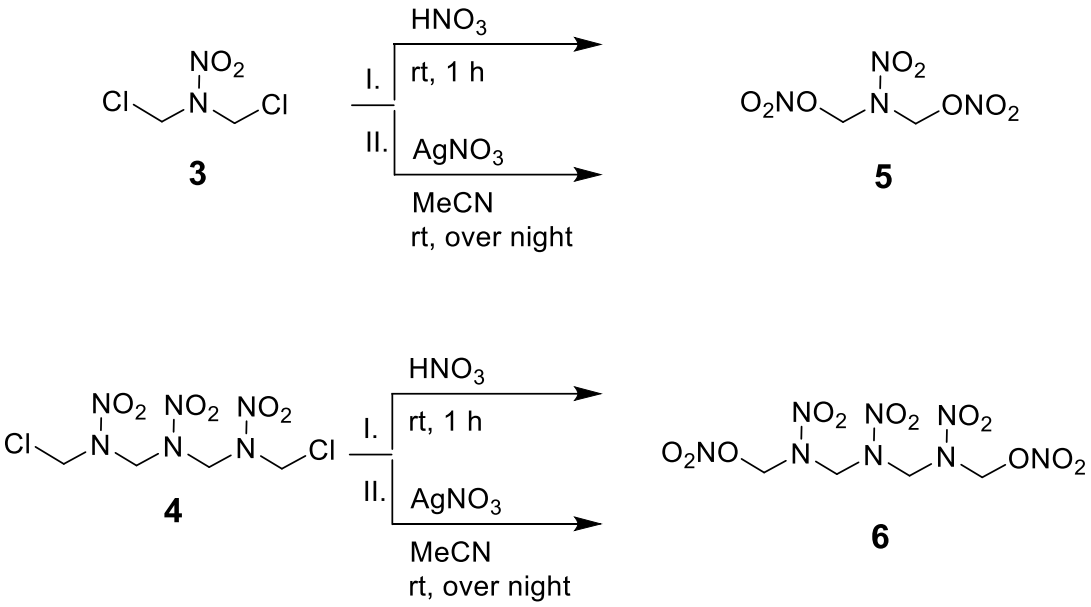

Scheme 2. Conversion of **3** and **4** into the nitro esters **5** and **6**.

Both routes work different for **5** and **6**; whereas **5** is obtained in larger yields *via* nitration with $AgNO_3$ (60 % *vs*. 30 %), **6** is the opposite *via* nitration with HNO_3 (75 % *vs*. 34 %).

For the nitration of **3** *via* pathway II different reaction times were tested to determine the best conditions. It was found that if **3** is stirred with silver nitrate for only 2 hours, an inseparable mixture is observed and not only the desired product. In this mixture, a cyclized product is formed in very small amounts identified by X-ray diffraction as 3,7-dinitro-1,5,3,7-dioxadiazocane, shown in Scheme 3 and Figure 7. However, it was not possible to specifically prepare and isolate the compound, therefore it was treated as a by-product with no further analysis possible. Thus, to obtain pure **6**, a reaction time of at least 12 h is necessary.

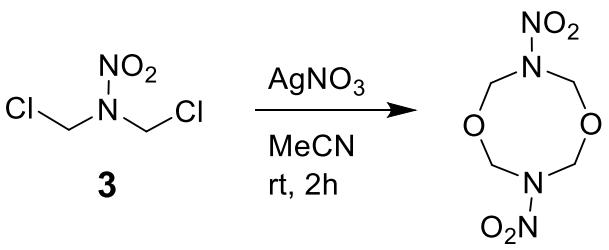

Scheme 3. 3,7-Dinitro-1,5,3,7-dioxadiazocane as a product of nitration after short reaction time.

1,3-Dichloro-2-oxapropane (bischloromethyl ether) was prepared according to a literature procedure.[23] Here as well, the nitration of the chloromethyl group was attempted *via* two different pathways as shown in Scheme 4.

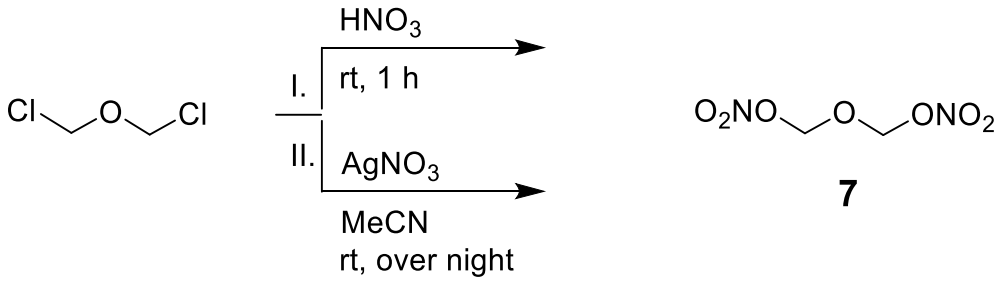

Scheme 4. Nitration of bis-chloromethyl ether to form the corresponding nitrate **7**.

A comparison of both options shows that nitration with silver nitrate is preferable. While the nitration with fuming nitric acid results in only low yields of an impure product, the Victor-Meyer reaction[22] with silver nitrate furnished in good yields (82 %) the pure nitro ester 1,3-dinitroxy-2-oxapropane **7**.

8.2.2 Characterization

All synthesized compounds were characterized by ^{1}H, ^{13}C{^{1}H} and ^{14}N NMR spectroscopy in acetone-d_6. In addition, ^{15}N NMR spectra of **5** and **6** as well as a ^{17}O NMR spectrum of **7** were recorded, and are shown and discussed in more detail in the following. All other spectra and assignments can be found in the Experimental Section and in the Supporting Information.

Figure 2 shows the ^{15}N NMR spectrum of **5**. The singlet at −188.6 ppm can be assigned to the nitramine nitrogen (denoted as N1). The resonances of the nitro groups appear as multiplets due to coupling with the methylene hydrogen atoms in the typical regions at lower field at −39.6 ppm for the nitro group (N2) of the nitramine moiety as a quintet ($^{3}J_{N,H}$=3.4 Hz), and at −48.5 ppm for the nitro ester nitrogen (N3) as a triplet ($^{3}J_{N,H}$=4.8 Hz).

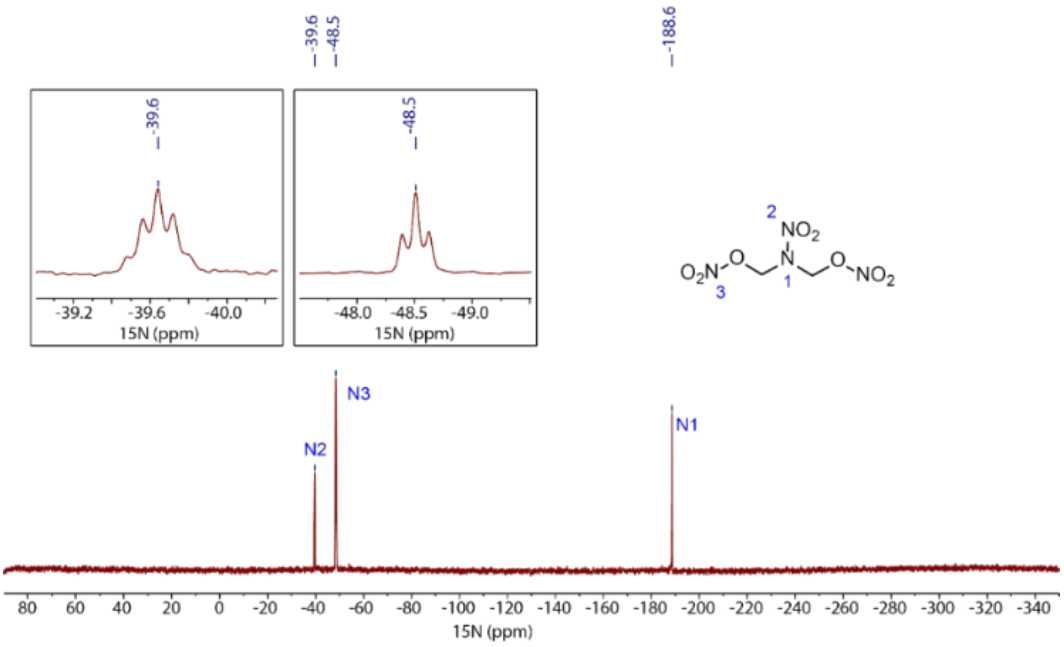

Figure 2. ^{15}N NMR spectrum of 1,3-dinitrooxy-2-nitrazapropane (**5**) in acetone-d_6.

The ^{15}N NMR spectrum of **6** is displayed in Figure 3, and shows the five resonances as to be expected due to the symmetry. The two singlets at −189.5 (denoted as N2) and −191.0 (N1, central nitrogen) ppm are found for the nitramine nitrogen atoms in a 2 : 1 ratio. Accordingly, the two nitro nitrogen resonances of the nitramine moieties are detected at −33.5 ppm (N3, quintet, $^3J_{N,H}$=3.2 Hz) and at −36.0 ppm (N4, quintet, $^3J_{N,H}$=3.1 Hz), as well with a 1 : 2 ratio. The triplet (N5, $^3J_{N,H}$=4.7 Hz) at −47.2 ppm is assigned to the nitro ester nitrogen resonances.

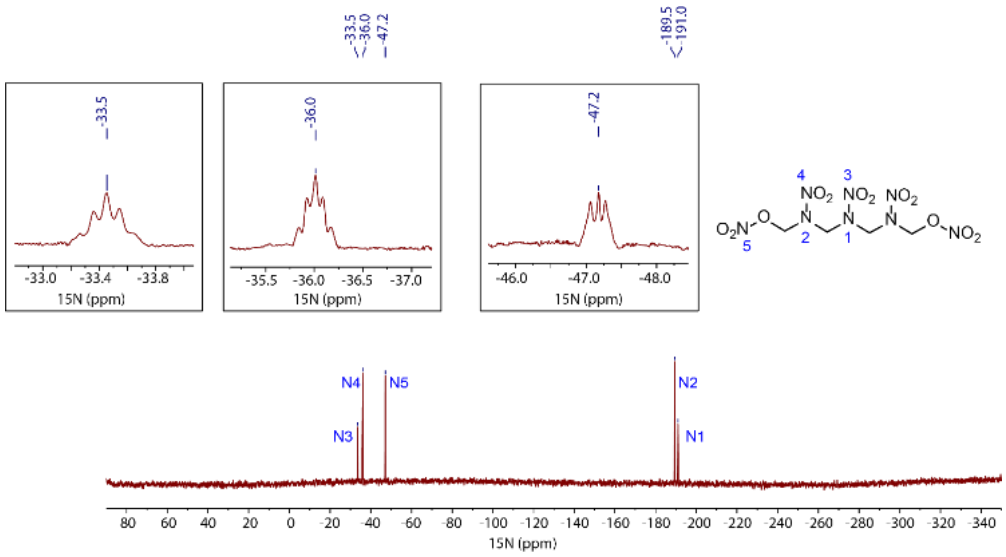

Figure 3. ^{15}N NMR spectrum of 1,7-dinitroxy-2,4,6-trinitrazaheptane (**6**) in acetone-d_6.

Figure 4 shows the ^{17}O NMR spectrum of the nitro ester substituted ether **7**. Since this compound is liquid at ambient temperature, and due to the low abundance of the ^{17}O isotope and the quadrupolar nature (0.037 %, I=−5/2), the spectrum was recorded as neat liquid. Due to the symmetry of the compound, three resonances with significant broadening are detected, as to be expected by the symmetry. The resonance at 73 ppm is assigned to the central ether oxygen atom (denoted as O1), that at 358 ppm corresponds to the ester oxygen (O2). The most intense (four oxygen atoms) resonances at lowest field at 452 ppm is assigned to the nitro oxygen atoms (O3). The shift of the nitro oxygen resonance is in good agreement for that of methyl nitrate.[24]

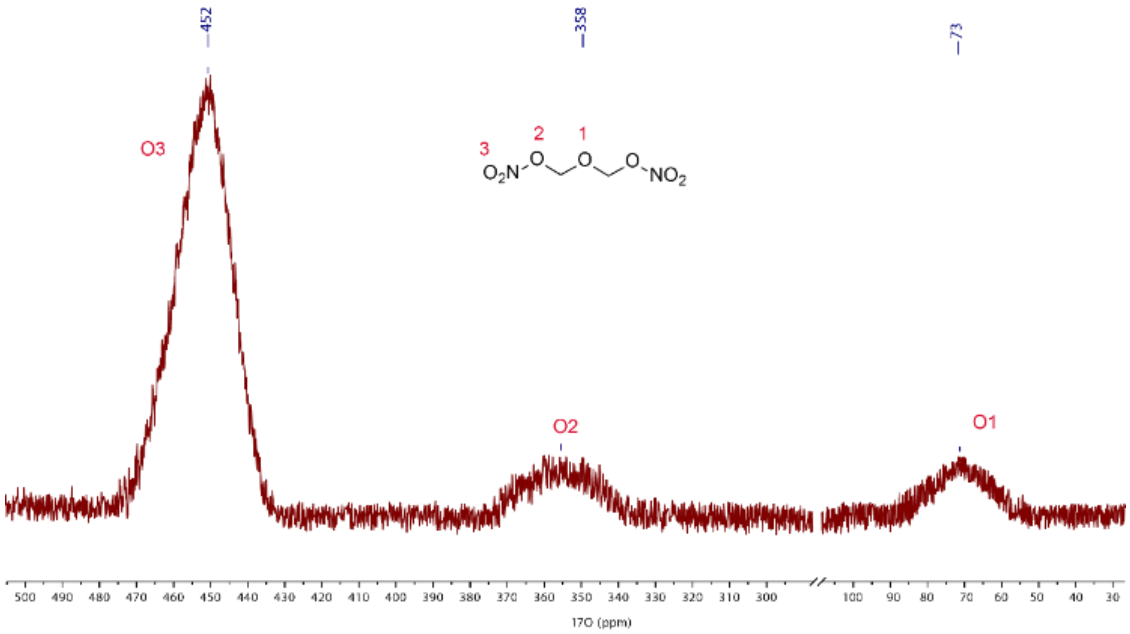

Figure 4. ^{17}O NMR spectrum of 1,3-dinitroxy-2-oxapropane (**7**) as a neat liquid.

8.2.3 X-ray Diffraction

Low temperature single-crystal X-ray diffraction experiments were performed on single crystals of **5**, **6** and the side product 3,7-dinitro-1,5,3,7-dioxadiazocane.[25] The crystal structures with selected bond lengths and angles are shown and discussed in the following, more information about the crystallographic data and structure refinement can be found in the Supporting Information.

The crystal structures of 1,3-dinitroxy-2-nitrazapropane (**5**, left) and 1,7-dinitroxy-2,4,6-trinitrazaheptane (**6**, right) are shown in Figure 5.

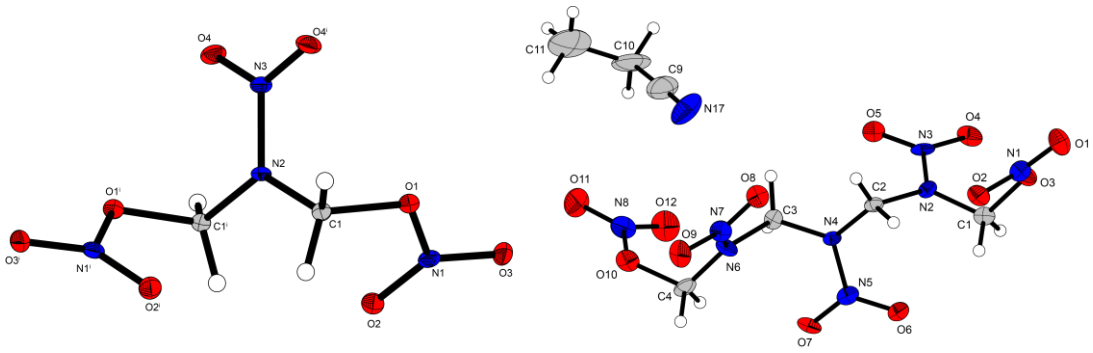

Figure 5. Crystal structure of **5** and **6** with selected bond lengths (Å): **5** O2−N1 1.2104(15), O1−N1 1.4100(15), O3−N1 1.1989(15); **6** O1−N1 1.201(9), O2−N1 1.214(10), O3−N1 1.413(10), O11−N8 1.199(9), O12−N8 1.219(10), O10−N8 1.403(10) (For compound **6**, selected values of one of the two independent molecules in the unit cell are given).

The azapropane **5** was recrystallized from acetonitrile and crystallizes as colorless plates in the orthorhombic space group *Pbcn* with a recalculated density of 1.874 g cm^{-3} at 298 K and four molecules per unit cell. The azaheptane **6** crystallizes as colorless plates in the orthorhombic space group $P2_12_12_1$ with a recalculated density of 1.578 g cm^{-3} at 298 K. Moreover, it crystallizes with a propionitrile solvate and two different molecules in its unit cell. Both structures, **5** and **6**, show a noticeable twisted character, due to the repulsion of the nitro groups. For **5** both nitro groups are arranged *trans* to each other to keep a maximum distance. Nevertheless, the structure is symmetrical when viewed from the nitrogen (N2) in the center, and the twisting of the two nitrato groups occurs with the same angle (N1−O1−C1−N2 −73.53(14)). In Figure 6 the unit cell of compound **5** along the *b* axis is shown.

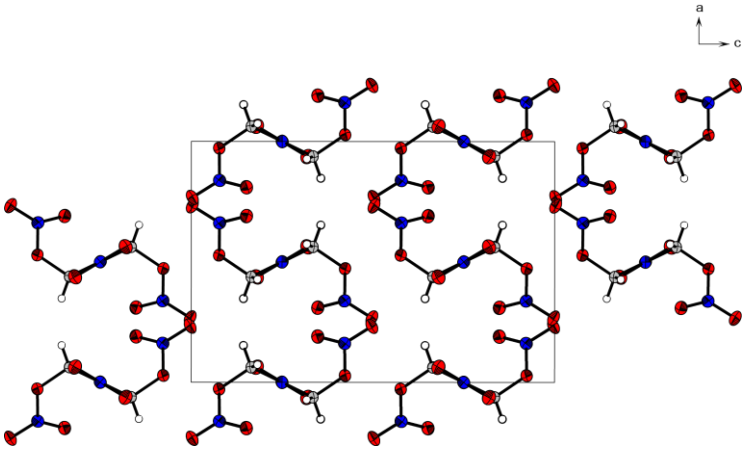

Figure 6. Molecular structure of compound **5** along the *b* axis with selected angles (°): N1−O1−C1−N2 −73.53(14), N3−N2−C1−O1 −68.68(11).

For **6** also a noticeable twist is obvious. A view at the nitro groups reveals a slight twist away from each other due to repulsion. Thus, viewed from left to right, the first nitro group is oriented backward, the second forward, then the third in the center upward, the fourth backward again, and the last again forward. As a result, a *zigzag*-type structure of the C−N backbone is formed.

The crystal structure of the unexpected side product 3,7-dinitro-1,5,3,7-dioxadiazocane is shown in Figure 7. Crystallization was obtained from ethyl acetate as a colorless plate in the orthorhombic space group *Fmm*2 with a recalculated density of 1.679 g cm^{-3} at 298 K and four molecules per unit cell, which can be seen in Figure 7 on the right.

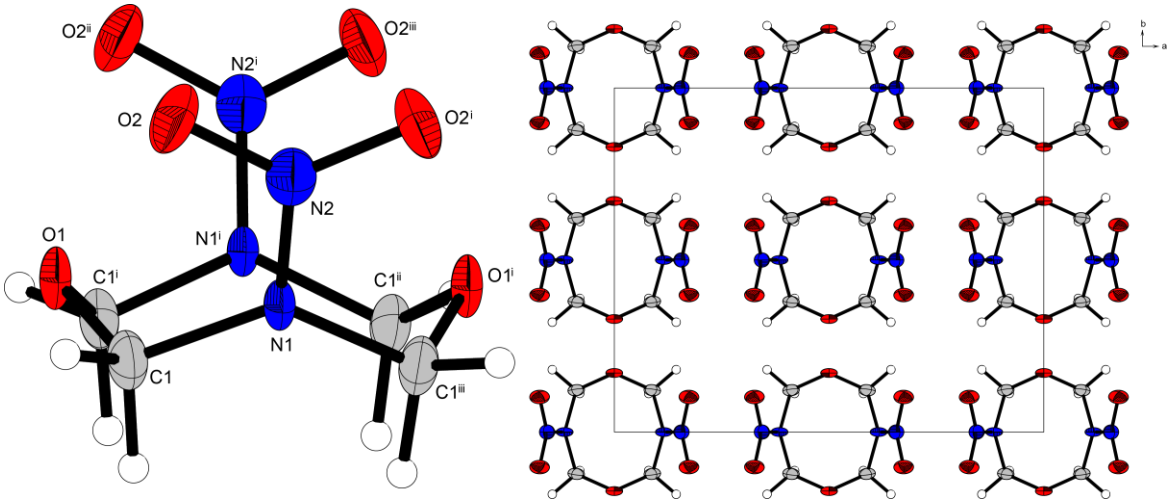

Figure 7. Crystal structure of 3,7-dinitro-1,5,3,7-dioxadiazocane (left) and molecular structure of its unit cell along the *c* axis (right) with selected values: bond lengths (Å): N2−N1 1.349(8), O2−N2 1.236(4); angles (°): O2−N2−N1 118.2(3), N2−N1−C1 117.3(3), C1−N1−C1 124.8(6).

On the left in Figure 7, the chair-chair (CC) structure of the diazocane backbone of 3,7-dinitro-1,5,3,7-dioxadiazocanes can be seen. The two nitro groups, which are attached to the ring nitrogen atoms, are aligned *cis* to each other in the same axial direction.

8.2.4 Thermal Analyses

Thermal characterization of **5**, **6** and **7** was performed using differential thermal analysis (DTA) and thermogravimetric analysis (TGA) with a heating rate of 5 °C min^{-1}. Because of the liquid character and high vapor pressure of **7** it was

necessary to increase the heating rate up to 20 °C min^{-1} for the determination of the decomposition temperature. The melting and decomposition points are shown explicitly in Table 1.

Table 1. Melting and decomposition temperatures of **5**, **6** and **7**.

	5	**6**	**7**
T_{melt} [°C]	44[a]	150[a]	−23[c]
T_{dec} [°C]	117[b]	155[b]	177[d]

[a] Onset point of the endothermic event of the DTA measurement. [b] Onset point of the exothermic event of the DTA measurement. [c] Measured with a low-temperature thermometer. [d] Decomposition temperature from the TGA measurement.

In addition, the DTA plot in combination with the TGA plot of 1,3-dinitroxy-2-nitrazapropane (**5**) is shown in Figure 8. A comparison of the two nitraza bridged **5** and **6** show that the melting point of **5** is significantly lower than the melting point of **6** with a difference of more than 100 °C. However, the decomposition temperatures differ by only 33 °C. While **5** does not decompose until 117 °C, **6** melts at 150 °C and then decomposes immediately. Thus, it can be assumed that the endothermic event initiates the exothermic decomposition of the compound.

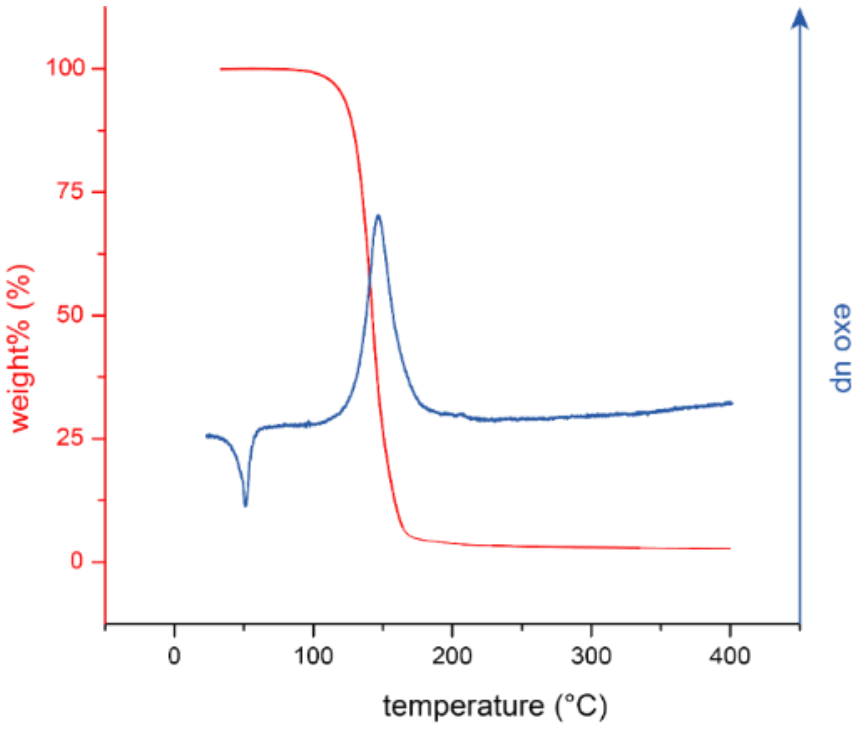

Figure 8. DTA and TGA measurement of 1,3-dinitroxy-2-nitrazapropane (**5**).

In addition, Figure 9 shows the TGA measurement of **7** at different heating rates. On the left, at a heating rate of 10 °C min^{-1} or less, the compound evaporates and therefore does not decompose, which can be seen from the permanent loss of mass starting already at the beginning of the measurement. However, if heated fast enough, the decomposition temperature can be reached before the complete sample is evaporated. In Figure 9 on the right, at a heating rate of 20 °C min^{-1}, the decomposition temperature of **7** is at 177°C.

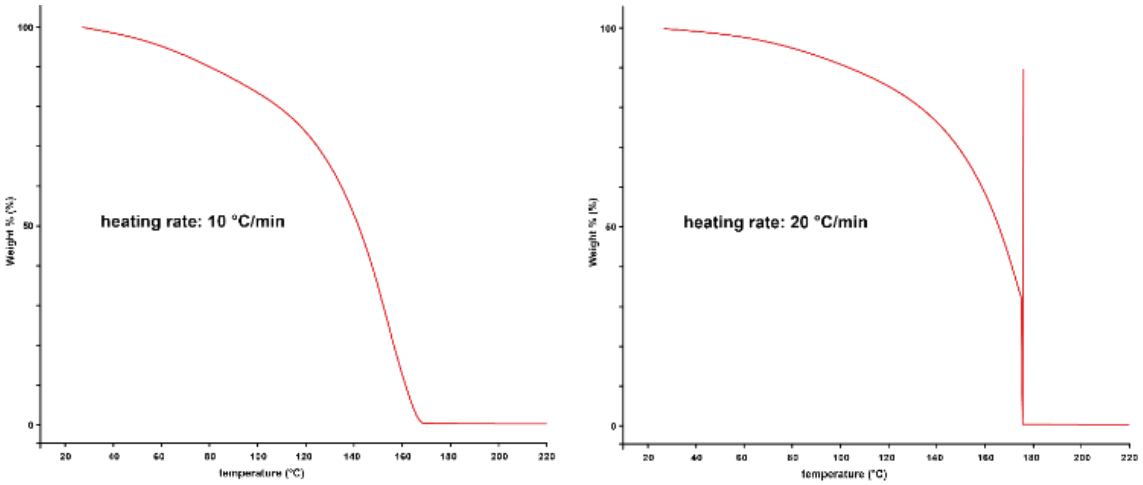

Figure 9. TGA measurements of 1,3-dinitroxy-2-oxapropane (**7**) with a heating rate of 10 °C min^{-1} (left) and 20 °C min^{-1} (right).

Upon comparison of the thermal stabilities of **5** and **7**, which differ only in the different bridging unit, the oxapropane-bridged compounds are shown to be more stable, as already described.[17]

8.2.5 Sensitivities and Energetic Properties

The sensitivities towards impact and friction of **5**, **6** and **7** were measured, the determined values are shown in Table 2 compared to prominent examples of the group of nitro esters (NG, EGDN and PETN).

When considering impact sensitivities, **5** and **6** show a value of 2 J, whereas a value lower than 1 J was observed for **7**. According to the UN Recommendations on the Transport of Dangerous Goods[26], these compounds are classified as very sensitive. The friction sensitivity value of **6** is 120 N and is therefore classified as

sensitive, whereas **5** and **7** with a friction sensitivity of 20 N are classified as very sensitive.[26]

Table 2. Sensitivities towards impact and friction of **5**, **6** and **7**.

	5	**6**	**7**	**PETN**[26,27]	**NG**[26,27]	**EGDN**[18]
IS[a] [J]	2	2	<1	3	<1	5
FS[b] [N]	20	120	20	60	>360	>360

[a] Impact sensitivity according to the BAM drop hammer (method 1 of 6). [b] Friction sensitivity according to the BAM friction tester (method 1 of 6).

In addition, the energetic properties of **5**, **6,** and **7** were calculated using the EXPLO5 code version 6.06.01.[27] The calculated EXPLO5 values are based on the density of the compounds and their enthalpy of formation. All relevant values are shown in Table 3 compared to pentaerythritol tetranitrate (PETN), nitroglycerine (NG), and ethylene glycol dinitrate (EGDN), three well-known and widely applied examples of the group of nitro esters.[28-29]

A closer look at the values in Table 3 reveals a similarity of **6** with PETN, while the values of **5** are between PETN and NG. The combined nitrogen and oxygen contents of **5**, **6** and **7** are higher compared to those of PETN, NG, and EGDN. As well, the values of the oxygen balance assuming the formation of CO and CO_2 are clearly positive for **5** and **7** and even slightly better than NG. The oxygen balance of **6** is slightly lower but with Ω_{CO2} of 0% better than the oxygen balance of PETN. Considering the detonation parameters, the velocity of detonation of **6** is 341 m s^{-1} higher than the value of PETN. The value of **5** is around 8500 m s^{-1}, which is in the same range as PETN, but still significantly better than NG. Due to the low heat of formation, the detonation velocity of **7** unfortunately cannot exceed the values of NG and EGDN.

Table 3. Energetic properties of **5**, **6** and **7** compared to PETN, NG and EGDN.

	5	**6**	**7**	**PETN**[25,26]	**NG**[25,26]	**EGDN**[18]
Formula	$C_2H_4N_4O_8$	$C_4H_8N_8O_{12}$	$C_2H_4N_2O_7$	$C_5H_8N_4O_{12}$	$C_3H_5N_3O_9$	$C_2H_4N_2O_6$
FW [g mol^{-1}]	212.08	360.16	168.06	316.14	227.09	152.06
$\rho_{calc.}$ (298 K) [g cm^{-3}]	1.87[a]	1.75[b]	1.52[c]	1.78	1.60	1.49
N + O [%][d]	86.77	84.42	83.31	78.45	81.91	81.55
Ω_{CO} [%][e]	+30	+18	+29	+15	+25	+21
Ω_{CO2} [%][e]	+15	0	+10	–10	+4	0
$T_{dec.}$ [°C][f]	117	155	177	180	143	190
$\Delta_f H°(s/l)$ [kJ mol^{-1}][g]	–194.5 (s)	+21.2 (s)	–367.6 (l)	–533.7 (s)	–370.8 (l)	–241.0 (l)
EXPLO5 V6.06.01						
P_{CJ} [GPa][h]	31	33	19	31	23	21
V_{det} [m s^{-1}][i]	8494	8753	7167	8412	7694	7519
$-\Delta_{ex}U°$ [kJ kg^{-1}][j]	6799	6531	5206	5962	5911	6426
T_{det} [K][k]	3583	4431	3869	3941	4225	4441
V_0 [dm^3 kg^{-1}][l]	782	805	796	742	779	810

[a] determined by gas-pycnometer; [b] recalculated from X-Ray density; [c] liquid at room temperature, therefore determined experimentally through the formula ρ=m/V; [d] Combined nitrogen and oxygen content; [e] oxygen balance assuming the formation of CO or CO_2; [f] temperature of decomposition (at a heating rate of 5 °C min^{-1} for **5** and **6** and 20 °C min^{-1} for **7**); [g] calculated (CBS-4M) heat of formation; [h] detonation pressure; [i] detonation velocity; [j] energy of explosion; [k] explosion temperature; [l] volume of detonation gases at standard temperature and pressure condition.

8.3 Conclusion

In this work, the three energetic materials 1,3-dinitroxy-2-nitrazapropane (**5**), 1,7-dinitroxy-2,4,6-trinitrazaheptane (**6**) and 1,3-dinitroxy-2-oxapropane (**7**) were synthesized and fully characterized. Importantly, that the precursor acetates **1** and **2** are obtained by a reaction condition modification of the Bachmann process and thus can be synthesized in already existing plants. The two new nitro esters **5** and **6** can be obtained in a simple two-step synthesis *via* the corresponding chloromethyl derivatives **3** and **4**. For the synthesis of the nitrazapropane-bridged **5** the route *via* a Viktor-Meyer reaction and for the trinitrazaheptane-bridged **6** the nitration by using fuming nitric acid is preferable in terms of better yields. Both

compounds are classified as sensitive due to their sensitivities towards impact and friction and also show only moderate thermal stability of 117 °C (**5**) and 155 °C (**6**). These properties are very similar to the explosive PETN, which is widely used as a booster and obtains its energetic character also through functionalization with nitro ester groups. If the energetic parameters of these three compounds are compared, it can be seen that both 1,3-dinitroxy-2-nitrazapropane (**5**) and 1,7-dinitroxy-2,4,6-trinitrazaheptane (**6**) show higher values, such as a higher detonation velocity than PETN. A possible application of **5** and **6** as booster explosives in booster charges would be therefore conceivable. Furthermore, 1,3-dinitroxy-2-oxapropane (**7**), which is liquid at room temperature and melts at −23 °C, can be obtained in a simple two-step synthesis from formaldehyde in good yields. As in the case of **5**, nitration with silver nitrate (Viktor-Meyer reaction) leads to better yields. This route represents an advantage over nitration with nitric acid, since no acidic conditions are used here. In the past, accidents have occurred because residual acid in nitro esters has led to uncontrolled autocatalytic decomposition. The synthesis of **5** and **7** *via* pathway II would avoid this risk. The properties of **7** show a strong similarity to nitroglycerin, which is still used today in double-base and triple-base propellants. A comparison of both compounds reveal, that the oxygen balance of **7** exceeds that of NG but due to its lower heat of formation shows a lower detonation velocity. Nevertheless, a possible application or 1,3-dinitroxy-2-oxapropane (**7**), in propellant mixtures or as an energetic plasticizer such as EGDN would be conceivable.

8.4 Experimental Section

CAUTION! All investigated compounds are potentially explosive energetic materials, which show partly (especially **5** and **7**) increased sensitivities towards various stimuli (e. g. elevated temperatures, impact or friction). Therefore, proper security precautions (safety glass, face shield, earthed equipment and shoes, leather coat, Kevlar gloves, Kevlar sleeves, and ear plugs) have to be applied while synthesizing and handling the described compounds. The synthesis procedure and analytics can be found in the Supporting Information.

1,3-Diacetoxy-2-nitrazapropane (1): 1,3-Diacetoxy-2-nitrazapropane was synthesized according to a modified literature procedure.[12-13] Acetic anhydride (384 mL, 4.1 mol) was cooled while fuming nitric acid (144 mL, 3.5 mol) was slowly added. A solution of hexamine (94.9 g, 0.68 mol) and acetic acid (176 mL) was added to the mixture dropwise while cooling to 0-10 °C. The solution was stirred for 12 h at room temperature. The precipitate was filtered (which was used for the preparation of **2**) and dichloromethane (150 mL) was added to the filtrate and the organic phase was washed with water, sodium hydroxide solution (0.1 M, 150 mL) and water. The organic phase was dried over magnesium sulfate and the solvent was removed *in vacuo*. Through vacuum distillation, (oil bath temperature 177 °C, until 100 °C/21 mbar) 1,3-diacetoxy-2-nitrazapropane (21.7 g, 16%) was obtained, as a colorless liquid. **^{1}H NMR** (400 MHz, acetone-D_6, ppm) δ = 6.11 (s, 4H, NCH_2O), 2.13 (s, 6H, OC(O)CH_3); **^{13}C{^{1}H} NMR** (101 MHz, acetone-D_6, ppm) δ = 169.7 (OC(O)CH$_3$), 85.0 (NCH$_2$N), 20.4 (OC(O)CH$_3$); **^{14}N NMR** (29 MHz, acetone-D_6, ppm) δ = –49 (NNO$_2$); **IR** (ATR, cm^{-1}): $\tilde{\nu}$ = 3064 (w), 3011 (vw), 2995 (vw), 2829 (vw), 1575 (m), 1559 (s), 1448 (s), 1417 (m), 1322 (s), 1271 (vs), 1169 (m), 1068 (s), 1059 (m), 899 (vs), 865 (s), 762 (s), 677 (vs), 632 (m), 600 (s), 432 (w), 410 (m). **Elemental Analysis** ($C_8H_{14}N_6O_{10}$): calcd: C 27.13, H 3.98, N 23.73 %; analyzed: C 27.32, H 3.76, N 23.35 %.

1,7-Diacetoxy-2,4,6-trinitrazaheptane (2): 1,7-Diacetoxy-2,4,6-trinitrazaheptane was synthesized according to a modified literature procedure.[12-13] The filtered precipitate from the synthesis of **1** (see above) was washed with a small amount of water and recrystallized from glacial acetic acid. 1,7-Diacetoxy-2,4,6-trinitrazaheptane (123 g, 52%) was obtained, as a colorless solid. **^{1}H NMR** (400 MHz, acetone-D_6, ppm) δ = 6.01 (s, 4H, NCH_2N), 5.90 (s, 4H, NCH_2O), 2.07 (s, 6H, OC(O)CH_3); **^{13}C{^{1}H} NMR** (101 MHz, acetone-D_6, ppm) δ = 171.2 (OC(O)CH$_3$), 72.9 (NCH$_2$N), 65.7 (NCH$_2$O), 20.6 (OC(O)CH$_3$); **^{14}N NMR** (29 MHz, acetone-D_6, ppm) δ = –34, –35 (OCH$_3$NNO$_2$, NCH$_2$NNO$_2$); **IR** (ATR, cm^{-1}): $\tilde{\nu}$ = 3038 (w), 1744 (s), 1667 (w), 1656 (w), 1574 (s), 1549 (s), 1451 (s), 1417 (m), 1392 (w), 1383 (w), 1367 (m), 1317 (w), 1281 (vs), 1262 (s), 1215 (s), 1198 (s), 1180 (vs), 1131 (s), 1101 (m), 1042 (w), 1018 (s), 990 (m), 960 (s), 933 (vs), 880 (m), 862 (s), 836 (s), 767 (s), 724 (w), 707 (w), 650 (m), 644 (m), 617 (s), 598 (s),

502 (m), 476 (m), 448 (w), 425 (m). **Elemental Analysis** ($C_6H_{10}N_2O_6$): calcd: C 34.96, H 4.89, N 13.59 %; analyzed: C 34.70, H 4.81, N 13.70 %.

1,3-Dichloro-2-nitrazapropane (3): 1,3-Dichloro-2-nitrazapropane was synthesized according to a modified literature procedure.[12-13] A solution of 1,4-dioxane (150 mL) and 1,3-diacetoxy-2-nitrazapropane (11.0 g, 53.0 mmol) was cooled and hydrogen chloride was bubbled through for 30 min. The solution was stored for 48 h at 4 °C. The obtained mixture was reduced *in vacuo* and further purified by performing a vacuum distillation (oil bath temp. 80 °C, up temp. 37 °C, < 1 x 10^{-3} mbar). 1,3-Dichloro-2-nitrazapropane (1.6 g, 19 %) was obtained as a colorless oil. **^{1}H NMR** (400 MHz, acetone-D_6, ppm) δ = 5.96 (s, 2H, CH_2); **^{13}C{^{1}H} NMR** (101 MHz, acetone-D_6, ppm) δ = 58.9 (NCH$_2$N); **^{14}N NMR** (29 MHz, acetone-D_6, ppm) δ = –40 (NNO$_2$); **IR** (ATR, cm^{-1}): $\tilde{\nu}$ = 3063 (w), 3010 (vw), 2923 (vw), 2853 (vw), 1575 (s), 1560 (s), 1448 (s), 1417 (m), 1322 (s), 1271 (vs), 1168 (m), 1067 (s), 1058 (m), 905 (vs), 899 (vs), 865 (s), 762 (s), 677 (vs), 632 (m), 600 (vs), 432 (w), 410 (m). **Elemental Analysis** ($C_2H_4Cl_2N_2O_2$): calcd: C 15.11, H 2.54, N 17.62 %; analyzed: C 15.28, H 2.81, N 17.62 %.

1,7-Dichloro-2,4,6-trinitrazaheptane (4): 1,7-Dichloro-2,4,6-trinitrazaheptane was synthesized according to a modified literature procedure.[12-13] A solution of 1,4-dioxane (200 mL) and 1,3-diacetoxy-2,4,6-trinitrazaheptane (19.0 g, 53.6 mmol) was cooled and hydrogen chloride was bubbled through for 30 min. The solution was stored for 48 h at 4 °C. The colorless solid was filtered and washed with diethyl ether. 1,7-Dichloro-2,4,6-trinitrazaheptane (8.9 g, 54%) was obtained, as a colorless solid. **^{1}H NMR** (400 MHz, acetone-D_6, ppm) δ = 5.96 (s, 4H, NCH_2Cl), 6.05 (s, 4H, NCH_2N); **^{13}C{^{1}H} NMR** (101 MHz, acetone-D_6, ppm) δ = 65.3 (ClCH$_2$N), 59.9 (NCH$_2$N); **^{14}N NMR** (29 MHz, acetone-D_6, ppm) δ = –36 (ClCH$_2$NNO$_2$), –35 (CH$_2$NNO$_2$); **IR** (ATR, cm^{-1}): $\tilde{\nu}$ = 3078 (w), 3031 (w), 2980 (vw), 2860 (vw), 1585 (m), 1542 (m), 1463 (w), 1442 (s), 1411 (m), 1394 (w), 1359 (w), 1311 (w), 1292 (m), 1259 (vs), 1241 (s), 1173 (m), 1124 (s), 1173 (m), 1124 (s), 1064 (s), 943 (s), 909 (vs), 888 (w), 863 (m), 857 (m), 768 (m), 758 (s), 660 (s), 634 (m), 601 (s), 475 (m), 425 (m). **Elemental Analysis** ($C_4H_8Cl_2N_6O_6$): calcd: C 15.65, H 2.63, N 27.37, Cl 23.09 %; analyzed: C 15.81, H 2.66, N 27.46, Cl 22.72 %.

1,3-Dinitroxy-2-nitrazapropane (5):

Pathway I.: 1,3-Dichloro-2-nitrazapropane (0.250 g, 1.57 mmol) was added to cooled fuming nitric acid (10 mL). The solution was stirred for 2 h at room temperature. The mixture was quenched on ice and the resulting solution was extracted with ethyl acetate (2 x 100 mL). The organic phase was washed with sodium hydrogen carbonate (150 mL) and water (150 mL). The organic phase was dried over magnesium sulfate and reduced *in vacuo*. 1,3-Dinitroxy-2-nitrazapropane (0.100 g, 30%) was obtained as a colorless oil.

Pathway II.: 1,3-Dichloro-2-nitrazapropane (0.250 g, 1.57 mmol) was dissolved in acetonitrile (100 mL) and silver nitrate (0.668 g, 3.93 mmol) was added. The reaction was stirred protected from light overnight at room temperature. The resulting precipitate was separated and the filtrate was concentrated *in vacuo*. The crude product was dissolved in ethyl acetate (100 mL) and washed once with saturated sodium chloride solution (150 mL) and twice with water (100 mL). The organic phase was dried over magnesium sulfate and again reduced *in vacuo*. 1,3-Dinitroxy-2-nitrazapropane (0.203 g, 61 %) was obtained as a colorless oil. Crystals suitable for X-ray diffraction were obtained by recrystallization from acetonitrile.

^{1}H NMR (400 MHz, acetone-D_6, ppm) δ = 6.44 (s, 2H, NCH_2O); **^{13}C{^{1}H} NMR** (101 MHz, acetone-D_6, ppm) δ = 79.1 (NCH$_2$O); **^{15}N NMR** (41 MHz, acetone-D_6, ppm) δ = –39.6 ($^{3}J_{N,H}$ = 3.4 Hz, ONO$_2$), –48.5 ($^{3}J_{N,H}$ = 4.8 Hz, CH$_2$NNO$_2$), –188.6 (CH$_2$$NNO_2$). **IR** (ATR, cm^{-1}): $\tilde{\nu}$ = 3062 (w), 2930 (vw), 1644 (vs), 1582 (s), 1564 (s), 1450 (m), 1412 (s), 1377 (w), 1306 (m), 1272 (vs), 1233 (m), 1223 (m), 1171 (s), 1019 (w), 997 (m), 923 (s), 816 (vs), 769 (s), 750 (vs), 717 (m), 641 (s), 611 (m), 583 (vs), 457 (m), 407 (w). **Elemental Analysis** ($C_2H_4N_4O_8$): calcd: C 11.33, H 1.90, N 26.42 %; analyzed: C 11.39, H 2.12, N 26.70 %.

1,7-Dinitroxy-2,4,6-trinitrazaheptane (6):

Pathway I.: 1,7-Dichloro-2,4,6-trinitrazaheptane (0.500 g, 1.63 mmol) was added to fuming nitric acid (10 mL). The solution was cooled and stirred for 10 min and then stirred for 2 h at room temperature. The mixture was quenched on ice and the colorless solid was filtered. 1,7-Dinitroxy-2,4,6-trinitrazaheptane (0.440 g, 75%)

was obtained. Via recrystallization from propionitrile crystals suitable for X-ray diffraction were obtained.

Pathway II.: 1,7-Dichloro-2,4,6-trinitrazaheptane (0.500 g, 1.63 mmol) was dissolved in acetonitrile (500 mL) and silver nitrate (0.692 g, 4.08 mmol) was added. The reaction was stirred under exclusion of light overnight at room temperature. The resulting precipitate was separated and the filtrate was concentrated *in vacuo*. The crude product was dissolved in ethyl acetate (100 mL) and washed once with saturated sodium chloride solution (150 mL) and twice with water (100 mL). The organic phase was dried over magnesium sulfate and again reduced *in vacuo*. 1,7-Dinitroxy-2,4,6-trinitrazaheptane (0.211 g, 36 %) was obtained as a colorless solid.

^{1}H NMR (400 MHz, acetone-D_6, ppm) δ = 6.41 (s, 4H, NCH_2O), 6.12 (s, 4H, NCH_2N); **^{13}C{^{1}H} NMR** (101 MHz, acetone-D_6, ppm) δ = 79.6 (NCH$_2$O), 65.9 (NCH$_2$N); **^{15}N NMR** (41 MHz, acetone-D_6, ppm) δ = –33.5 ($^{3}J_{N,H}$ = 3.2 Hz, CH$_2$NNO$_2$), –36.0 ($^{3}J_{N,H}$ = 3.1 Hz, CH$_2$NNO$_2$), –47.2 ($^{3}J_{N,H}$ = 4.7 Hz, ONO$_2$), –189.5 (CH$_2$$NNO_2$), –191.0 (CH$_2$$NNO_2$); **IR** (ATR, cm^{-1}): $\tilde{\nu}$ = 3069 (vw), 3048 (vw), 2913 (vw), 1731 (vw), 1668 (m), 1646 (m), 1574 (s), 1558 (s), 1446 (w), 1451 (m), 1441 (m), 1415 (m), 1398 (w), 1387 (w), 1374 (w), 1328 (w), 1317 (vw), 1267 (vs), 1258 (vs), 1205 (m), 1176 (s), 1132 (s), 1104 (m), 984 (m), 951 (s), 922 (s), 879 (m), 864 (m), 837 (vs), 769 (s), 752 (s), 731 (w), 706 (w), 661 (m), 647 (m), 609 (m), 591 (vs), 478 (w), 447 (m), 419 (w). **Elemental Analysis** ($C_4H_8N_8O_{12}$): calcd.: C 13.34, H 2.24, N 31.11 %; analyzed: C 13.44, H 2.30, N 30.85 %.

1,3-Dinitroxy-2-oxapropane (7):

Pathway I.: 1,3-Dichloro-2-oxapropane was synthesized as described in the literature.[24] 1,3-Dichloro-2-oxapropane (0.500 g, 4.35 mmol) was added to cooled fuming nitric acid (10 mL) and the solution was stirred afterward for 2 h at room temperature. After quenching the reaction mixture on ice, the resulting solution was extracted with ethyl acetate (2 x 100 mL). Then the organic phase was washed with sodium hydrogen carbonate (150 mL) and water (150 mL). The organic phase was dried over magnesium sulfate and reduced *in vacuo*. 1,3-Dinitroxy-2-oxapropane (0.387 g, 53 %) was obtained with small impurities as a yellowish oil.

Pathway II.: 1,3-Dichloro-2-oxapropane[20] (0.500 g, 4.35 mmol) was dissolved in acetonitrile (40 mL) and silver nitrate (1.55 g, 9.14 mmol) was added. The reaction

mixture was stirred overnight at room temperature protected from light. The resulting precipitate was filtered and the filtrate was concentrated *in vacuo*. The crude product was dissolved in ethyl acetate (100 mL) and washed once with saturated sodium chloride solution (150 mL) and twice with water (100 mL). Afterward, the organic phase was dried over magnesium sulfate and again reduced *in vacuo*. 1,3-Dinitroxy-2-oxapropane (0.600 g, 82 %) was obtained as a colorless oil.

^{1}H NMR (400 MHz, acetone-D_6, ppm) δ = 5.88 (s, 4H, OCH_2O); **^{13}C{^{1}H} NMR** (101 MHz acetone-D_6, ppm) δ = 93.9 (OCH$_2$O); **^{15}N NMR** (41 MHz, neat, ppm) δ = –49.3 ($^{3}J_{N,H}$ = 4.2 Hz, OCH$_2$ONO$_2$); **^{17}O NMR** (54 MHz, neat, ppm) δ = 452 (ONO_2), 358 (ONO$_2$), 73 (OCH$_2$ONO$_2$); **IR** (ATR, cm^{-1}): $\tilde{\nu}$ = 2976 (vw), 2931 (vw), 2576 (vw), 1642 (vs), 1466 (w), 1449 (w), 1408 (vw), 1394 (vw), 1286 (vs), 1144 (s), 1064 (m), 924 (s), 836 (m), 804 (vs), 753 (s), 669 (s), 623 (m), 591 (s), 496 (w), 470 (w), 445 (vw), 425 (vw), 410 (w). **Elemental Analysis** ($C_2H_4N_2O_7$): calcd.: C 14.29, H 2.40, N 16.67 %; analyzed: C 14.34, H 2.35, N 16.58 %.

8.5 Acknowledgements

For financial support of this work the Ludwig Maximilian University (LMU), EMTO GmbH, the Office of Naval Research (ONR) under grant no. ONR N00014-19-1-2078 and the Strategic Environmental Research and Development Program (SERDP) under contract no. W912HQ19C0033 are gratefully acknowledged.

8.6 References

[1] a) T. M. Klapötke, *Chemistry of High-Energy Materials*. 6th ed., de Gruyter, Berlin/Boston **2022**; b) Agrawal, J. P.; Hodgson, R. D. *Organic Chemistry of Explosives*. 1st ed., Wiley-VCH, Weinheim **2007**.

[2] T. M.Klapötke, J. T. Lechner, L. W. B. Stanislawski, J. Stierstorfer, M. Mühlemann, G. Lemarchand, *Propellants Explos. Pyrotech.* **2023**, e202300062.

[3] A. Kumar, V. Rao, R. Sinha, A. Rao, *Propellants Explos. Pyrotech.* **2010**, *35,* 359–364.

[4] W. de. C. Crater, *Ind. Eng. Chem.* **1948**, *40*, 1627–1635.

[5] W. E. Bachmann, J. C. Sheehan, *J. Am. Chem. Soc*. **1949**, *71*, 1842–1845.

[6] J. P. Baxter, Scientists Against Time, M. I. T. Press, Cambridge, United Kingdom, **1968**.

[7] a) W. E. Bachmann (United States Secretary of WAR), US 2680671, **1954**; b) W. E. Bachmann (United States Secretary of WAR), US 2798870, **1957**.

[8] Y.Zhang, Z. Xu, J. Ruan, X. Wang, L. Zhang, J. Luo, *Propellants Explos. Pyrotech.*, **2018**, *43*, 1287–1295.

[9] Z. Matys, D. Powala, A. Orchechowski, A. Maranda, *Chemik*, **2012**, *66*, 61–63.

[10] S. Epstein, C. A. Winkler, *Can. J. Chem.*, **1952**, *30*, 734–742.

[11] W. E. Bachmann, W. J. Harton, E. L. Jenner, N. W. Mac Naughton, L. B. Scott, *J. Am. Chem. Soc.* **1951**, *73*, 2769–2773.

[12] T. M. Klapötke, B. Krumm, F. X. Steemann, *Propellants Explos. Pyrotech*., **2009**, *34*, 13–23.

[13] T. M. Klapötke, A. Penger, C. Pflüger, J. Stierstorfer, M. Sućeska, *Eur. J. Inorg. Chem.*, **2013**, 4667–4678.

[14] J. J. Sabatini, E. C. Johnson, *ACS Omega* **2021**, *6*, 11813–11821.

[15] T. M. Klapötke, B. Krumm, J. T. Lechner, C. Riedelsheimer, *ChemistrySelect* **2022**, *7*, e202202232.

[16] S. G. Il'yasov, E. O. Danilova, *Propellants Explos. Pyrotech.* **2012**, *37*, 427–431.

[17] L. T. Eremenko, A. M. Korolev, V. N. Grebennikov, G. M. Nazin, *Izvestiya Akademii Nauk SSSR, Seriya Khimicheskaya,* **1971**, *3*, 627–629.

[18] J. T. Lechner, A. Neuer, V. Bockmair, J. Stierstorfer, T. M. Klapötke, *Cryst. Growth Des.* **2022**, *22*, 6215–6223.

[19] A. G. Harter, T. M. Klapötke, B. Krumm, J. T. Lechner, C. Riedelsheimer, *Eur. J. Org. Chem.* **2023**, e202300302.

[20] T. M. Klapötke, G. Lemarchand, T. Lenz, M. Mühlemann, J. Stierstorfer, F. Venetz, R. Weber, J. Wutke, *Propellants, Explos., Pyrotech.* **2023**, *48*, e202200288.

[21] M. N. Boers, W. P. C. de Klerk, *Propellants, Explos., Pyrotech*. **2005**, *30*, 356−362.

[22] V. Meyer, *Justus Liebigs Ann. Chem.* **1874**, *171*, 1–56.

[23] S. R. Buc, *Org. Synth.* **1956**, *36*, 1–4.

[24] M. Reichel, B. Krumm, Y. V. Vishnevskiy, S. Blomeyer, J. Schwabedissen, H.-G. Stammler, K. Karaghiosoff, N. W. Mitzel, *Angew. Chem. Int. Ed.* **2019**, *58*, 18557–18561.

[25] Deposition numbers 2279205 (for **5**), 2279206 (for **6**), and 2279207 (for 3,7-Dinitro-1,5,3,7-dioxadiazocane) contain the supplementary crystallographic data for this paper. These data are provided free of charge by the joint Cambridge Crystallographic Data Centre and Fachinformationszentrum Karlsruhe Access Structures service.

[26] Impact: insensitive > 40 J, less sensitive ≥ 35 J, sensitive ≥ 4 J, very sensitive ≤ 3 J; Friction: insensitive > 360 N, less sensitive = 360 N, sensitive < 360 N and > 80 N, very sensitive ≤ 80 N, extremely sensitive ≤ 10 N. According to the UN Recommendations on the Transport of Dangerous Goods, (+) indicates not safe for transport.

[27] M. Sućeska, *Explo5 V6.06.01*, Zagreb (Croatia), **2021**.

[28] T. M. Klapötke, *Energetic Materials Encyclopedia* ,2nd ed., DEGRUYTER, Berlin/Boston, **2021**.

[29] J. Liu, Nitrate Esters Chemistry and Technology, Springer Nature, Singapore, **2019**.

[30] NATO standardization agreement (STANAG) on explosives, impact sensitivity tests, no. 4489, 1st ed, Sept. 17, **1999**.

[31] WIWEB-Standardarbeitsanweisung 4-5.1.02, Ermittlung der Explosionsgefährlichkeit, hier der Schlagempfindlichkeit mit dem Fallhammer. Nov. 8, **2002**.

[32] "http://www.bam.de", accessed March **2022**.

[33] NATO standardization agreement (STANAG) on explosive, friction sensitivity tests. no. 4487, 1st ed., Aug. 22, **2002**.

[34] WIWEB-Standardarbeitsanweisung 4-5.1.03, Ermittlung der Explosionsgefährlichkeit oder der Reibeempfindlichkeit mit dem Reibeapparat. Nov. 8, **2002**.

[35] Impact: insensitive > 40 J, less sensitive ≥ 35 J, sensitive ≥ 4 J, very sensitive ≤ 3 J, Friction: insensitive > 360 N, less sensitive = 360 N, sensitive < 360 N and > 80 N, very sensitive ≤ 80 N, extremely sensitive ≤ 10 N. According to the UN Recommendations on the Transport of Dangerous Goods, (+) indicates not safe for transport.

[36] CrysAlisPro, Oxford Diffraction Ltd., version 171.33.41, **2009**.

[37] A. Altomare, G. Cascarano, C. Giacovazzo, A. Guagliardi, *J. Appl. Crystallogr* **1993**, *26*, 343−350.

[38] a) A. Altomare, G. Cascarano, C. Giacovazzo, A. Guagliardi, A. G. G. Moliterni, SIR97 **1997**; b) A. Altomare, M. C. Burla, M. Camalli, G. L. Cascarano, C. Giacovazzo, A., *J. Appl. Crystallogr*. **1999**, *32*, 115−119.

[39] G. M. Sheldrick, *Acta Crystallogr. Sect. A* **2008**, *A64*, 112−122.

[40] G. M. Sheldrick, SHELXL-97, Program for the Refinement of Crystal, University of Göttingen, Germany, **1997**.

[41] A. L. Spek, PLATON, A Multipurpose Crystallographic Tool, Utrecht University **1999**.

[42] L. J. Farrugia, *J. Appl. Cryst.* **2012**, *45*, 849−854.

[43] a) Empirical absorption correction using spherical harmonics, implemented in SCALE3 ABSPACK scaling algorithm (CrysAlisPro Oxford Diffraction Ltd., Version 171.33.41, 2009); b) APEX3. Bruker AXS Inc., Madison, Wisconsin, USA.

[44] M. J. Frisch, G. W. Trucks, H. B. Schlegel, G. E. Scuseria, M. A. Robb, J. R. Cheeseman, G. Scalmani, V. Barone, B. Mennucci, G. A. Petersson, H. Nakatsuji, M. Caricato, X. Li, H.P. Hratchian, A. F. Izmaylov, J. Bloino, G. Zheng, J. L. Sonnenberg, M. Hada, M. Ehara, K. Toyota, R. Fukuda, J. Hasegawa, M. Ishida, T. Nakajima, Y. Honda, O. Kitao, H. Nakai, T. Vreven, J. A. Montgomery, Jr., J. E. Peralta, F. Ogliaro, M. Bearpark, J. J. Heyd, E. Brothers, K. N. Kudin, V. N. Staroverov, R. Kobayashi, J. Normand, K. Raghavachari, A. Rendell, J. C. Burant, S. S. Iyengar, J. Tomasi, M. Cossi, N. Rega, J. M. Millam, M. Klene, J. E. Knox, J. B. Cross, V. Bakken, C. Adamo, J. Jaramillo, R. Gomperts, R. E. Stratmann, O. Yazyev, A. J. Austin, R. Cammi, C. Pomelli, J. W. Ochterski, R. L. Martin, K. Morokuma, V. G. Zakrzewski, G. A. Voth, P. Salvador, J. J. Dannenberg, S. Dapprich, A. D. Daniels, O. Farkas, J.B. Foresman, J. V. Ortiz, J. Cioslowski, D. J. Fox, Gaussian 09 A.02, Gaussian, Inc., Wallingford, CT, USA, **2009**.

[45] a) J. W. Ochterski, G. A. Petersson, and J. A. Montgomery Jr., *J. Chem. Phys.* **1996**, *104*, 2598−2619; b) J. A. Montgomery Jr., M. J. Frisch, J. W. Ochterski G. A. Petersson, *J. Chem. Phys.* **2000**, *112*, 6532−6542; c) L. A. Curtiss, K. Raghavachari, P. C. Redfern, J. A. Pople, *J. Chem. Phys.* **1997**, *106*, 1063−1079; d) E. F. C. Byrd, B. M. Rice, *J. Phys. Chem. A* **2006**, *110*, 1005–1013; e) B. M. Rice, S. V. Pai, J. Hare, *Comb. Flame* **1999**, *118*, 445–458.

[46] F. Trouton, *Philos. Mag.* (1876-1900) **1884**, *18*, 54-57; b) M. S. Westwell, M. S. Searle, D. J. Wales, D. H. Willimas, *J. Am. Chem. Soc.* **1995**, *117*, 5013-5015.

[47] M. Sućeska, EXPLO5 V6.06.01, Zagreb (Croatia) **2021**.

[48] M. Sućeska, *Propellants, Explos., Pyrotech.* **1991**, *16*, 197–202.

8.7 Supporting Information

8.7.1 Experimental Information

All chemicals and solvents were employed as received (Sigma-Aldrich, Fluka, Acros, ABCR). ^{1}H, ^{13}C, ^{14}N, ^{15}N and ^{17}O NMR spectra were recorded at ambient temperature using a Bruker TR 400 instrument and are referenced with respect to Me_4Si ($^{1}H/^{13}C$), $MeNO_2$ ($^{14}N/^{15}N$) and H_2O (^{17}O). Melting and decomposition temperatures of the described compounds were measured through differential thermal analysis (DTA) with an OZM Research DTA 552-Ex instrument. The samples were measured in a range of 25–400 °C at a heating rate of 5 °C min^{-1}. Partly the compounds were measured also by thermal gravimetric analysis (TGA) with a PerkinElmer TGA4000. Infrared spectra were measured with pure samples on a Perkin-Elmer BXII FT-IR system with a Smith DuraSampler IR II diamond ATR. Determination of the carbon, hydrogen, and nitrogen contents was carried out by combustion analysis using an Elementar Vario El (nitrogen values determined are often lower than the calculated due to their explosive behavior). Impact sensitivity tests were carried out according to STANAG 4489[1] modified instruction[2] using a BAM (Bundesanstalt für Materialforschung) drophammer.[3] Friction sensitivity tests were carried out according to STANAG 4487[4] modified instruction[5] using the BAM friction tester. The classification of the tested compounds results from the “UN Recommendations on the Transport of Dangerous Goods”.[6]

8.7.2 NMR Spectroscopy

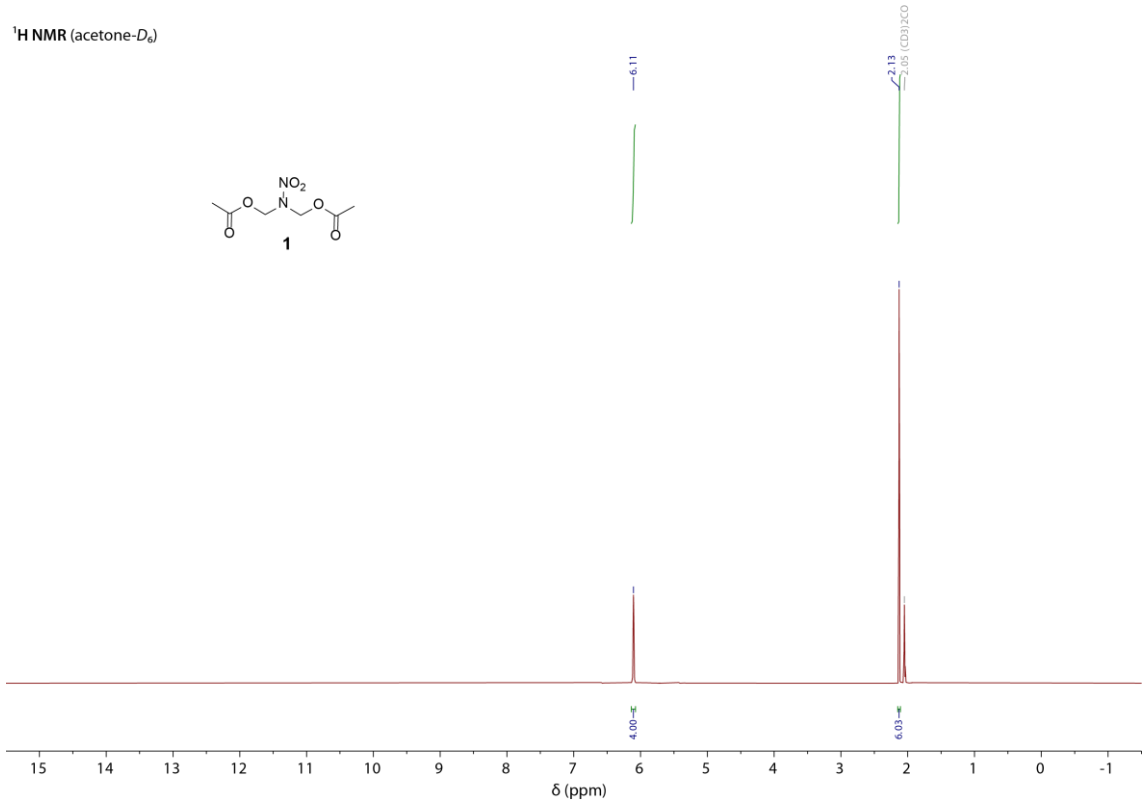

Figure S1. ^{1}H NMR spectrum of **1** in acetone-D_6.

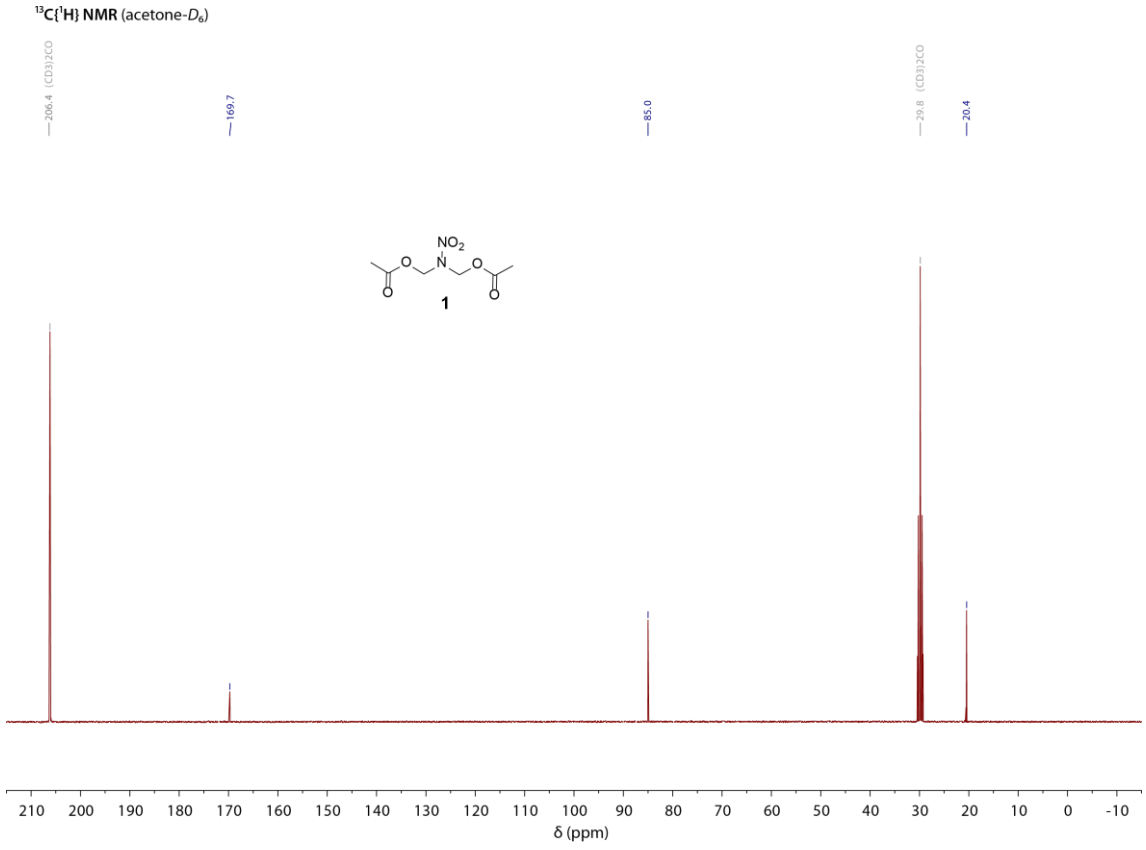

Figure S2. ^{13}C{^{1}H} NMR spectrum of **1** in acetone-D_6.

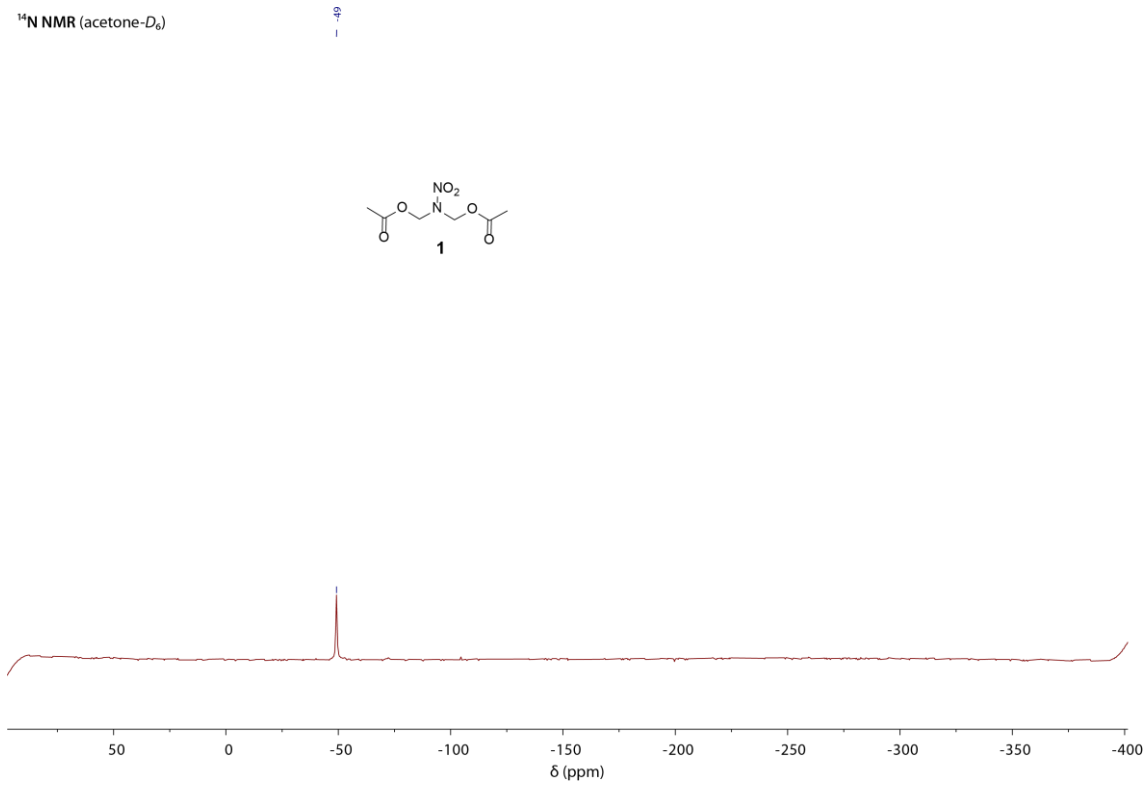

Figure S3. ^{14}N NMR spectrum of **1** in acetone-D_6.

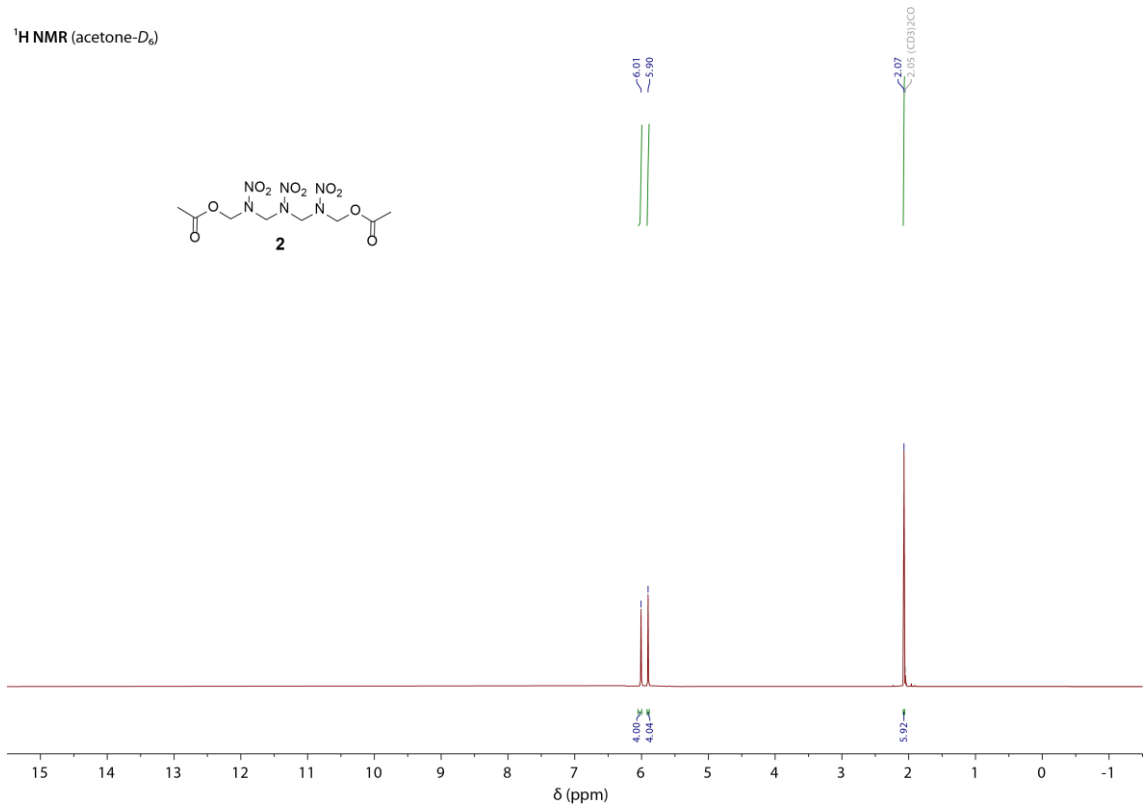

Figure S4. ^{1}H NMR spectrum of **2** in acetone-D_6.

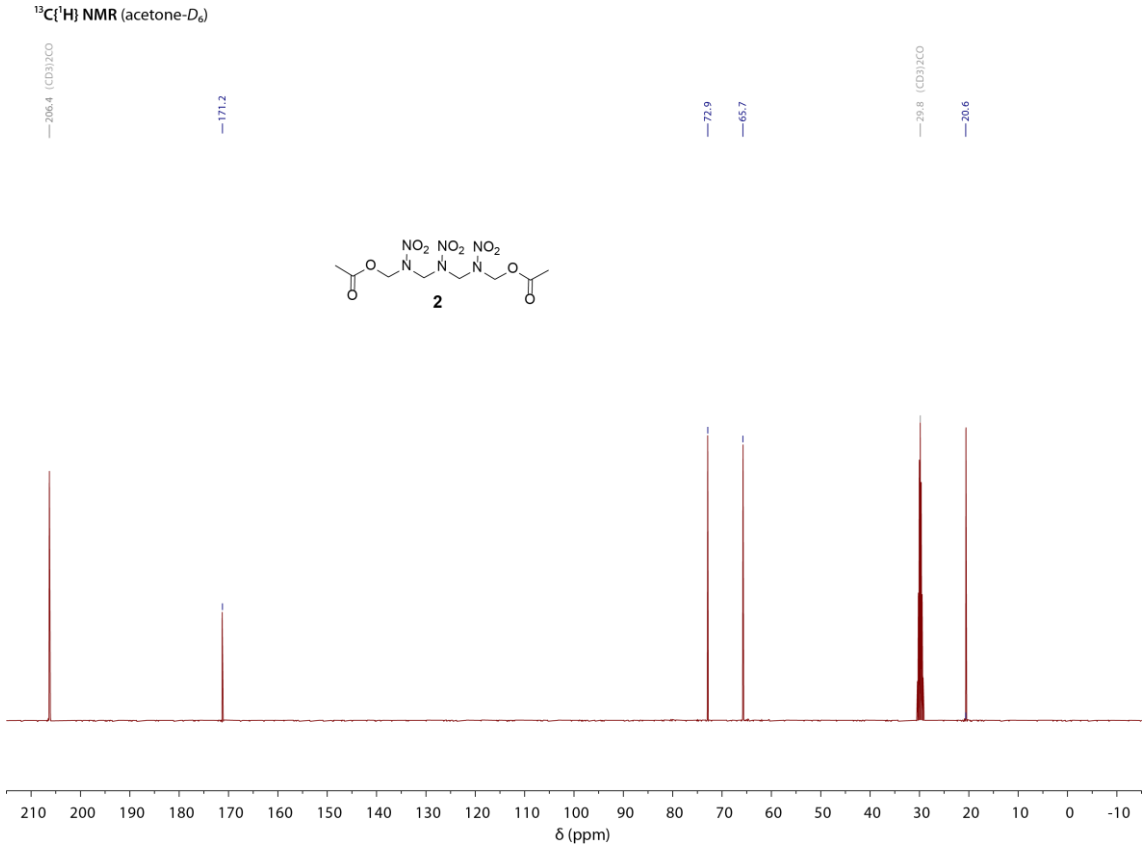

Figure S5. $^{13}C\{^{1}H\}$ NMR spectrum of **2** in acetone-D_6.

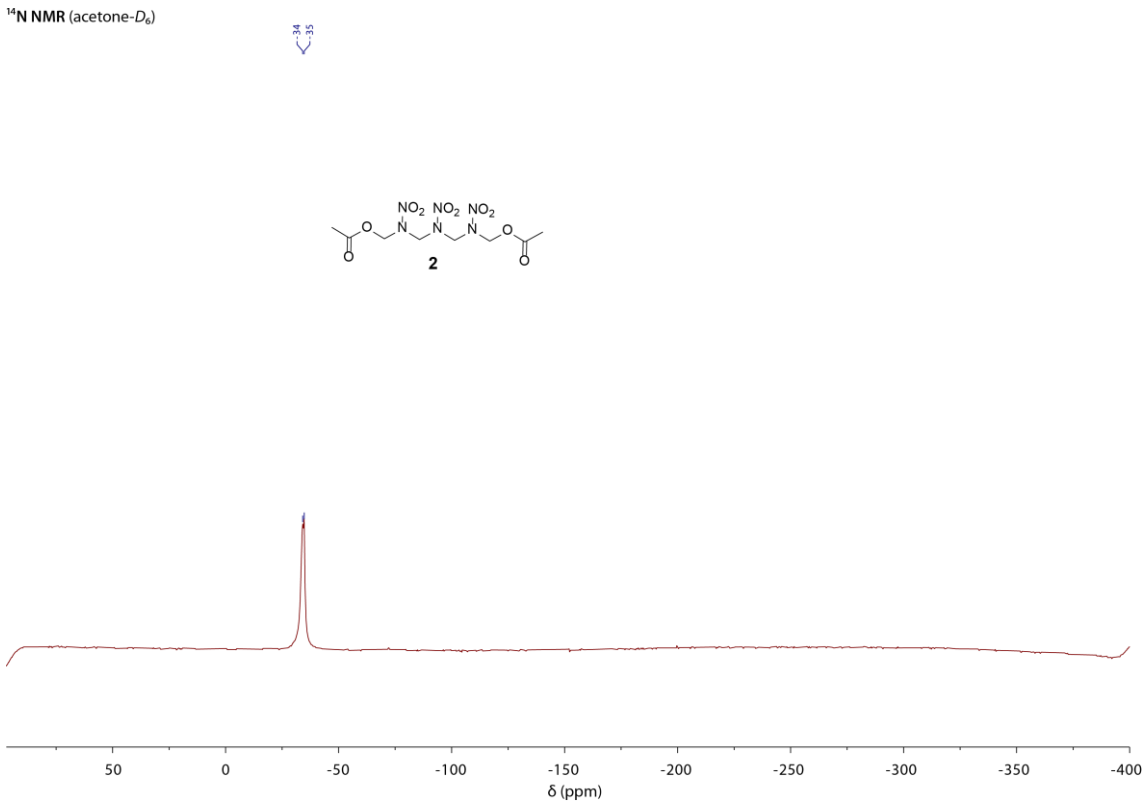

Figure S6. ^{14}N NMR spectrum of **2** in acetone-D_6.

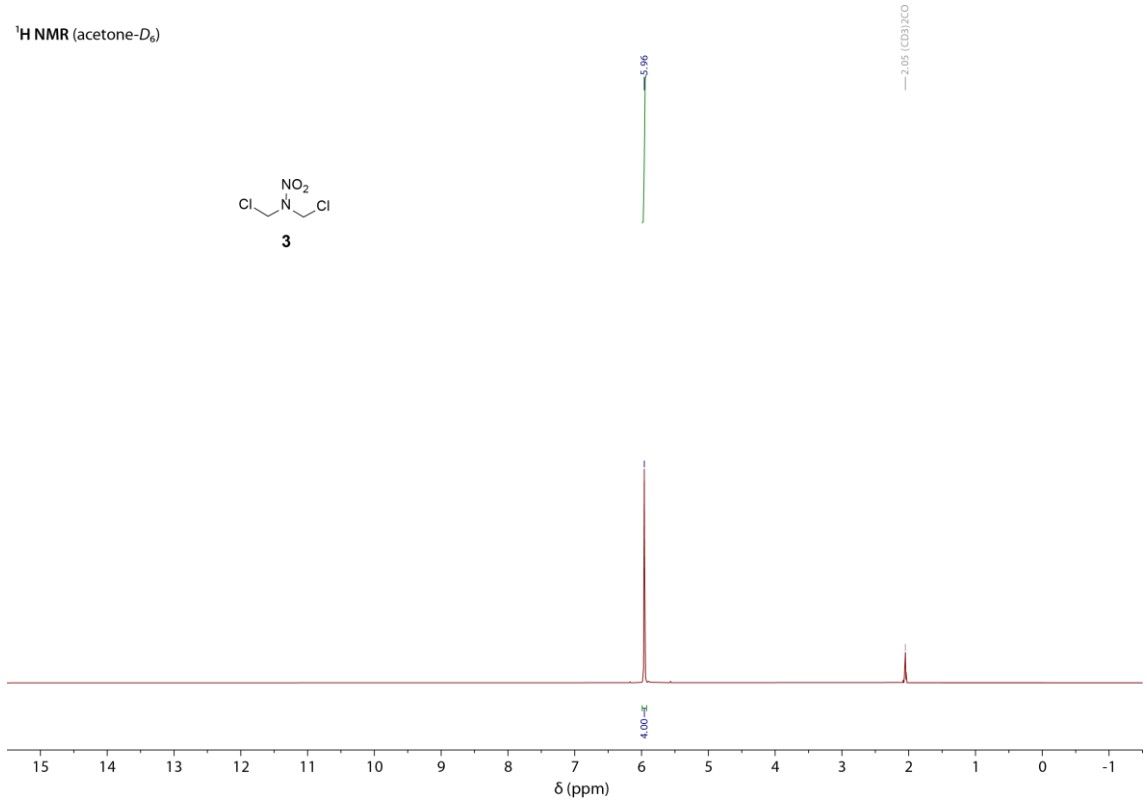

Figure S7. ^{1}H NMR spectrum of **3** in acetone-D_6.

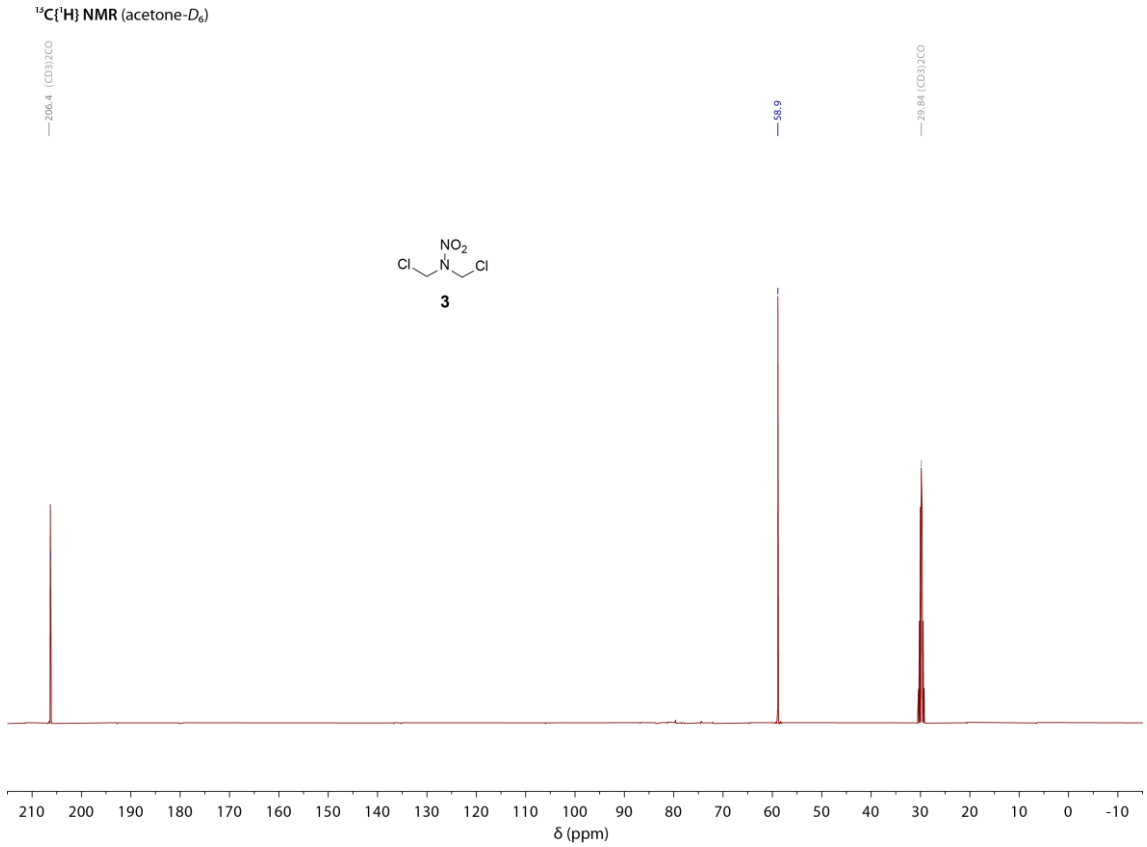

Figure S8. ^{13}C{^{1}H} NMR spectrum of **3** in acetone-D_6.

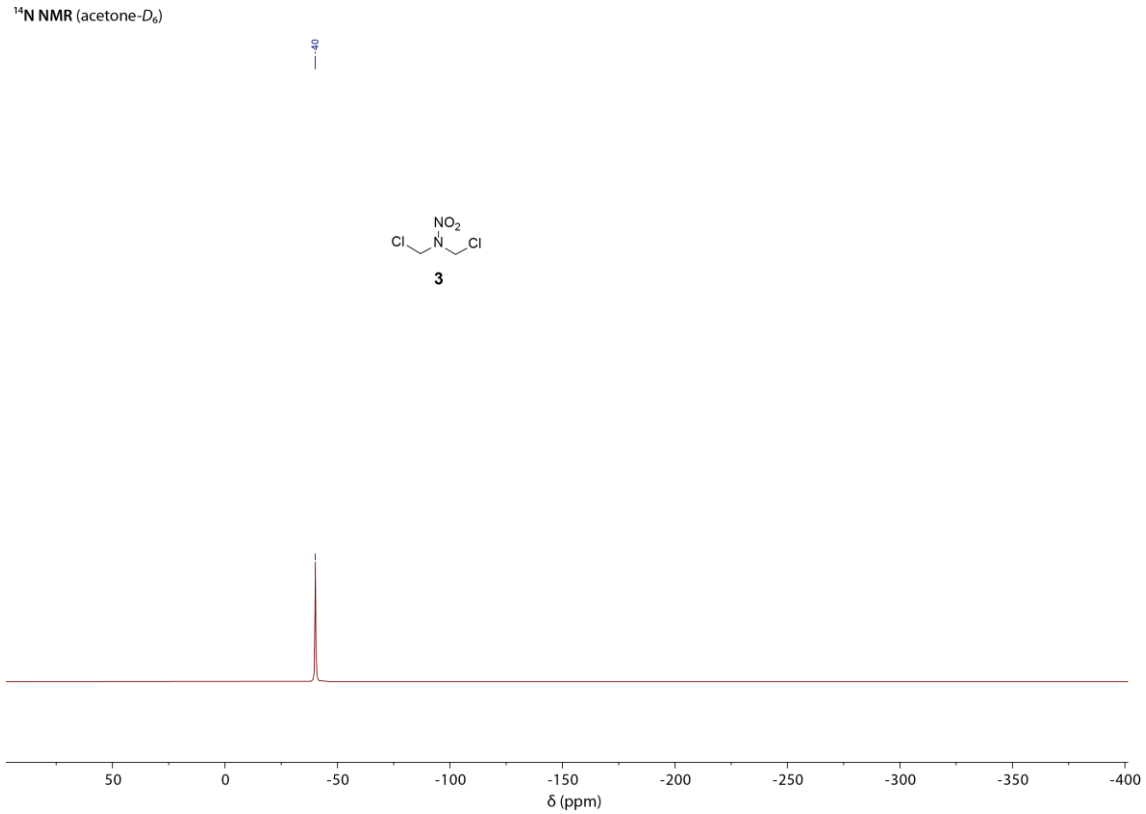

Figure S9. ^{14}N NMR spectrum of **3** in acetone-D_6.

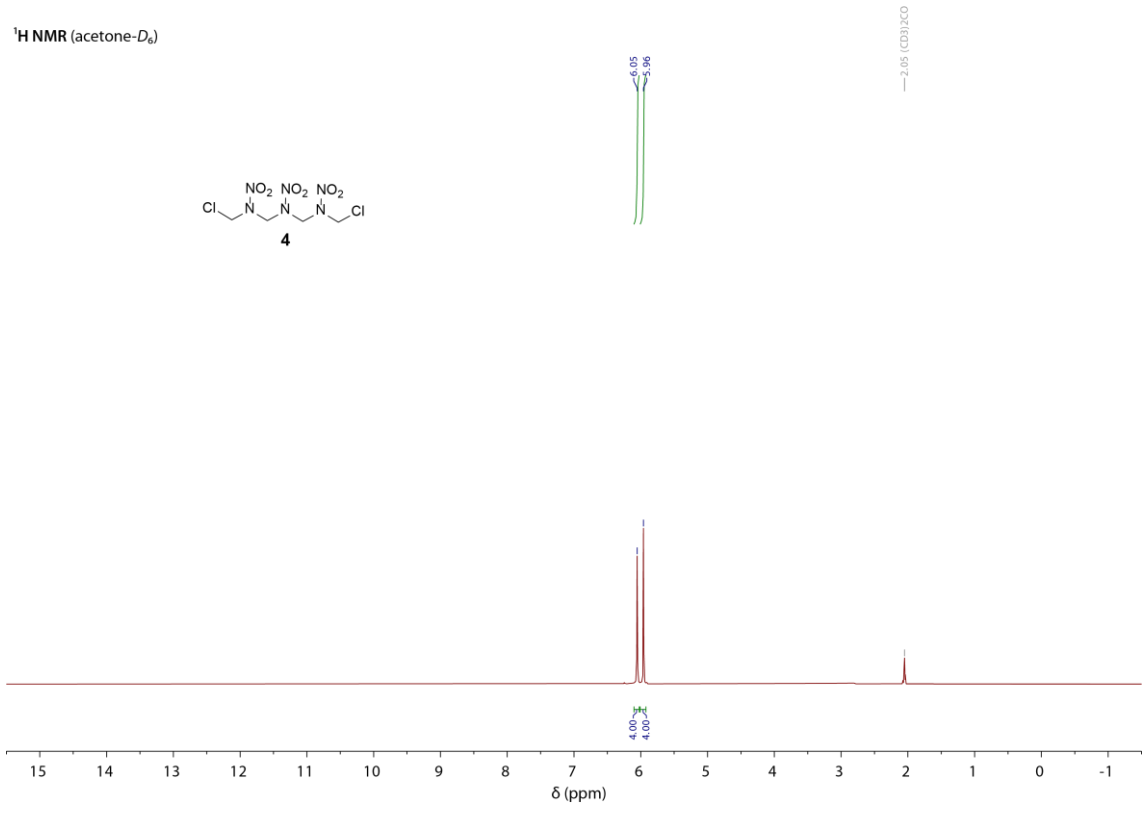

Figure S10. ^{1}H NMR spectrum of **4** in acetone-D_6.

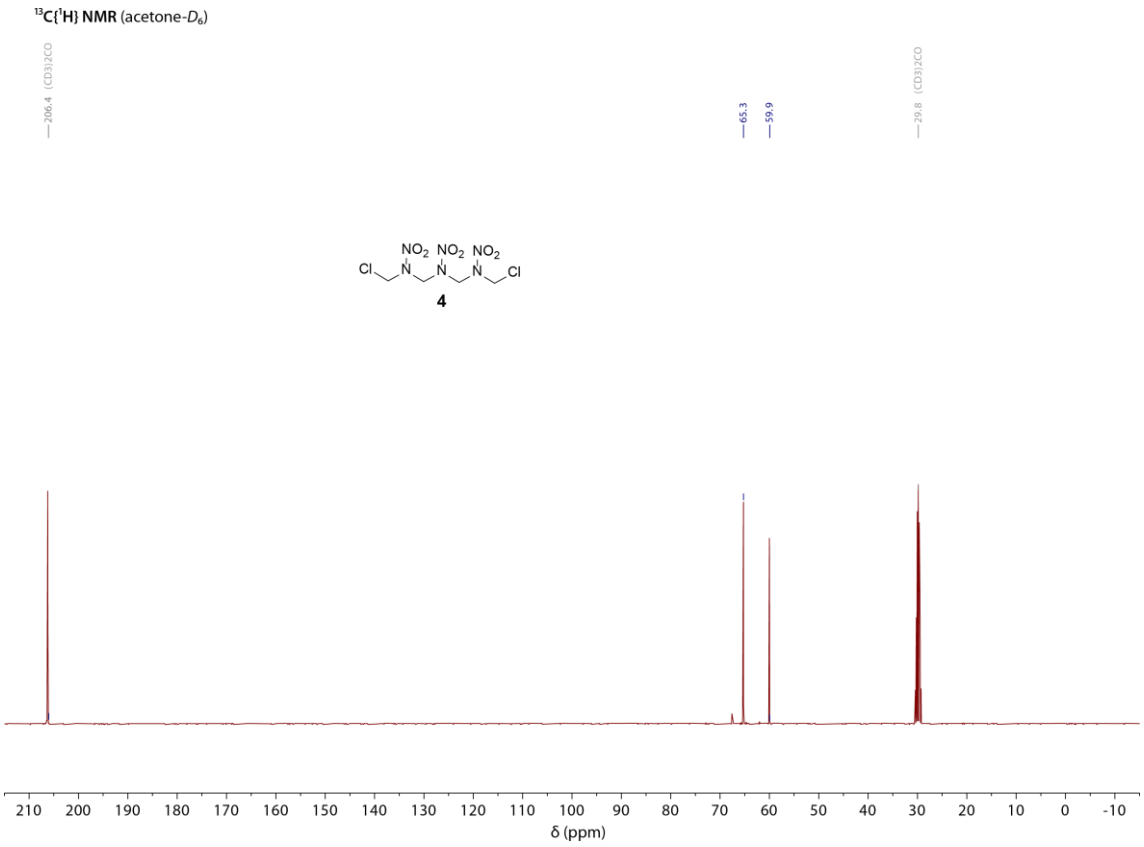

Figure S11. $^{13}C\{^{1}H\}$ NMR spectrum of **4** in acetone-D_6.

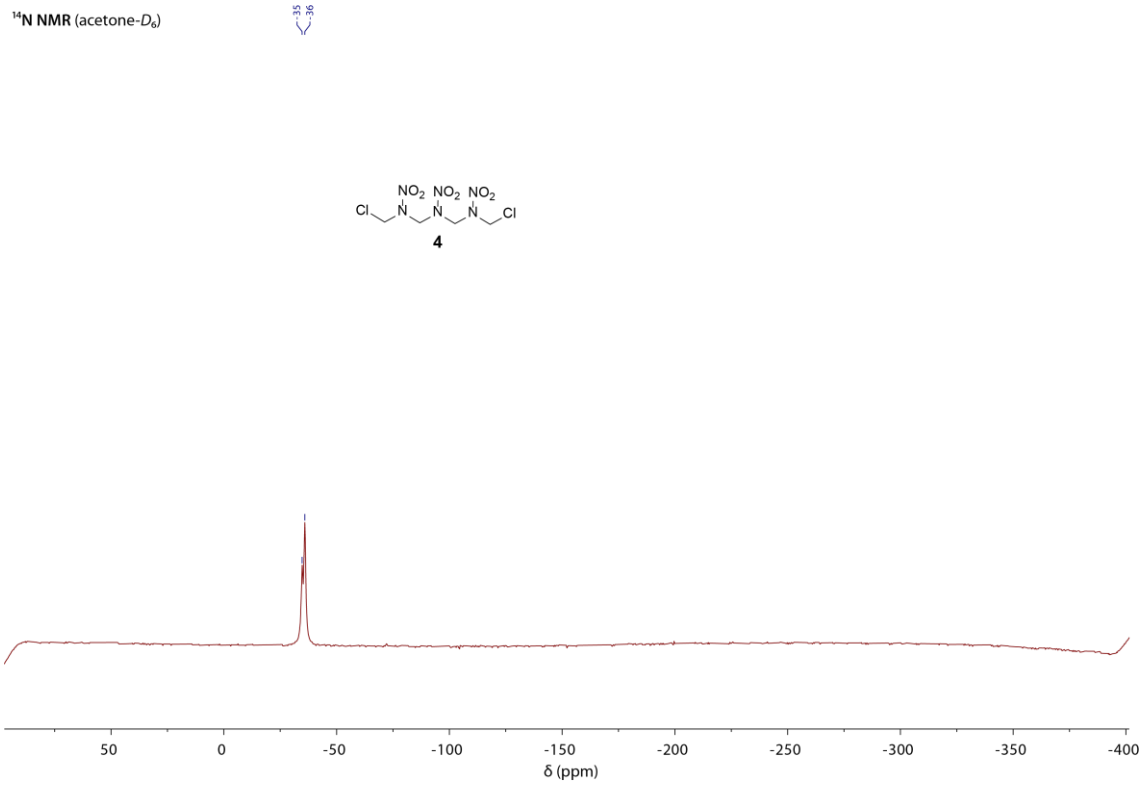

Figure S12. ^{14}N NMR spectrum of **4** in acetone-D_6.

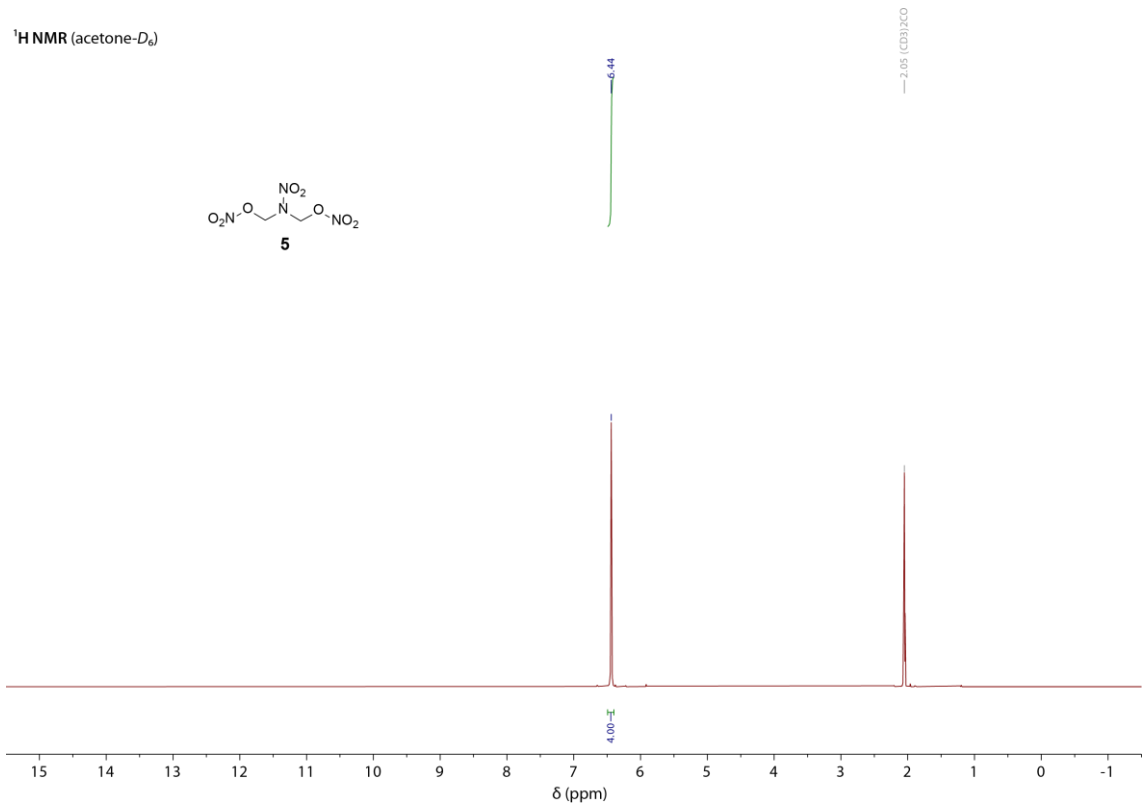

Figure S13. ^{1}H NMR spectrum of **5** in acetone-D_6.

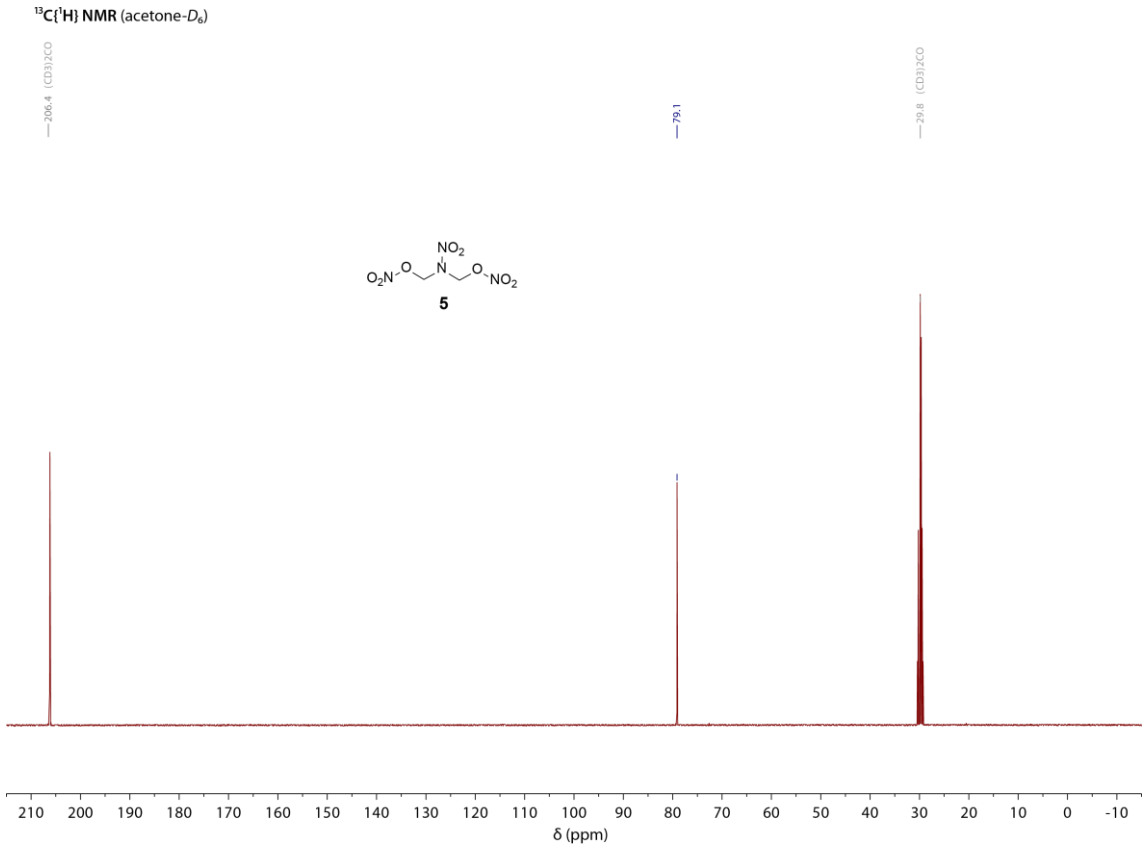

Figure S14. ^{13}C{^{1}H} NMR spectrum of **5** in acetone-D_6.

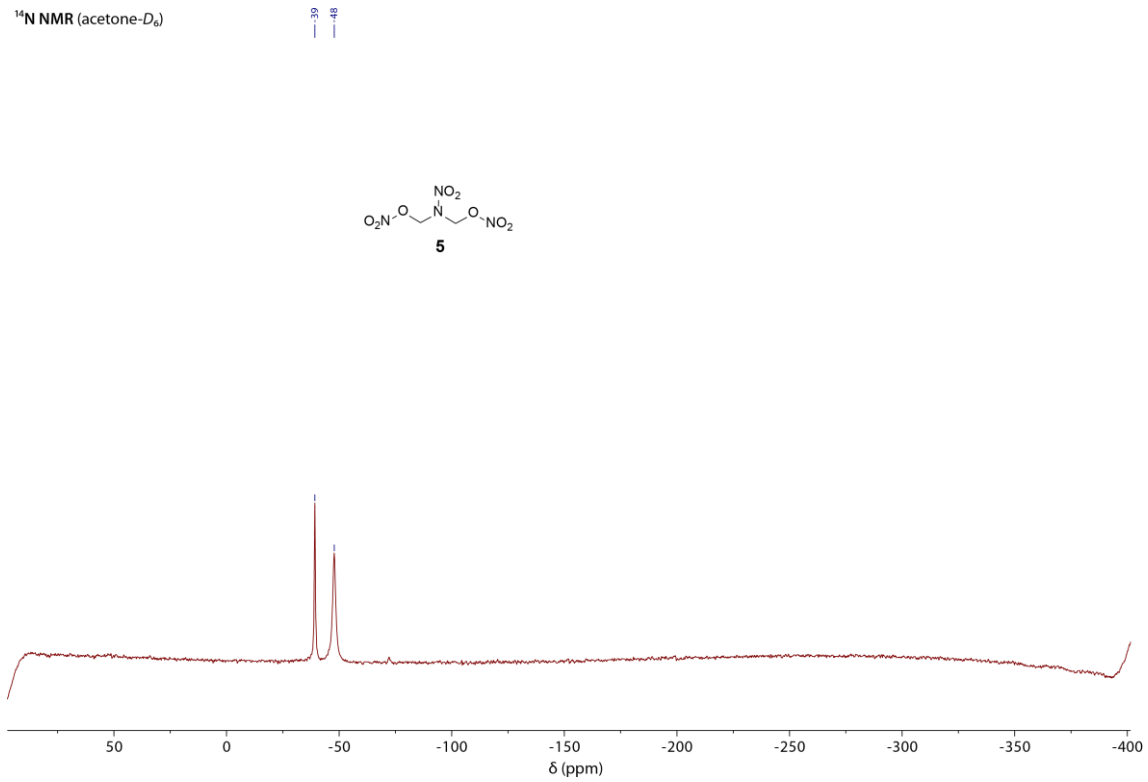

Figure S15. ^{14}N NMR spectrum of **5** in acetone-D_6.

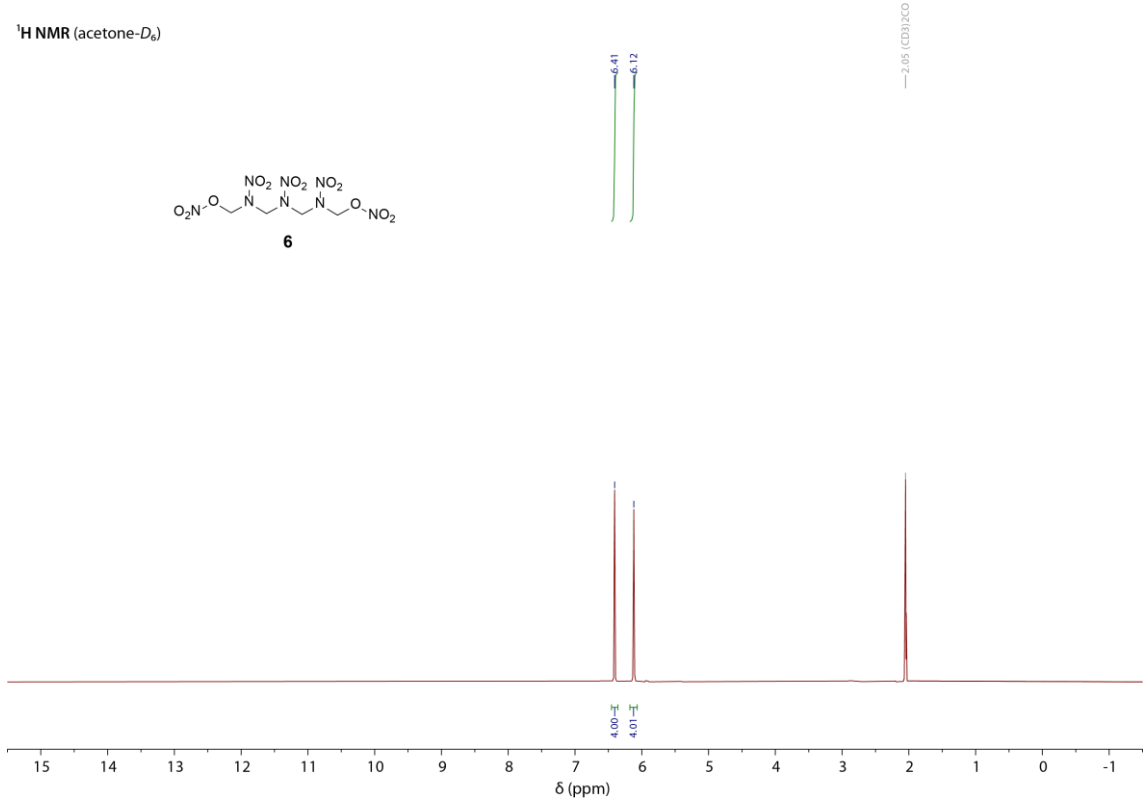

Figure S16. ^{1}H NMR spectrum of **6** in acetone-D_6.

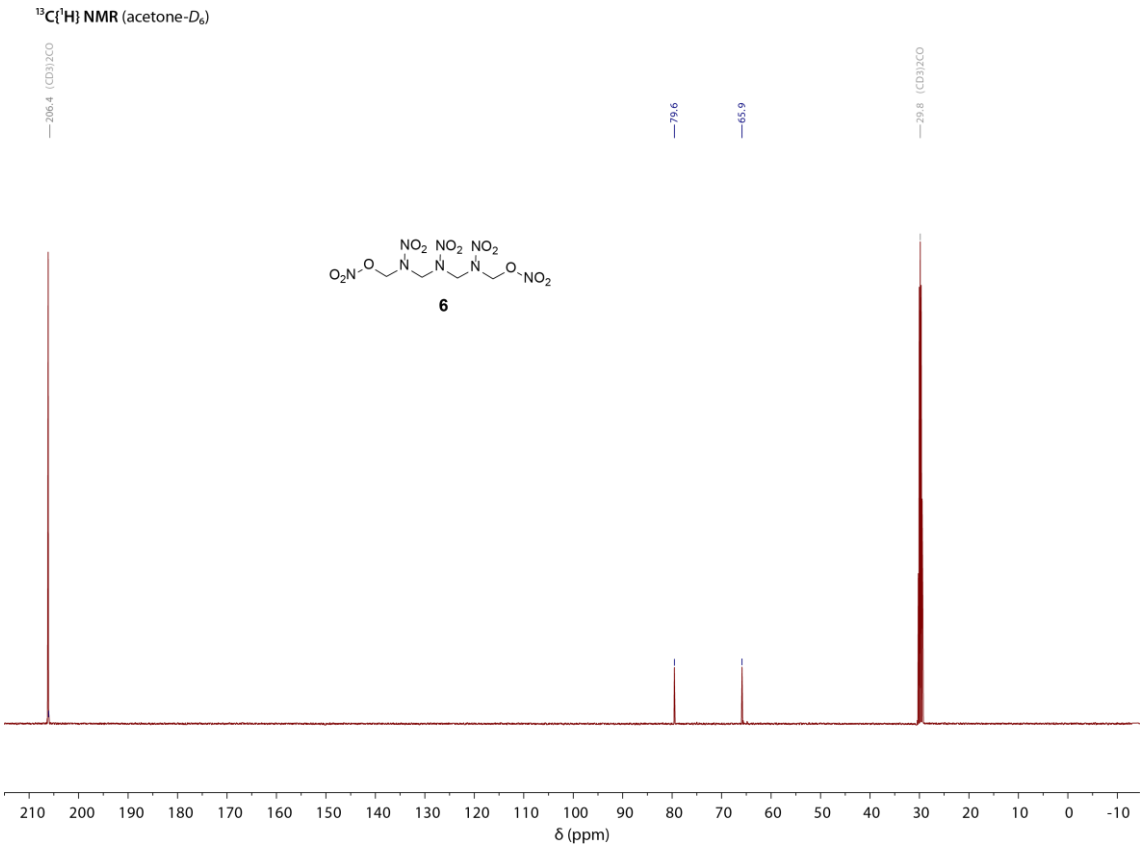

Figure S17. $^{13}C\{^{1}H\}$ NMR spectrum of **6** in acetone-D_6.

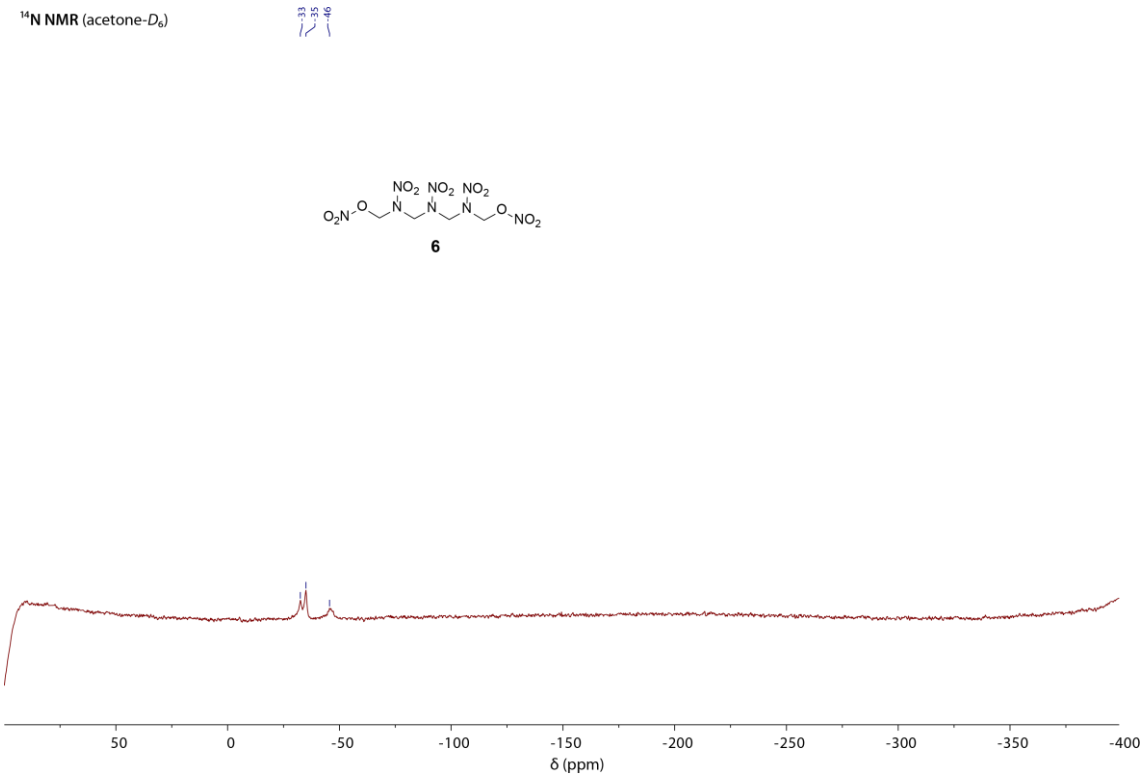

Figure S18. ^{14}N NMR spectrum of **6** in acetone-D_6.

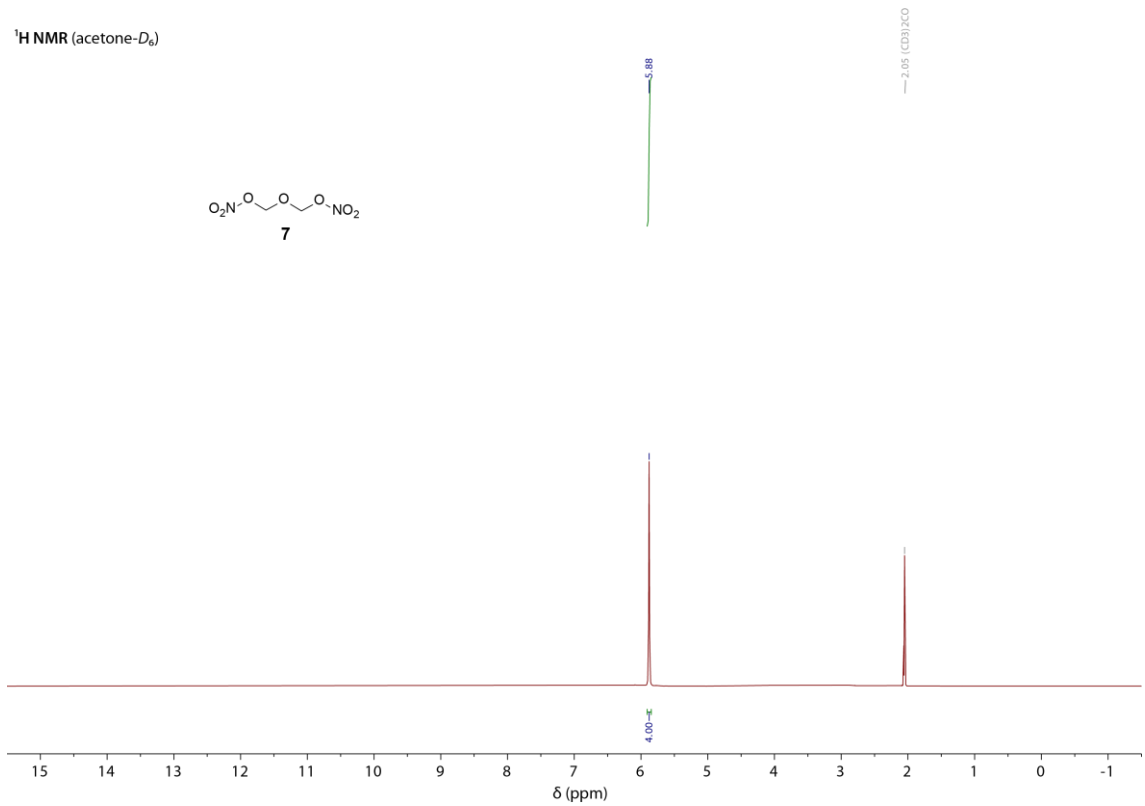

Figure S19. ^{1}H NMR spectrum of **7** in acetone-D_6.

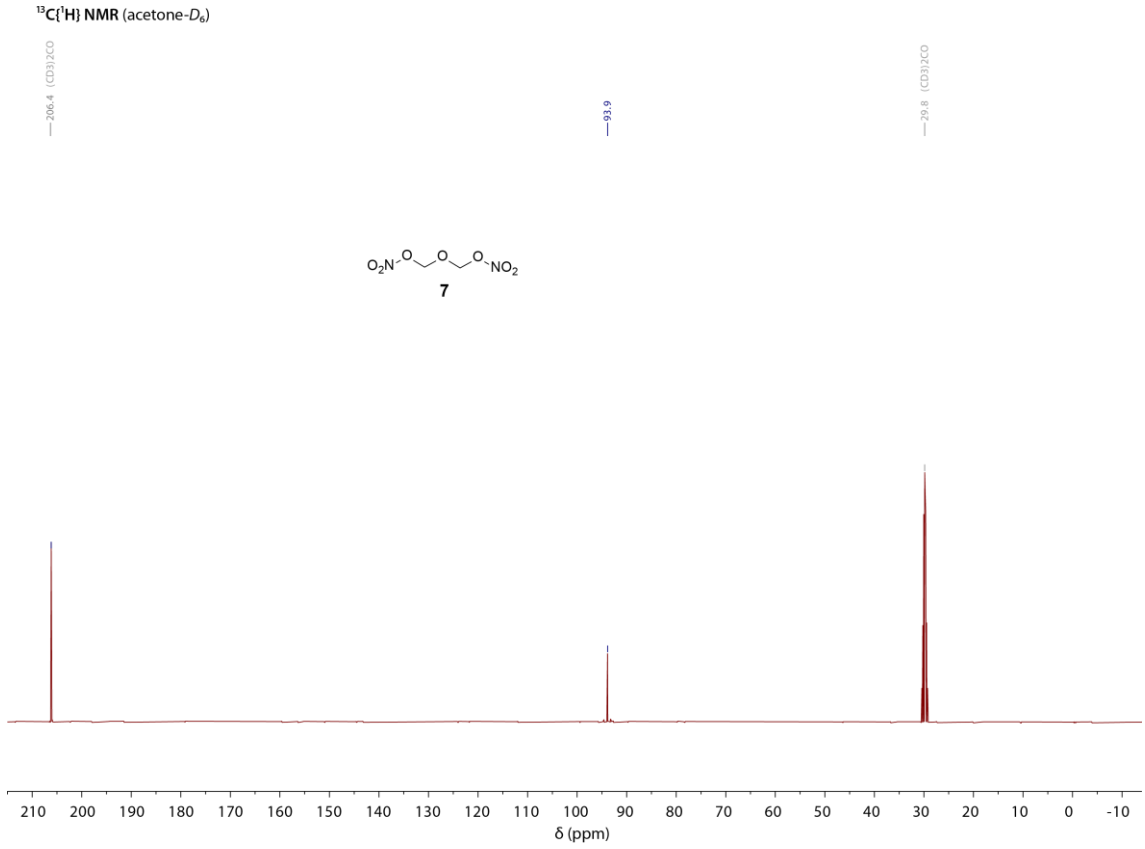

Figure S20. $^{13}C\{^{1}H\}$ NMR spectrum of **7** in acetone-D_6.

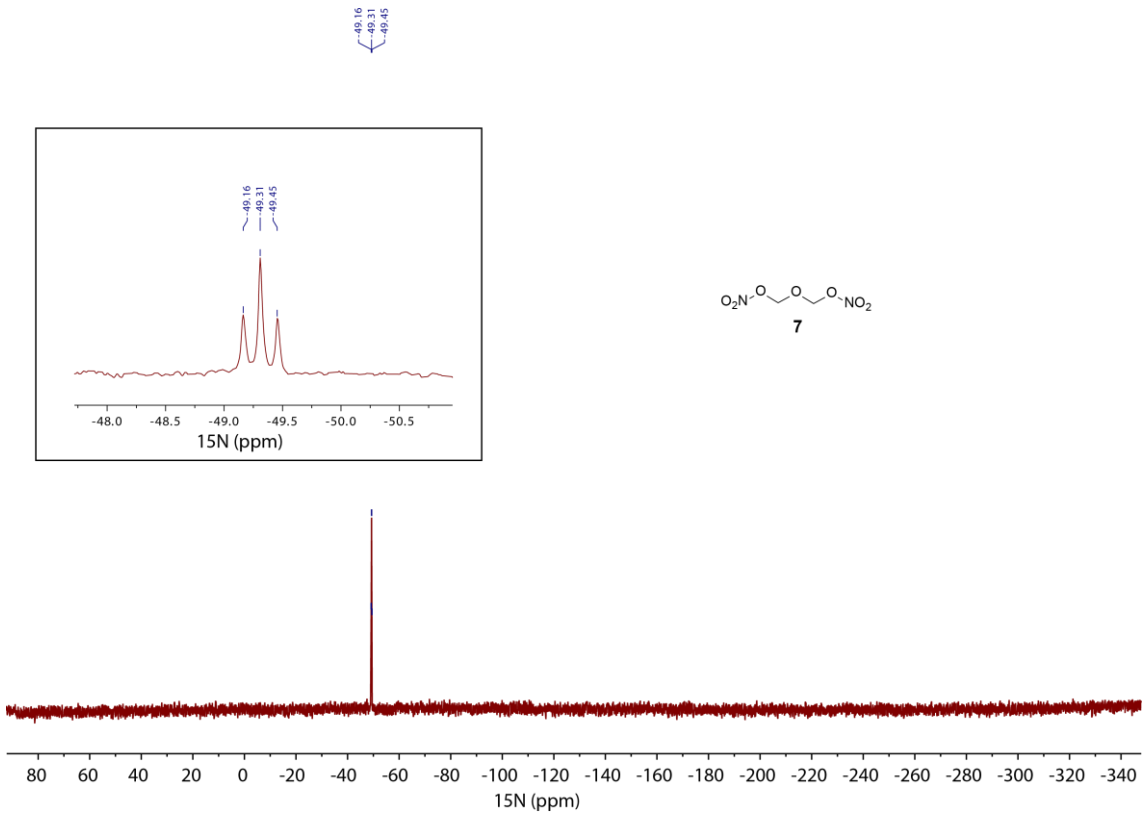

Figure S21. ^{15}N NMR spectrum of **7** in acetone-D_6.

8.7.3 IR Spectroscopy

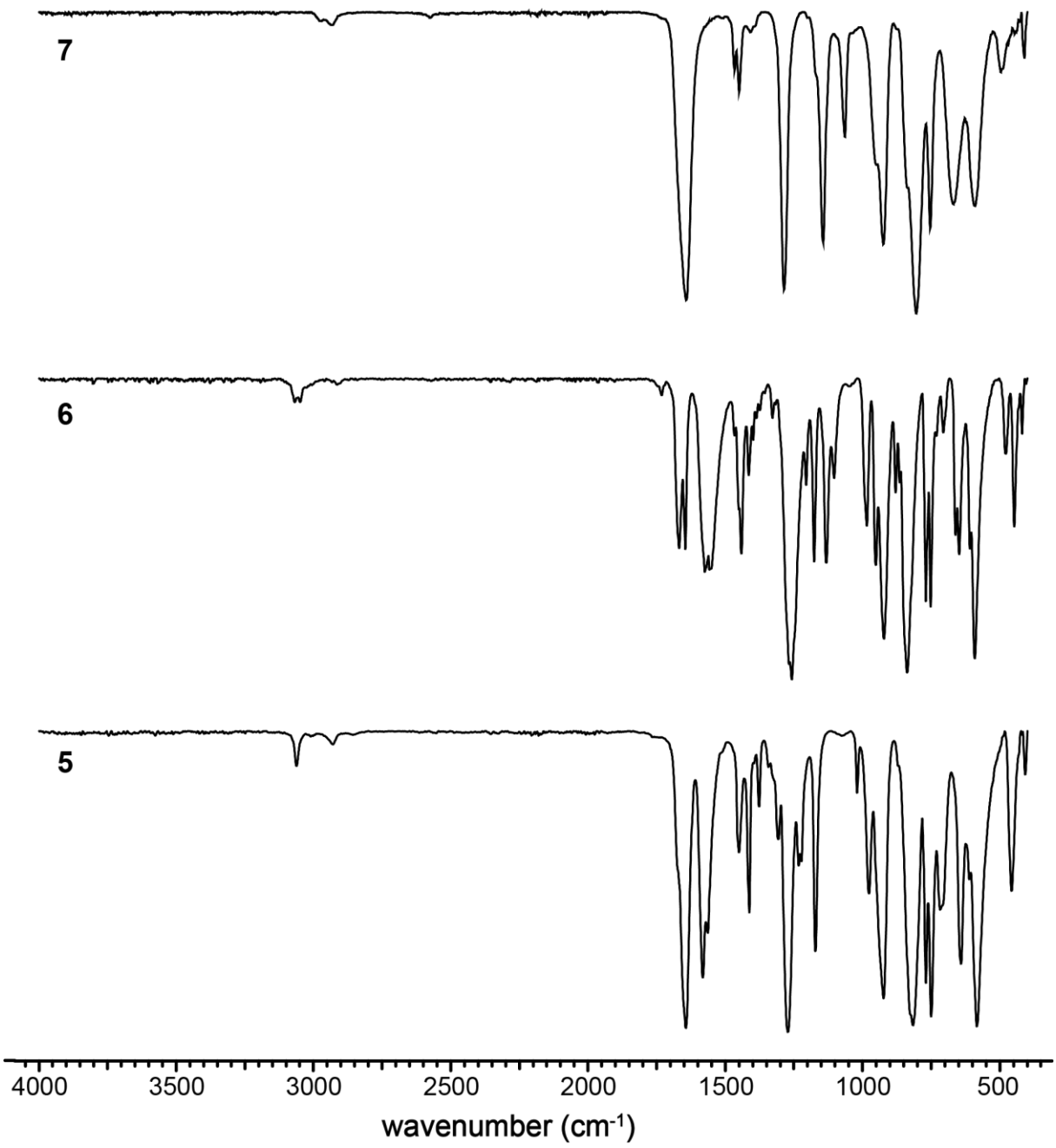

Figure S22. IR spectra of **5** (bottom), **6** (middle) and **7** (top).

8.7.4 DTA Measurements

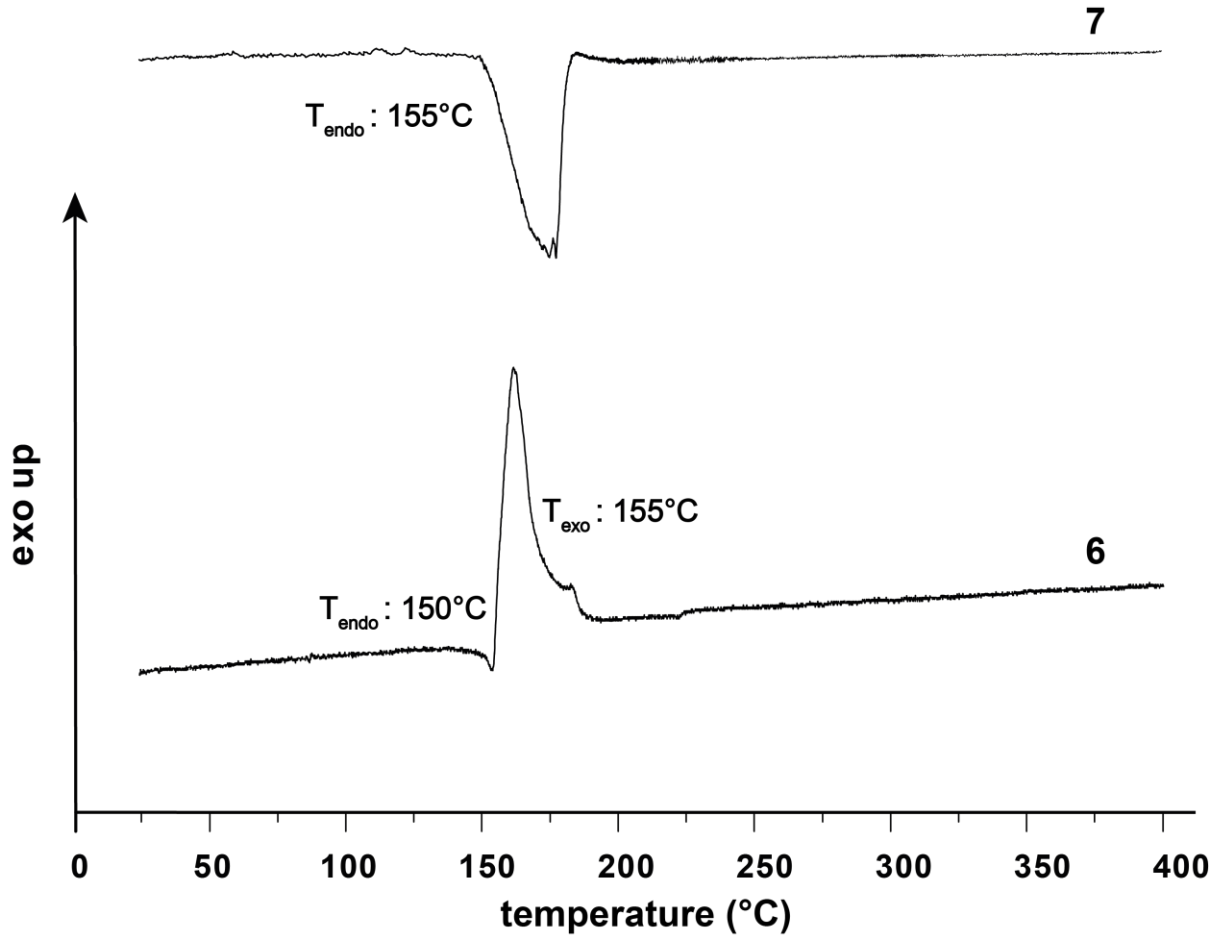

Figure S23. DTA measurements of **6** and **7** with a heating rate of 5 °C min^{-1}.

8.7.5 TGA Measurement

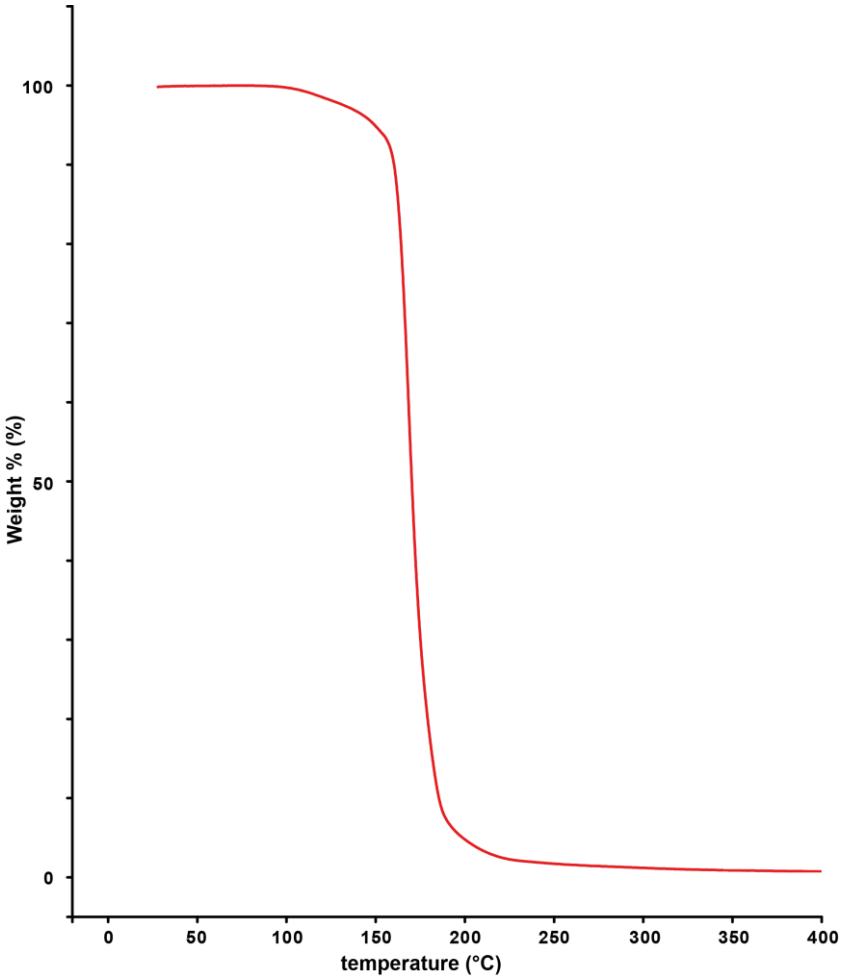

Figure S24. TGA measurement of **6** with a heating rate of 5 °C min^{-1}.

8.7.6 X-Ray Diffraction

For all crystalline compounds, an Oxford Xcalibur3 diffractometer with a CCD area detector or Bruker D8 Venture TXS diffractometer equipped with a multilayer monochromator, a Photon 2 detector, and a rotating-anode generator was employed for data collection using Mo-Kα radiation (λ = 0.71073 Å). On the Oxford device, data collection and reduction were carried out using the CRYSALISPRO software.[7] On the Bruker diffractometer, the data were collected with the Bruker Instrument Service v3.0.21, the data reduction was performed using the SAINT V8.18C software (Bruker AXS Inc., 2011). The structures were solved by direct methods (SIR-92, [8] SIR-97[9] or SHELXT[9,10]) and refined by full-matrix least-squares on F2 (SHELXL[10,11]) and finally checked using the PLATON software[12] integrated into the WinGX[13] software suite. The non-hydrogen atoms were refined anisotropically and the hydrogen atoms were located and freely refined. The absorptions were corrected by a SCALE3 ABSPACK or SADABS Bruker APEX3 multiscan method. [14] All DIAMOND2 plots are shown with thermal ellipsoids at the 50 % probability level and hydrogen atoms are shown as small spheres of arbitrary radius.

Table S1. Crystallographic data and structure refinement of **5** and **6**·EtCN.

	5	**6·EtCN**
Formula	$C_2H_4N_4O_8$	$C_4H_8N_8O_8 \cdot C_3H_5N$
FW [g mol^{-1}]	212.09	351.24
Crystal system	orthorhombic	orthorhombic
Space group	*Pbcn*	$P2_12_12_1$
Color / Habit	colorless plate	colorless plate
Size [mm]	0.10 x 0.20 x 0.25	0.05 x 0.20 x 0.60
a [Å]	8.9270(6)	10.1790(16)
b [Å]	6.0614(4)	11.1002(16)
c [Å]	13.4724 (11)	30.000(5)
α [°]	90	90
β [°]	90	90
γ [°]	90	90
V [Å^3]	728.99 (9)	3389.7(9)
Z	4	8
$\rho_{calc.}$ [g cm^{-3}]	1.933	1.627
μ [mm^{-1}]	0.200	0.155
F(000)	432	1712
$\lambda_{MoK\alpha}$ [Å]	0.71073	0.71073
T [K]	92	93
θ Min-Max [°]	3.0, 26.4	2.1, 26.4
Dataset	-11: 11 ; -7: 7 ; -16: 16	-12: 6 ; -13: 13 ; -37: 37
Reflections collected	5432	14767
Independent refl.	748	6921
R_{int}	0.048	0.110
Observed reflections	634	3292
Parameters	73	515
R_1 (obs)[a]	0.0299	0.0816
wR_2 (all data)[b]	0.0752	0.1316
S [c]	1.04	0.96
Resd. dens [e Å^{-3}]	-0.19, 0.23	-0.35, 0.32
Device type	Xcalibur Sapphire 3	Xcalibur Sapphire 3
Solution	SHELXT 2018/2	SHELXT 2018/2
Refinement	ShelXL 2018/3	ShelXL 2018/3
Absorption correction	multi-scan	multi-scan
CCDC	2279207	2279206

[a] $R_1 = \Sigma||F_o|-|F_c||/\Sigma|F_o|$; [b] $wR_2 = [\Sigma[w(F_o^2-F_c^2)^2]/\Sigma[w(F_o)^2]]^{1/2}$; $w = [\sigma c^2(F_o^2)+(xP)^2+yP]^{-1}$ and $P=(F_o^2+2F_c^2)/3$; [c] $S = \{\Sigma[w(F_o^2-F_c^2)^2]/(n-p)\}^{1/2}$ (n = number of reflections; p = total number of parameters).

Table S2. Crystallographic data and structure refinement of 3,7-dinitro-1,5,3,7-dioxadiazocane.

	3,7-Dinitro-1,5,3,7-dioxadiazocane
Formula	$C_4H_8N_4O_6$
FW [g mol^{-1}]	208.13
Crystal system	orthorhombic
Space group	*Fmm*2
Color / Habit	colorless plate
Size [mm]	0.05 x 0.10 x 0.10
a [Å]	13.360(3)
b [Å]	10.6877(18)
c [Å]	5.5944(9)
α [°]	90
β [°]	90
γ [°]	90
V [Å^3]	798.8(3)
Z	4
$\rho_{calc.}$ [g cm^{-3}]	1.731
μ [mm^{-1}]	0.162
F(000)	432
$\lambda_{MoK\alpha}$ [Å]	0.71073
T [K]	91
θ Min-Max [°]	3.0, 26.4
Dataset	-16: 16 ; -13: 12 ; -6: 6
Reflections collected	1617
Independent refl.	450
R_{int}	0.077
Observed reflections	341
Parameters	37
R_1 (obs)[a]	0.0541
wR_2 (all data)[b]	0.1096
S [c]	1.05
Resd. dens [e Å^{-3}]	-0.17, 0.30
Device type	Xcalibur Sapphire 3
Solution	SHELXT 2018/2
Refinement	ShelXL 2018/3
Absorption correction	multi-scan
CCDC	2279205

[a]$R_1 = \Sigma||F_0|-|F_c||/\Sigma|F_0|$; [b]$wR_2 = [\Sigma[w(F_0^2-F_c^2)^2]/\Sigma[w(F_0)^2]]^{1/2}$; $w = [\sigma c^2(F_0^2)+(xP)^2+yP]^{-1}$ and $P=(F_0^2+2F_c^2)/3$; [c]$S = \{\Sigma[w(F_o^2-F_c^2)^2]/(n-p)\}^{1/2}$ (n = number of reflections; p = total number of parameters).

8.7.7 Heat of Formation Calculations

All quantum chemical calculations were carried out using the Gaussian G09 program package.[15] The enthalpies (H) and free energies (G) were calculated using the complete basis set (CBS) method of *Petersson* and coworkers to obtain very accurate energies.[16] The CBS models are using the known asymptotic convergence of pair natural orbital expressions to extrapolate from calculations using a finite basis set to the estimated CBS limit. CBS-4 starts with an HF/3-21G(d) geometry optimization; the zero-point energy is computed at the same level. It then uses a large basis set SCF calculation as base energy, and an MP2/6-31+G calculation with a CBS extrapolation to correct the energy through second order. A MP4(SDQ)/6-31+(d,p) calculation is used to approximate higher-order contributions. In this study, we applied the modified CBS-4M method.
Heats of formation were calculated using the atomization method (Equation S1) using room temperature CBS-4M enthalpies, which are summarized in Table S3.[16]

$$\Delta_f H°_{(g,\,M,\,298)} = H_{(Molecule,\,298)} - \sum H°_{(Atoms,\,298)} + \sum \Delta_f H°_{(Atoms,\,298)} \quad (S1)$$

Table S3. CBS-4M enthalpies for atoms C, H, N, and O and their literature values for atomic $\Delta H°_f{}^{298}$ / kJ mol^{-1}.

	$-H^{298}$ / a.u.	NIST
H	0.500991	218.2
C	37.786156	717.2
N	54.522462	473.1
O	74.991202	249.5

The standard molar enthalpy of formation were calculated using $\Delta_f H(g)$ subtracting the enthalpy of sublimation estimated by applying Trouton´s rule.[17]

8.7.8 Calculation of Energetic Performance Parameters

The detonation parameters were calculated with the EXPLO5 (version 6.06.01) computer code.[18] This calculation code is based on the steady-state model of equilibrium and uses the Becker–Kistiakowski–Wilson equation of state.[19] It calculates the detonation parameters at the Chapman–Jouguet (CJ) point, which itself is found from the Hugoniot curve of the system by its first derivative. These calculations are based on the density recalculated from the corresponding crystal densities by Equation S2 (av = 1.5x10^{-4} K) and on the calculated enthalpies of formation.

$$d_{298K} = \frac{d_T}{1+ \alpha_v(298-T_0)} \quad \text{(S2)}$$

d_T = insert X-ray density in g cm^{-3}

T_0 = insert X-Ray temperature in K

α_v = correction factor

Table S4. X-Ray and recalculated densities of **5**, **6** · EtCN and 3,7-dinitro-1,5,3,7-dioxadiazocane.

	X-Ray density [g cm-3]	Density recalculated to 298K [g cm^{-3}]
5	(@ 92K) 1.932	1.874
6 · EtCN	(@ 93K) 1.627	1.578
3,7-Dinitro-1,5,3,7-dioxadiazocane	(@ 91K) 1.731	1.679

8.7.9 References SI

[S1] NATO standardization agreement (STANAG) on explosives, impact sensitivity tests, no. 4489, 1st ed, Sept. 17, **1999**.

[S2] WIWEB-Standardarbeitsanweisung 4-5.1.02, Ermittlung der Explosionsgefährlichkeit, hier der Schlagempfindlichkeit mit dem Fallhammer. Nov. 8, **2002**.

[S3] "http://www.bam.de", accessed March **2022**.

[S4] NATO standardization agreement (STANAG) on explosive, friction sensitivity tests. no. 4487, 1st ed., Aug. 22, **2002**.

[S5] WIWEB-Standardarbeitsanweisung 4-5.1.03, Ermittlung der Explosionsgefährlichkeit oder der Reibeempfindlichkeit mit dem Reibeapparat. Nov. 8, **2002**.

[S6] Impact: insensitive > 40 J, less sensitive ≥ 35 J, sensitive ≥ 4 J, very sensitive ≤ 3 J, Friction: insensitive > 360 N, less sensitive = 360 N, sensitive < 360 N and > 80 N, very sensitive ≤ 80 N, extremely sensitive ≤ 10 N. According to the UN Recommendations on the Transport of Dangerous Goods, (+) indicates not safe for transport.

[S7] CrysAlisPro, Oxford Diffraction Ltd., version 171.33.41, **2009**.

[S8] A. Altomare, G. Cascarano, C. Giacovazzo, A. Guagliardi, *J. Appl. Crystallogr* **1993**, *26*, 343−350.

[S9] a) A. Altomare, G. Cascarano, C. Giacovazzo, A. Guagliardi, A. G. G. Moliterni, SIR97 **1997**; b) A. Altomare, M. C. Burla, M. Camalli, G. L. Cascarano, C. Giacovazzo, A., *J. Appl. Crystallogr*. **1999**, *32*, 115−119.

[S10] G. M. Sheldrick, *Acta Crystallogr. Sect. A* **2008**, *A64*, 112−122.

[S11] G. M. Sheldrick, SHELXL-97, Program for the Refinement of Crystal, University of Göttingen, Germany, **1997**.

[S12] A. L. Spek, PLATON, A Multipurpose Crystallographic Tool, Utrecht University **1999**.

[S13] L. J. Farrugia, *J. Appl. Cryst.* **2012**, *45*, 849−854.

[S14] a) Empirical absorption correction using spherical harmonics, implemented in SCALE3 ABSPACK scaling algorithm (CrysAlisPro Oxford Diffraction Ltd., Version 171.33.41, 2009); b) APEX3. Bruker AXS Inc., Madison, Wisconsin, USA.

[S15] M. J. Frisch, G. W. Trucks, H. B. Schlegel, G. E. Scuseria, M. A. Robb, J. R. Cheeseman, G. Scalmani, V. Barone, B. Mennucci, G. A. Petersson, H. Nakatsuji, M. Caricato, X. Li, H.P. Hratchian, A. F. Izmaylov, J. Bloino, G. Zheng, J. L. Sonnenberg, M. Hada, M. Ehara, K. Toyota, R. Fukuda, J. Hasegawa, M. Ishida, T. Nakajima, Y. Honda, O. Kitao, H. Nakai, T. Vreven, J. A. Montgomery, Jr., J. E. Peralta, F. Ogliaro, M. Bearpark, J. J. Heyd, E. Brothers, K. N. Kudin, V. N. Staroverov, R. Kobayashi, J. Normand, K. Raghavachari, A. Rendell, J. C. Burant, S. S. Iyengar, J. Tomasi, M. Cossi, N. Rega, J. M. Millam, M. Klene, J. E. Knox, J. B. Cross, V. Bakken, C. Adamo, J. Jaramillo, R. Gomperts, R. E. Stratmann, O. Yazyev, A. J. Austin, R. Cammi, C. Pomelli, J. W. Ochterski, R. L. Martin, K. Morokuma, V. G. Zakrzewski, G. A. Voth, P. Salvador, J. J. Dannenberg, S. Dapprich, A. D. Daniels, O. Farkas, J.B. Foresman, J. V. Ortiz, J. Cioslowski, D. J. Fox, Gaussian 09 A.02, Gaussian, Inc., Wallingford, CT, USA, **2009**.

[S16] a) J. W. Ochterski, G. A. Petersson, and J. A. Montgomery Jr., *J. Chem. Phys.* **1996**, *104*, 2598−2619; b) J. A. Montgomery Jr., M. J. Frisch, J. W. Ochterski G. A. Petersson, *J. Chem. Phys.* **2000**, *112*, 6532−6542; c) L. A. Curtiss, K. Raghavachari, P. C. Redfern, J. A. Pople, *J. Chem. Phys.* **1997**, *106*, 1063−1079; d) E. F. C. Byrd, B. M. Rice, *J. Phys. Chem. A* **2006**, *110*, 1005–1013; e) B. M. Rice, S. V. Pai, J. Hare, *Comb. Flame* **1999**, *118*, 445–458.

[S17] F. Trouton, *Philos. Mag.* (1876-1900) **1884**, *18*, 54-57; b) M. S. Westwell, M. S. Searle, D. J. Wales, D. H. Willimas, *J. Am. Chem. Soc.* **1995**, *117*, 5013-5015.

[S18] M. Sućeska, EXPLO5 V6.06.01, Zagreb (Croatia) **2021**.

[S19] M. Sućeska, *Propellants, Explos., Pyrotech.* **1991**, *16*, 197–202.

9 Synthesis of Bridged Tetrazoles with Promising Properties and Potential Applications by a One-Step Finkelstein Reaction

Jasmin T. Lechner, Christian Riedelsheimer, Simon M. J. Endraß, Nina M. Gerold, Jennifer Heidrich, Burkhard Krumm, Jörg Stierstorfer and Thomas M. Klapötke*

as published in *Chemistry − a European Journal* **2023**, e202303021

DOI: 10.1002/chem.202303021

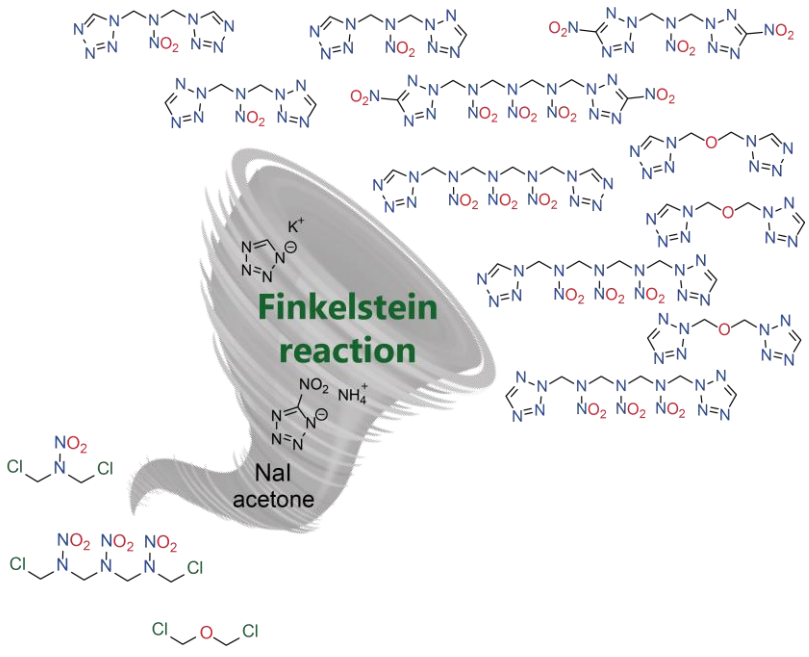

Abstract: Numerous nitramine bridged compounds which show promising combinations of properties have already been identified in the area of energetic materials. In this work, four new nitrazapropane bridged tetrazoles, as well as four new trinitrazaheptane tetrazoles and three oxapropane bridged tetrazoles were synthesized and fully characterized. These new compounds can all be synthesized by a simple, one-step synthesis using Finkelstein conditions. All of these new energetic materials were characterized using NMR spectroscopy, single crystal X-ray diffraction, vibrational analysis and elemental analysis. The thermal behaviour of these compounds was studied by differential thermal analysis (DTA) and partly by thermogravimetric analysis (TGA). The BAM standard method was used to determine the sensitivities towards impact (IS) and friction (FS). The enthalpies of formation were calculated at the CBS-4M level, and the energetic performances were calculated using the EXPLO5 (V6.06.01) computer code. The properties of the new compounds were compared to each other as well as to the known energetic material RDX. Moreover, the iron(II) and copper(II) perchlorate complexes with 1,3-bis-1,1'-tetrazolylnitrazapropane as ligand were prepared and investigated.

9.1 Introduction

The demands on new energetic materials are diverse and difficult to reconcile. There are not only demands on the synthetic process - which should be cost-efficient and environmentally friendly - there are also demands on the properties of new compounds, such as reconciling a high performance with low sensitivity.[1-4] Therefore, to obtain a compound which can be more easily handled, the right compromise between energy and stability has to be found.

Various synthetic strategies have been described for creating new energetic materials, such as the introduction of ring and cage strain, or aiming to reach the highest possible nitrogen content.[5-8] In order to achieve these properties in a compound, the same energetic building blocks are often used.[1-2] Well-known examples are functionalization with nitro, nitrato, nitrimino and nitramino groups, or the addition of covalent azides.[1,9-14] However, not only incorporation of the functional groups described above is used for the design of energetic materials.

The inclusion of different building blocks like arenes or different heterocycles can increase the energy content in a molecule as well.[1,15-20] Azoles such as pyrazoles, triazoles or tetrazoles are often used due to their positive enthalpies of formation. Examples of such novel energetic materials are TKX-50 (dihydroxylammonium-5,5-bistetrazolyl-1,1-diolat) or the primary explosive DBX-1 (copper(I) 5-nitrotetrazolate).[21-22]

The nitramine functional group is also widely used as an energetic building block in energetic materials, and many compounds which incorporate this building block are known and show promise for use in applicaions. Examples of cyclic nitramines are the two secondary explosives (1,3,5-trinitro-1,3,5-triazinane, RDX) and octogen (1,3,5,7-tetranitro-1,3,5,7-tetrazocane, HMX), both of which are mainly used in the military sector in warheads or propellant formulations.[23-25] In addition, there are also open-chain nitramine energetic compounds such as the nitroxyethyl nitramines (NENAs). Important examples of NENAs are BuNENA (*n*-butyl nitroxyethylnitramine) or DINA (dioxyethylnitramine dinitrate), both of which are used as plasticizers in propellant formulations.[26-27]

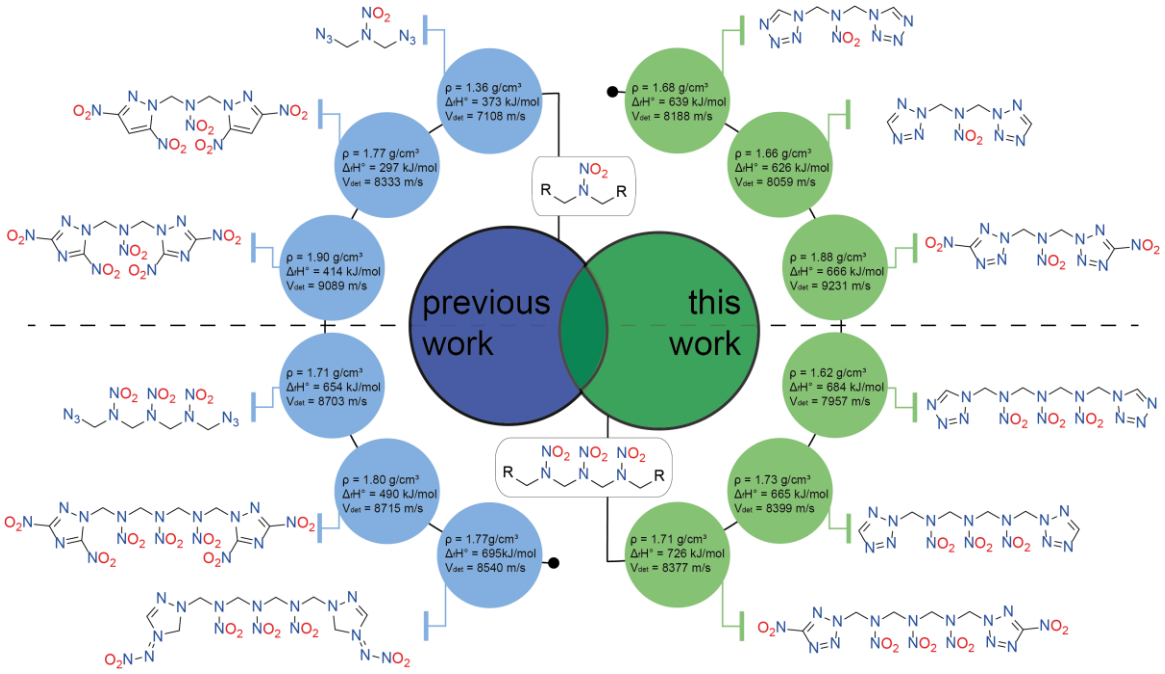

Figure 1. New nitramine-bridged compounds as well as those previously reported in the literature with their density, solid-state heat of formation (HoF) and detonation velocity (V_{det}).[33-36]

In the literature it is reported that bridged energetic materials show a higher stability.[28-30] In the previously reported compounds, simple saturated carbon chains have usually been used to act as bridging units, but also oxa, azo or nitramine bridged compounds have been reported.[30-32] As is shown on the left side of Figure 1, many compounds with nitrazapropane or trinitrazaheptane as the bridging unit have been reported. Open-chain nitramine compounds such as the bridged *bis*-(azides) or bridged azoles are already known in literature (Figure 1).[33-36]

A closer look at the density, solid-state enthalpy of formations (HoF) and detonation velocities (V_{det}) of the compounds in shown Figure 1 shows that most exhibit promising properties. The 1,3-*bis*(3,5-dinitro-1,2,4-triazol-1-yl)-2-nitrazapropane stands out in this respect, because of its remarkable high density of 1.90 g cm^{-3}, which results in a calculated detonation velocity of 9089 m s^{-1}.[34] However, the corresponding trinitrazaheptane-bridged compound 1,7-*bis*(3,5-dinitro-1,2,4-triazol-1-yl)-2,4,6-trinitrazaheptane also shows promising properties with a HoF of 490 kJ $mol^{-}1$ and a detonation velocity of 8715 m s^{-1}.[35]

So far, only nitramine-bridged pyrazoles and triazoles are known in the literature, while the corresponding tetrazole compounds remain elusive.[34-37] Therefore, in this work, the corresponding nitramine bridged tetrazole isomers and 5-nitrotetrazoles were synthesized, characterized, and their properties compared with those of known secondary explosives. In addition, 1,3-*bis*-1,1'-tetrazolylnitrazapropane was used to act as a ligand in energetic coordination compounds (ECCs), and the properties of the new complex compounds were investigated.[38]

Since the literature suggests that oxapropane-bridged compounds are more stable than nitrazapropane-bridged compounds, the three isomers of oxapropane-bridged tetrazole were also synthesized and compared with the nitramine-bridged compounds.[30] The 1,1'-isomer **9** has been mentioned once before in the literature, however, in this work it was prepared *via* an alternative route and was fully characterized for the first time in terms of its energetic properties.[39]

9.2 Results and Discussion

9.2.1 Synthesis

The syntheses of compounds **1** to **11** were all performed using a Finkelstein reaction, as shown in Scheme 1-3.[40-42] Starting from the chloride, first a chloride-iodide exchange (S_N2 mechanism) is carried out by adding sodium iodide. This halide exchange is carried out to exploit the solubility differences of the halide salts in the corresponding solvent, which is in most cases acetone. While sodium iodide dissolves well in acetone, sodium chloride is almost insoluble. Therefore, the equilibrium of the nucleophilic substitution reaction is shifted, and the reaction to attach the tetrazole rings on the nitramine bridge is favored. In general, it is known that the Finkelstein reaction proceeds best for primary halides. In our work primary halides were used, therefore reaction times of no longer than 12 h were required and no raised temperatures were necessary.[40-42]

From Scheme 1 it can be seen that in the reaction of 1,3-dichloro-2-nitrazapropane with potassium tetrazolate under Finkelstein conditions, all three possible isomers are formed. The 1,2-isomer (**2**) was obtained as the main component (60%), followed by the 2,2'-isomer (**3**, 25%) and the 1,1'-isomer (**1**, 15%). The isomers were obtained with a moderate overall yield of 62% and can be easily separated by column chromatography. In contrast, only one isomer was formed in the reaction with ammonium nitrotetrazolate. Due to the electron withdrawing effect of the nitro group on the tetrazole ring, only the 2,2'-isomer (**4**) is formed, leading to an almost quantitative conversion with a yield of 98%.

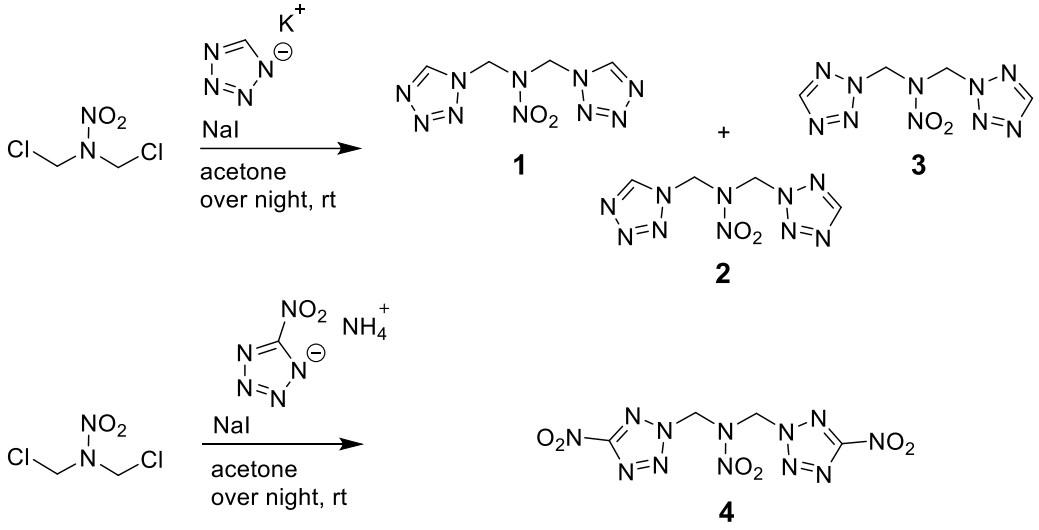

Scheme 1. Synthetic route of 1,3-*bis*-1,1'-tetrazolylnitrazapropane (**1**), 1,3-*bis*-1,2-tetrazolylnitrazapropane (**2**), 1,3-*bis*-2,2'-tetrazolylnitrazapropane (**3**) and 1,3-*bis*-2,2'-nitrotetrazolylnitrazapropane (**4**).

Similar results were observed for the reaction of 1,7-dichloro-2,4,6-trinitrazaheptane with potassium tetrazolate under Finkelstein conditions as shown in Scheme 2. All three isomers were again formed, with a ratio of 27% of 1,1'-isomer (**5**), 43% of 1,2-isomer (**6**) and 30% of 2,2'-isomer (**7**). The isomers can again be separated using column chromatography and are obtained with a moderate overall yield of 60%. For the nitrotetrazole derivative **8**, again only one isomer is obtained with a very good yield of 92%.

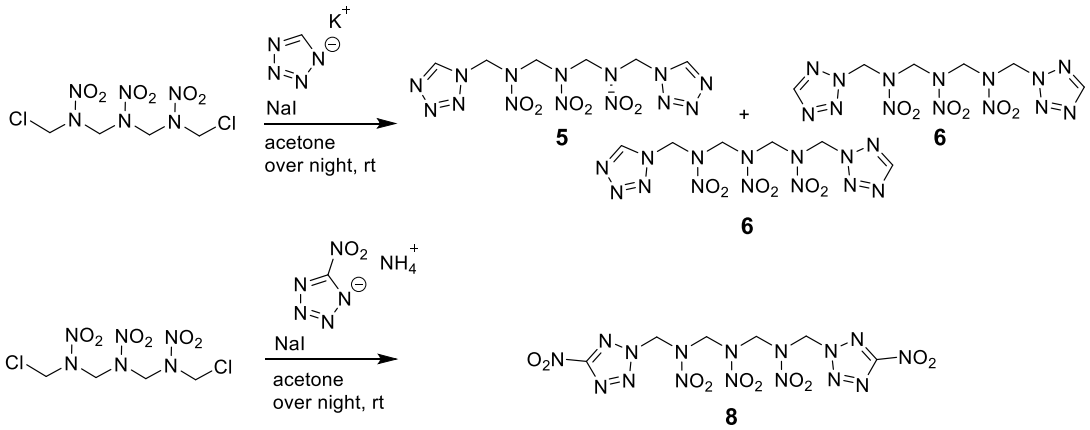

Scheme 2. Synthetic route of 1,7-*bis*-1,1'-tetrazolyltrinitrazaheptane (**5**), 1,7-*bis*-1,2-tetrazolyltrinitrazaheptane (**6**), 1,7-*bis*-2,2'-tetrazolyltrinitrazaheptane (**7**) and 1,7-*bis*-2,2'-nitrotetrazolyltrinitrazaheptane (**8**).

Scheme 3 shows the reaction of 1,3-dichloro-2-oxapropane with potassium tetrazolate under Finkelstein conditions. Here, again, all three isomers are formed with a total yield of 78%. The isomers can be seorated using column chromatography, and are formed in the ratio of 14% of 1,1'-isomer (**9**), 50% of 1,2-isomer (**10**) and 36% of 2,2'-isomer (**11**).

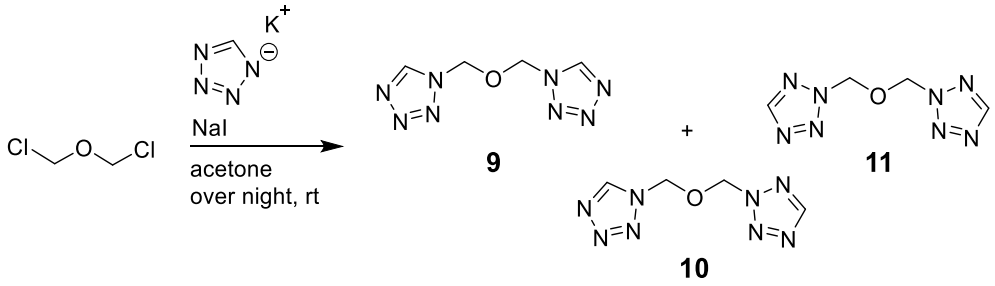

Scheme 3. Synthetic route of 1,3-*bis*-1,1'-tetrazolyloxapropane (**9**), 1,3-*bis*-1,2-tetrazolyloxapropane (**10**) and 1,3-*bis*-2,2'-tetrazolyloxapropane (**11**).

In addition, 1,3-*bis*-1,1'-tetrazolylnitrazapropane (**1**) was used as a ligand in ECCs. In order to synthesize the ECCs shown in scheme 4, three equivalents of **1** were reacted with one equivalent of the corresponding copper(II) or iron(II) perchlorate, which resulted in the formation of the energetic complexes **12** and **13**.

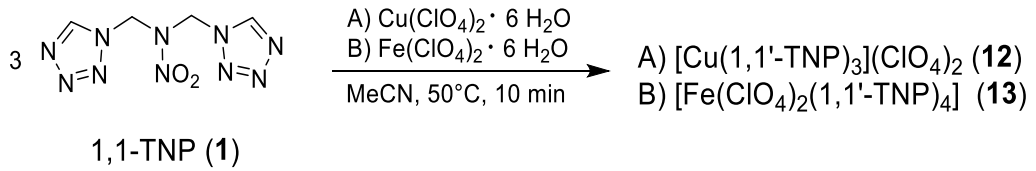

Scheme 4. Synthesis of energetic coordination compounds (ECCs) **12** and **13** using 1,3-*bis*-1,1'-tetrazolylnitrazapropane (**1**) as the energetic ligand.

9.2.2 NMR Spectroscopy

Compounds **1** to **11** were characterized by ^{1}H, $^{13}C\{^{1}H\}$ and ^{14}N NMR spectroscopy in acetone-D_6. Moreover, ^{15}N NMR spectra of compounds **4** and **8** wereobtained, which are discussed in more detail in the following section. All other spectra and assignments can be found in the Experimental Section or in the Supporting Information.

In Figure 2, the ^{15}N NMR spectrum of **4** is shown. The signal at –191.6 ppm can be assigned to the nitramine nitrogen (N1). The quintet ($^{3}J_{N,H}$ = 2.7 Hz) at –41.1 ppm corresponds to the nitro group (N2) of the nitramine moiety, while the signal at –35.1 ppm can be assigned to the nitro group (N7) which is attached to the tetrazole ring. The signals corresponding to the remaining four tetrazole nitrogen atoms can be assigned as follows based on the assignments made for similar compounds previously in the literature: N3 at –78.8 ppm, N4 at –95.0 ppm, N5 at 8.6 ppm and N6 at –52.2 ppm.[38]

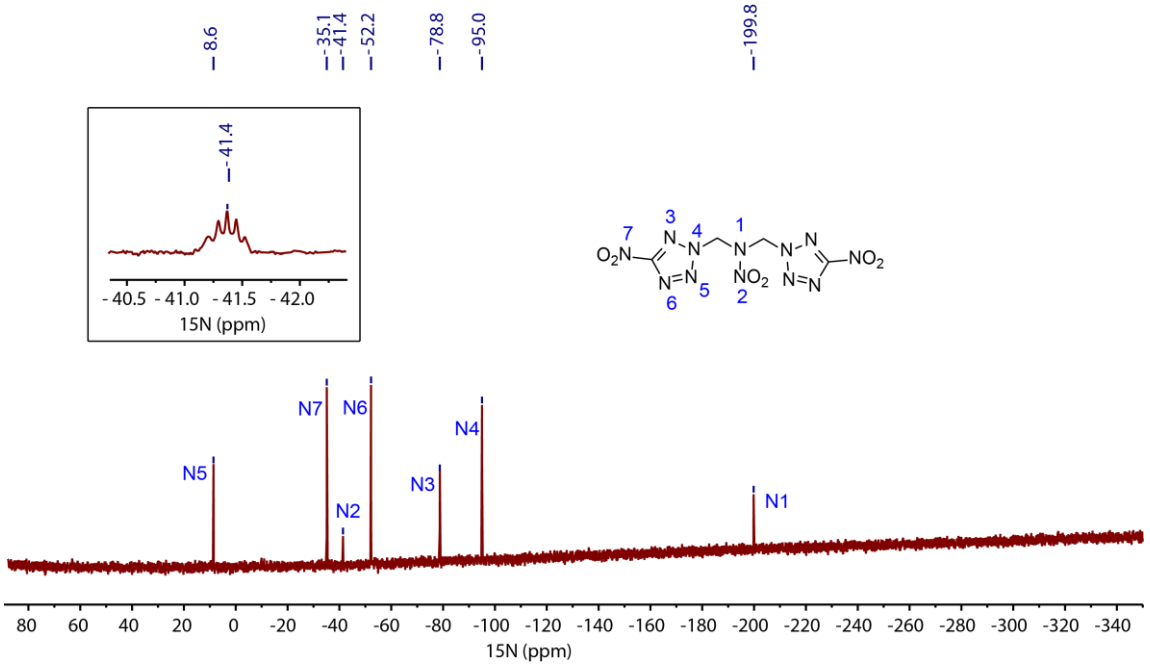

Figure 2. ^{15}N NMR spectrum of 1,3-*bis*-2,2'-nitrotetrazolylnitrazapropane (**4**) in acetone-D_6.

The ^{15}N spectrum of compound **8** is shown in Figure 3. The signals corresponding to the two nitramine N atoms can be assigned as follows: –191.6 ppm (N1) and –195.5 ppm (N2) because of the signal intensity of 1:2. The nitro groups of the nitramine moieties are observed at –34.0 ppm (N3, quintet, $^{3}J_{N,H}$ = 2.5 Hz) and at –36.8 ppm (N4, quintet, $^{3}J_{N,H}$ = 2.5 Hz). Here, as well, the assignment can be made based on the signal intensity. The signal at –34.8 ppm can be assigned to the nitrogen group (N9) attached to the tetrazole ring. The assignment of the signals corresponding to the N atoms within the tetrazole ring is similar to that of compound **4**, and is as follows: N5 at –78.9 ppm, N6 at –93.9 ppm, N7 at 7.7 ppm and N8 at –52.8 ppm.[38]

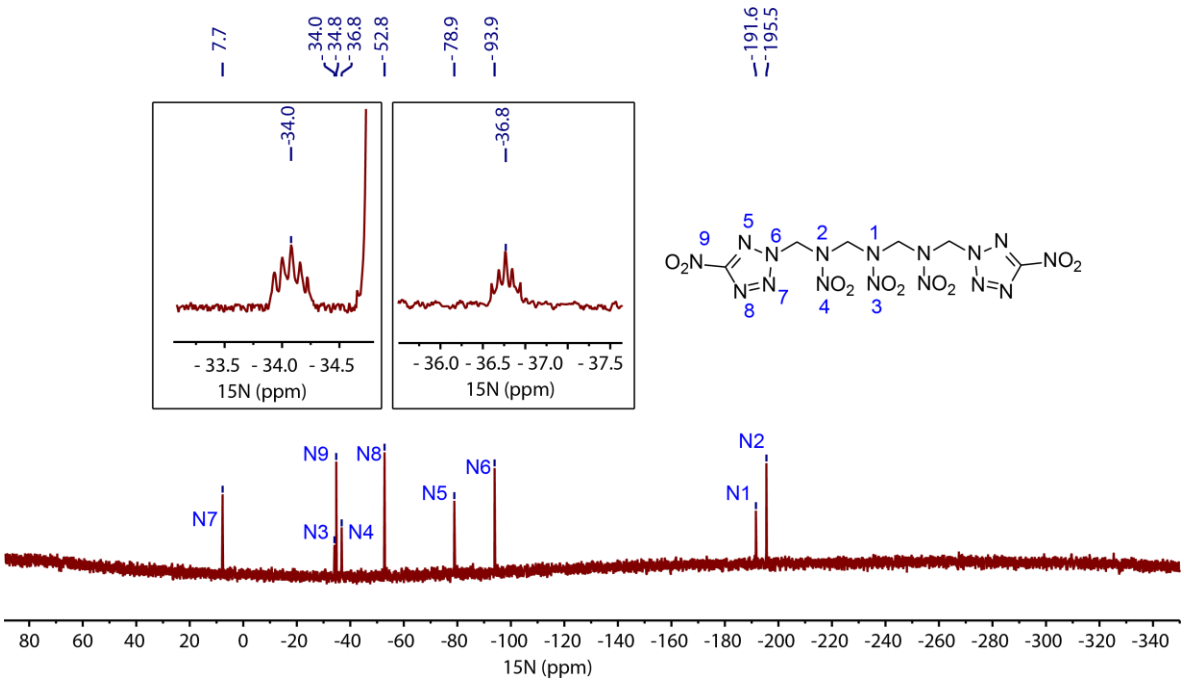

Figure 3. ^{15}N NMR spectrum of 1,7-*bis*-2,2'-nitrotetrazolyltrinitrazaheptane (**8**) in acetone-D_6.

9.2.3 Single Crystal Analysis

The single crystal structures of compounds **1**, **3**, **4**, **7** and **9** were determined using low temperature X-ray diffraction. The individual crystal structures are shown and discussed in the following section, However, additional information about the measurements and refinements can be found in the Supporting Information.

The crystal structures of 1,3-*bis*-1,1'-tetrazolylnitrazapropane (**1**, left) and 1,3-*bis*-2,2'-tetrazolylnitrazapropane (**3**, right) are shown in Figure 3.

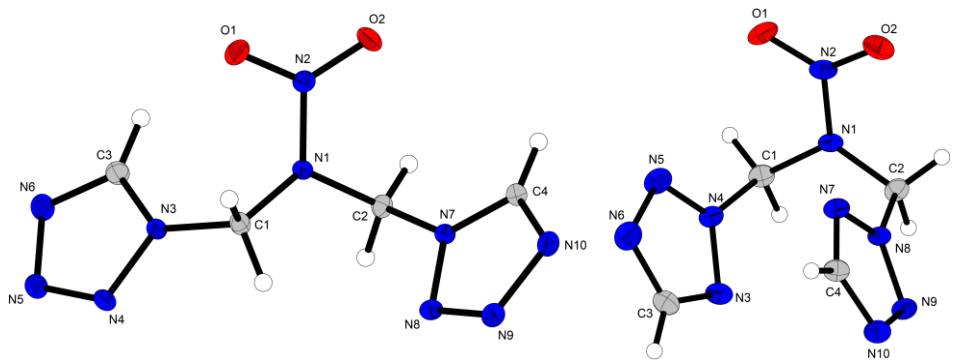

Figure 4. Crystal structures of **1** (left) and **3** (right) with selected bond lengths (Å) and selected angles (°): **1** N1−N2 1.3857 (14), N3−C1 1.4748 (15), N7−C2 1.4596 (15), C3−N3−C1−N1 −28.99 (17),

C4−N7−C2−N1 −98.52(14); **2** N1−N2 1.392 (2), N4−C1 1.463 (2), N8−C2 1.482 (2), N3−N4−C1−N1 –91.0 (2), N7−N8−C2−N1 –37.1 (2).

Compound **1** crystallizes in the monoclinic space group $P2_1/c$ with four molecules per unit cell and a re-calculated density of 1.68 g cm^{-3} at room temperature. The corresponding 2,2'-isomer **3** has similar structural parameters, also crystallizing in the monoclinic space group $P2_1/c$ with four molecules per unit cell. 1,3-*Bis*-2,2'-tetrazolylnitrazapropane, however, has a slightly lower re-calculated density of 1.66 g cm^{-3} at room temperature. The spatial arrangement of the two isomers shows clear differences. While the tetrazole rings in the 1,1'-isomer are aligned as far away from each other as possible, in the 2,2'-isomer (**3)** they are arranged in such a way that they align themselves parallel to each other in a pincer-like manner.

In Figure 4, the crystal structures of 1,3-*bis*-2,2'-nitrotetrazolylnitrazapropane (**4**, left) and 1,7-*bis*-2,2'-tetrazolyltrinitrazaheptane (**7**, right) are shown.

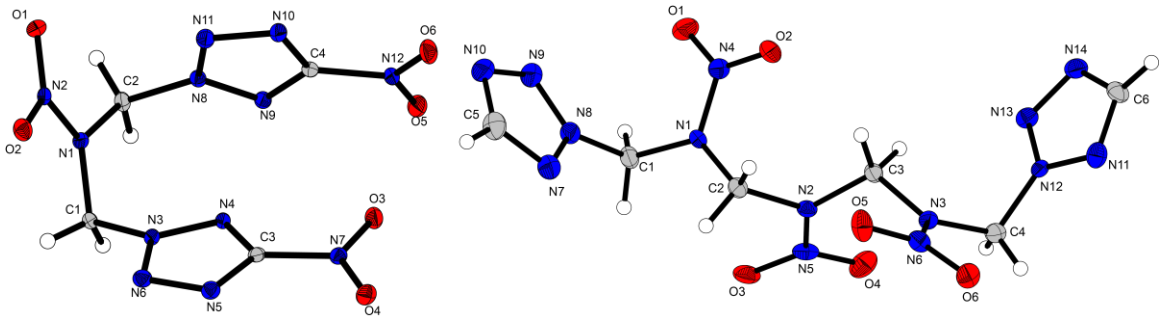

Figure 5. Crystal structures of **4** (left) and **7** (right) with selected bond lengths (Å): and selected angles (°): **4** N2−N1 1.404 (2), N3−C1 1.476 (3), N8−C2 1.482 (3), N4−N3−C1−N1 -62.9 (3), N9−N8−C2−N1 121.7(2); **7** N8−C1 1.450 (7), N12−C4 1.464 (7), N7−N8−C1−N1 –77.7(6), N13−N12−C4−N3 –78.0(6).

1,3-*Bis*-2,2'-nitrotetrazolylnitrazapropane (**4**) crystallizes in the monoclinic space group *Cc*, with four molecules per unit cell. However, **(4)** shows a relatively high density of 1.88 g cm^{-3} at room temperature. In **(4)** the tetrazole rings are twisted towards each other in a pincer-like manner, similar to that observed in **3**.

Due to the longer trinitrazaheptane bridge in compound **7**, the tetrazole rings are no longer twisted towards each other. 1,7-*Bis*-2,2'-tetrazolyltrinitrazaheptane (**7**) crystallizes in the monoclinic space group $P2_1/c$ with four molecules per unit cell and a re-calculated density of 1.73 g cm^{-3} at room temperature.

Figure 6 shows the crystal structure of 1,3-*bis*-1,1'-tetrazolyloxapropane (**9**). Compound (9) crystallizes in the orthorhombic space group $P2_12_12_1$ with four molecules per unit cell and has a re-calculated density of 1.53 g cm^{-3} at room temperature.

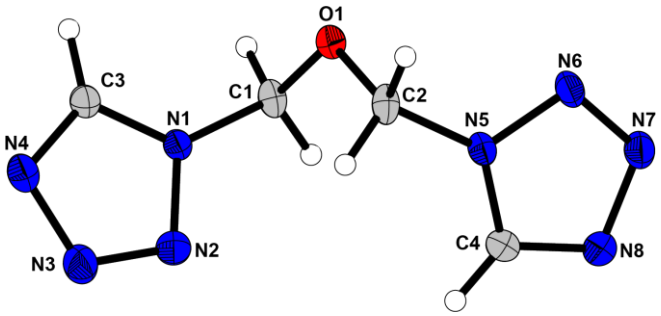

Figure 6. Crystal structure of **9** with selected bond lengths (Å) and selected angles (°): N1−C1 1.464 (2), N5−C2 1.466 (2), N2−N1−C1−O1 –102.1 (2), N6−N5−C2−O1 76.3 (2).

The 1,1'-oxa-bridged bistetrazole **9** shows a similar spatial arrangement to that of the 1,1'-nitrazapropane-bridged compound **1**. The tetrazole rings are arranged in such a way that they are as far away from each other as possible.

9.2.4 Thermal Analyses

In order to investigate the thermal behavior of the compounds prepared in this work, compounds **1** to **13** were all analyzed by differential thermal analysis (DTA). DTA measurements were carried out in the range from 25 to 400°C with a heating rate of 5°C min^{-1}. The results of these measurements are shown in Table 1. Figure 7 shows the DTA plots of **4** and **8**, while the plots of the DTA measurements of the other compounds can be found in the SI (Figures S33–S36).

Table 1. Endothermic[a] and exothermic[b] onset points of the DTA measurements of compounds **1** to **13** compared to RDX.[43]

	T_{endo}[a] [°C]	T_{exo}[b] [°C]
1	167	171
2	99	154
3	72	173
4	157	213
5	–	187
6	–	194
7	193	212
8	210	217
9	98	168
10	–	180
11	–	185
12	–	246
13	–	220
RDX[43]	7.5	209

All compounds (1 – 13) were found to decompose above 150°C. In general, it can be seen that the *bis*nitrotetrazolyl derivatives (**4**, **8**) are thermally more stable than the *bis*-tetrazolyl compounds (**1**–**3**, **5**–**7**). Moreover, it can be seen that the trinitrazaheptane-bridged compounds (**5**–**8**) are more thermally stable than the nitrazapropane-bridged compounds (**1**–**4**). The trend that oxapropane bridged compounds are more thermally stable compared to the corresponding nitrazapropane bridged compounds is shown for the 1,2'-isomer (**2** vs. **10**) and 2,2'-isomer (**3** vs. **11**), but not for the 1,1'-isomer (**1** vs. **9**).

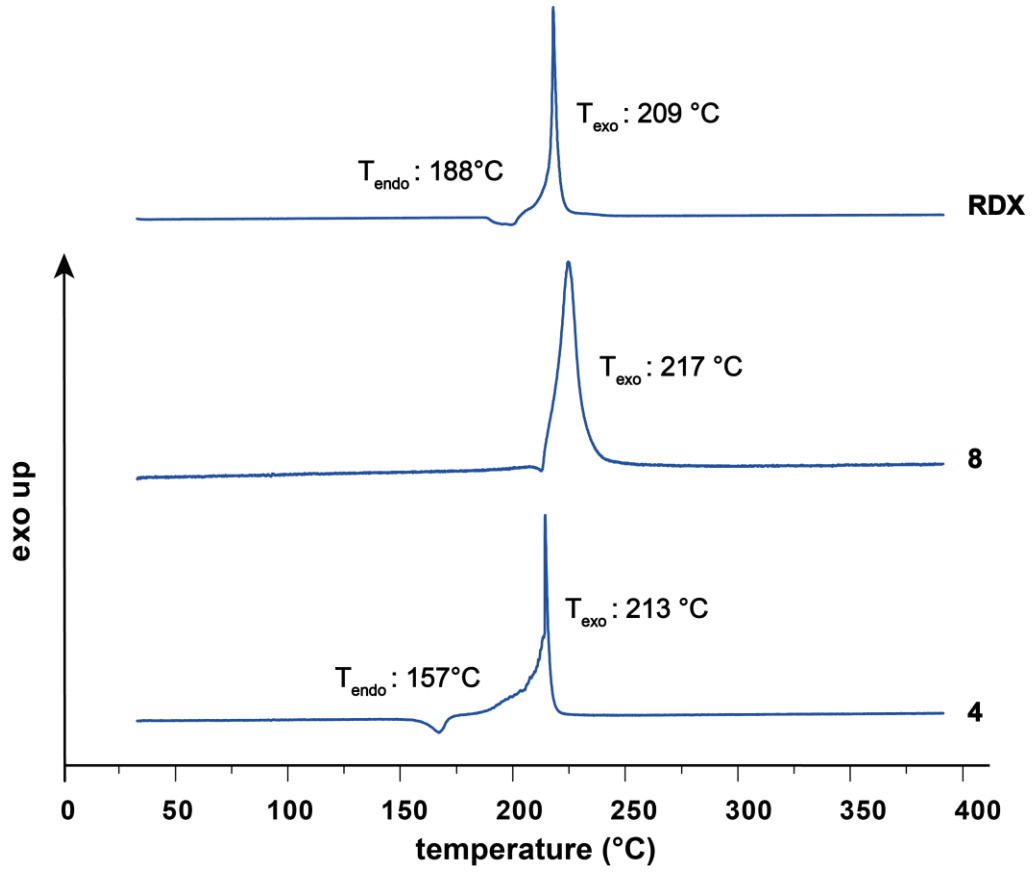

Figure 7. DTA measurements of **4** (bottom) and **8** (middle), as well as of RDX[43] for comparison, with a heating rate of 5°C min^{-1}.

Furthermore, all of the compounds which showed an endothermic signal in the DTA (**1**–**4** and **7**–**9**) were additionally examined using thermogravimetric analysis (TGA). The TGA measurements confirmed that all of the endothermic signals in the DTA measurements correspond to melting points. The TGA plots are shown in the Supporting information (Figures S37–S41).

Based on the thermal stability of the two ECCs (**12** and **13)**, it can be concluded that the decomposition temperature of the ligand can be significantly increased by coordination to the metals copper and iron.

9.2.5 Sensitivities and Energetic Properties

The sensitivities of all compounds **1** to **13** towards impact (IS) and friction (FS) were determined according to BAM standard methods[44-48] and all values are shown in Table 2.

It is notable that the *bis*-nitrotetrazolyl derivatives (**4**, **8**) are significantly more sensitive towards impact and friction than the *bis*-tetrazolyl derivatives (**1**–**3**, **5**–**7**). According to the UN Recommendations on the Transport of Dangerous Goods,[49] **4** and **8** are classified as being very sensitive towards impact. With respect to friction, **8** is classified as sensitive, and **4** even as very sensitive.

Comparing the sensitivities of the oxa-bridged compounds with those of the nitrazapropane-bridged compounds confirms the results in the literature [30]: **9** to **11** are clearly less sensitive than **1** to **3**. The sensitivities of the two ECCs (**12** and **13)** stand out showing very low values, both of which are in the range of primary explosives, with sensitivities towards impact being classified as very sensitive and towards friction as extremely sensitive.

Table 2. Sensitivities towards friction and impact of compounds **1**–**13** compared to that of RDX.[43]

	IS [J][a]	**FS [N][b]**
1	30	> 360
2	20	120
3	30	72
4	3	60
5	30	> 360
6	25	288
7	30	> 360
8	3	160
9	40	> 360
10	40	> 360
11	40	288
12	< 1	10
13	< 1	9
RDX[43]	8	120

[a] impact sensitivity according to the BAM drophammer (method 1 of 6); [b] friction sensitivity according to the BAM friction tester (method 1 of 6).

Furthermore, hot needle and hot plate tests were performed on **12** and **13** to investigate their possible application as primary explosives. Both the copper and iron complexes showed deflagration in both tests, as is shown in Figure 8.

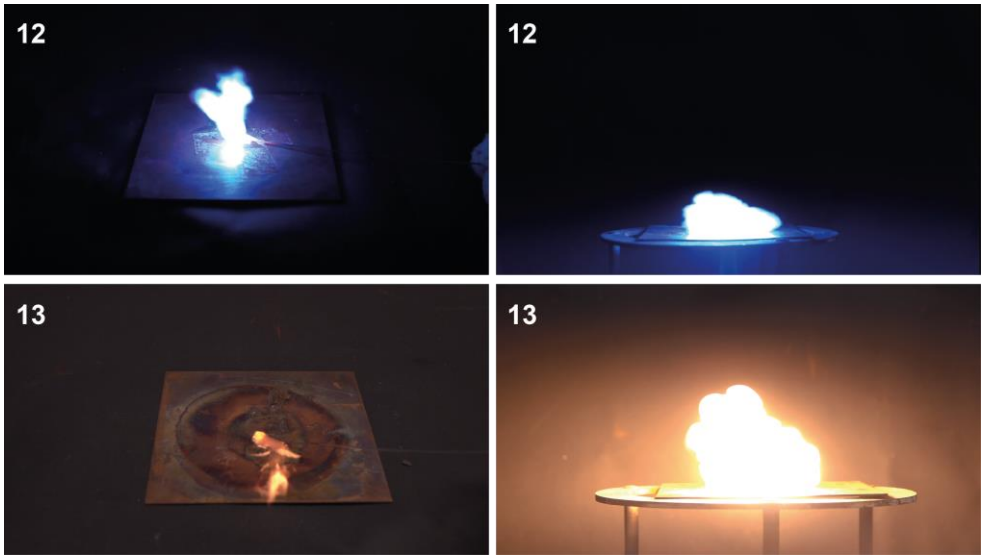

Figure 8. Hot needle (left) and hot plate (right) tests of the energetic coordination compounds (ECCs) **12** and **13**.

In addition, the energetic properties of compounds **1** to **11** were calculated using the EXPLO5 code version 6.06.01.[50] These values were calculated based on the density of the compounds, as well as on their enthalpy of formation which was calculated at the CBS-4M level. The results are shown in Table 3 and further details about the calculations can be found in the Supporting Information.

With a nitrogen plus oxygen content of over 70 percent in all compounds, they all look promising at first glance. However, when a closer look at the values is taken, the oxapropane-bridged compounds **9** to **11** show a noticeably lower density and heat of formation (HOF), and thus give significantly lower performanc parameters compared to the nitramine-bridged compounds **1** to **8**. It can be observed that the *bis*-nitrotetrazolyl derivatives **4** and **8** show higher HOFs compared to the corresponding *bis*-tetrazolyl derivatives. Due to the rather low densities of the latter (densities between 1.65 g cm^{-3} and 1.68 g cm^{-3}), this results in calculated detonation velocities for the nitrazapropane-bridged compounds **1** to **3** of between 8000 - 8200 m s^{-1}. In the case of the trinitrazaheptane bridged compounds, larger differences between the isomers can be seen. While the 1,1'-isomer **5** has a density of only 1.62 g cm^{-3}, the 2,2'-isomer **7** has a considerably higher density of 1.73 g cm^{-3}. Thus, for the trinitrazaheptane-bridged compounds, the best values are obtained for the 2,2'-isomer (**7)** which has a calculated detonation velocity of almost 8400 m s^{-1}. The compound which shows the highest HOF in this work is

the trinitrazaheptane bridged *bis*-nitrotetrazolate **8,** with a value of 725.8 kJ mol^{-1}. However, since 8 shows only a moderate density of 1.71 g cm^{-3}, a detonation velocity of 8377 m s^{-1} is obtained, which is somewhat lower compared to that of compound **7** which has been described previously. Overall, the best detonation parameters in this work were obtained for compound **4**. Due to its high density of 1.88 g cm^{-3} and good solid-state enthalpy of formation of 665.7 kJ mol^{-1}, an outstanding detonation velocity of 9231 m s^{-1} was predicted for **4**.

Table 3. Energetic properties of compounds **1** – **11** and RDX.[43]

	1	**2**	**3**	**4**	**5**	**6**
Formula	$C_4H_6N_{10}O_2$	$C_4H_6N_{10}O_2$	$C_4H_6N_{10}O_2$	$C_4H_4N_{12}O_6$	$C_6H_{10}N_{14}O_6$	$C_6H_{10}N_{14}O_6$
FW [g mol^{-1}]	226.07	226.07	226.07	316.04	374.24	374.24
$\rho_{calc.}$ (298 K) [g cm^{-3}]	1.68[a]	1.65[b]	1.66[a]	1.88[a]	1.62[b]	1.72[b]
N + O [%][d]	76.1	76.1	76.1	83.5	78.1	78.1
Ω_{CO2} [%][e]	–64	–64	–64	–20	–47	–47
$T_{dec.}$ [°C][f]	171	154	173	213	187	194
$\Delta_fH°(s/l)$ [kJ mol^{-1}][g]	638.7 (s)	634.9 (s)	625.7 (s)	665.7 (s)	684.2 (s)	680.1 (s)
EXPLO5 V6.06.01[44]						
P_{CJ} [GPa][h]	24.4	23.6	23.7	38.2	24.2	27.3
V_{det} [m s^{-1}][i]	8188	8027	8059	9231	7957	8368
$-\Delta_{ex}U°$ [kJ kg^{-1}][j]	4621	4596	4560	5692	5021	5055
T_{det} [K][k]	3178	3195	3168	4051	3503	3443
V_0 [dm^3 kg^{-1}][l]	804	806	805	762	822	810

	7	**8**	**9**	**10**	**11**	**RDX**[43,50]
Formula	$C_6H_{10}N_{14}O_6$	$C_6H_8N_{16}O_{10}$	$C_4H_6N_8O$	$C_4H_6N_8O$	$C_4H_6N_8O$	$C_3H_6N_6O_6$
FW [g mol^{-1}]	374.24	464.23	182.15	182.15	182.15	236.15
$\rho_{calc.}$ (298 K) [g cm^{-3}]	1.73[a]	1.71[b]	1.53[a]	1.50[c]	1.51[c]	1.80
N + O [%][d]	78.1	82.7	70.3	70.3	70.3	81.1
Ω_{CO2} [%][e]	–47	–21	–88	–88	–88	–22
$T_{dec.}$ [°C][f]	212	217	168	180	185	209
$\Delta_fH°(s/l)$ [kJ mol^{-1}][g]	665.1 (s)	725.8 (s)	446.8 (s)	442.7 (l)	439.5 (l)	70.3 (s)
EXPLO5 V6.06.01[44]						
P_{CJ} [GPa][h]	27.5	28.4	17.4	16.5	16.7	33.6
V_{det} [m s^{-1}][i]	8399	8377	7216	7068	7108	8794
$-\Delta_{ex}U°$ [kJ kg^{-1}][j]	5020	5224	3618	3595	3579	5717
T_{det} [K][k]	3418	3766	2582	2579	2567	3734
V_0 [dm^3 kg^{-1}][l]	809	795	789	791	790	784

[a] re-calculated from X-ray density; [b] determined by gas-pycnometer; [c] liquid at room temperature, therefore determined experimentally through the formula ρ=m/V; [d] Combined nitrogen and oxygen content; [e] oxygen balance assuming the formation of CO_2; [f] onset temperature of decomposition (at a heating rate of 5 °C min^{-1}); [g] calculated (CBS-4M) heat of formation; [h] detonation pressure; [i] detonation velocity; [j] energy of explosion; [k] explosion temperature; [l] volume of detonation gases at standard temperature and pressure condition.

It was also found that $[Fe(ClO_4)_2(1,1'\text{-TNP})_4]$ shows a thermochromic effect due to spin crossover, when cooled with liquid nitrogen. Therefore, magnetic properties of **13** were investigated and can be found in Figure S42 and S43 in the SI.

9.3 Conclusion

In this work, 11 new nitramine and oxa bridged energetic materials as well as two new energetic coordination compounds were synthesized and fully characterized. **1** to **11** can be prepared from the corresponding dichloro compounds by a one-step Finkelstein reaction. While the reaction to yield the corresponding *bis*-tetrazolyl compounds **1**–**3**, **5**–**7** and **9**–**11** always forms all three possible isomers, the reaction to yield the *bis*-nitrotetrazolyl compounds **4** and **8** only forms the preferred 2,2'-isomer.

Figure 8 shows the two best compounds of this work, 1,3-*bis*-2,2'-nitrotetrazolylnitrazapropane (**4**) and 1,7-*bis*-2,2'-tetrazolyltrinitrazaheptane (**7**), compared to the commonly used secondary explosive RDX. As described in the introduction, it is difficult to achieve the right balance between performance and stability when designing new energetic materials. Compound **4**, for example, shows a higher detonation velocity than RDX (**4**: V_{det} = 9231 m s^{-1} vs. RDX: V_{det} = 8794 m s^{-1}) with comparable thermal stability (**4**: T_{dec} = 213°C vs. RDX: T_{dec} = 209°C) as can be seen in Figure 9. However, **4** is more sensitive towards impact and friction than RDX. Compound **7**, on the other hand, has a lower sensitivity compared to RDX and is therefore safer to handle, but has a 400 m s^{-1} lower detonation velocity compared to RDX due to its lower density.

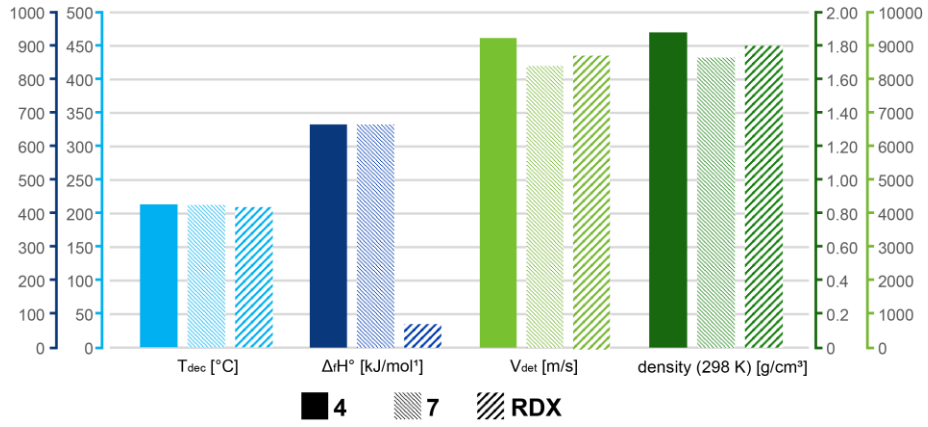

Figure 9. Bar chart comparing important properties of compounds **4** and **7** with RDX.

Nevertheless, both compounds show promising properties and are of interest as replacements for RDX, especially due to their easy synthesis.
Furthermore, 1,3-*bis*-1,1'-tetrazolylnitrazapropane (**1**) was used as ligand in energetic coordination compounds (ECCs) to investigate its possible application in detonators. Both the sensitivities and thermal stabilities of **12** and **13** are in a good range. However, the hot needle and hot plate tests showed that the compounds deflagrate and do not detonate, which makes their use as ignition agents more promising.

9.4 Acknowledgements

For financial support of this work the Ludwig Maximilian University (LMU), EMTO GmbH, the Office of Naval Research (ONR) under grant no. ONR N00014-19-1-2078 and the Strategic Environmental Research and Development Program (SERDP) under contract no. W912HQ19C0033 are gratefully acknowledged.

9.5 References

[1] T. M. Klapötke, *Chemistry of High-Energy Materials*. 6th ed., de Gruyter, Berlin/Boston **2022**.
[2] Agrawal, J. P.; Hodgson, R. D. *Organic Chemistry of Explosives*. 1st ed., Wiley-VCH, Weinheim **2007**.
[3] A. A. Larin, D. D. Degtyarev, I. V. Ananyev, A. N. Pivkina, L. L. Fershtat *Chem. Eng*. *J.* **2023**, *470*, 144144.
[4] A. G. Harter, T. M. Klapötke, J. T. Lechner, J. Stierstorfer, *Propellants, Explos., Pyrotech.* **2022**, *47*, e202200031.
[5] J. A. Bumpus, *Adv. Phys. Chem.* **2012**, 175146–175153.
[6] Z. Xu, T. Hou, F. Yang, L. Zhang, X. Zhang, W. Liu, Q. Lang, M. Lu, Y. Xu, *ACS Appl. Mater. Interfaces* **2023**, https://doi.org/10.1021/acsami.3c09652.
[7] M. Benz, T. M. Klapötke, J. Stierstorfer, M. Voggenreiter, *J. Am. Chem. Soc.* **2022**, *14*, 6143–6147
[8] Y. Qu, S. P. Babailov, *J. Mater. Chem. A*, **2018**, *6*, 1915-1940.

[9] S. Manzoor, Q. Tariq, X. Yin, J.-G. Zhang, *Def. Technol.* **2021**, *17*, 1995–2010.

[10] D. Kumar, Y. Tang, C. He, G. H. Imler, D. A. Parrish, J. M. Shreeve, *Chem. Eur. J.* **2018**, *24*, 17220–17224.

[11] S. Gayathri, S. Reshmi, *Polym. Adv. Technol.* **2017**, *28*, 1539–1550.

[12] Y. Wang, L. Hu, S. Pang, J. M. Shreeve, *J. Mater. Chem. A* **2023**, *11*, 13876–13888.

[13] H. Huamg, Y. Li, J. Yang, R. Pan, X. Lin, *New J. Chem.* **2017**, *41*, 7697–7704.

[14] M. Benz, T. M. Klapötke, J. Stierstorfer, *ChemPlusChem* **2022**, *87*, e202200186.

[15] C. Lei, H. Yang, Q. Zhang, G. Cheng, *Cryst. Growth Des.* **2022**, *22*, 2594–2601.

[16] F. Chen, S. Song, K. Wang, Y. Wang, Q. Zhang, *J. Chem. Eng*. **2022**, *435*, 135053.

[17] C. Lei, H. Yang, G. Cheng, *Dalton Trans.* **2020**, *49*, 1660–1667.

[18] S. Seth, C. Pathak, *Cryst. Growth Des.* **2023**, *23*, 4669–4679.

[19] J. Tang, H. Xiong, Y. Tang, H. Yang, G. Cheng, Dalton Trans. **2023**, *52*, 3169–3175.

[20] T. Wang, H. Gao, J. M. Shreeve, *Z. Anorg. Allg. Chem.* **2021**, *647*, 157–191.

[21] N. Fischer, D. Fischer, T. M. Klapötke, D. G. Piercy, J. Stierstorfer, *J. Mater. Chem.* **2012**, *22*, 20418–20422.

[22] J. W. Fronabarger, M.D. Williams, W. B. Sanborn, J. G. Bragg, D. A. Parrish, M., Bichay, *Propellants, Explos., Pyrotech.* **2011**, *36*, 541–550.

[23] F. Majiet, F. J. Mostert, *Def. Technol.* **2019**, *15*, 802–807.

[24] Y. Liu, J. Yin, Z. Wang, X. Zhang, G. Bi, *Materials* **2020**, *13*, 4519–4530.

[25] G. Jaiswal, M. A. R. Shaikh, S. D. Shelar, V. Ramavath, S. Roy, *Propellants, Explos., Pyrotech.* **2020**, *45*, 472–479.

[26] J. Sabatini, E. C. Johnson, A*CS Omega* **2021**, *6*, 11813–11821.

[27] K. A. Fredriksen, T. E.Kristensen, *Propellants, Explos., Pyrotech.* **2023**, *48*, e202200321.

[28] P. Yin, D. A. Parrish, J. M. Shreeve, *Angew. Chem. Int. Ed.* **2014**, *53*, 12889–12892.

[29] J. Zhang, S. Dharavath, L. A. Mitchell, D. A. Parrish, J. M. Shreeve*, J. Mater. Chem. A* **2016**, *4*, 16961–16967.

[30] A. G. Harter, T. M. Klapötke, B. Krumm, J. T. Lechner, C. Riedelsheimer, *Eur. J. Org. Chem.* **2023**, *26*, e202300302.

[31] S. Feng, F.-S. Li, X.-Y. Zhao, Y.-D. Qian, T. Fei, P. Yin, S.-P. Pang, *Energetic Materials Frontiers*, **2021**, *2*, 125–130.

[32] A. A. Larin, A. V. Shaferov, A. S. Kulikov, A. N. Pivkina, K. A. Monogarov, A. O. Dmitrienko, I. V. Ananyev, D. V. Khakimov, L. L. Fershtat, N. N. Makhova, *Chem. Eur. J.* **2021**, *27*, 14628–14637.

[33] T. M. Klapötke, B. Krumm, F. X. Steemann, *Prop., Explos., Pyrotech.* **2009**, *34*, 13–23.

[34] T. M. Klapötke, A. Penger, C. Pflüger, J. Stierstorfer, M. Suceska, *Eur. J. Inorg. Chem.* **2013**, *2013*, 4667–4678.

[35] T. K. Highsmith, J. M. Hanks, S. P. Velarde, J. C. Bottaro (Alliant Techsystems Inc.), WO2002060881, **2002.**

[36] O. P. Shitov, V. L. Korolev, V. A. Tartakovsky, *Russ. Chem. Bull. Int. Ed*. **2009**, *58*, 2347–2355.

[37] J. Zhang, C. He, D. A. Parrish, J. M. Shreeve, *Chem. Eur. J.* **2013**, *19*, 8929–8936.

[38] N. Szimhardt, M. H. H. Wurzenberger, T. M. Klapötke, J. T. Lechner, H. Reichherzer, C. C. Unger, J. Stierstorfer*, J. Mater. Chem. A* **2018**, *6*, 6565–6577.

[39] T. V. Golobokova, F. A. Pokatilov, A. G. Proidakov, L. I. Vereshchagin, V. N. Kizhnyaev, *Russ. J. Org. Chem*., **2013**, *49*, 130–137.

[40] H. Finkelstein, *Chem. Ber.* **1910**, *43*, 1528–1532.

[41] A. Streitwieser, *Chem. Rev.* **1956**, 56, 571–752.

[42] F. G. Bordwell, W. T. Brannen, *J. Am. Chem. Soc.* **1964**, *86*, 4645–4650.

[43] T. M. Klapötke, *Energetic Materials Encyclopedia* ,2nd ed., de Gruyter, Berlin/Boston, **2021**.

[44] NATO standardization agreement (STANAG) on explosives, impact sensitivity tests, no. 4489, 1st ed, Sept. 17, **1999**.

[45] WIWEB-Standardarbeitsanweisung 4-5.1.02, Ermittlung der Explosionsgefährlichkeit, hier der Schlagempfindlichkeit mit dem Fallhammer. Nov. 8, **2002**.

[46] "http://www.bam.de", accessed March **2022**.

[47] NATO standardization agreement (STANAG) on explosive, friction sensitivity tests. no. 4487, 1st ed., Aug. 22, **2002**.

[48] WIWEB-Standardarbeitsanweisung 4-5.1.03, Ermittlung der Explosionsgefährlichkeit oder der Reibeempfindlichkeit mit dem Reibeapparat. Nov. 8, **2002**.

[49] Impact: insensitive > 40 J, less sensitive ≥ 35 J, sensitive ≥ 4 J, very sensitive ≤ 3 J; Friction: insensitive > 360 N, less sensitive = 360 N, sensitive < 360 N and > 80 N, very sensitive ≤ 80 N, extremely sensitive ≤ 10 N. According to the UN Recommendations on the Transport of Dangerous Goods, (+) indicates not safe for transport.

[50] M. Sućeska, *Explo5 V6.06.01*, Zagreb (Croatia), **2021**.

[51] CrysAlisPro, Oxford Diffraction Ltd., version 171.33.41, **2009**.

[52] A. Altomare, G. Cascarano, C. Giacovazzo, A. Guagliardi, *J. Appl. Crystallogr.* **1993**, *26*, 343−350.

[53] a) A. Altomare, G. Cascarano, C. Giacovazzo, A. Guagliardi, A. G. G. Moliterni, SIR97 **1997**; b) A. Altomare, M. C. Burla, M. Camalli, G. L. Cascarano, C. Giacovazzo, A., *J. Appl. Crystallogr*. **1999**, *32*, 115−119.

[54] G. M. Sheldrick, *Acta Crystallogr. Sect. A* **2008**, *A64*, 112−122.

[55] G. M. Sheldrick, SHELXL-97, Program for the Refinement of Crystal, University of Göttingen, Germany, **1997**.

[56] A. L. Spek, PLATON, A Multipurpose Crystallographic Tool, Utrecht University **1999**.

[57] L. J. Farrugia, *J. Appl. Cryst.* **2012**, *45*, 849−854.

[58] a) Empirical absorption correction using spherical harmonics, implemented in SCALE3 ABSPACK scaling algorithm (CrysAlisPro Oxford Diffraction Ltd., Version 171.33.41, 2009); b) APEX3. Bruker AXS Inc., Madison, Wisconsin, USA.

[59] M. J. Frisch, G. W. Trucks, H. B. Schlegel, G. E. Scuseria, M. A. Robb, J. R. Cheeseman, G. Scalmani, V. Barone, B. Mennucci, G. A. Petersson, H. Nakatsuji, M. Caricato, X. Li, H.P. Hratchian, A. F. Izmaylov, J. Bloino, G. Zheng, J. L. Sonnenberg, M. Hada, M. Ehara, K. Toyota, R. Fukuda, J. Hasegawa, M. Ishida, T. Nakajima, Y. Honda, O. Kitao, H. Nakai, T. Vreven, J. A. Montgomery, Jr., J. E. Peralta, F. Ogliaro, M. Bearpark, J. J. Heyd, E. Brothers, K. N. Kudin, V. N. Staroverov, R. Kobayashi, J. Normand, K. Raghavachari, A. Rendell, J. C. Burant, S. S. Iyengar, J. Tomasi, M. Cossi, N. Rega, J. M. Millam, M. Klene, J. E.

Knox, J. B. Cross, V. Bakken, C. Adamo, J. Jaramillo, R. Gomperts, R. E. Stratmann, O. Yazyev, A. J. Austin, R. Cammi, C. Pomelli, J. W. Ochterski, R. L. Martin, K. Morokuma, V. G. Zakrzewski, G. A. Voth, P. Salvador, J. J. Dannenberg, S. Dapprich, A. D. Daniels, O. Farkas, J.B. Foresman, J. V. Ortiz, J. Cioslowski, D. J. Fox, Gaussian 09 A.02, Gaussian, Inc., Wallingford, CT, USA, **2009**.

[60] a) J. W. Ochterski, G. A. Petersson, and J. A. Montgomery Jr., *J. Chem. Phys.* **1996**, *104*, 2598−2619; b) J. A. Montgomery Jr., M. J. Frisch, J. W. Ochterski G. A. Petersson, *J. Chem. Phys.* **2000**, *112*, 6532−6542; c) L. A. Curtiss, K. Raghavachari, P. C. Redfern, J. A. Pople, *J. Chem. Phys.* **1997**, *106*, 1063−1079; d) E. F. C. Byrd, B. M. Rice, *J. Phys. Chem. A* **2006**, *110*, 1005–1013; e) B. M. Rice, S. V. Pai, J. Hare, *Comb. Flame* **1999**, *118*, 445–458.

[61] F. Trouton, *Philos. Mag.* (1876-1900) **1884**, *18*, 54-57; b) M. S. Westwell, M. S. Searle, D. J. Wales, D. H. Willimas, *J. Am. Chem. Soc.* **1995**, *117*, 5013-5015.

[62] M. Sućeska, *Propellants, Explos., Pyrotech.* **1991**, *16*, 197–202.

9.6 Supporting Information

9.6.1 Experimental Information

All chemicals and solvents were employed as received (Sigma-Aldrich, Fluka, Acros, ABCR). ^{1}H, $^{13}C\{^{1}H\}$, ^{14}N, and ^{15}N NMR spectra were recorded at ambient temperature using a Bruker TR 400 instrument and are referenced with respect to Me_4Si ($^{1}H/^{13}C$), $MeNO_2$ ($^{14}N/^{15}N$). Melting and decomposition temperatures of the described compounds were measured through differential thermal analysis (DTA) with an OZM Research DTA 552-Ex instrument. The samples were measured in a range of 25–400 °C at a heating rate of 5°C min^{-1}. Selected compounds were also investigated using thermal gravimetric analysis (TGA) with a PerkinElmer TGA4000. Infrared spectra were measured on pure samples using a Perkin-Elmer BXII FT-IR system with a Smith DuraSampler IR II diamond ATR. Determination of the carbon, hydrogen, and nitrogen contents was carried out by combustion analysis using an Elementar Vario El (nitrogen values determined are often lower than the calculated due to their explosive behavior). Impact sensitivity tests were carried out according to STANAG 4489[1] modified instruction[2] using a BAM (Bundesanstalt für Materialforschung) drophammer.[3] Friction sensitivity tests were carried out according to STANAG 4487[4] modified instruction[5] using the BAM friction tester. The classification of the tested compounds results from the “UN Recommendations on the Transport of Dangerous Goods”.[6]

Nitrazapropane-bridged tetrazoles (1–3)

1,3-Dichloro-2-nitrazapropane (1.00 g, 6.29 mmol, 1.0 eq) was dissolved in acetone (80 mL). Potassium tetrazolate (1.36 g, 12.58 mmol, 2.0 eq) and sodium iodide (1.89 g, 12.58 mmol, 2.0 eq) were added and the reaction was stirred for 12 h at 25°C. The suspension was filtered and the filtrate was evaporated *in vacuo*. The residue was extracted with ethyl acetate (100 mL) and washed with water (3 x 100 mL). The organic phase was dried over magnesium sulfate. The dried solution was filtered and the filtrate was concentrated. The crude product was purified by column chromatography on silica gel (80/20 → 90/10 ethyl acetate/isohexane) to yield **1** (226 mg, 16%), **2** (509 mg, 36%), **3** (124 mg, 9%) as off-white/yellowish solids.

1,3-*Bis*-1,1'-tetrazolylnitrazapropane (1)

TLC (90/10 ethyl acetate/isohexane): R_f = 0.24.

^{1}H NMR (400 MHz, acetone-D_6, ppm): δ = 9.39 (s, 1H), 6.85 (s, 2H); ^{13}C{^{1}H} NMR (101 MHz, acetone-D_6, ppm): δ = 145.1, 61.3; ^{14}N NMR (29 MHz, acetone-D_6, ppm): δ = −37, −152; IR (ATR, cm^{-1}): 3127 (m), 3109 (m), 3054 (w), 3027 (w), 2989 (w), 2922 (w), 2853 (vw), 2168 (vw), 1812 (vw), 1765 (vw), 1748 (vw), 1704 (vw), 1572 (s), 1478 (m), 1446 (m), 1434 (m), 1418 (m), 1389 (w), 1354 (m), 1340 (m), 1320 (w), 1283 (vs), 1261 (m), 1261 (m), 1248 (m), 1208 (m), 1170 (s), 1152 (s), 1116 (m), 1104 (s), 1085 (s), 1042 (w), 1015 (m), 969 (m), 951 (m), 937 (s), 906 (m), 885 (m), 767 (s), 727 (m), 717 (m), 661 (vs), 634 (s), 569 (w), 550 (w), 530 (w), 453 (m), 439 (m); elemental analysis calcd. (%) for $C_4H_6N_{10}O_2$ (226.07 g mol^{-1}): C 21.24, H 2.67, N 61.93; found: C 21.64, H 2.89, N 61.36; DTA (5°C min^{-1}): onset: 166.7 °C (endo.), 170.5°C (dec.); BAM drophammer: 30 J; Friction tester: >360 N.

1,3-*Bis*-1,2-tetrazolylnitrazapropane (2)

TLC (90/10 ethyl acetate/isohexane): R_f = 0.44.

^{1}H NMR (400 MHz, acetone-D_6, ppm): δ = 9.39 (s, 1H), 8.82 (s, 1H), 7.01 (s, 2H), 6.88 (s, 2H); ^{13}C{^{1}H} NMR (101 MHz, acetone-D_6, ppm): δ = 154.3, 145.0, 65.3, 61.2; ^{14}N NMR (29 MHz, acetone-D_6, ppm): δ = −37, −98, −149; IR (ATR, cm^{-1}): 3151 (w), 3122 (w), 3049 (w), 3033 (w), 2986 (w), 2847 (vw), 1818 (vw), 1717 (vw), 1566 (s), 1476 (m), 1444 (s), 1415 (m), 1374 (w), 1357 (w), 1327 (m), 1279 (vs), 1232 (m), 1189 (m), 1173 (s), 1163 (s), 1146 (m), 1121 (m), 1100 (s), 1089 (s), 1070 (s), 1033 (m), 1020 (s), 1000 (w), 963 (s), 93 (s), 900 (s), 892 (m), 869 (w), 761 (vs), 741 (m), 717 (m), 704 (m), 678 (s), 665 (s), 645 (s), 632 (s), 550 (w), 502 (vw), 451 (m), 436 (w); elemental analysis calcd. (%) for $C_4H_6N_{10}O_2$ (226.07 g mol^{-1}): C 21.24, H 2.67, N 61.93; found: C 22.40, H 3.01, N 60.28; DTA (5°C min^{-1}): onset: 98.6 °C (endo.), 154.3 °C/162.1°C (exo.); BAM drophammer: 20 J; Friction tester: 120 N.

1,3-*Bis*-2,2'-tetrazolylnitrazapropane (3)

TLC (90/10 ethyl acetate/isohexane): R_f = 0.77.

^{1}H NMR (400 MHz, acetone-D_6, ppm): δ = 8.78 (s, 1H), 7.04 (s, 2H); ^{13}C{^{1}H} NMR (101 MHz, acetone-D_6, ppm): δ = 154.3, 65.0; ^{14}N NMR (29 MHz, acetone-D_6,

ppm): δ = −39, −99; IR (ATR, cm^{-1}): 3147 (w), 3055 (w), 3041 (w), 3003 (w), 2994 (w), 2920 (vw), 2852 (vw), 2168 (vw), 2005 (vw), 1808 (vw), 1719 (vw), 1574 (s), 1458 (w), 1437 (s), 1421 (m), 1400 (w), 1367 (m), 1339 (m), 1327 (m), 1272 (vs), 1237 (m), 1193 (m), 1181 (s), 1181 (s), 1144 (m), 1130 (m), 1081 (s), 1022 (s), 1008 (s), 953 (m), 932 (vs), 903 (s), 879 (w), 765. (vs), 741 (m), 705 (s), 680 (m), 673 (m), 651 (s), 620 (s), 550 (w), 448 (m); elemental analysis calcd. (%) for $C_4H_6N_{10}O_2$ (226.07 g mol^{-1}): C 21.24, H 2.67, N 61.93; found: C 21.57, H 2.76, N 61.12; DTA (5°C min^{-1}): onset: 71.6°C (endo.), 173.1°C (dec.); BAM drophammer: 30 J; Friction tester: 80 N.

1,3-*Bis*-2,2'-nitrotetrazolylnitrazapropane (4)

1,2-Dichloro-2-nitrazapropane (1.0 g, 6.29 mmol, 1.0 eq) was dissolved in acetone (80 mL). Ammonium-5-nitrotetrazolate hemihydrate (1.78 g, 12.58 mmol, 2.0 eq) and sodium iodide (1.89 g, 12.58 mmol, 2.0 eq) were added and the reaction was stirred for 12 h at 25°C. The suspension was filtered and the filtrate was evaporated *in vacuo*. The residue was extracted with ethyl acetate (100 mL) and washed with water (1 x 100 mL). The organic phase was dried over magnesium sulfate. The dried solution was filtered and the filtrate was concentrated. The crude product was purified by flash column chromatography on silica gel (50/50 ethyl acetate/isohexane) to obtain **4** (1.87 g, 95%) as a yellowish solid.
TLC (50/50 ethyl acetate/isohexane): R_f = 0.39.

^{1}H NMR (400 MHz, acetone-D_6, ppm):δ = 7.30 (s, 1H); $^{13}C\{^{1}H\}$ NMR (101 MHz, acetone-D_6, ppm): δ = 66.8; ^{15}N NMR (41 MHz, acetone-D_6, ppm): δ = 8.6, −35.1, −41.4, −54.9, −78.8, −95.0, −199.8; IR (ATR, cm^{-1}): 3148 (vw), 3067 (w), 3054 (w), 3047 (w), 2992 (w), 2925 (vw), 2877 (vw), 2736 (vw), 2168 (vw), 1729 (w), 1589 (s), 1566 (vs), 1492 (m), 1479 (m), 1439 (m), 1424 (m), 1413 (m), 1400 (m), 1369 (w), 1350 (w), 1326 (s), 1276 (vs), 1250 (s), 1250 (s), 1209 (m), 1197 (m), 1181 (w), 1139 (w), 1130 (w), 1085 (m), 1073 (w), 1058 (m), 1019 (m), 1009 (w), 948 (m), 925 (s), 904 (w), 881 (vw), 843 (m), 779 (m), 769 (s), 755 (s), 741 (m), 705 (w), 687 (m), 663 (m), 645 (m), 628 (s), 548 (w), 542 (w), 474 (w), 450 (m), 423 (w); elemental analysis calcd. (%) for $C_4H_4N_{12}O_6$ (316.04 g mol^{-1}): C 15.20, H 1.28, N 53.17; found: C 16.75, H 1.77, N 51.17; DTA (5°C min^{-1}): onset: 157.2°C (endo.), 212.6°C (dec.); BAM drophammer: 3 J; Friction tester: 60 N.

Trinitrazapropane-bridged tetrazoles (5–7)

1,7-Dichloro-2,4,6-trinitrazaheptane (1.0 g, 3.26 mmol, 1.0 eq) was dissolved in acetone (80 mL). Potassium tetrazolate (705 mg, 6.25 mmol, 2.0 eq) and sodium iodide (977 mg, 6.25 mmol, 2.0 eq) were added and the reaction was stirred for 12 h at 25°C. The suspension was filtered and the filtrate was evaporated *in vacuo*. The yellowish solid was washed with water and ethanol. The crude product was purified by column chromatography on silica gel (50/50 → 70/30 ethyl acetate/isohexane) to obtain **5** (223 mg, 19%), **6** (315 mg, 26%) and **7** (200 mg, 17%) as off-white/yellowish solids.

1,7-Bis-1,1'-tetrazolyltrinitrazaheptane (5)

TLC (70/30 ethyl acetate/isohexane): R_f = 0.39.

^{1}H NMR (400 MHz, acetone-D_6, ppm): δ = 9.32 (s, 1H), 6.72 (s, 2H), 6.22 (s, 2H); ^{13}C{^{1}H}NMR (101 MHz, acetone-D_6, ppm): δ = 145.0, 66.2, 61.7; ^{14}N NMR (29 MHz, acetone-D_6, ppm): δ −35; IR (ATR, cm^{-1}): 3146 (w), 3044 (w), 2995 (vw), 2926 (w), 2854 (vw), 1741 (vw), 1591 (m), 1571 (s), 1543 (s), 1467 (w), 1435 (s), 1414 (m), 1370 (w), 1353 (w), 1327 (w), 1269 (vs), 1229 (m), 1211 (s), 1190 (m), 1154 (s), 1121 (m), 1094 (s), 1073 (s), 1073 (s), 1021 (m), 966 (m), 928 (vs), 892 (m), 876 (m), 856 (m), 763 (s), 755 (s), 716 (m), 708 (m), 700 (m), 679 (w), 659 (m), 640 (m), 610 (s), 532 (vw), 479 (w), 447 (w); elemental analysis calcd. (%) for $C_6H_{10}N_{14}O_6$ (374.24 g mol^{-1}): C 19.26, H 2.69, N 52.40; found: C 19.41, H 2.88, N 52.67; DTA (5°C min^{-1}): onset: 187.0°C (dec.); BAM drophammer: 40 J; Friction tester: >360 N.

1,7-*Bis*-1,2-tetrazolyltrinitrazaheptane (6)

TLC (70/30 ethyl acetate/isohexane): R_f = 0.61.

^{1}H NMR (400 MHz, acetone-D_6, ppm): δ = 9.32 (s, 1H), 8.82 (s, 1H), 6.89 (s, 2H), 6.73 (s, 2H), 6.26 (d, 4H); ^{13}C{^{1}H} NMR (101 MHz, acetone-D_6, ppm): δ = 154.2, 145.0, 66.2, 65.9, 65.7, 61.8; ^{14}N NMR (29 MHz, acetone-D_6, ppm): δ = −34; IR (ATR, cm^{-1}): 3147 (w), 3044 (w), 2994 (vw), 2925 (w), 2854 (vw), 2168 (vw), 1790 (vw), 1729 (vw), 1590 (m), 1571 (s), 1541 (m), 1468 (w), 1436 (s), 1412 (m), 1370 (w), 1342 (w), 1270 (vs), 1212 (s), 1190 (m), 1153 (m), 1118 (m), 1103 (m), 1094 (s), 1094 (s), 1073 (s), 1063 (m), 1020 (m), 1001 (w), 966 (m), 927 (vs), 906 (m), 892 (m), 877 (m), 855 (m), 763 (s), 755 (s), 717 (w), 708 (m), 700 (m), 678 (m),

660 (m), 641 (m), 634 (m), 609 (s), 480 (w), 447 (w); elemental analysis calcd. (%) for $C_6H_{10}N_{14}O_6$ (374.24 g mol^{-1}): C 19.26, H 2.69, N 52.40; found: C 19.92, H 2.87, N 52.12; DTA (5°C min^{-1}): onset: 194.2°C (dec.); BAM drophammer: 25 J; Friction tester: 288 N.

1,7-*Bis*-2,2'-tetrazolyltrinitrazaheptane (7)

TLC (70/30 ethyl acetate/isohexane): R_f = 0.78.

^{1}H NMR (400 MHz, acetone-D_6, ppm): δ = 8.83 (s 1H), 6.89 (s, 2H), 6.29 (s, 2H); ^{13}C{^{1}H} NMR (101 MHz, acetone-D_6, ppm): δ = 154.2, 65.9, 65.7; ^{14}N NMR (29 MHz, acetone-D_6, ppm): δ = −35; IR (ATR, cm^{-1}): 3156 (vw), 3149 (vw), 3067 (w), 3016 (vw), 2213 (vw), 2174 (vw), 2168 (vw), 1732 (w), 1574 (m), 1557 (s), 1539 (s), 1463 (w), 1452 (w), 1436 (m), 1427 (m), 1412 (m), 1404 (m), 1394 (m), 1380 (w), 1368 (w), 1354 (w), 1337 (w), 1274 (vs), 1274 (vs), 1247 (m), 1232 (s), 1194 (m), 1185 (m), 1152 (m), 1122 (w), 1099 (s), 1072 (m), 1021 (m), 1005 (m), 921(vs), 888 (m), 880 (m), 868 (m), 854 (m), 769 (s), 758 (s), 706 (m), 693 (w), 683 (m), 676 (m), 659 (w), 643 (m), 638 (m), 629 (w), 603 (s), 540 (vw), 503 (vw), 486 (w), 449 (m), 429 (vw), 424 (vw), 415 (w), 403 (vw); elemental analysis calcd. (%) for ($C_6H_{10}N_{14}O_6$ (374.24 g mol^{-1}): C 19.26, H 2.69, N 52.40; found: C 20.18, H 2.83, N 51.57; DTA (5 °C min^{-1}): onset: 193.1°C (endo.), 211.5°C (dec.); BAM drophammer: 30 J; Friction tester: 360 N.

1,7-*Bis*-2,2'-nitrotetrazolyltrinitrazaheptane (8)

1,7-Dichloro-2,4,6-trinitrazaheptane (1.0 g, 3.26 mmol, 1.0 eq) was dissolved in acetone (80 mL). Ammonium-5-nitrotetrazolate hemihydrate (920 mg, 6.25 mmol, 2.0 eq) and sodium iodide (977 mg, 6.25 mmol, 2.0 eq) were added and the reaction was stirred overnight at room temperature. The suspension was filtered and the filtrate was evaporated *in vacuo*. The residue was extracted with ethyl acetate (100 mL) and washed with water (1 x 100 mL). The organic phase was dried over magnesium sulfate. The dried solution was filtered and the filtrate was concentrated. The crude product was purified by column chromatography on silica gel (40/60 → 50/50 ethyl acetate/isohexane) to obtain **8** (1.32 g, 87%) as a white solid.

TLC (50/50 ethyl acetate/isohexane): R_f = 0.63.

^{1}H NMR (400 MHz, acetone-D_6, ppm): δ = 7.08 (s, 1H), 6.30 (s, 1H); ^{13}C{^{1}H} NMR (101 MHz, acetone-D_6, ppm): δ = 67.4, 65.9; ^{15}N NMR (41 MHz, acetone-D_6, ppm): δ = 4.5, −34.1, −34.8, −36.8, −51.4, −72.0, −93.9, −186.7, −195.1; IR (ATR, cm^{-1}): 3048.00 (vw), 3005.00 (vw), 2962.00 (vw), 2927.00 (vw), 2865.00 (vw), 2168.00 (vw), 1728 (w), 1563 (s), 1558 (vs), 1504 (vw), 1488 (w), 1455 (w), 1439 (m), 1436 (m), 1409 (m), 1385 (w), 1373 (w), 1315 (m), 1276 (vs), 1243 (m), 1231 (m), 1211 (w), 1195 (m), 1195 (m), 1154 (w), 1109 (m), 1078 (m), 1059 (m), 1018 (w), 925 (s), 875 (w), 837 (s), 764 (s), 703 (w), 692 (w), 664 (w), 644 (m), 610 (s), 542 (w), 502 (vw), 478 (w), 466 (w), 446 (w), 427 (vw); elemental analysis calcd. (%) for $C_6H_8N_{16}O_{10}$ (464.23 g mol^{-1}): C 15.52, H 1.74, N 48.28; found: C 19.78, H 2.38, N 43.82; DTA (5°C min^{-1}): onset: 210.3°C (endo.), 217.1°C (dec.); BAM drophammer: 3 J; Friction tester: 160 N.

Oxapropane-bridged tetrazoles (9–11)

Sodium iodide (2.61 g, 17.4 mmol, 2.0 eq) and potassium tetrazolate (1.88 g, 17.4 mmol, 2.0 eq) were added to 1,3-dichloro-2-oxapropane (1.0 g, 8.70 mmol, 1.0 eq) in acetone (80 mL). The suspension was stirred for 12 h at 25°C with the exclusion of light. The resulting precipitate was filtered and the filtrate was concentrated *in vacuo*. The crude product was dissolved in ethyl acetate (50 mL) and washed with saturated sodium thiosulfate solution (3 x 50 mL). The organic phase was dried over $MgSO_4$, and filtered afterwards. The solvent was removed under reduced pressure and the crude product was purified by column chromatography ($CHCl_3$: MeOH, 9:1) to separate the different isomers. Compounds **10** (180 mg, 11 %) and **11** (620 mg, 39 %) were obtained as colorless liquids and **9** was obtained as a colorless solid (0.45 g, 28 %).

1,3-*Bis*-1,1'-tetrazolyloxapropane (9)

^{1}H NMR (400 MHz, acetone-D_6, ppm) δ = 9.37 (s, 2H), 6.19 (s, 4H); ^{13}C{^{1}H} NMR (101 MHz, acetone-D_6, ppm) δ = 144.9, 75.7; IR (ATR, cm^{-1}): 3122 (w), 3101 (m), 1484 (m), 1451 (w), 1429 (m), 1373 (m), 1319 (w), 1300 (w), 1281 (w), 1224 (w), 1199 (m), 1178 (s), 1171 (s), 1117 (m), 1106 (m), 1083 (vs), 1054 (m), 1028 (m), 1008 (m), 983 (s), 962 (s), 931 (s), 888 (m), 753 (vs), 715 (s), 652 (vs), 480 (w); elemental analysis calcd. (%) for $C_4H_6N_8O$ (182.15 g mol^{-1}): C 21.24, H 2.67, N

61.93; found: C 22.64, H 2.89, N 60.06; DTA (5°C min^{-1}): onset: 97.5°C (endo.), 168.0°C (dec.); BAM drophammer: 40 J; Friction tester: >360 N.

1,3-*Bis*-1,2-tetrazolyloxapropane (10)

^{1}H NMR (400 MHz, acetone-D_6, ppm) δ = 9.35 (s, 1H), 8.84 (s, 1H), 6.31 (s, 2H,), 6.21 (s, 2H); $^{13}C\{^{1}H\}$ NMR (101 MHz, acetone-D_6, ppm) δ = 154.4, 144.88, 79.6, 76.0; IR (ATR, cm^{-1}): 3140 (w), 1483 (m), 1457 (w), 1428 (w), 1385 (w), 1338 (m), 1312 (w), 1283 (m), 1203 (w), 1166 (s), 1112 (s), 1085 (vs), 1049 (m), 1023 (s), 1002 (s), 953 (m), 934 (m), 886 (m), 766 (s), 755 (s), 715 (w), 707 (m), 677 (m), 653 (s), 492 (w), 479 (w); elemental analysis calcd. (%) for $C_4H_6N_8O$ (182.15 g mol^{-1}): 26.38, H 3.32, N 61.52; found: C 26.31, H 3.28, N 61.36; DTA (5°C min^{-1}): onset: 180.0°C (dec.); BAM drophammer: 40 J; Friction tester: >360 N.

1,3-*Bis*-2,2'-tetrazolyloxapropane (11)

^{1}H NMR (400 MHz, acetone-D_6, ppm) δ = 8.84 (s, 2H), 6.31 (s, 2H); $^{13}C\{^{1}H\}$ NMR (101 MHz, acetone-D_6, ppm) δ = 154.6, 79.6; IR (ATR, cm^{-1}): 3141 (vw), 1715 (s), 1463 (m), 1422 (w), 1394 (m), 1368 (s), 1284 (w), 1252 (w), 1234 (w), 1183 (m), 1169 (m), 1096 (vs), 1021 (m), 1002 (w), 972 (w), 956 (w), 940 (w), 875 (w), 772 (m), 751 (w), 708 (w), 682 (m), 654 (w), 631 (w), 580 (m), 549 (w), 500 (w), 483 (w), 473 (w), 455 (w); elemental analysis calcd. (%) for $C_4H_6N_8O$ (182.15 g mol^{-1}): C 26.38, H 3.32, N 61.52; found: C 26.21, H 3.23, N 61.28; DTA (5°C min^{-1}): onset: 185.0°C (dec.); BAM drophammer: 40 J; Friction tester: 288 N.

General Procedure for the synthesis of the ECCs $[Cu(1,1'\text{-TNP})_3](ClO_4)_2$ (12) and $[Fe(ClO_4)_2(1,1'\text{-TNP})_4]$ (13):

1,1'-TNP (169.6 mg, 0.75 mmol, 3 eq.) was suspended in 4 mL of MeCN and heated to 50°C until a clear solution was obtained. The respective perchlorate ($Cu(ClO_4)_2 \cdot 6\ H_2O$: 92.6 mg, 0.25 mmol, 1 eq; $Fe(ClO_4)_2 \cdot 6\ H_2O$: 90.7 mg, 0.25 mmol, 1 eq) was dissolved in 1 mL of MeCN at room temperature and added dropwise. The solution which was obtained was stirred at 50°C for 10 minutes and then allowed to cool down to room temperature. On cooling down, precipitation was observed in both cases. The precipitates were filtered off, washed with cold MeCN and dried in air.

[Cu(1,1'-TNP)$_3$](ClO$_4$)$_2$ (12)

Compound **12** was obtained as a light blue solid in a yield of 70 % (165.8 mg, 0.18 mmol). IR (ATR, cm^{-1}): $\tilde{\upsilon}$ = 3134 (w), 3047 (w), 2996 (vw), 1598 (m), 1496 (m), 1443 (m), 1420 (m), 1403 (w), 1335 (m), 1295 (s), 1256 (w), 1215 (m), 1180 (s), 1110 (m), 1079 (vs), 1018 (s), 995 (m), 979 (m), 937 (s), 904 (m), 872 (w), 761 (m), 749 (s), 714 (m), 672 (m), 662 (m), 639 (m), 621 (vs), 439 (m), 426 (w), 415 (w); elemental analysis calcd. (%) for $C_{12}H_{18}Cl_2CuN_{30}O_{14}$ (940.92 g mol^{-1}): C 15.32 H 1.93 N 44.66, found C 15.60 H 2.05 N 44.37; DTA (5°C min^{-1}) onset: 246.1 °C (dec.); BAM drop hammer: < 1 J; Friction tester: 10 N.

[Fe(ClO$_4$)$_2$(1,1'-TNP)$_4$] (13)

The compound was obtained as a colorless solid i53% yield (152.6 mg, 0.13 mmol). IR (ATR, cm^{-1}): $\tilde{\upsilon}$ = 3130 (w), 3045 (w), 2996 (w), 1600 (m), 1497 (m), 1443 (m), 1422 (w), 1403 (w), 1335 (w), 1295 (m), 1256 (w), 1215 (m), 1181 (m), 1110 (m), 1091 (vs), 1018 (m), 984 (m), 939 (m), 907 (w), 871 (w), 761 (m), 750 (s), 715 (m), 672 (m), 663 (m), 641 (w), 622 (s), 513 (w), 476 (vw), 437 (m), 419 (w). elemental analysis calcd. (%) for $C_{16}H_{24}Cl_2FeN_{40}O_{16}$ (1159.38 g mol^{-1}): C 16.58 H 2.09 N 48.33, found C 16.29 H 2.35 N 48.03; DTA (5°C min^{-1}) onset: 220.0°C (dec.); BAM drophammer: < 1 J; Friction tester: 9 N.

9.6.2 NMR Spectroscopy

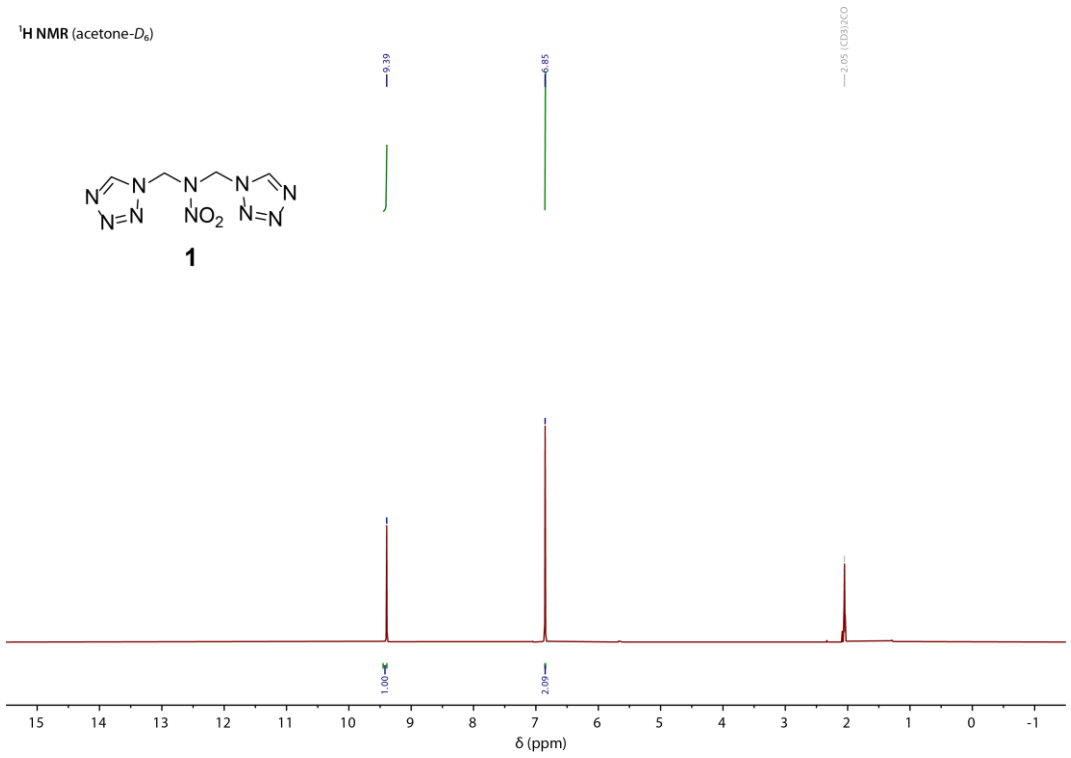

Figure S1. ^{1}H NMR spectrum of **1** in acetone-D_6.

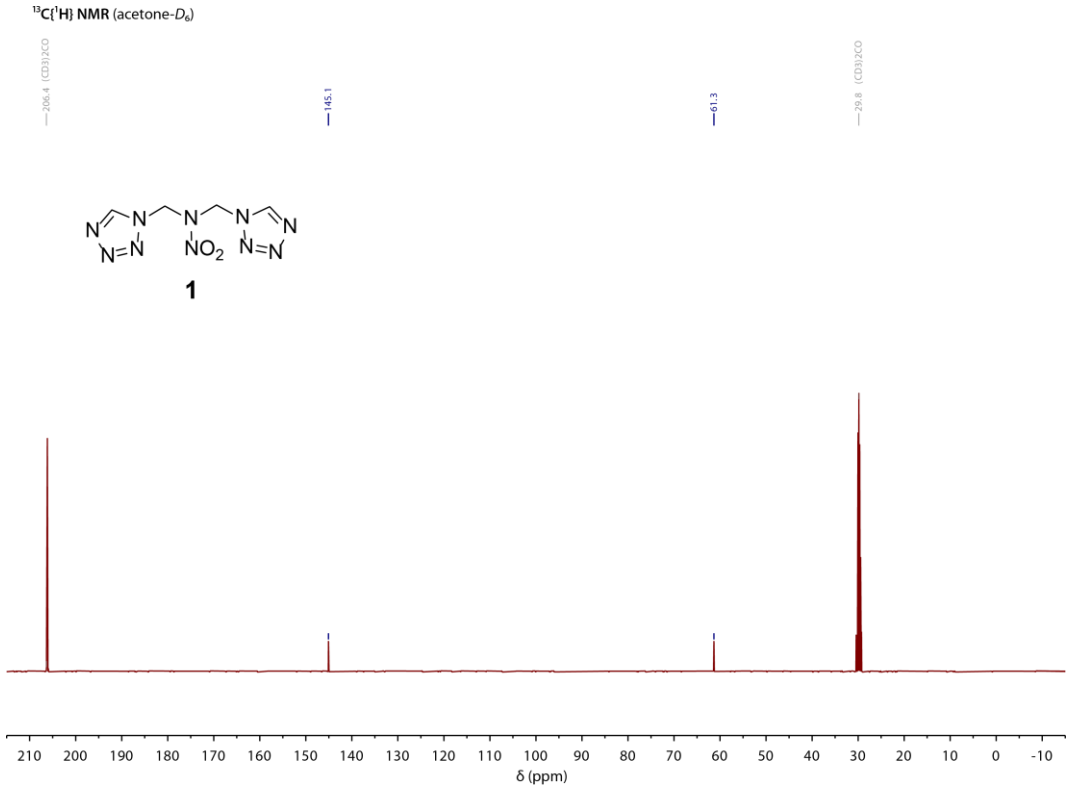

Figure S2. ^{13}C{^{1}H} NMR spectrum of **1** in acetone-D_6.

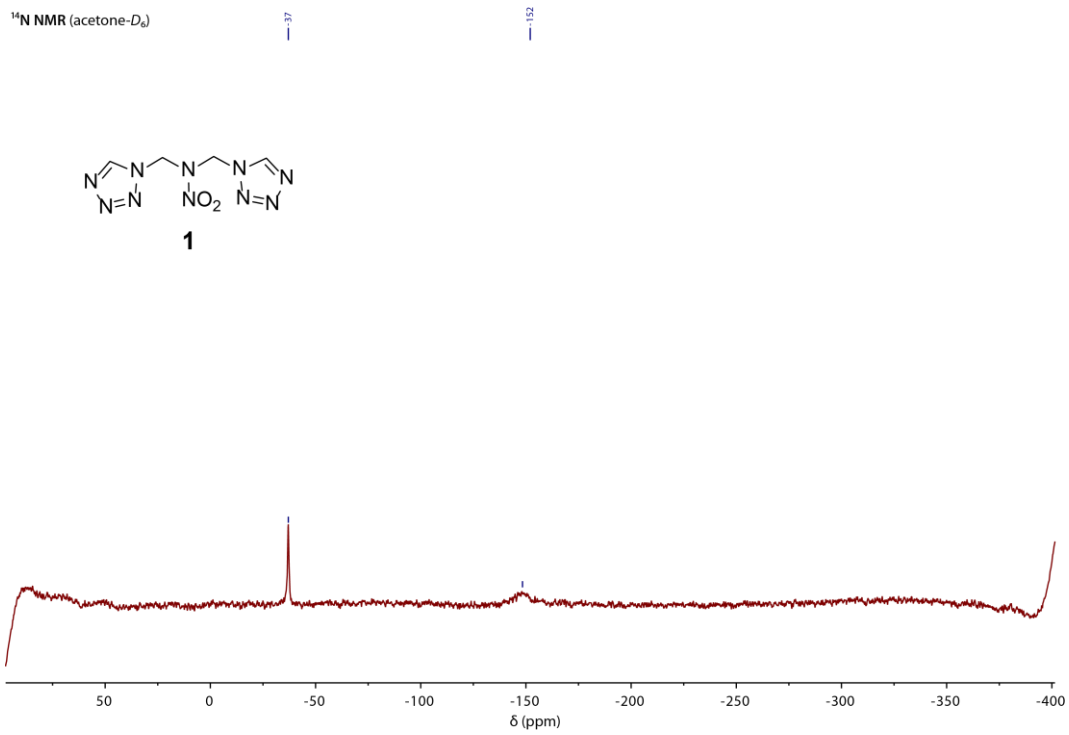

Figure S3. ^{14}N NMR spectrum of **1** in acetone-D_6.

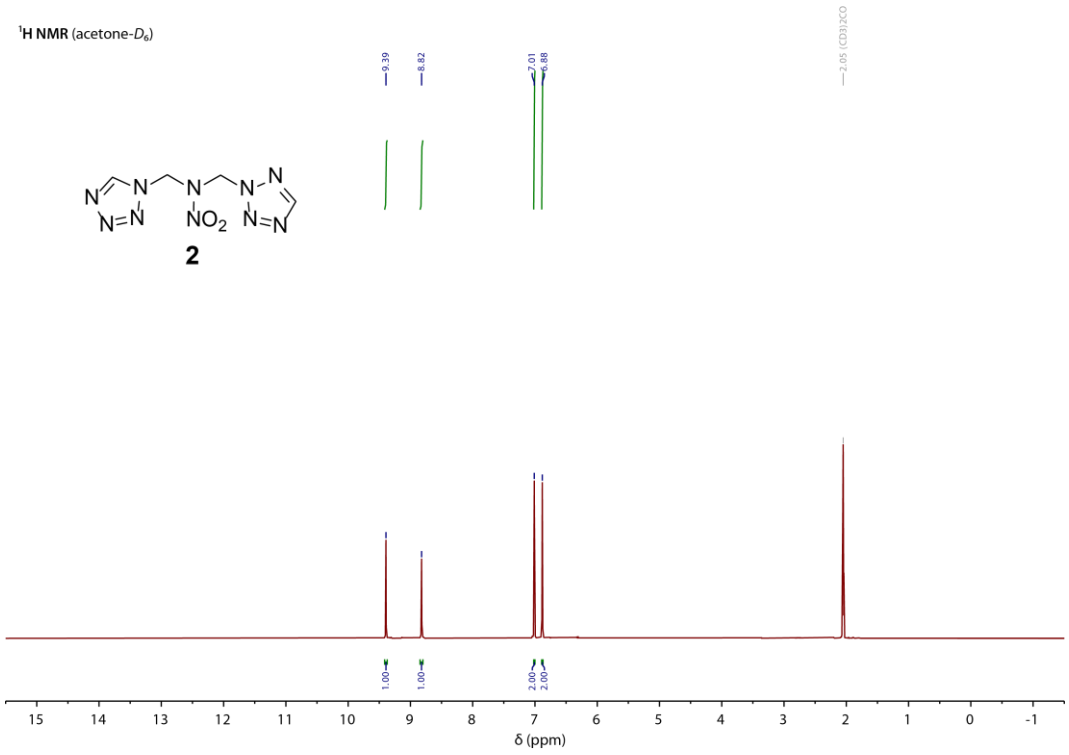

Figure S4. ^{1}H NMR spectrum of **2** in acetone-D_6.

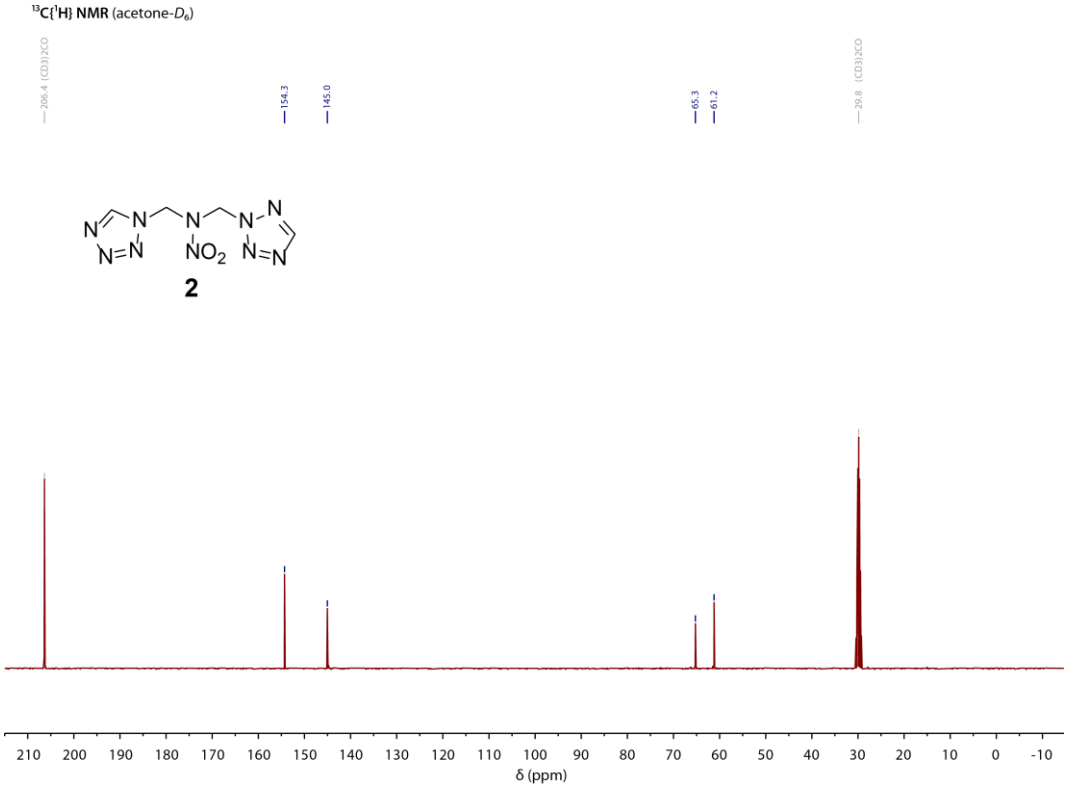

Figure S5. $^{13}C\{^{1}H\}$ NMR spectrum of **2** in acetone-D_6.

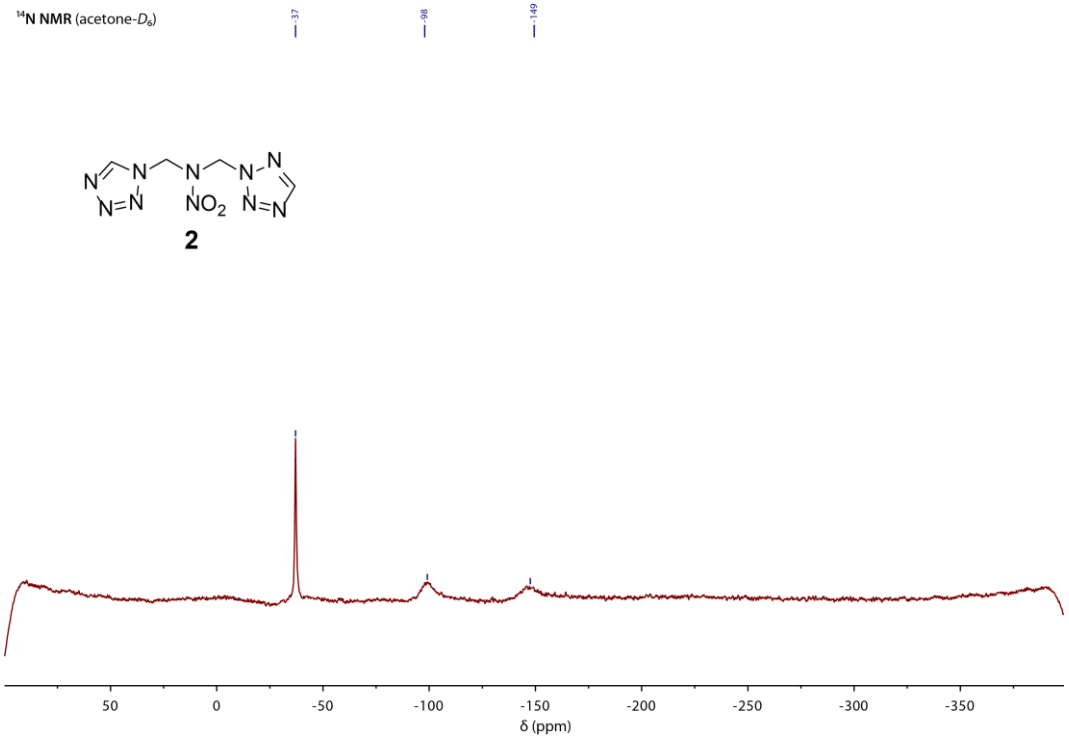

Figure S6. ^{14}N NMR spectrum of **2** in acetone-D_6.

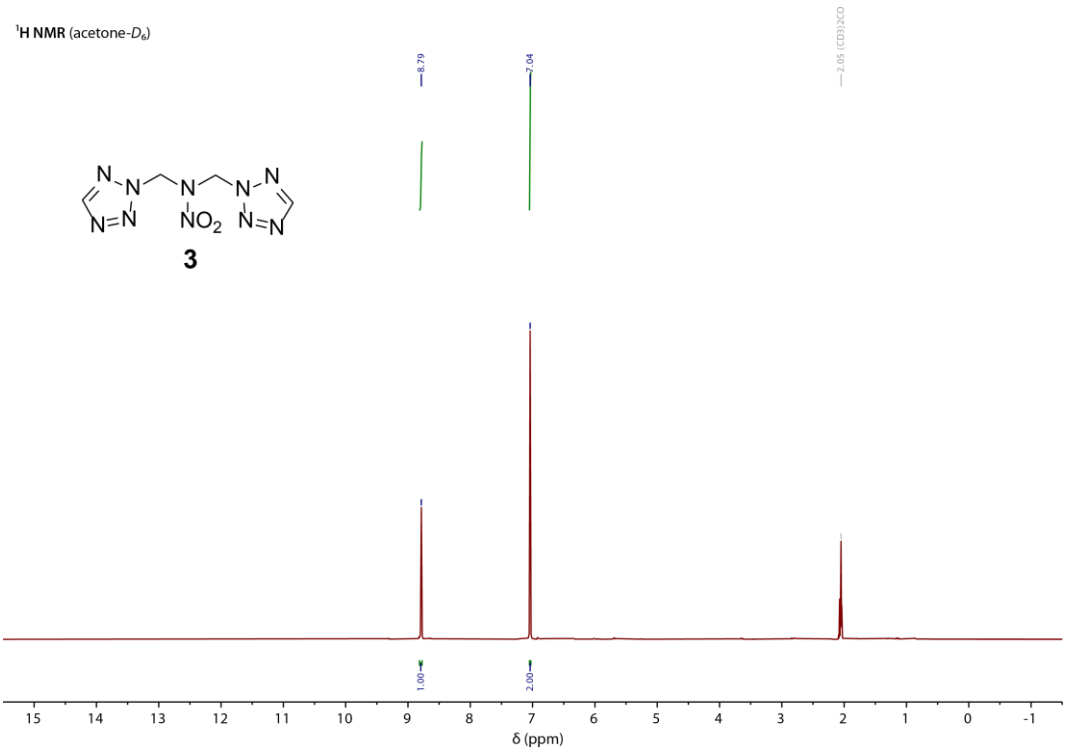

Figure S7. ^{1}H NMR spectrum of **3** in acetone-D_6.

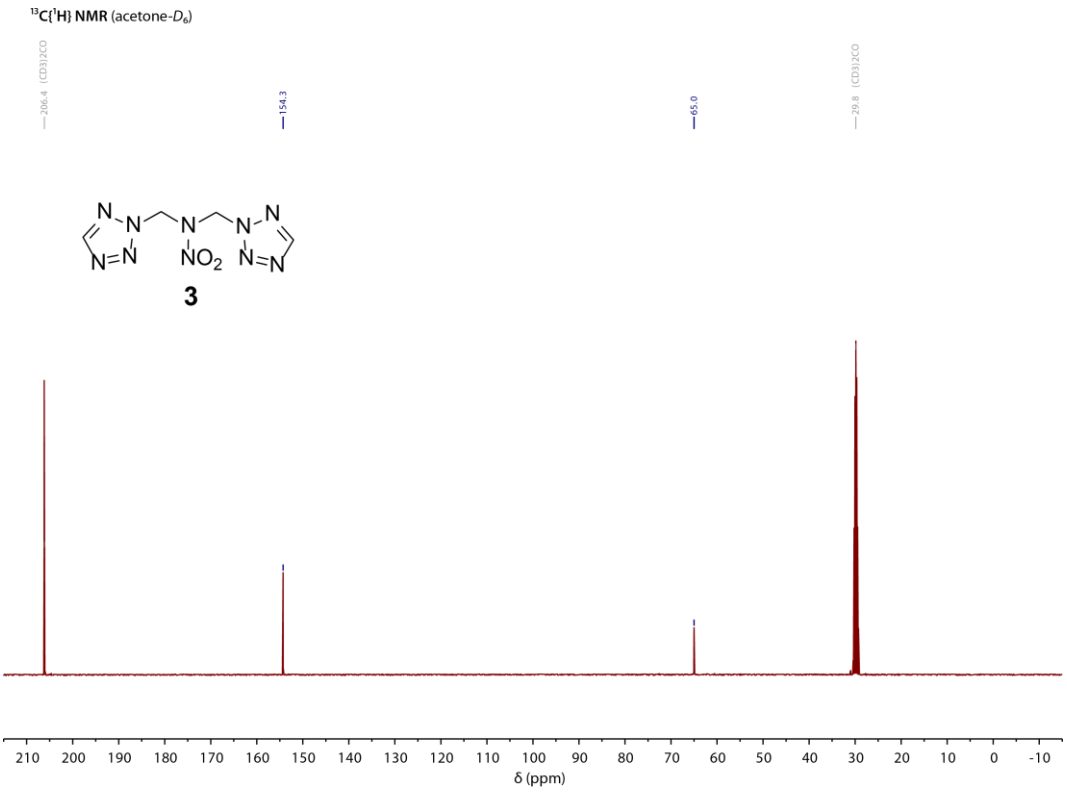

Figure S8. ^{13}C{^{1}H} NMR spectrum of **3** in acetone-D_6.

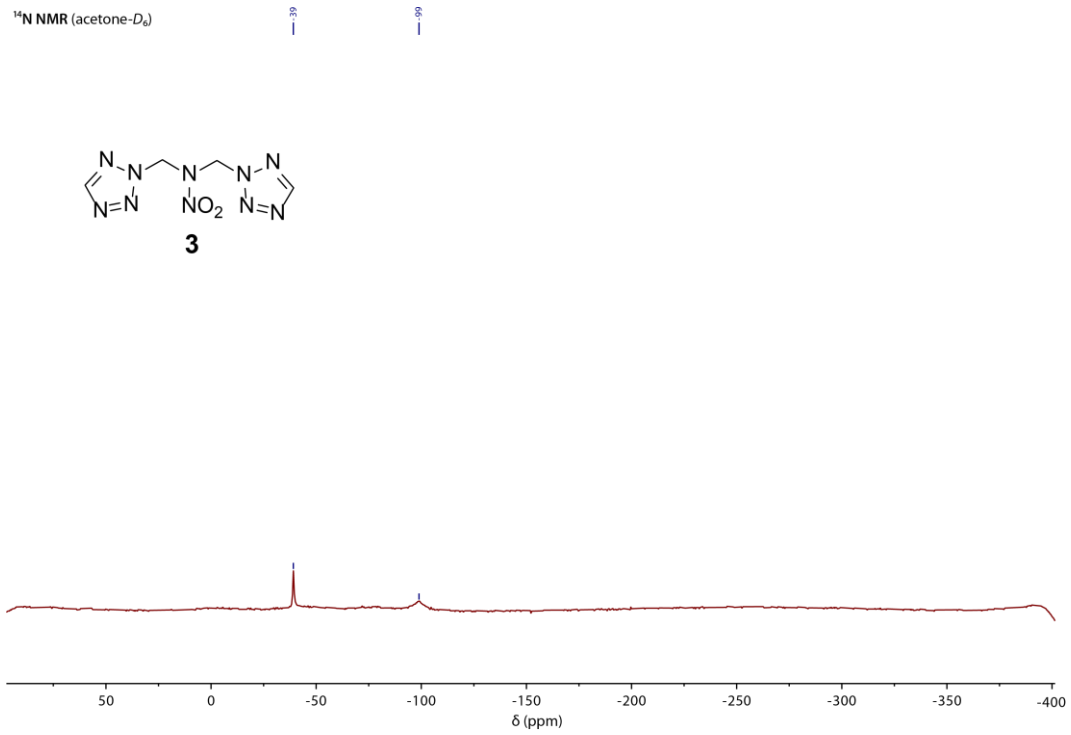

Figure S9. ^{14}N NMR spectrum of **3** in acetone-D_6.

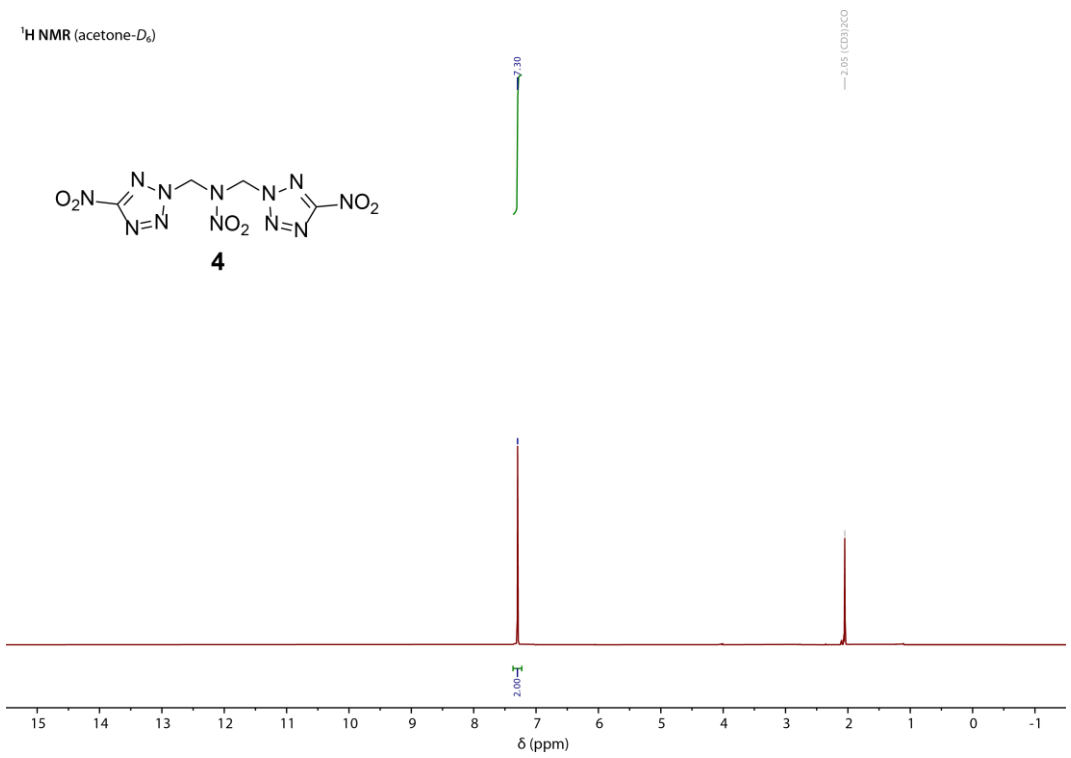

Figure S10. ^{1}H NMR spectrum of **4** in acetone-D_6.

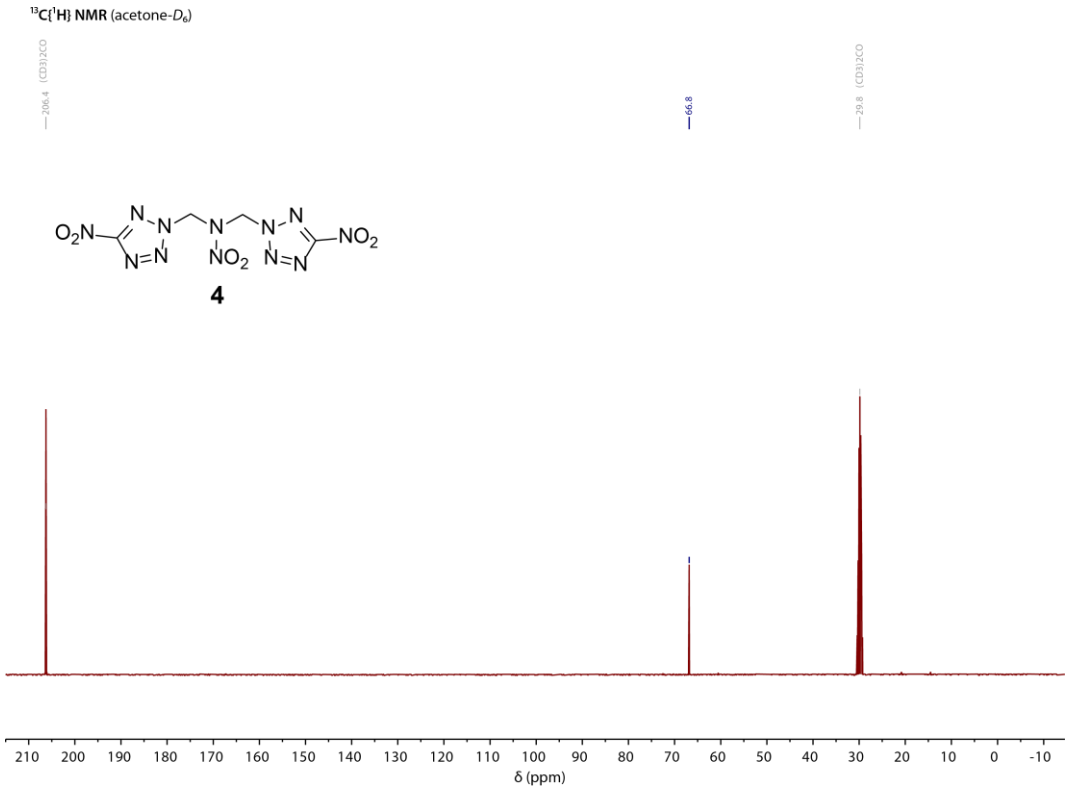

Figure S11. $^{13}C\{^{1}H\}$ NMR spectrum of **4** in acetone-D_6.

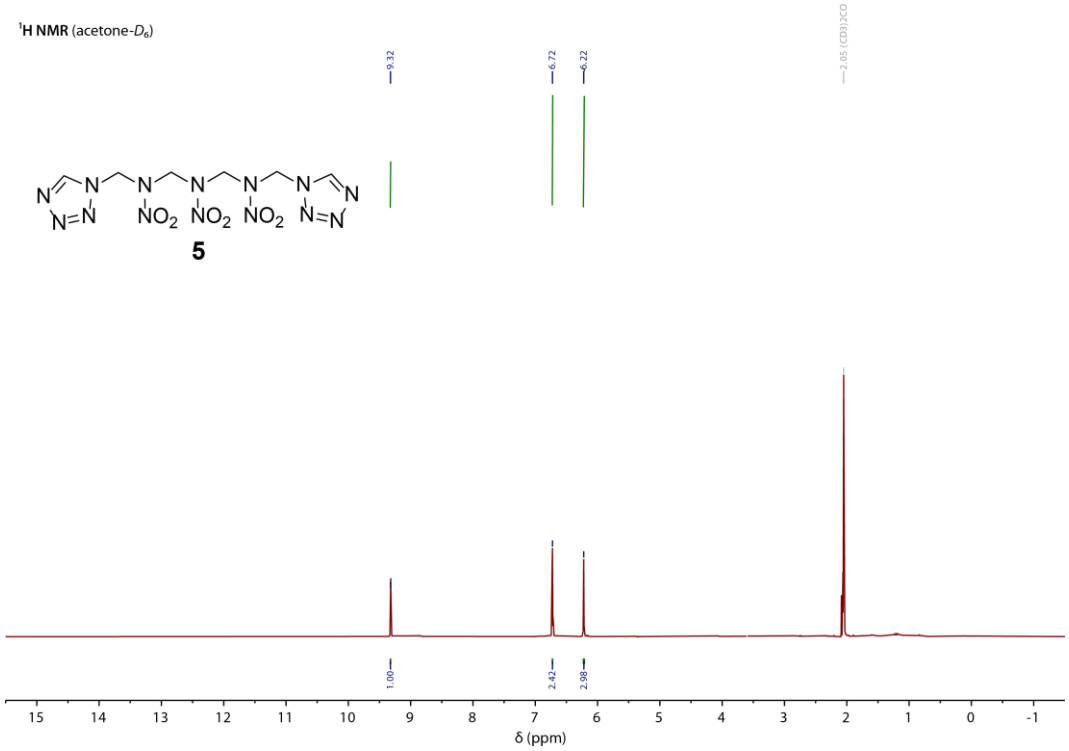

Figure S12. ^{1}H NMR spectrum of **5** in acetone-D_6.

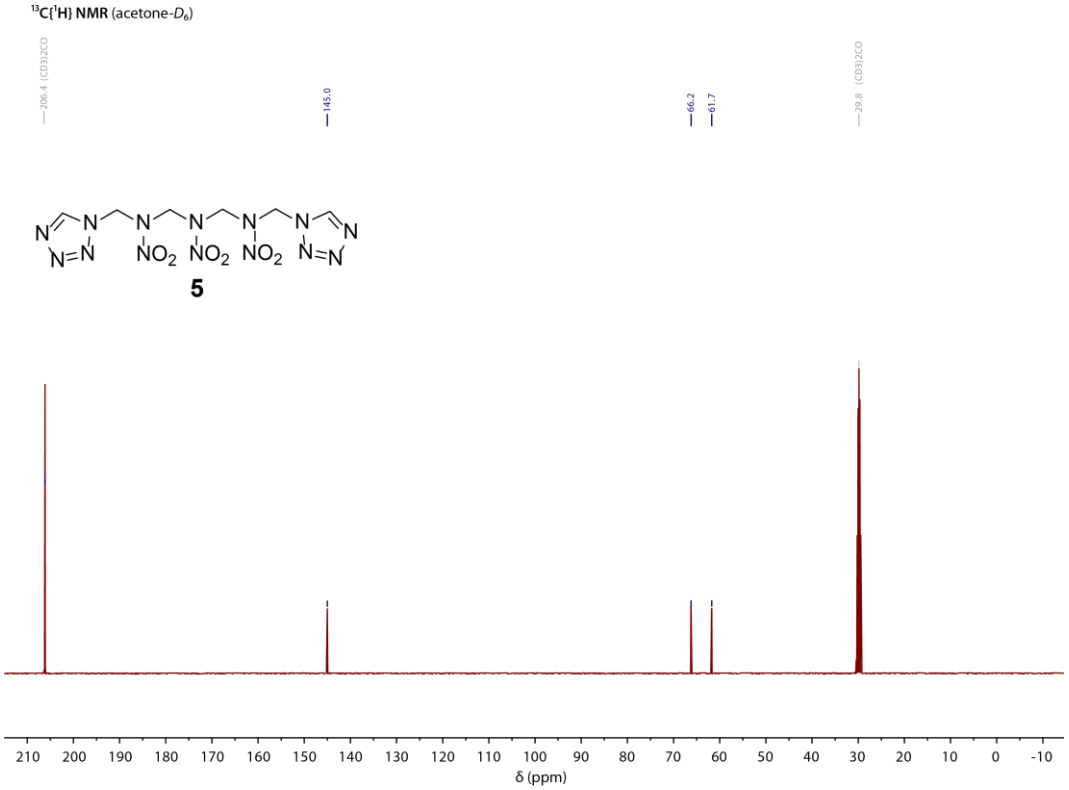

Figure S13. $^{13}C\{^{1}H\}$ NMR spectrum of **5** in acetone-D_6.

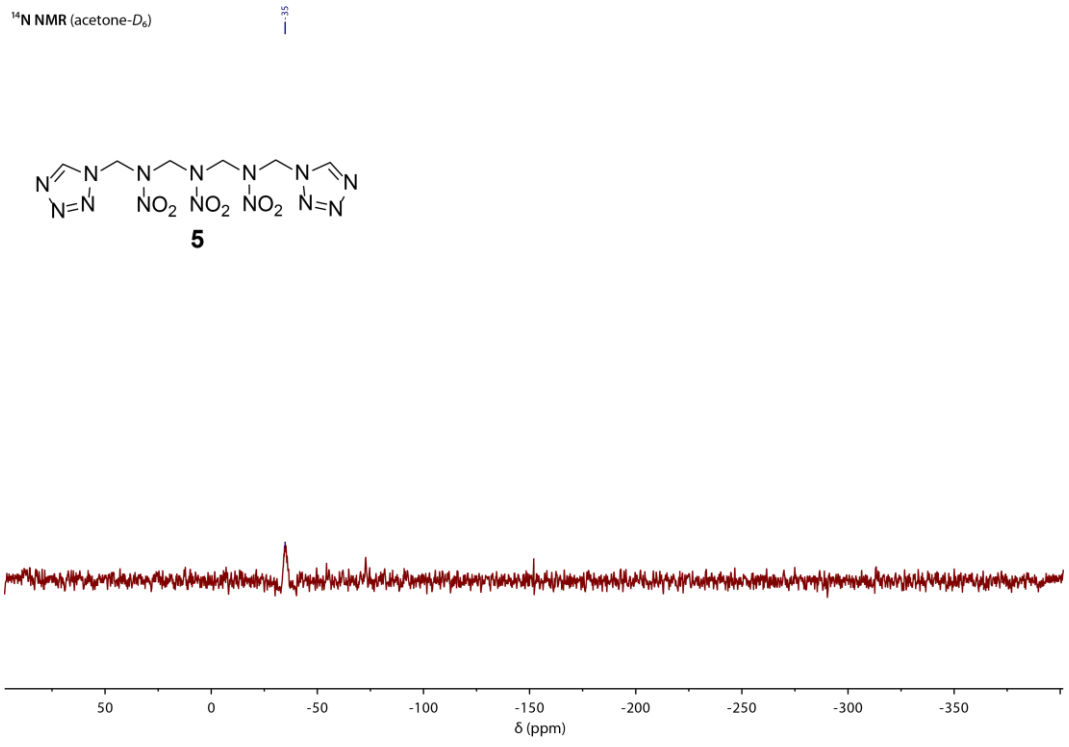

Figure S14. ^{14}N NMR spectrum of **5** in acetone-D_6.

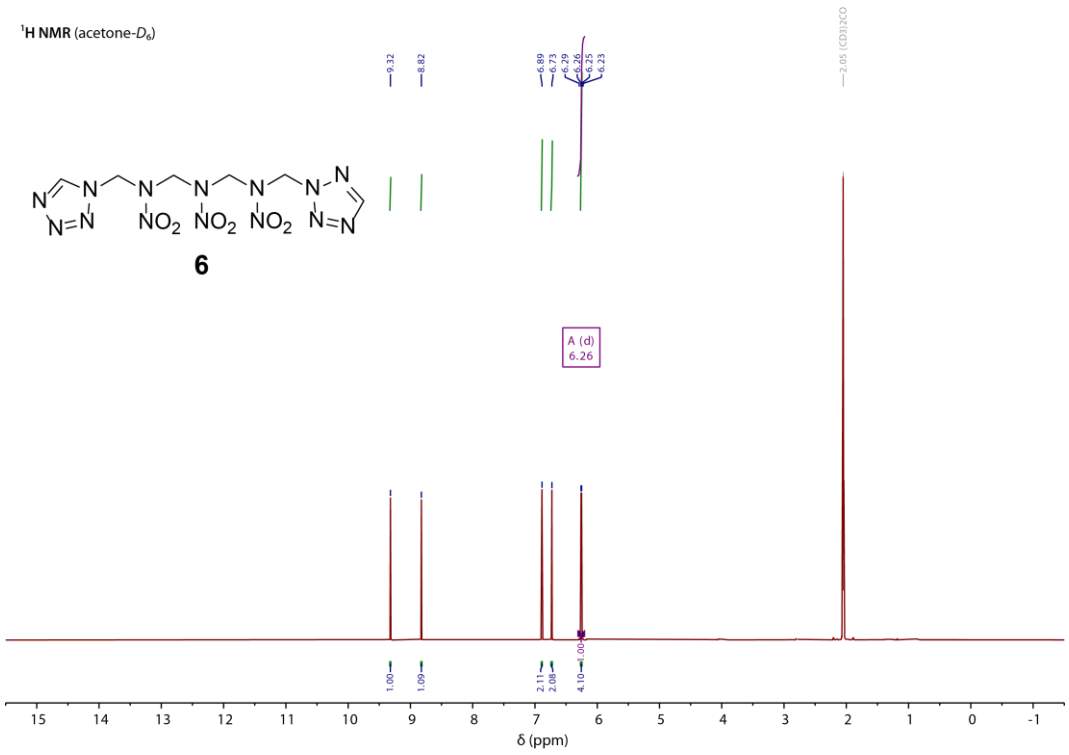

Figure S15. ^{1}H NMR spectrum of **6** in acetone-D_6.

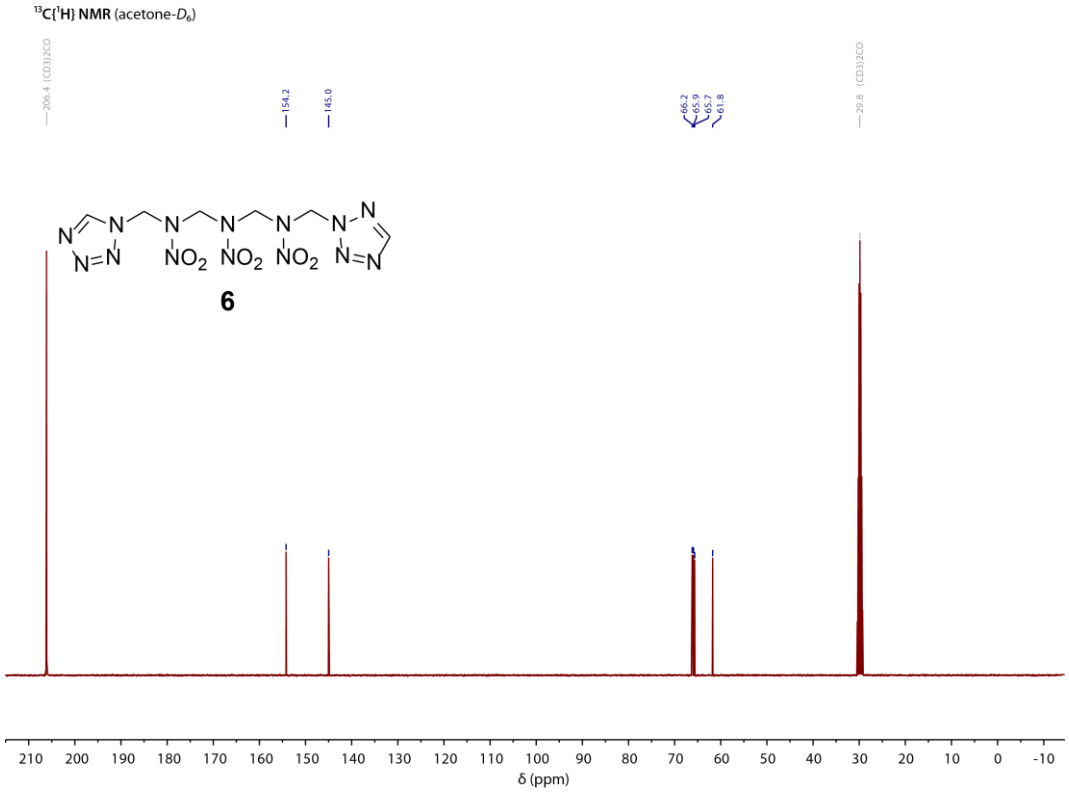

Figure S16. ^{13}C{^{1}H} NMR spectrum of **6** in acetone-D_6.

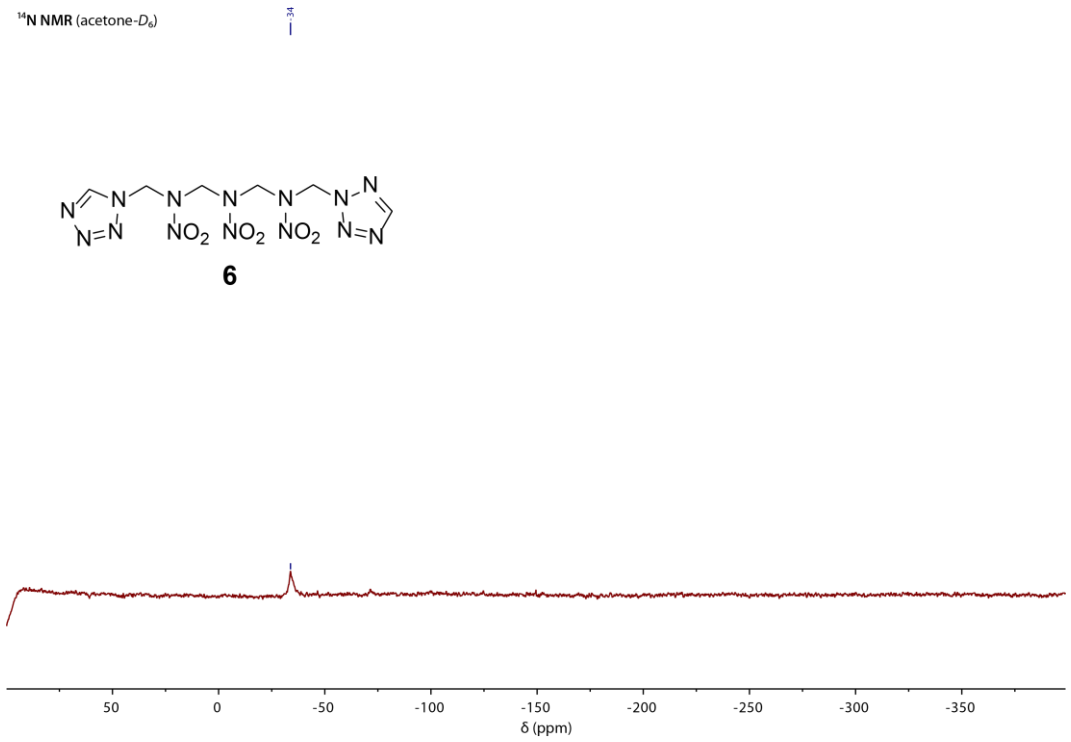

Figure S17. ^{14}N NMR spectrum of **6** in acetone-D_6.

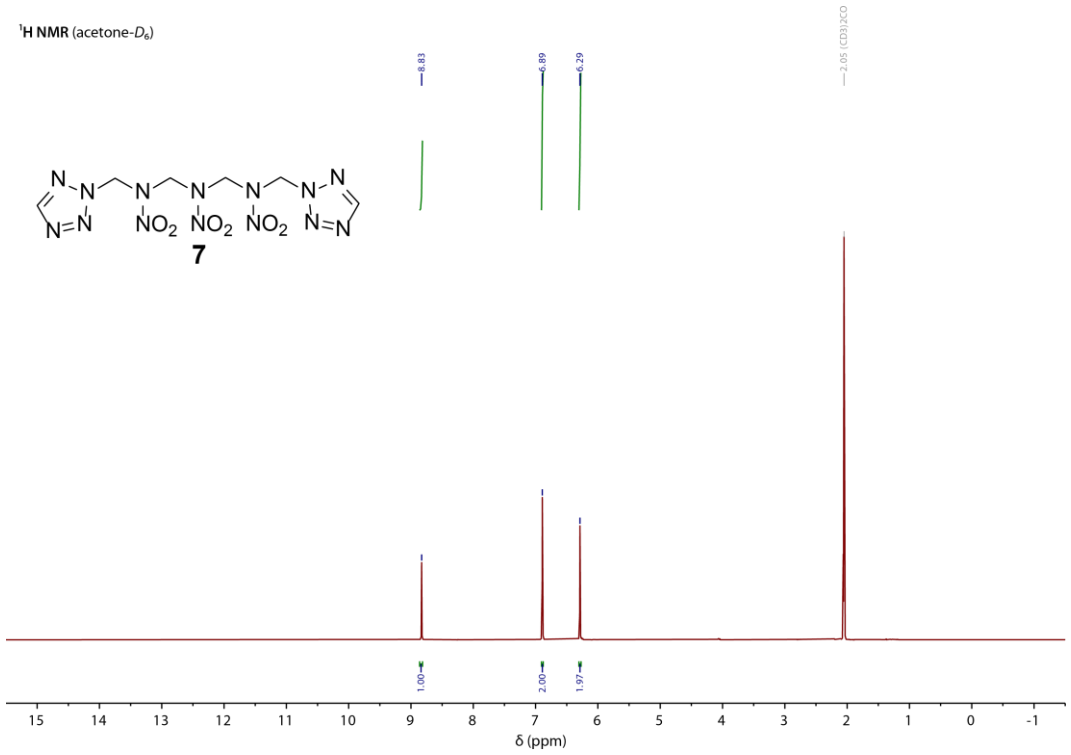

Figure S18. ^{1}H NMR spectrum of **7** in acetone-D_6.

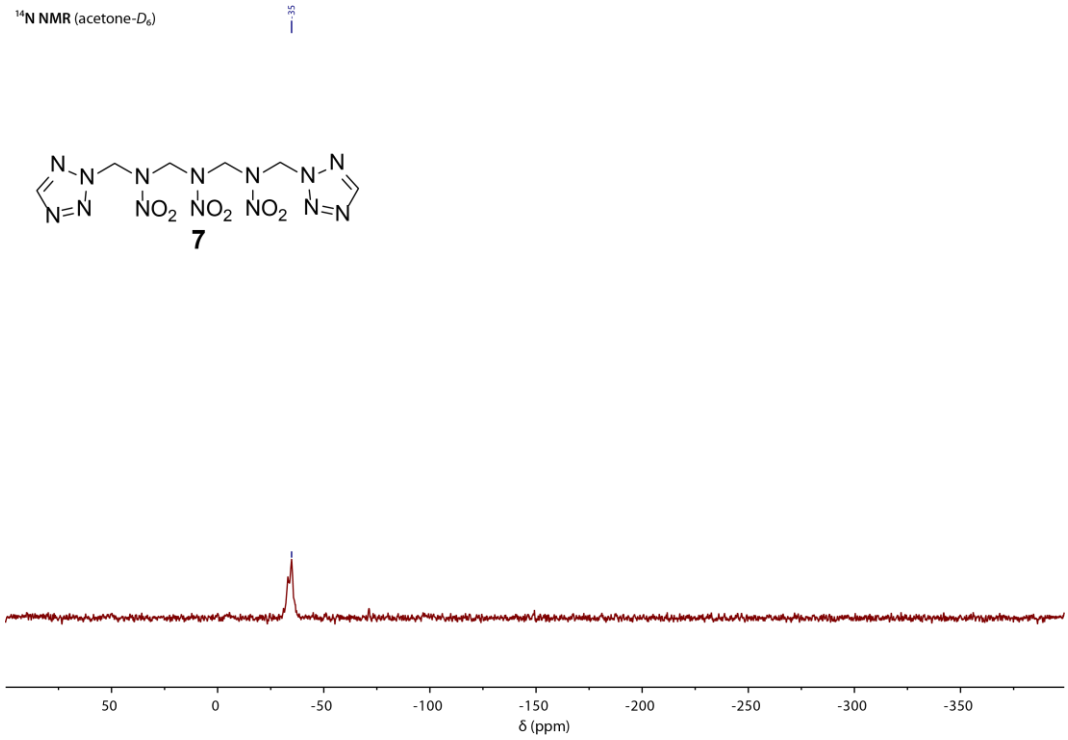

Figure S19. $^{13}C\{^{1}H\}$ NMR spectrum of **7** in acetone-D_6.

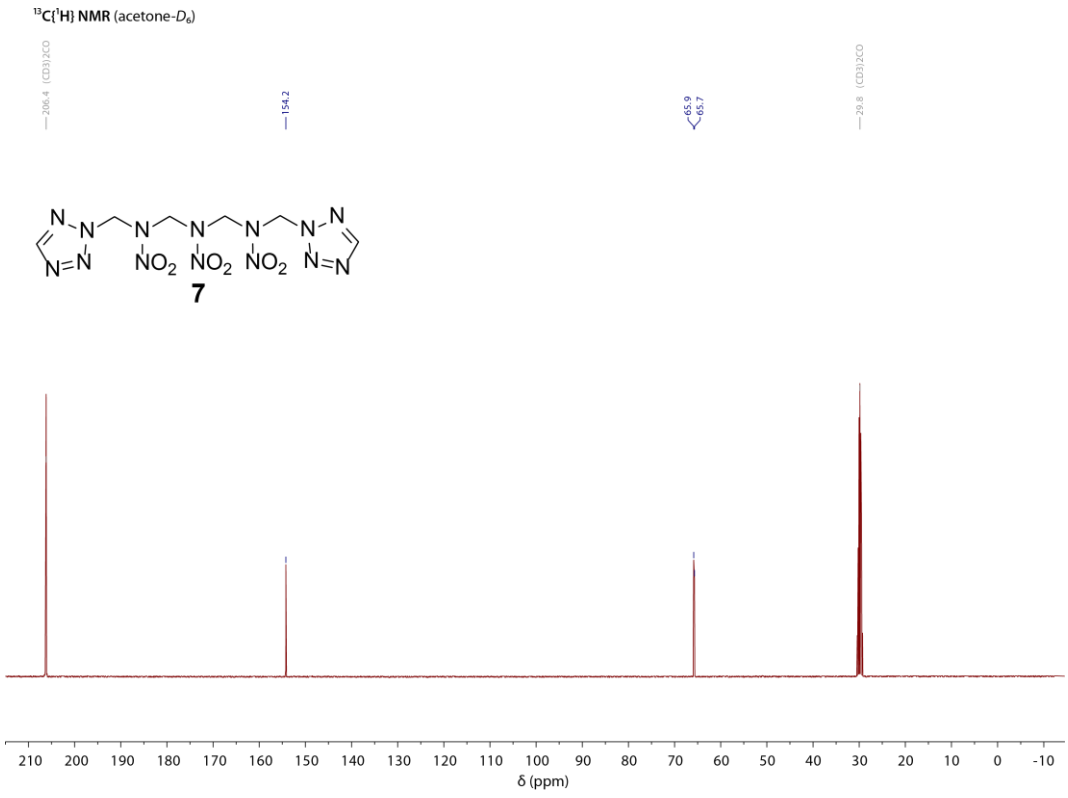

Figure S20. ^{14}N NMR spectrum of **7** in acetone-D_6.

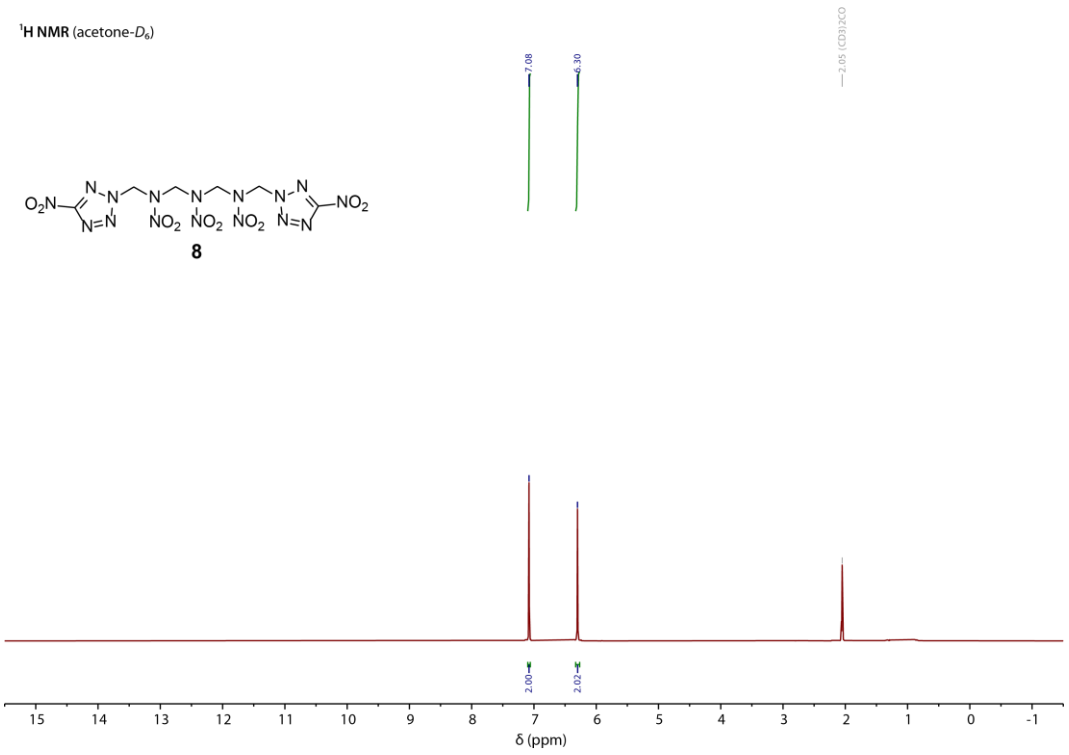

Figure S21. ^{1}H NMR spectrum of **8** in acetone-D_6.

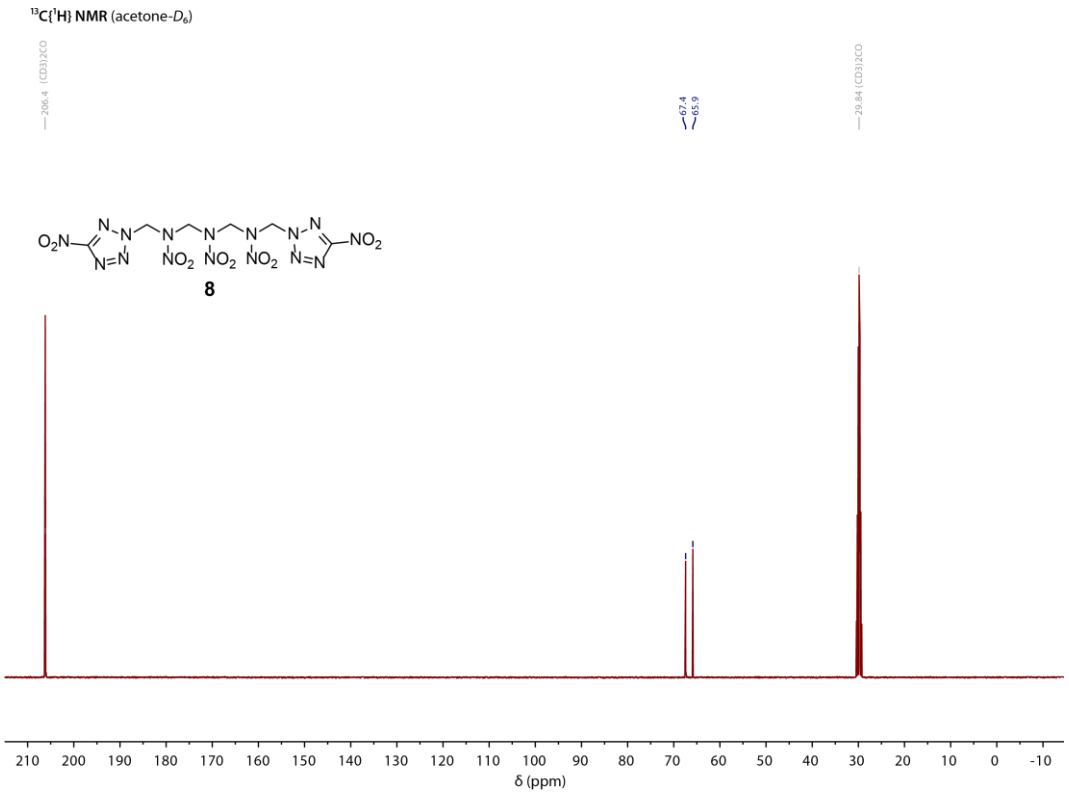

Figure S22. ^{13}C{^{1}H} NMR spectrum of **8** in acetone-D_6.

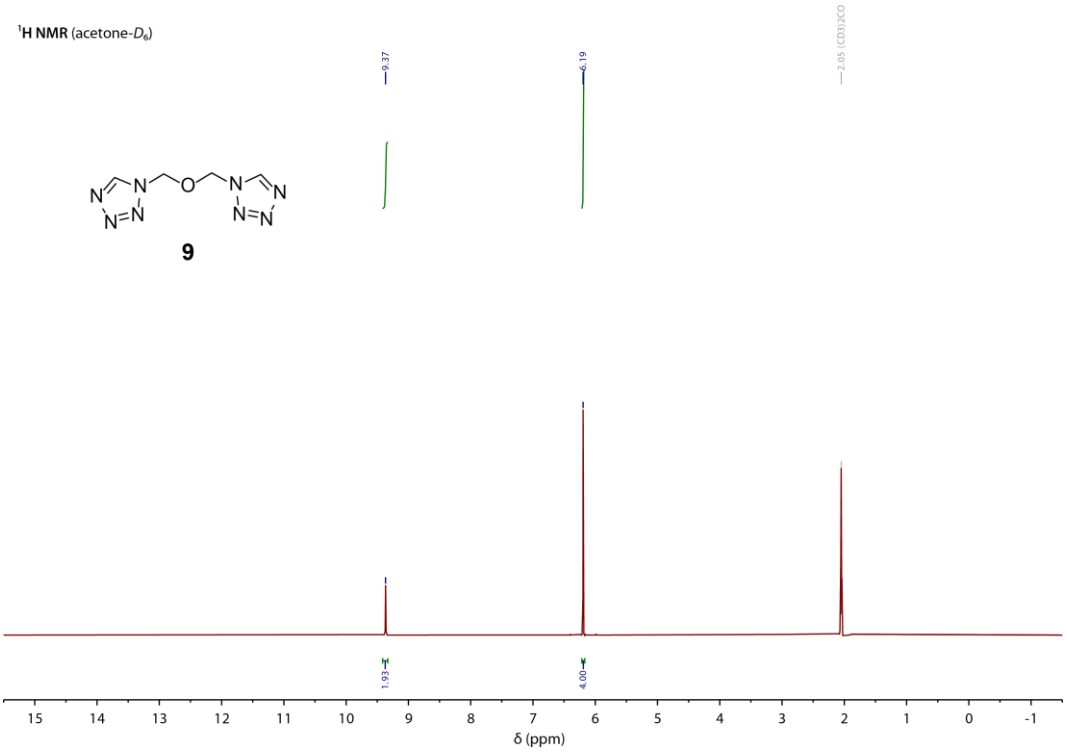

Figure S23. ^{1}H NMR spectrum of **9** in acetone-D_6.

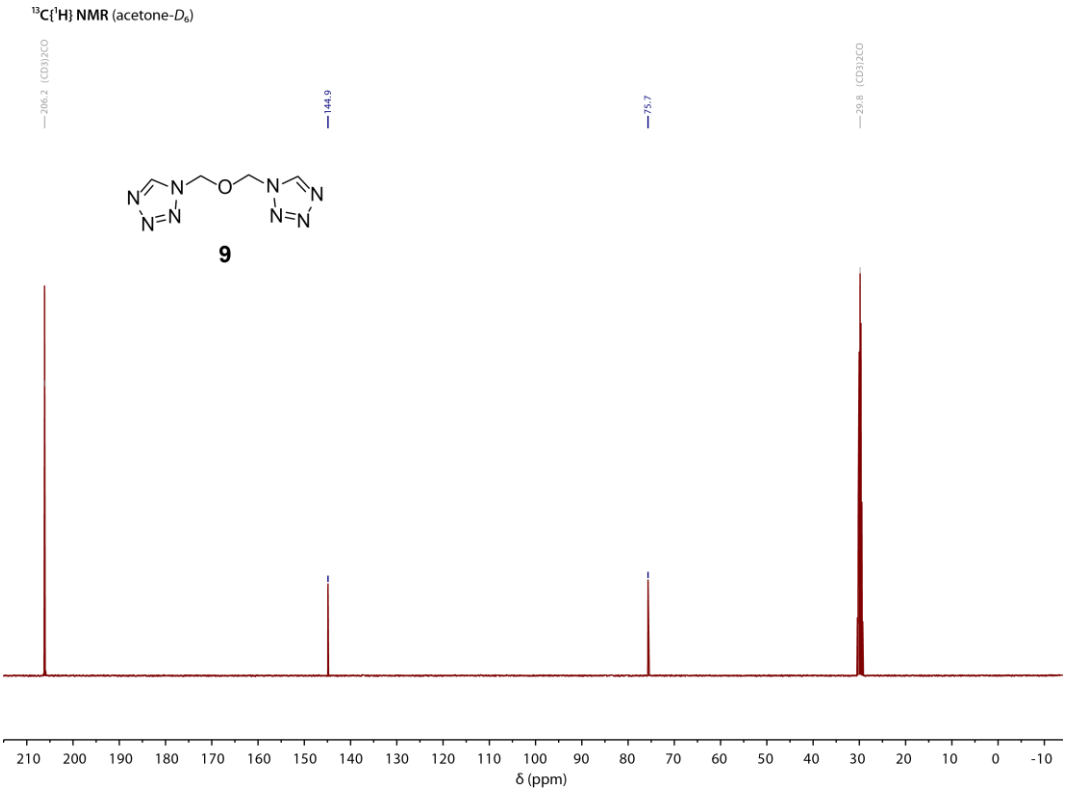

Figure S24. ^{13}C{^{1}H} NMR spectrum of **9** in acetone-D_6.

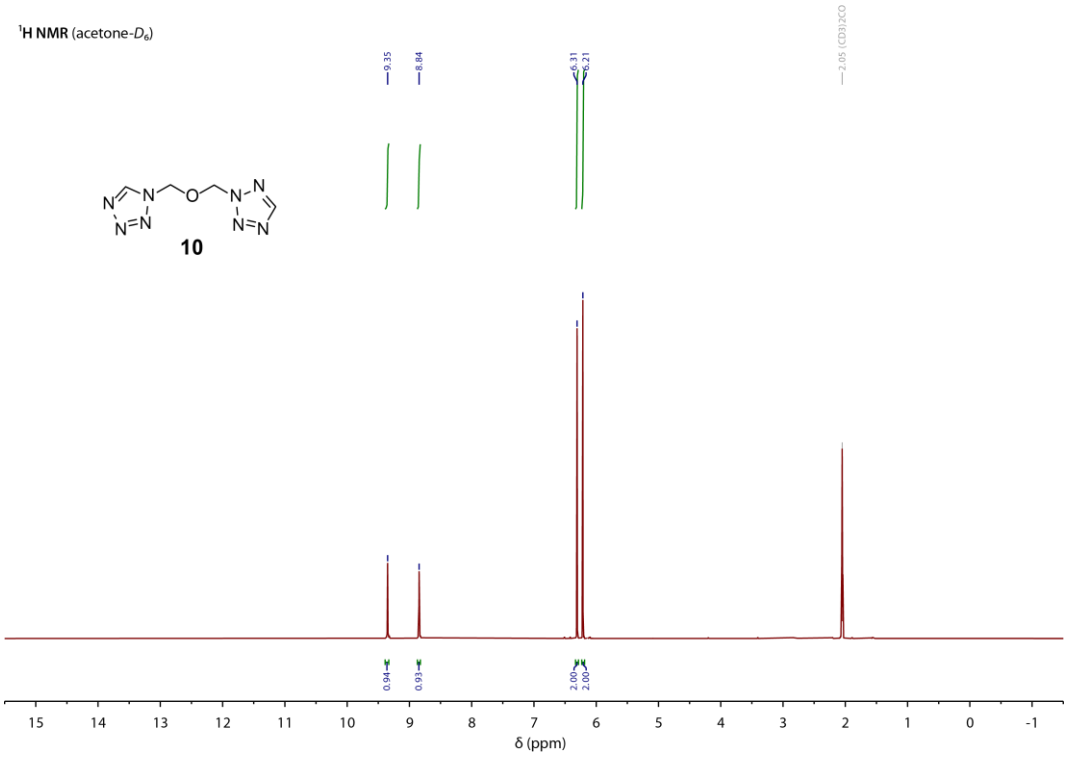

Figure S25. ^{1}H NMR spectrum of **10** in acetone-D_6.

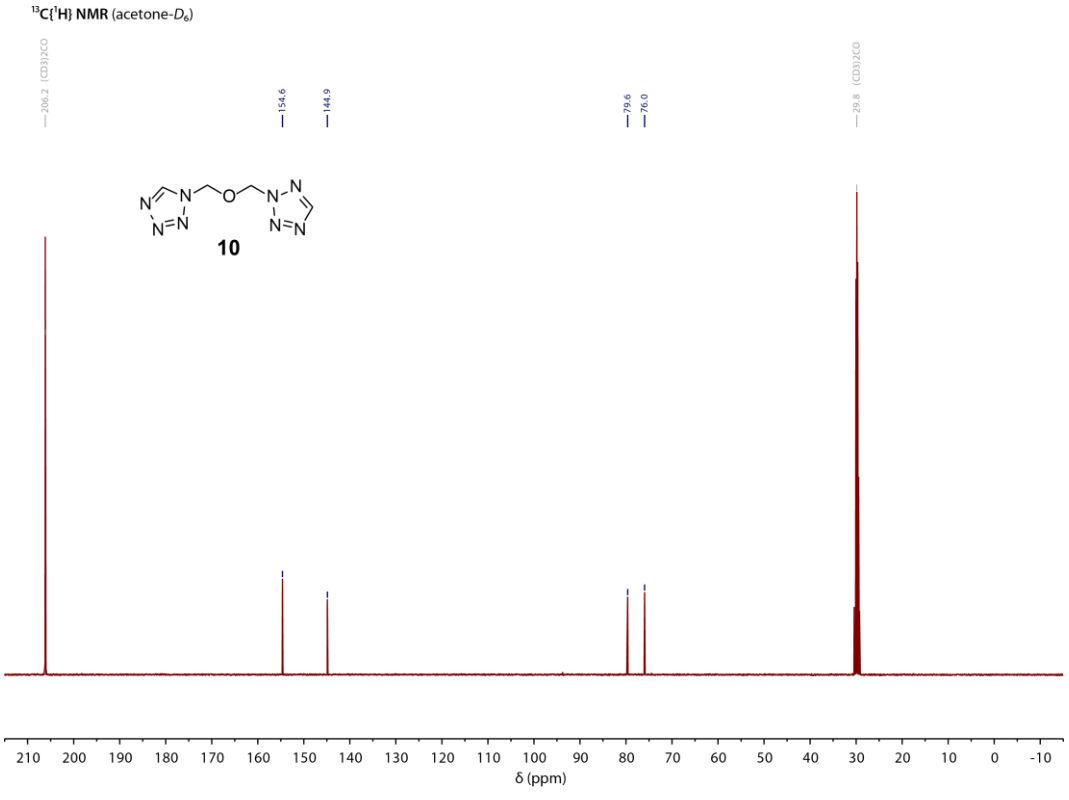

Figure S26. ^{13}C{^{1}H} NMR spectrum of **10** in acetone-D_6.

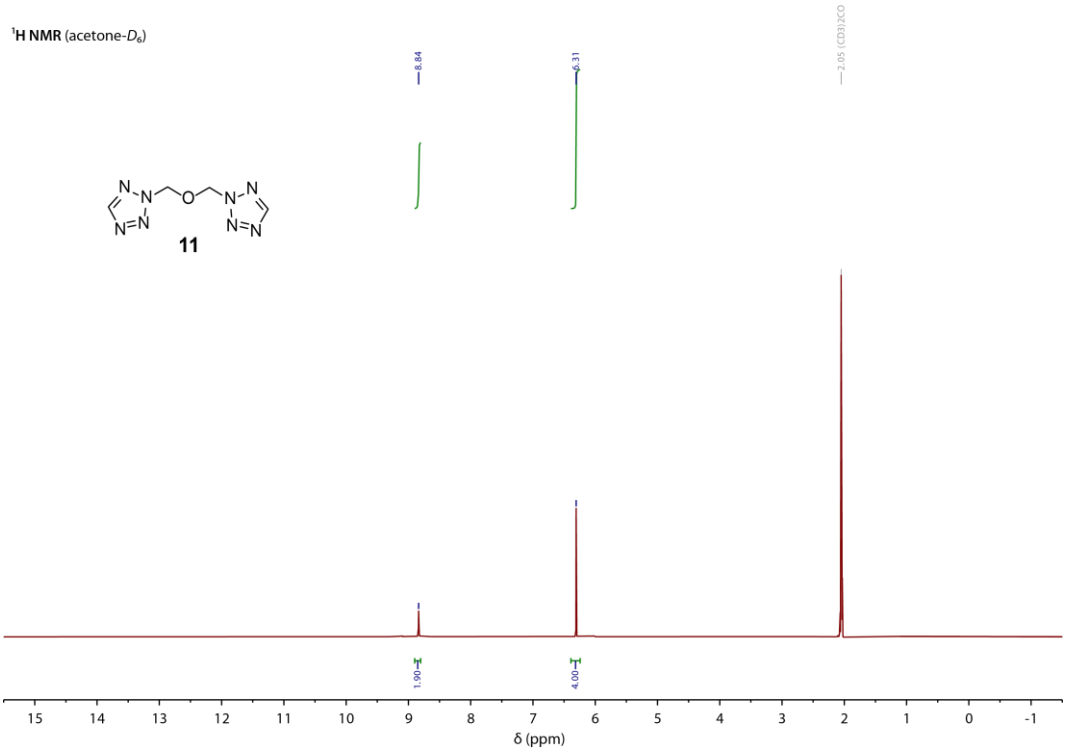

Figure S27. ^{1}H NMR spectrum of **11** in acetone-D_6.

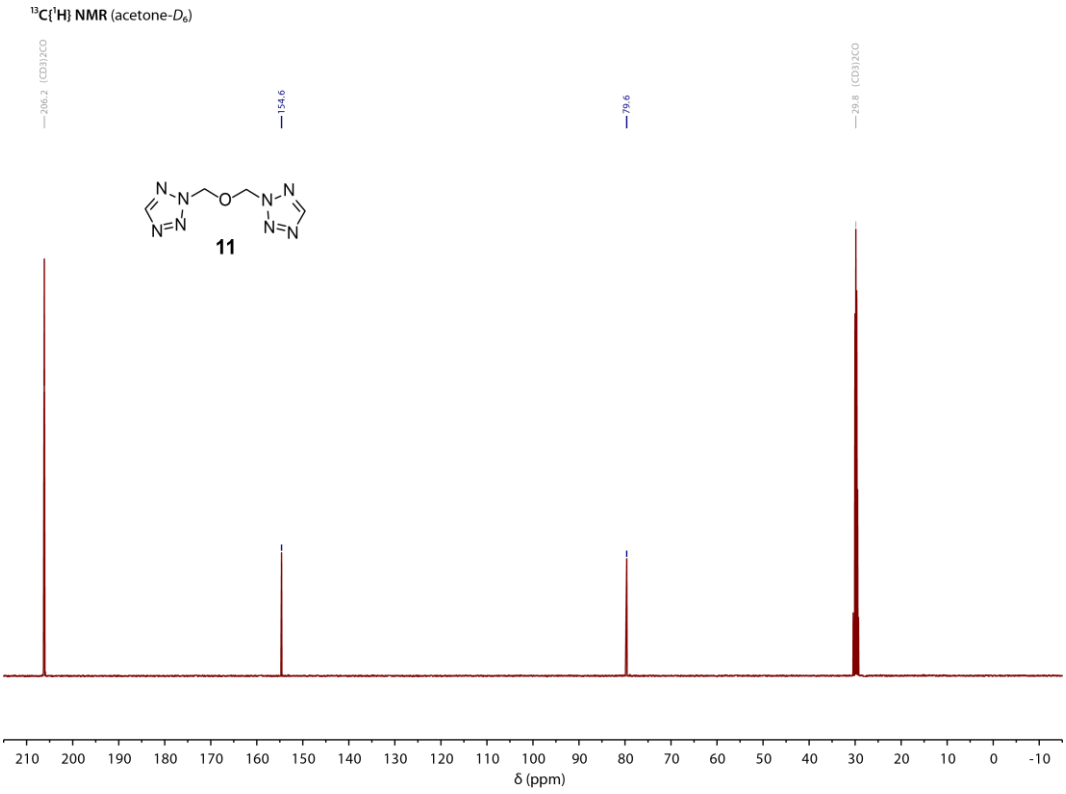

Figure S28. ^{13}C{^{1}H} NMR spectrum of **11** in acetone-D_6.

9.6.3 IR Spectroscopy

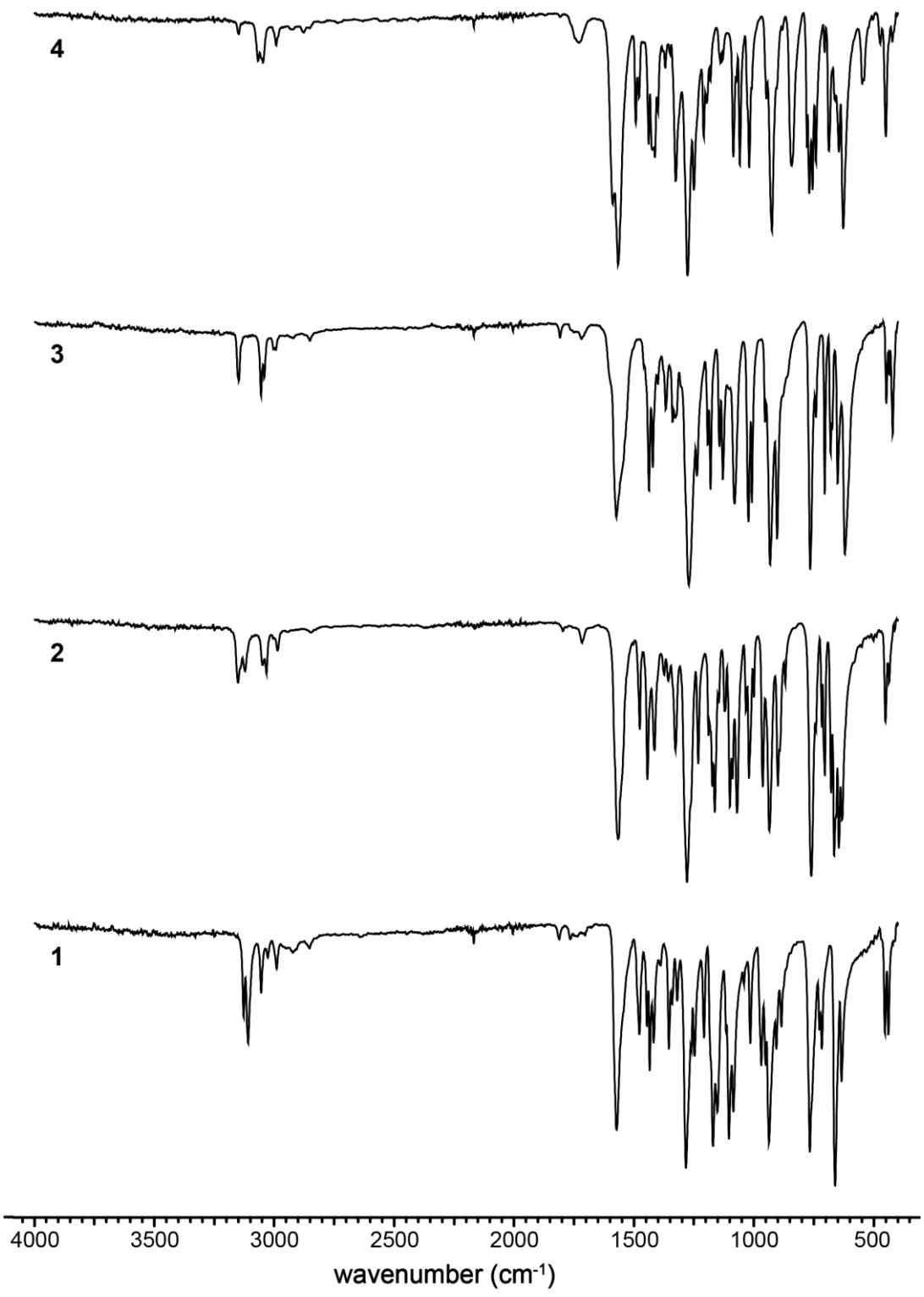

Figure S29. IR spectra of **1** to **4**.

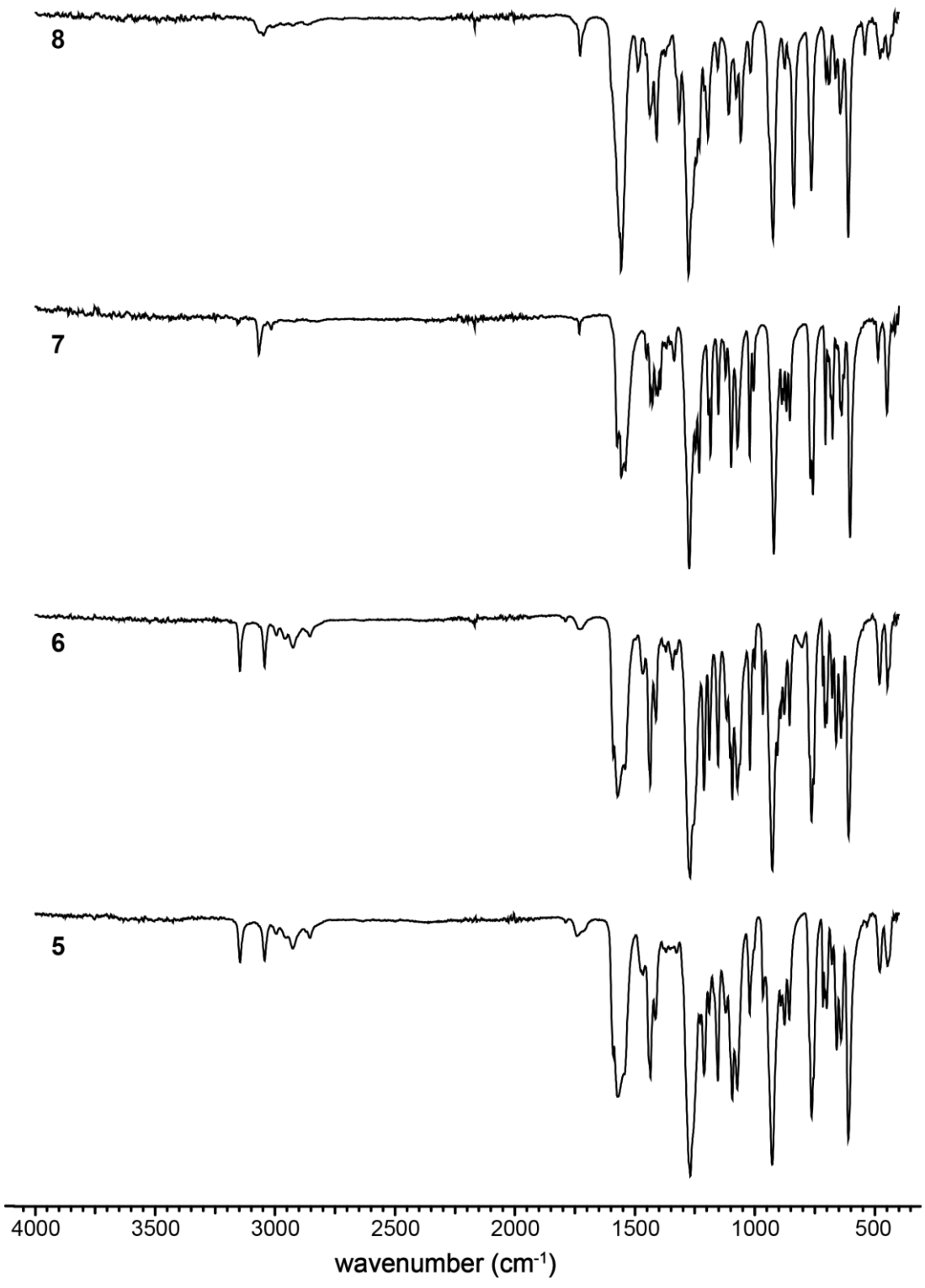

Figure S30. IR spectra of **5** to **8**.

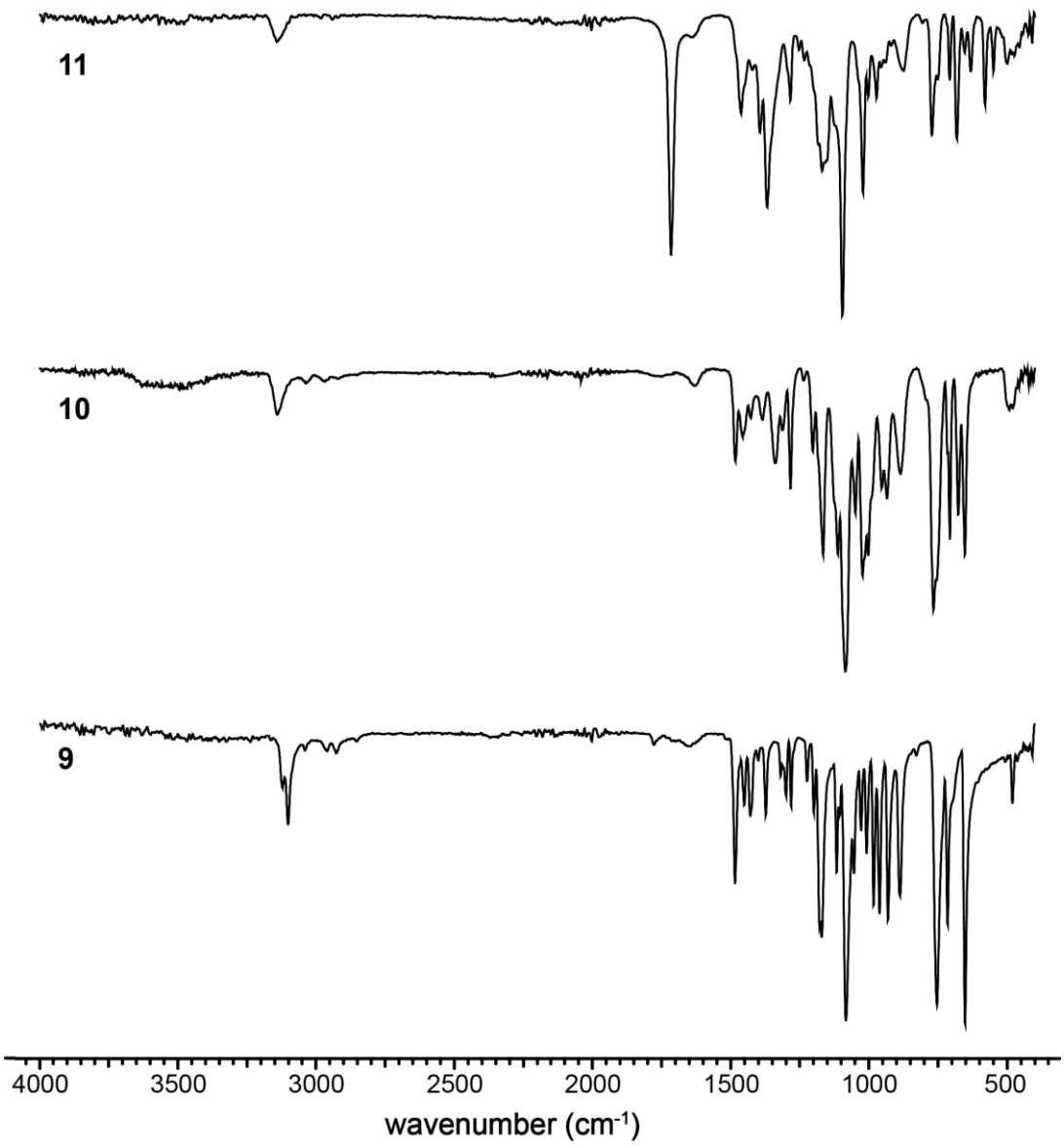

Figure S31. IR spectra of **9** to **11**.

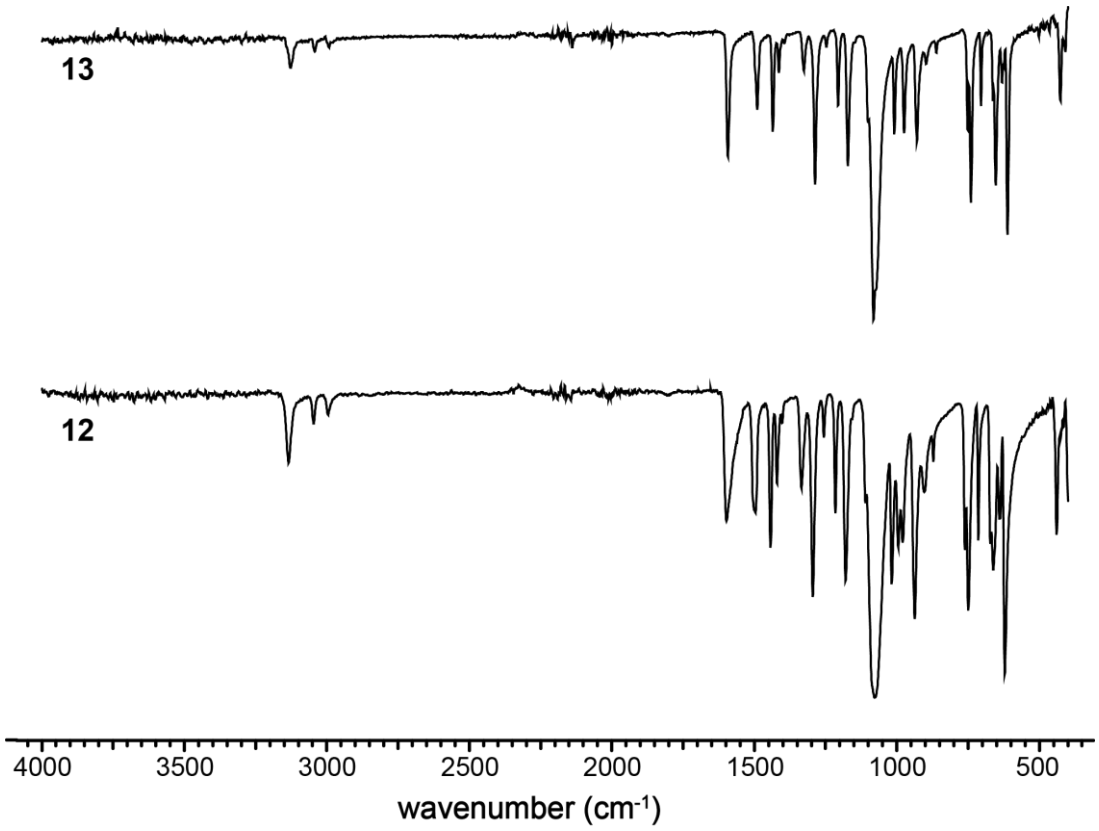

Figure S32. IR spectra of **12** and **13**.

9.6.4 DTA Measurements

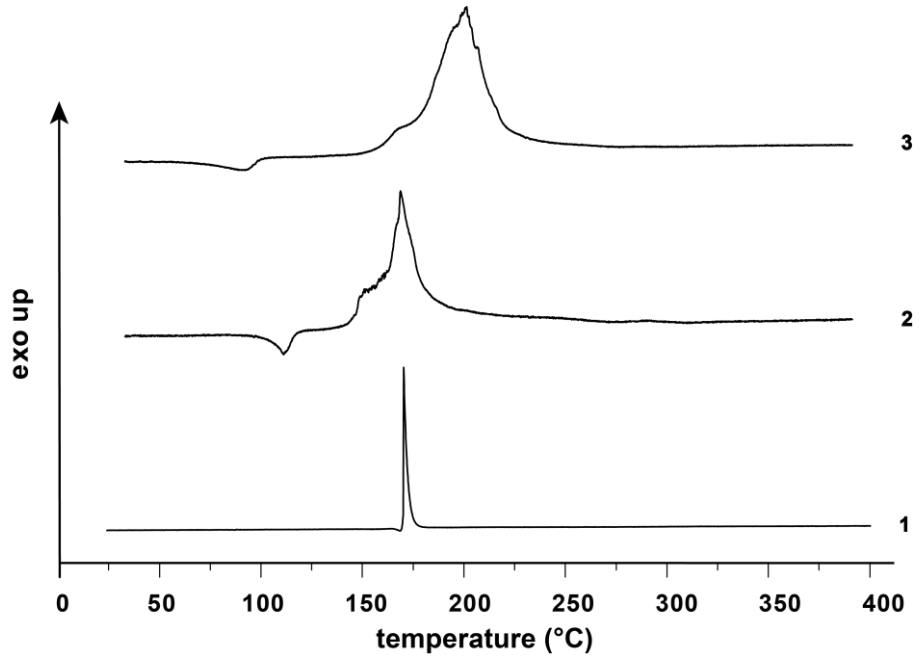

Figure S33. DTA measurements of **1** to **3** with a heating rate of 5°C min^{-1}.

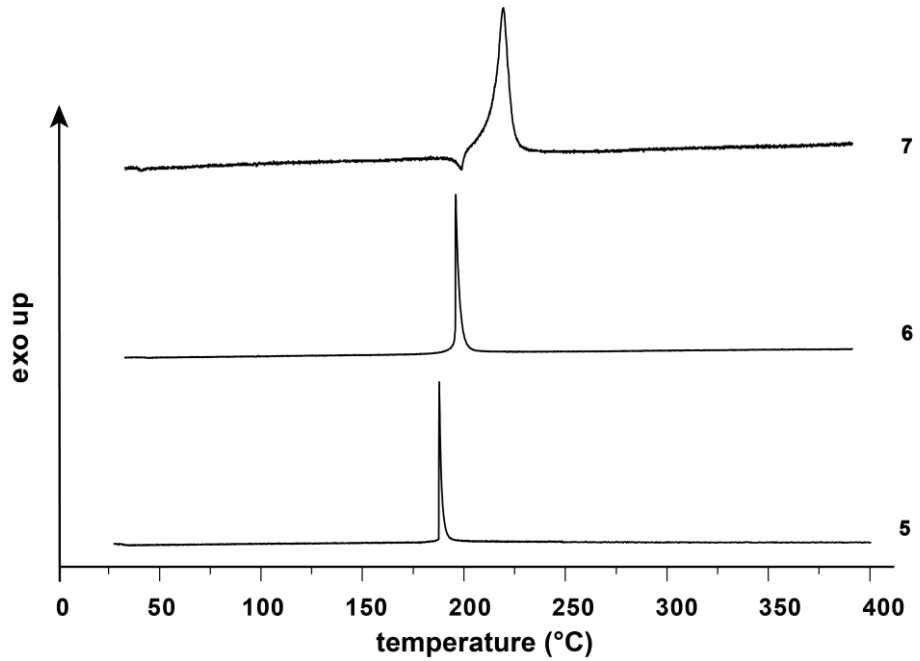

Figure S34. DTA measurements of **5** to **7** with a heating rate of 5°C min^{-1}.

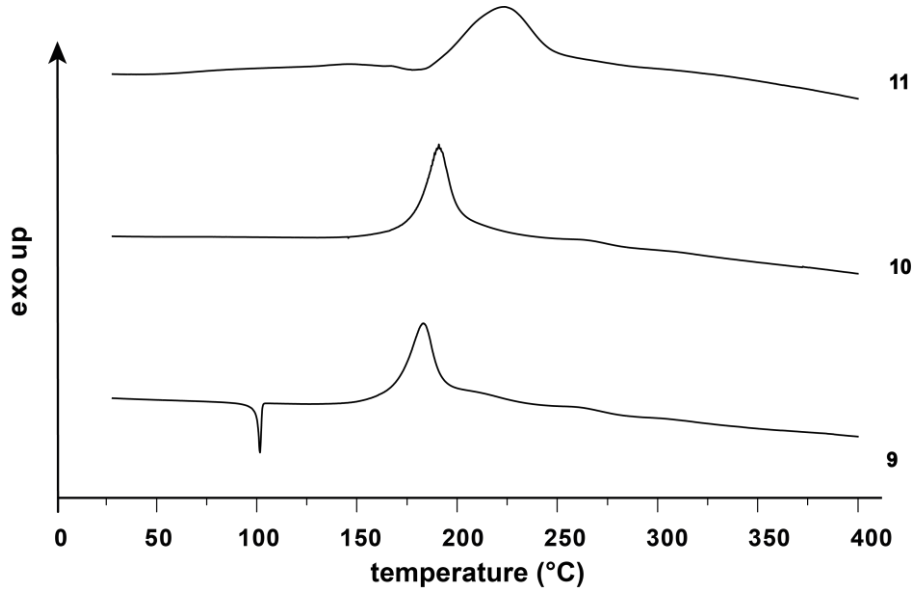

Figure S35. DTA measurements of **9** to **11** with a heating rate of 5°C min^{-1}.

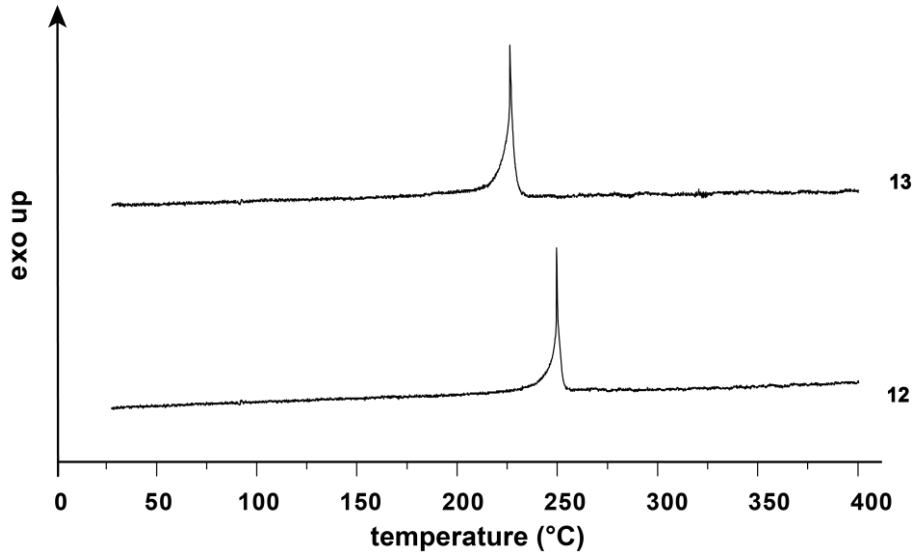

Figure S36. DTA measurements of **12** and **13** with a heating rate of 5°C min^{-1}.

9.6.5 TGA Measurements

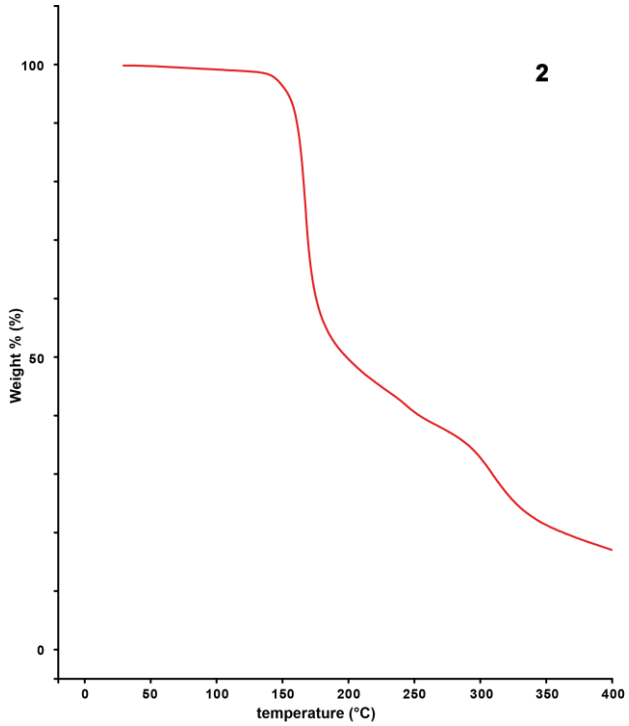

Figure S37. TGA measurement of **2** with a heating rate of 5°C min^{-1}.

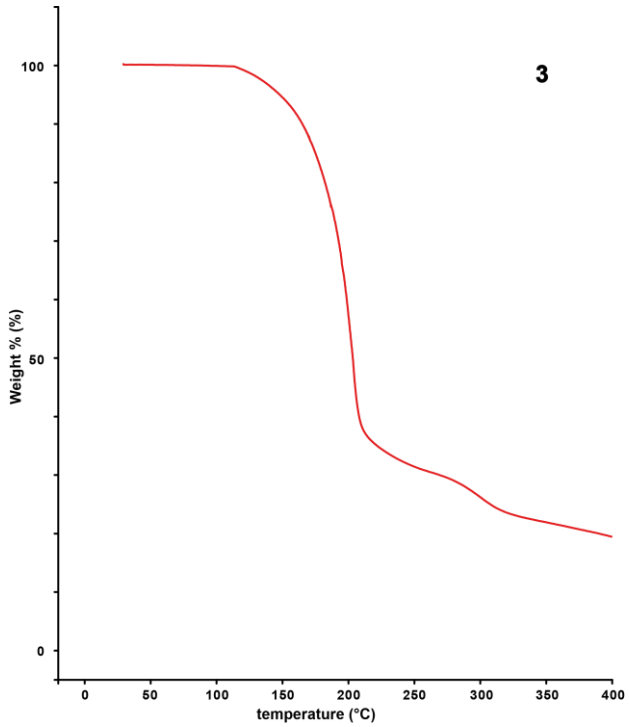

Figure S38. TGA measurement of **3** with a heating rate of 5°C min^{-1}.

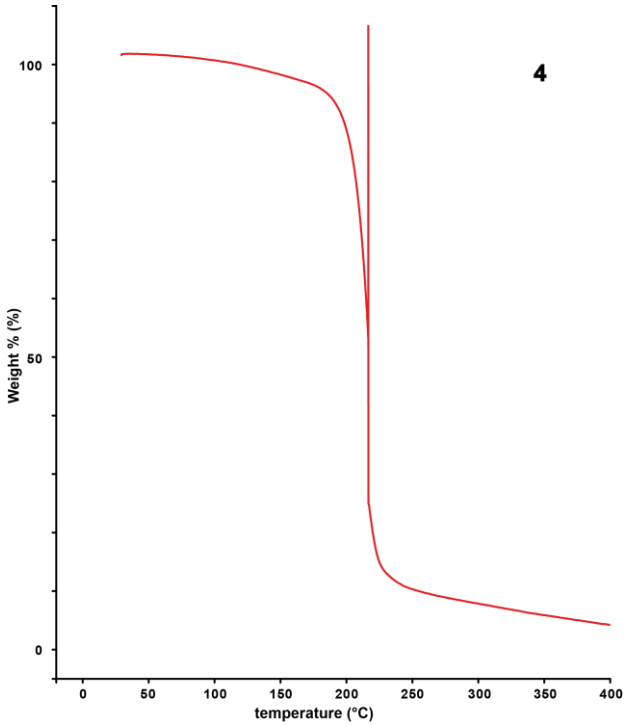

Figure S39. TGA measurement of **4** with a heating rate of 5°C min^{-1}.

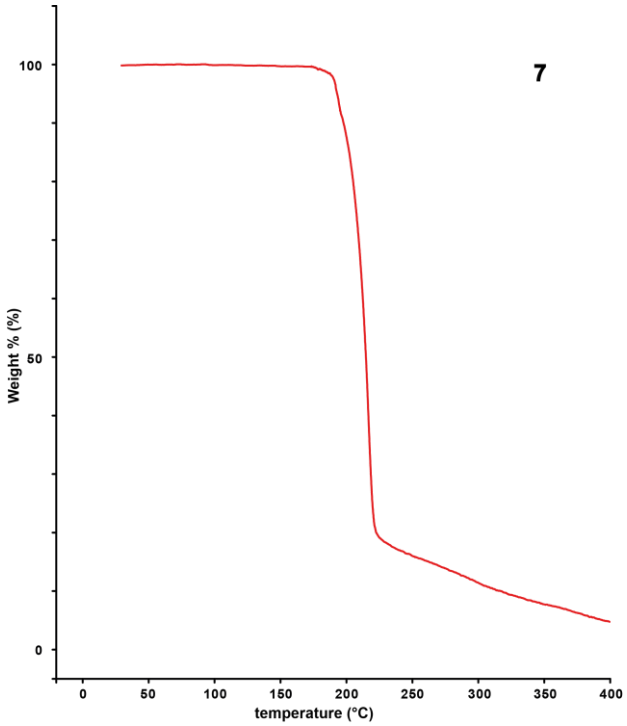

Figure S40. TGA measurement of **7** with a heating rate of 5°C min^{-1}.

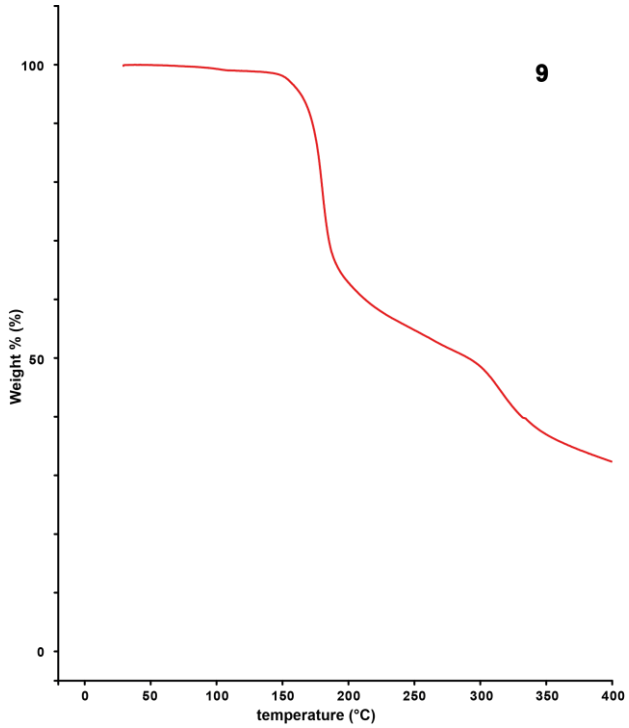

Figure S41. TGA measurement of **9** with a heating rate of 5°C min^{-1}.

9.6.6 X-Ray Diffraction

For all crystalline compounds, an Oxford Xcalibur3 diffractometer with a CCD area detector or Bruker D8 Venture TXS diffractometer equipped with a multilayer monochromator, a Photon 2 detector, and a rotating-anode generator was employed for data collection using Mo-Kα radiation (λ = 0.71073 Å). On the Oxford device, data collection and reduction were carried out using the CRYSALISPRO software.[7] On the Bruker diffractometer, the data were collected with the Bruker Instrument Service v3.0.21, the data reduction was performed using the SAINT V8.18C software (Bruker AXS Inc., 2011). The structures were solved by direct methods (SIR-92, [8] SIR-97[9] or SHELXT[9,10]) and refined by full-matrix least-squares on F2 (SHELXL[10,11]) and finally checked using the PLATON software[12] integrated into the WinGX[13] software suite. The non-hydrogen atoms were refined anisotropically and the hydrogen atoms were located and freely refined. The absorptions were corrected by a SCALE3 ABSPACK or SADABS Bruker APEX3 multiscan method. [14] All DIAMOND2 plots are shown with thermal ellipsoids at the 50 % probability level and hydrogen atoms are shown as small spheres of arbitrary radius.

Table S1. Crystallographic data and structure refinement of **1** and **3**.

	1	**3**
Formula	$C_4H_6N_{10}O_2$	$C_4H_6N_{10}O_2$
FW [g mol^{-1}]	226.19	226.19
Crystal system	monoclinic	monoclinic
Space group	$P2_1/c$	$P2_1/c$
Color / Habit	colorless plate	colorless plate
Size [mm]	0.20 x 0.50 x 0.50	0.05 x 0.30 x 0.30
a [Å]	12.8542 (6)	12.1943 (19)
b [Å]	6.3562 (3)	5.0811 (5)
c [Å]	10.9768 (5)	14.5457 (14)
α [°]	90	90
β [°]	104.966 (5)	101.525 (12)
γ [°]	90	90
V [Å^3]	866.43 (7)	883.09 (19)
Z	4	4
$\rho_{calc.}$ [g cm^{-3}]	1.734	1.701
μ [mm^{-1}]	0.143	0.141
F(000)	464	464
$\lambda_{MoK\alpha}$ [Å]	0.71073	0.71073
T [K]	96	111
θ Min-Max [°]	3.3, 26.4	2.9, 26.4
Dataset	-16: 15 ; -7: 7 ; -13: 13	-15: 15; -6: 6; -18: 18
Reflections collected	6934	7280
Independent refl.	1757	1807
R_{int}	0.024	0.046
Observed reflections	1546	1361
Parameters	169	169
R_1 (obs)[a]	0.0282	0.0404
wR_2 (all data)[b]	0.0714	0.1001
S [c]	1.03	1.04
Resd. dens [e Å^{-3}]	-0.22, 0.20	-0.21, 0.23
Device type	Xcalibur Sapphire 3	Xcalibur Sapphire 3
Solution	SHELXT 2018/2	SHELXT 2018/2
Refinement	ShelXL 2018/3	ShelXL 2018/3
Absorption correction	multi-scan	multi-scan
CCDC	2290727	2290728

[a] $R_1 = \Sigma||F_0|-|F_c||/\Sigma|F_0|$; [b] $wR_2 = [\Sigma[w(F_0^2-F_c^2)^2]/\Sigma[w(F_0)^2]]^{1/2}$; $w = [\sigma c^2(F_0^2)+(xP)^2+yP]^{-1}$ and $P=(F_0^2+2F_c^2)/3$; [c] $S = \{\Sigma[w(F_o^2-F_c^2)^2]/(n-p)\}^{1/2}$ (n = number of reflections; p = total number of parameters).

Table S2. Crystallographic data and structure refinement of **4**, **7** and **9**.

	4	**7**	**9**
Formula	$C_4H_4N_{12}O_6$	$C_6H_{10}N_{14}O_6$	$C_4H_6N_8O$
FW [g mol^{-1}]	316.19	374.28	182.15
Crystal system	monoclinic	monoclinic	orthorhombic
Space group	*Cc*	$P2_1/c$	$P2_12_12_1$
Color / Habit	colorless plate	colorless plate	colorless needle
Size [mm]	0.05 x 0.30 x 0.50	0.02 x 0.16 x 0.20	0.50 x 0.10 x 0.05
a [Å]	6.3565(4)	24.186(2)	6.5903(6)
b [Å]	18.1936(16)	9.0198(8)	10.6310(8)
c [Å]	9.3762(7)	6.4985(6)	10.9678(8)
α [°]	90	90	90
β [°]	90.735(7)	94.060(4)	90
γ [°]	90	90	90
V [Å^3]	1084.25(14)	1414.1(2)	768.42(11)
Z	4	4	4
$\rho_{calc.}$ [g cm^{-3}]	1.937	1.758	1.575
μ [mm^{-1}]	0.177	0.154	0.12
F(000)	640	768	376
$\lambda_{MoK\alpha}$ [Å]	0.71073	0.71073	0.71073
T [K]	100	173	91
θ Min-Max [°]	2.2, 30.5	2.5, 26.4	3.8, 29.0
Dataset	-9: 9 ; -25: 25 ; -12: 13	-30: 30 ; -11: 11 ; -8: 8	-9: 9 ; -15: 15 ; -15: 15
Reflections collected	6276	22471	14111
Independent refl.	2913	2762	2282
R_{int}	0.025	0.076	0.045
Observed reflections	2640	2271	1921
Parameters	215	275	143
R_1 (obs)[a]	0.0326	0.0912	0.0446
wR_2 (all data)[b]	0.0659	0.1987	0.0755
S [c]	1.03	1.22	1.08
Resd. dens [e Å^{-3}]	-0.18, 0.25	-0.38, 0.38	-0.22, 0.21
Device type	Xcalibur Sapphire 3	Bruker D8 Venture TXS	Xcalibur Sapphire 3
Solution	SHELXT 2018/2	SHELXT 2018/2	SHELXT 2018/2
Refinement	ShelXL 2018/3	ShelXL 2018/3	ShelXL 2018/3
Absorption correction	multi-scan	multi-scan	multi-scan
CCDC	2290729	2290730	2290731

[a] $R_1 = \Sigma||F_0|-|F_c||/\Sigma|F_0|$; [b] $wR_2 = [\Sigma[w(F_0^2-F_c^2)^2]/\Sigma[w(F_0)^2]]^{1/2}$; $w = [\sigma c^2(F_0^2)+(xP)^2+yP]^{-1}$ and $P=(F_0^2+2F_c^2)/3$; [c] $S = \{\Sigma[w(F_o^2-F_c^2)^2]/(n-p)\}^{1/2}$ (n = number of reflections; p = total number of parameters).

9.6.7 Heat of Formation Calculations

All quantum chemical calculations were carried out using the Gaussian G09 program package.[15] The enthalpies (H) and free energies (G) were calculated using the complete basis set (CBS) method of *Petersson* and coworkers to obtain very accurate energies.[16] The CBS models are using the known asymptotic convergence of pair natural orbital expressions to extrapolate from calculations using a finite basis set to the estimated CBS limit. CBS-4 starts with an HF/3-21G(d) geometry optimization; the zero-point energy is computed at the same level. It then uses a large basis set SCF calculation as base energy, and an MP2/6-31+G calculation with a CBS extrapolation to correct the energy through second order. A MP4(SDQ)/6-31+(d,p) calculation is used to approximate higher-order contributions. In this study, we applied the modified CBS-4M method.
Heats of formation were calculated using the atomization method (Equation S1) using room temperature CBS-4M enthalpies, which are summarized in Table S3.[16]

$$\Delta_f H^\circ_{(g,\,M,\,298)} = H_{(Molecule,\,298)} - \sum H^\circ_{(Atoms,\,298)} + \sum \Delta_f H^\circ_{(Atoms,\,298)} \quad (S1)$$

Table S3. CBS-4M enthalpies for atoms C, H, N, and O and their literature values for atomic $\Delta H^\circ_f 298$ / kJ mol−1.

	–*H*298 / a.u.	NIST
H	0.500991	218.2
C	37.786156	717.2
N	54.522462	473.1
O	74.991202	249.5

The standard molar enthalpy of formation were calculated using $\Delta_f H(g)$ subtracting the enthalpy of sublimation estimated by applying Trouton´s rule.[17]

9.6.8 Calculation of Energetic Performance Parameters

The detonation parameters were calculated with the EXPLO5 (version 6.06.01) computer code.[18] This calculation code is based on the steady-state model of equilibrium and uses the Becker–Kistiakowski–Wilson equation of state.[19] It calculates the detonation parameters at the Chapman–Jouguet (CJ) point, which itself is found from the Hugoniot curve of the system by its first derivative. These calculations are based on the density recalculated from the corresponding crystal densities by Equation S2 (av = 1.5x10^{-4} K) and on the calculated enthalpies of formation.

$$d_{298K} = \frac{d_T}{1+ \alpha_v(298-T_0)} \quad \text{(S2)}$$

d_T = insert X-ray density in g cm^{-3}
T_0 = insert X-Ray temperature in K
α_v = correction factor

Table S4. X-Ray and recalculated densities of **1**, **3**, **6** and **7**.

	X-Ray density [g cm^{-3}]	Density re-calculated to 298 K value [g cm^{-3}]
1	(@ 96 K) 1.734	1.68
3	(@ 111 K) 1.701	1.66
4	(@ 100 K) 1.937	1.88
7	(@ 173 K) 1.758	1.73
9	(@ 91 K) 1.575	1.53

9.6.9 Magnetic Properties

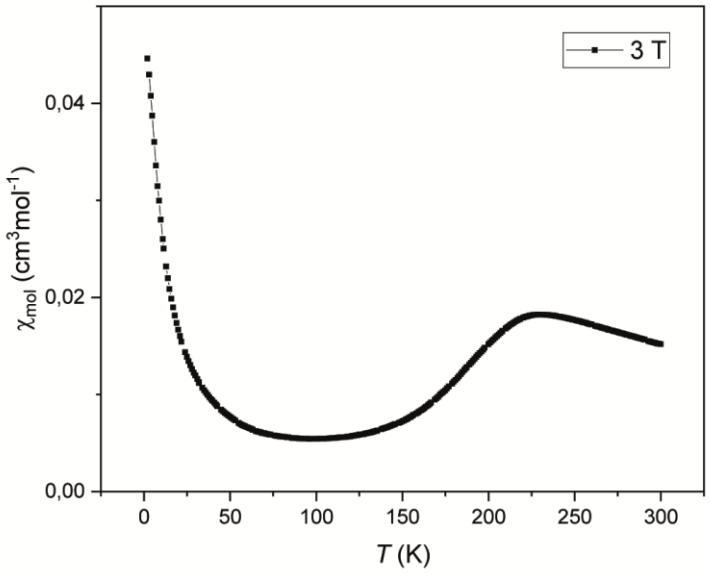

Figure S42. Molar magnetic susceptibility of $[Fe(ClO_4)_2(1,1'\text{-}TNP)_4]$ as a function of temperature.

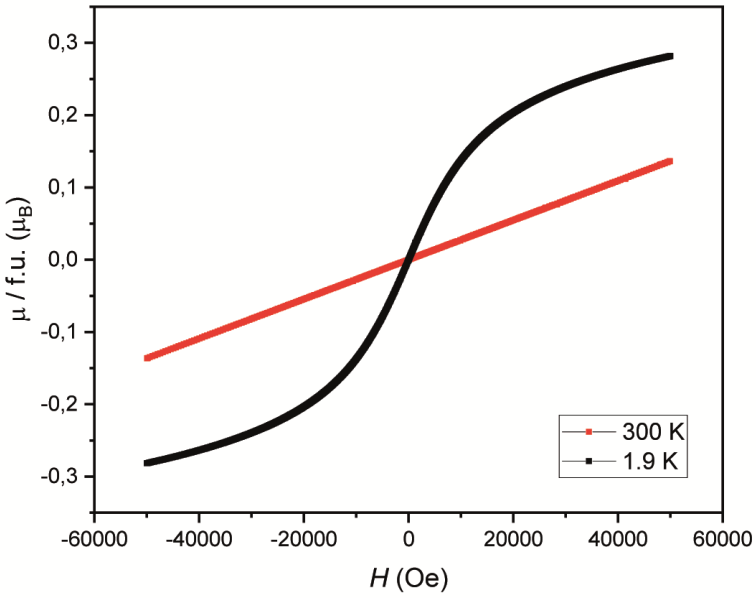

Figure S43. Magnetization isotherms of $[Fe(ClO_4)_2(1,1'\text{-}TNP)_4]$ at 300 K (red) and 1.9 K (black) per formula unit.

9.6.10 References SI

[S1] NATO standardization agreement (STANAG) on explosives, impact sensitivity tests, no. 4489, 1st ed, Sept. 17, **1999**.

[S2] WIWEB-Standardarbeitsanweisung 4-5.1.02, Ermittlung der Explosionsgefährlichkeit, hier der Schlagempfindlichkeit mit dem Fallhammer. Nov. 8, **2002**.

[S3] "http://www.bam.de", accessed March **2022**.

[S4] NATO standardization agreement (STANAG) on explosive, friction sensitivity tests. no. 4487, 1st ed., Aug. 22, **2002**.

[S5] WIWEB-Standardarbeitsanweisung 4-5.1.03, Ermittlung der Explosionsgefährlichkeit oder der Reibeempfindlichkeit mit dem Reibeapparat. Nov. 8, **2002**.

[S6] Impact: insensitive > 40 J, less sensitive ≥ 35 J, sensitive ≥ 4 J, very sensitive ≤ 3 J, Friction: insensitive > 360 N, less sensitive = 360 N, sensitive < 360 N and > 80 N, very sensitive ≤ 80 N, extremely sensitive ≤ 10 N. According to the UN Recommendations on the Transport of Dangerous Goods, (+) indicates not safe for transport.

[S7] CrysAlisPro, Oxford Diffraction Ltd., version 171.33.41, **2009**.

[S8] A. Altomare, G. Cascarano, C. Giacovazzo, A. Guagliardi, *J. Appl. Crystallogr* **1993**, *26*, 343−350.

[S9] a) A. Altomare, G. Cascarano, C. Giacovazzo, A. Guagliardi, A. G. G. Moliterni, SIR97 **1997**; b) A. Altomare, M. C. Burla, M. Camalli, G. L. Cascarano, C. Giacovazzo, A., *J. Appl. Crystallogr*. **1999**, *32*, 115−119.

[S10] G. M. Sheldrick, *Acta Crystallogr. Sect. A* **2008**, *A64*, 112−122.

[S11] G. M. Sheldrick, SHELXL-97, Program for the Refinement of Crystal, University of Göttingen, Germany, **1997**.

[S12] A. L. Spek, PLATON, A Multipurpose Crystallographic Tool, Utrecht University **1999**.

[S13] L. J. Farrugia, *J. Appl. Cryst.* **2012**, *45*, 849−854.

[S14] a) Empirical absorption correction using spherical harmonics, implemented in SCALE3 ABSPACK scaling algorithm (CrysAlisPro Oxford Diffraction Ltd., Version 171.33.41, 2009); b) APEX3. Bruker AXS Inc., Madison, Wisconsin, USA.

[S15] M. J. Frisch, G. W. Trucks, H. B. Schlegel, G. E. Scuseria, M. A. Robb, J. R. Cheeseman, G. Scalmani, V. Barone, B. Mennucci, G. A. Petersson, H. Nakatsuji, M. Caricato, X. Li, H.P. Hratchian, A. F. Izmaylov, J. Bloino, G. Zheng, J. L. Sonnenberg, M. Hada, M. Ehara, K. Toyota, R. Fukuda, J. Hasegawa, M. Ishida, T. Nakajima, Y. Honda, O. Kitao, H. Nakai, T. Vreven, J. A. Montgomery, Jr., J. E. Peralta, F. Ogliaro, M. Bearpark, J. J. Heyd, E. Brothers, K. N. Kudin, V. N. Staroverov, R. Kobayashi, J. Normand, K. Raghavachari, A. Rendell, J. C. Burant, S. S. Iyengar, J. Tomasi, M. Cossi, N. Rega, J. M. Millam, M. Klene, J. E. Knox, J. B. Cross, V. Bakken, C. Adamo, J. Jaramillo, R. Gomperts, R. E. Stratmann, O. Yazyev, A. J. Austin, R. Cammi, C. Pomelli, J. W. Ochterski, R. L. Martin, K. Morokuma, V. G. Zakrzewski, G. A. Voth, P. Salvador, J. J. Dannenberg, S. Dapprich, A. D. Daniels, O. Farkas, J.B. Foresman, J. V. Ortiz, J. Cioslowski, D. J. Fox, Gaussian 09 A.02, Gaussian, Inc., Wallingford, CT, USA, **2009**.

[S16] a) J. W. Ochterski, G. A. Petersson, and J. A. Montgomery Jr., *J. Chem. Phys.* **1996**, *104*, 2598−2619; b) J. A. Montgomery Jr., M. J. Frisch, J. W. Ochterski G. A. Petersson, *J. Chem. Phys.* **2000**, *112*, 6532−6542; c) L. A. Curtiss, K. Raghavachari, P. C. Redfern, J. A. Pople, *J. Chem. Phys.* **1997**, *106*, 1063−1079; d) E. F. C. Byrd, B. M. Rice, *J. Phys. Chem. A* **2006**, *110*, 1005–1013; e) B. M. Rice, S. V. Pai, J. Hare, *Comb. Flame* **1999**, *118*, 445–458.

[S17] F. Trouton, *Philos. Mag.* (1876-1900) **1884**, *18*, 54-57; b) M. S. Westwell, M. S. Searle, D. J. Wales, D. H. Willimas, *J. Am. Chem. Soc.* **1995**, *117*, 5013-5015.

[S18] M. Sućeska, EXPLO5 V6.06.01, Zagreb (Croatia) **2021**.

[S19] M. Sućeska, *Propellants, Explos., Pyrotech.* **1991**, *16*, 197–202.

10 Investigation of a New Promising Process for the RDX Synthesis via 1,3,5-Triacetyl-1,3,5-Triazinane (TRAT)

Thomas M. Klapötke*, Jasmin T. Lechner, Leon W. B. Stanislawski, Jörg Stierstorfer, Moritz Mühlemann and Guillaume Lemarchand

as published in *Propellants Explosives and Pyrotechnics* **2023**, *48*, e202300062

DOI: 10.1002/prep.202300062

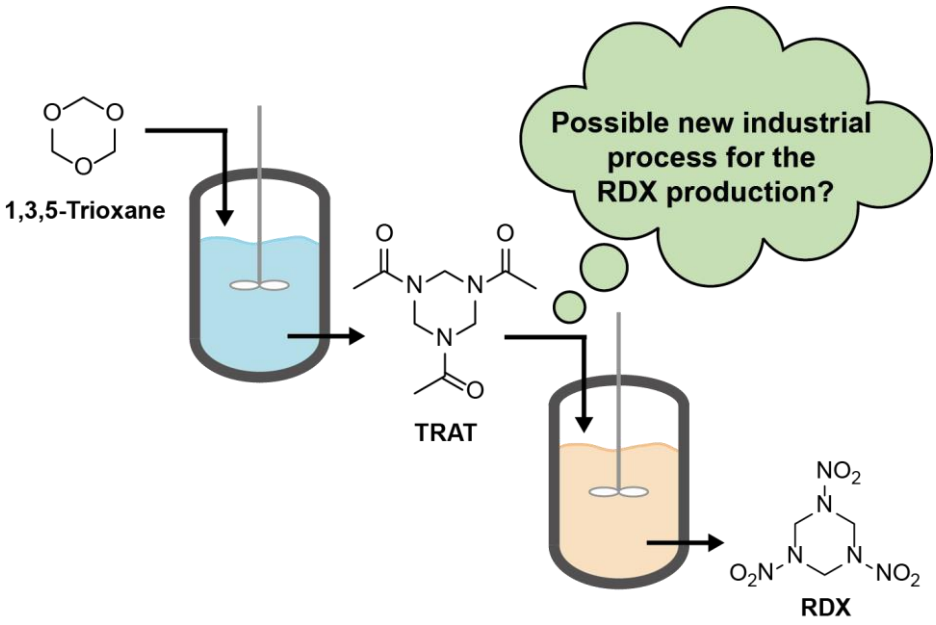

Abstract: Despite intensive research for possible replacements, RDX (1,3,5-trinitro-1,3,5-triazinane) is still considered to be one of the most important energetic materials because of its versatile application. Due to the high demand for RDX, optimization of synthesis and development of new methods are of great interest to both academia and industry. Therefore, in this work, the synthesis of RDX *via* the intermediate TRAT (1,3,5-triacetycl-1,3,5-triazinane) was investigated as a possible alternative industrial production method. In addition to the synthesis of TRAT starting from 1,3,5 trioxane, various feasible nitration methods from TRAT to RDX were investigated. Moreover, the suitability for large-scale production, the comparison of already established methods and the feasibility of a new flow process were discussed.

10.1 Introduction

In the context of its main application as military explosive, it is surprising that RDX was developed and patented as a urinary antiseptic. In 1899, Henning first synthesized RDX by the reaction of nitric acid with the previously known urinary antiseptic hexamine [1]. Its explosive properties and structure were not recognized until more than two decades later and arouse the interest of the military research establishments of several nations in the 1930s. With the start of World War II research in its production proliferated and the compound received various trivial names [2]. In the United Kingdom it was referred to as RDX, in the USA as cyclonite, in Germany as Hexogen and in Italy as T4 [3, 4]. Documentation reveals, that in 1941 the British began the large-scale production of RDX to meet the demand for a more powerful explosive than TNT (2,4,6-trinitrotoluene) on the battlefield [5]. For this the Woolwich method was applied, which is based on the treatment of hexamine with concentrated nitric acid [6]. Later that year, the USA started the industrial production utilizing the same method and proceeded the research in more efficient methods [5]. The following year, the Bachmann process was introduced, substantially reducing the required nitric acid and increasing the quantity of produced RDX content [7, 8]. Through this synthesis route the higher homologue 1,3,5,7-tetranitro-1,3,5,7-tetraazacyclooctane (high melting explosive, HMX) was first received [3, 9]. The Bachmann process, in contrast to the Woolwich

process, always yields a mixture of RDX with up to 19 % of HMX [10, 11]. Octogen (HMX) exhibits a higher density, melting point and detonation performance than Hexogen (RDX) [12]. However, due to its lower production cost, RDX is used predominantly. With regard to the global RDX market, its market size value in 2021 was reported to be 12.1 billion USD and it is predicted to reach 15.4 billion USD by 2030 [13]. The RDX market can be segmented among others by application or by type of use as shown in Figure 1 [14].

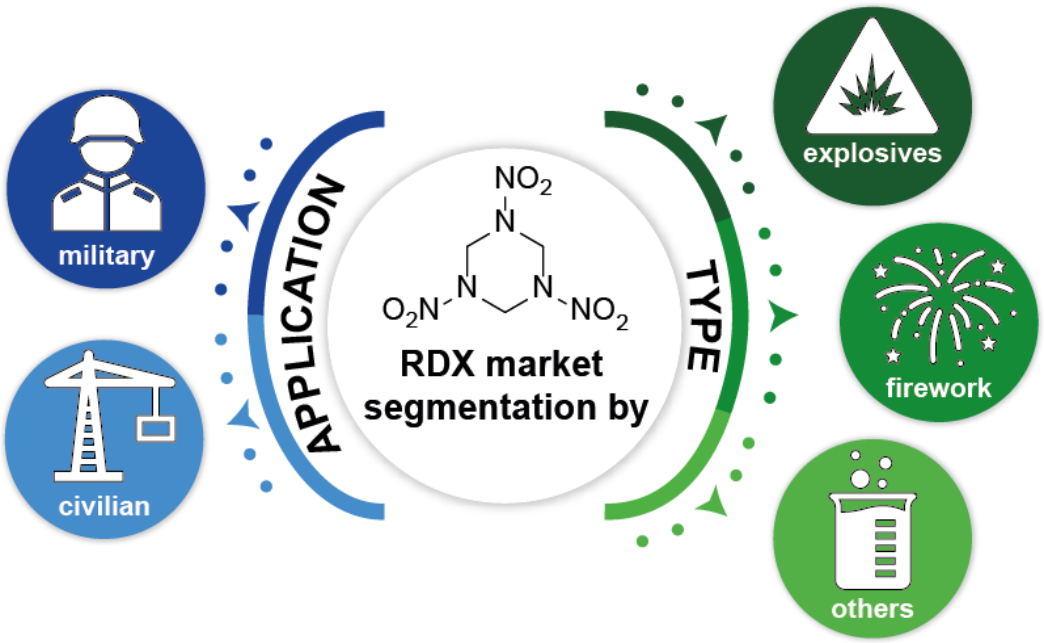

Figure 1. Different ways of RDX market segmentation.

The areas of application are divided into the civilian and military sectors, whereby the military sector dominates with a proportion of approximately 80 % [13, 14]. In the civil sector, RDX is mainly used in the construction and mining industries [13, 14]. Whereas in the military sector RDX is used for various applications, e. g. in its phlegmatized form in war heads and bombs or in propellant formulations (e. g. EX-99) [3, 15, 16]. Moreover, to reduce the risk of accidental detonation, RDX is often used in combination with a binder in plastic-bonded explosives (PBX) or with TNT as a less sensitive explosive, in an effort to desensitize the explosive charge. Examples of such explosive formulations are Composition A (RDX/Wax), Composition B (RDX/TNT/Wax) or the popular formulation Composition C4 (RDX/polyisobutylene) [3]. Dividing the RDX market by type of use, it can be split

into explosives, fireworks and others [17]. However, all these sectors are ongoingly increasing due to the growth of the defence, industrial and construction industries [13, 14].

Due to the high demand of RDX, synthesis optimization and the development of novel methods are of great interest by the scientific community and industry. Nowadays, there are various synthesis routes towards RDX known, [18, 19] Figure 2 shows the Bachmann and the Woolwich process, which are still used for industrial RDX synthesis in a continuous process with CSTR (continuous-stirred tank reactor) [20] systems.

Bachmann process for RDX synthesis:

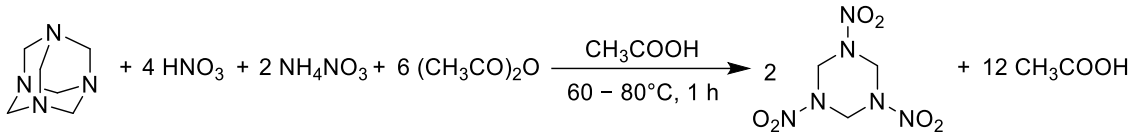

Woolwich process for RDX synthesis:

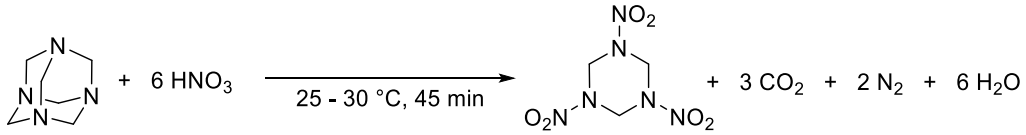

Figure 2. Industrial used processes for RDX synthesis.

In this work, the synthesis of RDX *via* the intermediate TRAT (1,3,5-triacetycl-1,3,5-triazinane) was investigated as a possible alternative industrial production method. This is of particular interest since in the literature this reaction pathway has been proposed as a continuous flow synthesis [21]. Due to the advantages in terms of safety and efficiency, the use of a continuous processes for the potential production of HEDMs (high energy dense material) is always preferable and therefore this possible new process attracted considerable interest in academia and industry[20, 22].

10.2 Experimental Section

All chemicals and solvents were employed as received. ^{1}H NMR spectra were recorded with neat solids as samples at ambient temperature using a Bruker TR 400 instrument. The chemical shifts quoted in ppm in the text refer to typical standards such as tetramethylsilane (^{1}H). All NMR spectra were analyzed with the software Mestrenova from Mestrelab Research S. L. Atom labelling and nomenclature are not in correspondence with IUPAC.

CAUTION! All investigated compounds and mixtures are potentially explosive energetic materials, which show partly increased sensitivities towards various stimuli (e. g. elevated temperatures, impact, friction, or electrostatic discharge). Therefore, proper security precautions (safety glass, face shield, earthed equipment and shoes, leather coat, Kevlar gloves, Kevlar sleeves, and ear plugs) have to be applied while synthesizing and handling the described compounds.

10.2.1 Synthesis of 1,3,5-Triacetycl-1,3,5-triazinane (TRAT)

TRAT was synthesized according to a modified literature procedure[23]. Ten drops of conc. sulphuric acid where added to acetonitrile (7.90 mL) and the mixture was heated to 50 °C. Trioxane (2.70 g, 30.0 mmol) was added slowly to the warm reaction mixture. Following 30 s of stirring, when a precipitate was visible, the reaction was rapidly cooled down with an ice bath mixed with NaCl. The reaction mixture was stirred for 30 min at 0 °C and NaOH (2 M, 5.00 mL) was added resulting in a large amount of colourless precipitate. The precipitate was isolated by filtration and was washed with ethyl acetate (100 mL). 1,3,5-Triacetycl-1,3,5-triazinane (3.20 g, 15.0 mmol, 50 %) was obtained as a colourless solid.

1,3,5-Triacetyl-1,3,5-triazinane (TRAT)

^{1}H NMR (400 MHz, DMSO-D_6, ppm) δ=5.21 (s, 6H, −CH_2−), 2.12 (s, 9H, −CH_3).

1,3,5,7-Tetraacetyl-1,3,5,7-tetrazocinane (TAT)

^{1}H NMR (400 MHz, DMSO-D_6, ppm) δ=4.99 (s, 8H, −CH_2−), 2.14 (s, 12H, −CH_3).

10.2.2 Nitration Attempts

Nitration of TRAT with HNO_3

TRAT (250 mg, 1.17 mmol) was added gradually while ice cooling to fuming nitric acid (15 mL, 360 mmol, 300 eq.). Following the complete addition, the ice bath was removed and stirred for 1 h at room temperature. The nitration mixture was then quenched on ice. No precipitation was observed and no product was obtained.

Nitration of TRAT with mixed acid (H_2SO_4/HNO_3)

Fuming nitric acid (9 mL, 215 mmol) was added gradually to concentrated sulfuric acid (6 mL, 112 mmol) while ice cooling. TRAT (250 mg, 1.17 mmol) was added slowly under cooling. Following the complete addition, the ice bath was removed and stirred for 1 h at room temperature. The nitration mixture was then quenched on ice. No precipitation was observed and no product was obtained.

Nitration of TRAT with N_2O_5

N_2O_5 (380 mg, 3.51 mmol, 3.00 eq.) was weighted under nitrogen and immediately dissolved in MeCN (10 mL). Parallel TRAT (250 mg, 1.17 mmol) was pre-dissolved in MeCN (10 mL) and added under cooling. Following the complete addition, the ice bath was removed. The reaction mixture was stirred for 1 h at room temperature, poured into a crystallization dish and allowed to evaporate overnight. A mixture of RDX and DANT as colorless oil was obtained.

1,3,5-Trinitro-1,3,5–triazinane (RDX)

^{1}H NMR (400 MHz, DMSO-D_6, ppm) δ=6.14 (s, 6H, −CH_2−).

1,3-Diacetyl-5-nitro-1,3,5-triazinane (DANT)

^{1}H NMR (400 MHz, DMSO-D_6, ppm) δ=5.64 (s, 4H, −CH_2−), 5.22 (s, 2H, −CH_2−), 2.12 (s, 6H, −CH_3).

Nitration of TRAT with TFAA & HNO_3

TRAT (1.4 g, 4.61 mmol) was dissolved in TFAA (15.5 g, 73.80 mmol) then fuming nitric acid (3.0 g, 2.0 mL) was added dropwise while cooling with a water bath (with a bit of ice). The water bath was removed and it was stirred for 1 h at room temperature. After that, the reaction mixture was quenched on ice water and the

precipitation was filtrated. A mixture of RDX and ADNT was obtained as a colorless solid.

1,3,5-Trinitro-1,3,5–triazinane (RDX)

^{1}H NMR (400 MHz, DMSO-D_6, ppm) δ=6.13 (s, 6H, −CH_2−).

5-Acetyl-1,3-dinitro-1,3,5-triazinane (ADNT)

^{1}H NMR (400 MHz, DMSO-D_6, ppm) δ=6.10 (s, 2H, −CH_2−), 5.63 (s, 4H, −CH_2−), 2.17 (s, 3H, −CH_3).

10.3 Results and Discussion

10.3.1 Synthesis

TRAT was synthesized according to a minimally modified method of Meng *et al*. (Scheme 1) [23].

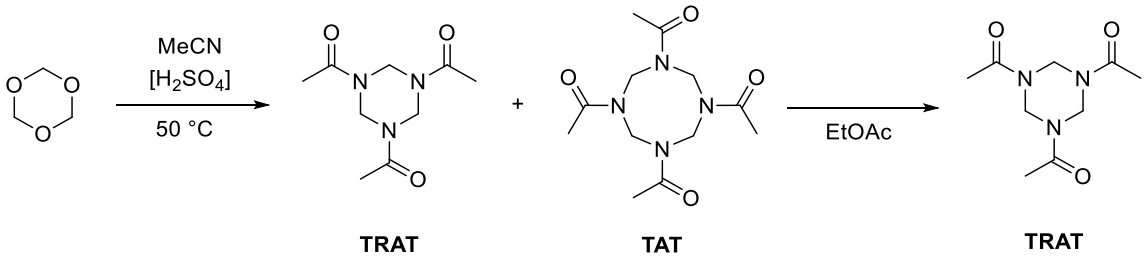

Scheme 1. Synthesis route towards TRAT and TAT starting from trioxane.

The mechanism of this reaction is also known from the literature [24]. Trioxane first undergoes a tautomeric reaction to form formaldehyde. The presence of acid then protonates formaldehyde to form its oxonium cation, which is in equilibrium with its carbocation. This reacts then with acetonitrile in a condensation reaction and after cyclization, TRAT is formed. However, not only the six-membered ring derivative was obtained, but also traces of the eight-membered ring compound TAT (1,3,5,7-tetraacetycl-1,3,5,7-tetrazocinane) were detected. TRAT could easily be isolated in 50 % yield by filtration and washing with a large amount of EtOAc. Purification by simple washing is possible because TAT and TRAT have different solubilities in EtOAc [21].

In the effort to find suitable nitration methods for the nitrolysis of TRAT to RDX, four typical nitration protocols were investigated (Scheme 2). The first implemented protocol was the nitration with nitric acid (100 %) from which no product could be obtained, this was also the case for the nitration trial with mixed acid (40 % H_2SO_4/60 % HNO_3). In the third protocol, N_2O_5 in MeCN was used as a nitration agent and a mixture of RDX and the mononitrated 1,3-diacetyl-5-nitro-1,3,5-triazinane (DANT) could be obtained. The received DANT contained about 5 % of RDX. So, it can be stated that the nitrolysis by N_2O_5 under the examined conditions was not suited for the synthesis of RDX and DANT can be considered the main product of this reaction. Additionally, the presence of ammonium was observed in the NMR spectrum which was suspected to be a decomposition product stemming from the cleavage of the ring. The fourth implemented protocol with nitration using fuming nitric acid and trifluoroacetic acid anhydride (TFAA) resulted in a mixture of RDX and 5-acetyl-1,3-dinitroo-1,3,5-triazinane (ADNT). In this case 29 % RDX content was obtained which is better than in the third nitration trials but also not good enough for industrial application.

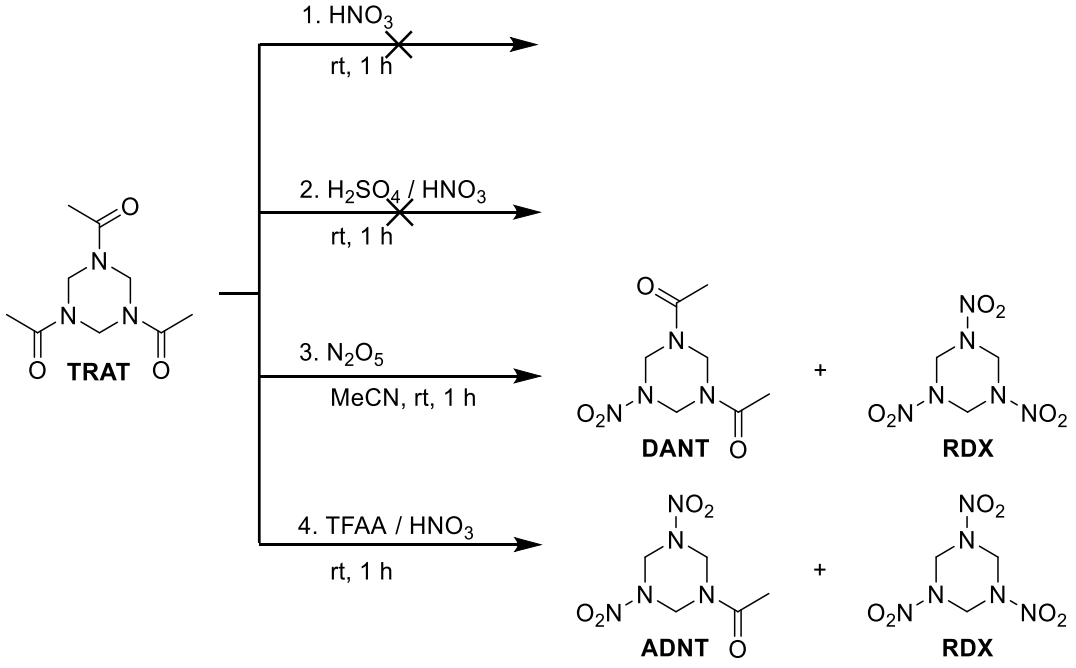

Scheme 2. Different nitration attempts of TRAT towards RDX.

In summary, it can be concluded that no optimal, inexpensive and simple way for the nitration of TRAT to RDX could be found. It can be seen that under almost

anhydrous conditions, as in protocols 3 and 4, product can be obtained, but in both cases complete conversion into the desired product is not possible. Even tests with longer reaction times or higher reaction temperatures could not improve this result.

10.3.2 NMR Characterization

The compounds were characterized by ^{1}H NMR spectroscopy. All compounds were measured in deuterated dimethyl sulfoxide (DMSO-D_6).

TRAT and TAT were identified in the crude ^{1}H NMR, see Figure 3. The singlet resonance at 5.21 ppm and 2.11 ppm can be assigned to the methylene (−CH_2) and methyl (−CH_3) groups TRAT. The remaining two singlet resonances at 4.99 ppm and 2.14 ppm can be assigned to the methylene (−CH_2) and methyl (−CH_3) groups of TAT. The amount of two signals per compound indicates the symmetrical property resulting in the magnetic equivalence of the -CH_2 and -CH_3 groups in both compounds. The ratio of compound TRAT to TAT can be determined by an equation (1) derived from the formula used to determine purities by *q*-NMR [25].

$$\%\text{m TRAT} = \frac{\frac{\text{NMR integral}_{TRAT}}{\text{number of protons}_{TRAT}} \times M_{TRAT}}{\frac{\text{NMR integral}_{TRAT}}{\text{number of protons}_{TRAT}} \times M_{TRAT} + \frac{\text{NMR integral}_{TAT}}{\text{number of protons}_{TAT}} \times M_{TAT}} \quad (\mathbf{1})$$

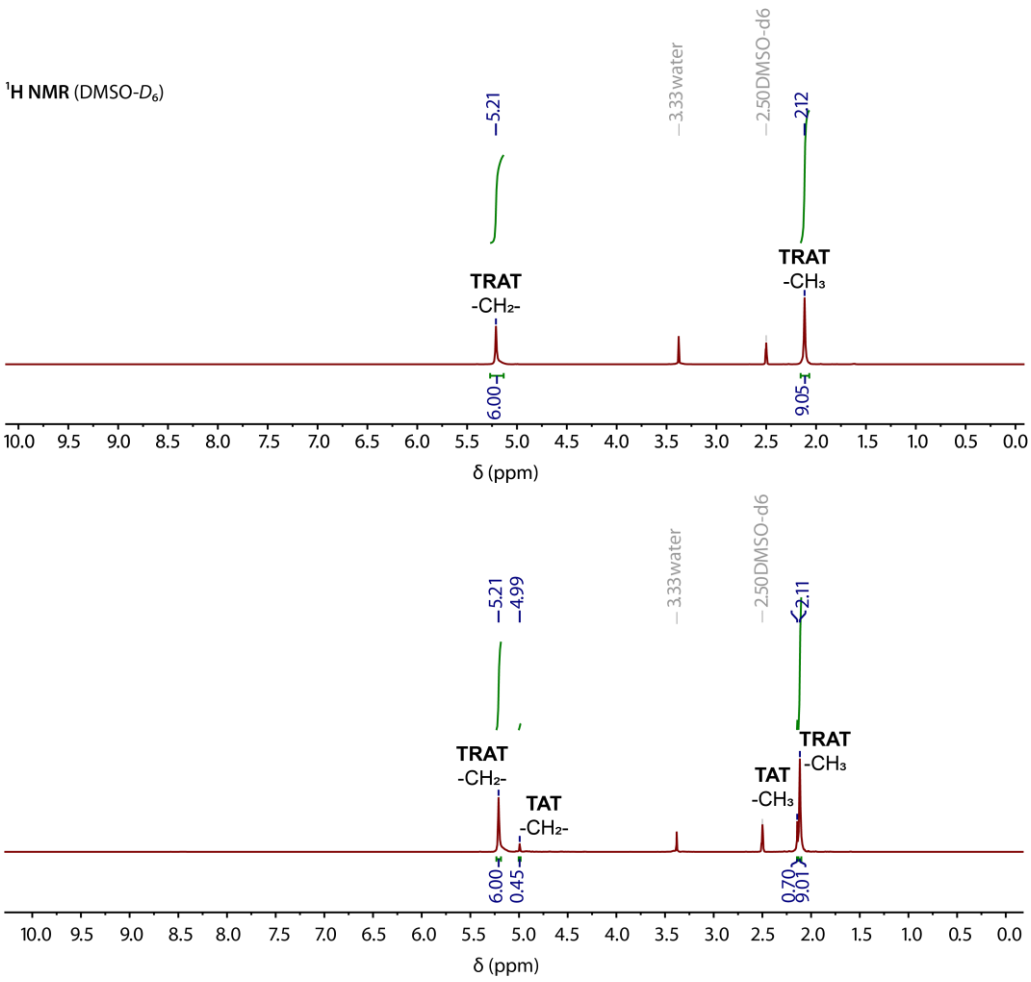

Figure 3. NMR spectra of TRAT and TAT.

The obtained crude product contained 93 % of TRAT and 7 % of TAT. Following washing with EtOAc, pure TRAT is visible in the measured ^{1}H NMR spectra.

The NMR spectra after the nitration trial with N_2O_5 shows different signals, see Figure 4. The singlet signal at 6.14 ppm can be assigned to the methylene group of RDX. While the singlet signal at 5.64 ppm can be assigned to the protons of the methylene groups in the alpha position to the nitro group of DANT. The singlet signal at 2.11 ppm can be assigned to the methyl groups of the acetyl moiety and the last singlet signal at 5.22 ppm is that of the protons from the methylene group in the alpha position to the carbonyl carbons. A ratio of 5 to 95 can be determined for RDX to DANT by a similar calculation like in equation 1 derived from the formula used to determine purities by *q*-NMR [25]. The triplet signal at 7.13 ppm can be identified as ammonium which indicates decomposition.

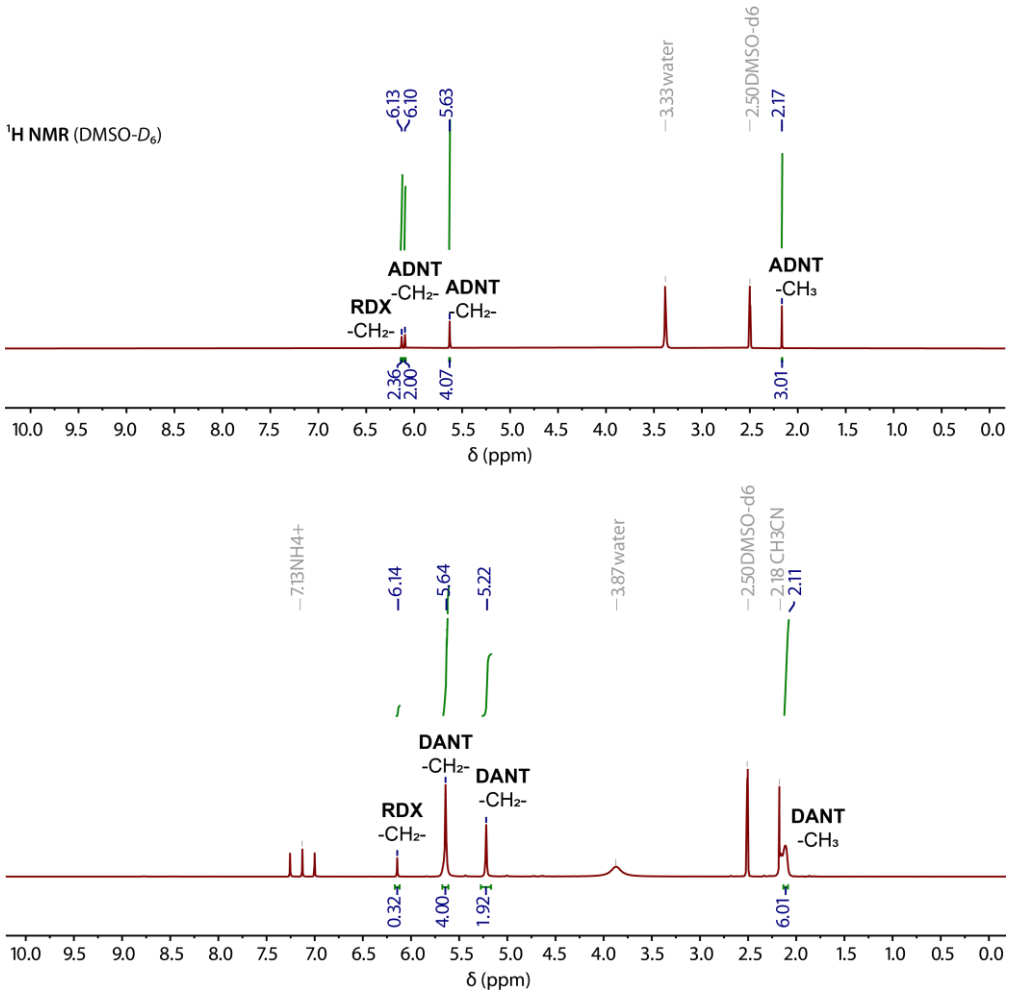

Figure 4. NMR spectra after the nitration trials 3 and 4.

After the nitration trial with TFAA and nitric acid, the NMR spectrum shows two compounds. The singlet signal at 6.13 ppm shows again RDX. While the other signals show the presence of ADNT. The singlet at 6.10 ppm can be assigned to the methylene group between the two nitro groups, and the singlet at 5.63 ppm belongs to the remaining two methylene groups from the trioxane ring between the acetyl and the nitro group. The last singlet at 2.17 ppm is from the methyl group of the acetyl moiety. Through the calculation of the ratio using the *q*-NMR formula a ratio of 71 % ADNT to 9 % RDX can be determined [25].

10.3.3 Crystal Structures

For the first time, the single crystal X-ray structure of TRAT tetrahydrate, DANT, and ADNT could be measured at low temperatures. The parameters of the crystal structures are shown in Table 1.

Table 1. Crystallographic data of TRAT tetrahydrat, DANTand ADNT.

	TRAT ·4 H_2O	**DANT**	**ADNT**
Formula	$C_9H_{15}N_3O_3 \cdot 4\ H_2O$	$C_7H_{12}N_4O_4$	$C_5H_9N_5O_5$
FW [g mol^{-1}]	285.30	216.20	219.17
Crystal system	trigonal	monoclinic	monoclinic
Space group	*R*−3	$P2_1/c$	$P2_1$/n
Color / Habit	colorless block	colorless block	colorless plate
Size [mm]	1.00 x 0.50 x 0.50	0.08 x 0.09 x 0.15	0.50 x 0.50 x 0.10
a [Å]	12.0327(13)	7.8404(4)	8.6532(17)
b [Å]	12.0327(13)	8.4558(5)	10.036(3)
c [Å]	17.709(2)	15.1713(8)	9.8564(12)
α [°]	90	90	90
β [°]	90	91.688(2)	99.349(15)
γ [°]	120	90	90
V [$Å^3$]	2220.5(6)	1005.37(9)	844.6(3)
Z	6	4	4
ρ_{calc} [g cm^{-3}]	1.280	1.428	1.724
μ [mm^{-1}]	0.109	0.118	0.153
F (000)	924	456	456
$\lambda_{MoK\alpha}$ [Å]	0.71073	0.71073	0.71073
T [K]	96	173	92
θ Min-Max [°]	3.0, 26.4	2.8, 27.5	2.9, 26.4
Dataset	−9:14; −14:6; −22:11	−10:9; −10:10; −19:19	−10:10; −12:8; −10:12
Reflections coll.	1461	16834	3765
Independent refl.	999	2296	1734
R_{int}	0.011	0.047	0.060
Parameters	90	184	148
*R*1 (obs)[a]	0.0359	0.0390	0.0679
wR2 (all data)[b]	0.0978	0.1017	0.1555
Resd. Dens. [e $Å^{-3}$]	−0.17, 0.31	−0.19, 0.20	−0.24, 0.33
Device type	Xcalibur, Sapphire 3	D8 Venture	Xcalibur, Sapphire 3
Solution	SHELXT 2018/2	SHELXT 2018/2	SHELXT 2018/2
Refinement	ShelXL 2018/3	ShelXL 2018/3	ShelXL 2018/3
CCDC	2241832	2241833	2241834
Absorption corr.	multi-scan	multi-scan	multi-scan

[a] *R*1 = Σ||F0|−|Fc||/Σ|F0|; [b] w*R*2 = [Σ[w(F02−Fc2)2]/ Σ[w(F0)2]]1/2; w = [σc2(F02)+(xP)2+yP]−1 and P=(F02+2Fc2)/3.

TRAT tetrahydrate crystallizes in the trigonal space group *R*-3, with six molecules in its unit cell and a recalculated density of 1.24 g cm^{-3} at room temperature. The crystal structure of TRAT is shown in Figure 5.

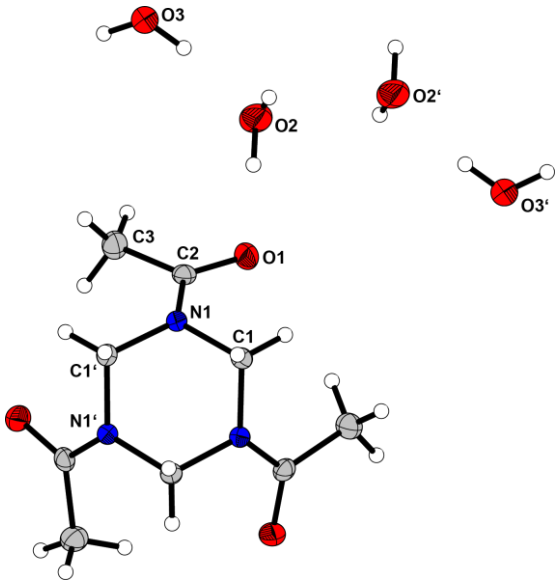

Figure 5. Molecular structure of TRAT tetrahydrat.

Figure 6 shows the three-dimensional structure of TRAT tetrahydrate. It is noticeable that the crystal water is tightly bound between the ring planes as well as between the acetyl groups.

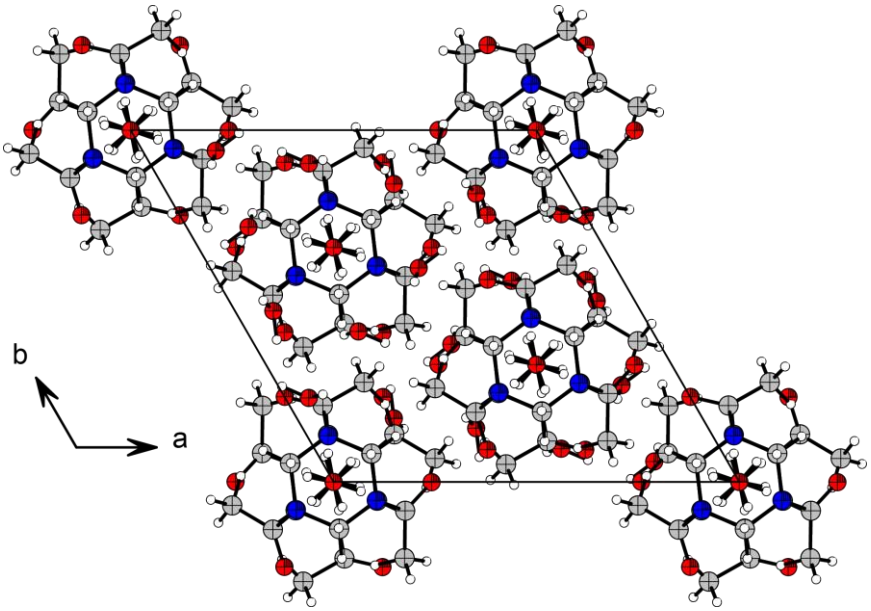

Figure 6. Three-dimensional structure of TRAT tetrahydrat along the *c* axis.

DANT crystallizes in the monoclinic space group $P2_1/c$, with four independent molecules in the asymmetric unit and a recalculated density of 1.40 g cm^{-3} at room temperature. The crystal structure of DANT is shown in Figure 7 on the left side while on its right side, the chair configuration of the triazine ring from DANT is highlighted in green. Here it can be seen that the three-ring substituted groups are arranged all in the same direction viewed from the ring plane.

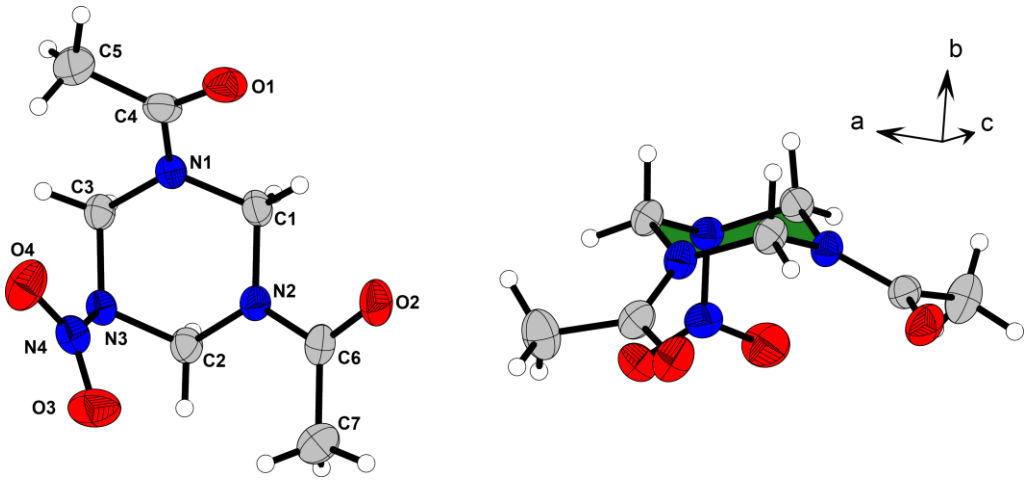

Figure 7. Molecular structure of DANT (left) in the crystal structure and chair configuration of its triazinane ring (right).

The same arrangement of the substituted groups on the triazine ring can also be seen in the ADNT crystal structure, as shown in Figure 8 highlighted in green on the right. ADNT crystallizes in the monoclinic space group $P2_1/n$, with four molecules in its unit cell and a recalculated density of 1.67 g cm^{-3} at room temperature. The crystal structure of ADNT is shown in Figure 8 on the left side.

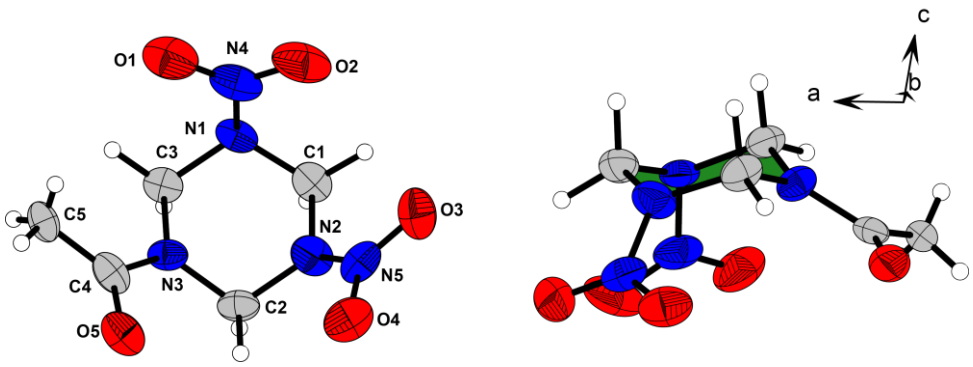

Figure 8. Molecular structure of ADNT (left) in the crystal structure and chair configuration of its triazinane ring (right).

10.3.4 Energetic Properties

The energetic properties were calculated using the EXPLO5 code version 6.06.01[26] and can be found in Table 2. The EXPLO5 calculations are based on the X-ray density recalculated to room temperature, as well as the enthalpy of formation calculated on CBS-4 M level using the Gaussian software.[27]

Table 2. Energetic properties of compounds DANT, ADNT and RDX.

	DANT	**ADNT**	**RDX[12]**
Formula	$C_7H_{12}N_4O_4$	$C_5H_9N_5O_5$	$C_3H_6N_6O_6$
FW [g mol^{-1}]	216.19	219.16	222.12
$\rho_{calc.}$ (298 K) [g cm^{-3}] [a]	1.40	1.67	1.80
$T_{melt.}$ [°C][b]	85	143	188
$T_{dec.}$ [°C][c]	177	228	209
$\Delta_f H°$ [kJ mol^{-1}][d]	−412.9	−165.8	70.3
EXPLO5 V6.06.01			
P_{CJ} [GPa][e]	11.7	20.9	33.6
V_{det} [m s^{-1}][f]	5879	7518	8794
$-\Delta_{ex}U°$ [kJ kg^{-1}][g]	2158	3982	5717
T_{det} [K][h]	1741	2689	3734
V_0 [m^3 kg^{-1}][i]	775	798	784

[a] X-ray density converted to RT [b] melting point indicated by endothermic event according to DTA (onset temperatures at a heating rate of 5 °Cmin^{-1}) [c] temperature of decomposition indicated by exothermic event according to DTA (onset temperatures at a heating rate of 5 °Cmin^{-1}) [d] calculated (CBS-4 M) heat of formation converted to the solid state HOF [e] detonation pressure [f] detonation velocity [g] Energy of explosion [h] Explosion temperature [i] Assuming only gaseous products.

Comparing the energetic parameters of the three compounds, it can be seen that, as expected, the calculated detonation velocity decreases from RDX *via* ADNT to DANT. ADNT with a velocity of detonation of 7518 m s^{-1} still has a moderate performance which is better than that of TNT (6793 m s^{-1}) at a comparable density[12]. In contrast, the value for the mono-nitro derivative DANT with 5879 m s^{-1} is clearly too low for use as an energetic material.

10.4 Conclusion

The objective of this work was to assess the synthesis of RDX *via* the intermediate TRAT (1,3,5-triacetyl-1,3,5-triazinane) as a potential alternative industrial production method. This route was stated to be a promising method for the production of pure RDX (without HMX impurities) under industrial conditions [21]. Therefore, this work was made in an effort, to evaluate the synthesis route with regard to its efficiency, to identify suitable nitration methods, and to estimate its potential.

This method has various advantages, including cheap starting materials and reactants as well as easy separation of TAT (1,3,5,7-Tetraacetyl-1,3,5,7-tetrazocinane) and TRAT by solubility differences. Due to the similar chemical and physical properties of RDX and HMX the isolation of both is very hard, so it would be favorable to separate the precursor TAT and TRAT from each other to obtain pure RDX in the next step. This aspect was successfully confirmed in this work where no trace of TAT was detected in TRAT following washing with ethyl acetate. However, for the synthesis of TRAT in this work only a moderate yield of 50 % was obtained. This presents a serious obstacle and suggests the need for further optimization or a change in the reaction and the reactants.

The main challenge of this work was the search for a feasible nitration method from TRAT to RDX, in the evaluation process this was identified as the main challenge of this method. Every tested method of nitration either gives no nitration product or merely leads to incomplete nitration with a low percentage of RDX. Further optimization of the reaction conditions and other methods could increase the ratio of RDX but for this process to be viable solely RDX has to be obtained. Otherwise, the main objective to yield pure RDX is missed. The option to develop a purification method to isolate RDX from the incompletely nitrated by-products would run the risk of making the process too complicated and therefore inferior to the well-established methods of the Bachmann and Woolwich processes.

However, from an academic standpoint, this work resulted not only in the determination of the undefined crystal structure of TRAT tetrahydrate, but also in the first-ever recorded synthesis of DANT and the determination of its crystal structure as well as the low-temperature measured crystal structure of ADNT. This

may advance the understanding of this process and promote its improvement to make it a feasible alternative.
In conclusion, the production of RDX *via* TRAT holds great potential but is not yet a viable method for industrial application.

10.5 Acknowledgments

For financial support of this work the Ludwig Maximilian University (LMU), EMTO GmbH, and BIAZZI SA are gratefully acknowledged.

10.6 References

[1] G. F. Henning, German Patent DE104280, The representation of a nitro body made of hexamethylenetetramine by entering nitric acid hexamethylenetetramine into cold smoke Nitric acid, Berlin, Germany, **1899**.
[2] J. T. Edward, Wartime Research on RDX, *J. Chem. Educ.* **1987**, *64*, 599−603.
[3] T. M. Klapötke, *Chemistry of High-Energy Materials*, 6th ed., DE GRUYTER, Berlin/Boston, **2022**.
[4] J. P. Agrawal; R. D. Hodgson, *Organic Chemistry of Explosives*, John Wiley & Sons, Hodgson, **2007**.
[5] C. F. Baxter, *The Secret History of RDX: The Super-Explosive that Helped Win World War II*, University Press of Kentucky, USA, **2018**.
[6] J. P. Baxter, *Scientists against tim*e, M.I.T. Press, Cambridge, United Kingdom, **1968**.
[7] W. E. Bachmann, J. C. Sheehan, A new method of preparing the high explosive RDX, *J. Am. Chem. Soc.*, **1949**, *71*, 1842–1845.
[8] a) W. E. Bachmann, US2680671, Method of treating cyclonite mixtures, USA, **1954**; b) W. E. Bachmann, US2798870, Method for preparing explosives, USA, **1957**.
[9] Z. Matys, D. Powala, A. Orzechowski, A. Maranda, Methods for obtaining octogen (HMX), *CHEMIK*, **2012**, *66*, 58–63.

[10] NATO, Explosives specification for RDX (Hexogene), STANAG 4022, draft 6th edition 4, June **2009**.

[11] Detail Specification − RDX (Cyclotrimethylene-trinitramine), MIL-DTL 398D, Dec. **1966**.

[12] T. M. Klapötke, Energetic Materials Encyclopedia, 2nd ed.DE GRUYTER, Berlin/Boston, **2021**.

[13] Acumen Research and Consulting, Research Department Explosive (RDX) Market Size - Global Industry, Share, Analysis, Trends and Forecast 2022 – 2030, Pune, India, Nov. **2022**.

[14] S. Abhay, M. Sonia, Allied Market Research, Research Department Explosive (RDX) Market by Type (Explosives, Pyrotechnics, and Others), Application (Military and Civilian), and Sales Channel (Domestics and International): Global Opportunity Analysis and Industry Forecast, 2021-2030, USA, Oct. **2021**.

[15] J. P. Agrawal, *High energy materials: propellants, explosives and pyrotechnics*, 1st ed., John Wiley & Sons, Hoboken, **2010**.

[16] J. Köhler, R. Meyer, A. Homburg, *Explosivstoffe*, 10th ed., Wiley-VCH, Weinheim, **2008**.

[17] J A Conkling, C. J. Mocella, *Chemistry of Pyrotechnics*, 3rd ed., CRC press, **2019**, Boca Raton, Fl., 222−223.

[18] W. de. C. Crater, Nitration, *Ind. Eng. Chem*., **1948**, *40*, 1627–1635.

[19] F. J. Brockman, D. C. Downing and G. F. Wright, Nitrolysis of hexamethylenetetramine: III. Preparation of pure cyclonite, *Canad. J. of Research*, **1949**, 27b, 469−474.

[20] E. Commission, J. R. Centre, D. Kyprianou, G. Rarata, G. Emma, G. Diaconu, M. Vahčič, D. Anderson, in *Flow chemistry and the synthesis of energetic materials*, Publications Office of the European Union, **2022**.

[21] D. O. J. Pöhlmann, S. Glante, *New Continuos Process For The Production Of RDX/HMX*, 51st International Annual Conference of the Fraunhofer ICT, Karlsruhe, Germany June 28 – July 1, **2022**.

[22] D. Kyprianou, M. Berglund, G. Emma, G. Rarata, D. Anderson, G. Diaconu, V. Exarchou, Synthesis of 2,4,6-Trinitrotoluene (TNT) Using Flow Chemistry, *Molecules* **2020**, *25*, 3586−3601.

[23] L. Wang, Z. Xu, P. Wang, L. Wang, Z. Lin, Z. Meng, Investigation of the solubility of Octahydro-1,3,7,9-tetranitro-1,3,5,7-tetrazocine and 1,3,5-triacetyl-hexahyrdo-s-triazine, *J. Chem. Eng. Data* **2013**, *58*, 737–740.

[24] J. Yang, Q. Yu, F. Zhao, J. Lu, Z. Ge, Triacylperhydro-1,3,5-triazines over Phenylsulfonic Acid Functionalized Mesoporous Silica, *Synthetic Communications*, **2011**, *41*, 3455−3461.

[25] S. Mahajan, I. P. Singh, Determining and reporting purity of organic molecules: why qNMR, *Magn. Reson. Chem.* **2013**, *51*, 76–81.

[26] M. Sućeska, Explo5V6.06.01, Zagreb, Croatia, **2021**.

[27] M. J. Frisch, G. W. Trucks, H. B. Schlegel, G. E. Scuseria, M. A. Robb, J. R. Cheeseman, G. Scalmani, V. Barone, B. Mennucci, G. A. Petersson, H. Nakatsuji, M. Caricato, X. Li, H.P. Hratchian, A. F. Izmaylov, J. Bloino, G. Zheng, J. L. Sonnenberg, M. Hada, M. Ehara, K. Toyota, R. Fukuda, J. Hasegawa, M. Ishida, T. Nakajima, Y. Honda, O. Kitao, H. Nakai, T. Vreven, J. A. Montgomery, Jr., J. E. Peralta, F. Ogliaro, M. Bearpark, J. J. Heyd, E. Brothers, K. N. Kudin, V. N. Staroverov, R. Kobayashi, J. Normand, K. Raghavachari, A. Rendell, J. C. Burant, S. S. Iyengar, J. Tomasi, M. Cossi, N. Rega, J. M. Millam, M. Klene, J. E. Knox, J. B. Cross, V. Bakken, C. Adamo, J. Jaramillo, R. Gomperts, R. E. Stratmann, O. Yazyev, A. J. Austin, R. Cammi, C. Pomelli, J. W. Ochterski, R. L. Martin, K. Morokuma, V. G. Zakrzewski, G. A. Voth, P. Salvador, J. J. Dannenberg, S. Dapprich, A. D. Daniels, O. Farkas, J.B. Foresman, J. V. Ortiz, J. Cioslowski, D. J. Fox, Gaussian 09 A.02, Gaussian Inc., Wallingford, USA, **2009**.

11 Bachmann Process for RDX and HMX Synthesis

The following results are unpublished and are derived from a cooperation project with the Swiss company BIAZZI S.A.

11.1 Overview of the Processes for RDX and HMX Synthesis

The molecular structures of the high energetic compounds **RDX** (Cyclonite, Hexogen) and **HMX** (Octogen) are shown in Figure 1.

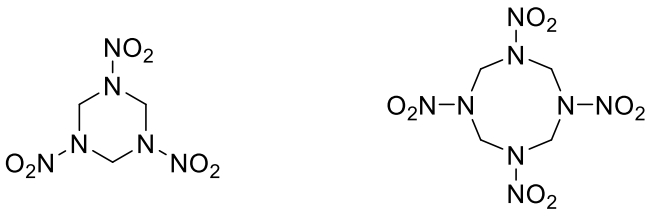

RDX **HMX**

Figure 1. Molecular structure of RDX (Research Department Explosive) and HMX (High Melting Explosive).

11.1.1 RDX Synthesis[1,2]

In the following six processes for the synthesis of RDX are shown:

1. **K−Process (Köffler)**
2. **E−Process (Ebele)**
3. **W−Process (Wolfram)**
4. **SH−Process (Schnurr)**
5. **KA−Process / Bachmann Process**
6. **Woolwich Process**

11.1.1.1 K−Process

- Discovered by Köffler
- use of ammonium nitrate to compensate the nitrogen deficiency in hexamine (Scheme 1)

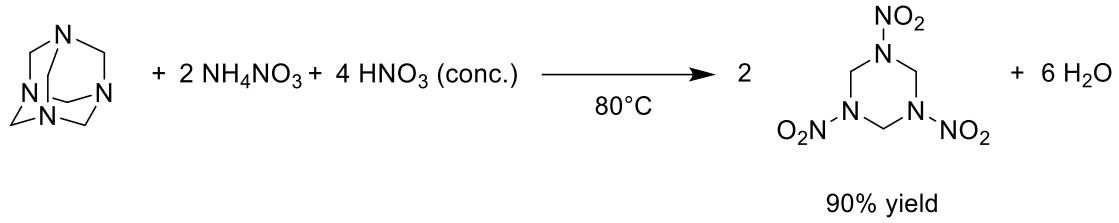

Scheme 1. Reaction scheme of RDX synthesis according to the K−Process.

→ The work up of the spent acids gave considerable difficulties.

11.1.1.2 E−Process (McGill Process)

- Discovered by M. Ebele (McGill, Schiessler and Ross)
- Dehydration of paraformaldehyde and ammonium nitrate in the presence of acetic anhydride (Scheme 2)

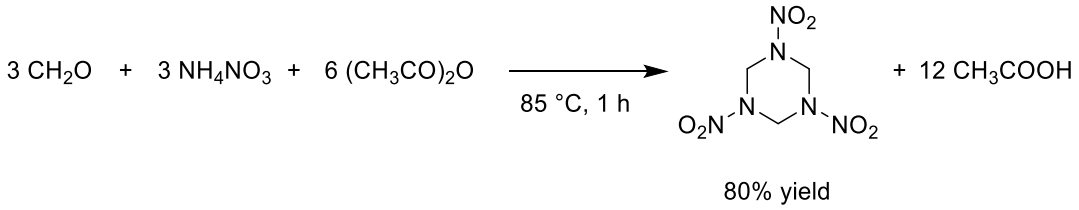

Scheme 2. Reaction scheme of RDX synthesis according to the E−Process.

→ Expensive, because of the relatively large amount of acetic anhydride.

→ Low acidity favors the formation of HMX as by-product.

11.1.1.3 W−Process

- Discovered by Wolfram
- condensation of potassium sulfamic acid with formaldehyde and subsequent nitration with nitric acid (Scheme 3)

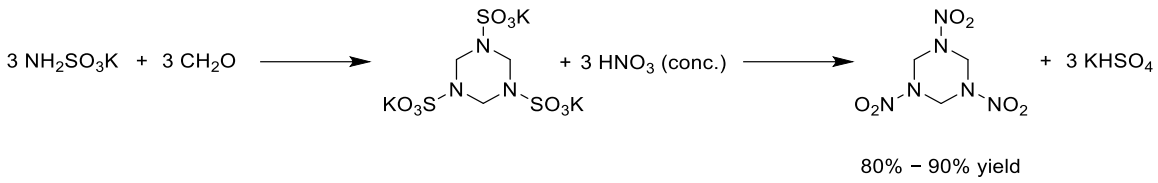

Scheme 3. Reaction scheme of RDX synthesis according to the W−Process.

→ Intermediate is very sensitive towards hydrolysis, therefore nitration must be carried out under anhydrous conditions.

11.1.1.4 SH−Process/ Woolrich Process:

- Developed by Schnurr (SH−Process) and Woolrich (Hale)
- Direct nitration of hexamine with nitric acid (Scheme 4)

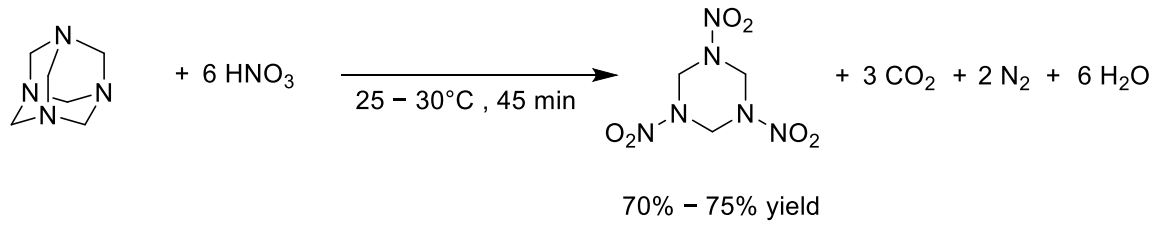

Scheme 4. Reaction scheme of RDX synthesis according to the SH−Process/ Woolwich Process.

→ One mole of hexamine can only form one mole of RDX.

→ Large excess of nitric acid has to be used.

→ SH−Process achieved stabilization of the spent acid by introducing a controlled cook-off step immediately after the nitration process.

11.1.1.5 KA−Process/ Bachmann Process:

- Discovered by Bachmann (Köffler)
- Combination of K− and E−Process
- Also called Combination-Process
- First the dinitrate salt of hexamine is formed which then reacts to RDX (Scheme 5)

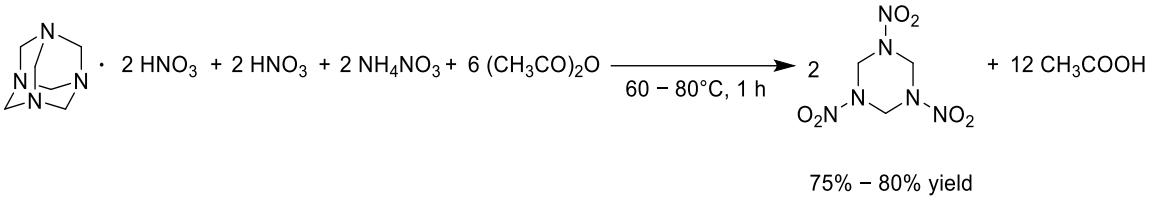

Scheme 5. Reaction scheme of RDX synthesis according to the KA−Process.

→ One mole of hexamine can produce two mole of RDX.

→ Dilution of the reaction mixture with water before removing the RDX produces a very impure product containing numerous unstable linear nitramine-nitrates.

11.1.1.6 Brockmann Process[3]

- Discovered by Brockman
- Oxidation of 1,3,5-trinitroso-1,3,5-triazacyclohexane with hydrogen peroxide in nitric acid (Scheme 6)

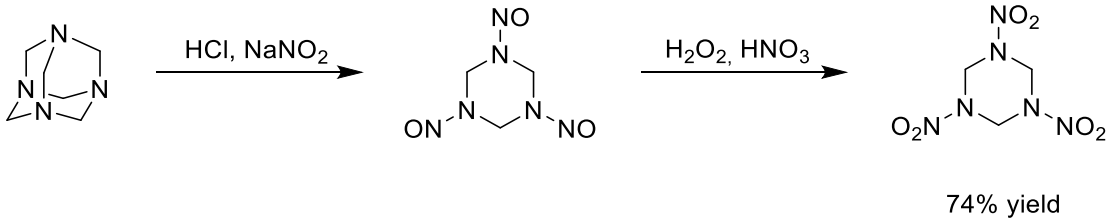

Scheme 6. Reaction scheme of RDX synthesis according to the Brockman−Process.

→ Yield pure RDX free from HMX.

→ 1,3,5-Trinitroso-1,3,5-triazacyclohexane has a low chemical stability.

11.1.1.7 Additional Information

According STANAG 4022[4] (Explosives specification for RDX) there are different types of RDX:

Type A: RDX made by the nitric acid process, (Woolrich Process)

Type B: RDX made by the acetic anhydride process (Bachmann Process)

According to MILITARY SPECIFICATION[5] there are again different Types of RDX:

Type I: HMX content of 0−5%

Type II: HMX content of 4−17%

→ Type A is usually Type I and Type B is usually Type II.

Table 1. Overview of HMX content during the different RDX syntheses.

RDX process type	HMX content
KA−Process/ Bachmann Process	~ 10%
E−Process	~ 6%
Brockman Process	0%

11.1.2 HMX Synthesis[6]

The conditions during nitrolysis of hexamine have an influence on whether and in which ratio RDX and HMX are formed. If milder conditions are used, the formation of HMX is preferred. For example, at lower temperatures, under less acidic conditions or with less addition of ammonium nitrate during the Bachmann process, a higher yield of HMX could be obtained.

In the following two alternatives for the synthesis of HMX are shown:

11.1.2.1 Two-stage synthesis with the formation of DPT as intermediate

- First stage is the preparation of DPT (dinitropentamethylene tetramine), for example from hexamine (Scheme 7)

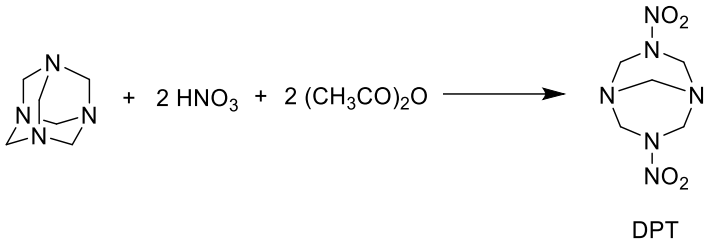

DPT

Scheme 7. Synthesis of DPT (dinitropentamethylene tetramine) from hexamine.

- Second stage is the preparation of HMX from DPT through nitrolysis (Scheme 8)

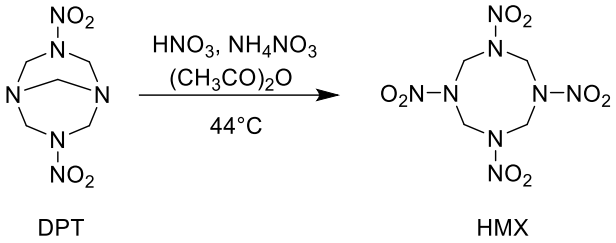

DPT HMX

Scheme 8. Synthesis of HMX from DPT.

11.1.2.2 Two-stage synthesis without the formation of an intermediate (Bachmann Process)

- Process is continuously without the separation of DPT (Scheme 9)

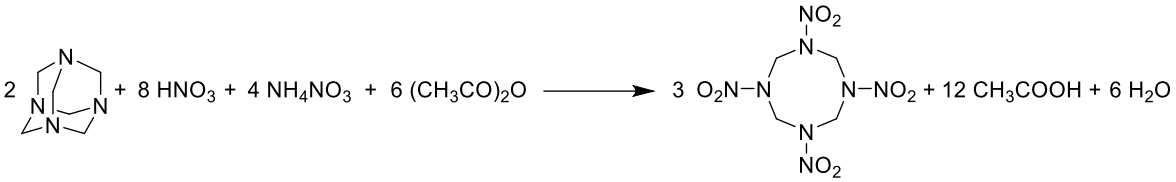

HMX

Scheme 9. Synthesis of HMX from hexamine without the isolation of DPT.

- There are a lot of side products like linear nitramines and RDX

11.1.2.3 Additional Information

There are a lot of different side reactions were for example linear nitramines could be formed. To prevent this, the step of oxidative crystallization is introduced, in which these linear products decompose to nitric oxides and carbon dioxide and should evaporate from the reaction mixture.

HMX occurs in four different polymeric crystal forms: alpha, beta, gamma and delta. They differ in their physical properties, as shown in Table 2:

Table 2. Different forms of HMX and their densities.[7]

HMX form	Density [g cm^{-3}]
alpha	1.84
beta	1.90
gamma	1.78
delta	1.79

Mostly in synthesis the temperature and environmental conditions leads to HMX in the alpha form but in industrial applications only the beta form is used. However, easy conversion from the alpha to the beta form could be made by recrystallization from acetone, acetonitrile or cyclohexanone.

11.1.3 References

[1] J. P. Agrawal; R. D. Hodgson, Organic Chemistry of Explosives. **2007**.

[2] W. de. C. Crater, *Ind. Eng. Chem.*, **1948**, *40*, 1627–1635.

[3] F. J. Brockman, D. C. Downing and G. F. Wright, *Cand. J. of Research*, **1949**, *27b*, 469−474.

[4] NATO, Explosives specification for RDX (Hexogene), STANAG 4022, draft 6 edition 4.

[5] Detail Specification – RDX (Cyclotrimethylenetrinitramine), MIL-DTL 398D, Dec. 1966.

[6] Z. Matys, D. Powala, A. Orchechowski, A. Maranda, *CHEMIK*, **2012**, *66*, 61–63.

[7] T. M. Klapötke, *Energetic Materials Encyclopedia*, DE GRUYTER, Berlin/Boston, **2021**.

11.2 Small Scale Synthesis for the evaluation of the critical process steps

Both the RDX and HMX synthesis in the Bachmann process is divided into four steps, as shown in Figure 2.

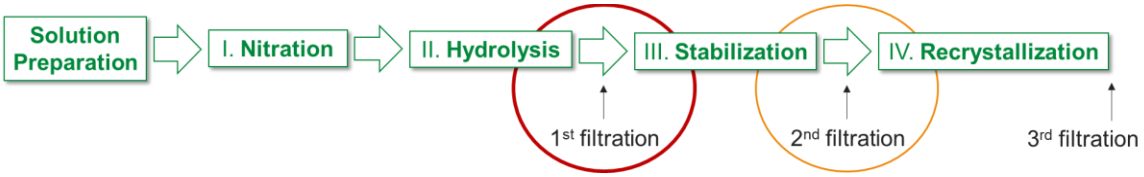

Figure 2. Synthesis steps of the RDX and HMX production according to the Bachmann Process.

However, before these synthesis steps, different solutions are prepared first. This is mainly done to dissolve all reactants that are present as solids, since it is advantageous to work only with liquids for process and dosing reasons. Then the first step is the nitration step, where hexamine is nitrated by generating acetyl nitrate. During the nitration step, the tree previously prepared solutions are added to the reaction mixture at certain intervals and in certain amounts. This is done for safety reasons, so that there is not a large excess of the nitration reagent present and the reaction generates too much heat and a runaway reaction occurs. The second step is called hydrolysis. Here, the product obtained from the nitration step is boiled in diluted acetic acid. The aim and purpose of this step is to eliminate the open-chain by-products which are formed in addition to RDX and HMX. These decompose in the hydrolysis step to various gaseous decomposition products and simply evaporate out of the reaction mixture. After this step, the first filtration step occurs. For the general synthesis, the filter cake is then processed further and the stabilization step follows. In the HMX synthesis, however, a so-called secondary product can also be obtained from the filtrate after the hydrolysis step. The stabilization step simply involves heating the product in water to get rid of the remaining acid residues and thus stabilize the product. After the stabilization step, the second filtration step takes place. Finally, the recrystallization step is performed to obtain the desired modification (beta HMX) and the desired particle size of the product. After recrystallization, the third and final filter step follows.

11.2.1 RDX Small Scale Synthesis

11.2.1.1 Synthesis

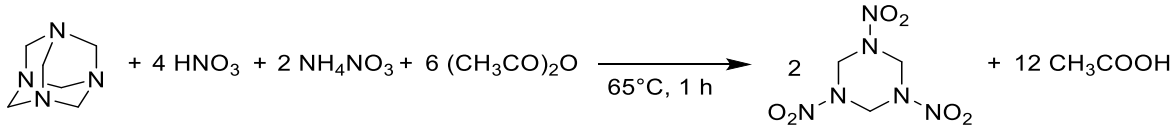

chemicals	M [g mol^{-1}]	ρ [g cm^{-3}]	conc.	n [mol]	m [g]	V [mL]
ammonium nitrate	80.04	–	–	0.15	11.8	–
nitric acid	63.01	1.51	100 %	0.20	12.8	8.5
hexamine	140.19	–	–	0.04	6.25	–
acetic anhydride	102.09	1.08	100 %	0.44	45.3	41.9
acetic acid	60.05	1.05	100 %	0.71	42.7	40.7

Solution preparation

Solutions 1 to 3 were prepared in three different beakers. Therefore, acetic anhydride (0.44 mol, 45.3 g, 41.9 mL) was measured (solution 1), ammonium nitrate (0.13 mol, 10.3 g) was dissolved in concentrated nitric acid (0.20 mol, 12.8 g, 8.5 mL) (solution 2)[1] and hexamine (0.04 mol, 6.25 g) was dissolved in glacial acetic acid (0.21 mol, 12.7 g, 12.1 mL) (solution 3)[2].

The densities of the solutions were then determined to 1.68 g cm^{-3} for solution 2 and 1.26 g cm^{-3} for solution 3.

I Nitration

In a 250 mL three-neck flask glacial acetic acid (0.5 mol, 30.0 g, 28.6 mL) was provided. While stirring, it was heated up to 65°C with an oil bath. Afterwards, the prepared solution 1 (1.8 g, 1.7 mL), solution 2 (2.7 g, 1.6 mL) and ammonium nitrate (0.02 mol, 1.5 g) were added to the warm reaction solution. It was left and stirred at 65°C until the reactants had completely dissolved in the reaction solution[3]. Solution 1 (43.5 g, 40.27 mL), solution 2 (20.4 g, 12.1 mL) and solution 3 (18.95 g, 15.0 mL) were then added in parallel to the reaction solution. For this

purpose, they were each separated into 15 parts and one part each of solution 1 (2.7 mL), solution 2 (0.8 mL) and solution3 (1.0 mL) were added in parallel and slowly to the reaction mixture[4]. After complete addition, the mixture was stirred at 65°C for 60 minutes.

II Hydrolysis

In a second 500mL flask, glacial acetic acid (7.12 g, 6.8 mL) was mixed with water (34.08 g, 34.08 mL) and heated to 95 °C while stirring. The still warm (65°C) reaction solution of the nitration reaction was slowly added to the hot diluted acetic acid[5]. The nitration flask was additionally washed with glacial acetic acid (5.0 g, 4.8 mL), which was also transferred to the hydrolysis flask. Afterwards, the reaction mixture was stirred at 95°C for 60 minutes[6]. It was allowed to cool down to 40°C and filtered using vacuum. The filter cake was then washed twice with water (2 x 20 mL).

III Stabilization

The filter cake obtained during hydrolysis was suspended in water (40 mL) and heated to 85°C using an oil bath. It was stirred at this temperature for 60 minutes and then cooled down to 50°C. After filtration under vacuum, crude RDX (12.8 g, 0.06 mol, 75%) was obtained as a colorless solid.

IV Recrystallization

The crude RDX was dissolved in acetone (90.0 g, 113.9 mL) and the reaction solution was heated for 60 minutes under reflux (58°C). Using a distillation reflux separator, approximately 70% (80 mL) of the acetone was distilled[7]. Under full reflux, an acetone-water mixture (5% acetone, 40 mL) was added slowly and after that, the residual acetone was distilled off at 98°C. The obtained suspension was allowed to cool to 60°C and filtered under vacuum. RDX (12.4 g, 0.056 mol, 70%, 17% HMX[8]) was obtained as a colorless solid.

---

[1] Slight gas development and heating during preparation. If the solution is stored for too long, ammonium nitrate starts to crystallize (NH_4NO_3 dissolves again when stirred briefly at 35°C).

[2] Highly viscous but stable solution.

[3] While the solid ammonium nitrate is dissolving, there is a strong heat development and a slight development of nitrous gases.

[4] At the beginning slowly and carefully addition, later faster addition is possible. After approx. $^{1}/_{3}$ of the addition, a precipitate is formed which does not dissolve any more, from that point further reaction as suspension.

[5] Content of the nitration flask is a suspension.

[6] Slight reflux was visible at the neck of the flask.

[7] During the distillation of acetone, precipitation occurs. From this point, the reaction mixture is a suspension.

[8] Determined by integration in ^{1}H NMR, more precise determination by HPLC follows.

11.2.1.2 Characterization

NMR spectroscopy:

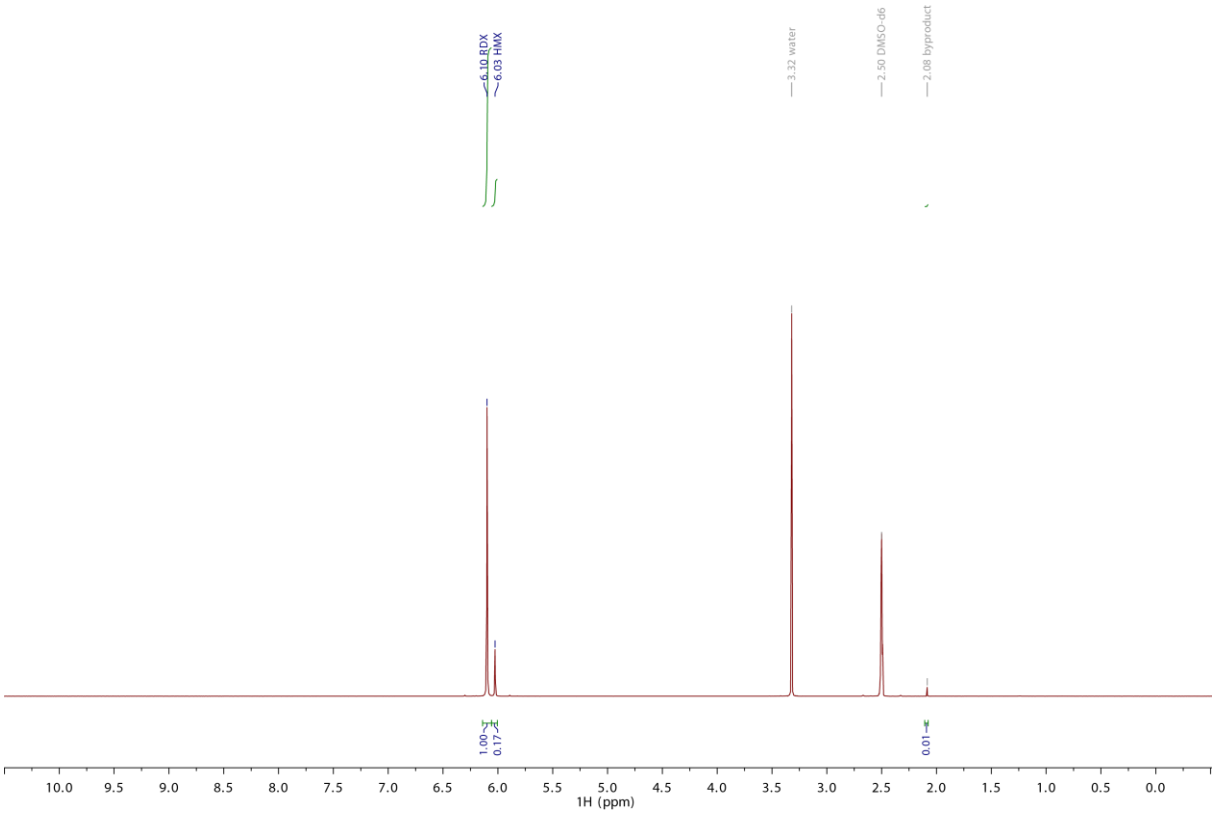

Figure 3. ^{1}H NMR in DMSO-d_6 from the RDX small scale synthesis.

Example calculation RDX to HMX ratio from ^{1}H NMR:

Molar mass (RDX): 222,12 g mol^{-1}

Molar mass (HMX): 296,16 g mol^{-1}

NMR integral (RDX): 0,16

NMR integral (HMX): 1,00

Number of protons (RDX): 6

Number of protons (HMX): 8

$$\%m\ RDX = \frac{{NMR\ Integral_{RDX}}/{Protonenanzahl_{RDX}} \times M_{RDX}}{{NMR\ Integral_{RDX}}/{Protonenanzahl_{RDX}} \times M_{RDX} + {NMR\ Integral_{HMX}}/{Protonenanzahl_{HMX}} \times M_{HMX}}$$

$$= \frac{{0,16}/{6} \times 222,12}{{0,16}/{6} \times 222,12 + {1,00}/{8} \times 296,16}$$

$$= 0.14$$

→ 14% RDX und 86% HMX

Elemental analysis:

EA for $C_3H_6N_6O_6$ calculated: C 16.22, H 2.72, N 37.84 %; found: C 16.02, H 2.64, N 37.67 %.

Differential thermal analysis:

Onset temperatures measured in the range from 25°C to 400°C with a heating rate of 5°C min^{-1}.

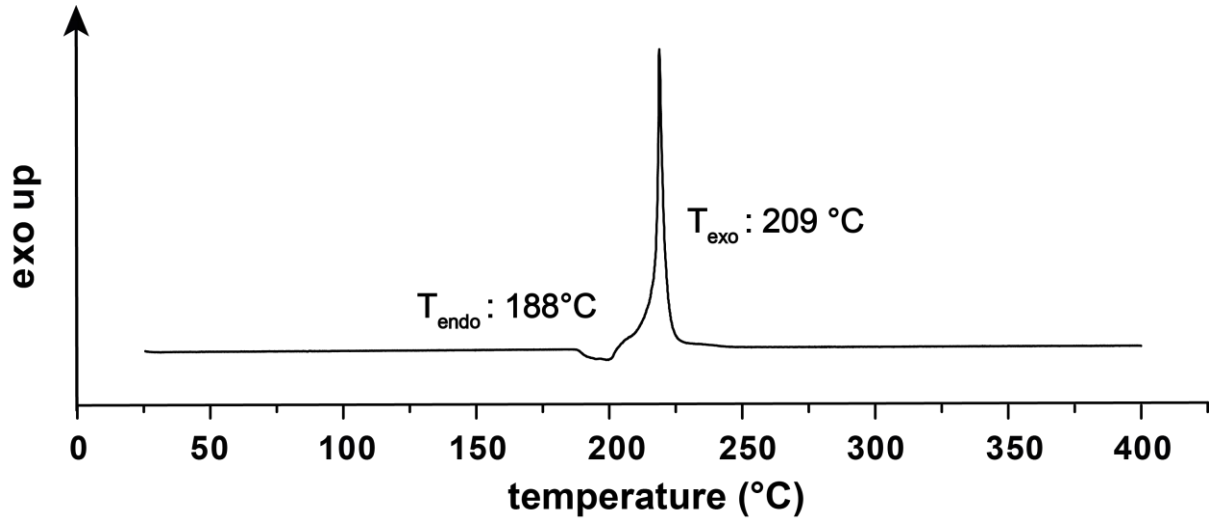

Figure 4. DTA measurement after the RDX small scale synthesis.

11.2.1.3 Small Scale Granulometry

Sieved by hand with Retsch Test Sieves with a Steel Body of 100 mm x 25 mm.

Table 2. Granulometry of the small scale RDX synthesis.

	Granulometry in %
> 1000 µm	0
1000 µm – 600 µm	0
600 µm – 500 µm	0,1
500 µm – 300 µm	0,3
300 µm – 106 µm	47,8
< 106 µm	51,8

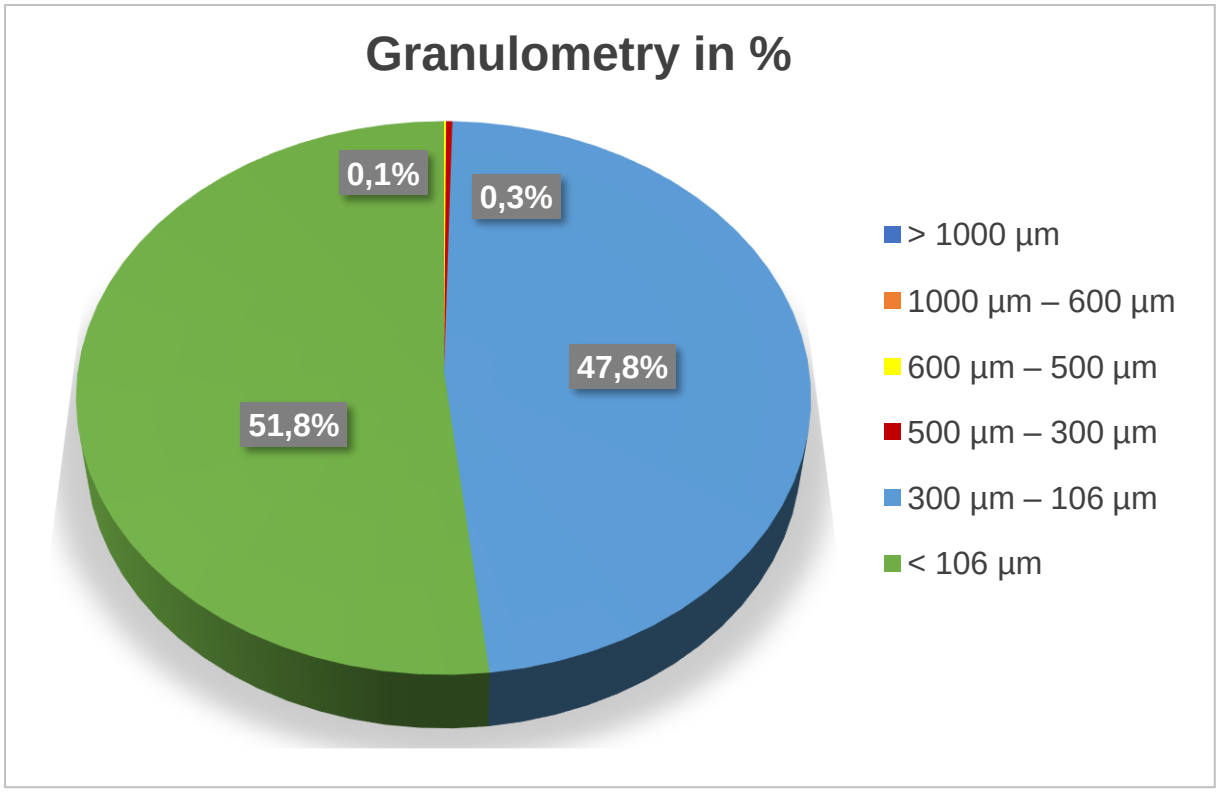

Figure 5. Granulometry of the small scale RDX synthesis.

11.2.2 HMX Small Scale Synthesis

11.2.2.1 Synthesis

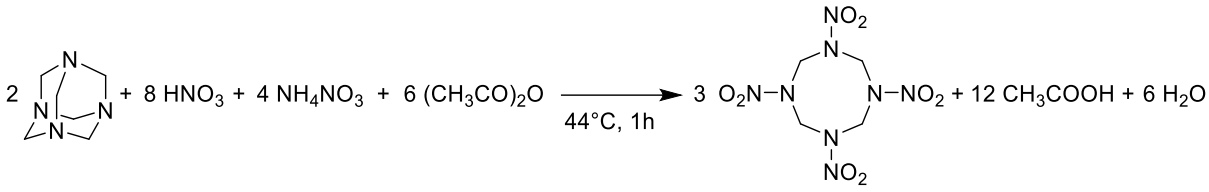

chemicals	M [g mol^{-1}]	ρ [g cm^{-3}]	conc.	n [mol]	m [g]	V [mL]
ammonium nitrate	80.04	–	–	0.13	10.7	–
nitric acid	63.01	1.51	100 %	0.22	13.7	9.1
hexamine	140.19	–	–	0.05	6.5	–
acetic anhydride	102.09	1.08	100 %	0.50	50.7	46.9
acetic acid	60.05	1.05	100 %	0.66	39.5	37.6

Solution preparation

Solutions 1 to 3 were prepared in three different beakers. Therefore, acetic anhydride (0.50 mol, 50.7 g, 46.9 mL) was measured (solution 1), ammonium nitrate (0.13 mol, 10.7 g) was dissolved in concentrated nitric acid (0.22 mol, 13.7 g, 9.1 mL) (solution 2)[1] and hexamine (0.05 mol, 6.5 g) was dissolved in glacial acetic acid (0.22 mol, 13.2 g, 12.6 mL) (solution 3)[2].

The densities of the solutions were then determined to 1.63 g cm^{-3} for solution 2 and 1.21 g cm^{-3} for solution 3.

I Nitration

In a 250 mL three-neck flask glacial acetic acid (0.44 mol, 26.3 g, 25.0 mL) was provided. While stirring, it was heated up to 44°C with an oil bath. Afterwards, the prepared solution 1 (1.6 g, 1.4 mL) and solution 3 (3.1 g, 2.6 mL) were added to the warm reaction solution. It was left and stirred until the temperature of the reaction solution was stable at 44°C. Solution 1 (20.5 g, 19.0 mL), solution 2 (9.7 g, 6.0 mL) and solution 3 (16.6 g, 13.7 mL) were then added in parallel to the reaction solution.[3] After this addition it was stirred at 44°C for 10 minutes[4].

Thereafter, solution 1 (8.3 g, 7.7 mL) and solution 2 (3.0 g, 1.8 mL) were added in parallel to the reaction mixture. And after this addition again solution 1 (20.3 g, 18.8 mL) and solution 2 (11.7 g, 7.2 mL) were added in parallel to the reaction. After complete addition, the mixture was stirred at 44°C for 60 minutes.

II Hydrolysis

In a second 500mL flask, glacial acetic acid (7.6 g, 7.2 mL) was mixed with water (29.7 g, 29.7 mL) and heated to 95 °C while stirring. The still warm (44°C) reaction solution of the nitration reaction was slowly added to the hot diluted acetic acid[5]. The nitration flask was additionally washed with glacial acetic acid (5.0 g, 4.8 mL), which was also transferred to the hydrolysis flask. Afterwards, the reaction mixture was stirred at 95°C for 60 minutes[6]. It was allowed to cool down to 65°C and filtered using vacuum. The filter cake was then washed twice with water (2 x 20 mL).

III Stabilization

The filter cake obtained during hydrolysis was suspended in water (42.5 mL) and heated to 85°C using an oil bath. It was stirred at this temperature for 60 minutes and then cooled down to 50°C. After filtration under vacuum, crude HMX (7.7 g, 0.03 mol, 35%) was obtained as a colorless solid.

IV Recrystallization

The crude HMX was suspended in acetone (161.5 g, 204.4 mL) and the reaction solution was heated for 60 minutes under reflux (58°C)[7]. Using a distillation reflux separator, approximately 80% (164 mL) of the acetone was distilled. Under full reflux, an acetone-water mixture (5% acetone, 40 mL) was added and then the residual acetone was distilled off at 98°C. The obtained suspension was allowed to cool to 60°C and filtered under vacuum. HMX (12.4 g, 0.024 mol, 32%, 0% RDX[8]) was obtained as a colorless solid.

V Secondary Product

To the still warm filtrate obtained at the end of II hydrolysis, an aqueous sodium hydrogen carbonate (1.68 g, 0.02 mol) solution (10 mL) was added under ice cooling. The solution was allowed to settle and cool down (ice cooling). After about

30 minutes, the precipitate was filtered under vacuum. The secondary product (RDX:HMX ratio 22:78) was obtained as a colorless crystalline powder.

---

[1] Slight gas development and heating during preparation.

[2] Highly viscous but stable solution.

[3] During the feeding, in order to maintain the temperature at 44°C, alternating cooling with an ice bath and heating with an oil bath was used.

[4] During the feeding a precipitation occurred and thus a suspension was formed. From here, the reaction was continued as a suspension.

[5] Content of the nitration flask is a suspension.

[6] Colorless vapors have evaporated from the open flask.

[7] The Crude HMX did not dissolve completely in the acetone. The recrystallization was carried out as suspension.

[8] Determined by integration in ^{1}H NMR, more precise determination by HPLC follows.

11.2.2.2 Characterization

NMR spectroscopy:

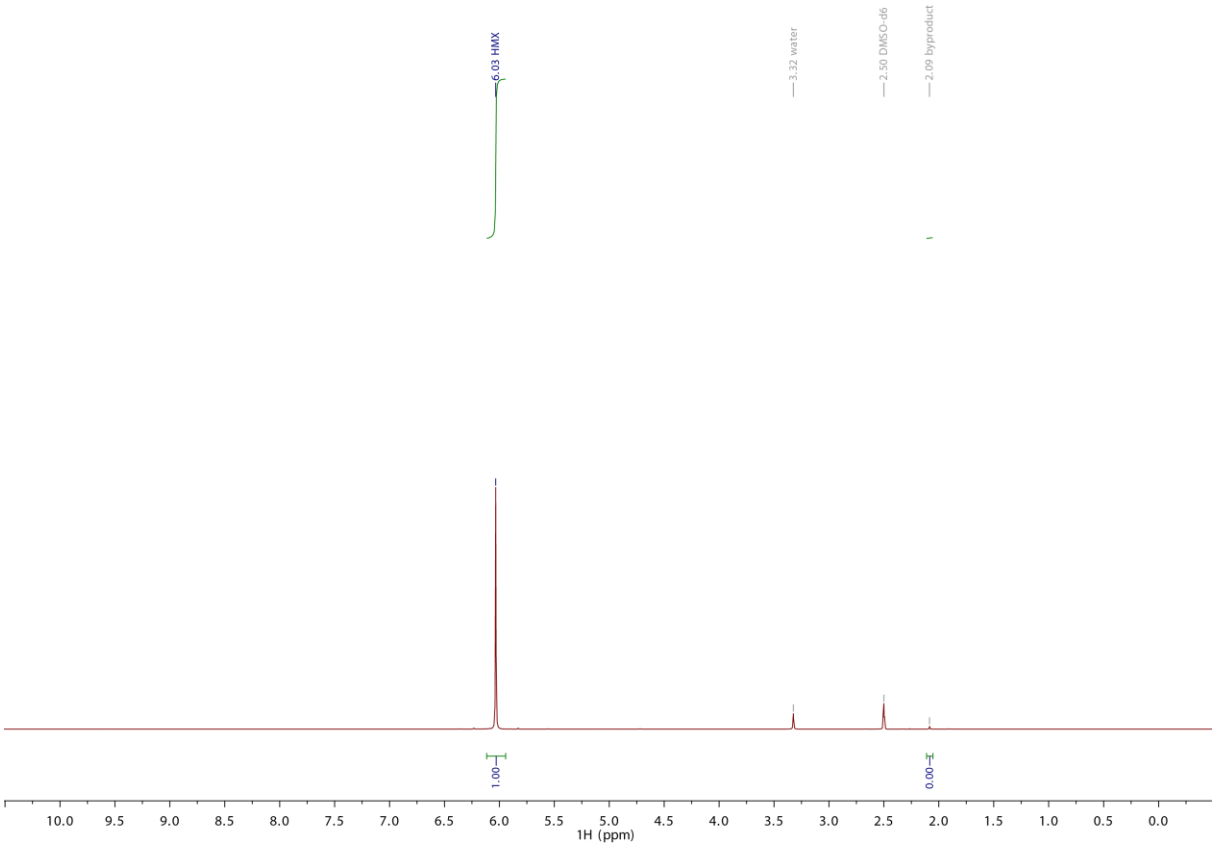

Figure 6. ^{1}H NMR in DMSO-d_6 from the HMX small scale synthesis.

Elemental analysis:

EA for $C_3H_6N_6O_6$ calculated: C 16.22, H 2.72, N 37.84 %; found: C 16.12, H 2.65, N 37.51 %.

Differential thermal analysis:

Onset temperatures measured in the range from 25°C to 400°C with a heating rate of 5°C min^{-1}.

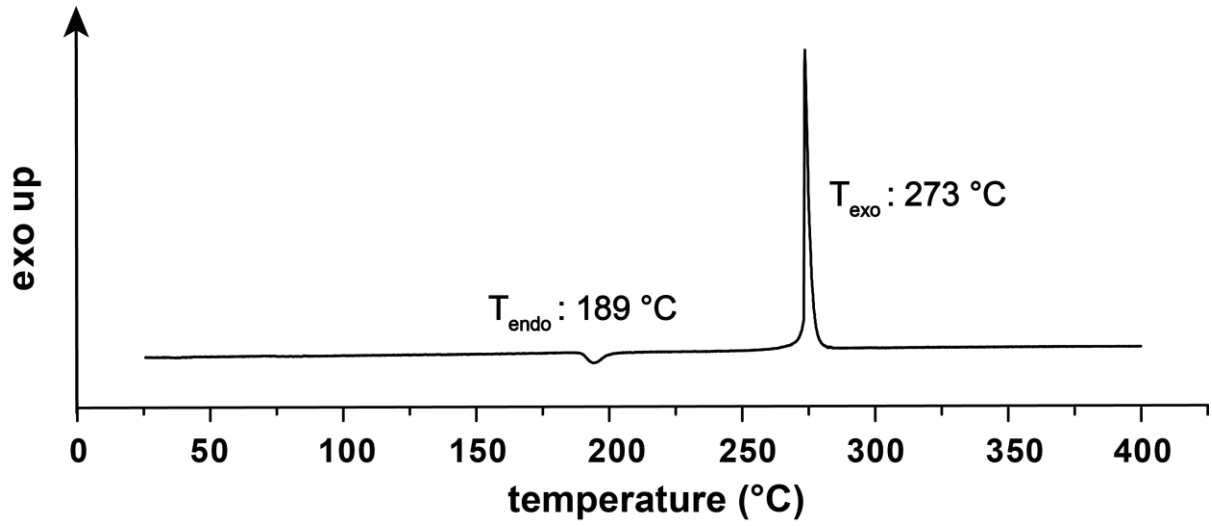

Figure 7. DTA measurement after the HMX small scale synthesis.

11.2.2.3 Small Scale Granulometry

Sieved by hand with Retsch Test Sieves with a Steel Body of 100 mm x 25 mm.

Table 3. Granulometry of the small scale HMX synthesis.

	Granulometry in %
> 1000 µm	0
1000 µm – 600 µm	0
600 µm – 500 µm	0
500 µm – 300 µm	0,3
300 µm – 106 µm	1,0
< 106 µm	98,7

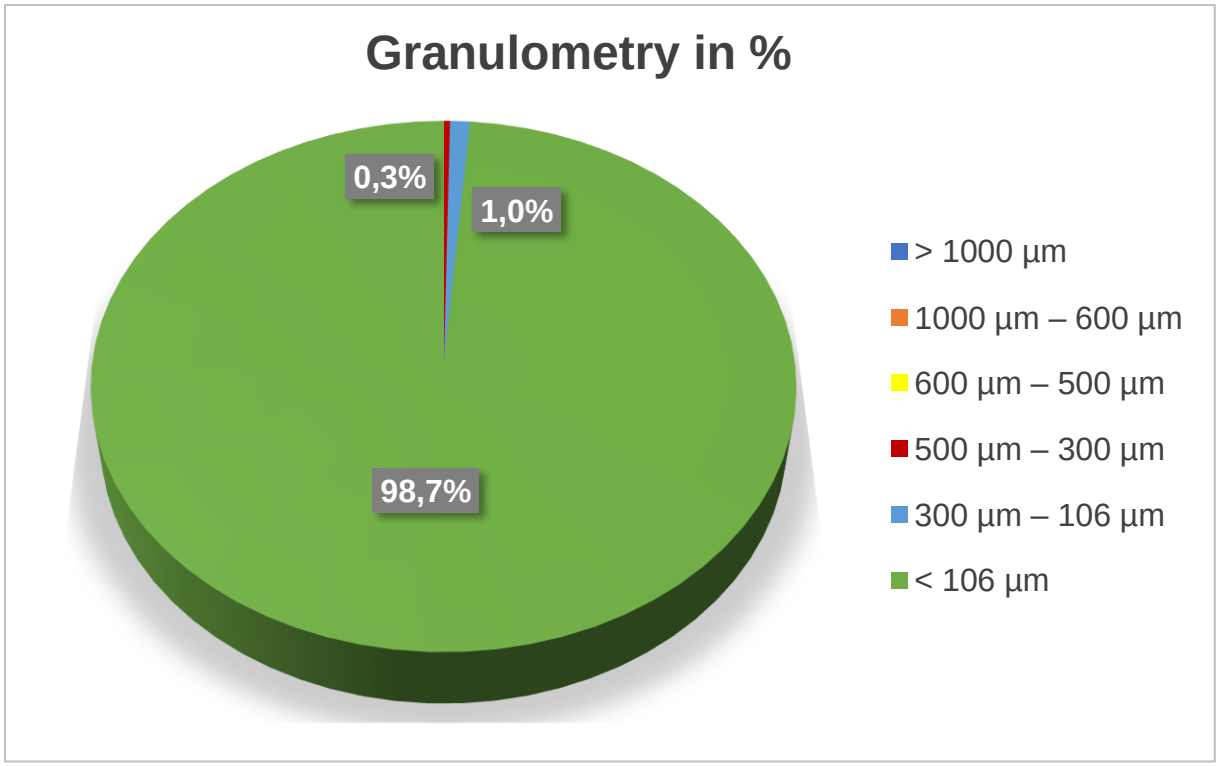

Figure 8. Granulometry of the small scale HMX synthesis.

11.3 Investigation of the variation of the filter temperature after II Hydrolysis in the HMX Small scale synthesis

To investigate the effect of different filter temperatures on yield, HMX:RDX ratio and the secondary product, the above described small scale synthesis of HMX was performed with different filter temperatures. The results are shown in the following table.

Table 4. Results from the variation of the filter temperature after II Hydrolysis in the HMX Small scale synthesis.

Trial No.	Filter temperature [°C]	Yield [%]	Ratio HMX:RDX	Yield Sec. product	Ratio HMX:RDX in Sec. product
1	65	31.6 %	100:0	1.45 g for 7.01g HMX	22:78
2	60	33.1 %	100:0	1.41 g for 7.37 g HMX	07:93
3	55	34.7 %	88:12	1.23 g for 7.73 g HMX	05:95
4	50	35.2 %	86:14	1.21 g for 7.84 g HMX	05:95
5	45	56.0 %	42:58	0.92 g for 8.23 g HMX	05:95

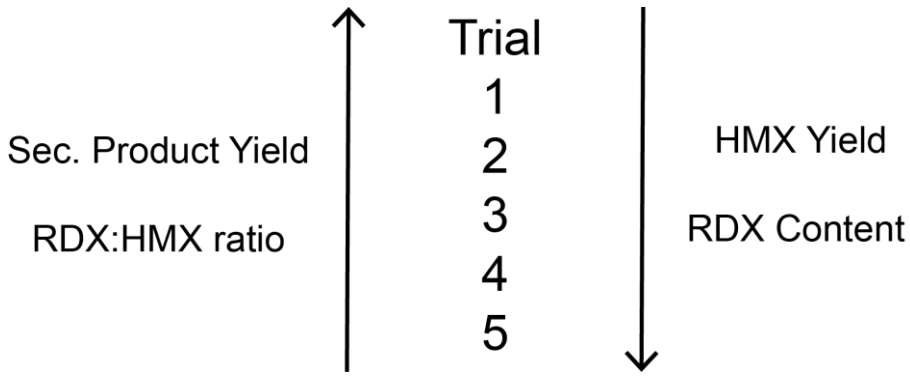

Figure 3. Results from the variation of the filter temperature after II Hydrolysis in the HMX Small scale synthesis.

12 Summary and Conclusion

In this dissertation, research was done in all three areas of the high-energy materials research domains shown in Figure 1.

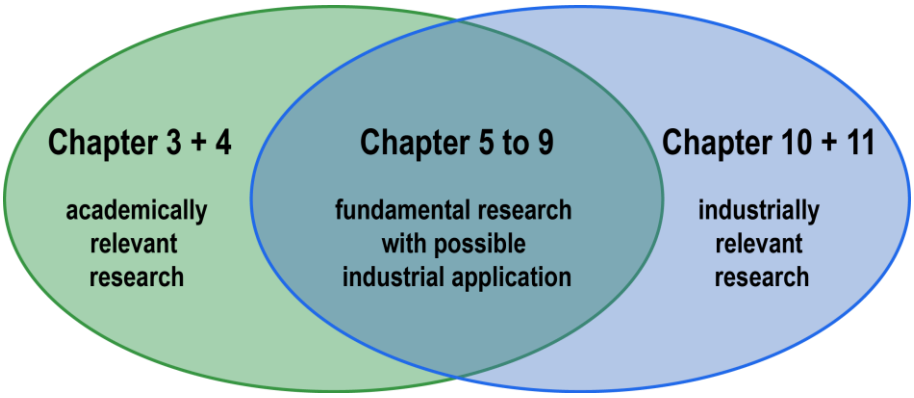

Figure 1. Research focus of the different chapters of this thesis in the area of energetic materials.

In chapters 3 and 4, research was conducted into modifying the properties in the academic field of the energetic material FOX-7 by isotopic labeling. The main part of the thesis (chapters 5 to 9) deals with fundamental research that could either have a potential industrial application or contribute information about already used materials to the industry. Mainly, new high-energy materials were synthesized and fully characterized. This includes the investigation of their thermal properties as well as their sensitivities towards external stimuli. But also spectroscopic measurements (NMR and IR) and if possible single crystal X-ray diffraction. In addition, the performance parameters were also determined by quantum chemical calculations. The last part, chapters 10 and 11, refers to the industrially relevant part of the research domains. On the one hand, a possible new route for RDX synthesis was investigated and evaluated for its industrial applicability. On the other hand, the Bachman process for industrial RDX and HMX synthesis was investigated and different process properties, such as filter temperatures, were studied. In the following, the essential aspects of the individual chapters are summarized and particularly promising compounds are highlighted.

In **Chapter 3** of this thesis, the known secondary explosive FOX-7 was deuterated. The deuteration level was determined to be greater than 95% by ^{1}H *q*-NMR. It was also possible to determine the crystal structure of FOX-7-D_4, which crystallized in

a different space group than the classical, non-deuterated FOX-7. FOX-7-D_4 was found to have a higher density of 1.90 g cm^{-3} compared to 1.87 g cm^{-3} of FOX-7 at room temperature. Their thermal stability was also compared, and it was found that the decomposition temperature of the deuterated FOX-7-D_4 is about 30°C higher than that of the hydrogenated form. This can be explained by the kinetic isotope effect. In addition, the activation energy of thermal decomposition of both compounds was determined, and the enthalpies of formation and zero-point energies of both were calculated. This showed that the previously established theory that deuterated compounds, in contrast to their hydrated derivatives, have a lower zero-point energy but a higher activation energy also applies for FOX-7-D_4. **Chapter 4** deals with the ^{13}C isotopic labeling of FOX-7. Starting from double ^{13}C-labeled acetonitrile, the isotopically labeled FOX-7 was isolated in a four-step synthesis. It was studied by IR and NMR spectroscopy, and due to ^{13}C labeling, a splitting was observed in the ^{13}C NMR spectrum of this compound. Thermal studies by differential thermal analysis (DTA) revealed that, similar to previously reported in Chapter 3, the thermal stability of the ^{13}C-labeled FOX-7 was enhanced by the kinetic isotope effect, increasing the decomposition temperature by about 30°C compared to the unlabeled FOX-7. Figure 2 shows the studied compounds of chapters 3 and 4 with their decomposition temperatures.

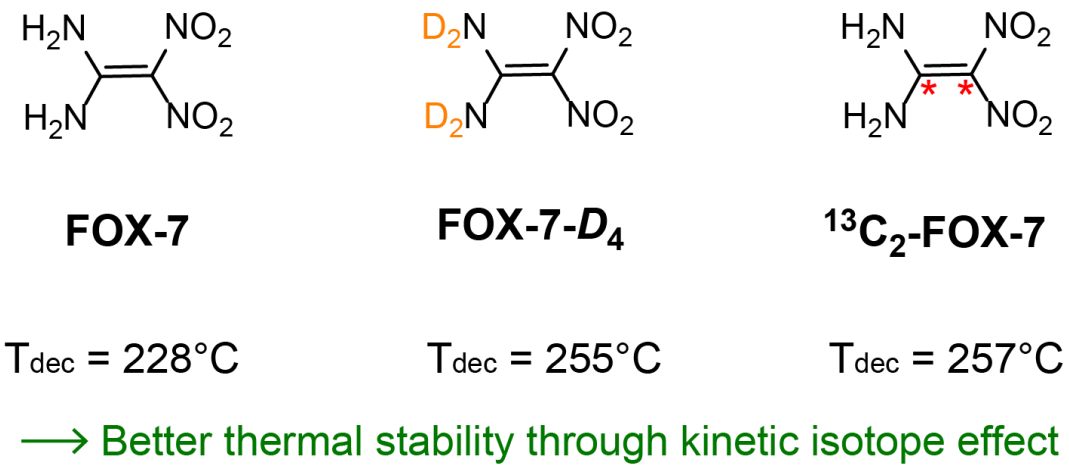

Figure 2. Main compounds of chapter 3 and 4 with their decomposition temperatures.

In **Chapter 5** of this dissertation, the crystal structures of the energetic plasticizers EGDN, DEGDN and TEGDN were determined for the first time using a low-temperature crystallization method. From these crystal structures (Figure 3), new

information about the properties in the solid state could be obtained, for which *Hirshfeld* analyses were performed. These have shown that, as for in the liquid compounds at room temperature, EGDN is most sensitive followed by DEGDN and then by TEGDN. Vapor pressure measurements of the three compounds were also performed and compared. The study showed a trend that the introduction of more ethylene glycol bridges leads to a decrease in volatility while increasing the molar enthalpy of vaporization.

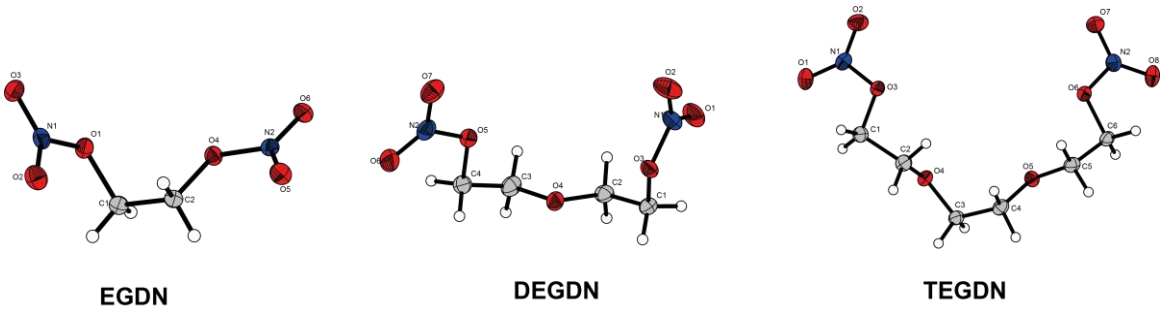

Figure 3. Crystal structures of the energetic plasticizers EGDN, DEGDN and TEGDN.

Chapter 6 deals with the synthesis and characterization of the corresponding nitrocarbamate of the nitric ester DINA (dinitroxyethyl nitramine dinitrate), which is widely used as an energetic plasticizer in composite compositions. Nitrocarbamates generally show a higher thermal stability than the corresponding organic nitrates, which would make them promising compounds. However, this statement could not be confirmed by analytical measurements. On the contrary, DTA measurements showed that DINA (184°C) indeed exhibits higher thermal stability than its nitrocarbamate counterparts bis (nitrocarbamoylethyl) ammonium nitrate (150°C) and bis (nitrocarbamoylethyl) nitramine (BNCEN) (153°C). However, if the detonation parameters are compared, it can be seen that the higher nitrogen content and increased density of bis (nitrocarbamoylethyl) nitramine nitrocarbamate lead to better detonation velocity compared to DINA. Figure 4shows some values of DINA compared to its corresponding nitrocarbamate BNCEN.

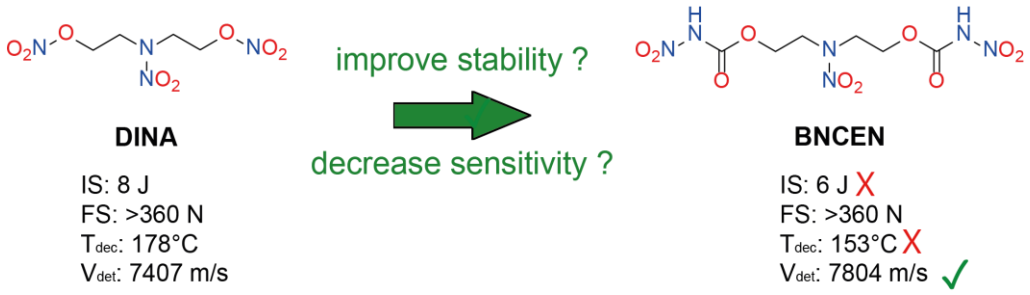

Figure 4. Properties of DINA in comparison with its corresponding nitrocarbamate BNCEN.

In **Chapter 7**, two new nitrazapropyl- and oxapropyl-bridged nitraminotriazoles were synthesized. In addition, some salts with both compounds and the hydrazonmethylene-bridged derivative were prepared and characterized. From the comparison of the bridging moieties, it is found that the nitrazapropylene bridge (1,3-*bis*(3-nitramino-4*H*-1,2,4-triazole-5-yl) 2-nitrazapropane, BNATNAP) has the lowest thermal stability. This is probably due to the thermally labile nitramino group, although it improves the energetic parameters. The oxapropylene bridge (1,3-*bis*(3-nitramino-4*H*-1,2,4-triazole-5-yl) 2-oxapropane, BNATOP) prevents a decrease in energetic properties but increases thermal stability. The overall most balanced nitraminotriazole is the hydrazonemethylene-bridged derivative (1,3-*bis*(3-nitramino-4*H*-1,2,4-triazole-5-yl) hydrazonemethane, BNATHM) with moderate thermal stability and the best energetic properties. The salts confirm the same trends, but with increased thermal stability. Selected properties of the three different bridged triazoles are shown in Figure 5.

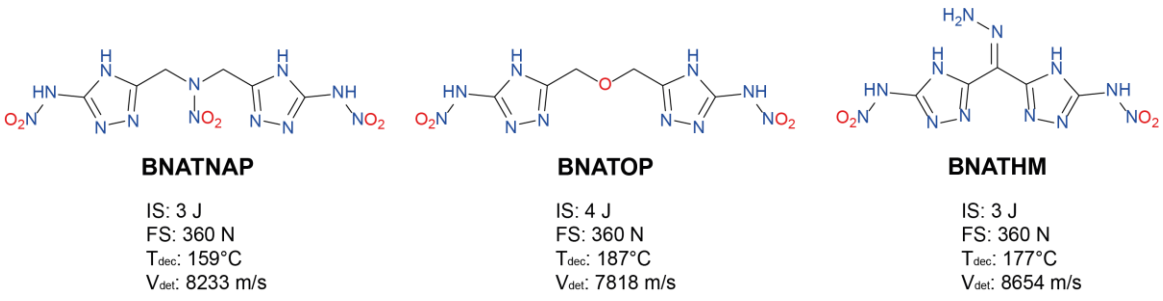

Figure 5. Compared properties of the three different bridged triazoles BNATNAP, BNATOP and BNATHM.

Chapter 8 includes the synthesis of three new energetic materials, 1,3-dinitroxy-2-nitrazapropane, 1,7-dinitroxy-2,4,6-trinitrazaheptane, and 1,3-dinitroxy-2-

oxapropane, which were synthesized as well as fully characterized and show promising properties. Importantly, the precursors of 1,3-dinitroxy-2-nitrazapropane and 1,7-dinitroxy-2,4,6-trinitrazaheptane can be obtained by modifying the reaction conditions of the Bachmann process and thus can be synthesized in existing plants. The syntheses of each of the three new compounds were tested by two different routes and compared. The modified Bachmann process for the synthesis of the two new nitric esters is shown in Figure 6.

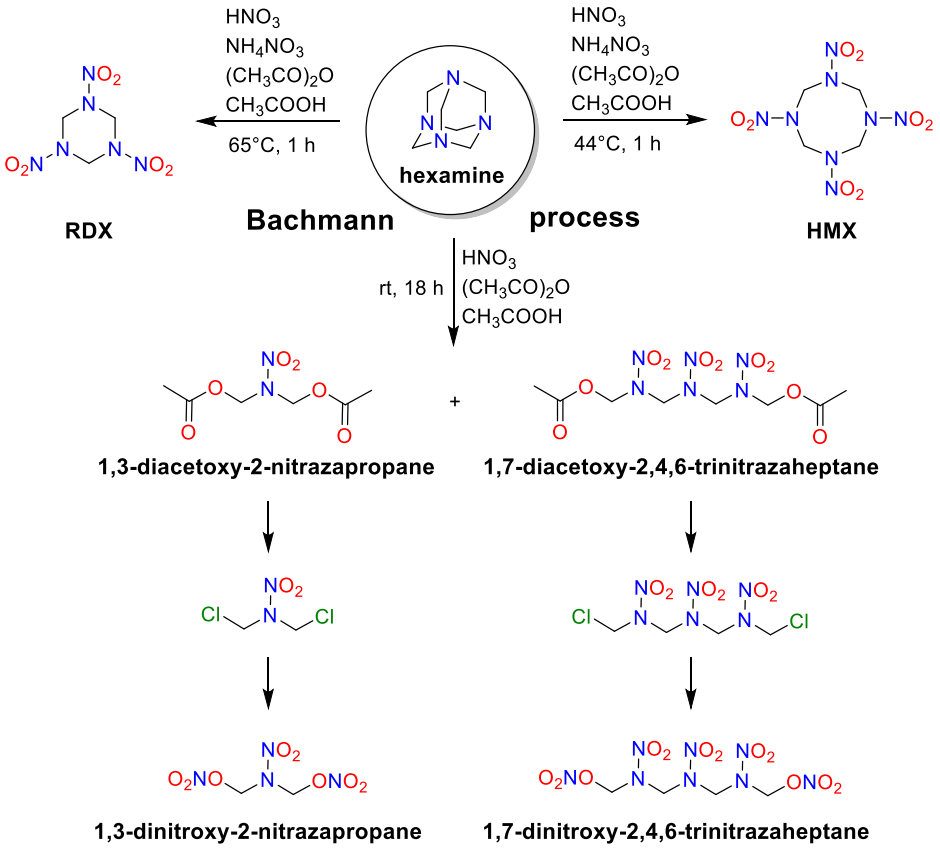

Figure 6. Modified Bachmann process for the synthesis of 1,3-dinitroxy-2-nitrazapropane and 1,7-dinitroxy-2,4,6-trinitrazaheptane.

The properties of 1,3-dinitroxy-2-nitrazapropane and 1,7-dinitroxy-2,4,6-trinitrazaheptane are very similar to the explosive PETN, which is often used as a booster and obtains its energetic character by functionalization with nitric ester groups. Comparing the energetic parameters of these three compounds, it can be seen that both 1,3-dinitroxy-2-nitrazapropane and 1,7-dinitroxy-2,4,6-trinitrazaheptane, have higher performance values, for example a higher detonation velocity than PETN. Selected values can be seen in Figure 7.

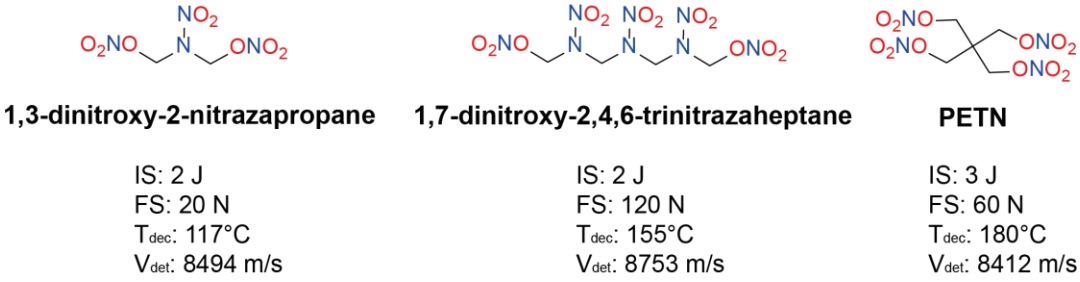

Figure 7. Compared properties of 1,3-dinitroxy-2-nitrazapropane, 1,7-dinitroxy-2,4,6-trinitrazaheptane and PETN.

A closer look at the properties of 1,3-dinitroxy-2-oxapropane reveals a strong similarity to nitroglycerin, which is still used today in double- and triple-base propellants. Comparing these two compounds shows that the oxygen balance of 1,3-dinitroxy-2-oxapropane exceeds that of NG, but it has a lower detonation velocity due to its lower heat of formation. Nevertheless, 1,3-dinitroxy-2-oxapropane could be used in propellant mixtures or as an energetic plasticizer such as EGDN.

In **Chapter 9** of this thesis, new nitramine- and oxa-bridged energetic materials as well as two new energetic coordination compounds were synthesized and fully characterized. As mentioned in the chapter above, the starting materials can be prepared by a modified Bachmann Process and further used by a one-step Finkelstein reaction (Figure 8).

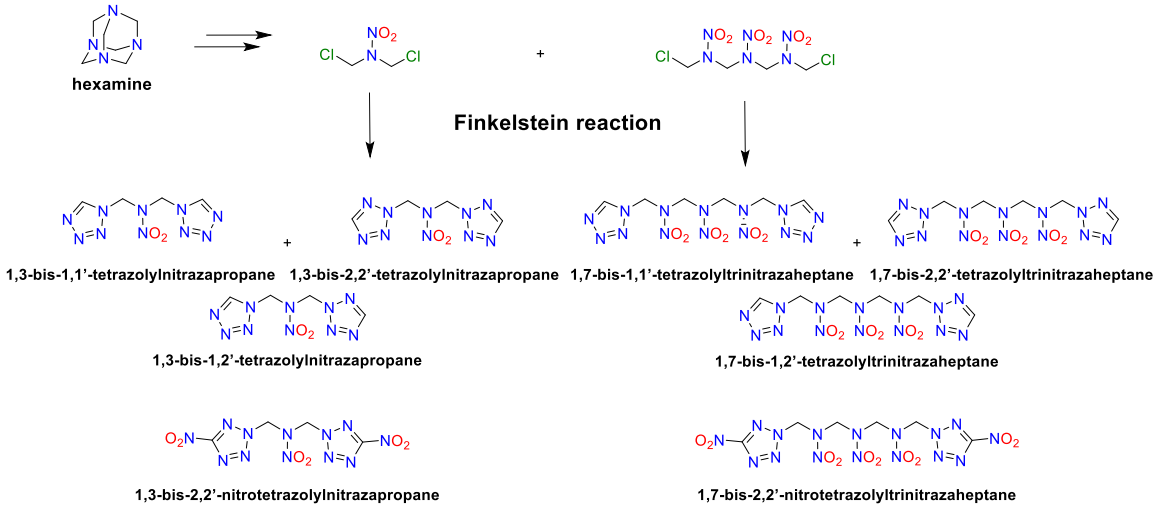

Figure 8. Synthesis of the new nitramine bridged tetrazoles.

Especially 1,3-*bis*-2,2'-nitrotetrazolylnitrazapropane and 1,7-*bis*-2,2'-tetrazolyltrinitrazaheptane stand out with their promising properties as possible RDX substitutes. 1,3-*Bis*-2,2'-nitrotetrazolylnitrazapropane shows very good values compared to RDX in terms of its performance parameters. It has a higher detonation velocity than RDX and comparable thermal stability, but is more sensitive towards impact and friction than RDX. 1,7-*Bis*-2,2'-tetrazolyltrinitrazaheptane, is less sensitive compared to RDX. However, due to its lower density, it has a calculated detonation velocity 400 m s^{-1} lower than RDX. Furthermore, 1,3-*bis*-2,2'-tetrazolylnitrazapropane shows promising properties as a possible TNT substitute as a melt-castable explosive. It is in a good temperature range with a melting point of 72°C and decomposes 100 degrees higher at 173°C. It also performs significantly better than TNT, as shown in Figure 9.

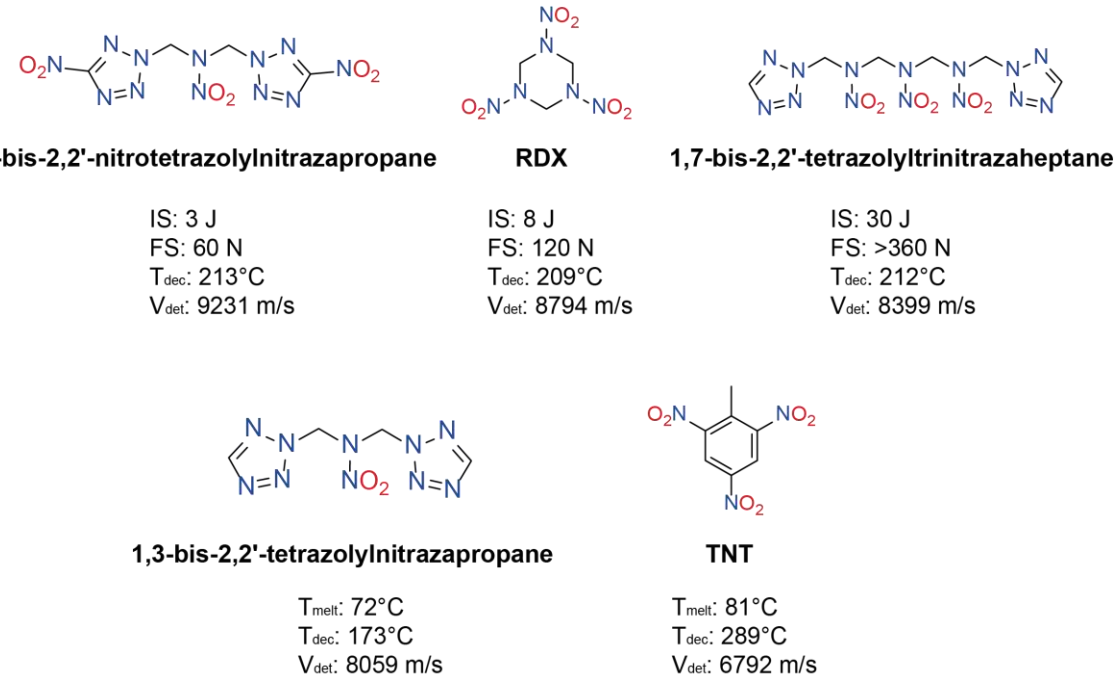

Figure 9. Compared properties of new compounds of chapter 9 with RDX and TNT.

In **Chapter 10**, the synthesis of RDX *via* the intermediate TRAT (1,3,5-triacetyl-1,3,5-triazinane) was investigated as a possible alternative industrial production method. This route was touted as a promising method to produce pure RDX (without HMX impurities) under industrial conditions. This method has several advantages, including cheap starting materials (1,3,5-trioxane) and reactants, and easy separation from the intermediate products TAT (1,3,5,7-tetraacetyl-1,3,5,7-

tetrazocinane) and TRAT by solubility differences. Due to the similar chemical and physical properties of RDX and HMX, isolation of both is very difficult, so it would be advantageous to separate the precursors TAT and TRAT from each other to obtain pure RDX in the next step. This aspect was successfully confirmed in this work, as no traces of TAT were detected in TRAT after washing with ethyl acetate. However, only a moderate yield of 50% was obtained in the synthesis of TRAT, which represents a serious drawback in the synthesis of TRAT.

However, the biggest challenge is in the next step of finding a feasible nitration method from TRAT to RDX. Every tested nitration method either does not yield a nitration product or results only in a incomplete nitration with 1,3-diacetyl-5-nitro-1,3,5-triazinane (DANT) and 5-acetyl-1,3-dinitroo-1,3,5-triazinane (ADNT) as main product with a small amount of RDX as by-product, as can be seen in Figure 10. So, it summary, this method will certainly not replace the established processes.

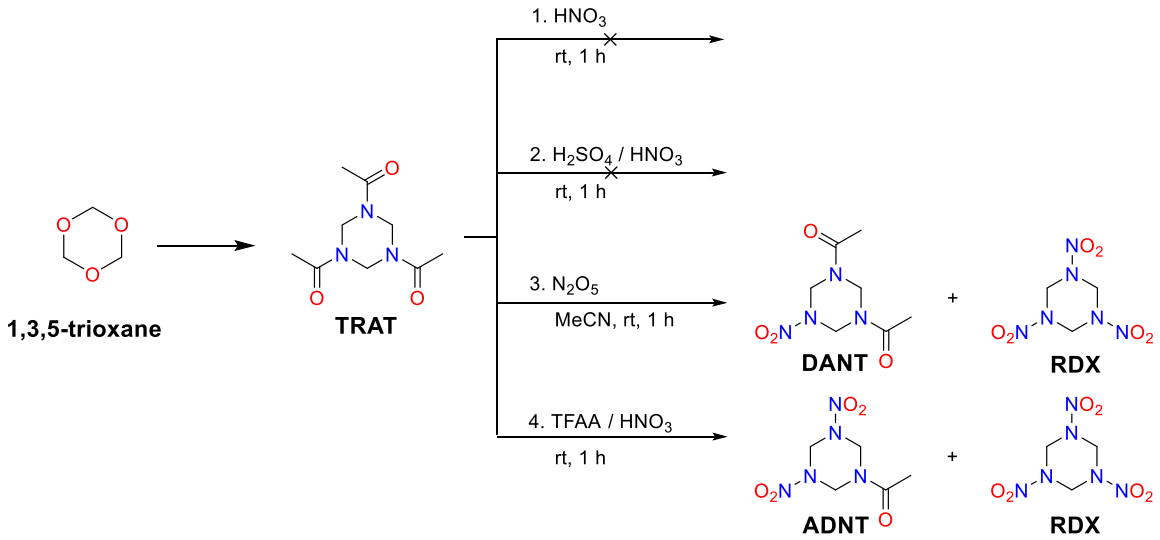

Figure 10. Synthesis of RDX *via* the intermediate TRAT (1,3,5-triacetyl-1,3,5-triazinane).

Chapter 11 shows parts of a collaborative project with industry. This involves the investigation and study of the Bachmann process for RDX and HMX synthesis. It includes, on the one hand, the investigation of the individual process steps on a small scale and, on the other hand, the investigation and characterization of the products. It has been shown that the filtration steps, especially the first filtration step, are very crucial for the purity and yield of the final product. It is therefore

important to ensure that the filtration parameters are strictly adhered to. The steps of the industrial used Bachman process are shown in Figure 11.

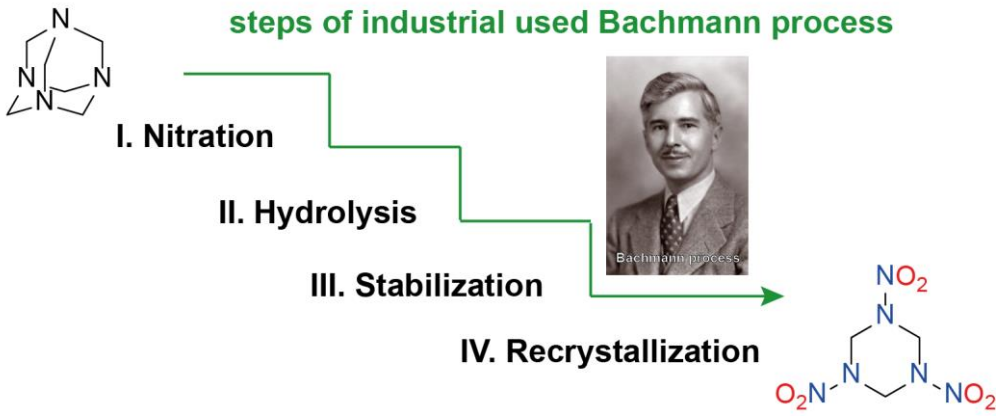

Figure 11. Step of the industrial used Bachmann process for RDX syntehsis.

Overall, it can be said that this dissertation has contributed different research results to all three research areas of energetic materials. Particularly promising are the results of chapters 8 and 9, since on the one hand the first synthesis steps can be carried out on existing Bachmann plants and on the other hand a large number of different compounds from different areas of application can be produced. The nitric esters described in chapter 8 show promising properties for their use as booster explosives. The two most promising compounds from chapter 9 1,3-*bis*-2,2'-nitrotetrazolylnitrazapropane and 1,7-*bis*-2,2'-tetrazolyltrinitrazaheptane could be possible RDX substitutes due to their properties. In addition, the nitramine-bridged tetrazoles in combination with the right metal and anion could have suitable properties for use as primary explosive.

13 Appendix

13.1 List of Co-Author Publications

13.1.1 Highly functional energetic complexes: stability tuning through coordination diversity of isomeric propyl-linked ditetrazoles

Norbert Szimhardt, Maximilian H. H. Wurzenberger, Thomas M. Klapötke, Jasmin T. Lechner, Hannes Reichherzer, Cornelia C. Unger and Jörg Stierstorfer*

published in *Journal of Materials A* **2018**, *6,* 6565−6577

DOI: 10.1039/C8TA01412D

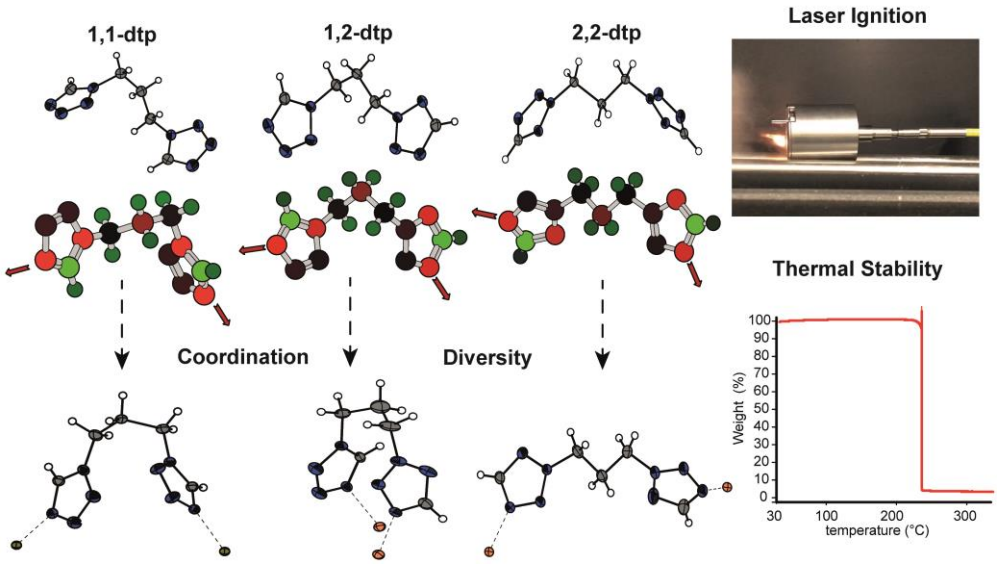

Abstract: Currently used primary explosives suffer not only from various drawbacks like insidious sensitivities toward mechanical stimuli and electrostatic discharge, but also from environmental concerns largely attributed to toxic lead

compounds. These issues can directly be related to higher risk during processing and handling of these sensitive materials. In this research, 12 new lead-free energetic coordination compounds (ECCs) based on three isomeric propyl-linked ditetrazoles as ligands with moderate sensitivities are described, which can be initiated reliably and safely by irradiation with near infrared light (NIR). Excellent thermal stabilities for all complexes up to an outstanding decomposition temperature of 297 °C for compound **7** could be achieved through the formation of stable polymeric networks. The optical and energetic properties of these complexes can easily be customized by variation of various building blocks like different transition metals (Mn^{2+}, Fe^{2+}, Ni^{2+}, Co^{2+}, Cu^{2+}, Zn^{2+}, and Ag^{+}) and anions (perchlorate, styphnate, cyanodinitromethanide and dinitramide) and for the first time by the use of three different isomeric ditetrazole ligands. 1,3-Di(tetrazol-1-yl)propane (1,1-dtp), 1-(tetrazol-1-yl)-3-(tetrazol-2-yl)propane (1,2-dtp) and 1,3-di(tetrazol-2-yl)propane (2,2-dtp) were prepared in a convenient and straightforward one-step alkylation reaction of 1,5*H*-tetrazole. The obtained compounds were extensively characterized by *e.g.* XRD, IR, EA, UV/Vis and DTA. In addition, the sensitivities toward external stimuli (impact, friction and electrostatic discharge) were determined according to Bundesamt für Materialforschung und -prüfung (BAM) standard methods. Iron(II) **5** and copper(II) perchlorate complexes **8**, **11** and **12** show promising characteristics and could be potential candidates for possible applications in the future.

13.1.2 Copper(II) Dicyanamide Complexes with N-Substituted Tetrazole Ligands – Energetic Coordination Polymers with Moderate Sensitivities

Maximilian H. H. Wurzenberger, Jasmin T. Lechner, Dr. Jörg Stierstorfer*

published in *ChemPlusChem* **2020**, *85*, 769−775

DOI: 10.1002/cplu.202000156

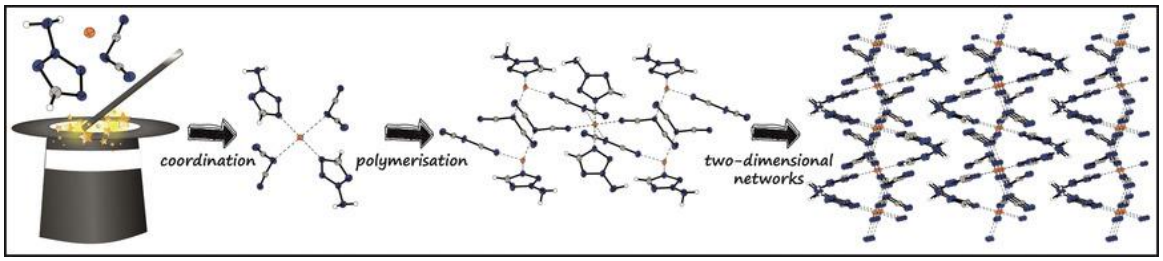

Abstract: Following the useful concept of energetic coordination compounds (ECC), copper(II) dicyanamide was used as a building block for the synthesis of eight new complexes. As ligands, six different *N*-substituted tetrazoles were applied, leading to the formation of high-nitrogen containing complexes. The obtained compounds were characterized in detail by single crystal as well as powder XRD, IR, EA, DTA, and TGA. In addition, the sensitivities towards impact and friction were determined with BAM standard techniques as well as the sensitivity towards electrostatic discharges. All compounds show moderate sensitivities (*IS*>6, *FS*>80 N) and energetic properties but differ in their polymeric structures forming polymeric chains or layers up to 3D networks.

13.1.3 Salts of Picramic Acid – Nearly Forgotten Temperature-Resistant Energetic Materials

Maximilian H. H. Wurzenberger, Jasmin T. Lechner, Marcus Lommel, Thomas M. Klapötke, Jörg Stierstorfer

published in *Propellants Explosives and Pyrotechnics* **2021**, *45,* 898–907

DOI: 10.1002/prep.201900402

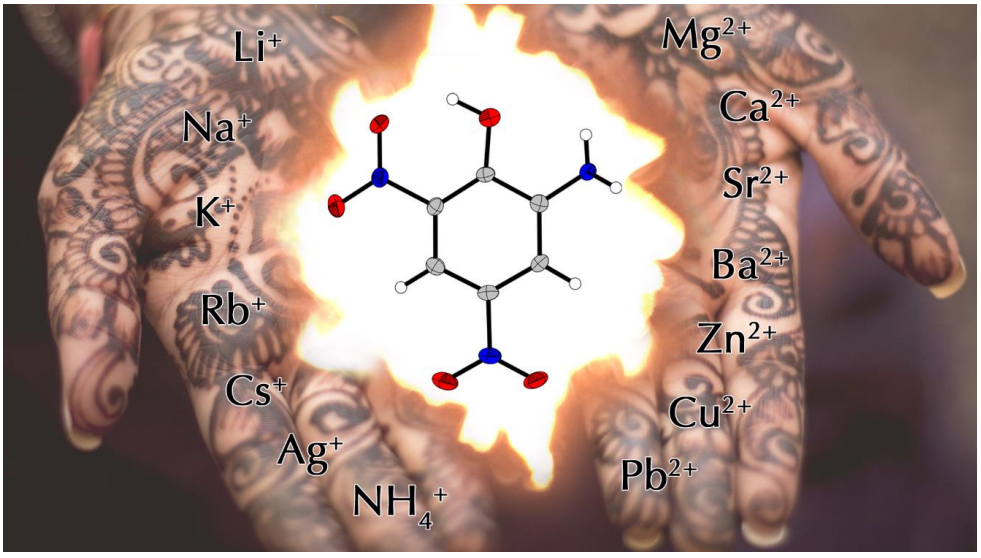

Abstract: Thermally stable explosives are becoming more and more important nowadays due to their important role in the oil and mining industry. The requirements of these explosives are constantly changing. Picramate-based compounds are poorly investigated towards their energetic properties as well as sensitivities. In this work, 13 different salts of picramic acid were synthesized as potential energetic materials with high thermal stability in a simple one-step reaction and compared with commercially used lead picramate. The obtained compounds were extensively characterized by e. g. XRD, IR, EA, DTA, and TGA.

In addition, the sensitivities towards impact and friction were determined with the BAM drop hammer and the BAM friction tester. Also, the electrostatic discharge sensitivity was explored. Calculations of the energetic performance of selected compounds were carried out with the current version of EXPLO5 code. Therefore, heats of formation were computed and X-ray densities were converted to room temperature. Some of the synthesized salts show promising characteristics with high exothermic decomposition temperatures. Especially, the water-free rubidium, cesium, and barium salts **5**, **6** and **10** with decomposition temperatures of almost 300 °C could be promising candidates for future applications.

13.1.4 Synthesis, Characterization and Derivatives of Iso-Picramic Acid

Thomas M. Klapötke*, Jasmin T. Lechner and Jörg Stierstorfer

as published in *Propellants Explosives and Pyrotechnics* **2022**, *47*, e2021002

DOI: 10.1002/prep.202100205

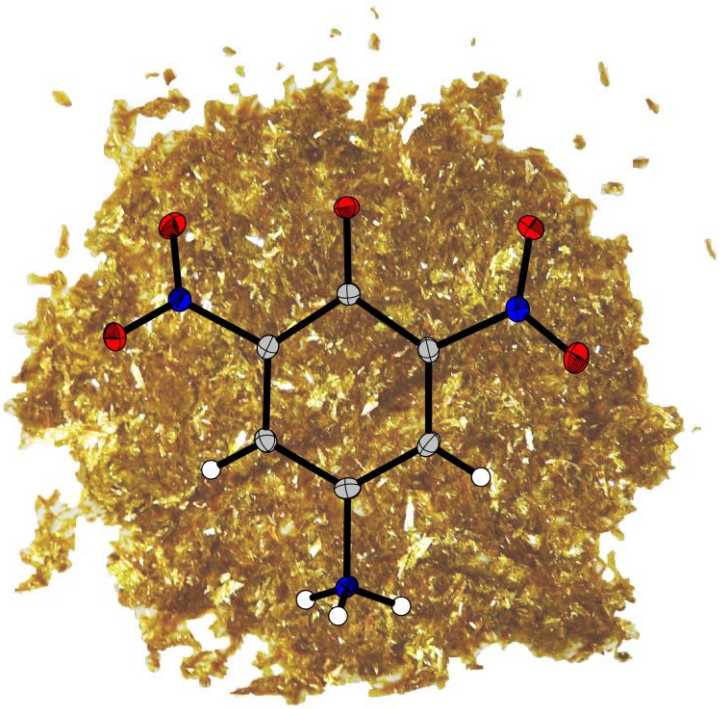

Abstract: Comparing the sensitive explosives DDNP (2-diazonium-4,6-dinitrophenolate) with iso-DDNP (para-DDNP, 4-diazonium-2,6-dinitrophenolate), it seems obvious that with increasing symmetry in the molecule, the energetic parameters also increase. This work therefore investigates whether the same trend can be applied for the isomers picramic acid (2-amino-4,6-dinitrophenol) and iso-picramic acid (para picramic acid, 4-amino-2,6-dinitrophenol). For this purpose,

iso-picramic acid was synthesized and compared with the properties of picramic acid. In addition, selected ionic and other energetic derivatives such as 2,6-dinitro-4-(5*H*-tetrazol-1-yl)phenol were synthesized. The compounds were extensively studied by XRD, IR, EA, DTA and TGA. Further, their sensitivities towards impact and friction were investigated and the energetic properties were computed using the EXPLO5 code.

13.1.5 Kinetic Predictions Concerning the Long-Term Stability of TKX-50 and Other Common Explosives Using the NETZSCH Kinetics Neo Software

Alexander G. Harter, Thomas M. Klapötke,* Jasmin T. Lechner, Jörg Stierstorfer

published in *Propellants Explosives and Pyrotechnics* **2022**, *47*, e2022000

DOI: 10.1002/prep.202200031

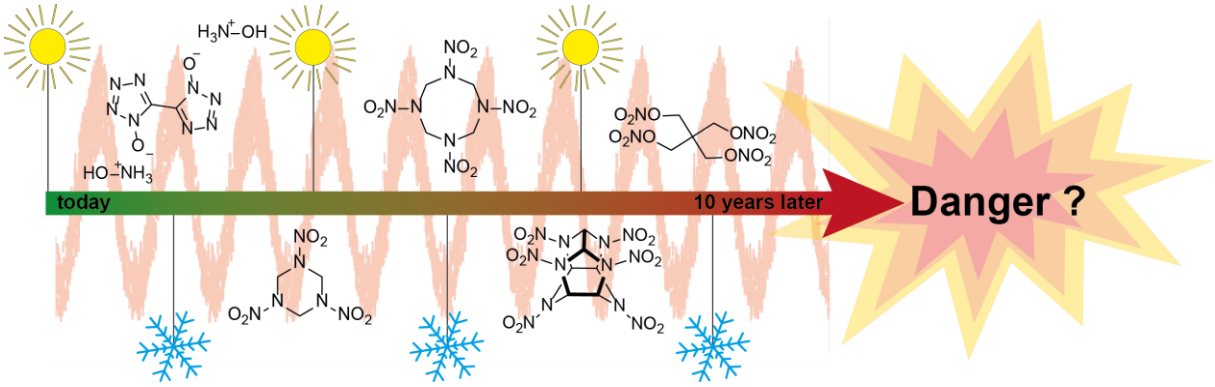

Abstract: Explosives are used in both military and civilian applications all over the world. Sufficient longevity and good thermal stability are therefore essential for safe handling and safe storage of energetic materials. In this work, five well-known compounds, TKX-50, RDX, HMX, CL-20 and PETN, were investigated by means of different kinetic models, in order to make predictions about their long-term stability. For this purpose, the compounds were synthesized according to literature-known procedures and thermogravimetric (TG) measurements were performed. The TG plots were analyzed using the Ozawa-Flynn-Wall, Friedman and ASTM E698 kinetic models with the NETZSCH Kinetics Neo software and the activation energy and isothermal long-term stability were determined. Moreover, various climatic predictions of different countries were made.

13.1.6 Exploring the Photochemistry of Solid 1,1-Diamino-2,2-dinitroethylene (FOX-7) Spanning Simple Bond Ruptures, Nitro-to-Nitrite Isomerization, and Nonadiabatic Dynamics

Andrew M. Turner, Yuheng Luo, Joshua H. Marks, Rui Sun*, Jasmin T. Lechner, Thomas M. Klapötke* and Ralf I. Kaiser*

published *in Journal of Physical Chemistry A* **2022,** *126*, 4747–4761

DOI: 10.1021/acs.jpca.2c02696

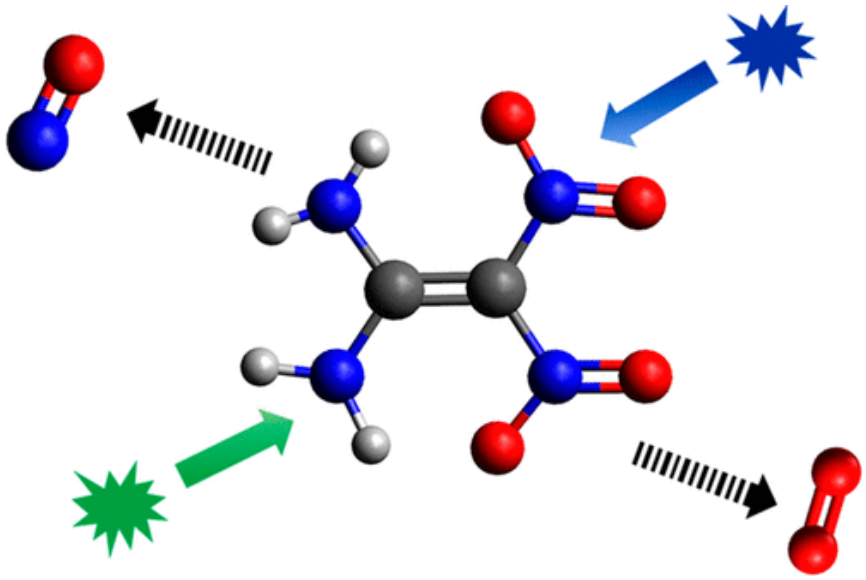

Abstract: The UV photolysis of solid FOX-7 at 5 K with 355 and 532 nm photons was investigated to unravel initial isomerization and decomposition pathways. Isomer-selective single photon ionization coupled with reflectron time-of-flight mass spectrometry (ReTOF-MS) documented the nitric oxide (NO) loss channel at 355 nm along with a nitro-to-nitrite isomerization, which was observed by using infrared spectroscopy, representing the initial reaction pathway followed by O–NO bond rupture of the nitrite moiety. A residual gas analyzer detected molecular oxygen for the 355 and 532 nm photolysis at a ratio of 4.3 ± 0.3:1, which signifies FOX-7 as an energetic material that provides its own oxidant once the

decomposition starts. Overall branching ratios for molecular oxygen versus nitric oxide were derived to be 700 ± 100:1 at 355 nm. It is notable that this is the first time that molecular oxygen was detected as a decomposition product of FOX-7. Computations show that atomic oxygen, which later combines to form molecular oxygen, is likely released from a nitro group involving conical intersections. The condensed phase potential energy profile computed at the CCSD(T) and CASPT2 level correlates well with the experiments and highlights the critical roles of conical intersections, nonadiabatic dynamics, and the encapsulated environment that dictate the mechanism of the reaction through intermolecular hydrogen bonds.

13.1.7 Electron-Induced Decomposition of Solid 1,1-Diamino-2,2-Dinitroethylene (FOX-7) at Cryogenic Temperatures

Andrew M. Turner, Joshua H. Marks, Yuheng Luo, Jasmin T. Lechner, Thomas M. Klapötke,* Rui Sun,* and Ralf I. Kaiser*

published *in Journal of Physical Chemistry A* **2023,** *127*, 3390–3401

DOI: 10.1021/acs.jpca.3c01035

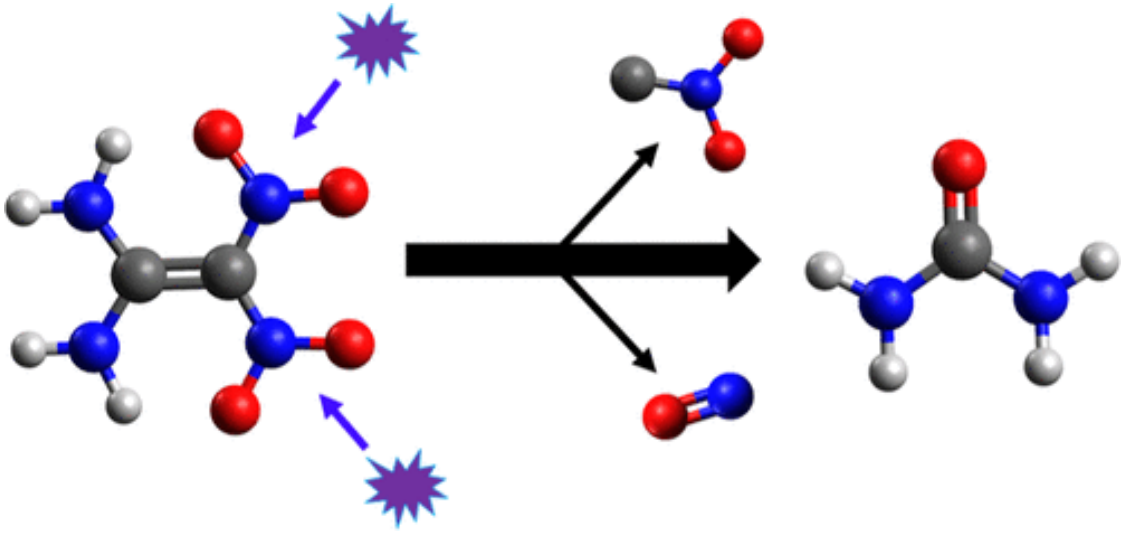

Abstract: Solid FOX-7 (1,1-diamino-2,2-dinitroethylene), an energetic material of interest due to its high stability and low shock/thermal sensitivity, was exposed to energetic electrons at 5 K to explore the fundamental mechanisms leading to decomposition products and provide a better understanding of the reaction pathways involved. As a result of the radiation exposure, infrared spectroscopy revealed carbon dioxide (CO_2) and carbon monoxide (CO) trapped in the FOX-7 matrix, while these compounds along with water (H_2O), nitrogen monoxide (NO), and cyanogen (C_2N_2) were detected exploiting quadrupole mass spectrometry both during irradiation and during the warming phase from 5 to 300 K. Photoionization reflectron time-of-flight mass spectrometry detected small molecules such as ammonia (NH_3), nitrogen monoxide (NO), and nitrogen dioxide (NO_2) as well as

more complex molecules up to 96 amu. Potential reaction pathways are presented and assignments are discussed. Among the reaction mechanisms, the importance of an initial nitro-to-nitrite isomerization is highlighted by the observed decomposition products.

13.1.8 Ultraviolet-Initiated Decomposition of Solid 1,1-Diamino-2,2-Dinitroethylene (FOX-7)

Andrew M. Turner, Joshua H. Marks, Jasmin Lechner, Thomas M. Klapötke,* Rui Sun,* Ralf I. Kaiser*

published *in Journal of Physical Chemistry A* **2023,** *127*, 7707–7717

DOI: 10.1021/acs.jpca.3c03215

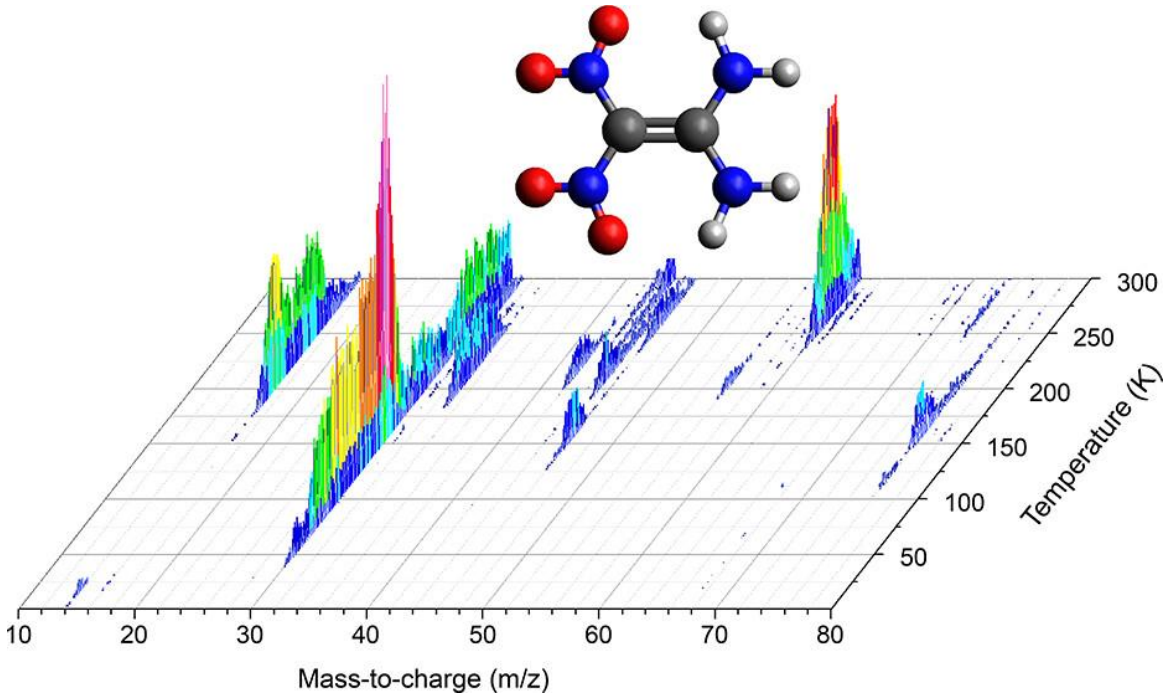

Abstract: FOX-7 (1,1-diamino-2,2-dinitroethylene) was photolyzed with 202 nm photons to probe reaction energies leading to the decomposition of this energetic material and to compare results from irradiations using lower energy 532 nm and 355 nm photons as well as higher energy electrons. The photolysis occurred at 5 K to suppress thermal reactions and the solid samples were monitored using Fourier transform infrared spectroscopy (FTIR), which observed carbon dioxide (CO_2), carbon monoxide (CO), cyanide (CN^-), and cyanate (OCN^-) after irradiation.

During warming to 300 K, subliming products were detected using electron-impact quadrupole mass spectrometry (EI-QMS) and photoionization time-of-flight mass spectrometry (PI-ReTOF-MS). Five products were observed in the QMS: water (H_2O), carbon monoxide (CO), nitric oxide (NO), carbon dioxide (CO_2), and cyanogen (NCCN). The ReTOF-MS results showed overlap with electron irradiation products but also included three intermediates for the oxidation of ammonia and nitrogen monoxide: hydroxylamine (NH_2OH), nitrosamine (NH_2NO), and the largest product at 76 amu with the proposed assignment of hydroxyurea ($NH_2C(O)NHOH$). These results highlight the role of reactive oxygen intermediates and nitro-to-nitrite isomerization as key early reactions that lead to a diverse array of decomposition products.

13.1.9 Performance of TKX-50 in Thermobaric Explosives

Thomas M. Klapötke,* Stanisław Cudziło,* Waldemar A. Trzciński, Józef Paszula, Lukas Bauer, Christian Riedelsheimer, Jasmin T. Lechner

published in *Propellants Explosives and Pyrotechnics* **2023**, *48,* e202300010

DOI: 10.1002/prep.202300010

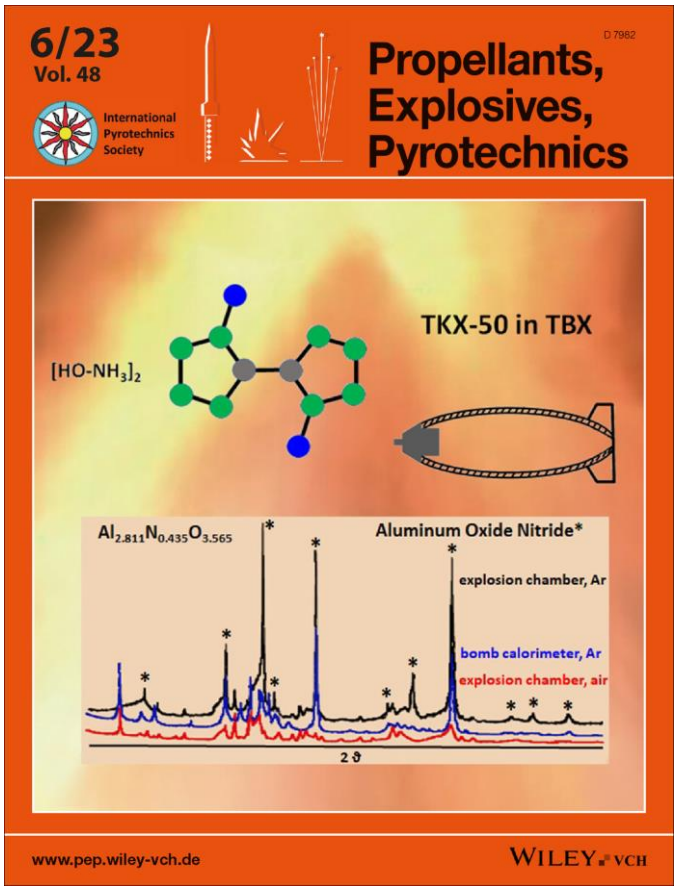

Abstract: In this study, the behavior of the high-nitrogen compound TKX-50 in model thermobaric formulations was investigated. The addition of 10 % Al to TKX-50 reduces the heat of detonation by approximately 90 J/g. Despite this, Al reacts with the detonation products of TKX-50 in an exothermic manner, and the energy

contribution was calculated to be approx. 375 J/g. In addition, the overpressure in the explosion chamber filled with argon after detonation of aluminized TKX-50 charges containing 27 % Al is approx. 20 % higher than in the case of neat TKX-50. Also the maximum temperature of the TKX-50/Al explosion products in the argon filled chamber is higher by 370 K than that of measured after detonating TKX only. What is more aluminum oxynitride with a low nitrogen content has been identified in the solid detonation products of aluminized TKX-50, but only for detonations in argon. Of course, charges made of TKX-50/Al mixture generate significantly higher overpressure and radiant temperature values in a confined space when they are detonated in an air atmosphere. It all means that burning aluminum in nitrogen provides little energy, and even if the concentration of nitrogen in the post-detonation products is much higher than that of oxygen, aluminum oxides are preferentially formed.

13.1.10 Application of 1- and 2-propargyltetrazole in laser-ignitable energetic coordination compounds

Simon M. J. Endraß, Thomas M. Klapötke, Jasmin T. Lechner, Jörg Stierstorfer,*

published in *FirePhysChem* **2023**, *48,* e202300010

DOI: 10.1016/j.fpc.2023.03.005

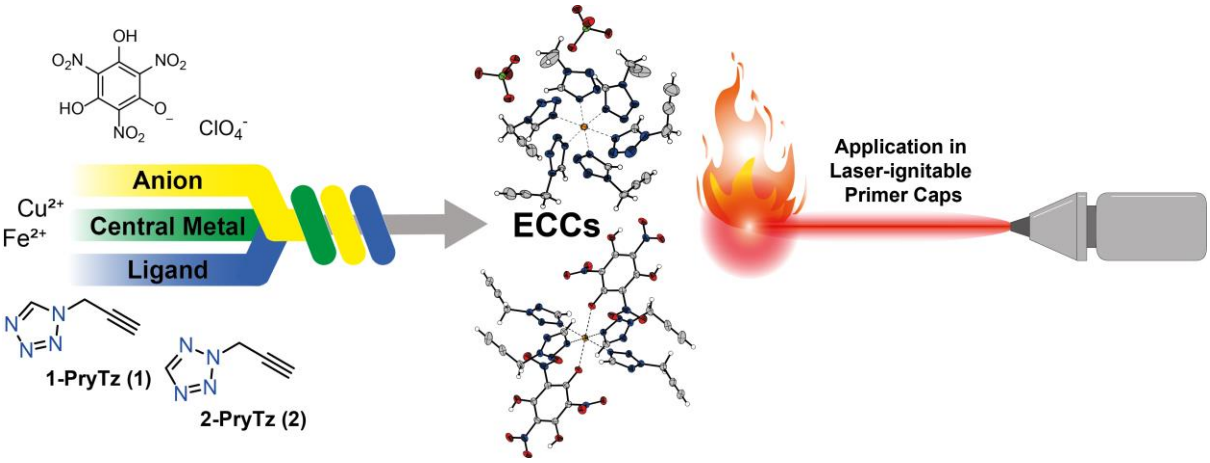

Abstract: 1- and 2-Propargyl-tetrazole (1- and 2-PryTz) were synthesized by reaction of propargyl bromide with sodium tetrazolate and used as ligands in energetic coordination compounds (ECCs) and evaluated concerning their thermal and mechanical sensitivities. Furthermore, the two nitrogen-rich compounds 1-((1*H*-1,2,3-triazol-4-yl)methyl)-1*H*-tetrazole (TriMT, 3) and 1-((1-(2-(1*H*-tetrazol-1-yl)ethyl)-1*H*-1,2,3-triazol-4-yl)methyl)-1*H*-tetrazole (TriMTET, 4) were prepared. Both were characterized by IR spectroscopy, NMR measurements, and low-temperature X-Ray diffraction analysis. Due to the highly endothermic enthalpy of formation of the propargyl-tetrazole ligands, powerful, yet relatively safe to handle, laser-ignitable ECCs were obtained.

13.2 List of Conferences

1 24th International Seminar: New Trends in Research of Energetic Materials (NTREM), Pardubice (Czech Republic) 06.04.2022 − 08.04.2022:

Poster presentation:

Comparing long-term stability predictions of commonly known secondary explosives.

2 1st International Explosives Conference (IEC), London (United Kingdom) 22.06.2022 − 24.06.2022:

Oral presentation:

Crystal Structure and Characterization of the Well-Known Plasticizers Ethylene Glycol Dinitrate, Diethylene Glycol Dinitrate and Triethylene Glycol Dinitrate.

3 10th INTERNATIONAL SCIENTIFIC CONFERENCE ON DEFENSIVE TECHNOLOGIES (OTEH), Belgrad (Serbien) 13.10.2022 − 14.10.2022:

Oral presentation:

SYNTHESIS – The Core Component of Energetic Materials Research.

4 25th International Seminar: New Trends in Research of Energetic Materials (NTREM), Pardubice (Serbia) 19.04.2023 − 21.04.2023:

Oral presentation:

Investigation of a New Promising Process for RDX and HMX Synthesis via TRAT and TAT.

5 52nd International ICT-Conference, Karlsruhe (Germany) 27.06.2023 − 30.06.2023:

Oral presentation:

Investigation of some new nitrazapropyl- and trinitrazaheptyl-bridged energetic molecules.